CHARACTERIZATION OF XYLOGLUCAN ENDOTRANSGLYCOSYLASE (XET) ENZYMES FROM DIFFERENT PLANT SPECIES

by

Merve Seven

Submitted to Graduate School of Natural and Applied Sciences
in Partial Fulfillment of the Requirements
for the Degree of Doctor in Philosophy in
Biotechnology

Yeditepe University

2017

CHARACTERIZATION OF XYLOGLUCAN ENDOTRANSGLYCOSYLASE (XET) ENZYMES FROM DIFFERENT PLANT SPECIES

APPROVED BY:

Assist. Prof. Dr. Andrew John Harvey .....
(Thesis Supervisor)

Prof. Dr. Berna Sarıyar Akbulut .....

Prof. Dr. Işıl Aksan Kurnaz .....

Assist. Prof. Dr. Hüseyin Çimen .....

Assist. Prof. Dr. Sanem Argın .....

DATE OF APPROVAL: .../.../2017

ACKNOWLEDGEMENTS

It is with immense gratitude that I acknowledge the support and help of my Assist. Prof. Dr. Andrew John Harvey. Pursuing my thesis under his supervision has been an experience which broadens the mind and presents an unlimited source of learning.

During my PhD journey, I had chances to meet and work with wonderful people whom I would like to mention and thank in person; Burcu Gür, my first lab mate; Ümit Cem Derman, a true and understanding friend; Dr. Hülya Pınar Akdemir Koç, who is more than an associate and collaborator; Ezgi Türksever, always there for a warm hug; Michael Banner Wells, despite miles of distance he always believed in me and my work; Emrah Özcan for helping me see that it is never the end; my valuable jury members for their worthy comments throughout my thesis course; Prof. Dr. Ece Genç and Prof. Dr. İnci Özden for sharing their lab and HPLC instrument; Prof. Dr. Murat Kasap and Assist. Prof. Dr. Gürler Akpınar, they were very welcoming and helpful with proteomic work; Assoc. Prof. Ferruh Özcan, always welcomed me in his lab; valuable faculty members of Yeditepe University Genetic and Bioengineering Department Prof Dr. Fikrettin Şahin, Prof. Dr. Gamze Torun Köse, Prof. Dr. Mustafa Çulha, Assoc Prof Dilek Telci, Assist. Prof. Dr. Bahar Soğutmaz Özdemir, Assist. Prof. Dr. Emrah Nikerel, Assist. Prof. Dr. Hüseyin Çimen and Assist. Prof. Dr. Ali Özhan Aytekin for their valuable advices and my dear friends Ezgi Avşar Abdik, Hüseyin Abdik, Görkem Cemali, Başak Kandemir, members of Bioprocess Group and members of Bahar's Lab, office mates, many undergraduate students who helped me survive the day; Rüyam Fettahoğlu, Algan Göksan, Onurcan Özbolat, Beyza Mat, Melis Süleymangil, Kübra Öztürk, Büşra Ülger, Dilara Tüzün. I would also like to thank my sisters-from-other-misters Emel Ünal and Cansu Ebren for always being there for me without any hesitation. And a one more gratitude to a wonder woman, whom I am so fortunate to come across in my journey, Ekin Akbaş Arpacı.

Last but not the least, I would like to thank my mother, my father, my lovely sister and my aunty for their endless love and support, which makes everything possible and more beautiful.

ABSTRACT

CHARACTERIZATION OF XYLOGLUCAN ENDOTRANSGLYCOSYLASE (XET) ENZYMES FROM DIFFERENT PLANT SPECIES

Kingdom Plantae, which has extensive variety between species and provides the planet with most of the fixed organic carbon, is a very important kingdom with a specific distinctive feature; cell walls made of polysaccharides and functional and structural proteins. Plant cell walls are made of cellulose microfibrils embedded in a matrix of pectic polysaccharides and cross-linked with non-cellulosic β-linked polysaccharides. Xyloglucan is a major non-cellulosic β-linked polysaccharide, it is ubiquitous in the cell walls of non-graminaceous, graminaceous and evolutionarily distant species like *Equisetum* plants, and it links cellulose microfibrils to form load-bearing structures in the primary cell wall.

The cell wall changes during the lifespan of a plant. This change, or adaptation, is achieved by enzymes that are capable of modifying cell wall polysaccharides. Xyloglucan endotransglycosylase/hydrolase enzymes (XTH), found as multi-member isozyme families in most plant species, including agriculturally important species, catalyse endotransglycosylation and/or hydrolysis of xyloglucan and possibly other polysaccharides within the plant cell wall, resulting in modifications of the wall.

XTH enzymes group into six phylogenetic clades depending on their amino acid sequences, which are also proven to differ in their substrate specificity. As demonstrated in this thesis, Group I XTH family members show dominant preference to xyloglucan whereas ancestral clade members have a broader substrate specificity, with *Arabidopsis* ATXTH3 members acting preferentially on mixed-linked β-glucan. On the other hand, with the discovery of mixed-linked β-glucan in *Equisetum fluviatile*, a new enzyme was identified named as mixed-linked β-glucan: xyloglucan endotransglycosylase (MXE). *E. telmateia*, an *Equisetum* species commonly found in Turkey, was used as an explant in order to purify, characterize and identify an MXE-like enzyme. With enzyme characterizations of MXE, ancestral clade and Group I members, evolution of XTHs in plants from bacterial licheninase ancestors is aimed to be enlightened.

ÖZET

FARKLI BİTKİ TÜRLERİNDEN KSİLOGLUKAN ENDOTRANSGLİKOZİLAZ (XET) ENZİMLERİNİN KARAKTERİZASYONU

Türler arası engin çeşitlilik gösteren ve Dünya üzerindeki bağlı organik karbonun büyük kısmını sağlayan Bitkiler Alemi, özgül ayırt edici bir özelliğe sahiptir; polisakkaritlerden ve fonksiyonel ve yapısal proteinlerden oluşmuş bir hücre duvarı. Bitki hücre duvarları, pektik polisakkaritlerinden oluşmuş bir matriks içine gömülmüş ve selülozik olmayan β-bağlı polisakkaritler ile çapraz bağlanmış selüloz mikrofibrillerinden oluşmuştur. Ksiloglukan, otsu olan, otsu olmayan ve *Equisetum* gibi evrimsel olarak uzak türlerde çokça bulunan, başlıca selülozik olmayan β-bağlı polisakkaritlerden biridir ve yük taşıyıcı bir yapı oluşturmak üzere primer hücre duvarında selüloz mikrofibrillerini çapraz bağlamaktadır.

Hücre duvarı, bitkinin yaşamı boyunca değişmektedir. Bu değişim, veya adaptasyon, hücre duvarını değiştirebilen enzimler ile sağlanmaktadır. Tarımsal öneme sahip bitki türleri de dahil olmak üzere çoğu bitkide çok üyeli izozim aileleri şeklinde bulunan ksiloglukan endotransglikozilaz/ hidrolaz (XTH) enzimleri, hücre duvarında ksiloglukanın ve büyük ihtimalle diğer polisakkaritlerin endotransglikozilasyonu ve/veya hidrolizini katalizleyerek hücre duvarını değiştirmektedir.

XTH enzimleri, amino asit dizileri temel alınarak altı adet filogenetik grup oluşturmaktadır ki enzimlerin substrat özgüllüklerinin de gruplar arası değiştiği gösterilmiştir. Bu çalışmada gösterildiği gibi Grup I XTH enzimleri baskın bir ksiloglukan tercihi gösterirken atasal grup üyeleri daha geniş bir substrat tercihi sergilerler ki *Arabidopsis* AtXTH3 üyesinin tercihi substratı karışık-bağlı β-glukandır. Bir diğer yandan, *Equisetum fluviatile* bitksinde karışık-bağlı β-glukanın keşfi ile, karışık-bağlı β-glukan; ksiloglukan endotransglikozlaz (MXE) olarak isimlendirilen bir enzim tanımlanmıştır. Türkiye'de yaygın olarak bulunan *E. telmateia* eksplant olarak kullanılıp MXE-benzeri enzim saflaştırılmış, karakterize edilmiş ve tanımlanmıştır. MXE, atasal grup ve Grup I üyesi enzimlerin karakterizasyonu ile bitki XTH'lerinin bakteri likeninaz atalarından evriminin aydınlatılması hedeflenmiştir.

TABLE OF CONTENTS

LIST OF FIGURES

LIST OF TABLES

LIST OF SYMBOLS/ABBREVIATIONS

ACN	Acetonitrile
AOX1	*Alcohol oxidase 1*
APS	Ammonium per sulphate
BA	1,3:1,4-β-glucotetraose A
BB	1,3:1,4-β-glucotetraose B
BB	1,3:1,4-β-glucotetraose C
BBG	Barley β-glucan
BLAST	Basic Local Alignment Search Tool
BMGY	Buffered glycerol complex medium
BMMY	Buffered methanol complex medium
BR	Brassinosteroid
BSA	Bovine serume albumin
CAZymes	Carbohydrate-Active enzymes
cDNA	complementary DNA
CESA	Cellulose Synthase
CSL	Cellulose Synthase Like
CelS	Cellulose synthase enzyme complex
CM	Carob galactomannan
CMC	Carboxymethyl Cellulose
CT	1,4-β-cellotetraose
CV	Column volume
CXE	Cellulose: xyloglucan endotransglycosylase
DGM	Di-galactosyl mannopentaose
DNA	Deoxyribonucleic acid
dNTP	Deoxynucleotide triphosphate
DP	Degree of polymerization
DTT	Dithiothreitol
ECL	Enhanced chemiluminescence
EDTA	Ethylenediaminetetraacetic acid
EG16	Endoglucanase 16
FLD	Fluorescence detector

FPLC	Fast protein liquid chromatography
FTIR	Fourier transform infrared spectroscopy
GHs	Glycoside hydrolases
Glc	1,4-β-D-glucosyl
GGM	Guar galactomannan
GM	Galactosyl mannotriose
GPa	Gigapascal
GSP	Gene specific primer
HEC	Hydroxyl-ethyl cellulose
HPLC	High pressure liquid chromatography
HRP	Horseradish peroxidase
HTG	Hetero-trans-β-glucanase
IAA	indole-3-acetic acid
IPTG	Isopropyl β-D-1-thiogalactopyranoside
Kb	Kilobase
kDa	Kilodalton
KM	Konjac glucomannan
KPa	Kilopascal
LB	Luria Bertani broth
LBA	Luria Bertani agar
LC-MS	Liquid chromatography-mass spectrometry
LG	Lupin galactan
LT	Laminaritetraose
MALDI-TOF MS	Matrix-assisted laser desorption/ionization time-of-flight mass spectrometry
MC	Methyl Cellulose
MLG	Mixed linked β-glucan
MT	1,4-β-mannotetraose
MXE	Mixed linked β-glucan; xyloglucan endotransglycosylase
NCBI	National Center for Biotechnology Information
NEB	New England Biolabs
OD	Optic density
PBS	Phosphate buffer saline

PCR	Polymerase chain reaction
PDB	Protein Data Bank
PMSF	Phenylmethane sulfonyl fluoride
RACE	Rapid amplification of cDNA ends
RC	Regenerative cellulose
RNA	Ribonucleic acid
rpm	Rounds per minute
RT-PCR	Reverse Transcriptase PCR
SDS-PAGE	Sodium dodecyl sulphate polyacrylamide gel electrophoresis
TBS-T	Tris buffer saline tween 20
TCA	Trichloroacetic acid
TXG	Tamarind seed xyloglucan
UDP-α-glucose	Uridine diphosphate glucose
UPLC	Ultra performance liquid chromatography
UV	Ultra violet
WA	Wheat arabinoxylan
XEH	Xyloglucan endohydrolase
XET	Xyloglucan endotransglycosylase
XyG	Xyloglucan
Xyl*p*	1,6-α-xylopyranose
XT	1,4-β-D-xylotetraose
XTH	Xyloglucan endotransglycosylase/hydrolase
X7	Xyloglucan heptasaccharide
XGO	Xyloglucan oligosaccharide
YPD	Yeast extract peptone dextrose medium
YPDS agar	Yeast extract peptone dextrose sorbitol medium

1. INTRODUCTION

1.1. PLANT CELL WALL

Kingdom Plantae is one of the main kingdoms of living organisms on earth. World's molecular oxygen is provided by green plants and algae. They convert sunlight energy to chemical energy via photosynthesis reactions and store the chemical energy within sugar molecules. Due to this characteristic, plants have been an important source of food, feed, fibre and building materials for humankind throughout the civilization history.

An important feature and a distinctive character of plants is that plant cells have cell wall as a surrounding outer layer of their cells. The plant cell wall is observed outside of all cells of vascular plants [1]. Plant cells synthesize and deposit this extracellular matrix outside of cell's plasma membrane. Cell wall thickness can range between 0.1 μm to 0.3 μm but can also exceed 1 μm in some examples [2]. The plant cell wall is made of polysaccharides, glycosylated proteins and lignins in a general view [3]. Primary cell walls are highly complex structures composed of inextensible, immobilized, nanometre sized cellulose microfibrils that are cross-linked by and embedded in a gel-like, heterogeneously mobile matrix made of non-cellulosic β-linked polysaccharides and pectins. Alongside to the carbohydrate composition of plant cell walls, there are also proteins and glycoproteins that function as enzymes or structural proteins [4-8]. All of these components give shape to plant cell protoplast and bring mechanical properties to the cell. Thickness of the cell wall composition differs in-between plant cell types [9]. However, cell walls are more than just a physical barrier or mechanical protector for plant cells, they have many more crucial roles due to determining feature of a plant as a whole through giving shape to individual cells [10]. The cell wall provides necessary strength and flexibility for cells to withstand harsh environmental conditions. By the help of cell wall, plants can grow in environments with less osmotic strength than that of their cytosol. It helps plant cells to withstand turgor pressure as high as 5-20 atmospheres which is created when plants encounter osmotic water flow inside the cell when placed in a hypotonic medium [9, 11]. It protects plant cells from impacts of environmental effects like hard rain or wind gusts and it plays an important role in plant-microbe interactions and defence responses against pathogens

[12](). It is thought that during the cell wall degradation under a pathogen attack, released oligosaccharide can act as latent signal molecules and this can be a result of complex structure of the cell walls [3]. By assuring cell-to-cell adhesion, it contributes to mechanical robustness of growing cells [13]. Through structural elements like plasmodesmata or pores inside the cell wall matrix, it allows transfer of solutes and signalling molecules between cells [14]. Since plant cell wall constitutes the interface between neighbouring cells, it is also responsible for intercellular communication of plant cells [7, 11]. Growth and development of plant cells is not only controlled by genes, but also controlled by cellulose in the cell wall. The plane of cell division and axis along which cell elongation takes place determines direction of growth [15]. Plant cell walls have changing structure which evolve throughout the life of a cell depending on growth and organ development [16].

Increase in cell volume happens after cellular water uptake. While resisting turgor pressure caused by cellular water uptake, wall polymers stretch and this situation creates a wall stress which provides necessary mechanical energy that is required to extend the cell wall. Cellulose microfibrils are aligned in one direction within the cell wall and turgor pressure generally cause a stress perpendicular to direction of cellulose microfibrils. This situation results in pectin and non-cellulosic β-linked polysaccharide cross-linked matrix bearing the stress [6]. Plant cells can grow up to a thousand-fold of their initial volume during maturation and to prevent cell wall from becoming too thin and weak, new polymers are integrated into the wall during controlled and selective polymer creep/loosening of cellulose microfibrils. Wall loosening is a modification, like scission of stress-bearing crosslinks, of the wall network that results in a reduction in wall stress without a dimensional change of the cell [17].

In addition to being a very important molecule for turgor pressure in plant cells, water is also an important player in structure and mechanics of primary cell walls. It is also essential for the activity of wall loosening / wall degrading enzymes [8].

Cell elongation and expansion are two biochemically and physiologically important metabolism features that are strictly controlled at cell wall level.

It is possible to see two different and distinct types of cell walls in plants; primary cell wall and secondary cell wall. These different cell wall types have differences in matrix polymer

structures, mechanical properties and functions [18]. It should be kept in mind that cell walls of different plants have distinct characteristics, yet more or less they are placed in the spectrum with 2 extreme ends as primary and secondary cell walls [7].

1.1.1. Primary Cell Wall

Primary cell wall is the cell wall layer formed during the cell formation, expansion and development [19]. Structurally, it is a highly-hydrated matrix of pectin polysaccharides with cellulose microfibrils that are cross-linked by non-cellulosic β-linked polysaccharides embedded within. In some specialized plants, primary cell wall can also comprise lignin, suberin, cutin or silica polymers [18-20]. Polysaccharide composition of primary walls differ in-between grasses and dicot plants. Primary cell wall is stable enough to prevent cells from rupturing under turgor pressure and also extensible enough to permit cell expansion while keeping plant cells intact [21]. Likewise, plant cell wall growth and differentiation are affected by structural modifications in the primary cell wall [22]. Importance of cell wall modification was shown in many processes in life cycle of plants such as cell growth, organ abscission, fruit softening and ripening and pathogen response [23-26].

Primary cell wall components form a complex matrix structure by cross linking to each other via non-covalent interactions or covalent linkages. Cellulose microfibrils hydrogen-bond to each other and some other non-cellulosic β-linked polysaccharides. Pectic polysaccharide content of the primary cell wall was also shown to form covalent cross-links between each other through borate diester cross-links and this is said to have a structural importance for the cell wall [19, 27]. Another example of covalent interactions within the cell wall is the linkage between xyloglucan and pectins in the cell walls of suspension-cultured rose cells [28].

Primary cell walls of flowering plants can be subsumed into two categories based on structural differences; Type I cell walls and Type II cell walls. Ratios of cellulose, pectins and non-cellulosic β-linked polysaccharides differ in these cell wall types [29]. Type I cell wall is found in dicots, noncommelinoid monocots and gymnosperms. Type II cell wall is found in commelinoid monocots.

1.1.2. Secondary Cell Wall

In some cell types like fibre cells of woods and xylem-phloem tissue cells, secondary cell wall is deposited after termination of cell growth, between the primary cell wall and the plasma membrane [3, 30]. Secondary cell wall deposition happens in cells that require great mechanical strength and structural reinforcement [17]. It confers mechanical stability to some specialized cell types like xylem elements and sclerenchyma cells. Different from primary cell walls, it contains lignin and much higher proportion of cellulose to non-cellulosic β-linked polysaccharides and it is reported that xyloglucan and pectin components of secondary cell wall are usually replaced by xylans and glucomannans [31]. In addition to polysaccharide structure of the cell wall, there are also some structural proteins and cell modifying enzymes [21] .

1.2. PLANT CELL WALL STRUCTURE

Plant cell walls are composed of a wide variety of polysaccharides and composition of these polysaccharides within a wall change within the lifespan of a plant.

Cellulose is very important for plants in that it not only helps plants to withstand the internal turgor pressure but also helps plant cells to maintain size, shape and division/differentiation potential [15]. While the atmospheric pressure on earth at sea level is 101 kPa, the stiffness of cellulose is said to be 130 GPa [32]. In the structure of the plant cell wall, cellulose microfibrils are embedded into a matrix made non-cellulosic β-linked polysaccharides or so called hemicellulose polymers (xyloglucan, glucomannans, xylans, mixed-linked glucans) and of pectins (homogalacturonan, rhamnogalacturonan I and II) that also help in binding the walls of neighbouring cells together (Figure 1.1) [7]. Non-covalent interactions between matrix polysaccharides and cellulose microfibrils and between different non-cellulosic β-linked polysaccharides keep cell wall building blocks together [1, 17].

Mentioning the group of sugars as ‘non-cellulosic β-linked polysaccharides’ is a truer abbreviation than the term ‘hemicelluloses’, however they are generally mentioned as hemicelluloses in the literature. It should be kept in mind that even if the hemicelluloses

name is used throughout this text or elsewhere, it always refers to non-cellulosic β-linked polysaccharides.

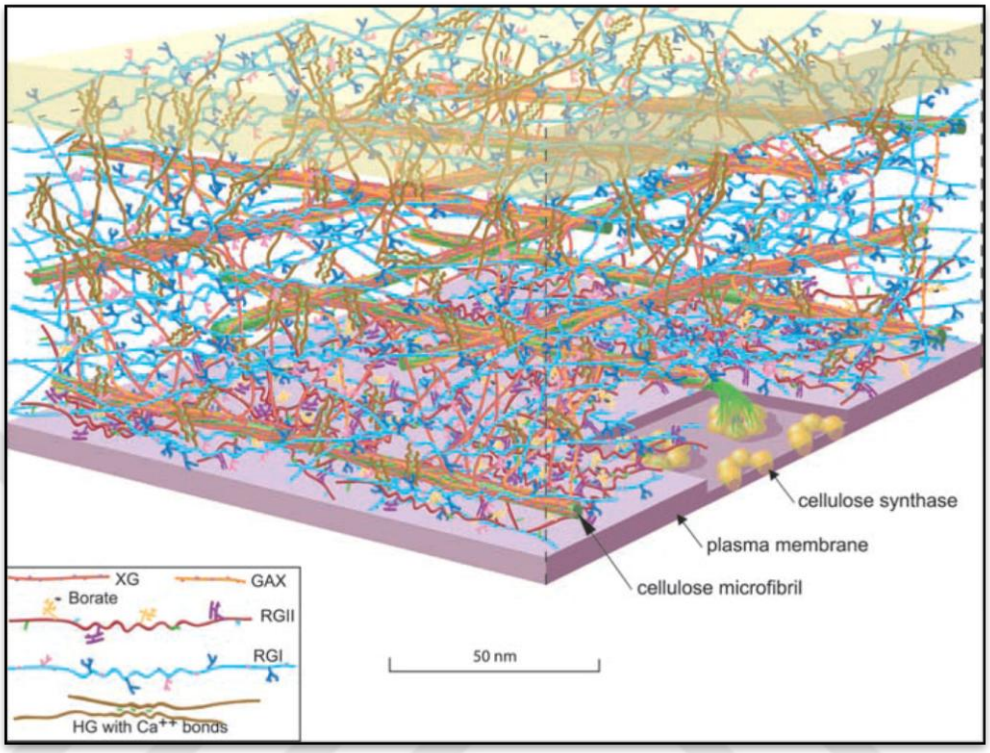

Figure 1.1. Proportional model showing polysaccharides in Arabidopsis leaf cell. Cellulose microfibril amount is reduced for clarity. Non-cellulosic polysaccharide amounts are shown relative to cellulose [3].

Non-cellulosic β-linked polysaccharides are branched polysaccharides. Their backbone is composed of neutral sugars and they form covalent cross-links with cellulose fibrils [3]. Xyloglucan and arabinoxylan are the most abundant non-cellulosic β-linked polysaccharides. Their chemical structure and abundance may vary among different plant species, among different tissues of the same plant, among different cells of the same tissue and during different developmental stages [1, 17, 33].

Different tissue types have different polysaccharide composition, and regulation of cell wall composition also depends on growth and development. This variation is proposed to be caused by different requirements of elasticity and strength of cell walls under different conditions [3].

Cell wall composition varies between monocot and dicot plants. There is not much difference between cellulose percentages between primary cell walls of monocots and dicots; cellulose ratio is ~20-30 per cent in monocots and ~15-30 per cent in dicots. However, percentages and composition of non-cellulosic β-linked polysaccharide ratios differ. While xylans, like arabinoxylan, form ~20-40 per cent of the primary cell wall in monocots, they compose ~5 per cent of dicot primary cell wall. Just the opposite, xyloglucans consist ~1-5 per cent of primary cell wall of monocots and ~20-25 per cent of primary cell wall of dicots. Grass plants also contain ~10-30 per cent of mixed-link glucans, especially (1,3;1,4)-β-D-glucans, which are absent in dicots [29]. Cell wall composition of the same specie's different tissues also shows a variation. For example, *Hordeum vulgare* coleoptile tissue is composed of 35 per cent cellulose 32 per cent heteroxylan and 10 per cent xyloglucan. On the other hand for stem tissues of barley, these values are 65 per cent of cellulose, 28 per cent of heteroxylan and xyloglucan couldn't be detected [34].

1.3. CELLULOSE

Plant cell wall mainly consists of cellulose molecules. Cellulose usually accounts for about 20 per cent of the primary cell wall and 50 per cent of the secondary cell wall in higher plants [35]. It is implied as the most abundant macromolecule on earth. It is a huge linear polysaccharide made of β-1,4 linked glucosyl units. This crystalline state of cellulose is determined by the arrangement of the glucan chains with respect to each other in a unit cell. Insolubility of cellulose is due to hydrogen bonds and van der Waals forces between the glucan chains. These forces cause glucan chains to form aggregates and produce crystalline structures. Molecular weight and degree of crystallinity varies among different cellulose molecules from different species in nature [3, 15]. β-1,4 Linkages between glucosyl sugars make a strong linear polysaccharide that forms stable fibers and 36 parallel cellulose chains build a microfibril [21].

Cellulose synthase (CESA) enzymes are responsible for cellulose synthesis at the plasma membrane and their substrate is cytosolic uridine diphospho-α-glucose (UDP-α-glucose) [15]. The CesA enzyme family belongs to the Cellulose Synthase-Like (CSL) superfamily [17]. Cellulose synthesis is believed to happen in membrane-bound cellulose synthase

enzyme complexes (CelS) which are hexameric rosettes and consists of 36 cellulose synthase (CesA) proteins per rosette (Figure 1.2) [35]. Cellulose synthase A, is the catalytic subunit of the cellulose synthase complex [36]. It has been observed that 3 different *CesA* gene products are required to make a functional CelS [17]. Cellulose synthase enzymes can do cellulose synthesis *de novo* without needing a primer [15]. Glycosyl transfer by inversion of configuration at the anomeric carbon is the process of synthesis as a summary.

During synthesis, monomolecular β-1,4-linked glucan chains are formed and six separate β-1,4-linked glucan chains are directed towards the exit of this complex and then hydrogen-bonded into the crystalline cellulose microfibrils. Throughout the reaction, non-reducing end of the chain is associated to catalytic region of cellulose synthase and addition of new glucose from UDP-glucose donor happens at this end. An interesting thing about cellulose synthase is that synthesized β-1,4-glucan chains have a two-fold symmetry. It is thought that UDP-glucose addition to the non-reducing end of the β-1,4-glucan chain happens in a simultaneous and sequential manner. In this model, newly added glucose residue was inverted 180° with respect to its neighbouring residue. The model also proposes that two-fold symmetry can be provided by a single enzyme with two catalytic sites but this is still debated [15].

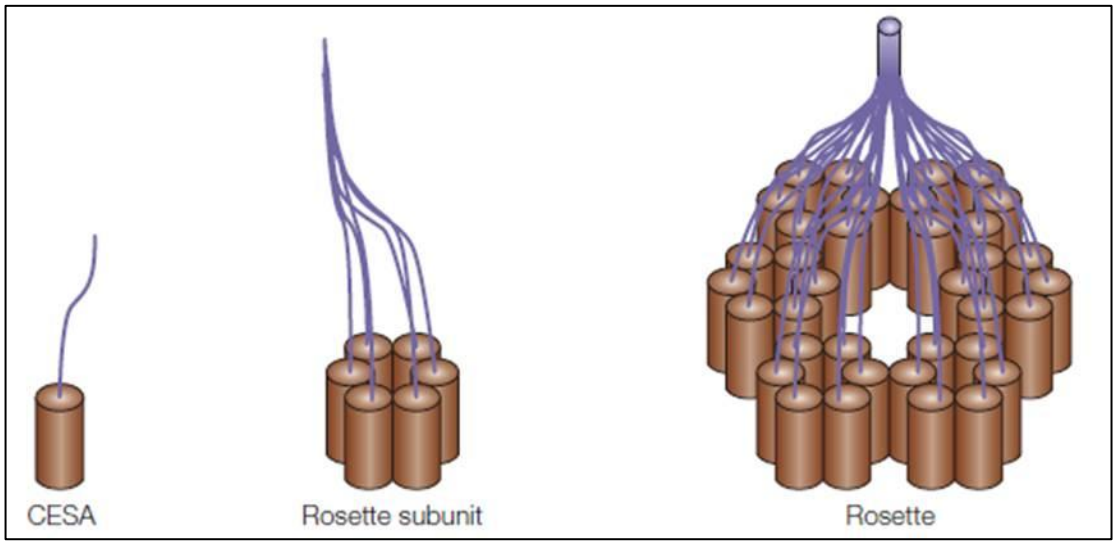

Figure 1.2. Representation of cellulose synthase enzyme complexes (CelS). One CesA can synthesize a β-1,4-linked glucan chain. 36 CesA subunits forming a rosette structure are responsible of cellulose microfibril synthesis [17].

Different families of CesA and Csl enzymes have different catalytic activities, gene expression and regulation characteristics [17, 37].

The *Csl* gene super-family is a huge family made of 9 Csl members, *CslA, CslB, CslC, CslD, CslE, CslF, CslG, CslH, CslJ,* and *CesA* families (Figure 1.3) [34]. Depending on their cell wall compositions, plants can have members of different Csl subgroups [38]. *CesA* genes are responsible of coding enzymes necessary for cellulose synthesis. Due to their phylogenetic similarities to *CesA* members, *Csl* member are thought to be responsible of coding enzymes involved in synthesis of other cellulosic or non-cellulosic polysaccharides of the cell wall in the Golgi [39]. It was observed that *CslF* and *CslH* genes from rice were able to synthesize (1,3;1,4)-β-D-glucan in walls of transgenic Arabidopsis, which natively don't have any *CslF* genes or (1,3;1,4)-β-D-glucan in its walls, containing *CslF* genes of rice [1, 40]. Members of CslA family are linked with β-1,4-mannan backbone synthesis of mannans [41, 42] and members of the CslC family are proposed to be responsible for the synthesis of the xyloglucan backbone [1]. It has been shown that some *Csl* gene products can be associated with synthesis of polysaccharides other than β-1,4-linked glycans. Thus, the reason of wide structural variety and branched structure of polysaccharides of the cell wall can be linked to various members of Csl subfamilies' gene products being responsible of synthesis of differently linked polysaccharide backbones made of different sugars. Three of *Csl* families, *CslF, CslH* and *CslJ* were found to be specific to cereals [34, 39].

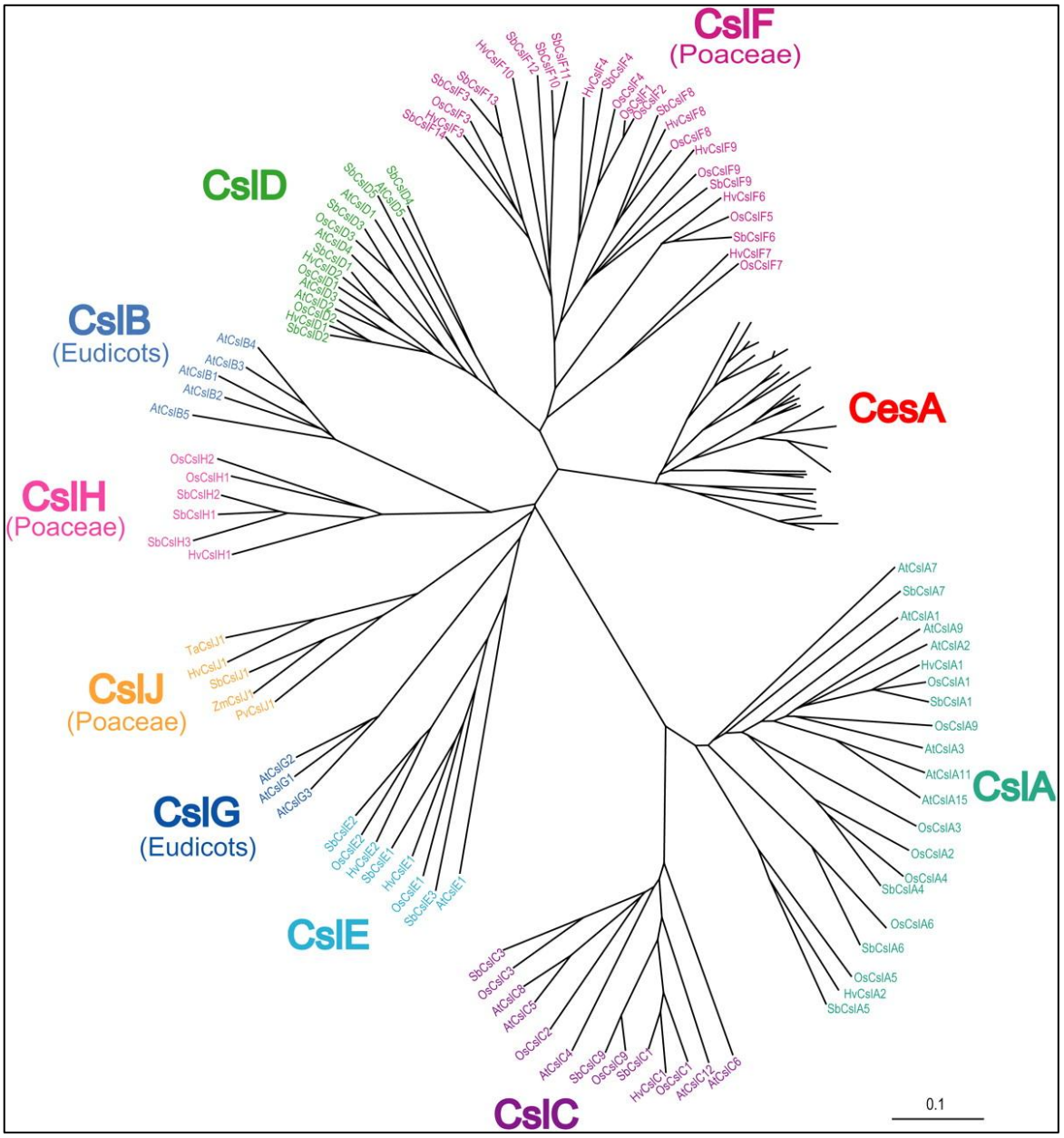

Figure 1.3. Phylogenetic tree of cellulose synthase and cellulose synthase like genes in higher plants. Poaceae is a family under Poales order. It can also be called as grasses. [34].

CesA genes are responsible of encoding probable catalytic subunits of the plant cellulose synthase enzyme complex [37]. In many plant species there are different *CesA* genes but there are also different isoforms generated by splicing that have differential expression patterns in different tissues during different developmental stages [35]. The first plant *CesA* genes were identified in cotton fibre, a tissue highly rich in cellulose, and are renamed as *GhCesA1* and *GhCesA2 [43]*.

Trapping of non-cellulosic β-linked polysaccharides such as xyloglucan in cellulose microfibrils during synthesis is proposed to explain disordered regions in fibril structure [17].

The difference between enzymes responsible for cellulose synthesis in primary and secondary cell walls cause difference between the degree of polymerization and crystallinity of cellulose fibrils in primary and secondary cell walls [30]. A mutation observed in any of three different enzymes building up the rosette structure leads to loss of function and this clearly states that all three different enzymes are necessary for cellulose synthesis in rosettes [15].

In studies on *Oryza sativa*, it was revealed that not only dicots but also monocots harbour multi *CesA* and *Csl* family members. It is seen that plant CesA and Csl enzymes contain the characteristic "D,D,D,QxxRW" motif and this is the conserved region of these proteins [37].

During primary cell wall cellulose synthesis, newly made CelS are needed to be distributed uniformly at the plasma membrane and actin cytoskeleton of the cell is responsible for that distribution [44]. Direction of cellulose synthesis is determined by the microtubules of the individual cell and the role of microtubules is suggested as providing guide channels for setting up the direction of initial microfibril synthesis and also membrane flow within these channels [15]. Cortical microtubules that lie under the plasma membrane of the cell is thought to provide tracks for cellulose synthase complexes [30]. It is also suggested that microfibrils can be providing cues for the orientation of the cortical microtubules [15].

1.4. XYLOGLUCAN

Xyloglucan (XyG) is the major non-cellulosic β-linked polysaccharide, present in primary cell walls of non-graminaceous species, that cross-links cellulose microfibrils and forms a load-bearing structure [1, 17, 45]. Studies with Arabidopsis *xxt1 xxt2* mutants suggest that xyloglucan in the primary cell wall acts as a spacer molecule that reduces interactions of cellulose microfibrils as absence of xyloglucan in these mutants results in aggregation of cellulose microfibrils rather than a multilamellar cell wall formation [46]. Arabidopsis *xxt1 xxt2* mutant was observed to be showing disrupted organization of outer epidermal cell

wall, indicating absence of xyloglucan molecules in primary cell wall structure changes molecular interactions between cellulose microfibrils [46]. It is found in secondary cell wall of seeds of many dicot species (ex. Tamarind, *Tropaeolum*, and *Hymenaea*) as storage polysaccharide and it can be covalently linked to pectins in the wall [1, 28, 47]. It can be seen as a bridge between cellulose microfibrils and between cellulose and other cell wall polysaccharides, around cellulose microfibrils like a cover and entrapped in cellulose microfibrils [48]. Xyloglucan can also act as a spacer molecule by preventing cellulose microfibrils to form interactions and aggregate [1]. Cellulose and xyloglucan comprise nearly two thirds of the dry wall mass of dicot cell walls [49]. Cellulose and xyloglucan polysaccharides form a network matrix by non-covalent/ covalent linkages [50, 51].

Xyloglucan consists of a 1,4-β-D-glucosyl (Glc) backbone with 1,6-α-xylopyranose (Xyl*p*) residues on three out of four glucosyl residues in most dicots and non-graminaceous monocots but plants including other monocots and the Solanales can have two 1,6-α-xylopyranose (Xyl*p*) residues instead of three residues as a basic repeating unit [1, 52]. However, xyloglucans containing repeats of five β-D-glucan residues in the backbone were also seen [53]. Xyloglucan molecules can differ in their degree of polymerization between different tissues of the same plant and between different plant species. This means that not all xyloglucans are synthesized in the same way. In some examples, xylosyl residues can be further decorated by galactosyl and fucosyl residues [17]. (1,4)-β-glucan synthase enzymes, members of CSLC family have role in synthesis of xyloglucan backbone [54]. An α-1,2-fucosyltransferase adds terminal fucosyl residues to the xyloglucan chain. There can also be *O*-acetyl substituent linked to C-2 of galactosyl linked to xylosyl residue of the backbone. *O*-acetylation location can vary depending on species; in *Arabidopsis*, *O*-acetyl residues are observed specifically in the galactosyl residues and in *Nicotiana plumbaginifolia O*-acetylation was observed at the C-6 of the fourth glucosyl residue of the backbone [1, 55]. Xylosyl side chains and other substitutions prevent hydrogen bonding of xyloglucan molecules along the length of the molecule, resulting in a more soluble and flexible macromolecule. Like other non-cellulosic β-linked polysaccharides, is thought to be synthesized in golgi apparatus and then transported to cell wall where it is linked to other polysaccharides *in muro* [3]. Enzymes responsible for its synthesis are not all clear but some recent studies are brightening this area. CslC family members have role in synthesis of the β-(1-4)-glucan backbone of xyloglucan [1]. In Arabidopsis, a member of

the CslC group, AtCslC4, is responsible for the synthesis of β-1,4-glucan backbone of xyloglucan [54] and is localized in the golgi. CslC enzymes are integral membrane enzymes with putative multiple transmembrane domains. Both C- and N- termini and active site of the enzyme are predicted to be facing the cytosol, so they can be using cytosolic UDP-glucose for synthesizing β-(1-4)-glucan chains just like cellulose synthase (CesA) enzymes [56]. Besides the AtCslC4 β-glucan synthase or its equivalents, there are many more enzymes playing roles in xyloglucan synthesis since it is made of many different sugar subunits; three α-1,6-xylosyltranferases names as XXT1, XXT2 and XXT5 [57, 58], an α-fucosyltranferase [59] and a β-1,2-galactosyltranferases named as MUR3 [60], have been identified in *Arabidopsis thaliana*.

Xyloglucans are highly substituted molecules, but contain a repeating subunit structure. So called XXXG type xyloglucan is the subunit structure most commonly seen in higher plants. To help clarify this, the nomenclature used here is based on abbreviating backbone monosaccharides or oligosaccharides with one letter. Representation of sugar residues with letters is a widely-used method. Each backbone β-D-glucosyl residue is connected to the next via a β-1-4 linkage, and if they are unsubstituted, i.e. they have no sidechain or acetyl residues attached, are represented with a ‘G’ letter (Figure 1.4a). When an α-D-xylosyl residue is attached to one of the backbone β-D-glucosyls via an α-1-6 linkage, it is represented by an ‘X’ (Figure 1.4b). If there is a β-D-galactosyl residue attached to xylosyl of X with β-1-2 linkage, this newly formed structure is shown with an ‘L’ (Figure 1.4c). When an α-L-fucosyl residue is attached to the ‘L’ trisaccharide via α-1-2 linkage as a forth residue, it is represented as an ‘F’ (Figure 1.4d). These four sub-structures, G, X, L and F, are the most abundant ones in xyloglucan chemistry but there are some rare residues too. If an α-L-arabinosyl is linked on an X via α-1-2 linkage, an ‘S’ is formed (Figure 1.4e). With one more α-L-arabinosyl addition to an ‘S’ by a 1-3 linkage, ‘T’ is formed (Figure 1.4f). If a further β-D-galactosyl residue is linked to an L trisaccharide by a 1-2 linkage, ‘J’ is formed (Figure 1.4g) [61].

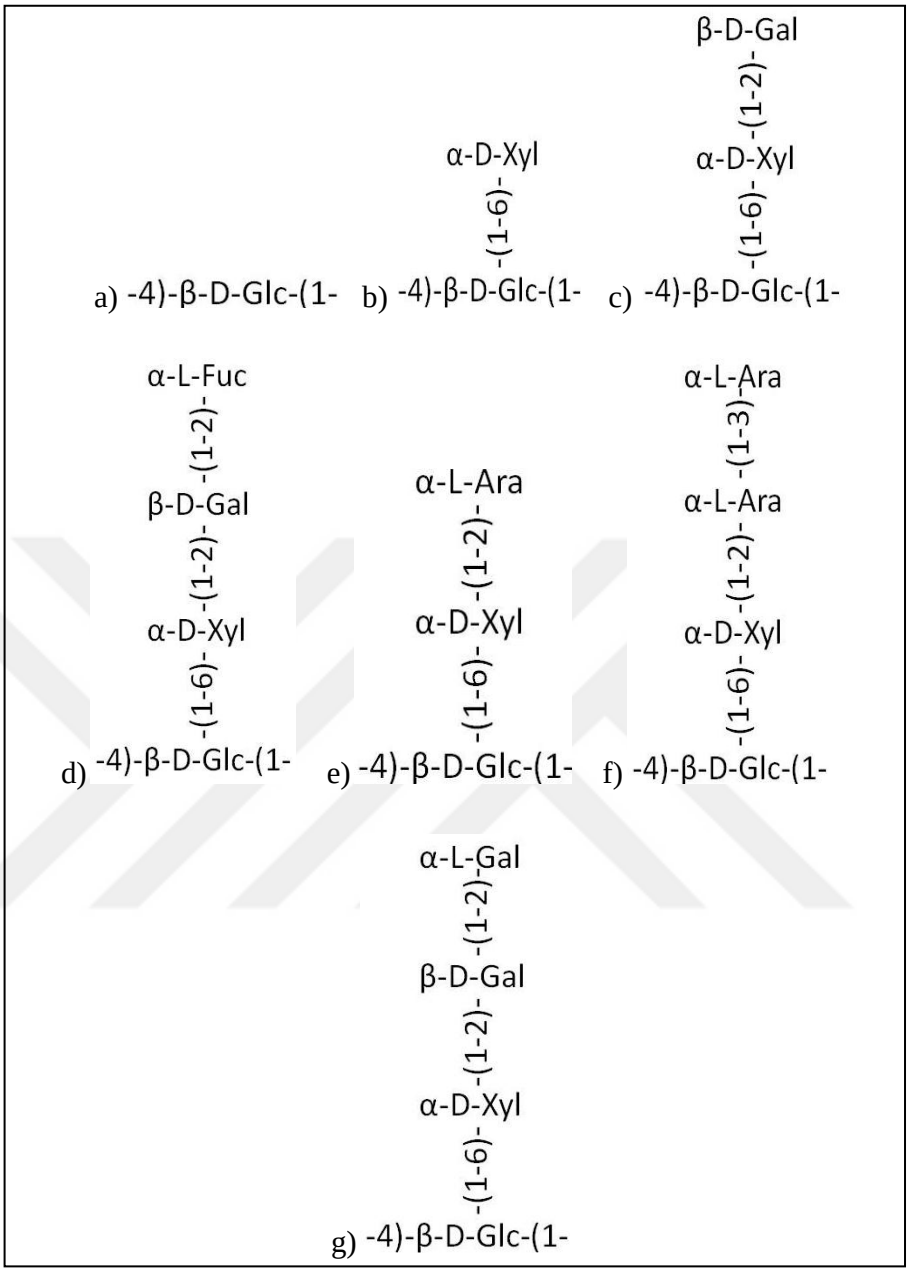

Figure 1.4: Legends of different subunits of xyloglucan saccharides. a) glucose residue is shown as ‘G’, b) xyl-glc residue is shown as ‘X’, c) gal-xyl-glc residue is shown as ‘L’, d) fuc-gal-xyl-glc residue is shown as ‘F’, e) ara-xyl-glc residue is shown as ‘S’, f) ara-ara-xyl-glc residue is shown as ‘T’, g) gal-gal-xyl-glc residue is shown as ‘J’.

Thus, the subunit structure XXXG represents four β-1,4-linked β-D-glucosyl residues, the first three of which are substituted with β-D-xylosyl residues (Figure 1.5a). There can be additional subunits to this main structure; sometimes a galactose can be added to the second and/or third xylosyl forming XXLG (Figure 1.5b) XLXG or XLLG, and a fucose

may be linked onto a galactosyl at the third position forming XLFG (Figure 1.5c) or XXFG (figure 1.5d).

The xyloglucan polysaccharides of a plant can be composed of one or more of the xyloglucan oligosaccharides subunit types described above. For example, it is possible to see XLFG, XXFG, XXLG/XLXG and XXXG structures in *Gossypium* (cotton) fibers but *Nerium oleander* leaves hosts a wider structural polymorphism; it contains XLFG, XXFG, XXXG, XLSG, and XXSG. Fucosylated XXXG (XLFG or XXFG) is a common feature in most dicots and non-graminaceous monocots. However, in Solanaceae members such as tobacco and tomato, it is more likely to see xyloglucan subunits of XXGG and a *O*-acetyl group at O-6 of a non-branched glucose residue. Members of Solanaceae and Oleaceae produce xyloglucans with arabinosyl residues but no fucosyl residues. Even though four glucosyl-based xyloglucan molecules are mostly seen, XXGGG-based xyloglucans (cellopentaose based) are observed in *Plantago major* and *Ocimum basilicum* [53]. Storage xyloglucan seen in seeds of some plant species are usually non-fucosylated and they have high molecular weight around 2000 kDa [47]. Endo-(1→4)-β-glucanase enzyme or named as cellulase enzyme can be used to fragment xyloglucan polysaccharides and analyse building block oligosaccharides of the chain [33]. This enzyme carries out endohydrolysis of 1-4-β-glucosidic linkages in 1-4-β-linked glucans. As a result of hydrolysis reaction, xyloglucan oligosaccharides with a non-branched glucose at the reducing end are observed however there are XXXX-type xyloglucans, with 1-2 linked α-L-arabinoxylan at every glucosyl residue, is reported in the literature [48].

The xyloglucan pool of the dicot *Arabidopsis thaliana* consists of 33 per cent of XXXG, 6.5 per cent of XXLG, 22 per cent XXFG and 25.3 per cent of XLFG as the main subunits present. Whereas the xyloglucan pool of *Hordeum vulgare*, a monocot species, consists of 44.4 per cent of XXG, 39.1 per cent of XXGG, 6.6 per cent of XXGGG as the main xyloglucan oligosaccharides that built up the xyloglucan polysaccharides [62].

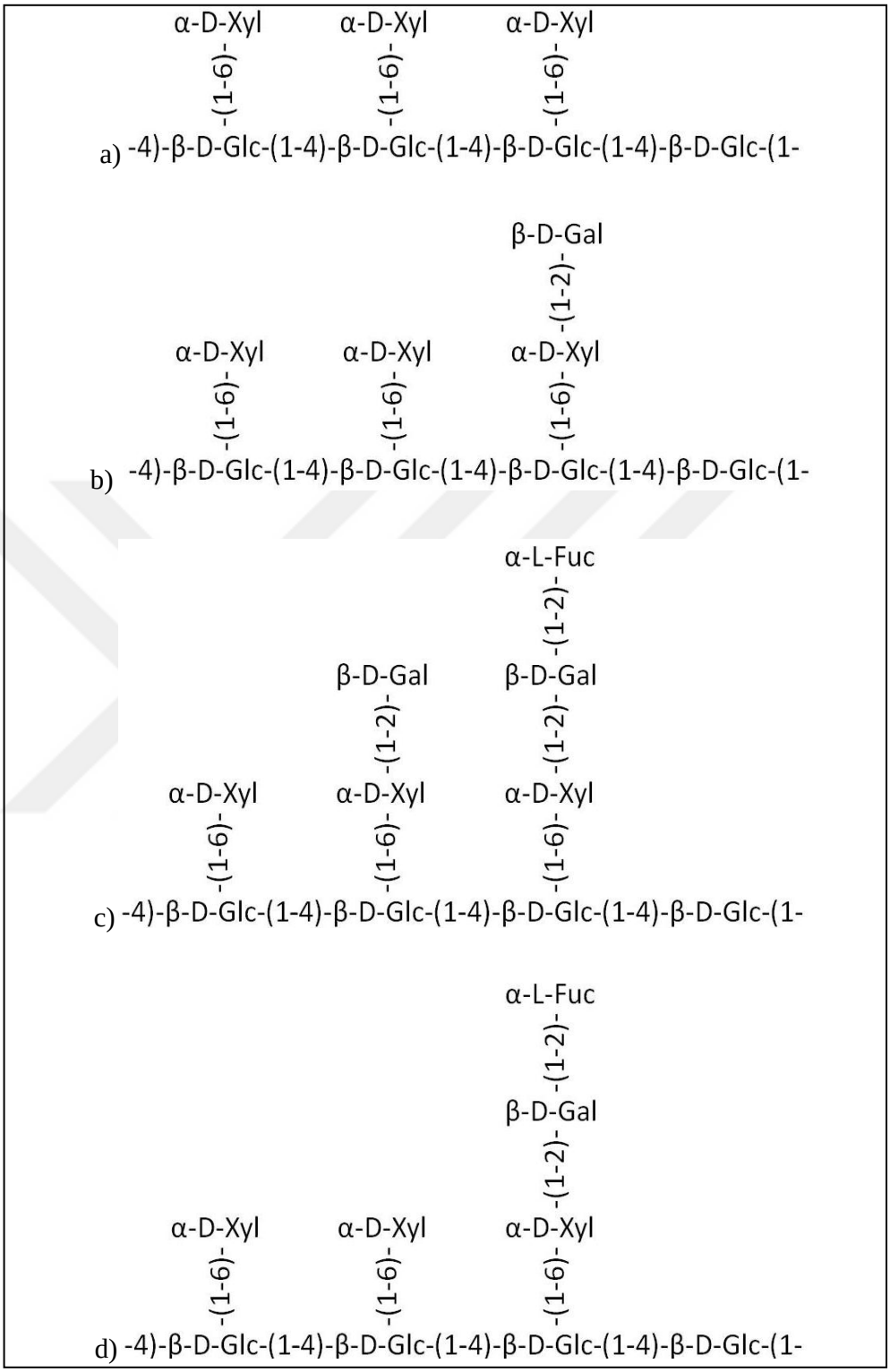

Figure 1.5. Representative structure of xyloglucan oligosaccharides. a) XXXG, b) XXLG, c) XLFG, d) XXFG.

Difference in fine structure, branching and molecular weight of xyloglucan effects binding capacity of xyloglucan to cellulose and this influence strength of the cell wall. For example, fucosylation of xyloglucan chains is proposed to increase their binding capacity to cellulose microfibrils. However, it has been observed that if non-fucosylated xyloglucan has the same molecular weight with the fucosylated form, cellulose binding capacity is not altered, but fucosylation effects cellulose binding energy. It has been reported that xyloglucans with lower molecular weight have a higher binding capacity to cellulose. When a xyloglucan with lower molecular weight is compared with a fucosylated xyloglucan with a relatively higher molecular weight, the lower molecular weight xyloglucan is seem to bind better to cellulose [47].

It should be kept in mind that since XXXG is composed of seven sugar residues, it can be also mentioned as a xyloglucan heptasaccharide or X7 or xyloglucan DP-7 standing for degree of polymerization 7. XXLG and XLXG are examples of xyloglucan octasaccharides since they are composed of eight sugar residues and all octasaccharide xyloglucans can be grouped as X8 or xyloglucan DP-8 standing for degree of polymerization 8. XXFG is an example of xyloglucan nonasaccharide and all xyloglucans made of nine sugar residues like XXFG can be grouped as X9 or xyloglucan DP-9 standing for degree of polymerization 9.

The xyloglucan-cellulose network is the main load bearing structure of primary cell walls, at least in dicot species. It has been shown that xyloglucans covalently link to rhamnogalacturonans which proposes that xyloglucan-cellulose network is also connected to pectins chemically [63]. Cell walls change during the lifetime of plants in order to adapt to changing environmental conditions and since structural changes in cellulose-xyloglucan network are considered to be regulated by enzymatic modifications, wall-modifying enzymes are expected to play an important role in regulation of cell wall modifications [25], thus helping plants to withstand change. As Charles Darwin once said “It is not the strongest of the species that survives, nor the most intelligent that survives. It is the one that is the most adaptable to change.”

Non-cellulosic β-linked polysaccharide chains bind to cellulose microfibrils tightly via hydrogen-bonds, cross-linking cellulose microfibrils together and the mechanical strength of the cell wall depends on these cross-linkages [7]. They can be named as cellulose-

binding polysaccharides too [17]. Although details about matrix formation are not clear, there are some models about linkages between cellulose microfibrils. One of the proposed ideas is that non-cellulosic β-linked polysaccharides can spontaneously bind to the surface of cellulose microfibrils and link them together. Another suggests that xyloglucan chains become trapped into cellulose microfibrils during synthesis and the untrapped end of that xyloglucan chain can bind to another cellulose microfibril or another non-cellulosic β-linked polysaccharide, thus connecting microfibrils together. A similar idea is that cellulose microfibrils might be covered with xyloglucans and those xyloglucans can be attached to other matrix polysaccharides. By this way, microfibrils are connected to each other through several molecules [17].

1.5. XYLANS

Xylans in all higher plants have a backbone of xylopyranosyl units linked via β-(1→4) linkages and they can be substituted by various monosaccharides/oligosaccharides [64]. They are specifically found in secondary walls of eudicots, in glucuronoxylan form, acting as strengthening load-bearing structure, in secondary walls of commelinoid monocots and a major polymer of starchy endosperm in cereals [16, 64]. A β-(1,4)-linked xylosyl backbone with α-(1,2)-linked glucuronic acid or 4-*O*-methyl-glucuronic acid substitutes is named as glucuronoxylan. In grasses, the β-(1,4)-linked xylosyl backbone can have *O*-acetyl groups, α-(1,3)- and/or α-(1,2)-arabinosyl and α-(1,2)-linked glucuronic acid or 4-*O*-methyl-glucuronic acid [1].

Structure of arabinoxylan differs between different cereal species; mono-substitution of xylans with 1-2 linked α-L-arabinosyl is a common structural feature in barley however it is rare in wheat and rye [34, 65]. Especially arabinoxylan in cereal grasses also carry glucuronic acid and ferulic acid ester residues [17](α-L-arabinosyl residues increase the solubility of arabinoxylan molecule and the highly branched nature of arabinoxylan molecules provide resistance against enzymatic degradation. It is found in primary and secondary cell walls of starchy endosperm and aleurone layer of cereals. It dominates endosperm cell walls of cereals except oats and barley; in these two cereals it makes up ~20 per cent of cell wall whereas it is ~60-70 per cent of rest of the cereals' cell walls [65].

1.5. MANNANS

Mannans are composed of a backbone of β-1,4-linked mannose residues or combination of β-1,4-linked mannose and glucose residues. α-1,6-linked galactose residue side chains are also a frequently seen structure. Existence of galactose residues in the structure increase solubility and interactions with other cell wall polysaccharides [66]. If the backbone has both β-1,4-linked mannan and glucose residues, then the polysaccharide is called glucomannan. They are found at the secondary cell wall of plants. Glucogalactomannans are formed when galactose residues are linked to the glucomannan backbone. Galactomannan has a β-1,4-linked mannan backbone with α-1,6-linked galactosyl residues [67].

Acetylation of galactosyl residues of galactomannans at O-2 and O-3 position is also observed. It is in abundance at the secondary cell wall of gymnosperms, especially in xylem tissue. It is also storage polysaccharide in guar-bean seeds and many other legume and palm members of angiosperms [1, 17, 66].

1.6. MIXED LINKED B-GLUCANS

Poaceae (grasses), *Equisetum* species, some fungi, algae and bryophytes contain mixed linked β-glucans (MLG) in their cell walls resulting in an asymmetrical distribution of MLG among plant kingdom. Out of these species, Poales and *Equisetum* spp. are the only vascular plants that possess MLG [68-70]. They are especially abundant in starchy endosperm walls of cereal grains that commonly consume every day, making it a very important part of daily diets of humankind and an important molecule as glucose storage for plant itself too [16, 68]. It is also found in the developing tissues of cereals like coleoptiles. Presence of MLG is evident in vascular tissues of Poales too, suggesting a structural and strengthening role of cell wall matrix [71].

(1,3;1,4)-β-D-glucans are made of glucosyl residues that are linked by 1,3-β and 1,4-β links. Distribution and ratios of β-1,3-glucosyl and β-1,4-glucosyl along the whole glucan chain differs between different species but general range of β-1,4-glucosyl residues to β-1,3-glucosyl residues is 2.2 to 2.6:1 in cereal. Even though distribution of the two different

glucosyl linkages are not clear yet and said to be random, two or more β-1,3-glucosyl residues are not likely to be seen linked to each other in species screened, two β-1,3-linkages are always separated by two or more β-1,4-l-linkages. Introduction of β-1,3-linkages into the long glucan chain causes formation of many kinks in the structure, decreasing or even eliminating inter-chain hydrogen bonding, resulting in the solubility of these large glucan molecules in water. Irregular distribution of β-1,3-linkages contribute to solubility and gel formation of MLG [68]. Yet, number of sequential 1,4-β links effect solubility of MLG, thus function and properties of the polysaccharide. MLGs form cross-links between cellulose microfibrils in Poales cell wall and chemical property of cross-links within cell wall structure confers to flexibility and porosity of the cell wall, showing the importance of chemical structure on function [68].

1.7. XYLOGLUCAN ENDOTRANSGLYCOSYLASE/HYDROLASE (XTH) ENZYMES

Developmental processes and physiological changes such as fruit ripening or abscission (detachment) of leaves in the fall season are all related to cell wall modifications. This situation makes plant cell walls and their structural regulation highly important topics for overall plant world.

One of the main aims of the cell wall is keeping the cell intact, in shape and keeping it away from expanding uncontrollably. However, it must be loosened and modified controllably while the cells grow. The polysaccharide network making up the cell wall that is helping the cell to protect its integrity under normal turgor conditions should relax during cell expansion, in order to allow an increase in the cell volume. While cell expansion, new polysaccharides must be synthesized and added into the cell wall [3, 21, 63] .

During growth of plant cells, elongation happens in a perpendicular manner to cellulose microfibrils. For elongation to happen, cellulose microfibrils should separate. Since microfibrils are generally cross-linked to each other by xyloglucan chains, xyloglucan endotransglycosylase enzymes are proposed to have an important role in cell wall elongation via controlled cell wall loosening [52]. Also, part of the fruit ripening process is

known to be as a result of enzymatic depolymerisation of xyloglucan in the cell wall which leads to wall-softening [72].

An important group of enzymes responsible for modification of cell wall are the Xyloglucan Endotransglycosylase (XET) enzymes (EC 2.4.1.207) [3]. They are apoplastic enzymes, having pH optima appropriate for this location which is typically between pH 5 and pH 6 [49]. XETs are classified as one of many Carbohydrate-Active Enzymes (CAZymes). CAZymes are the enzymes that cleave and build glycosidic bonds between saccharides in nature [73]. Plant XTH enzymes belong to the Glycosyl Hydrolase 16 (GH16) family in the CAZy classification [63]. Beside XTH enzymes from plants, there are also algal, bacterial and fungal hydrolases in GH16 family. However, amongst other enzymes, *XTH* gene products are most closely related to bacterial β-1,3;1,4-glucan hydrolases. This relationship suggests possible evolution of XTH enzymes from bacterial licheninase precursors [74, 75].

There are many enzyme families and groups under the CAZy classification that breakdown or modify oligosaccharides and polysaccharides; there are glycoside hydrolases, glycosyltransferases, polysaccharide lyases, carbohydrate esterases and carbohydrate-binding modules [76, 77]. Glycoside hydrolases (GH) (EC 3.2.1-) consists of 133 protein families based on amino acid sequences that are responsible for hydrolysis and/or transglycosylation of glycosidic bonds [76]. The GH family can also be divided into 14 clans from GH-A to GH-N depending on sequence and folding similarities of the enzymes.

XETs use xyloglucan as a substrate and have effects on the mechanical properties of the cell wall. They cleave the backbone of a xyloglucan molecule and add that cleaved chain with the reducing end to a non-reducing end of another polymeric or oligomeric xyloglucan chain [25] (Figure 1.6).

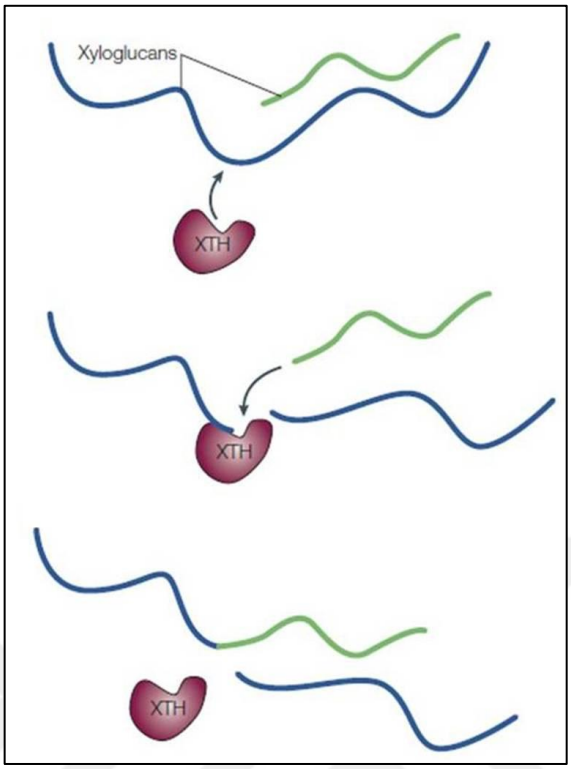

Figure 1.6. Endotransglycosylation activity of XTH enzymes. The top figure shows XTH enzyme breaking the glycosidic bond of a xyloglucan chain. The middle image shows reducing end of the cut chain in covalently linked to the enzyme and a free non-reducing end bearing xyloglucan moves to the catalytic site. The bottom figure shows newly formed hybrid xyloglucan and a xyloglucan chain is released [17].

Xyloglucan molecules can be integrated in two different ways. The first one is encounter of newly synthesized xyloglucans and nascent cellulose microfibrils via hydrogen bonding at the surface of the plasma membrane. Xyloglucan chains will become a part of the microfibril. The second way of integration of xyloglucan chains is via an XET enzyme. Exogenous xyloglucan is thought to be endotransglycosylated to anchored xyloglucan by the enzyme.

Endotransglycosylation happens at fourth glucose unit of xyloglucan 1,4-linked glucose backbone [52]. Endotransglycosylation reaction can be represented by 2 equations as in Figure 1.7.

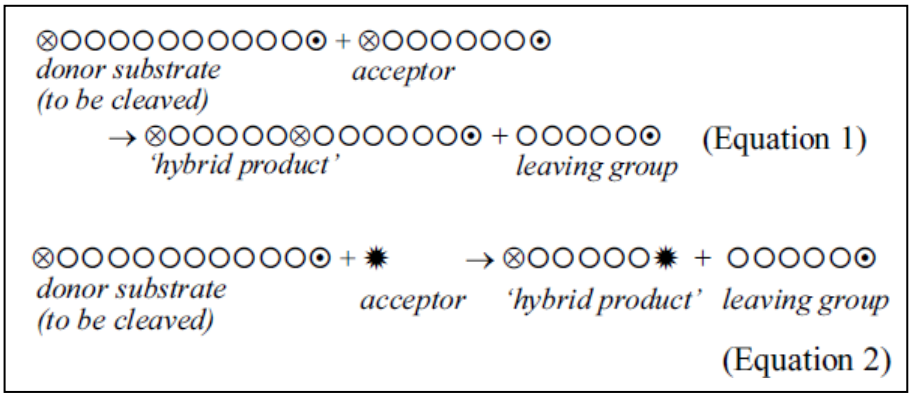

Figure 1.7. Representation of enzymatic reaction of endotransglycosylation. Each empty circle represents a xyloglucan oligosaccharide. Circles with dots in them represent reducing sugars. Equation 1 is the endotransglycosylation reaction happening between two xyloglucan chains. Equation 2 is the endotransglycosylation reaction happening between a xyloglucan polysaccharide and a xyloglucan oligosaccharide.

In the Equation 1, a glycosyl bond is broken and a new one is made in endotransglycosylation reaction. Endotransglycosylation can happen between polysaccharide-oligosaccharide or polysaccharide-polysaccharide. Equation 1 is a representative for polysaccharide-polysaccharide endotransglycosylation. When [^{3}H]Glc was used at the reducing terminus of xyloglucan acceptor, this is transglycosylated to the donor ^{1}H-xyloglucan molecule, leading to production of ^{3}H-xyloglucans with high molecular weight. However, an increase in the molecular weight is not always the case. Polysaccharide-oligosaccharide endotransglycosylation is shown in Equation 2 (Figure 1.7). [^{3}H]XGO (^{3}H labelled xyloglucan oligosaccharide mixture that consists of xyloglucan heptasaccharide, xyloglucan octasaccharide and xyloglucan nonasaccharide) acceptor is transglycosylated to high molecular weight xyloglucan donor chain in this reaction and it can be released by cellulase in intact form afterwards showing it is attached via β-(1→4) glycosidic bond. . Transglycosylation of xyloglucan oligosaccharides can be more preferential due to favourable kinetics for the smaller molecules as acceptors. Oligosaccharide-oligosaccharide endotransglycosylation is not a common event because XTH enzymes don't prefer small donors [49].

XET enzymes can also display hydrolase activity and since it is hard to determine whether an enzyme has hydrolysis activity as xyloglucan endohydrolase (XEH) and/or transglycosylation activity as xyloglucan endotransglycosylase (XET), the enzyme family is often named as xyloglucan endotransglycosylase/hydrolase (XTH) [78].

During hydrolysis activity (XEH) with the enzymes, the acceptor is H_2O instead of XGOs or other saccharide molecules. Some XTH enzymes have true XEH activity where as some show XEH activity during the absence of abundant XGO acceptor molecules. Hydrolase activity of XEH shouldn't be mixed with endo-β-1,4-glucanases, or in other words cellulases [49, 79].

Nasturtium seed xyloglucanase can use water molecules as substrate and at low xyloglucan acceptor concentrations; it acts as a hydrolytic enzyme [45].

While the donor preferences of XET/XTH enzymes are not clear, it is known that they prefer xyloglucan as donor. Xyloglucans' chemical composition and molecular weight can differ between different plants and different XTH enzymes seem to have specific preferences. Glc_4-based XGOs with Xyl/Glc-rich backbone are general acceptors and all known XET enzymes are able to use them. The preference of donor and acceptor saccharides can be relevant to an enzyme's function in a particular tissue. For example, some prefer relatively high molecular weight donors while some can tolerate low molecular weight ones [80, 81] . Some can show higher affinity to high molecular weight xyloglucans while other can have higher affinity to XGOs like XXXG. Some tend to show less reaction rates with xyloglucans containing fucose residues. In some cases, non-reducing end of donor can act as acceptor, competing with real labelled-acceptor. Such competition can be prevented by using high concentration of acceptor molecule [49].

If the target xyloglucan molecule of XET enzymes is acting as a tether between cellulose molecules, the reaction with xyloglucan oligosaccharides (XGO) might result in the cleavage of the tether. If endogenous xyloglucans are endotransglycosylated consecutively with xyloglucan oligosaccharides, that results in decrease of their molecule size in the wall but it will increase their solubility [52].

Theoretically, cell wall extension is achieved if the cellulose-xyloglucan network is modified [78]. It has been shown that cell wall elongation can be accelerated and

suppressed by integration of xyloglucan and xyloglucan oligosaccharides, respectively, to the cell wall [52].

XTH enzymes modify cell walls via causing cell wall loosening or adding xyloglucan chains to extending walls [45]. They make up 1.2 per cent by weight of apoplastic proteins in *Vigna angularis Ohwi and Ohashi cv.* Takara hypocotyls [80]. XTH enzymes have role/s in the construction and modification of the cell wall. These enzymes are encoded by members of multigene families in higher plants [82]. An important point that should be kept in mind is that if cell wall loosening happens without wall synthesis and reinforcement, it can lead to disastrous structural failure [49].

XTH enzymes are implicated during different physiological events and they can be listed as wall loosening, wall strengthening, wall restructuring, integration of new xyloglucans into the wall, trimming xyloglucan strands that are not tightly stuck to the surface of cellulose, fruit softening and hydrolysis of xyloglucans. They have affects that result in changes in the mechanical properties of the cell wall [17, 49, 83]. By usage of fluorescently labelled XGOs, XET activity was monitored at the elongation zone of Arabidopsis and tobacco roots [84]. Additionally, *XTH* gene expression is usually found during rapid cell expansion or cell division sites. Increases in XTH activity and/or *XTH* expression level was observed during formation of root aerenchyma [85], mesophyll air space, abscission zones and vascular tissues [86]. These experimental evidences suggest that XTH enzymes may be important in catalysing xyloglucan depolymerisation and/or solubilisation during cell wall disassembly [49]. However, there is not always a correlation between growth and *XTH* gene expression [63]. A study with tomato *LeXTH2* gene showed that the gene was expressed in the mature nonelongating regions of the hypocotyls whereas its mRNA abundance decreased after auxin treatment of etiolated hypocotyls segments [87].

XET gene expression was observed especially in rapidly elongating cotton fibre cells [88]. XET enzyme action was also visualized by fluorescently labelled XGO integration into root elongation zones of Lycopodiopsida and Polypodiopsida and various mono- and dicotyledonous angiosperm representatives, independent from any evolutionary distance between species [89]. A tomato *XTH* gene expression was found to be higher in tissues with higher elongation and growth rate and in relation with that, transgenic lines over-expressing *SlXTH* were observed to have a higher cell wall extensibility in the apical

hypocotyl segment. Also, FTIR analysis of cell wall polysaccharide linkages revealed that *SlXTH* overexpressing lines show differences in cellulose-xyloglucan regions [10].

XTH transcript levels were found to be the highest in early stage cotton fibre elongation, which can be interpreted as *XTH*s playing an important role in cell wall loosening during cell elongation [90]. As a study reinforcing such a theory, *GhXTH1* transgenic cotton plants, a *XTH* gene natively highly expressed in elongating cotton fibers, resulted in 15-20 per cent longer fibers compared to control plants [91]. This transgenic approach supports the idea of *XTH* expression being differentiated into tissues and XTHs taking role in cell elongation in cotton fibre elongation.

Also, XET activity was reported during secondary growth within the vascular region in poplar stem which was supported with the presence of fucosylated xyloglucan presence in secondary vascular tissues. Xyloglucan was observed during early secondary wall formation in xylem fibre and at primary-secondary wall junction. It was proposed that newly synthesized xyloglucan sugars are secreted to primary cell wall, passing through secondary cell wall and this situation creates strengthened links between microfibrils of primary and secondary walls [92]. Moreover, XET activity and *XTH* gene products were found to be present in mature, several years old gelatinous fibers, which are formed during the final stage of fibre differentiation, of poplar branches indicating post-mortem arrangement of the cell wall [93].

XTH gene expression and/or XTH enzyme activity is also affected by different plant hormones or biotic/abiotic stresses [49]. XTH enzymes are proposed to be related to effects driven by growth-enhancing hormones such as auxins and brassinosteroids [63]. Endogenous treatment of ethylene, a plant hormone that has role in abscission and fruit ripening, is seen to induce expression of several different *XET* genes (*SlXTH5*, *SlXTH8* and *MdXTH10*) and increase XET activity in tomato and apple [94].

An *XET* gene from *Cicer arietinum* (chickpea) expression was high in elongating tissues; apical epicotyls and lesser in roots. Gene expression was also up-regulated by exogenous IAA (indole-3-acetic acid; has role in growth) and BR (brassinosteroid; induce elongation) treatment and this finding points out relationship between *CaXTH1* and growth [63].

Expression of a hot pepper (*Capsicum annuum*) *XTH* gene, *CaXTH3*, was found to be induced by abiotic stresses such as salt and drought stress [95]. Constitutive expression of

the hot pepper *CaXTH3* gene in transgenic tomato plants is seen to enhance tolerance of tomato plants to salt and drought stress too. Abiotic stress tolerance is a widely-studied topic in the literature but significance of this study is that expression of *CaXTH3* transgene in tomato host didn't cause any phenotypic defects, like altering leaf or root morphology, that are almost always found in other similar studies. Under the stress conditions, width/length ratios of stomatal apertures of the transgenic tomato plants were smaller [96]. Even though it is not known in details, expression of *CaXTH3* might affect cell wall structure and cause guard cells of stomatal apertures to expand causing them to close in transgenic plants. *Populus euphratica XTH* (*PeXTH*) overexpression in tobacco cells increased tolerance of transgenic tobacco plants against salinity stress. Overexpression of *PeXTH* resulted in increased water content per unit area, higher ratio of fresh weight to dry weight compared to wild type plants and these changes result in an increase in water-retaining capacity in the leaf [97].

XTH enzyme activity was also found to be related to physiological trait of crop plants. In lettuce salad plants, down regulation of a member of *XTH* gene family, *LsXTH16*, generated plants with improved shelf life. This effect was proposed to be due to reduced leaf expansion and increased leaf strength. Also, *XTH* down regulated lines showed less susceptibility against bacterial invasion [98].

There are some experimental methods for detecting and quantifying XET activity. The most sensitive method is the usage of a ^{3}H-labeled acceptor. When radioactively labelled xyloglucan oligosaccharide acceptor and normal xyloglucan donor are incubated in the presence of XET enzyme, donor xyloglucan chain should become radioactively labelled if the enzyme has true endotransglycosylation activity. When the reaction mixture is dried on filter paper and then rinsed with water, hybrid product stays attached to the paper and rest of the reaction components are washed away. By using scintillation-counting, the amount of enzyme activity can be quantified. However, since it is a radioactive method, it can be hard to apply in basic laboratories. So, to overcome security problems, there are also fluorescent methods. Fluorescently labelled XGO with pyridylamino, sulforhodamine or fluorescein can be used as acceptor molecules. Just like radioactive methods, reaction mixture containing fluorescently labelled XGO can be spotted on paper and then analysed [49]. Additionally, since molecules used in the reaction mixture have different molecular

sizes, they can be separated and analysed using size-exclusion liquid chromatography methods.

XEH activity can be detected using colorimetric or viscometric methods. In the absence of XGOs, enzymes showing XEH activity will produce new reducing termini using xyloglucan and production of new reducing termini can be detected colourimetrically [49, 99].

XTH enzymes have a (D/N)-E-(I/L/F/V)-D-(F/I/L/M)-E-(F/L)-(L/M)-G motif that is highly conserved and contains the catalytic site for enzyme activity [49, 74]. Another structural feature is the signalling peptide of ~20 amino acids sequence at the 5' end of first exon that targets synthesized enzyme to the cell wall. XTH-donor linkage was proposed as a glycosyl ester bond between reducing end of the donor and first glutamate residue in the DEID-F/I-EFLG active site. XTH-donor complex can be stable for a period of time and it breaks down when an acceptor molecule is added that enables transglycosylation to be completed. In cell walls, this can be rephrased as XTH-donor molecule can be stable until this complex finds an appropriate acceptor molecule in the wall [49]. So we can assume that enzyme firstly binds donor molecule, forms a reducing end by splitting donor molecule into two parts, then binds acceptor and carries out enzymatic reaction [100].

XTH enzymes are glycosylated for their activities [49]. Glycosylation is mentioned in protein folding and stability and it is also referred that this modification serves as a primary determinant for specific molecular recognition [101]. Removal of N-linked glycosylation by enzymatic treatment causes decrease in transglycosylation activity [102]. Most of the XET enzymes have a conserved potential N-linked glycosylation site/s. One site is found near the C-terminus of the conserved catalytic domain and there are 5-15 residues between catalytic site and glycosylation site. It is proposed to be located near the acceptor binding end of active site. N-glycosylation usually happens at asparagine residue of Asn-X-Ser/Thr motif. A study done with heterologously expressed cauliflower BobXET16A enzyme in *P. pastoris* revealed that glycosyl groups were $Man_{8-12}GlcNAc_2$, but glycan group of the native enzyme usually is $Man_6GlcNAc_2$. Though, it was observed that this change in glycan structure doesn't affect activity [72, 102].

It was observed that XTH enzymes can also target non-cellulosic β-linked polysaccharides other that xyloglucan like arabinoxylan and (1,3;1,4)-β-D-glucan [103].

Studies on the model plant system *Arabidopsis thaliana* help by revealing candidate enzymes and genes that modify plant cell walls [21]. *A. thaliana* is preferred as the model system due to its relatively small genome, availability of established transformation and modification protocols, availability of many mutants, short life cycle (~ 6 weeks), has a similar growth and development strategy to other higher plants, ability of self-fertilization [104, 105].

Studies done with Arabidopsis show that *XTH* genes have different expression profiles. For example, it was seen that expression of *AtXTH22* gene was induced in response to mechanical effects like wind or touch. As a result, we can say that XTH enzymes can have role in adaptation of plant to mechanically stressful environments by manipulating cellulose microfibril/xyloglucan network in primary cell wall that is thought to contribute to the mechanical properties of primary cell walls. Another example is *ATXTH24*; studies done with the help of reporter genes showed that the gene is expressed at organ/tissue branching sites [82].

It has been estimated that cell wall synthesis and metabolism requires more than 2000 genes, which represents almost 10 per cent of all genes for an organism such as Arabidopsis. Identification of these genes and characterization of biochemical and biological functions of the gene products are important areas [7].

There are multiple XTH enzymes and *XTH* genes in different plant species. Existence of many different isoenzymes points out XTH enzymes can have activities other than the ones related to growth or they can have more complex expression and regulation mechanisms [63]. This diversity is proposed to be a result of gene/genome duplication and genes coming from same origin (residing on same chromosome and/or being closely similar) can show different expression patterns [82]. For example, *Arabidopsis thaliana* genome has 33 *XTH* genes [78, 82]. Different genes can show tissue specific and/or developmental stage specific expression or their expression can be effected by external plant hormones application. For example, *Arabidopsis thaliana* genes *AtXTH5, AtXTH12, AtXTH13, AtXTH14, AtXTH17, AtXTH18, AtXTH19, AtXTH20, AtXTH26* and *AtXTH31* shows root-specific expression. Expression of *AtXTH3, AtXTH17, AtXTH22* and *AtXTH23* were upregulated by both auxin and brassinolide. When solely auxin was applied, it only upregulated expression of *AtXTH19* and when solely brassinolide was applied, it increased expression of *AtXTH4* and *AtXTH5*. At the same time, hormones can down-regulate

expression of some genes; transcription of *AtXTH15* and *AtXTH21* were decreased under auxin treatment [82]. However, *XTH* gene expression was also observed in tissues in which cell expansion has completely ceased. Additionally, they were also observed in the cell plate during cytokinesis, which points out that they have variable functions [82].

In tomato (*Solanum lycopersecum*), 25 *XTH* genes have been identified so far and 29+ *XTH* genes in rice (*Oryza sativa*) [106, 107]. Forty-one genes were found in poplar genome [108]. An EST database search revealed 23 possible *XET* members in cotton [91].

Even though the amount of xyloglucan is much less in monocots than dicots (xyloglucans consist ~1-5 per cent of primary cell wall of monocots and ~20-25 per cent of primary cell wall of dicots), monocots also have large *XTH* families. This fact raises the questions of why monocots need many different XTH enzymes and is it possible that XTH enzyme can use substrates other than xyloglucan chains in the cell wall. They are hypothesized to link different polysaccharides in the cell wall [34]. A molecular modelling study done with poplar XTH shows that there are structural similarities at the active site and the substrate-binding clefts of XTH enzymes and (1,3;1,4)-β-D-glucan endohydrolases and xylan endohydrolases [103]. This finding also supports the idea that XTHs can use saccharides other than xyloglucan as substrates.

XET enzymes were mentioned to be playing a part in many physiological roles. In *Arabidopsis thaliana* plants, during metal toxicity caused by aluminium accumulation, it was seen that XET activity decreased and this decrease in enzyme activity was paralleled to apoplastic lesion. Expression of *AtXTH14*, *AtXTH15* and *AtXTH31* were reduced after 24 hour aluminium treatment and inhibition of root elongation was also observed simultaneously. On the other hand, *AtXTH5* expression was increased under aluminium treatment. However, individual roles of enzymes are not clear, so it is not easy to assign exact mechanism of each enzyme during different circumstances like metal toxicity or stresses. Decrease in XET activity will lead to failure of cleavage of the xyloglucan backbone and linking of new xyloglucans and this will prevent cell wall extension [78]. *AtXTH27* gene was shown to mostly be expressed in immature tracheary elements in which secondary wall thickening occurs and less in differentiating vasculature of roots and hypocotyls. Null mutation of *ATXTH27* gene in Arabidopsis plants cause defect in

tracheary elements formation in Arabidopsis rosette leaves, short-shaped tracheary elements in tertiary veins and reduction in the number of tertiary veins [109].

Assigning physiological roles of XTH enzymes or enlightening *XTH* gene expression patterns are hard because these enzymes have a multifunctional nature of transglycosylation/hydrolysis and they are a huge family which makes their analysis even harder. Elucidating XET enzymes' action patterns (acceptor and donor preferences) will be a huge step towards understanding their roles in the plants.

1.8. XYLOGLUCAN ENDOTRANSGLYCOSYLASE/HYDROLASE ENZYME CLASSIFICATION AND EVOLUTIONARY LINKAGES

XTH enzymes are classified into subfamilies based similarities in their amino acid sequences; Group I, Group II, Group III-A, Group III-B, Ancestral Group and EG16 [49, 75, 82] (Figure 1.8). There is no distinction between XTH enzymes belonging to different groups based on their biochemical characteristics or mechanism of action however it was observed that Group I, Group II and Group III-B enzymes predominantly have XET activity whereas Group III-A enzymes show XEH activity [49, 110]. However, when examined deeply, groups might seem to have an organ-specific expression pattern. Some researchers proposed Group I genes tend to show expression in young developing tissues while Group II genes are expressed in response to mechanical and hormonal stimuli [63].

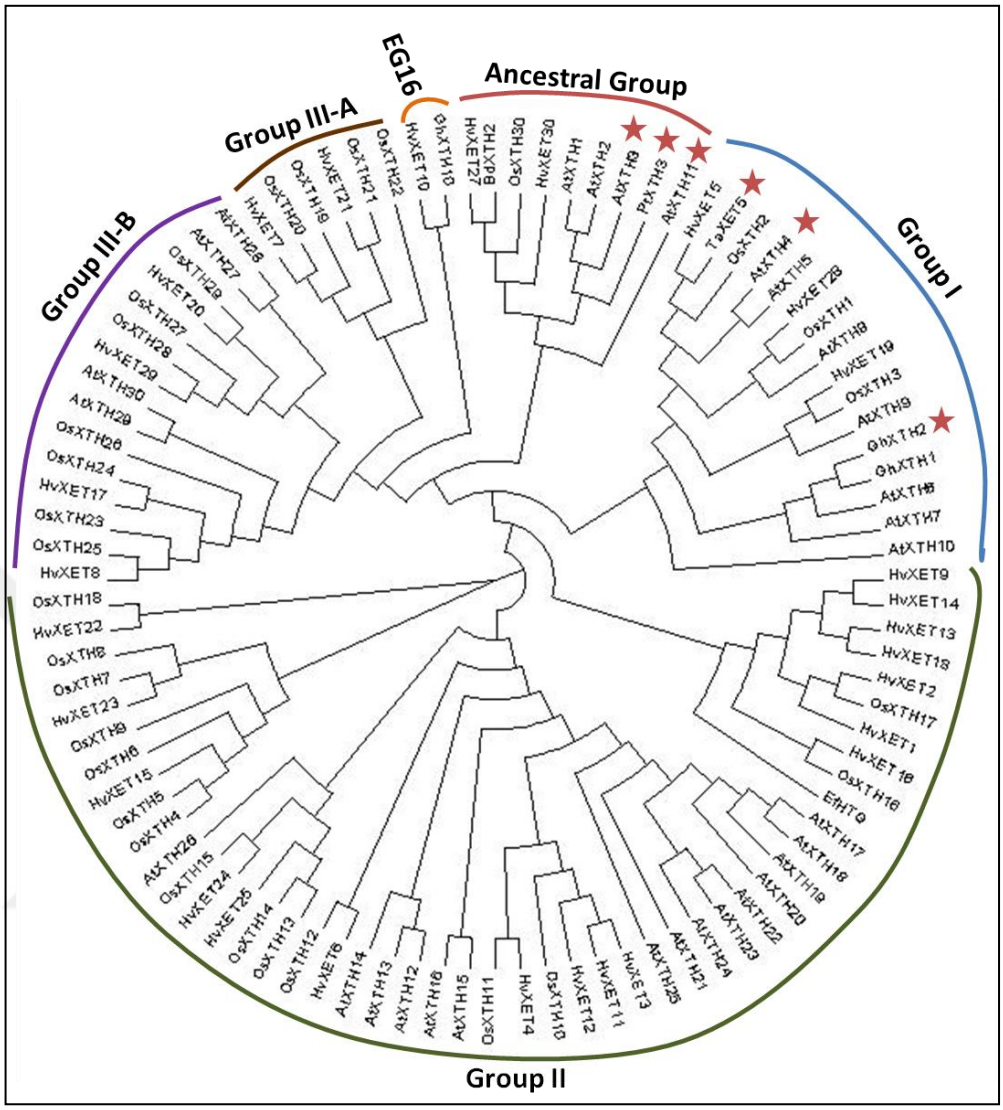

Figure 1.8. Phylogenetic Tree of selected XET enzymes based on their amino acid sequences. Red stars indicate sequences studied in the thesis.

XTH enzymes are member of GH16 family, which also hosts additional enzymes with different catalytic activities. Within the family, XTH proteins and bacterial licheninases (EC 3.2.1.73) were found to be the closest relatives [111], both sequences possessing 'DEIDFEFLG' catalytic site. As a common feature of GH16 family, both XTHs and bacterial licheninases share β-jellyroll fold. When protein models of representatives of XTH family and bacterial licheninases compared, major structural element differences are visible in structures (Figure 1.9, [74]). With existing sequence data and protein model information, it is possible to observe structural changes that took place during XTH

evolution throughout time (Figure 1.10). With a structure analysis of a poplar endo-β-glucanase (*Pt*EG16), the link between licheninases and EG16 endoglucanases was uncovered; loss of a loop which is present in licheninases towards N-terminal end was observed in EG16 [75]. A loop deletion from licheninases provided a wider substrate-binding cleft whereas acquiring a C-terminal domain is recognized as characteristic feature of XET proteins.

Another feature commonly seen in XTH enzymes is conserved Cys residues seen after active site that are thought to help stabilize C-terminal domain. XTH enzymes, except some members of Group III-A, also share a N-linked glycosylation site after active site that is thought to be important for stability of protein and its catalytic properties [74, 75, 110]. Aside from these common features, XTH clades are showing differences especially in loop 1 and loop 2; usually Group III-A and Group III-B members carry insertions in loop 1 and loop 2 [74].

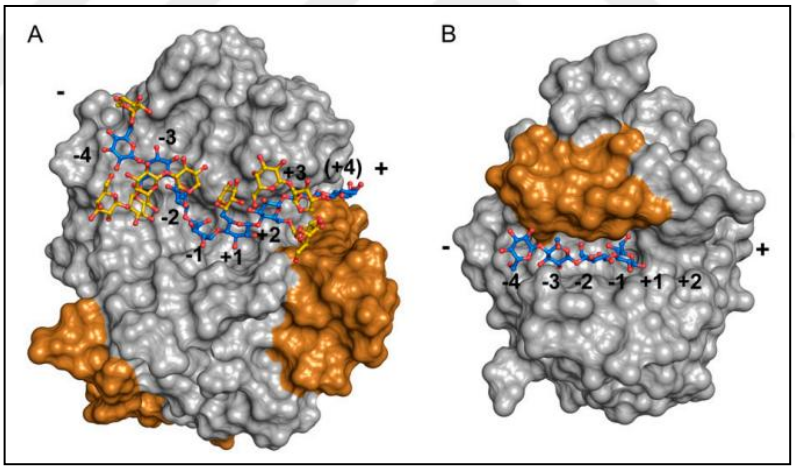

Figure 1.9. Structures of a XTH enzyme and β-1,3;1,4-glucanase. a) PttXET16-34 (PDB ID 1un1, 1umz) model with XLLGXLLG substrate bound to substrate binding cleft, b) β-1,3;1,4-glucanase (PDB ID 1u0a) [74].

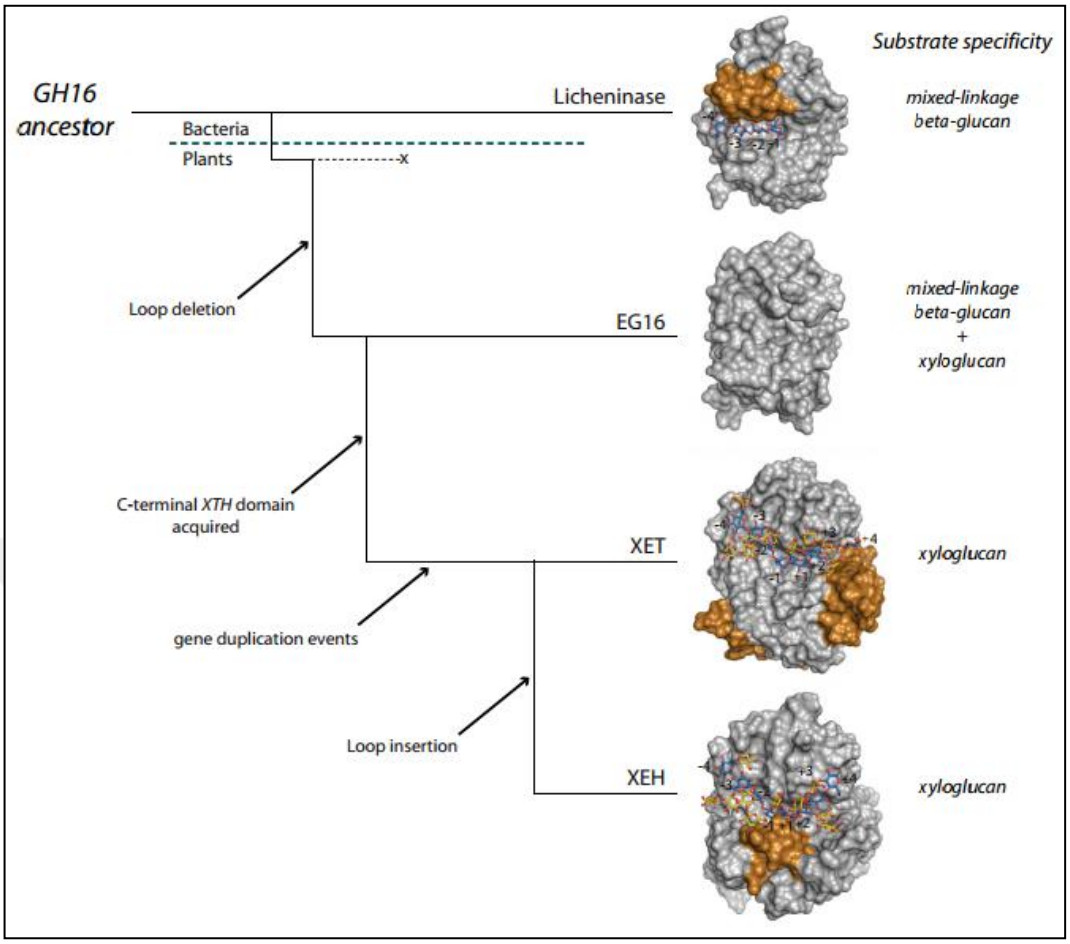

Figure 1.10. Evolution and changes in protein structure of *XTH* gene products from licheninase ancestor [75].

Ancestral clade in XTH phylogenetic tree is the clade whose members are showing amino acid differences in their active site. Due to this difference and their similarity to β-1,3;1,4-glucanase ancestors compared to other clade members, ancestral clade members were grouped separately. This group it thought to be a linking step in evolution of XTHs from precursors. Considering this, substrate specificity of this clade is proposed to be wider. Enzyme characterization of ancestral group members possess an important point in understanding and interpreting evolution of cell wall modifying enzyme.

1.9. *EQUISETUM* AND MIXED-LINKAGE GLUCAN: XYLOGLUCAN ENDOTRANSGLYCOSYLASE (MXE)

Equisetum, known as horsetail in common language, is a living member of Polypodiopsida, which is distant relative of land plants that diverged >380 million years ago [112]. A member of *Equisetum* family, *E. hyemale* was investigated and galacturonosyl and glucuronosyl residues were found to be the most abundant glycosyl residues in *E. hyemale* imidazole and NaOH soluble fractions [113]. However, in a different study, both xyloglucan and mixed-linkage glucan were proven to be present in primary cell walls of several different *Equisetum* species. As a summary of all these findings, *Equisetum* cell wall is made of high ratios of pectins, cellulose, MLG and low ratio of xyloglucan [70, 114, 115]. MLG ratio was more abundant in mature stem base section [114] which can implicate role of MLG in strengthening of cell walls in *Equisetum*.

MLG presence in *Equisetum* raised curiosity because this polysaccharide was only shown in Poales among vascular plants and these two families are not close to each other on an evolutionary scale. Comparison of lichenase digestions of both poalean MLG and *Equisetum* resulted in differences in saccharide compositions; G4G4G4G3 tetrasaccharide is the major component of *Equisetum* MLG whereas G4G4G3 trisaccharide is the most frequently found one in Poaceae primary cell wall. Also, longer than 8 subunit MLG oligosaccharides were absent in analysis of *E. arvense* MLG structure [70, 114]. Another difference from Poales' cell wall, *E. arvense* MLG co-exist with high levels of pectin and cellulose, unlike high content of glucuronoarabinoxylans. Difference in structure can be due to evolutionary dissociation of MLG synthesis system of *Equisetum* plants and Poales. One of the only apparent similarity between *Equisetum* and Poales is their high silica content [116, 117]. This common ground can be interpreted to a relation between MLG spacing and silicification [70].

Another difference *Equisetum* cell wall possess is difference in xyloglucan structural subunits. New xyloglucan structural repeat-units were identified in *E. hyemale* and *Selaginella kraussiana* and they are abbreviated as D and E. D is composed of α-1,2-L-Ara*p* on α-1,6-D-Xyl*p* that is linked to glucose residue. E subunit has an additional α-1,2-L-Fuc*p* linked to arabinosyl residue (Figure 1.11) [118].

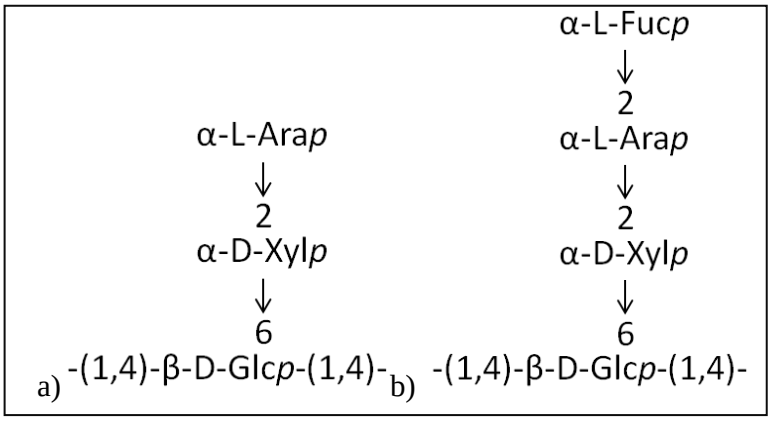

Figure 1.11. Structural subunits of *Equisetum* xyloglucan. a) Subunit D, b) Subunit E.

Additional to finding of MLG in *Equisetum*, a new endotransglycosylase enzyme activity apart from XET activity was identified in various *Equisetum* species crude extracts named as MLG:xyloglucan endotransglycosylase (MXE). Even though MXE and XET enzymes use same acceptor during their catalytic action, there is enough evidence to separate two enzyme activities, making MXE activity a novel one. Ratio of MXE activity over XET activity was reported to be higher in mature tissues of *Equisetum* and older plants and this finding implicate that MXE enzyme might have a wall strengthening role in *Equisetum* cell wall rather than a wall loosening role seen with various XETs [119, 120]). Since both MLG content and MXE activities are reported to be higher in older mature tissues, it can be interpreted than cells synthesize MXE parallel to MLG in order to integrate new MLGs into cell wall structure and strengthen it. This point is a very important point where *Equisetum* cell wall and Poales cell wall differentiate from each other, Poales have high MLG content but lack MXE activity whereas *Equisetum* plants have both MLG substrate and MXE activity. This can also be explained by evolutionary difference between two plant groups.

Plant callus systems are proposed to be good models for studying *in vivo* primary cell structure and metabolism, thus a study was carried with *E. fluviatile* calli in order to visualize both MLG, xyloglucan polysaccharides and MXE, XET enzyme activities by The Edinburgh Cell Wall Group [120]Studies on *Equisetum* calli cell wall fraction resulted in presence of abound xyloglucan compared to *Equisetum* stem cell wall fraction and interestingly no MLG was detected from *Equisetum* callus samples. Also, MXE activity

was not detected from *Equisetum* callus samples that also don't show any MLG presence, and this situation once more certify XET and MXE activities are generated by completely different enzymes [120]. Callus tissue is a non-differentiated group of plant cells and due to lack of differentiation into tissues, they don't have to provide additional strength to organism itself. These findings confirm the hypothesis of MLG's role in primary cell wall strengthening in order to participate in load bearing role of primary cell wall.

Observations of MXE activity was from crude extract of several *Equisetum* samples. Even-though enzyme activity was proven to be originating from a different molecule than XET, no genomic or proteomic characterization was done for MXE. In a latter study [121], late-season *E. fluviatile* were used as explants for purifying MXE. Interestingly, additional to MXE and XET activities, a new catalytic activity was observed with *E. fluviatile* extract, named as cellulose: xyloglucan endotransglycosylase (CXE) activity (Figure 1.12). All three catalytic activities, XET, MXE and CXE, were observed to be caused by a single protein band observed in native-PAGE studies and protein purification assays, thus this new enzyme was named hetero-trans-β-glucanase (HTG) [121].

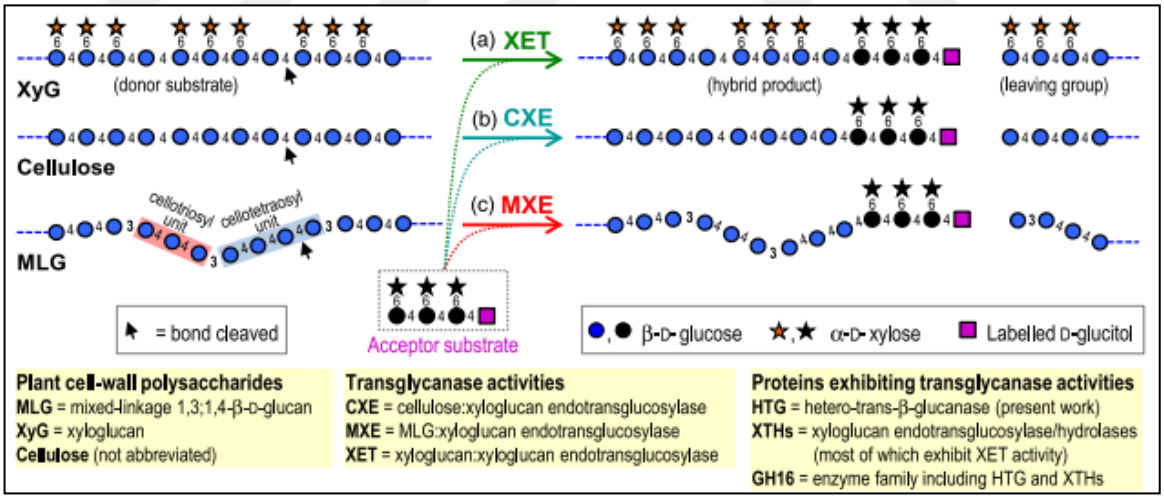

Figure 1.12. Proposed catalytic activities of native *Equisetum* HTG [121].

HTG from *E. fluviatile* was identify by LC-MS/MS analysis of HTG tryptic fragments and then matching these fragments to *in silico* translation products of *E. fluviatile* transcriptome. Full-length *EfHTG* sequence was obtained via 5' and 3'-RACE approaches

and HTG catalytic activities were confirmed by heterologous expression studies with *P. pastoris* [121].

Parallel to experimental trials in order to identify MXE/HTG enzyme of *Equisetum*, two different *Equisetum* species, *E. hyemale* and *E. diffusum*, transcriptomes were sequences within '1000 plants' (oneKP) initiative project. For sequencing, developing shoots of *E. diffusum* and sterile leaves/branches of *E. hyemale* were employed by project leaders. Using blast tool of project web site (https://db.cngb.org/blast4onekp/), putative XET/MXE sequences were extracted by searching database for sequences similar to XET sequences from other plants.

1.10. HETEROLOGOUS EXPRESSION AND PICHIA PASTORIS SYSTEM

To be able to modify plants to produce plant-based products such as foods, feed, textile products, fibre, and wood depending on the usage area, its structure and enzymatic modifications should be studied in detail. However, studying a living organism is not easy. It is not possible to observe every molecular change in the wall under a microscope during a time interval. So, *in vitro* and *in vivo* studies should be carried out simultaneously and obtained data can be pieced together to create the whole image.

For enzymatic characterization of the proteins, they should be obtained in a purified state. Growing plant samples and purifying target protein is a time consuming and difficult procedure. Purification of individual isoenzymes from a large family of highly similar proteins may be impossible. An alternative is heterologous expression of target proteins in a host system. Microbial hosts such as bacteria or yeast are preferred due to ease of handling and short time requirement for growth. For expression of XET enzymes, bacterial hosts are not a good choice because like mentioned before, these enzymes are glycosylated and bacterial expression systems lack glycosylation mechanisms. *Pichia pastoris* is one of the yeast hosts used for production of foreign proteins. It has many advantages when compared to mammalian systems; it is easier to do genetic manipulation and *P. pastoris* cells can be grown to higher cell densities. Since it is a eukaryotic host, it carries out post-translational modifications (glycosylation, sulphation, phosphorylation etc.) necessary to produce soluble, correctly folded eukaryotic recombinant proteins. Linearized foreign DNA is inserted into the yeast genome by homologous recombination to generate stable

transgenic lines. Also there are strong promoters of *P. pastoris* that yield large amounts of target protein [122].

One of the most important driving forces of choosing *P. pastoris* as host system is its ability of *N*-linked glycosylation. As mentioned above most of the XET enzymes are *N*-glycosylated proteins and it has been demonstrated that they need glycosylation for stability and optimum activity [102]. Thus, host system for heterologous expression should be able to carry out glycosylation of the protein after translation. It has been previously observed that native XET enzyme and recombinant enzyme produce in *P. pastoris* don't have any recorded difference in enzyme activity [72]. This feature makes *P. pastoris* a good host for XET expression.

Pichia pastoris SMD1168H is the host strain chosen for heterologous expression. This strain is defective in vacuole peptidase A (*pep4*) and since this enzyme is required for activation of carboxypeptidase Y and protease B1, this strain is also defective in the aforementioned proteolytic enzymes [122].

A preferred promoter for this work is the AOX1 promoter. AOX1 (Alcohol oxidase 1) enzyme is a key enzyme in methanol utilization; it catalyses oxidation of methanol [123]. AOX1 is induced by methanol and other primary alcohols, and repressed by many other carbon sources such as glucose and glycerol. This enzyme has a poor affinity for oxygen, thus *P. pastoris* up-regulates the AOX1 promoter to increase gene expression to balance the poor affinity [122].

Heterologous proteins expressed by yeast cells can be intracellular proteins or they can be secreted outside as extracellular proteins. Secretion of produced proteins is a desired feature for avoiding the usual first step of purification which is lysis of the cell to release cellular contents and clearance of cell debris. *P. pastoris* has low levels of native secreted proteins and this characteristic makes purification process a lot easier [124]. A preferred secretion signal is *Saccharomyces cerevisiae* α-factor prepro-peptide. It consists of 19 amino acids of pre-sequence (signal peptide) and 60 hydrophilic amino acids of pro-region. After translation, signal sequence is removed by signal peptidase and pro-region is removed by kex2 protease (kex2p) resulting in mature protein. Kex2 protease recognize Lys-Arg or Arg- Arg amino acid pairs and recognition site has two Glu-Ala repeats at the

C-terminal in general and this site consists of Glu-Lys-Arg*Glu-Ala-Glu-Ala amino acids in the chosen expression vector pPicZα-C (Invitrogen), * indicating cleavage point [122].

1.11. AIM OF THE STUDY

The composition of plant cell walls differs hugely between Type I cell walls (seen in dicots) and Type II cell walls (seen in Poales); the main non-cellulosic β-linked polysaccharide in dicots is XyG where as it is MLG and arabinoxylan in Poales. Despite this difference, XTH enzymes are represented by large multigene families in both monocots and dicots and the XTHs from various plant species are distributed throughout the different phylogenetic clades. By choosing a total of six enzymes representing different clades, we aimed to elucidate the catalytic potentials of these XTHs on different polysaccharides and oligosaccharides that represent a range of plant cell wall compositions, and to create an understanding of the way that XTHs are grouped. More, learning the broader substrate specificities of XTHs from different groups and comparing these enzymes' protein structures would help us to understand the evolution of XTHs from ancestral bacterial genes and the evolution of the catalytic action of XTHs.

On the other hand, MLG polysaccharide, previously thought to be present only in grasses, has also been observed in the evolutionarily distant genus of the vascular, non-seed plants of *Equisetum.* After discovery of MLG, a new enzyme activity was reported from *Equisetum fluviatile* crude extracts that had transferase ability, but with a preference for MLG as a donor substrate rather than XyG and thus was labelled as mixed-link glucan endotransglycosylase (MXE). Such an enzyme activity in an ancient plant can be a bridge in XTH evolution, thus we aimed to purify, identify and characterize putative MXE from *Equisetum telmateia* species that is growing in Istanbul, Turkey. By combining two strategies, XTH evolution and variance in their substrate preferences were enlightened.

2. MATERIALS

2.1. CHEMICALS

ClaI, DraI and XbaI restriction enzymes were supplied from New England Biolabs. FastDigest NotI restriction enzyme was purchased from Fermentas. All buffer salts and media components were purchased as pure molecular biology grade chemicals from Sigma-Aldrich (Germany) and Merck (Merck KGaA Darmstadt Germany). Organic solvents (ethanol, methanol, isopropanol, acetonitrile) and ammonium acetate were all HPLC grade and purchased from Sigma-Aldrich. Zeocin antibiotic was purchased from Invitrogen and all other antibiotics were from Sigma-Aldrich.

Macharey-Nagel Nucleospin Plasmid Kit (Catalogue No. 740588.50) and Invitrogen Purelink Quick Plasmid Miniprep Kit (Catalogue No. K210010) were used for plasmid isolation from *E. coli* transformants according to manufacturer's instructions. Macherey-Nagel NucleoSpin Gel and PCR Clean-up Kit (Catalogue no. 740609.50) was used for gel purification of DNA samples according to manufacturer's instructions.

Generuler 1Kb Plus DNA Ladder (Invitrogen Catalogue. No. 10787-018), 100 bp DNA Ladder (Invitrogen Catalogue No. 15628-019) and PageRuler Prestained Protein Ladder (Thermo Scientific Catalogue No. 26616) were used as markers in electrophoresis studies.

Sigma dialysis membrane Sigma cat. No. D9402-100ft was employed during dialysis of ammonium sulphate precipitated protein samples.

pCR 8/TOPO TA Cloning Kit (Invitrogen Catalogue No. 45-0642) and pGEM-T Easy Vector System (Promega Catalogue No. A1360) were used for cloning. Maximo Taq DNA Polymerase (GeneON Catalogue No. S101) and Phusion Hot Start II DNA Polymerase (ThermoFisher Catalogue No. F549L) were used as DNA polymerases within the study.

During Western Blotting studies, heterologously expressed proteins were detected using Anti-6X His tag antibody (HRP) (Abcam Catalogue No. ab1187). For Western Blotting imaging, Amersham ECL prime western blotting detection reagent (GE Healthcare Life Sciences Catalogue No. Rpn 2232) was utilized.

BioSep-SEC-s3000 (Phenomenex Catalogue No. 03C-2146-K0) size exclusion HPLC column was employed during enzyme activity reactions' analysis. Protein purification from plant extracts and heterologous expression media were carried using FPLC technique with GE Healthcare Life Sciences AktaPrime Plus instrument and various chromatographic separation columns (Table 2.1).

Table 2.1. Chromatographic separation columns supplied from GE Healthcare

Column name	**Catalogue Number**
HiScreen Capto Q	28-9269-78
HiScreen Capto S	28-9269-79
HiScreen Capto DEAE	28-9269-82
HiScreen Capto Butyl	28-9924-73
HiScreen Capto MMC	28-9269-80
HisTrap FF	17-5255-01
HiPrep 26/10 DeSalting	17508701
Superdex 75 16/100	
HiPrep 26/60 Sephacryl S-200 HR	17119501

2.2. EQUIPMENT

Biorad GenePulser II equipment was used for electroporation of *P. pastoris* cells. Biorad T100 Thermal Cycler was used for conventional PCR, nested-PCR, gradient PCR and enzyme activity tests.

Wealtec Elite 300 plus and Biorad Powerpac Universal power supplies were used for electrophoresis. Semi-Dry Western Blotting was carried using Biorad TransBlot Turbo or ThermoFisher Pierce Power Blotter.

All broth incubations of *E. coli* and *P. pastoris* cultures were done with New Brunswick Scientific Innova 44 shaking incubators. For protein purification, GE Healthcare Life Sciences AktaPrime Plus instrument and PrimeView software were utilized. Enzyme

reactions were analysed using Agilent 1100 Series HPLC system and ChemStation software or Waters Acquity UPLC system and Empower software.

2.3. OLIGOSACCHARIDE ACCEPTORS

Endotransglycosylase enzymes' ability of using different acceptor molecules was evaluated using oligosaccharides representing common polysaccharides in the cell wall during *in vitro* enzyme activity assays. All of the acceptor oligosaccharides are supplied from Megazyme Company (Ireland). Names, abbreviations and catalog numbers are given below (Table 2.2).

Table 2.2. Lists of acceptors, their abbreviations, catalog numbers and lot numbers.

Acceptors	Acceptor Abbreviations	Catalog #	Lot #
1,3:1,4-β-glucotetraose A	BA	O-BGTETA	70504A
1,3:1,4-β-glucotetraose B	BB	O-BGTETB	70507B
1,3:1,4-β-glucotetraose C	BC	O-BGTETC	70508C
1,4-β-cellotetraose	CT	O-CTE	110804
Galactosyl mannotriose	GM	O-GM3	10404a
1,4-β-mannotetraose	MT	O-MTE	30304
Di-galactosyl mannopentaose	DGM	O-GGM5	10407a
Laminaritetraose	LT	O-LAM4	51104
1,4-β-D-xylotetraose	XT	O-XTE	100504
Xyloglucan heptasaccharides	X7	O-X3G4	21207
Xyloglucan oligosaccharides	XGOs	O-XGHON	20509

Differences between these oligosaccharides are the glycosidic bonds in their structures and their building blocks. 1,3:1,4-β-glucotetraose A, B and C are all consists of four glucosyl residues linked together. The differences are; BA linkage between glucosyl residues are β-1,3-, β-1,4-, β-1,4- respectively whereas these linkages are β-1,4-, β-1,4-, β-1,3- respectively in BB and β-1,4-, β-1,3- and β-1,4- respectively in BC (Figure 2.1 A, 2.1 B, 2.1 C) These three oligosaccharides with difference in -1,3-β-linkage represent β-1,3;1,4-

glucan polysaccharide in the cell wall. CT consists of four glucosyl residues linked by β-1,4-linkages (Figure 2.1 D) and it is used for representing cellulose. MT is made of four mannose residues linked by β-1,4-linkages (Figure 2.1 E). XT is four xylopyranosyl residues linked by β-1,4-linkages (Figure 2.1 F) is a representative of xylan backbone in the cell wall. DGM has a more complex structure; backbone consists of five mannose residues linked by β-1,4-linkages, and third and fourth mannose residues also forms linkages with galactose residues via α-1,6-linkages (Figure 2.1 G). GM is three mannose residues linked by β-1,4-linkage and a galactose residue linked by α-1,6-linkage (Figure 2.1 H). DGM and GM are building block of galactomannans Four glucosyl residues linked by β-1,3-linkages makes up LT (Figure 2.1 I). Xyloglucan oligosaccharide structure was mentioned above and a representation is given in Figure 2.1 J.

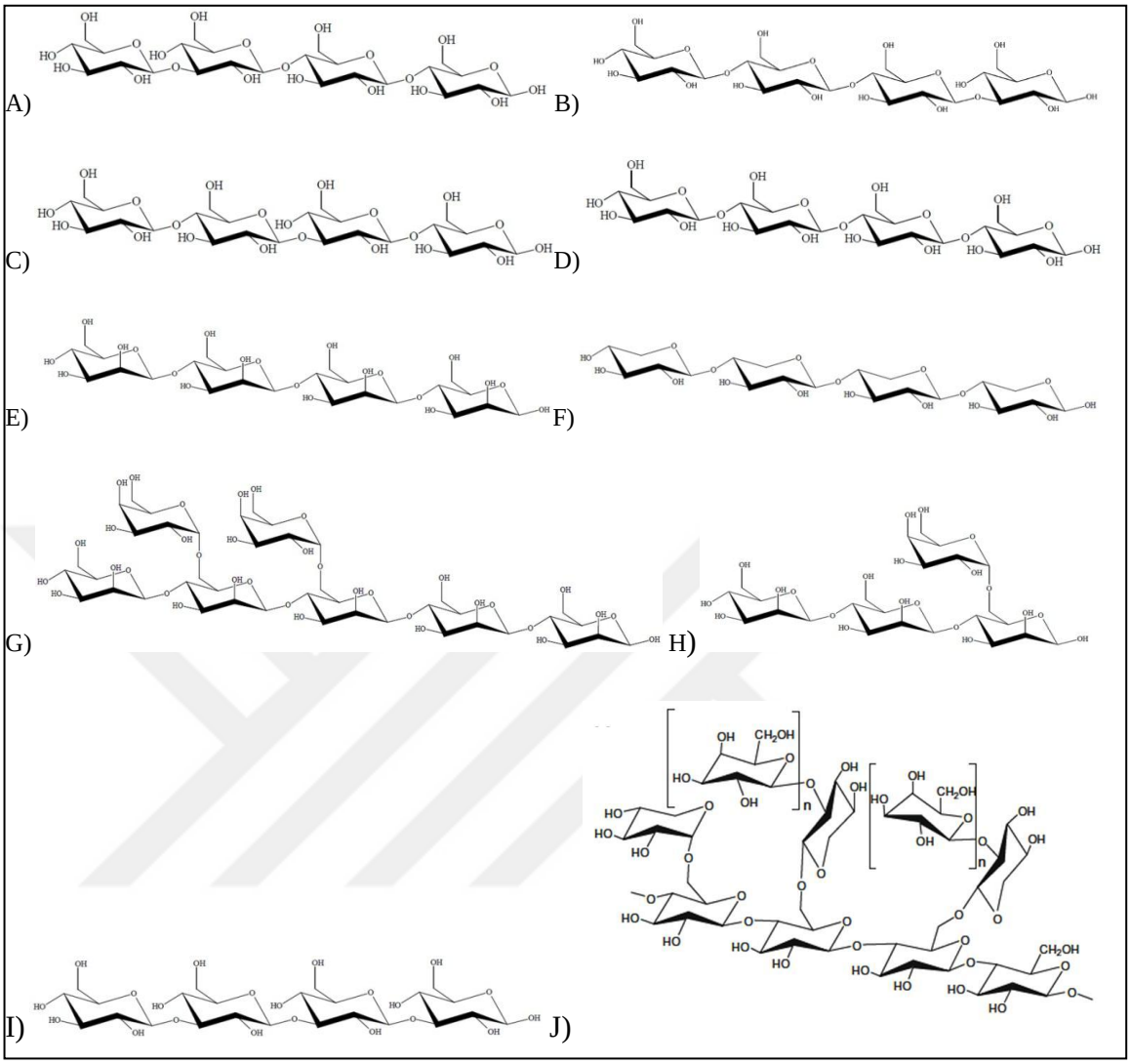

Figure 2.1. Representations of oligosaccharides used as acceptor substrates. Real chemical bond geometries are not included in the figures. (A)BA, (B)BB, (C)BC, (D)CT, (E)MT, (F)XT, (G)DGM, (H)GM, (I)LT, (J)XGO.

2.4. POLYSACCHARIDE DONORS

Polysaccharides used in the study were chosen specially in order to represent plant cell wall matrix components. XTH enzymes are known to be catalysing endotransglycosylation between xyloglucan chains. One of our main aims is to characterize susbtrat specificity of chosen XTH representatives, thus additionally to xyloglucan polysaccharide, main non-cellulosic β-linked polysaccharides were also chosen for the study. On the other hand, in order to test XTH enzymes tethering role between xyloglucan and cellulose microfibrils,

water-soluble cellulose analogues were included in the study. Polysaccharides used as donors are supplied from Megazyme Company (Ireland) except cellulose analogues; Hydroxyethyl-cellulose is supplied from Fluka and methyl-cellulose, carboxymethyl cellulose are supplied from Sigma-Aldrich, MO, USA (Table 2.3).

Table 2.3. List of donors, their abbreviations, catalog numbers and lot numbers.

Donors	**Donor Abbreviations**	**Catalog #**	**Lot #**
Hydroxyl-ethyl cellulose	HEC	54290	1146517
Methyl Cellulose	MC	274429	-
Carboxymethyl Cellulose	CMC	C9481	-
Konjac glucomannan	KM	P-GLCML	30401a
Tamarind seed xyloglucan	TXG	P-XYGLN	100402
Wheat arabinoxylan	WA	P-WAXYM	40302a
Barley β-glucan	BBG	P-BGBM	90801a
Carob galactomannan	CM	P-GALML	10501b
Guar galactomannan	GGM	P-GGMMV	00607a
Lupin galactan	LG	P-GALLU	101201

Donor substrates show many structural differences. Barley β-glucan is made of β-1,3- and β-1,4-linked D-glucosyl residues (Figure 2.2 A). Guar galactomannan is β-1,4-linked D-glucosyl residues with α-1,6-linked galactosyl residues as side chains (Figure 2.2 B). Hydroxyl-ethyl cellulose has a slightly different structure than normal cellulose. Some of –OH groups of glucose are $–OCH_2CH_2$ (Figure 2.2 C), this limits interchain hydrogen bonding, thus allowing the molecules to be soluble, as opposed to regular cellulose which is insoluble. In methyl cellulose structure, some H atoms of -OH groups are replaced with $-CH_3$ functional group and in carboxymethyl cellulose some H atoms of -OH groups are replaced with CH_2CO_2H group that is accompanied with Na^+ ion. Konjac glucomannan is made of β-1,4- linked glucosyl and mannosyl residues (Figure 2.2bD). Wheat arabinoxylan is β-1,4-linked D-xylan backbone with α-1,2- or α-1,3-linked L-arabinosyl residues (Figure 2.2 E).

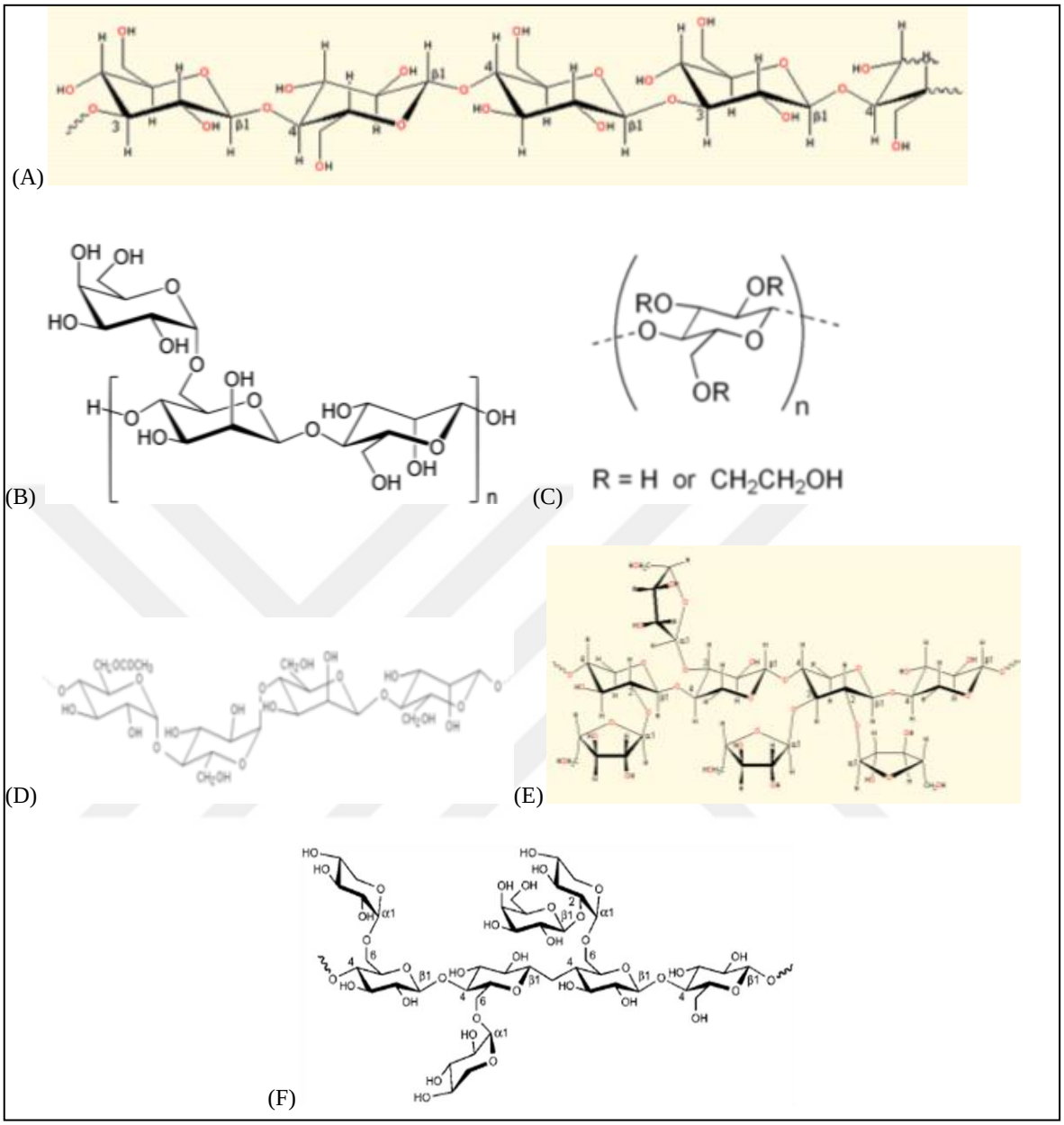

Figure 2.2. Representations of some of the donor polysaccharides. Real chemical bond geometries are not included in the figures. A)BG, (B)GM, (C)HC, (D)KM, (E)WA, (F)TXG.

3. METHODS

3.1. INITIAL BIOINFORMATIC ANALYSIS AND TARGET SELECTION

XTH enzyme amino acid sequences of model plants and agriculturally important plants were extracted from NCBI database. Target plants include *Arabidopsis thaliana, Brachypodium distachyon, Gossypium hirsutum, Hordeum vulgare, Populus trichocarpa, Oryza sativa, Triticum aestivum*. Gathered XTH sequences were used to generate a phylogenetic tree using ClustalX 2.1[125] and Dendroscope v 3.5.9 softwares. In order to study enzymatic roles and evolutionary background of XTH phylogenetic tree representatives, AtXTH3, AtXTH4, AtXTH11, BdXTH2, GhXTH2, PtXTH3, TaXTH5 enzymes were chosen from Group I which is known to have true XET role and Ancestral Group.

As the second part of study, reported *Equisetum* putative MXE was chosen as purification and characterization target.

3.2. CODON OPTIMIZED EXPRESSION TARGETS AND PREPARATION OF EXPRESSION PLASMIDS

Expression targets representing various branches of the XTH phylogenetic tree were chosen. Start codons and stop codons were removed from DNA sequences of targets. Any possible signal peptide of target XTH enzymes were detected and analysed using the SignalP 4.1 Server online tool [126]. Signal peptide coding regions were removed from *XTH* genes and the remaining coding regions were codon optimized for heterologous protein expression in *P. pastoris* by GenScript (NJ, USA). For cloning purposes, all sequences have ClaI restriction enzyme digestion site at their 5' end and XbaI restriction enzyme digestion site at their 3' end. Changes made on sequences were checked and altered coding regions were tsted for correct reading frames. *AtXTH4, AtXTH11, BdXTH2, GhXTH2, PtXTH3, TaXTH5* expression targets were cloned into pPicZα-C expression vector before shipment whereas *AtXTH3* and *OsXTH30* expression targets were cloned into pUC57 cloning vector and shipped.

AtXTH3 and *OsXTH30* genes needed to be cloned into pPicZα-C expression plasmid. For cloning, 1µg of pUC57-*AtXTH3* and pUC57-*OsXTH30* plasmids were separately digested using ClaI and XbaI restriction enzymes (NEB, MA, USA). Restriction reactions were run on 1 per cent w/v agarose gel and *AtXTH3* and *OsXTH30* genes separated from pUC57 were visualized. *AtXTH3* and *OsXTH30* DNA bands were excised from the agarose gel and gel purified using the Macherey-Nagel NucleoSpin Gel and PCR Clean-up Kit according to manufacturer's instructions. pPicZα-C expression plasmid was also digested by ClaI and XbaI enzymes in preparation for cloning. Digested and linearized pPicZα-C was run on a 1% w/v agarose gel and linearized plasmid band was excised from gel. pPicZα-C was gel purified using the Macherey-Nagel NucleoSpin Gel and PCR Clean-up Kit according to manufacturer's instructions. Cloning of *AtXTH3* and *OsXTH30* into pPicZα-C was carried out using T4 DNA Ligase (Thermo Scientific) according to manufacturer's instructions with a 1:2 molar ratio of vector:insert.

3.3. PHENOL EXTRACTION OF DNA

In order to fully purify the DNA sample, it was subjected to phenol extraction. DNA samples were mixed with equal amount of phenol solution and vortexed. Phase separation was achieved by centrifugation at 2,000 rpm for 5 minutes at room temperature. The separated aqueous layer was transferred into new microcentrifuge tube. Equal volume of phenol: chloroform 5:1 (Sigma Cat. No. P1944) was added and samples were mixed by vortexing. Then, DNA was separated from organic phase by centrifugation at 2,000 rpm 5 minutes at room temperature.

3.4. SODIUM ACETATE ETHANOL PRECIPITATION OF DNA

Sodium acetate ethanol precipitation was applied to concentrate DNA sample or as a control of phenol extraction of DNA. Each sample was mixed with 0.1 volume of 3 M sodium acetate pH 5.5 and 2.5 volumes of ice-cold absolute ethanol. After overnight incubation at -20°C, DNA in the sample was separated by centrifugation at +4°C 14,000 rpm for 15 minutes. Pelleted DNA was washed by addition of 2 volumes of 80 per cent v/v ethanol. The sample was incubated at room temperature for 5 minutes and then DNA was

centrifuged for 5 minutes at 14,000 rpm at +4°C. Any remaining ethanol was evaporated and DNA samples were resuspended in nuclease-free water.

3.5. BACTERIAL TRANSFORMATION

All ligation reactions and vector constructs were firstly transformed into *E. coli* DH5α for stock preparation and when necessary, blue-white selection.

An overnight grown DH5α *E. coli* colony was used to start a 10 ml LB culture. Bacteria cells were grown at 37°C with 200 rpm shaking until cultures were saturated. The overnight cultured 10-mL *E. coli* was used to inoculate a 100 mL LB broth and then grown until the OD_{600} value reached 0.4. Then, cells were pelleted by centrifugation for 10 minutes, 3,000 x *g* at 4°C and washed with ice-cold sterile 75 mM $CaCl_2$ + 15 per cent v/v glycerol twice. The cell pellet was resuspended in 2 mL ice-cold sterile 75 mM $CaCl_2$ + 15 per cent v/v glycerol, aliquoted, fast-frozen in liquid N_2 and stored at -80°C until use.

Heat stock transformation of chemically competent DH5α *E. coli* cells was employed to get plasmid DNA into the cells. Ligation reaction (2µl) was gently mixed with 50 µl competent cells and incubated on ice for 20 minutes. Heat shock was applied at 42°C for 45 seconds and cells were replaced back on ice for an additional 2 minutes. SOC media (950 µl) was added to each tube and the transformants were incubated at 37°C with 150 rpm shaking for 90 minutes. Then, for transformant selection, cells were plated on selective LBA plates and incubated at 37°C for 16-18 h, until transformant colonies appear.

3.6. YEAST TRANSFORMATION AND POSITIVE COLONY SELECTION

Expression constructs prepared in pPicZα-C expression plasmids were linearized using DraI restriction enzyme according to the manufacturer's instructions (New England BioLab Cat. No. R0129). Yeast transformation requires high quantities of DNA, thus for each transformation event 5-10 µg of plasmid was linearized using DraI and linearized plasmids were purified using the phenol extraction sodium acetate ethanol precipitation method and resuspended in nuclease-free water to final concentration of 1 µg DNA/µl.

Pichia pastoris SMD1168H strain was used for transformation and expression studies. Single *P. pastoris* SMD1168H colony was used to imbibe 10 ml YPD broth and yeast cells were grown overnight at 30°C with 200 rpm shaking. Overnight grown saturated culture was diluted to 1:99 ratio with YPD to final volume of 50 mL. Culture was grown till mid logarithmic growth phase (~ OD600 of 5.0) at 30°C with 200 rpm shaking. Then, cells were recovered from growth media by centrifugation and resuspended in 9 mL ice-cold BEDS solution supplemented with 1 mL of 1.0 M DTT. Cells were incubated at 30°C with 100 rpm shaking for 5 minutes and then pelleted by centrifugation at 4°C 500 x *g* for 5 minutes. Collected competent cells were resuspended in 1 mL BEDS solution and aliquoted in small amounts. They were slowly frozen for future uses.

For transformation of target DNA into competent *P. pastoris* cells, 1-4 µg of linearized plasmid was mixed with 40 µl of competent cells in a microcentrifuge tube. After incubation on ice for 2 minutes, they were transferred into an electroporation cuvette (cuvette gap 2,0 mm) and electroporated with setting of 1500 V, 200 Ω, 25 µF. Immediately 1.0 mL of YPD:1M sorbitol (1:1 v:v) mixture was added on electroporated cells in electroporation cuvette. Cells were transferred into 15 mL centrifuge tubes and incubated at 30°C with 150 rpm shaking for 2 hours before plating then on YPDS agar + zeocin (100µg/mL) plates. Transformant colonies become visible after incubating plates at 30°C incubator for 3-5 days.

Visible transformant *P. pastoris* colonies were restreaked on YPDS agar + zeocin (100µg/mL) plates for verification of antibiotic selection.

Obtained and verified transformant yeast colonies were screened for functional enzyme production by induction of gene expression according to EasySelect *Pichia* Expression Kit Manual (Invitrogen Cat. No. K1740-01, Manual part no. 25-0172) with a small scale induction model. Single colony taken from restreaking plates of each transformation event was used to inoculate 10 mL BMGY media. Cells were grown in BMGY media at 30°C 200 rpm until OD_{600} value reached 2-6. When aimed OD_{600} value was reached, cells were pelleted by centrifugation at 22°C 3200 x *g* for 10 minutes and they were resuspended in 10 mL BMMY media with an OD_{600} value of 1.0.BMMY samples were cultured at 22°C with 160 rpm shaking for 3-5 days with 1 per cent v/v methanol addition every 24 hours.

Methanol induction period lasts for 3-5 days and at the end of induction period cells were separated by centrifugation at 4°C 3200 x *g* for 10 minutes. Supernatants were screened for 6X-His tagged protein presence by SDS-PAGE and Western blotting and XET enzyme activity. Also, integrity of plant genes in *P. pastoris* genome were analysed by colony PCR.

3.7. SDS-PAGE AND WESTERN BLOTTING

Small scale induction samples were screened by SDS-PAGE and Western blotting. Firstly, proteins in supernatants were precipitated by TCA & acetone precipitation. 900 µL supernatant was mixed with 100 µL 133 per cent w/v TCA solution, vortexed and incubated on ice for an hour. Proteins were pelleted by centrifugation at 4°C 12 000 x *g* for 10 minutes. Supernatant was discarded and 800 µL of pure acetone was added on each pellet. They were vortexed back to resuspension and incubated at -20°C overnight. Protein samples were pelleted by centrifugation at 4°C 6500 x *g* for 10 minutes and washed with -20°C acetone twice by addition of 500µL acetone, vortexing, centrifugation. After washes, when remaining acetone was totally removed, protein pellets were dissolved in autoclaved ultrapure water and mixed with 2X Laemmli buffer. Samples were heated up to 95°C for 7 minutes to denature proteins for denaturing gel electrophoresis.

Polyacrylamide gel electrophoresis studies of heterologously expressed XETs and purified *Equisetum* MXEs were carried out with 5 per cent stacking - 12 per cent resolving gel. When performing colony screening or gel filtration fraction screening, 20 µL of denatured protein samples were loaded on gels. In other conditions, amount of protein loaded depends on aimed of PAGE study. Gel running systems were connected to a cooling system running at 4°C. Gels were run at 200 V until samples migrate into resolving gel and then, they were run at 300 V.

When gel running was completed, colony screening gels were stained with coomassie blue staining solution with an initial heating in microwave oven and incubation on a rocking platform for 45 minutes. Unbound dye molecules were destained with ultrapure water. Destained gels were visualized using Biorad ChemiDocX instrument via ImageLab software.

Gel filtration fraction gels and *Equisetum* purification gels, due to low amount of protein per sample and importance of samples, were stained by silver nitrate staining protocol. After the runs, gels were fixed with 1 ml/1 cm^3 gel volume, 30 per cent v/v ethanol 10 per cent v/v acetic acid fixation solution firstly for an hour, then with fresh 1 ml/1 cm^3 gel volume fixation solution for overnight. Fixed gels were sanitized using 1 ml/1 cm^3 gel volume 0.8 mM sodium thiosulfate solution for 1 minute and washed with 1.5 ml/1 cm^3 gel volume ultrapure water for 1 minute twice. Then, gels were stained with 1 ml/1 cm^3 gel volume 12 mM $AgNO_3$ solution for 40-45 minutes in dark on rocking platform. After $AgNO_3$ incubation was over, gel was washed with 1.5 ml/1 cm^3 gel volume ultrapure water for 15 seconds and band development was carried by incubating gels with 1 ml/1 cm^3 gel volume developer solution on rocking platform for 15 minutes. If band development reached intended intensity, developer incubation was finalized before incubation period was over, or if band intensity wasn't enough, an additional 15 minute incubation with fresh developer was done for each gel. When intended band development was reached, band formation was stopped by incubating gels in 1 ml/1 cm^3 gel volume stop solution (4 per cent w/v tris base, 2 per cent v/v acetic acid) on rocking platform for 30 minutes. Gels were washed with ultrapure water twice for 15 minute and visualized using Biorad ChemiDocX instrument via ImageLab software.

SDS-PAGE gels for Western blotting were blotted onto nitrocellulose membranes. Gels were transferred using Trans-Blot Turbo Mini Nitrocellulose Transfer Packs (Biorad, Cat. No. 1704158) and Trans-Blot Transfer System (Biorad Cat. No. 1704150) with default transfer program, 25 V 30 minutes. Also transfer was carried by manually preparing transfer sandwich and using Pierce Power Blotter at 25 V, 30 minutes. For manual transfer sandwich preparation, nitrocellulose membrane (SantaCruz Cat. No. Sc-3718) and Whatmann paper were equilibrated with transfer buffer for 15-20 minutes. After proteins were blotted on nitrocellulose membrane, membrane was blocked with 3 per cent w/v skimmed milk powder solution prepared with TBS-T overnight on rocking platform at room temperature. Anti 6X-His tag antibody (Abcam Cat. No. Ab1187) was used for detection. Antibody was diluted 1/7000 using TBS-T and membrane was incubated with this solution for an hour on rocking platform. Membrane was washed twice with TBS-T, once with PBS and visualized using Amersham ECL Prime Western Blotting Detection Reagent (GE Healthcare Cat. No. Rpn2232). ECL kit components were diluted 1/8 with

PBS each before usage. Membrane images were acquired by Biorad ChemiDocX instrument via ImageLab software.

3.8. COLONY PCR

Saturated, overnight grown transformant *P. pastoris* cultures were used for colony PCR. 10 µL of culture was mixed with 5 µL of 5 U/µL lyticase (Sigma-Aldrich Cat. No.) enzyme and incubated at 30°C for 20-30 minutes. Samples were immersed in liquid nitrogen for one minute and thawed on ice slowly. Then they were directly used in colony PCR mixes as templates with a solution composed of 10 nmoles $MgCl_2$, 4.5 nmoles dNTP mix, 7 pmoles of α-factor 5' and AOXI 3' primers, 2.2 µL template and 1.25 unit Maximo DNA taq polymerase in 20 µL 1X Reaction Buffer. PCR was carried out as initial denaturation at 95°C for 5 minutes; 40 cycles composed of 95°C 25 seconds denaturation, 64°C 20 seconds annealing, 72°C 60 seconds extension and a final extension at 72°C for 5 minutes. Results were visualized on a 1 per cent w/v agarose gel and imaged via ChemiDocX system ImageLab software.

3.9. GLYCEROL STOCK PREPARATION

Overnight grown, saturated cultures of *E.coli* and *P. pastoris* samples were used in glycerol stock preparation. 820 µL of culture was mixed with 180 µl sterile 87 per cent v/v glycerol in a 2 mL microcentrifuge tube. Sample tube was inverted for 5-6 times for thoroughly mixing of culture and glycerol. Tube was placed in -80°C freezer for long term storage.

3.10. HETEROLOGOUS PROTEIN PRODUCTION AND PURIFICATION

A positive colony was selected for each heterologous expression target gene. The positive colony per each gene was streaked on YPDS agar + zeocin (100µg/ml) plates and grown at 30°C for 4-5 days. A single transformant colony was used to start 10 mL BMGY culture and the culture was grown for 20-24 hours at 30°C 200 rpm. BMGY culture was scale-upped to 400-700 mL BMGY culture, using overnight grown small scale culture as

imbibition source. Large scale BMGY culture was grown for 20-22 hours at 30°C 200 rpm until OD_{600} value reaches 4.0-6.0. All of BMGY culture was used in starting BMMY culture with an OD_{600} of 1.0. BMMY culture was incubated at 22°C 160 rpm shaking for 3-5 days. Methanol addition to final volume of 1 per cent v/v was carried throughout incubation period every 24 hour in order to induce gene expression and protein production.

At the end of induction period cells were separated from culture media via centrifugation at 8000 x *g* 10 minutes roo temperature. Supernatant was filtered through 0.22 µm RC syringe filter to avoid any microbial contamination. Proteins in filtered supernatant were precipitated by ammonium sulphate precipitation method. 85 per cent ammonium sulphate saturation was aimed and ammonium sulphate was added into supernatant samples with slow mixing at +4°C. After all of $(NH_4)_2SO_4$ in samples was dissolved, proteins were precipitated by centrifugation at +4°C 8200 x *g* 60 minutes. Protein pellets were resuspended in 20 mM sodium phosphate pH 7.4 buffer. $(NH_4)_2SO_4$ was removed via dialysis of protein samples against 3 x 15 L 20 mM sodium phosphate pH 7.4 buffer at 4°C. After dialysis step, supernatant proteins were obtained in 20 mM sodium phosphate pH 7.4 buffer. NaCl and imidazole were added to protein samples to final concentrations of 0.5 M and 2 mM respectively.

Protein samples were firstly loaded on to HisTrap FF affinity column (GE Healthcare) to purify 6X-His tagged heterologously expressed proteins. HisTrap FF column was conditioned with binding buffer (20 mM sodium phosphate, 0.5 M NaCl, 2 mM imidazole pH 7.4) and protein sample was passed through column slowly. During sample loading, flow-through was collected. After protein sample was passed through the column, a wash with binding buffer was performed to wash away any nonspecific binding. Bound proteins were eluted from column by elution buffer (20 mM sodium phosphate, 0.5 M NaCl, 500 mM imidazole pH 7.4) into fractions. Chromatogram gathered during the run was investigated and fractions with 6X-His tagged protein were pooled down together. Thus, his-tagged protein was recovered in elution buffer from the column. However, despite affinity purification there can be some impurities such as immature protein products, protein aggregates. These impurities were removed via gel filtration chromatography step. Prior to gel filtration step, elution buffer was replaced by 0.1 M ammonium acetate pH 6.0 buffer via HiPrep 26/10 Desalting column (GE Healthcare Cat No. 17508701)

chromatography or by Amicon Ultra-15 centrifugal filter unit with ultracel-3 membrane (Merck Millipore Cat. No. UFC900324). (Before proceeding on with any chromatography method or any enzyme analysis study, protein buffer need to be changed to 0.1 M ammonium acetate pH 6.0). In column chromatography method, column is conditioned with 2 CV of buffer. Sample, at most 13 mL, is loaded onto column and fractionated into 2 mL tubes based on molecule sizes with 2 CV of buffer. GE Healthcare Life Sciences PrimeView software was used to monitor and record UV absorbance, conductivity (µS/cm), temperature and fractions during the run. By examining chromatograms of UV absorbance and conductivity, fractions with protein that have no increased conductivity were collected and pooled for the upcoming step of chromatography.

Heterologously synthesized proteins in 0.1 M ammonium acetate pH 6.0 buffer were loaded on Superdex 75 XK 16/100 hand casted column (GE Healthcare Cat. No. 17-1044-01) for gel filtration chromatography as polishing step. Run was carried with 0.1 M ammonium acetate pH 6.0 as mobile phase at 0.5 mL/min flowrate and sample was separated into 1.5 mL fractions. All of the fractions containing protein were collected and analysed for enzyme activity using TXG-XGO susbtrate couple and for protein purity by SDS-PAGE silver nitrate staining and Western blotting.

Gel filtration fractions with pure synthesized enzyme were pooled together and concentrated using Amicon Ultra-15 centrifugal filter unit with ultracel-3 membrane (Merck Millipore Cat. No. UFC900324). Purified, concentrated enzymes were stored at +4°C until used.

3.11. PROTEIN CONCENTRATION MEASUREMENTS

Protein amount and concentration calculations were carried using spectroscopic measurement. Two different assays were employed for this purpose; Bradford assay and BCA assay. Bradford assay depends on colorimetric detection of basic and aromatic amino acids, thus values obtained can be affected by protein amino acid composition whereas BCA assay color formation is influenced by prescence of cystene, tyrosine, tryptophan and overall peptide backbone. Preference between assays were done based on sample concentration; BCA assay was used with less concentrated samples.

Calibration curves were generated each time an assay was done. Bovine serum albumin (BSA) was used as standard in calibration curves. Any necessary BSA dilutions were done using 10 mg/mL BSA stock and ultrapure water as solvent. At least 5 different BSA concentrations, covering the range of sample concentration, were used and measurements were done in each assay, under conditions same as sample measurement conditions. Arithmetic average absorbance of 3 replicates were calculated and those averages were used to plot calibration curves. Slope equation of calibration curves were used during sample concentration calculations.

3.12. BRADFORD ASSAY

Bradford assay was carried using Bradford reagent (Sigma Cat. No. B6916). Samples and BSA standards were mixed with Bradford reagent with a ratio of 190 µL Bradford reagent and 10 µL sample / BSA solution in individual wells of sterile clear 96-well plate. After mixing thoroughly by pipetting, samples were incubated at room temperature on a slowly shaking rocking platform for 5 minutes in dark. At the end of incubation period, absorbances of samples were measured at 595 nm with Thermo Scientifi Multiskan Spectrum plate reader and obtained OD_{595} values were used in calibration curve generation and sample concentration calculations.

3.13. BCA ASSAY

Pierce BCA Protein Assay Kit was employed for BCA protein concentration assays. The kit consists of 2 reagents; BCA reagent A and BCA reagent B. Each time a BCA assay was done, working solution consisting of 50 volumes of BCA reagent A and 1 volume of BCA reagent B was prepared freshly. 10 µL of sample / BSA standard was mixed with 190 µL BCA working solution in a well of 96 well plate thoroughly by mixing. Samples were incubated at 37°C in dark for 2 hours. Spectroscopic absorbance measurements of samples were carried at 562 nm in Thermo Scientifi Multiskan Spectrum plate reader and obtained values were used in calibration curve generation and sample concentration calculations. Sample concentrations were calculated via slope equations of calibration curves.

3.14. PREPARATION OF DONOR AND ACCEPTOR MOLECULES

Acceptor oligosaccharides used in the study were tagged with fluorescent sulforhodamine B dye according to Kosik and Farkas, 2007 [127]. Excessive sulforhodamine dye was washed away with acetone. Labelled oligosaccharides were dried in freeze-dyer and then resuspended in 20 per cent v/v ethanol solution. Concentrations of labelled oligosaccharides were measured spectrophotometrically at 566 nm (molar absorption coefficient is 85 000)**.** These stock solutions were diluted to 50 µM working concentration using ultrapure water for all screening, pH optimization and enzyme substrate specificity studies. For kinetic calculations, acceptors were diluted to concentrations indicated in place with ultrapure water.

Donor polysaccharides were prepared according to manufacturer's instructions at 0.8 per cent w/v stock concentration. Before usage, for all screening studies they were diluted using pH 6.0 ammonium acetate buffer yielding 0.4 per cent w/v concentration donor in 0.1 M ammonium acetate and for pH optimization and enzyme substrate specificity studies, they were diluted using ammonium acetate buffer with indicated pH value yielding 0.4 per cent w/v concentration donor in 0.1 M ammonum acetate buffer at specific pH values. For enzyme kinetic studies, donors were used at pH optima of each enzyme. Different concentrations of donors were prepared in final 0.1 M ammonium acetate buffer using 0.8 per cent w/v stock.

3.15. ENZYME CHARACTERIZATION, ACTIVITY ANALYSIS AND KINETIC STUDIES

Endotransglycosylation capacity of a endotransglycosylase enzyme was detected and quantified by enzyme activity assay within this study. In oder to mimic plant cell wall environment, 8 donor polysaccharides and 11 sulforhodamine-labelled acceptor oligosaccharides were employed (Table 2.2 and 2.3). In individual 0.2 µL PCR tubes, 10 µL donor polysaccharide was mixed with 1 µL acceptor oligosaccharide and 2 µL of enzyme solution. They were mixed thoroughly and incubated at 30°C for given period of time. Colony screening reactions and donor-acceptor couple screening reactions were incubated for 24 hours. Substrate specificity calculation and pH optimization reactions

were incubated depending on enzyme's reaction capacity and concentration. Enzyme kinetic reactions were incubated for changing durations depending on donors used.

Enzyme activity reactions were performed as at least 3 repeats for substrate specificity characterization using at least 4 different time points, one being time zero. Repeat amounts were increased beyond 3 repeat for necessary donor-acceptor couples until obtaining a R^2 value >0.95 for linear slope equations.

At the end of enzyme activity reaction's incubation period, activity of the enzyme is ceased by decreaseing pH value of reaction environment with 6 µL formic acid addition. Then, reactions were analysed and produced hybrid product amounts were quantified by HPLC analysis.

3.16. pH OPTIMIZATION

For each enzyme studied, pH optimization was carried through a wide range between pH 4.0 to pH 8.0. In all pH optimization trials, pH 4.0, 4.1, 4.2, 4.3, 4.4, 4.5, 4.6, 4.7, 4.8, 4.9, 5.0, 5.1, 5.2, 5.3, 5.4, 5.5, 5.6, 5.7, 5.8, 5.9, 6.0, 6.2, 6.4, 6.5, 7.0, 8.0 values were employed. 0.8 per cent w/v stock TXG donor was diluted in 1:1 ratio using McIlvaine buffers prepared at given pH value. Enzyme activity trials were prepared with 0.4 per cent w/v TXG donor with given pH value and 50 µM XGO acceptor. These trials were done as 3 repeats and average of these 3 trials was taken in account during pH optimization analysis.

Enzyme characterization and kinetic studies were carried in 0.1 M ammonium acetate environment. Since McIlvaine and ammonium acetate buffer have different buffering capacities at different pH values, a narrow pH range was screened using ammonium acetate buffer as pH arranging buffer. For each enzyme, ±0.5 value of their McIlvaine pH optima was screened using 5-8 different ammonium acetate pH value (If pH optima of an enzyme is found as 5.5 with McIlvaine buffer, ammonium acetate screening was done between pH 5.0 and 6.0). pH arangement was done by mixing 0.8 per cent w/v TXG with 0.2 M ammonium acetate buffer in 1:1 ratio.

3.17. HPLC ANALYSES

Xyloglucan endotransglycosylation activity was measured by quantifying hybrid products formed during XET/MXE enzyme activity via HPLC system. Agilent 1100 HPLC system with Fluorescence Detector was employed for analyses. After enzyme incubation period, reactions were finalized by changing pH with formic acid addition and volume of the reactions were increased to 30 µl with ultrapure water. Then, they were transferred to Agilent HPLC vials and analysed freshly. Samples were run and separated on a Phenomenex BioSep 5 µm SEC-s 3000 75*7.8 mm LC column. System conditioning, sample loading and elution are all carried out with an isocratic composition of 20 per cent v/v ACN and 80 per cent v/v 0.1M ammonium acetate buffer, pH 6.0 at 0.5 ml/min flow rate, 25°C. Detection of separated oligosaccharides and polysaccharides were carried out at 570 nm and 590 nm as excitation and emission wavelengths respectively. Data analysis was carried using Agilent ChemStation software with manual integration of samples. Using standards, florescences of given amount of each acceptor were determined and using these values, amounts of hybrid products generated during enzyme activity assays were calculated.

3.18. DOT-BLOT ANALYSES

Dot-blot method was utilized for screening of polishing fractions of some enzymes used in the study. Performed enzyme activity reactions were terminated by formic acid addition and they blotted on Whatmann paper 1 µL at a time. When all of the reactions were blotted on the paper, unbound excess oligosaccharides were washed overnight under running tap water. Then, whatmann paper was dried for 2-4 hours at 60°C oven. Dot-blot papers were visualized on UV transilluminator.

3.19. EQUISETUM SAMPLE COLLECTION AND SPECIES ANALYSIS

Equisetum is a native weed specie growing in various regions of Turkey. It is a perennial plant, dying in winter and sprouting back to life in spring. Sample collection was firstly

done in May 2014 from Balıkesir region Turkey. Another sample was collected from Balıkesir region in October 2014 representing late stage plants from the same region.

Forest regions within Istanbul city borders were investigated for presence of wild native *Equisetum* populations and a growth area was found in Belgrad Forest Bahçeköy situs, Istanbul. This location was visited for several times to collect plant material (Table 3.1.). Individual plants were pulled out from soil without harming stem. Underground rhizome system is mostly disrupted and broken away during plant collection because of the depth and strength of this system. Uprooted plants were put into a plastic bag for transfer to laboratory. During plant collection, short newly sprouting plants were transferred to pots for cultivation trial with their own soil.

Table 3.1. Dates as month and year Belgrad Forest Bahçeköy region was visited for collecting *Equisetum* plants.

Date (month, year)	**Region**
September, 2014	Belgrad Forest Bahçeköy situs, Neşetsuyu track
June, 2015	Belgrad Forest Bahçeköy situs, Neşetsuyu track
November, 2015	Belgrad Forest Bahçeköy situs, Neşetsuyu track
April, 2016	Belgrad Forest Bahçeköy situs, Neşetsuyu track
June, 2016	Belgrad Forest Bahçeköy situs, Neşetsuyu track
July, 2016	Belgrad Forest Bahçeköy situs, Neşetsuyu track
September, 2016	Belgrad Forest Bahçeköy situs, Neşetsuyu track

Collected plant samples were used for protein extraction on the same day. For RNA extraction, samples from plants were dissected and frozen in liquid nitrogen, then stored at -80°C until experimentation.

Equisetum sample collected on September 2016 was used for species indication. Full physiological and close-up examination was done on samples. Stereomicroscope was also utilized for close-up examination. Gathered images and features were compared to identification key and descriptions which are kind sharing from Prof. Dr. Tamer Özcan (Istanbul University, Department of Botany).

3.20. PROTEIN SAMPLE PREPARATION FROM EQUISETUM

Freshly collected plant samples were used for extract preparation. After a literature research, two plant extraction methods were assigned as candidate extraction methods; Fincher method [128] and Fry method [120]. Both of the methods were used for preparation of plant extracts prior to protein purification. Thus, a comparison to find the working one and optimization of protocol can be done.

In Fincher method, 100 gr fresh plant sample was mixed with 250 ml of extraction buffer (0.1 M imidazole-HCl pH 6.0, 1 M NaCl, 2 mM EDTA, 1 mM β-mercaptoethanol, 1 mM PMSF) and homogenized at 4°C by Waring Blender for 5 times with 1-min intervals and 2-min intermittent cooling on ice. The homogenate was incubated at 4°C with mild mixing to ensure full solubilisation of proteins. Insoluble materials in homogenate were pelleted with centrifugation at 4000 x *g*, 60 min, at 4°C. Then, it was filtered through Miracloth. Proteins in plant extract were separated from the extract by ammonium sulphate precipitation. Solution was saturated by $(NH_4)_2SO_4$ addition up to 90 per cent saturation point. Then, proteins were pelleted by centrifugation at 4°C, 8000 x *g*, 45 minute. Precipitated protein sample was resuspended in buffer without NaCl (0.1 M imidazole-HCl pH 6.0, 2 mM EDTA, 1 mM β-mercaptoethanol, 1 mM PMSF).

In Fry method, extraction buffer (0.3 M succinate Na^+ pH 5.5, 10 mM $CaCl_2$, 20 mM ascorbate, 3 per cent w/v polyvinylpolypyrrolidone) was prepared and stirred overnight for complete hydration of water insoluble polyvinylpolypyrrolidone. For extraction, 100 gr fresh tissue was mixed with 500 ml buffer and homogenized at 4°C by Waring Blender for 5 times with 1-min intervals and 2-min intermittent cooling on ice. The homogenate was mixed slowly at 4°C for 2.5 hours. Then, homogenate was filtered through miracloth and impurities were separated by centrifugation at 4°C, 15 000 x *g*, 20 min.

Samples from both extraction methods were used in enzyme reactions with TXG-XGO and BBG-XGO as donor-acceptor couples to control efficiency of extraction protocol. Fry method was more efficient and requires less toxic chemical, thus it was used for all plant extract preparation studies.

*Equisetum p*lant collection was carried for many times. These plants are consisting of 3 main stuctural part; underground stem/rhisome, stem, leaves. In each plant extraction trial,

different plant sections were used (Table 3.2). Prior to proceeding with protein purification, they were all tested for prescence of MXE ativity by enzyme activity test.

Table 3.2. *Equisetum* plant sections used for extract preparation from plants collected at differet times.

Sampling time	**Parts used in extraction**
Mayıs 2014 (Balıkesir)	Young stem, rhisome
September 2014 (İstanbul Belgrad Forest)	Young stem, mature stem, leaves
October 2014 (Balıkesir)	Whole stem, leaves
June 2015 (İstanbul Belgrad Forest)	Stem, leaves
November 2015 (İstanbul Belgrad Forest)	
April 2016 (İstanbul Belgrad Forest)	Stem of young plants
June 2016 (İstanbul Belgrad Forest)	Stem, leaves
July 2016 (İstanbul Belgrad Forest)	Stem of young plants, leaves
September 2016 (İstanbul Belgrad Forest)	Stem of young plants and old plants

Prepared extracts were firstly processed by ammonium sulphate precipitation. Extracts were saturated with solid ammonium sulphate salt to indicated ratio by gentle stirring at +4°C. Ammonium sulphate additions were carried in small quantities. When all ammonium sulphate was dissolved, proteins were precipitated out of solution by centrifugation at +4°C 8200 *xg* for 75 minutes. Protein pellets were dissolved in first chromatography step's recommended starting buffer; 50 mM sodium acetate pH if first step is cation exchange chromatography with HiScreen Capto S column, 20 mM Tris HCl pH 8.0 if first step is anion exchange chromatography with HiScreen Capto Q column or weak anion exchange chromatography with HiScreen Capto DEAE column. Then protein solution is desalted into resolving buffer in order to remove ammonium sulphate salts that precipitated with proteins. Three different strategies were employed and selection was done considering sample size, molarity of buffer used and vulnerability of sample. These strategies are dialysis (carried at +4°C, 2 times 3 hour incubation in dialysis membrane in 15 L buffer of choice and an additional incubation at 15 L buffer overnight), using Amicon Ultra 15 mL Centrifugal Filters or using HiPrep 26/10 DeSalting column.

Target protein purification within precipitated total protein pool was carried using different chromatography methods in order to optimize a flow of purification. Utilized chromatography strategies include anion exchange (HiScreen Capto Q, HiScreen Capto DEAE), cation exchange (HiScreen Capto S), hydrophobic interaction (HiScreen Capto Butyl), multimodal cation exchange (HiScreen Capto MMC), size exclusion (Superdex 75 16/100).

Startig buffer of anion exchange columns HiScreen Capto Q and Capto DEAE is 20 mM Tris-HCl pH 8.0 and elution buffer of them is 20 mM Tris-HCl 1 M NaCl pH 8.0. For anion exchange chromatography step, column was conditioned with 5 CV of starting buffer at flowrate of 5 mL/min. Protein sample (30-50 mL) was loaded onto column at 1.2 mL/min flowrate. Column was washed with 10 CV starting buffer after sample loading in order to eliminate excess unbound proteins. Proteins were eluted from column based on their total charges with a linear gradient from 100 per cent starting buffer to 100 per cent elution buffer fro 15 CV into fractions of 1.5 mL with a flowrate of 3mL/min. Column was washed with 5 CV 100 per cent elution buffer in order to elute any strongly interacting proteins.

In cation exchange chromatography step, 50 mM sodium acetate pH 5.0 was utilized as starting buffer and 50 mM sodium acetate 1M NaCl pH 5.0 was utilized as elution buffer with HiScreen Capto S column. Column was equilibrated with 5 CV of starting buffer at flowrate of 3 mL/min. Protein sample (30-50 mL) was loaded onto column at 1.2 mL/min flowrate. Column was washed with 10 CV starting buffer after sample loading in order to eliminate excess unbound proteins. Proteins were eluted from column based on their total charges with a linear gradient from 100 per cent starting buffer to 100 per cent elution buffer fro 15 CV into fractions of 3 mL with a flowrate of 3mL/min. Column was washed with 5 CV 100 per cent elution buffer in order to elute any strongly interacting proteins.

HiScreen Capto MMC is a multimodal cation exchange column and was used with 25 mM sodium acetate pH 4.5 starting buffer and 25 mM sodium acetate 1 M NaCl pH 7.5 elution buffer. Column was conditioned with 5 CV of starting buffer at flowrate of 3 mL/min. Protein sample (30-50 mL) was loaded onto column at 1.2 mL/min flowrate. Column was washed with 10 CV starting buffer after sample loading in order to eliminate excess unbound proteins. Proteins were eluted from column based on their total charges with a linear gradient from 100 per cent starting buffer to 100 per cent elution buffer fro 15 CV

into fractions of 3 mL with a flowrate of 3mL/min. Column was washed with 5 CV 100 per cent elution buffer in order to elute any strongly interacting proteins.

Hydrophobic interaction chromatography was actualised by HiScreen Capto Butyl column accompanied by 1.7 M ammonium sulphate 50 mM sodium phosphate pH 7.0 starting buffer and 50 mM sodium phosphate pH 7.0 elution buffer. Column was equilibrated by passing 10 CV of starting buffer at 2 mL/min flowrate. Protein sample (30-50 mL) was loaded onto column at 1 mL/min flowrate. Column was washed with 10 CV starting buffer after sample loading in order to eliminate excess unbound proteins. Proteins were eluted from column based on their total charges with a linear gradient from 100 per cent starting buffer to 100 per cent elution buffer fro 15 CV into fractions of 3 mL with a flowrate of 2mL/min. Column was washed with 5 CV 100 per cent elution buffer in order to elute any strongly interacting proteins.

Mobile phase used with Superdex 75 16/100 column was 20 mM sodium citrate 100 mM NaCl pH 5.5 buffer in size exclusion chromatography step. Column was conditioned with 2 CV of mobile phase. 5 mL of protein sample was loaded onto column and separeted into 1.5 mL ractions based on their molecule sizes at flowrate of 0.5 mL/min**.**

In between different chromatography steps, sample buffer was changed into next step's starting buffer using Amicon Ultra 15 Centrifugal Filters.

Combinations of different chromatographic separation techniques were tested for efficiency during target MXE enyzme purification from *Equisetum* protein pools (Table 3.3). After various trials, a serial usage of HiScreen Capto S, HiScreen Capto Q and Superdex 75 16/100 columns were optimized for MXE enzyme purification. Thus, this strategy was employed on subsequent purifications.

Table 3.3. Flow of chromatographic separation methods employed for protein purification optimization.

Sample name		Employed chromatography Columns
May 2014		--
September 2014	Mature Stem	HiScreen Capto Q, HiScreen Capto Butyl,
	Young stem	HiScreen Capto DEAE, HiScreen Capto MMC
October 2014		--
June 2015		HiScreen Capto S, HiScreen Capto Q, Superdex 75 16/100,
November 2015		
April 2016		HiScreen Capto S, HiScreen Capto Q, Superdex 75 16/100
June 2016		--
July 2016		HiScreen Capto S, HiScreen Capto Q, Superdex 75 16/100
September 2016		HiScreen Capto S, HiScreen Capto Q, Superdex 75 16/100

3.21. EQUISETUM PROTEIN IDENTIFICATION

3.21.1. In-gel Tryptic digestion of protein bands

Protein sample was loaded in polyacrylamide gel and separated via SDS-PAGE. After running, gel was stained by coomassie brilliant blue dye and destained by 30 per cent v/v ethanol- 10 per cent v/v acetic acid solution. Visualized bands were cut using a clean scalpel and sliced into small pieces, then transferred into 1.5 ml microcentrifuge tube in a laminar flow. Rest of the protocol was also carried in a laminar flow specific for proteomic work in order to minimize possible keratin and/or other protein contamination. 300 µl of wash solution (50 per cent MeOH v/v & 5 per cent acetic acid v/v) was added onto gel pieces and tube was mixed by vortexing for 10 minutes. At the end of vortexing, wash solution was removed by pipetting. Then, fresh wash solution was added onto gel pieces and this washing step was repeated until coomassie dye was removed from proteins in the gel pieces. When washing of the gel piece was over, 200 µl of destaining solution (per cent50 100 mM ammonium bicarbonate and 50 per cent acetonitrile) was added and pipetted out for 5 times. Then, gel pieces were dehydrated by addition of 200 µl

acetonitrile and incubating for 5 minutes at room temperature for twice. Dehydrated gel pieces were reduced by adding 30 µl 10 mM DTT and incubating at room temperature for 30 min in dark. DTT solution was pipetted away and for alkylation, 30 µl 100 mM iodoacetamide was added and sample was incubated at room temperature for 30 minutes in dark. After pipetting iodoacetamide solution away, gel pieces were dehydrated again by 200 µl acetonitrile addition and incubation at room temperature for 5 min. Acetonitrile was removed and 200 µl of 100 mM ammonium bicarbonate was added. Gel pieces were incubated with ammonium bicarbonate for 10 minutes at room temperature and then 200 µl acetonitrile was put on gel pieces after ammonium bicarbonate was pipetted out. Gel pieces were incubated with acetonitrile for 5 minutes at room temperature. After incubation, acetonitrile was completely removed and 10 µl of trypsin solution was added on ice. Dehydrated gel pieces absorbed the trypsin solution. Until they become completely saturated, 50 mM ammonium bicarbonate was added in small batches while sample was on ice. Then gel pieces were incubated at 37°C for 18 hours for complete tryptic digestion of the fragments. Next, 20 µl of 50 mM ammonium bicarbonate was added and tube was mixed by vortexing for 10 min at room temperature. Supernatant was transferred into a glass vial insert in a microcentrifuge tube. Extraction buffer (20 µl, 50 per cent acetonitrile v/v 5 per cent formic acid v/v) was added to gel pieces and they were mixed by vortexing at room temperature for 10 minutes. Supernatant was transferred to glass insert. The last extraction step via vortexing was then repeated for a second time. At the third extraction step, 20 µl of extraction buffer was added and sample was sonicated for 10 minutes at 20 per cent power. Supernatant was pooled with the rest of the extracts in the glass insert and total volume of extracts were reduced to ~20 µl by vacuum concentrator at 30°C. Tryptic fragments were then stored at -20°C until analysis.

3.21.2. Native-PAGE

Native-PAGE gels were prepared as 4 per cent stacking gel and 12 per cent resolving gel (Table 3.4). Gel with donor barley β-glucan (BBG) was prepared with addition of BBG to a final concentration of per cent1 w/v in 12 per cent resolving gel. After pouring both resolving and stacking parts of the gels, they were polymerized overnight at +4°C. Before sample loading, gels were prerun for 30 minutes at 200 volts constant.

Table 3.4. Native-PAGE gel compositions w/ and w/o BBG donor.

	12 per cent resolving gel w/o BBG (ml)	**12 per cent resolving gel w/ BBG (ml)**	**4 per cent stacking Gel (ml)**
ddH_2O	2.02	1.29	3.57
30 per cent acrylamide mix	2.4	2.4	0.66
1.5 M Tris buffer pH 8.8	1.5	1.5	-
1 M Tris buffer pH 6.8	-	-	0.63
10 per cent APS	0.06	0.06	0.05
TEMED	0.0024	0.0024	0.005
0.8 per cent w/v BBG solution	-	0.75	-

Sample buffer of Native-PAGE (2X concentrate) consists of 100 mM Tris pH 6.8, 40 per cent v/v glycerol and 0.05 per cent w/v bromophenol blue. Protein samples were mixed with sample loading buffer and incubated on ice for 2-3 hours before the run. Gels were run in 25 mM Tris, 192 mM glycine pH 8.3 running buffer firstly at 80 volts (~11 mA) and then at 100 volts (~13 mA).

3.21.3. In-gel activity assay

Protein samples were separated by Native-PAGE protocol in w/ BBG gel for in-gel activity assay. Lanes spared for in-gel activity assay were incubated with 1 ml of 10 µM X7 in 20 mM ammonium acetate pH 7.0 buffer per 3 cm^3 gel volume on rocking platform at room temperature for 24 hours. After incubation, gels were washed with 20 ml of ultrapure water for 20 minutes twice and then fixed with fixation solution (30 per cent v/v ethanol and 10 per cent v/v acetic acid) for 40 minutes. Then they were rinsed with ultrapure water and visualized using Biorad ChemiDoc Imagelab software.

3.21.4. Database preparation for MALDI-TOF MS analysis

During MALDI-TOF MS analysis of tryptic protein fragments, measured fragment sizes are blasted against a prepared database by Mascot software. For blast search and identification of purified *Equisetum* MXE enzyme, a database consisting of various XET sequences of different plants were used. These sequences include both full and partial ones. *Equisetum* sequences in the database were extracted from NCBI database and "The 1000 plants" initiative transcript database belonging to *Equisetum hyemale, Equisetum diffusum, Equisetum, Equisetum fluviatile*. Additionaly, nasturtium, *Populus tremula x Populus tremuloides, Hordeum vulgare, Oryza sativa, Arabidopsis thaliana* sequences were included.

3.21.5. Edman degradation sample preparation

Protein sample for N-terminal Edman Sequencing was desalted into 25 mM sodium citrate 50 mM NaCl pH 5.5 buffer using Amicon Ultra 15 mL Centrifugal Filters. Concentrated and buffer exchanged sample was mixed with Laemmli denaturing buffer and denatured by heating up at 95°C for 7 minutes. After performing SDS-PAGE, gel was firstly incubated in 50 mM sodium borate pH 9.0 buffer and then blotted onto PVDF membrane by semidry blotting using 50 mM sodium borate 20 per cent v/v methanol pH 9.0 buffer for 100 minutes at 0.5 A constant. Membrane was stained with 0.1 per cent w/v coomassie brilliant blue R250 dye for 5 minute and destained using 10 per cent v/v acetic acid 40 per cent v/v methanol solution for 5 minutes three times. After the protein band was visualized on PVDF membrane, it was cut out of membrane and send for sequencing.

3.22. *EQUISETUM* ENZYME CHARACTERIZATION

Optimum pH value *Equisetum* MXE enzyme catalyses endotransglycosylation is studied for pH values between 4.0 and pH 7.0. For enzyme reactions, 0.4 per cent w/v TXG donor substrate is prepared using McIlvaine buffer (citrate-phosphate buffer). As for acceptor, 50μM XGO is used. TXG-XGO reactions were carried out using *Equisetum* September'16 sample Pool β. Hybrid product amouts at the end of three hour incubation period were

analysed by HPLC system coupled with FLD. pH value at which enzyme was producing the most hybrid product was assigned as optimum pH for *Equisetum* MXE.

Specific enzyme activity of different *Equisetum* MXE pools were investigated using different donors and xyloglucan acceptors. Hybrid product amounts were analysed using an HPLC system coupled with FLD. Product amounts were converted to specific enzyme activities as picokatal/mg enzyme.

3.23. RNA EXTRACTION AND CDNA SYNTHESIS

Gene coding *Equisetum* MXE remained as a mystery due to the lack of genomic, transcriptomic and proteomic information about *Equisetum* in general and about *E. telmaitea* in particular. In order to enlighten gene, RACE studies were carried out. Prior to RACE studies, RNA extraction and cDNA synthesis was done.

Total RNA extractions were carried from snap frozen *Equisetum* plant parts using IntronBio easy-spin IIp Plant RNA Extraction Kit. RNA samples were quantified by Thermo Nanodrop2000 instrument and their A260/A280 and A260/A230 purity ratios were also measured.

cDNA synthesis was carried using Thermo Fisher Scientific SuperScript IV First-Strand Synthesis System. Reverse transcription reactions were carried using oligo $(dT)_{20}$ primer according to manufacturer's instructions. After first-strand cDNA synthesis, RNA templates in DNA-RNA hybrids were digested by RNase treatment step. Synthesized cDNAs were stored at -20°C until being used.

3.24. 5'- AND 3'-RACE STUDIES

3.24.1. 3'-RACE study

Equisetum April'16 whole young plant, *Equisetum* September'16 whole young plant and *Equisetum* June'16 stem samples were used in 3'-RACE. RNA extractions from mentioned plant samples were done using IntronBio easy-spin IIp Plant RNA Extraction Kit. Concentration measurements were carried using ThermoScientific Nanodrop2000

instruments. Extracted RNA samples were used as templates in cDNA synthesis using oligo $(dT)_{20}$ adapter primer (Table 3.5). Firstly 11 µl of extracted RNA samples were mixed with 1 µl of 10 µM primer and incubated at 70°C for 10 minutes. Then, cDNA synthesis components from Invitrogen SuperScript III First-Strand Synthesis System for RT-PCR (cat. no. 18080-051) were included as mentioned in Table X. These reactions were incubated at 50°C prior to SuperScript III reverse transcriptase addition and after 1 µl SuperScript III addition, they were further incubated at 50°C for 50 minutes for cDNA synthesis. Reactions were terminated at 85°C for 5 minutes by heat inactivation and RNA templates in cDNA-RNA hybrids were digested using 1µl RNase H at 37°C for 20 minutes.

Table 3.5. cDNA synthesis reaction mixture for 3'-RACE.

Component name	**Amount (µl)**
10X RT Buffer	2
25 mM $MgCl_2$	2
10 mM dNTP	1
0.1 M DTT	2

Synthesized cDNAs were used in PCR studies as templates. For 3'-RACE studies, 2 sets of 5' primers were design. First set of primers (EqOnlyDegI, GroupIOnlyDegI, GroupIIIBOnlyDegI; GSPI, gene specific primer I) were for initial PCR and second set of primers (EqOnlyDegII, GroupIOnlyDegII, GroupIIIBOnlyDegII; GSPII, gene specific primer II) were for nested PCR. When *Equisetum* XTH enzymes were pulled out of database prepared for University of Alberta 1000 plants project BLAST webpage (https://db.cngb.org/blast4onekp/, Novmber 2016), it was seen that those sequences were settling in 3 different positions in XTH phylogenetic tree; GroupI, GroupIIIB and some of the sequences were forming a clade by their own. In order to design 3'-RACE primers, conserved nucleotide regions on 5' side of catalytic site were searched by ClustalX2 alignment of *Equisetum* XET sequences acquired from University of Alberta 1000 plants project BLAST webpage. Two target regions, one more towards 5'end of sequences compared to other, were chosen as primer design targets. First set of primers were designed as degenerated primers depending on above mentioned conserved region toward 5'end and

second set of primers were designed as degenerated primers based on conserved region closed to catalytic site (Table 3.6).

Table 3.6. Primers and their sequences used in 3'-RACE studies.

Primer name	Primer sequence
oligo $(dT)_{20}$ adapter	5' GCCACGCGTCGACTAGTACTTTTTTTTTTTTTTT
AUAP	5' GCCACGCGTCGACTAGTAC
EqOnlyDegI	5' ATGSARATBAAGCTIRTRYC
GroupIOnlyDegI	5' ATGGYTGGTTYAGYATGAAGCT
GroupIIIBOnlyDegI	5' TTTTAGTGCTKSRATMAAGCT
EqOnlyDegII	5' GAYGAGYTRGAYTTYGAGTTYYTIGG
GroupIOnlyDegII	5' GAGCTGGACTTYGAGTTYYTGG
GroupIIIBOnlyDegII	5' GGCTYARYYTYTGGTTTGATCC

An initial PCR using first primer set as 5' primer and AUAP primer as 3' primer was carried with synthesized cDNAs (Table 3.7). All PCR studies during 3'-RACE were done using GeneOn Maximo Taq DNA Polymerase (GeneOn, Germany). Gradient PCR application was carried in order to optimize annealing temperature (Table 3.8). PCR components final concentrations were as following; 0.2 mM of each dNTP (dATP, dCTP, dGTP, dTTP), 0.6µM of AUAP primer, 0.2µM of GSP primer, 0-0.167 mM $MgCl_2$, 1.5 unit DNA taq polymerase and 1:2 diluted cDNA templates in 30µL 1X Buffer I conditions. After PCR results were analysed by running on 1 per cent w/v agarose gel, PCR products were used as templates in nested PCR with second set of degenerate primers (GSPII).

Table 3.7. Primer couples used in initial PCR of 3'-RACE study.

Primer couple name	5' primer	3' primer
A	EqOnlyDegI	AUAP
B	GroupIOnlyDegI	AUAP
C	GroupIIIBOnlyDegI	AUAP

Table 3.8. Annealing temperatures during initial PCR of 3'-RACE.

	Annealing Temperatures (°C)				
Primer Couple A	49.8	52	53.9	58.1	62
Primer Couple B	50.5	52	55.8	58.1	62
Primer Couple C	48	50.5	52	55.8	58.1

Nested PCR trials were done using GSPII; EqOnlyDegII and GroupIOnlyDegII. Different annealing temperatures were tested (Table 3.9) in a PCR mixture of 0.2 mM of each dNTP (dATP, dCTP, dGTP, dTTP), 0.4 µM GSPII, 0.2 µM AUAP, 0-0.125 mM $MgCl_2$, 1.5 unit taq DNA polymerase and 1 µl template DNA (PCR product from initial PCR) in 30 µL 1X Buffer I per each tube. PCR results were analysed by running on 1 per cent w/v agarose gel. PCR bands acquired from initial PCR and nested PCR were excised separately and gel-purified using Macherey-Nagel PCR clean-up Gel extraction kit according to manufacturer's instructions. Concentration and purity measurements of gel-purified fragments were carried using ThermoScientific Nanodrop2000. Samples were precipitated and cleaned using sodium acetate ethanol precipitation method. Then, fragments were ligated into pGEM-T easy vector using pGEM-T Easy Vector System (Promega Cat. no. A1360) with 1:2 molar ratio of vector:insert according to manufacturer's instructions.

Table 3.9. Annealing temperatures during nested PCR of 3'-RACE.

	Annealing Temperatures (°C)							
EqOnlyDegII	52	54.3	55.8	56.6	59.3	60	61.6	64
GroupIOnlyDegII	53.9	58.1	62					

Ligation reactions were transformed into *E.coli* DH5α cells and transformant bacteria were selected on LBA+ampicillin+X-gal+IPTG plates. 3 different colonies per each transformation event were incubated in LB+ampicillin broth for plasmid isolation. PureLink Quick Plasmid Miniprep Kit (ThermoFisher Cat. No. K210011) was used for plasmid isolation from transformant cells. Isolated plasmids were digested by Fast Digest

NotI restriction endonuclease (ThermoFisher Cat. No. FD0596) in order to control insert size. Restriction results were separated depending on their sizes on a 1 per cent w/v agarose gel and plasmids with different inserts were sent for sequencing by Macrogen (Macrogen Inc., South Korea).

3.24.2. 5'-RACE study

Each 3'-RACE study positive result sequences were used for primer design. Nucleotide region 3' to conserved catalytic site was used as target for primer design. First set of primers (GSP1) were designed to be used in cDNA synthesis from total RNA tool and second set of primers (GSP2) were designed to be used in nested PCR from cDNAs synthesized by GSP1.

New total RNA was extracted from *Equisetum* September'16 whole young plant frozen stored sample using Plant/Fungi RNA Extraction Kit (Norgen, Cat. No. 25800) according to manufacturer's instructions. After RNA samples were quantified using ThermoFisher Nanodrop2000, they were used in first strand cDNA synthesis by 5'-RACE System for Rapid Amplification of cDNA Ends (Invitrogen, Cat. No. 18374-058) according to manufacturer instructions. 700 ng of RNA sample was mixed with 5 pmoles of GSP1 primers (Table 3.10) in a final volume of 15.5 µl and incubated at 70°C for 10 minutes. Then, 62.5 nanomoles of $MgCl_2$, 1 nanomole of dNTP mix, 0.25 µmoles DTT was added in 1X PCR Buffer and samples were incubated at 42°C for a minute. cDNA synthesis was done by 200 unit SuperScriptII addition and incubation at 42°C for 50 minutes. Reactions were terminated by heat inactivation of enzyme at 70°C for 15 minutes. RNA template in cDNA-RNA hybrid was digested by adding 1 µl of RNase mix and incubating at 37°C for 30 minutes.

Table 3.10. Primers used in 5'-RACE study.

Primer name	Primer sequence
Frg9 GSP1	5'- ACATTCATCCATTGGC
Frg9 GSP2	5'-GATTGTCGGGAAGGTAGTTGTTCC
Frg10-3 GSP1	5'-ATAGATACGTTGTTCTCG
Frg10-3 GSP1	5'-TGTAACCAAACGTGATACATTCCA
Frg12 GSP1	5'-GAAGGCATTTCTGGTT
Frg12 GSP2	5'-GCCATGTGCTAGTTGTATCTTCTGT
AAP	5'-GGCCACGCGTCGACTAGTACGGGIIGGGIIGGGIIG

Synthesized cDNAs were purified from reaction components by S.N.A.P. column purification according to manufacturer's instructions. Afterwards, they were TdT tailed according to manufacturer's instructions and used as template in PCR production of target DNA fragments. Different annealing temperatures were tested by gradient PCR (Table 3.11) using Maximo taq DNA polymerase (GeneOn, Germany) in PCR mixture composed of 12.5 nmoles of $MgCl_2$, 4 nmole of dNTP mix, 8 nmole GSP2 (GSP2 of each fragment was used with cDNA of specific fragment), 8 nmole AAP primer, 1.6 µL dC-tailed cDNA, 1 unit taq DNA polymerase in 20 µL 1X Reaction Buffer.

Table 3.11. Annealing temperatures during first PCR trial.

	Annealing temperatures (°C)						
Frg9 GSP2	58	58.8	60.5	61.2	61.6	64.9	
Frg10-3GSP2	60.5	62	64.5	64.9	66.4	68	
Frg12 GSP2	58	58.8	60	60.5	61.2	61.6	64.9

PCR results were analysed on 1 per cent w/v agarose gel by electrophoresis. Visualized PCR bands were excised from gel and purified using Macherey-Nagel PCR clean-up Gel extraction kit according to manufacturer's instructions. They were further concentrated and purified by sodium acetate ethanol precipitation method and dissolved in nuclease-free water. Fragments were quantified by Thermo NanoDrop2000 instrument and cloned into pGEM-T easy vector by 1:1 vector:insert molar ratio (Promega Cat. no. A1360). Ligation

reactions were incubated at room temperature for an hour and then at +4°C for 5 hours. pGEM-T easy plasmids with 5'-RACE products were transformed into chemically competent *E. coli* DH5α cells by heat shock and transformants were selected on LBA+ ampicillin (100µg/mL) + IPTG + X-Gal plates.

White transformant colonies were grown in LB + ampicillin (100µg/mL) broth overnight for plasmid isolation by PureLink Quick Plasmid Miniprep Kit (ThermoFisher Cat. No. K210011). Isolated plasmids were digested by Fast Digest NotI restriction endonuclease (ThermoFisher Cat. No. FD0596) according to manufacturer's instruction for controlling insertion event and insert size. Restriction results were separated depending on their sizes on a 1 per cent w/v agarose gel and plasmids with different inserts were sent for sequencing by Macrogen (Macrogen Inc., South Korea).

4. RESULTS

4.1. INITIAL BIOINFORMATIC ANALYSIS AND TARGET SELECTION

There are many papers about plant XTHs published in the past years. Sequences of various plant XTH enzymes were gathered from papers and rest were fished through NCBI database [99, 129] (https://www.ncbi.nlm.nih.gov/). It is known that in general XTH proteins have three highly conserved regions; DE-I/F-DFEFLG domain as catalytic site for enzymatic activity, a *N*-linked glycosylation site following catalytic domain usually as NL(V)SG and four cysteine residues in the C-terminal portion [97]. These three conserved motifs were referred during *XTH* sequence research. Amino acid sequences of XTH enzymes form various plant were gathered as a list and they were used for preparation of XTH phylogenetic tree by MEGA6 program (Table 4.1).

Table 4.1. XTH sequences;enzyme names, GenBank accession numbers, locus tags.

XTH enzymes	GenBank accession numbers	NCBI Reference Sequence	Locus Tag
AtXTH1	NM_117377.3	NP_193044.3	AT4G13080
AtXTH2	NM_117378.2	NP_193045.1	AT4G13090
AtXTH3	NM_113409.4	NP_189141.1	AT3G25050
AtXTH4	NM_126666.4	NP_178708.1	AT2G06850
AtXTH5	NM_001343297.1	NP_001331376.1	AT5G13870
AtXTH6	NM_125970.4	NP_569019.1	AT5G65730
AtXTH7	NM_119942.3	NP_195494.1	AT4G37800
AtXTH8	NM_101028.4	NP_563892.1	AT1G11545
AtXTH9	NM_116559.3	NP_192230.1	AT4G03210
AtXTH10	NM_127026.4	NP_179069.1	AT2G14620
AtXTH11	NM_114717.3	NP_566910.1	AT3G48580
AtXTH12	NM_125134.2	NP_200561.1	AT5G57530.1
AtXTH13	NM_125135.2	NP_200562.1	AT5G57540
AtXTH14	NM_118714.4	NP_194312.1	AT4G25820
AtXTH15	NM_117490.4	NP_193149.2	AT4G14130
AtXTH16	NM_113277.3	NP_566738.1	AT3G23730
AtXTH17	NM_105205.4	NP_176710.1	AT1G65310

AtXTH18	NM_119174.2	NP_194757.1	AT4G30280
AtXTH19	NM_119175.3	NP_194758.1	AT4G30290
AtXTH20	NM_124181.4	NP_199618.1	AT5G48070
AtXTH21	NM_127436.2	NP_179470.1	AT2G18800
AtXTH22	NM_125137.4	NP_200564.1	AT5G57560
AtXTH23	NM_118713.5	NP_194311.1	AT4G25810
AtXTH24	NM_119173.4	NP_194756.1	AT4G30270
AtXTH25	AY143939.1	AAN28878.1	
AtXTH26	NM_119029.3	NP_194614.1	AT4G28850
AtXTH27	NM_126246.4	NP_178294.1	AT2G01850
AtXTH28	NM_101341.4	NP_172925.1	AT1G14720
AtXTH29	NM_118017.3	NP_193634.1	AT4G18990
AtXTH30	NM_102950.4	NP_174496.1	AT1G32170
BdXTH2	XM_014896475.1	XP_014751961.1	
GhXTH1	NM_001327047.1	NP_001313976.1	
GhXTH2	NM_001327390.1	NP_001314319.1	
GhXTH10	XM_016839956.1	XP_016695445.1	
HvXET1	X91660.1	CAA62848.1	
HvXET2	AK367117.1	BAJ98320.1	
HvXET3	X93174.1	CAA63662.1 /	
HvXET4	AK367663.1	BAJ98866.1 /	
HvXET5	AK355355.1	CAA62847.1	
HvXET6	EU247793.1	ABY79073.1	
HvXET7	AK365879.1	BAJ97082.1	
HvXET8	FJ917201.1	ACS13756.1	
HvXET9	AK361278.1	BAJ92485.1	
HvXTH10	AK356496.1		
HvXET11	AK370212.1	BAJ89051.1	
HvXET12	AK358343.1	BAJ89557.1	
HvXET13	AK364758	BAJ95961.1	
HvXET14	AK371075.1	BAK02273.1	
HvXET15			MLOC_65419.6
HvXET16	AK365330.1	BAJ96533.1	
HvXET17	AK354927.1	BAJ86146.1	
HvXET18	AK360629.1	BAJ91838.1	
HvXET19	AK367091	BAJ98294.1	
HvXET20	AK373731.1	BAK04928.1	
HvXET21	AK357092.1	BAJ88307.1	
HvXET22	AK358294/ AK360254	BAJ89508.1	

HvXET23	AK252817.1		
HvXET24			MLOC_21703.1
HvXET25			MLOC_14992.1
HvXET26	AK354670.1	BAJ85889.1	
HvXET27			Morex contig 2552665
HvXET28	AK355309.1	BAJ86528.1	
HvXET29	AK376480.1	BAK07675.1	
HvXET30			Morex contig_8001
OsXTH1	XM_015789738.1	XP_015645224.1	OSNPB_070529700
OsXTH2	XM_015760099.1	XP_015615585.1	OSNPB_110539200
OsXTH3	XM_015778816.1	XP_015634302.1	OSNPB_040631200
OsXTH4	XM_015792907.1	XP_015648393.1	OSNPB_080240500
OsXTH5	XM_015793744.1	XP_015649230.1	OSNPB_080240566
OsXTH6	XM_015780208.1	XP_015635694.1	OSNPB_040604200
OsXTH7			
OsXTH8	XM_015793983.1	XP_015649469.1	OSNPB_080237800
OsXTH9	AK070734.1	BAG92117.1	OSNPB_040604300
OSXTH10	XM_015786197.1	XP_015641683.1	OSNPB_060697000
OsXTH11	XM_015785621.1	XP_015641107.1	OSNPB_060696400
OsXTH12	XM_015785680.1	XP_015641166.1	OSNPB_060696600
OsXTH13	XM_015768670.1	XP_015624156.1	OSNPB_020280200
OsXTH14	XM_015769254.1	XP_015624740.1	OSNPB_020280250
OsXTH15	XM_015785500.1	XP_015640986.1	OSNPB_060335900
OsXTH16	XM_015778700.1	XP_015634186.1	OSNPB_040604900
OsXTH17	XM_015795203.1	XP_015650689.1	OSNPB_080237000
OsXTH18	XM_015785620.1	XP_015641106.1	OSNPB_060696500
OsXTH19	XM_015773127.1	XP_015628613.1	OSNPB_030108300
OsXTH20	XM_015758855.1	XP_015614341.1	OSNPB_100545500
OsXTH21	XM_015789926.1	XP_015645412.1	OSNPB_070480800
OsXTH22	XM_015769458.1	XP_015624944.1	OSNPB_020823700
OsXTH23	XM_015767696.1	XP_015623182.1	OSNPB_020696500
OsXTH24			
OsXTH25	XM_015757492.1	XP_015612978.1	OSNPB_100577500
OsXTH26	XM_015769371.1	XP_015624857.1	OSNPB_020127800
OsXTH27			
OsXTH28	XM_015773815.1	XP_015629301.1	OSNPB_030239000
OsXTH29	XM_015755817.1	XP_015611303.1	OSNPB_090395600
OsXTH30	XM_015787289.1	XP_015642775.1	OSNPB_060237400
PtXTH3	XM_002301756.2	XP_002301792.2	POPTR_0002s24570g

TaXTH5	D16457.1	BAA03924.1	
EfHTG	LN626749.1	CEH24720.1	

XTH sequences fell into six groups which are GroupI, GroupII, GroupIIIA, GroupIIIB, EG16 and Ancestral Group. A narrower classification was shown by many different groups [49, 63, 82].

Sequences of expression targets, AtXTH3, AtXTH4, AtXTH11, BdXTH2, GhXTH2, OsXTH30, PtXTH3, TaXTH5, were acquired from NCBI Nucleotide database (https://www.ncbi.nlm.nih.gov/nuccore) as mRNA sequences (Table 4.2).

Table 4.2. Expression target names and GenBank accession numbers.

Expression targets	**GenBank accession numbers**	**NCBI Reference Sequence**	**Locus Tag**
AtXTH3	NM_113409.4 / DQ446697.1	NP_189141.1	AT3G25050
AtXTH4	NM_126666.4	NP_178708.1	AT2G06850
AtXTH11	NM_114717.3 / BT025721.1	NP_566910.1	AT3G48580
BdXTH2	XM_014896475.1	XP_014751961.1	
GhXTH2	NM_001327390.1	NP_001314319.1	
OsXTH30	XM_015787289.1	XP_015642775.1	OSNPB_060237400
PtXTH3	XM_002301756.2	XP_002301792.2	POPTR_0002s24570g
TaXTH5	D16457.1	BAA03924.1	

4.2. CODON OPTIMIZED EXPRESSION TARGETS AND PREPARATION OF EXPRESSION PLASMIDS

Signal peptides and signal peptide cleavage sites of protein sequences given in Table X were predicted via the SignalP 4.1 Server online tool [126] After the signal peptide tag is removed from the coding regions of proteins, the rest of the coding regions were codon optimized for heterologous protein expression in *P. pastoris* by GenScript (NJ, USA).

During codon optimization, ClaI restriction digestion enzyme recognition site was inserted at the 5'- end of the sequences and XbaI restriction digestion enzyme recognition site was

inserted at the 3'- end of the sequences. Prepared sequences were cloned into pUC57/pPicZα-C vectors by GenScript (NJ, USA). Codons of the original sequence may be rare in *P. pastoris* and low availability of aminoacyl-tRNA in the yeast cell may limit the expression causing premature proteins. There can be complications during synthesis/folding of the protein due to deceleration. Codon optimization can also increase expression levels. Since heterologous expression methods will be used for obtaining enzymes, it will be better to use codon optimized sequences of original *XET* genes.

After codon optimization and gene synthesis by GenScript, plasmids with genes of interest were received (Table 4.3). All of them were firstly transformed into *E. coli* DH5α cell and selected on LBA + zeocin (pPicZα-C plasmids) or LBA + ampicillin (pUC57 plasmids) plates. Transformant bacteria were grown in LB + zeocin (pPicZα-C plasmids) or LB + ampicillin (pUC57) broth overnight. Saturated cultures were used for 15 per cent v/v glycerol stock preparation . Plasmid isolation was done from the rest of the overnight cultures.

Table 4.3. Codon optimized *XET* sequences and their carrier vector system.

Name of the gene	**Name of the plasmid**	**Size of the insert after codon optimization**
AtXTH3	pUC57	819 bp
AtXTH4	pPicZα-C	828 bp
AtXTH11	pPicZα-C	786 bp
BdXTH2	pPicZα-C	816 bp
GhXTH2	pPicZα-C	828 bp
OsXTH30	pUC57	852 bp
PtXTH3	pPicZα-C	828 bp
TaXTH5	pPicZα-C	828 bp

Genes in pUC57 vector were released from the plasmid by a ClaI-XbaI double digestion. Restriction results were separated on 1 per cent w/v agarose gel and *AtXTH3* and *OsXTH30* genes were excised from agarose gel, and gel purified using the Macharey-Nagel PCR clean-up Gel extraction kit. Empty pPicZα-C plasmid was also digested using

ClaI-XbaI restriction endonuclease enzymes and gel purified by Macharey-Nagel PCR clean-up Gel extraction kit. Digested pPicZα-C plasmid and genes were ligated using Thermo Scientific T4 DNA ligase with 1:1 vector:insert molar ratio according to the manufacturer's instruction. Ligation reactions were transformed into DH5α *E. coli* and selection was done by plating transformation events onto LBA + zeocin plates. For each gene, 3 transformant colonies were chosen and grown in LB + zeocin overnight. Glycerol stock preparation and plasmid isolation were done from these cultures. Presence of *AtXTH2* and *OsXTH30* inserts in pPicZα-C was checked by ClaI-XbaI double digestion.

All of the expression plasmids were linearized, precipitated and purified by phenol extraction sodium acetate ethanol precipitation. They were resolubilized in nuclease-free water to a final concentration of 500 ng/µL and used immediately for yeast transformation.

4.3. YEAST TRANSFORMATION AND POSITIVE COLONY SELECTION

Heterologous expression system *pPicZα-C* has an α-factor signal sequence prior to the cloning site, separated from the insert by Kex2 and Ste13 signal cleavage sites (Figure 4.1) as well as a *c-myc* epitope and a polyhistidine tag after the cloning site. Thus, a protein expressed in *P. pastoris* by *pPicZα-C* expression system will have α-factor signal at N-terminal and *c-myc* epitope and polyhistidine tag at C-terminal. During secretion of synthesized protein outside the cells, the α-factor signal will be cleaved from Kex2 cleavage site firstly, leaving Glu-Ala-Glu-Ala repeats. Then, Glu-Ala repeats are further cleaved by Ste13 (Invitrogen Man0000042 Manual part no. 25-0172). The secreted mature protein can have Glu-Ala-Glu-Ala repeat remaining from Kex2 cleavage on their N-terminal end and will have a *c-myc* epitope and polyhistidine tag on their C-terminal end. These features will add to protein structure, changing the molecule size and charge. Heterologously synthesized proteins' theoretical molecular weights and pI values were calculated using Expasy Compute pI/Mw tool (Table 4.4).

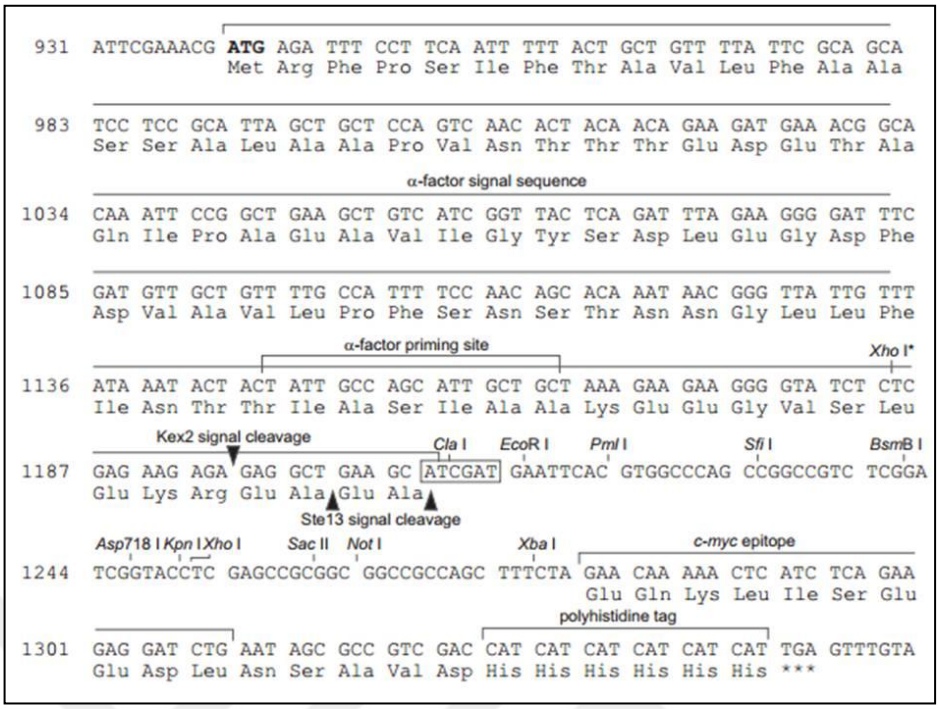

Figure 4.1. Expression casette sequence and features of *pPicZα-C* expression vector.

Table 4.4. Theoretical molecular weights and pI values of heterologously synthesized mature proteins.

Name of the protein	**Expected theoretical mature protein molecule size (Da)**	**Theoretical pI value of mature proteins**
AtXTH3	33908.34	5.89
AtXTH4	34923.32	8.30
AtXTH11	33003.98	7.29
BdXTH2	33196.64	5.23
GhXTH2	34633.43	6.10
OsXTH30	33954.52	5.04
PtXTH3	34302.73	6.27
TaXTH5	34633.43	6.10

Linearized expression plasmids were transformed into competent *P. pastoris* cells via electroporation. Transformant cells were selected on YPDSagar + zeocin (100 µg/mL) plates (Figure 4.2). More than 50 transformant colonies were obtained per each gene transformation event. At least 12 colonies per gene were screened for functional protein synthesis by different methods (Table 4.5).

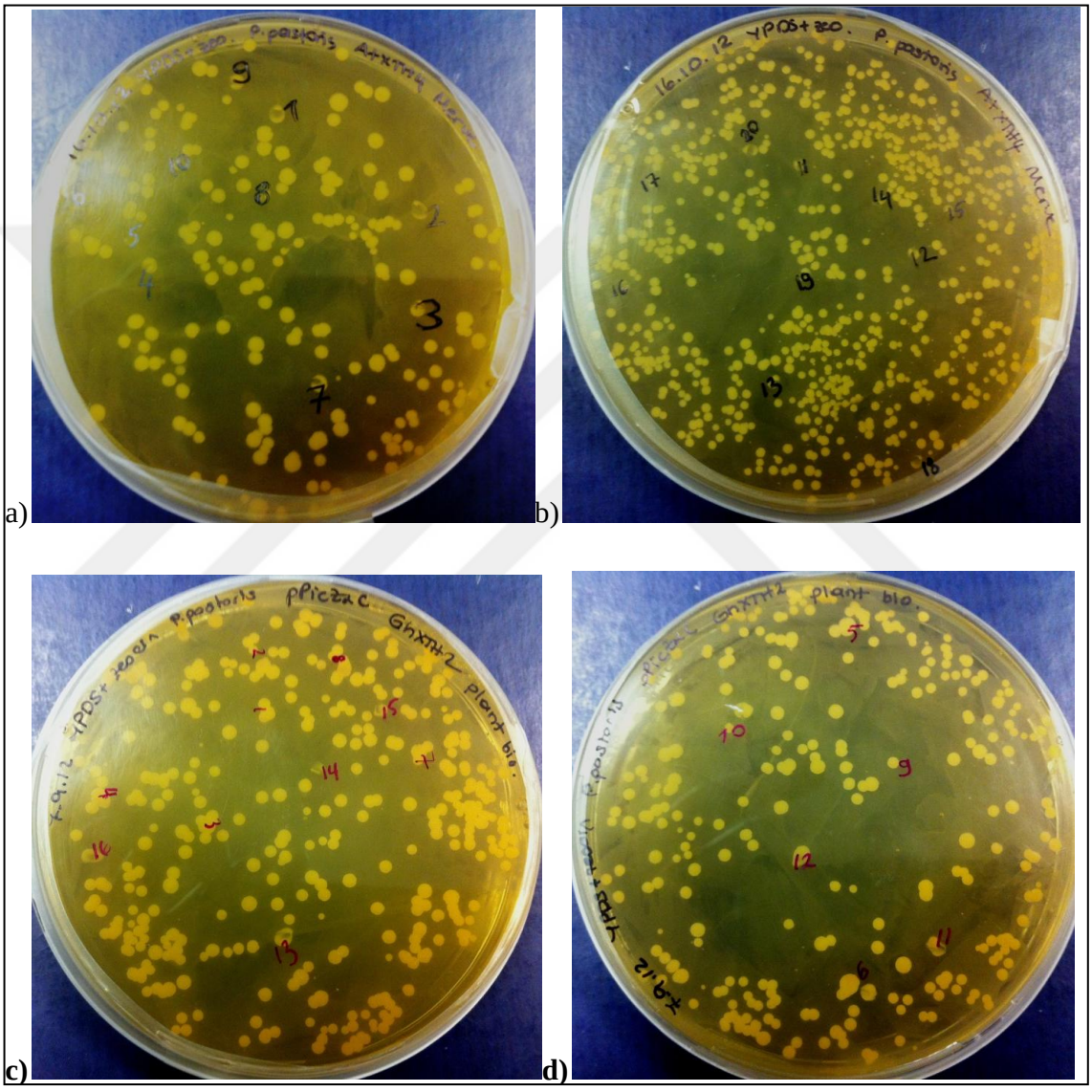

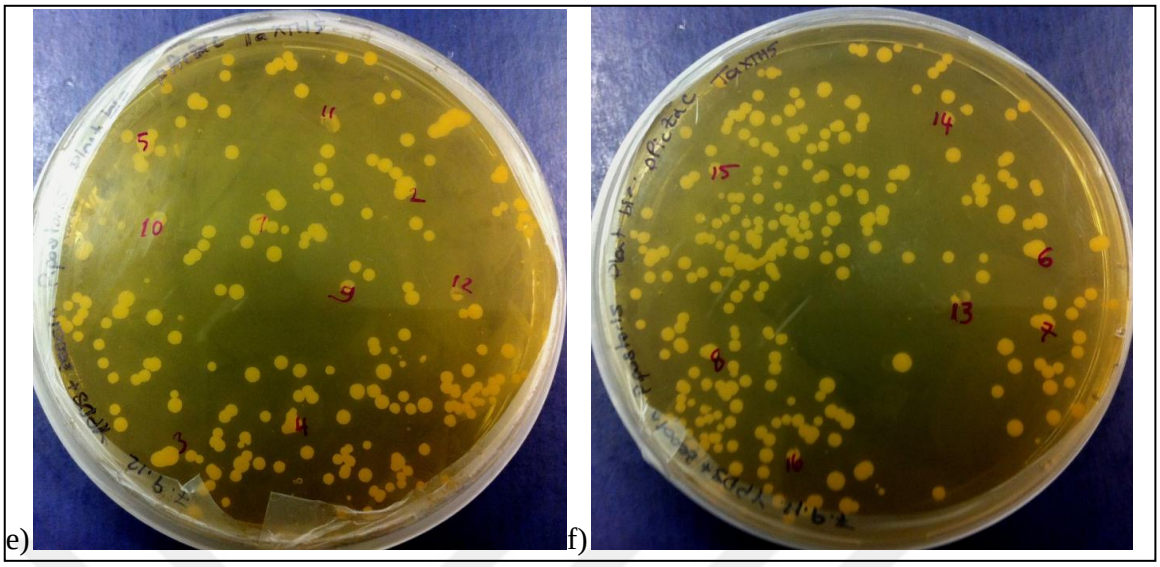

Figure 4.2. *P. pastoris* transformant selection on YPDSagar + zeocin plates, a and b) *AtXTH4* transformants, c and d) *GhXTH2* transformants, e and f)*TaXTH5* transformants.

Table 4.5. Number of transformants screened per gene.

Name of the gene	**Number of transformants screened**
AtXTH3	40
AtXTH4	22
AtXTH11	21
BdXTH2	22
GhXTH2	16
OsXTH30	40
PtXTH3	12
TaXTH5	49

As a background control, empty pPicZα-C was also linearized by DraI restriction enzyme and transformed into competent *P. pastoris* cells. Transformant cells were selected on YPDSagar + zeocin (100 ug/ml) plates (Figure 4.3). Three different transformants were selected for gene expression induction and analysis of induction products.

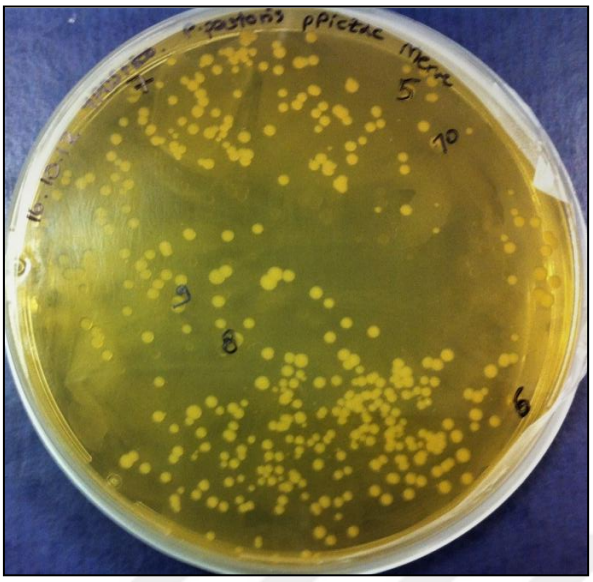

Figure 4.3. Linearized pPicZα-C transformant selection on YPDS agar + zeocin plates.

4.4. LINEARIZED PPICZA-C TRANSFORMANT COLONY SCREENING

Methanol induction of transformant *P. pastoris* cells result in expression of gene after *AOXI* promoter on the pPicZα-C plasmid, thus results in production of protein product. Without any insert after the promoter, it is not expected to observe production of any protein product with a 6X-his tag. By screening three different linearized pPicZα-C transformants, it was aimed to control if there is any background protein being expressed and produced by *P. pastoris* that is 6X-his tagged and interfere with affinity purification.. It was also aimed to verify *P. pastoris* transformation protocol by performing a colony PCR and analysing the result for integrity of linearized plasmid in transformant cells' chromosome.

Transformant colonies were firstly grown in 10 mL BMGY media at 30°C with 200 rpm shaking for 20-22 hours until OD_{600} value reaches 2.0-6.0. Then cells were used to start 10 mL BMMY induction culture with an OD_{600} value of 1.0. Gene expression was carried by 1 per cent v/v methanol addition every 24 hours for 5 days. At the end of day 5, cells were separated from supernatant by centrifugation. Proteins in supernatants of samples were precipitated and concentrated via TCA & acetone precipitation method and they were

analysed by SDS-PAGE and Western blotting. Induced cells were used in colony PCR studies by *5′ AOXI* and *3′ AOXI* primers (Figure 4.4, Figure 4.5).

Colony PCR results revealed a band sized 500-700 bp per colony. It is known that *5′ AOXI* priming site and *3′ AOXI* priming site are dissociated from each other on vector and the gap in between them is 593 bp. Obtained colony PCR results are proving that integration of expression vector into host genome via homologous recombination is successful because colony PCR results in bands at 593 bp (Figure 4.5).

Since analysed *P. pastoris pPicZα-C* transformants lack an insert, it is not expected to see any protein band from supernatants at same size with plant XETs or any positive Western Blotting bands. SDS-PAGE studies revealed only a visible protein bands >40 kDa, yet no protein band inbetween 35-40 kDa sizes and no positive results in Western blotting analysis (Figure 4.4). These findings confirm that *P. pastoris* host doesn't contain any protein at same size with XETs or with 6X-His tag. Thus, both host organism and expression vector system are safe and suitable for heterologous expression of different plant XETs.

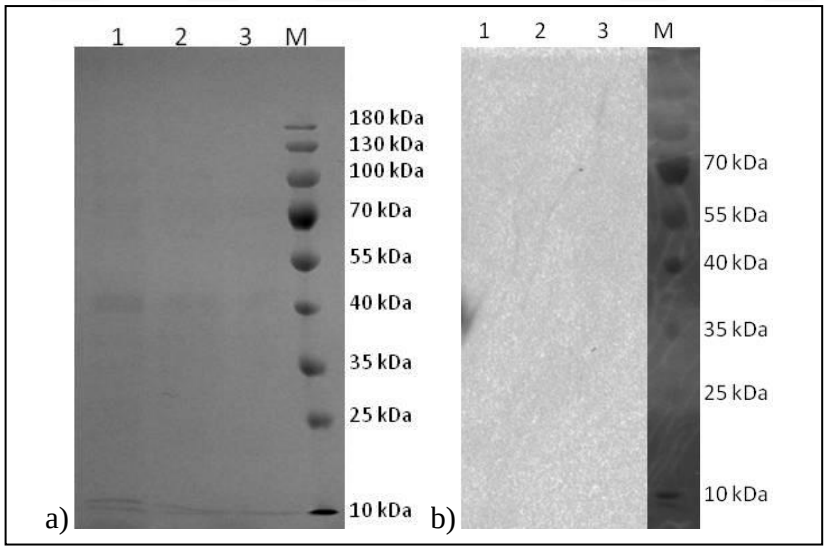

Figure 4.4. Protein analysis of *P. pastoris pPicZα-C* transformants. a) SDS- PAGE Coomassie blue staining, b)SDS-PAGE Western blotting with ant, 6X-His antibody. Transformant colony names and protein marker band sizes are given in the figure.

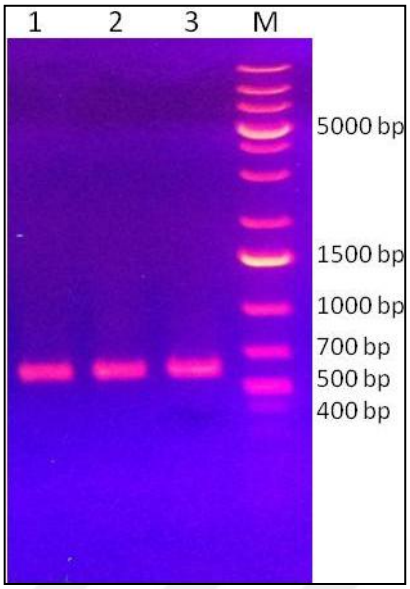

Figure 4.5. Colony PCR results of *P. pastoris pPicZα-C* transformants. *5' AOXI* and *3' AOXI* primers were used. Transformant colony names and DNA ladder band sizes are given in the figure.

4.5. POSITIVE EXPRESSION COLONY SCREENING

4.5.1. AtXTH3

Transformation of linearized pPicZα-C/*AtXTH3* into *P. pastoris* via electroporation yield more than 100 transformant colonies based on zeocin resistance selection on YPDS agar + zeocin (100 µg/ml) plates. 40 transformant colonies were selected and restreaked on YPDS agar + zeocin (100 µg/ml) plates for a second confirmation of transformation event. After single colonies appeared on plates, they were used to imbibe 10 mL BMMY cultures for colony screening. Transformant colonies were induced in BMMY media for 3 days, with 1 per cent v/v methanol addition every 24 hours. At the end of induction period, supernatant were screened by activity analysis, SDS-PAGE and Western blotting for presence of heterologoulsy produced 6X-His tagged AtXTH3. Firstly, all the colonies were screened for XET activity of AtXTH3 enzyme by TXG-XGO activity analysis. Hybrid products were analysed via HPLC. 18 *AtXTH3* transformant colonies were chosen based on their XET activity HPLC results. Proteins within supernatants of chosen samples were

precipitated by TCA & acetone precipitation and separated by SDS-PAGE. Gels with samples were stained by coomassie blue staining in order to visualize protein content and treated by anti 6X-His tagged antibody in Western blotting in order to detect heterologously produced protein (Figure 4.6).

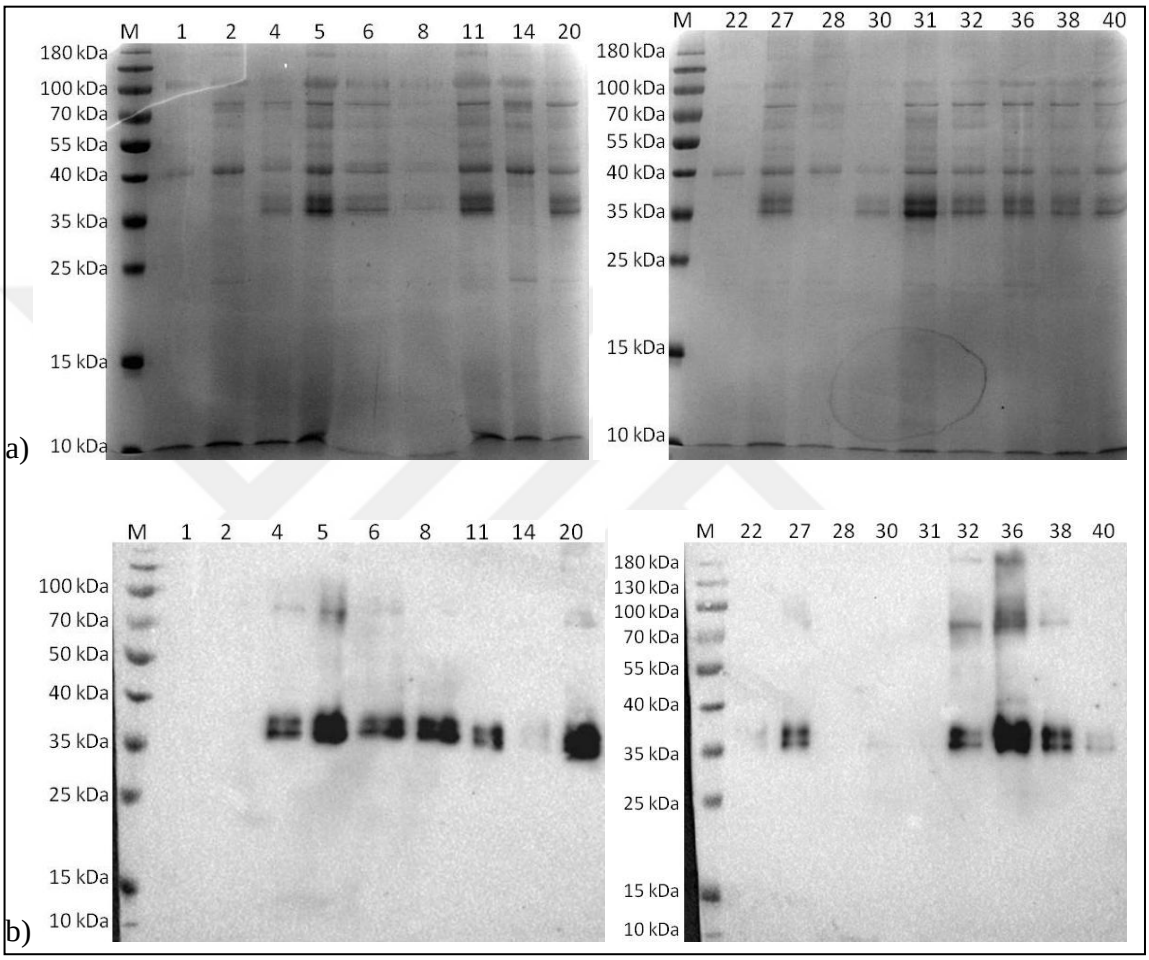

Figure 4.6. SDS-PAGE Western blotting analysis of *AtXTH3* transformant induced *P. pastoris* cells. a) SDS-PAGE analysis coomassie brilliant blue stained gels of chosen transformant colonies, b) SDS-PAGE Western Blotting with anti 6X-His tagged antibody of chosen transformant colonies. M; protein size marker. Colony numbers are indicated on the figure.

Colony 36 was the colony with highest XET activity on TXG-XGO donor-acceptor couple. This colony gave a positive strong band at Western blotting analysis. Double band observed at SDS-PAGE coomassie blue stained gels and Western blotting membranes are

due to glycosylated and non-glycosylated isomers of produced AtXTH3. Colony 36 with highest XET activity and detected 6X-His tag was chosen for large scale production of AtXTH3 protein.

4.5.2. AtXTH4

More than 50 transformant colonies were obtained for *AtXTH4* gene and 10 of those transformant colonies were restreaked on YPDS agar + zeocin (100µg/ml) plates for an additional antibiotic selection. Colonies were grown at 30°C for 5 days and a single colony per transformant was used to start 10 mL BMGY culture. The BMGY cultures were grown at 30°C 200 rpm for 20 hours. Their cell densities were measured using spectrophotometer at 600 nm wavelength. Cells were diluted to OD_{600} value of 1.0 in 10 mL BMMY media and induced by methanol for *AtXTH4* gene expression for 5 days at 22°C 160 rpm. When induction was finalized, cells were pelleted and 900 µL of supernatant was used in TCA & acetone protein precipitation. Supernatant samples were loaded on polyacrylamide gel for SDS-PAGE and Western blotting analysis (Figure 4.7). Transformant cells were also used in colony PCR studies with *5' AOXI* and *3' AOXI* primers (Figure 4.8). Codon optimized *AtXTH4* sequence and sequence from plasmid between primer binding sites result in PCR bands of 1132 bp in length. Except colony 2, all 9 colonies out of 10 screened transformant colonies, gave a PCR band at expected size. They all have insert integrated into their genome. Absence of a band sized 304 bp (in case of no insertion) or a band sized 1132 bp (in case of insertion) can be due to lack of template DNA is PCR mix. Brightness of PCR bands can be related to number of insert copies in the genomes of transformants (Figure 4.8).

Transformant colonies except colony 9 gave a strong Western blotting signal and this can relate to produced protein amount. Theoretical molecular weight of AtXTH4 is 34.9 kDa, yet post-translational glycosylation of protein will add to molecular size, resulting in protein bands to appear between 35-40 kDa size marker bands. All samples seem to have a contaminant between 10-25 kDa, this can be due to degradation of heterologously produced AtXTH4 protein. Colony 7 was the colony with a strong Western signal and less amount of contaminant degraded protein, thus this colony was chosen for initial large scale production.

When initial production trial was unsuccessful colony 6 was used for induction study.

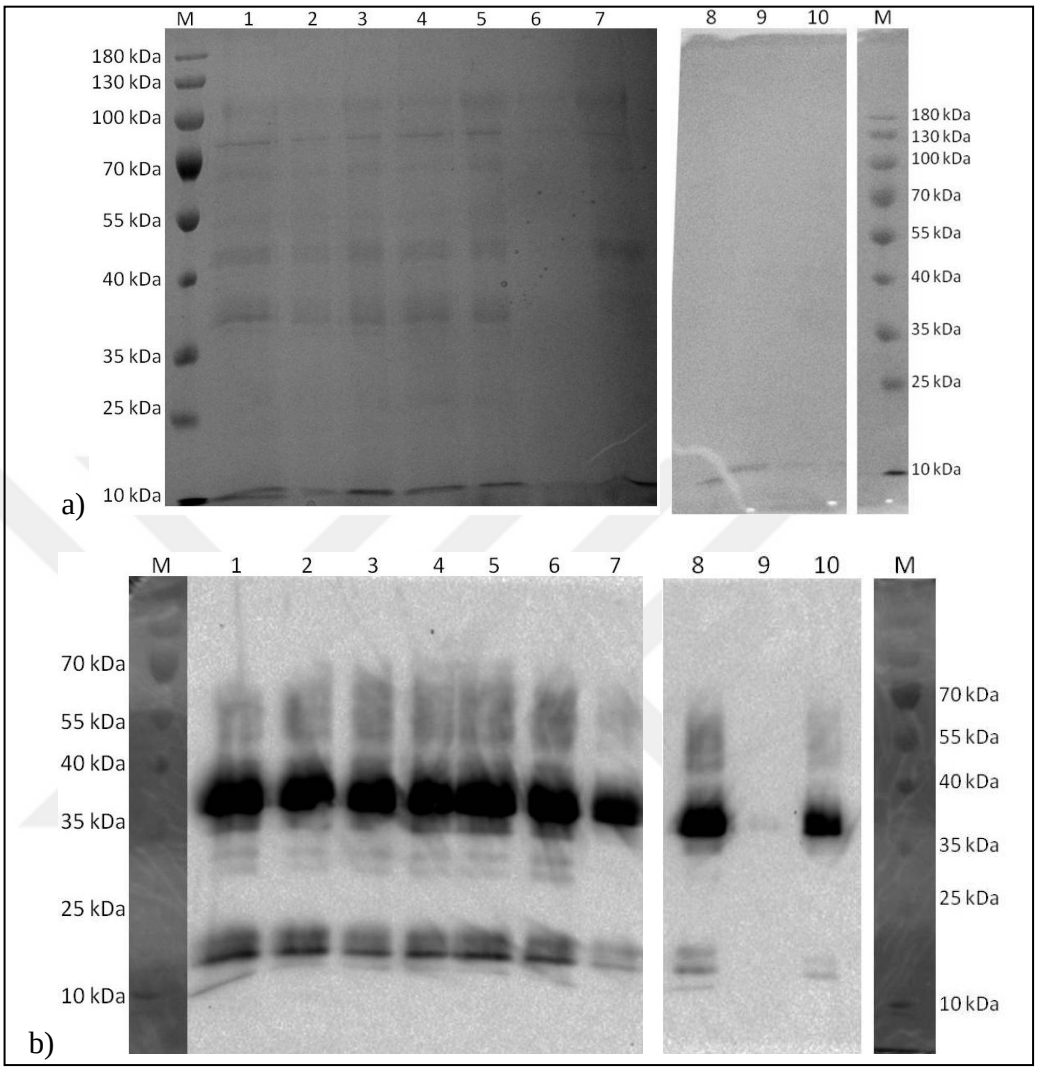

Figure 4.7. Protein analysis of *P. pastoris AtXTH4* colonies. a) Coomassie brilliant blue stained SDS-PAGE gels of colonies 1-10, b)SDS-PAGE Western blotting of colonies 1-10 with anti 6X-His tagged antibody. M; protein size marker, colony numbers are indicated on figure.

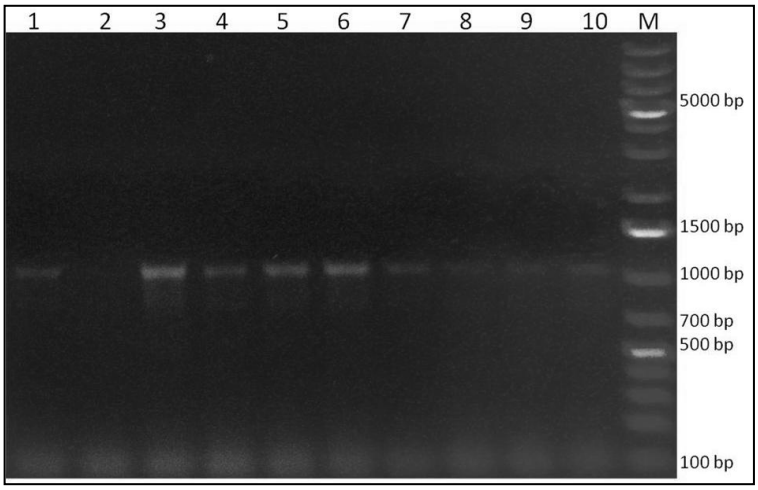

Figure 4.8. PCR results of *P. pastoris AtXTH4* transformants. *5' AOXI* and *3' AOXI* primers were used. Transformant colony names and DNA ladder band sizes are given in the figure.

Initial AtXTH4 production trials were unsuccessful, thus a new transformation with linearized plasmids were done and 12 new colonies were screened for protein synthesis via SDS-PAGE and Western blotting. Transformants were induced in 10 mL BMMY media by 1 per cent v/v methanol addition for 5 days and supernatant was analysed after TCA & acetone precipitation (Figure 4.9). Colonies were also screened for XET activity using TXG-XGO donor acceptor couple and colony 18 showed the highest activity. Colony 18 was the one with the highest activity however, Western band of colony 18 was one of the two low intensity bands. Yet, AtXTH4-18 was still used for large scale production. Also, a new large scale production trial was carried using AtXTH4-9 colony from first transformation event.

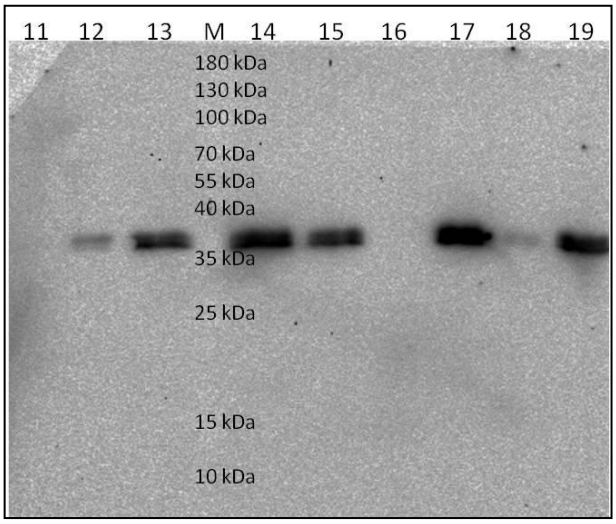

Figure 4.9. SDS-PAGE and Western blotting trials of new *AtXTH4* transformants. Colony numbers and protein size marker bands are shown in the figure.

Two final colonies used for large scale production, colonies 9 and 18, were used in colony PCR with *α-factor* and *3'AOXI* primer couple. PCR product sizes of both colonies were as expected, they both result in PCR bands at 1132 bp (Figure 4.10).

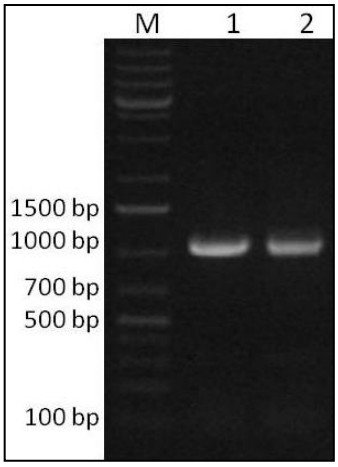

Figure 4.10. Agarose gel image result of colony PCR of AtXTH4-9 and AtXTH4-18 colonies using *α-factor* and *3'AOXI* primer couple. M; DNA size marker, 1;colony AtXTH4-9 as template, 2;colony AtXTH4-18 as template.

4.5.3. AtXTH11

DEIDFEFLG site is known to be very important for enzymatic activity. As a member of Ancestral clade, AtXTH11 enzyme has different amino acids in the active site found in all other XTH enzymes reported so far (Figure 4.11). Thus AtXTH11 was expected to show no XET activity. In order to test this hypothesis, firstly codon optimized AtXTH11 in pPicZα-C expression vector was obtained from GenScript company. Vector with the gene of interest was transformed into *E. coli* cells. Isolated plasmid, in large amount, was linearized using DraI restriction endonuclease and then transformed into competent *P. pastoris* cells via electroporation. More than 30 transformant colonies were obtained and 24 of them were restreaked on agar plates for a second round of antibiotic selection. At the end of incubation period of 3-4 days, single colonies for 21 colonies were obtained and they were used to imbibe 10 ml of BMGY culture. Transformant yeast cells were grown in BMGY for ~18-20 hours and after OD600 measurements, they were used to start 10 ml of BMMY culture with a starting OD600 value of 1.

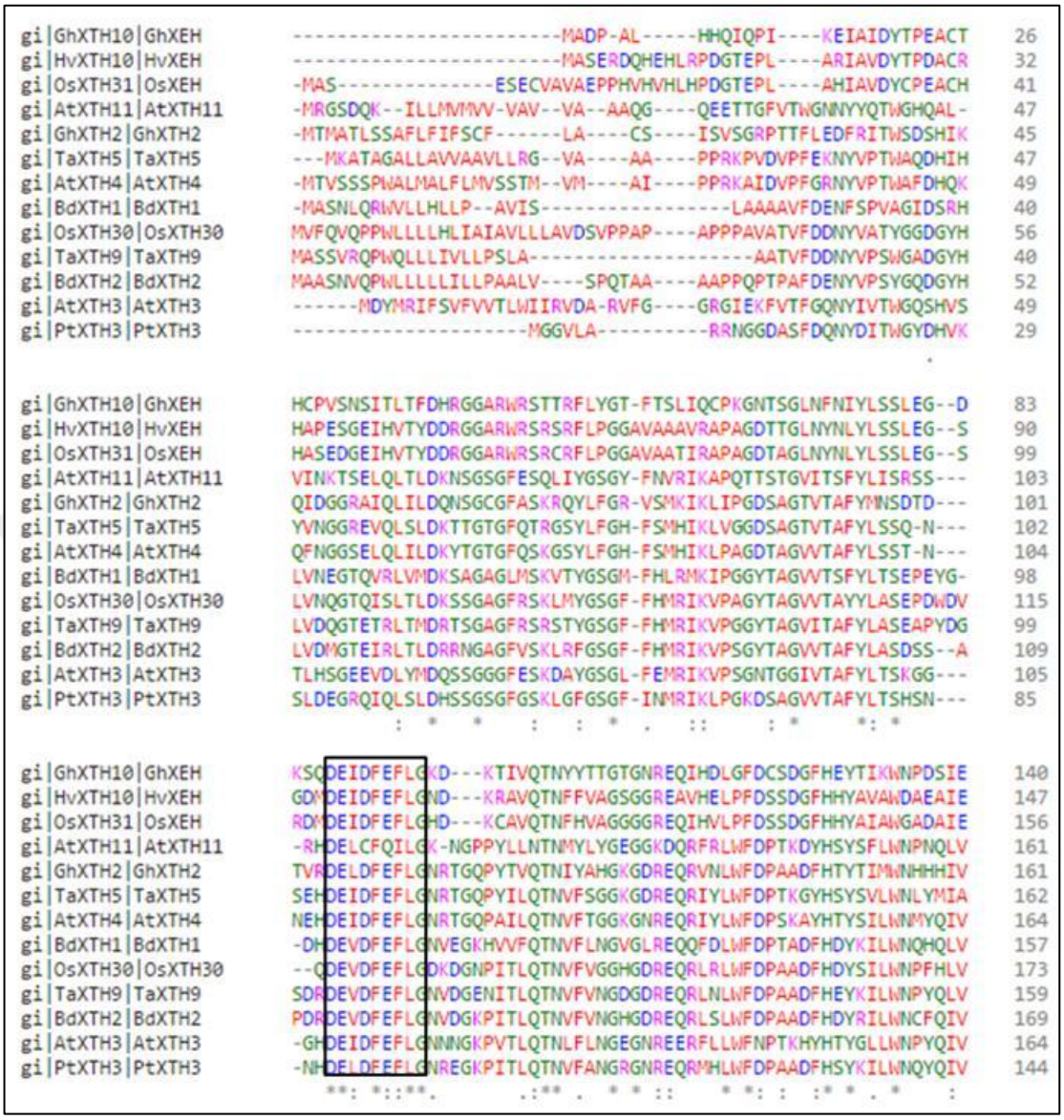
gi|GhXTH10|GhXEH
gi|HvXTH10|HvXEH
gi|OsXTH31|OsXEH
gi|AtXTH11|AtXTH11
gi|GhXTH2|GhXTH2
gi|TaXTH5|TaXTH5
gi|AtXTH4|AtXTH4
gi|BdXTH1|BdXTH1
gi|OsXTH30|OsXTH30
gi|TaXTH9|TaXTH9
gi|BdXTH2|BdXTH2
gi|AtXTH3|AtXTH3
gi|PtXTH3|PtXTH3

Figure 4.11. Alignment of various XTH proteins. Black rectangle indicates the active site.

At the end of total 5 days of methanol induction period, cells were separated from media by centrifugation and supernatant was used for tests. Part of the supernatant was used for SDS-PAGE studies. For this purpose, proteins in the supernatant were precipitated using TCA & acetone precipitation method and then loaded onto 12 per cent polyacrylamide gels. Gels were stained by coomassie brilliant blue staining solution after SDS-PAGE to visualize proteins in the expression environment at the end of expression period (Figure 4.12). Theoretical molecular weight of AtXTH11 enzyme without signal peptide and with

6X-His tag is 32.29 kDa. Protein bands seen on coomassie stained gels (Figure 4.12) were much larger in size, starting from ~55-70 kDa. This is highly likely to be due to N-linked glycosylation of synthesized protein or the smear seen on gels can be other proteins from supernatant and the amount of target protein's amount can be lower than coomassie stain's detection range. Thus, Western blotting studies with anti 6X-His tag antibody was also performed to detect target heterologously expressed 6X-His tagged protein (Figure 4.13). Colonies except 12, 18, 19 and 21 have positive results from Western blotting trials. These results suggest that 17/21 colonies synthesized 6X-His tagged AtXTH11 successfully.

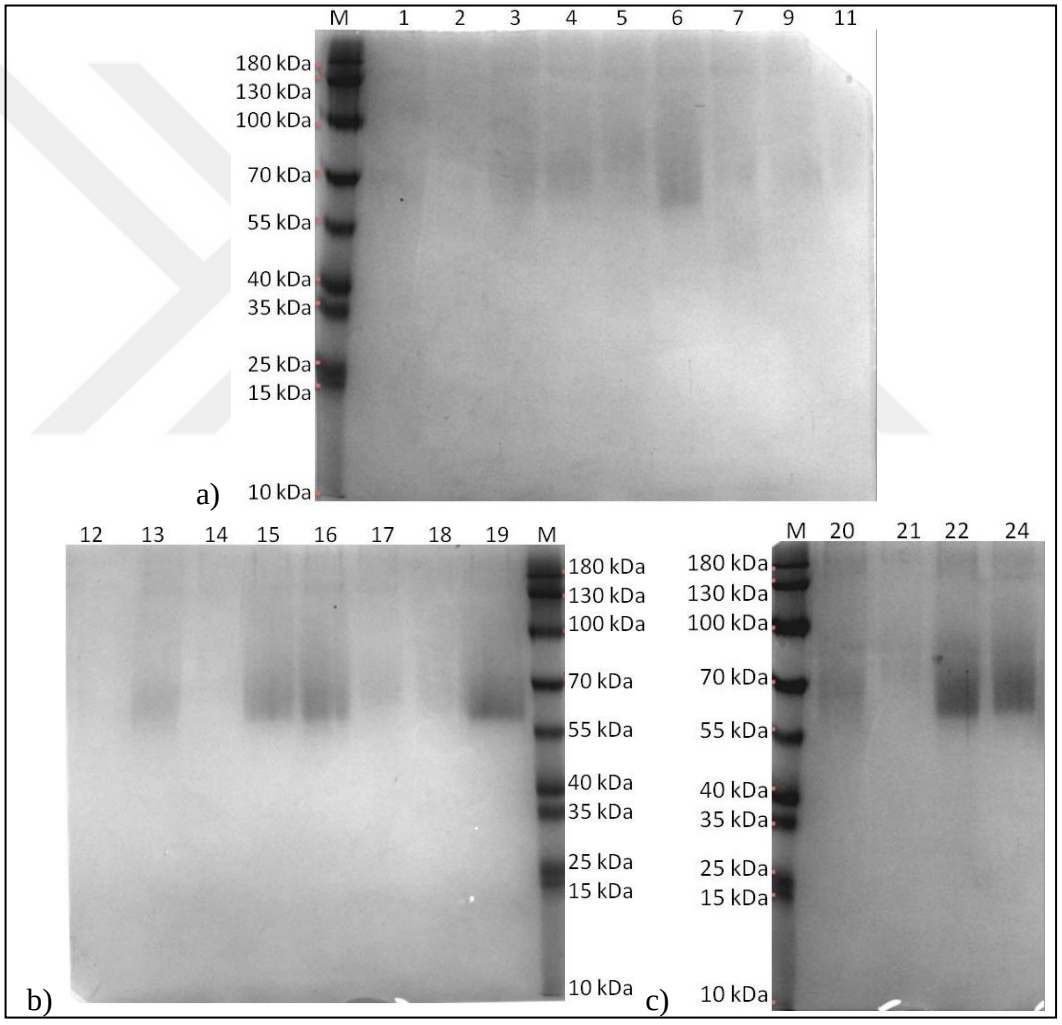

Figure 4.12. SDS-PAGE analysis of different transformant colonies expressing AtXTH11. Molecular size marker bands are indicated on the figures. Colony numbers are indicated on the figures. Gels were stained with silver nitrate.

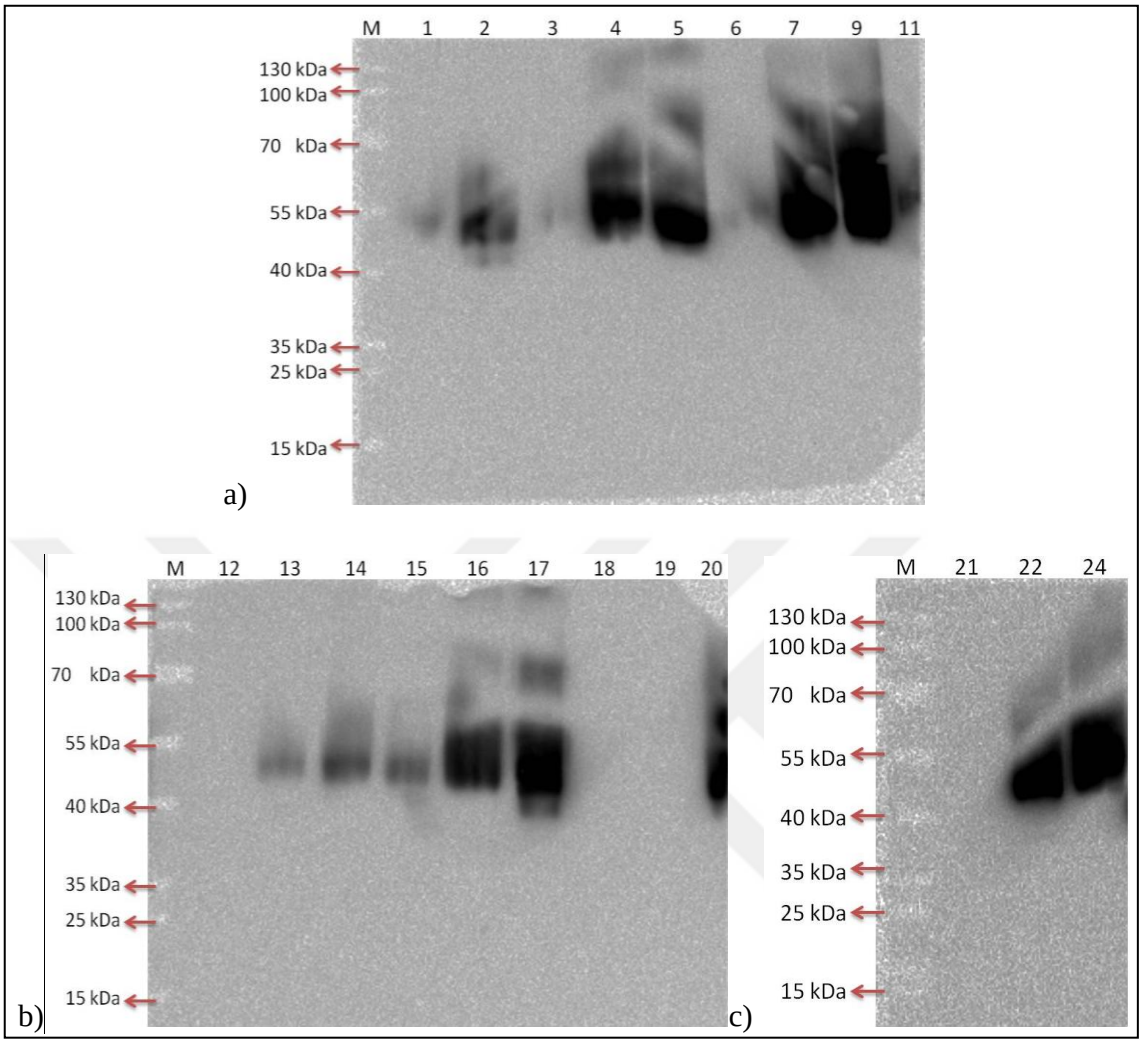

Figure 4.13. Western Blotting analysis of different transformant colonies expressing AtXTH11. Molecular size marker bands are indicated on the figures. Colony numbers are indicated on the figures. Gels were stained with silver nitrate.

After proving the presence of heterologously expressed protein, TXG-XGO and BBG-XGO enzyme activity tests was carried in order to see whether heterologously expressed and produced AtXTH11 enzyme possess any XET activity. Reactions were analysed using Waters UPLC system with fluorescence detector after 24 hours of incubation (Figure 4.14). As expected, no endotransglycosylase activity was seen. There was no change in the height or the area of the donor peak.

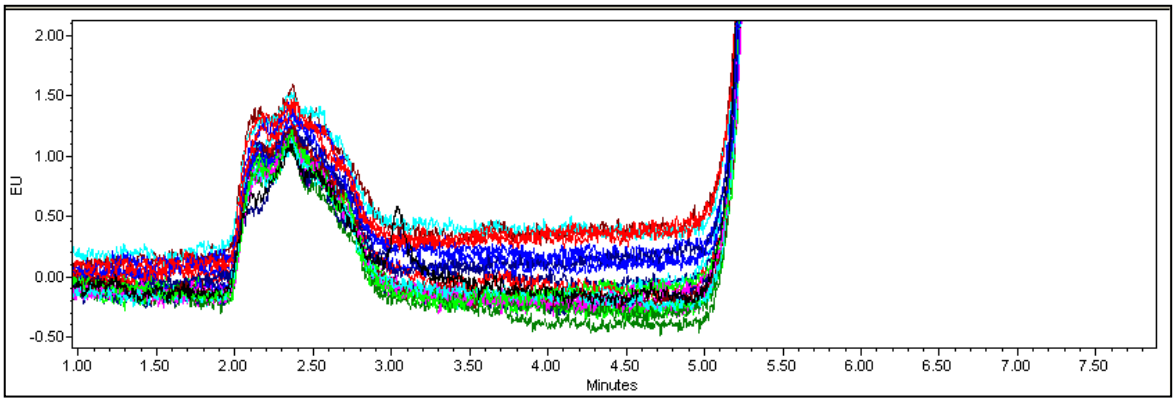

Figure 4.14. Chromatogram of AtXTH11 TXG-XGO enzyme activity results run on Waters UPLC system. Black line is TXG-XGO standard. Coloured lines indicate different samples.

4.5.4. BdXTH2

Codon optimized *BdXTH2* gene was transformed into *P. pastoris* yeast within pPicZα-C expression vector by electroporation. Transformant colonies were selected onYPDS agar + zeocin (100 µg/ml) plates. More than 50 transformant colonies were observed and 22 of them were restreaked on YPDS agar + zeocin (100 µg/ml) plates for confirmation of selection. Single colonies of all 22 transformants were screened for protein production by methanol induction. Colonies were induced in BMMY media for 5 days with 1 per cent v/v methanol addition every 24 hours. At the end of induction period, cells were separated by centrifugation and used for colony PCR for controlling integrity of *BdXTH2* in transformant cells' genome using α-factor 5' and *AOXI* 3' primers. Results were loaded on an agarose gel, separated and DNA fragments were visualized (Figure 4.15). Expected PCR product size is 1120 bp, consisting of 816 bp *BdXTH2* fragment and 304 bp of plasmid. Colonies 1, 2, 3, 5, 6, 7, 8, 9, 10, 11, 12, 13, 14 have a PCR band at expected size, meaning they are the transformants with *BdXTH2* insert.

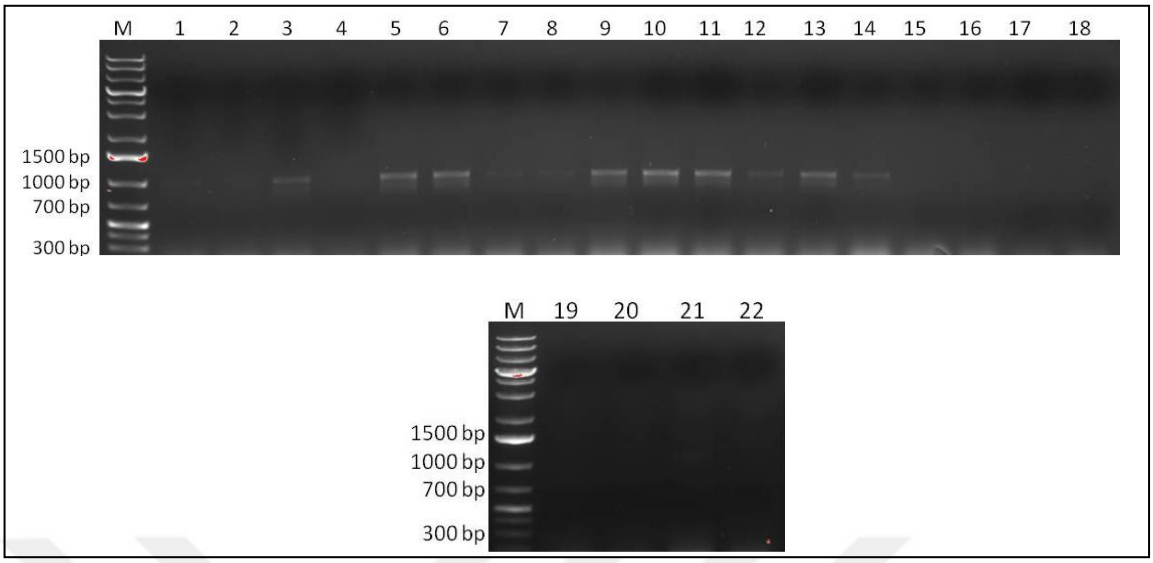

Figure 4.15. Colony PCR results of *BdXTH2* transformant induced *P. pastoris* cells using α-factor 5' and *AOXI* 3' primers analysed by agarose gel electrophoresis. M; DNA size marker. Colony numbers are indicated on figure.

Supernatants were analysed for the presence of 6X-his tagged heterologously produced BdXTH2 protein by activity test with TXG-XGO donor-acceptor couple. Hybrid TXG-XGO product amounts were measured by HPLC system and 9 colonies with and without activity (including the colony with highest XET activity on TXG-XGO) were chosen for SDS-PAGE and Western Blotting analysis.

Proteins in supernatant samples from small scale productions were precipitated by TCA & acetone precipitation. Then, they were separated by SDS-PAGE method. Separated proteins were both visualized by coomassie blue staining and Western blotting (Figure 4.16).

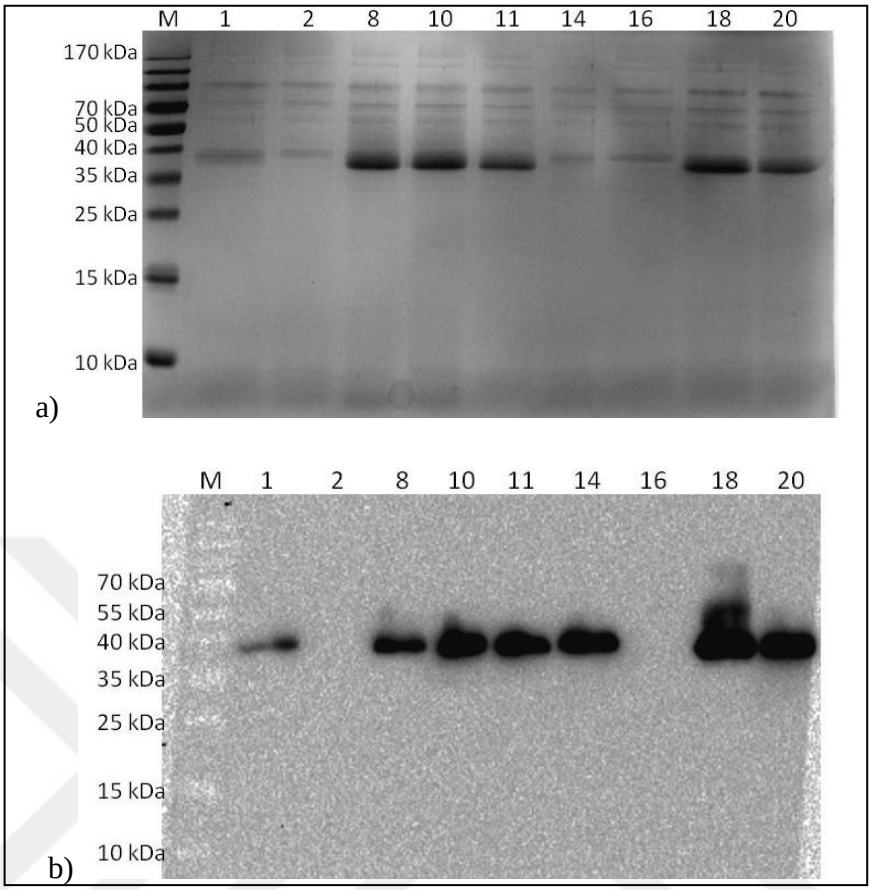

Figure 4.16. SDS-PAGE and Western Blotting analysis of selected *BdXTH2* transformant colonies. a) SDS-PAGE coomassie brilliant blue stained gel image, b) SDS-PAGE Western blotting result using anti 6X-His tag antibody. M; protein size marker, colony number are indicated on the figure.

Colonies except 2 and 16 gave a positive Western blotting band. Colony 14 amongst all colonies tested by activity test was the one showing highest XET activity on TXG-XGO. This colony also gave excepted band in colony PCR study, thus BdXTH21-14 colony was chosen for large scale BdXTH2 production.

4.5.5. GhXTH2

pPicZα-C/GhXTH2 expression construct was transformed into *P. pastoris* and more than 50 transformants were obtained. 16 of these transformants were restreaked on YPDS agar

+ zeocin plates for antibiotic reselection. Firstly transformants were screened for the presence of *GhXTH2* gene in their genome via colony PCR using *α-factor* and 3'*AOXI* primers. PCR results were analysed by agarose gel electrophoresis (Figure 4.17). *GhXTH2* insert length is 828 bp and additional 304 bp is added to PCR products due to primer binding sites on construct, thus resulting in 1132 bp expected PCR product size.Colonies except 14 gave expected positive result in colony PCR.

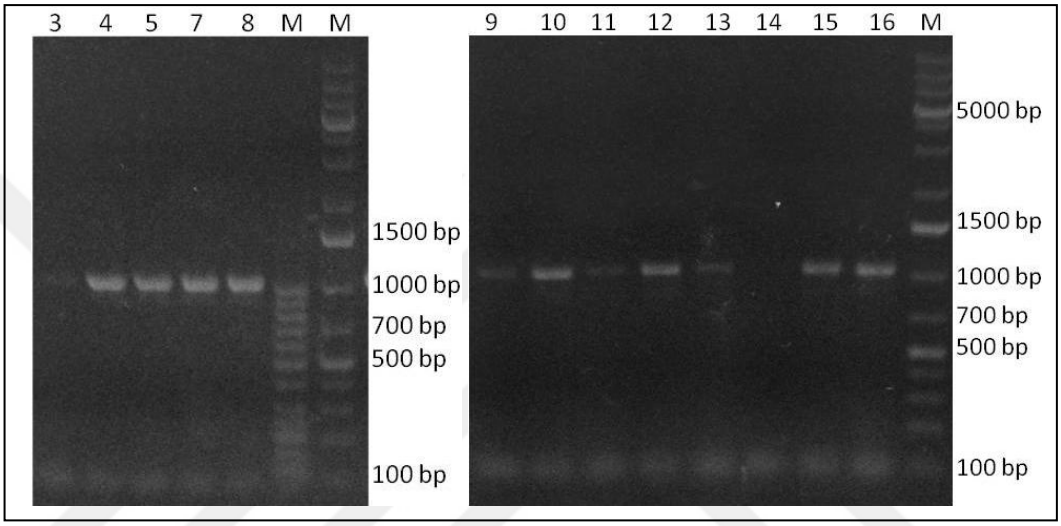

Figure 4.17. Colony PCR results of *GhXTH2* transformant induced *P. pastoris* cells using α-factor 5' and *AOXI* 3' primers analysed by agarose gel electrophoresis. M; DNA size marker. Colony numbers are indicated on figure.

All the restreaked colonies were incubated and induced in 10 mL BMMY media for 5 days, with 1 per cent v/v methanol addition every 24 hours. At the end of induction period, cells were separated from induction environment via centrifugation and supernatant was screened for presence of synthesized GhXTH2 by SDS-PAGE coomassie blue staining and Western Blotting (Figure 4.18).

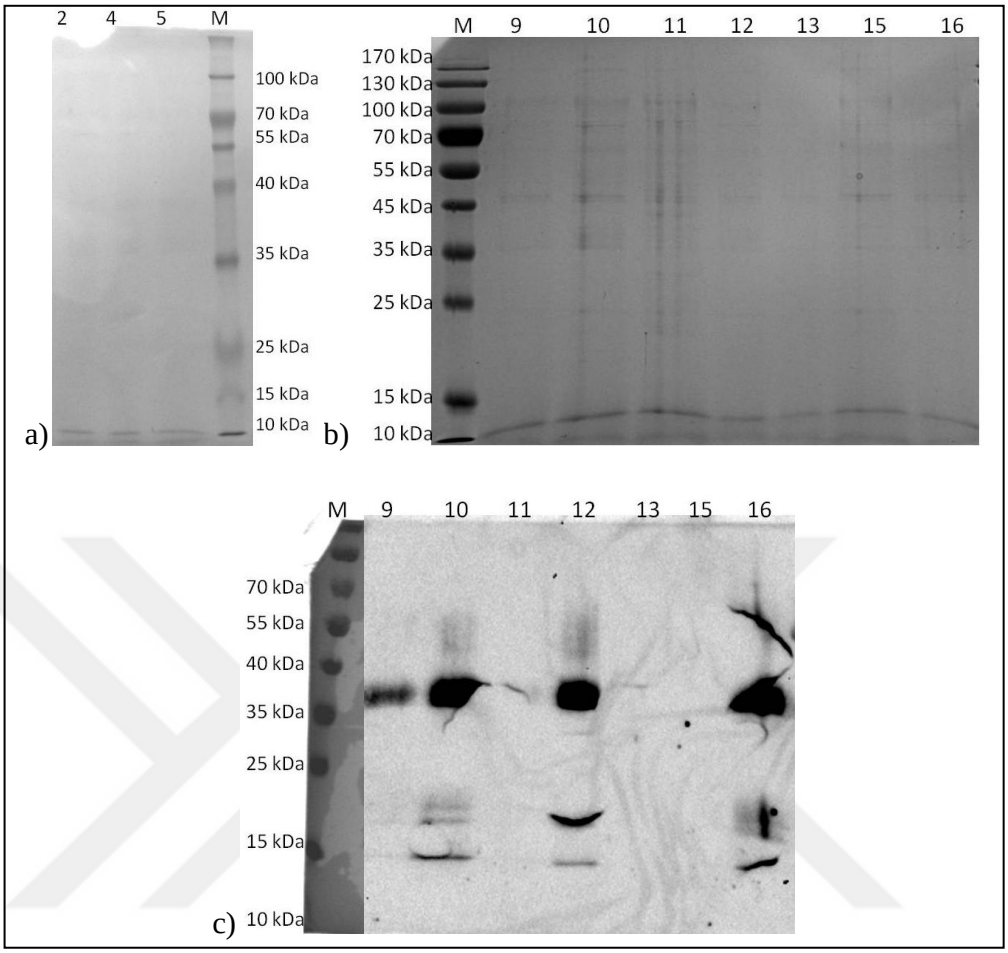

Figure 4.18. SDS-PAGE and Western Blotting analysis of selected *GhXTH2* transformant colonies. a) SDS-PAGE coomassie brilliant blue stained gel image of colonies 2, 4 and 5, b) SDS-PAGE coomassie brilliant blue stained gel image of colonies 9-16, c) SDS-PAGE Western blotting result using anti 6X-His tag antibody. M; protein size marker, colony number are indicated on the figure.

Colonies 9, 10, 12 and 16 synthesize 6X-His tagged GhXTH2 enzyme however no other colony gave positive result in Western blotting analysis. Out of these 4 colonies, when tested with TXG-XGO donor-acceptor, GhXTH2-10 colony produced the most GhXTH2 protein, thus GhXTH2-10 colony was chosen for large scale production.

4.5.6. PtXTH3

Codon optimized *PtXTH3* coding sequence within pPicZα-C expression vector was electroporated into competent *P. pastoris* cells and transformant yeast cells were selected on YPDS agar + zeocin (100 µg/ml) plates. More than 50 transformants were obtained and 12 transformant colonies were restreaked on YPDS agar + zeocin (100 µg/ml) plates for confirmation of antibiotic selection. These 12 colonies were confirmed for transformation event and they were screened for functional PtXTH3 protein synthesis. Transformant colonies were induced in BMMY media in small scale for 5 days by 1 per cent v/v methanol addition every 24 hours. At the end of induction period, cells were centrifuged and supernatants were analysed for presence of 6X-His tagged PtXTH3 and active PtXTH3 enzyme. TCA & acetone precipitation was utilized in order to precipitate and concentrate proteins in the induction media. After, samples were analysed by SDS-PAGE and Western blotting by anti 6X-His tag antibody. Gels and membranes were visualised (Figure 4.19) and it was seen that except colonies 2 and 10, all of them synthesized 6X-His tagged PtXTH3.

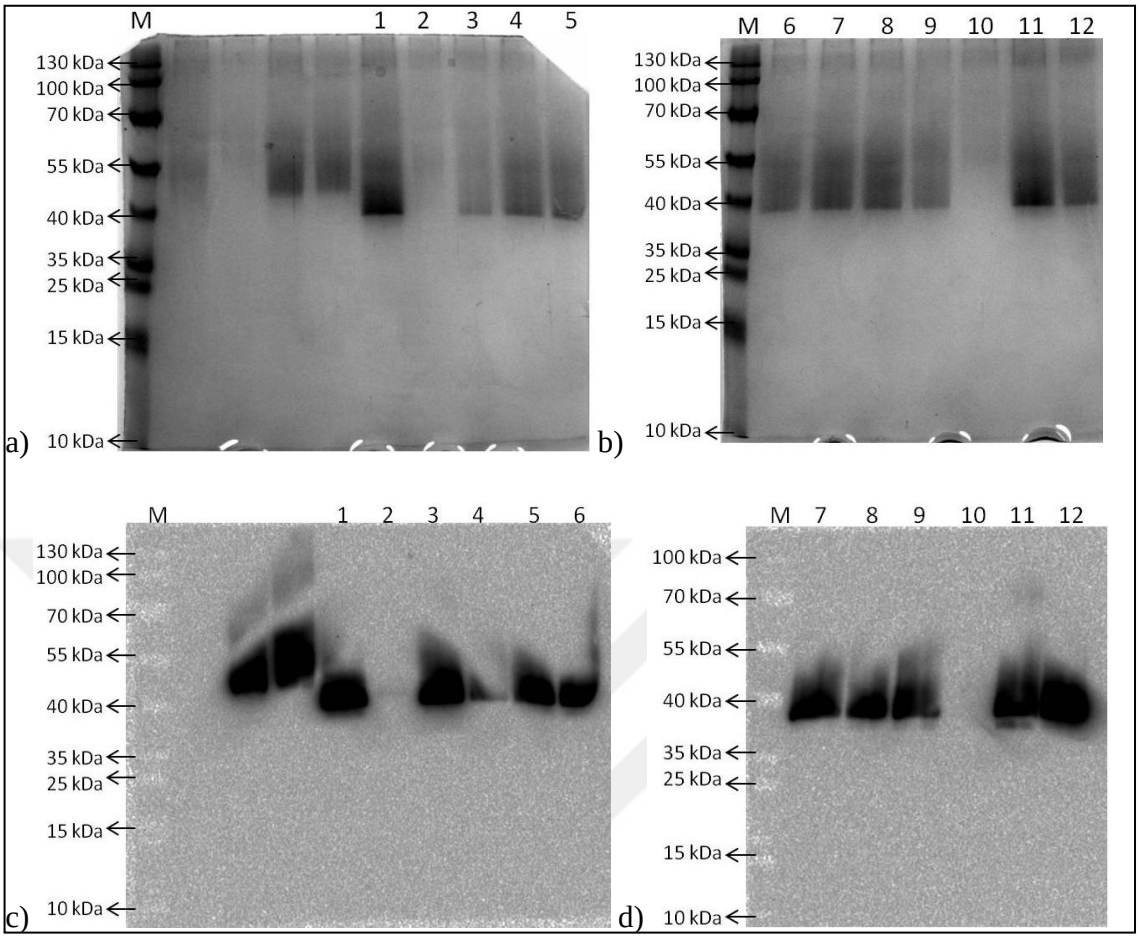

Figure 4.19. SDS-PAGE and Western Blotting analysis of selected *PtXTH3* transformant colonies. a) SDS-PAGE coomassie brilliant blue stained gel image of colonies 1-5, b) SDS-PAGE coomassie brilliant blue stained gel image of colonies 6-12, c) SDS-PAGE Western blotting result of colonies 1-6 using anti 6X-His tag antibody, d) SDS-PAGE Western blotting result of colonies 7-12 using anti 6X-His tag antibody. M; protein size marker, colony number are indicated on the figure.

Proving presence of heterologously synthesized PtXTH3 is not enough because folding of synthesized PtXTH3, thus activity of the enzyme can vary between colonies. Also amount of synthesized enzyme can differ depending on genomic insertion position and copy number, resulting in changing amounts of XET activity. With regards to these different points of views, all colonies were also screened for XET activity by enzyme activity test using TXG-XGO and BBG-XGO donor-acceptor couples. Hybrid TXG-XGO and BBG-XGO product amounts each colony produced were analysed by UPLC (Waters Acquity

UPLC) (Figure 4.20). All screened colonies showed higher activity on TXG-XGO substrate couple, by comparing hybrid product amounts.

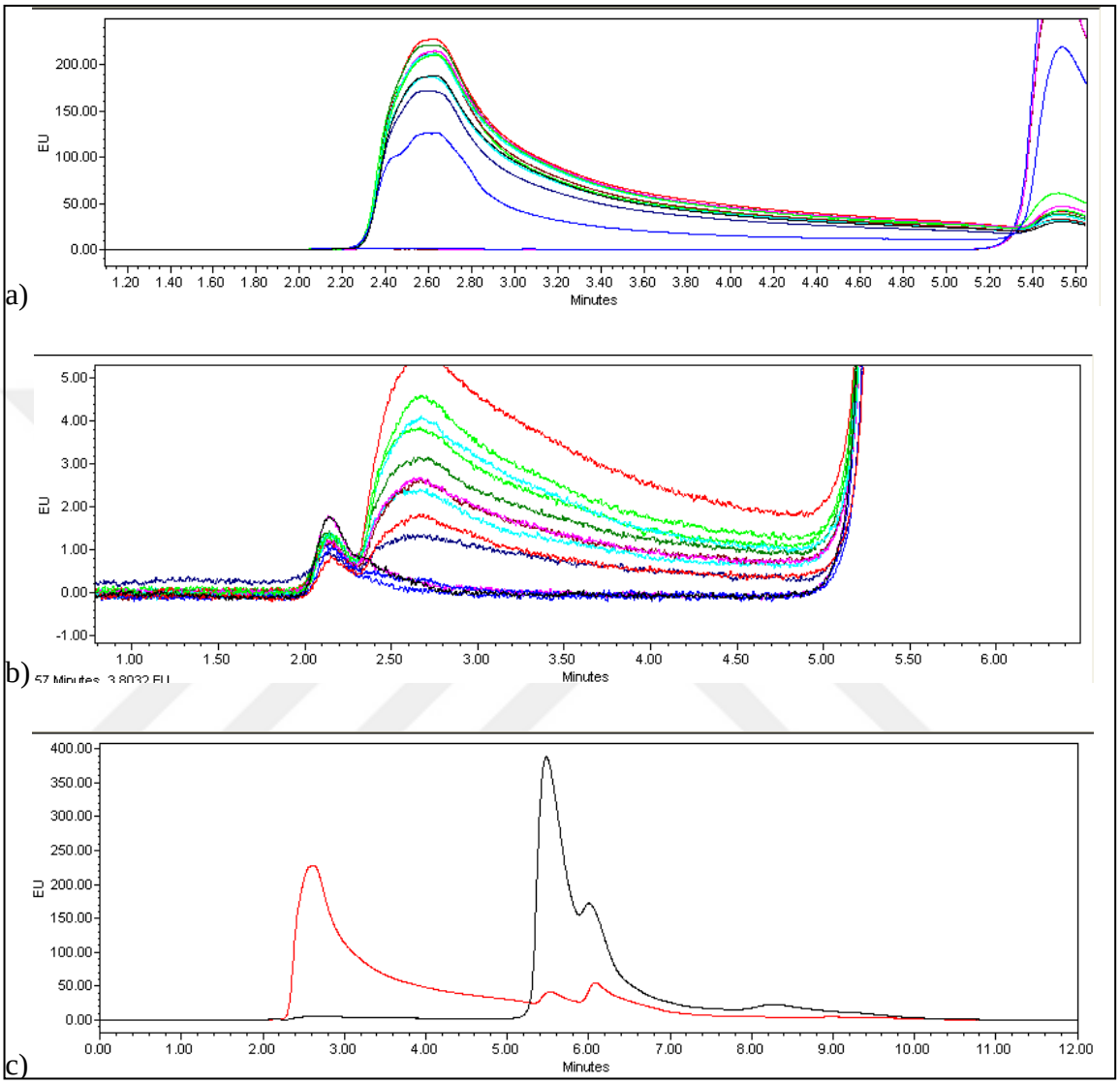

Figure 4.20. PtXTH3 active colony screening enzyme activity results. a) TXG-XGO enzyme activity results of different PtXTH3 transformant colonies, b) BBG-XGO enzyme activity results of different PtXTH3 transformant colonies, c) TXG-XGO and BBG-XGO enzyme activity result of colony number 9, red line is TXG-XGO activity result and black line is BBG-XGO activity result.

Within screened *PtXTH3* transformant colonies, colony number 9 showed highest XET activity on TXG-XGO compared to other transformant colonies, thus colony 9 was used in PtXTH3 protein production for characterization studies.

4.5.7. TaXTH5

pPicZα-C/*TaXTH5* transformation into *P. pastoris* resulted in more than 50 transformant colony. Firstly, 8 of these transformants were selected and restreaked on YPDS agar + zeocin (100µg/ml). A single colony of each transformant was grown in BMGY media, then yeast cells were transferred into BMMY media for TaXTH5 synthesis induction. They were incubated in BMMY media for 5 days, with 1 per cent v/v methanol addition every 24 hours. At the end of induction period cells were separated by centrifugation and supernatant was used for protein analysis. Proteins in media were precipitated by TCA & acetone precipitation and analysed by SDS-PAGE coomassie blue staining (Figure 4.21).

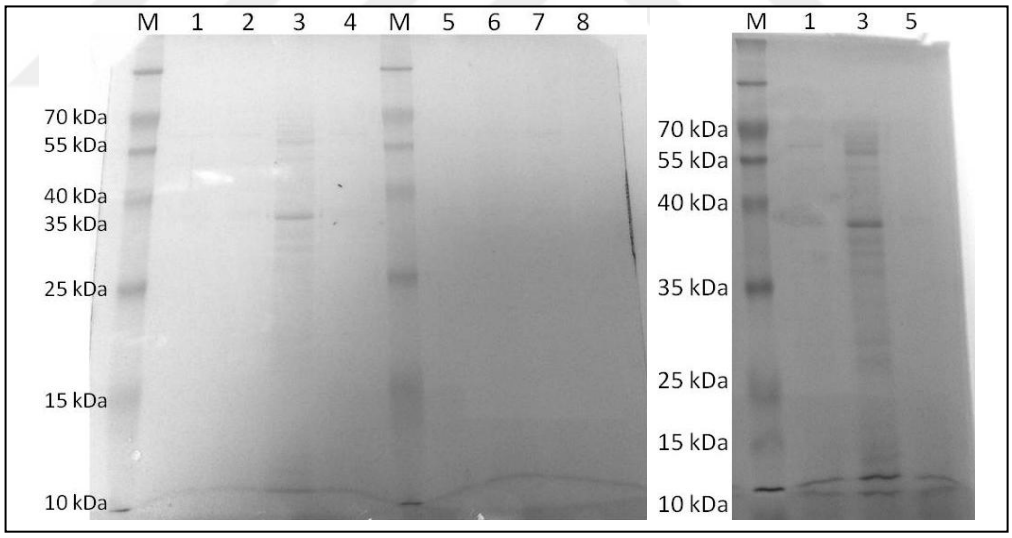

Figure 4.21. SDS-PAGE coomassie brilliant blue stained gel image of *TaXTH5* transformant colonies. M; protein size marker. Colony numbers are indicated on gel images.

Only colony 3 gave protein bands on SDS-PAGE analysis. In order to do a better screening for a colony with positive result, 8 more transformants were restreaked on YPDS agar +

zeocin plates and then induced for heterologous protein synthesis in BMMY media for 5 days, with 1 per cent v/v methanol addition every 24 hours. At the end of induction period, cells were separated by centrifugation. Supernatants were analysed for the presence of 6X-His tagged TaXTH5 by SDS-PAGE coomassie blue staining and Western blotting (Figure 4.22). Also, cells were used in colony PCR for screening of insert using α-factor 5' and AOXI 3' primers (Figure 4.23)

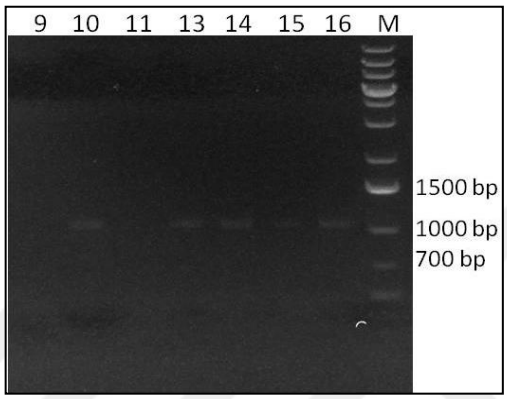

Figure 4.22. Colony PCR results of *TaXTH5* transformant induced *P. pastoris* cells using α-factor 5' and *AOXI* 3' primers analysed by agarose gel electrophoresis. M; DNA size marker. Colony numbers are indicated on figure.

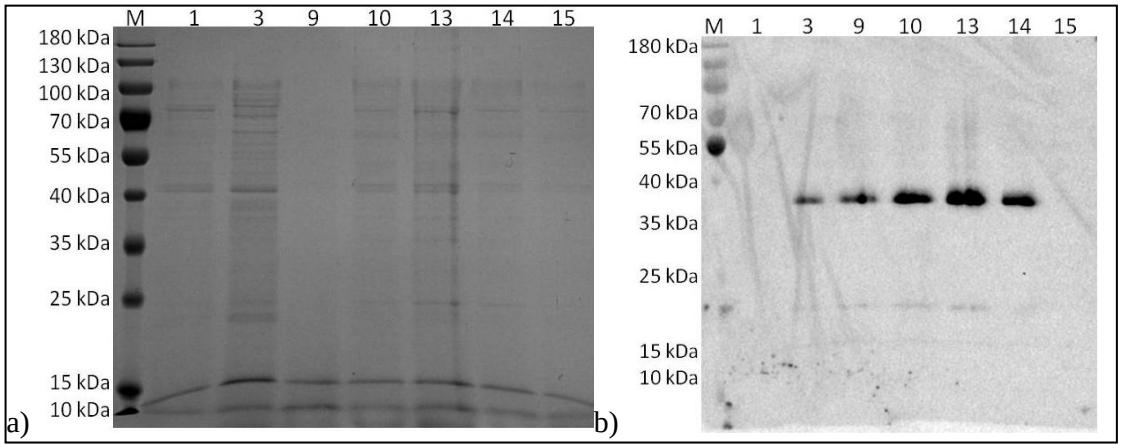

Figure 4.23. SDS-PAGE and Western Blotting analysis of selected *TaXTH5* transformant colonies. a) SDS-PAGE coomassie brilliant blue stained gel image of selected colonies, b) SDS-PAGE Western blotting result of selected colonies using anti 6X-His tag antibody. M; protein size marker, colony number are indicated on the figure.

Colony 13 was chosen as colony with the highest 6X-His tagged TaXTH5 since it gave the brightest Western signal in analysis (Figure 4.23). Thus, this colony was used in a pilot scale induction trial.

Another transformation was carried to obtained more colonies for screening. Transformation was successful, resulting in more than 50 colonies growing on YPDS agar + zeocin plate. 30 of these colonies were restreaked on YPDS agar + zeocin plates for confirmation of antibiotic selection. Then they were grown in BMMY media in order to induce *TaXTH5* gene expression, by addition of 1 per cent v/v methanol every 24 hours for 5 days. At the end of induction period, cells were centrifuged and supernatant was analysed for the presence of active TaXTH5 enzyme. Enzyme activity assay was carried using TXG-XGO donor-acceptor substrate couples for each colony. They were analysed by HPLC system and colonies showing XET activity on TXG-XGO substrate couple were further investigated for the presence of 6X-his tagged TaXTH5 by SDS-PAGE and Western blotting (Figure 4.24). Colony with the highest XET activity was colony number 46 and it gave positive result in Western blotting studies. This colony was also control by colony PCR for the *TaXTH5* insert using α-factor 5' and AOXI 3' primers (Figure 4.25). Size of PCR band was as expected. Thus, this colony was chosen for large scale production of TaXTH5 enzyme.

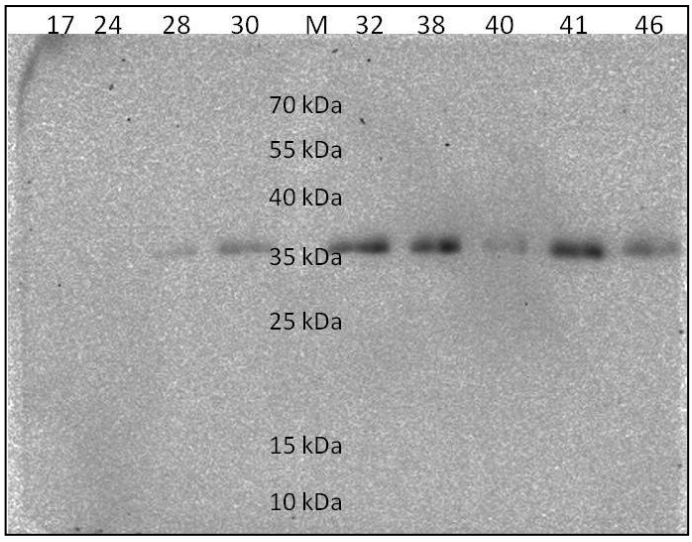

Figure 4.24. SDS-PAGE Western blotting of chosen *TaXTH5* transformant colonies. Codon numbers and protein size marker bands are shown in the figure.

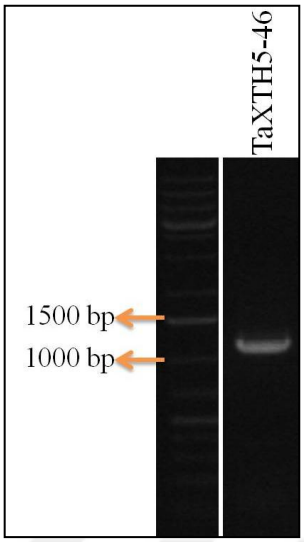

Figure 4.25. Colony PCR of *TaXTH5* transformant colony number 45 using α-factor 5' and *AOXI* 3' primers analysed by agarose gel electrophoresis. M; DNA size marker.

4.6. HETEROLOGOUS PROTEIN PRODUCTION AND PURIFICATION

4.6.1. AtXTH3

P. pastoris AtXTH3 transformant colony 36 was cultured and induced in 4 L BMMY media for 3 days with 1 per cent v/v methanol addition every 24 hours. 500 µl sample was collected from culture every 24 hours throughout 3 day induction period. Sample was used for OD_{600} absorbance measurement of culture (Table 4.6) and a representative growth rate plot was generated for the culture (Figure 4.26). Additionally protein concentration measurements and XET activity tests were performed with collected sample. Hybrid TXG-XGO product amount generated by AtXTH3 induction samples were analysed by HPLC and protein concentration measurement was done by Bradford assay (Table 4.7). It was clearly observed that cell density, protein concentration and synthesized AtXTH3 enzyme thus XET activity capacity increases throughout the induction period. Increase in cell number lead to more AtXTH3 enzyme and as a natural result, more hybrid TXG-XGO product florescence.

Table 4.6. Optic density measurement of induction media of *AtXTH3* daily at 600 nm wavelength.

Time (days)	OD600 absorbance
0	0.8
1	6.9
2	9.6
3	11.8

Table 4.7. Amount of hybrid TXG-XGO product generated by AtXTH3 enzyme produced during induction period of *AtXTH3* transformant and change of protein concentration during induction period.

Time (days)	TXG-XGO hybrid product fluorescence	Protein concentration of the induction media (mg/ml)
0	35	0.075
1	61.3	0.136
2	122.8	0.142
3	230	0.213

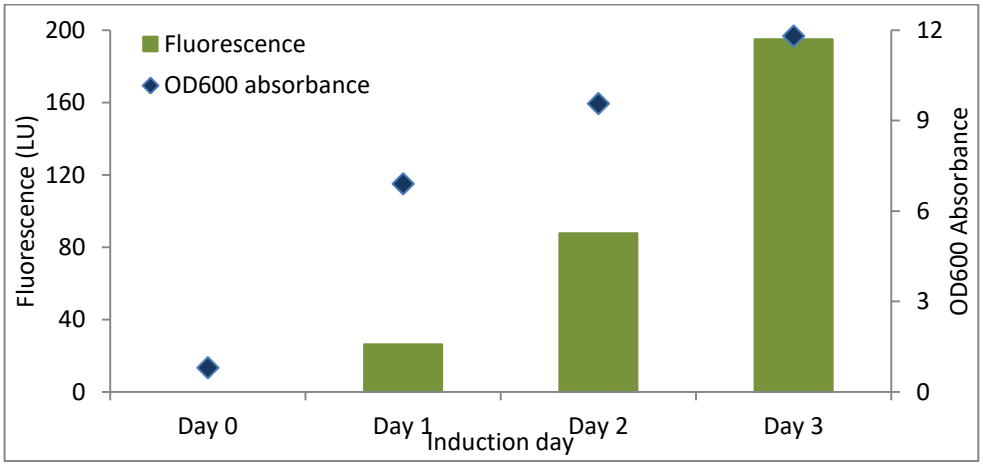

Figure 4.26. Relationship between the amount of TXG-XGO hybrid product generated by heterologously produced AtXTH3 and OD600 measurement of cell concentration during induction period of AtXTH3 induction culture.

At the end of induction period, cells were separated by centrifugation and protein content within supernatant was precipitated by ammonium sulphate protein precipitation method using 90 per cent ammonium sulphate saturation. Prior to dialysis, protein sample was filtered using 0.22 µm RC syringe filter. After dialysis, 6X-His tagged AtXTH3 was purified on HisTrap FF column (Figure 4.27). Flow-through during sample loading was collected and repurified on HisTrap FF column for maximum protein recovery.

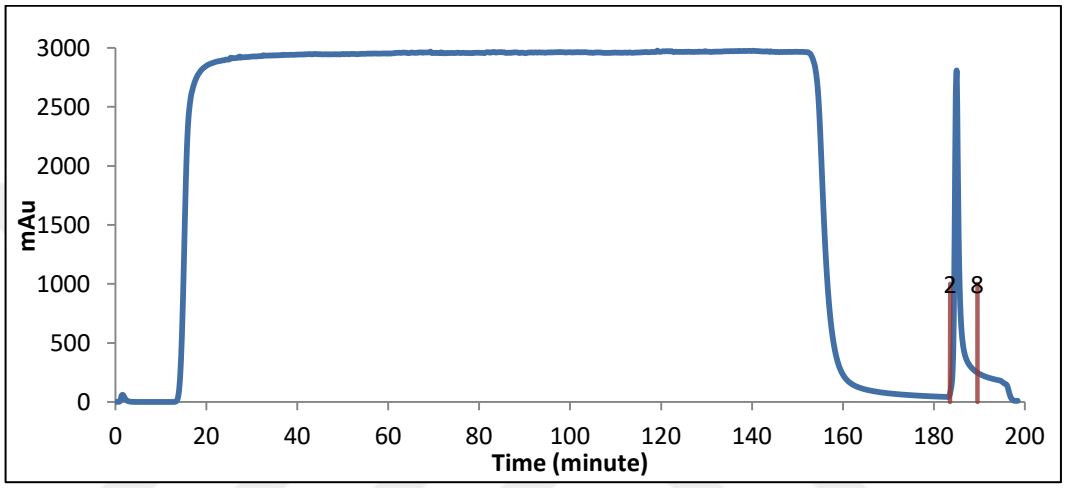

Figure 4.27. HisTrap FF column affinity chromatography of 6X-His tagged AtXTH3 sample from induction media.

Affinity purified AtXTH3 protein was polished using Superdex 75 16/100 size exclusion step. Sample was separated into 2 mL fractions (Figure 4.28). Fractions between 43-94 were analysed for their protein content by SDS-PAGE and Western blotting analysis. For this purpose, 1 in every 3 fraction between 43-94 were concentrated by Amicon ultra centrifugal filters and loaded on polyacyrlamide gels. After SDS-PAGE, gels were stained by silver nitrate and visualized (Figure 4.29). Also, AtXTH3 with 6X-His tag was detected by Western blotting (Figure 4.29).

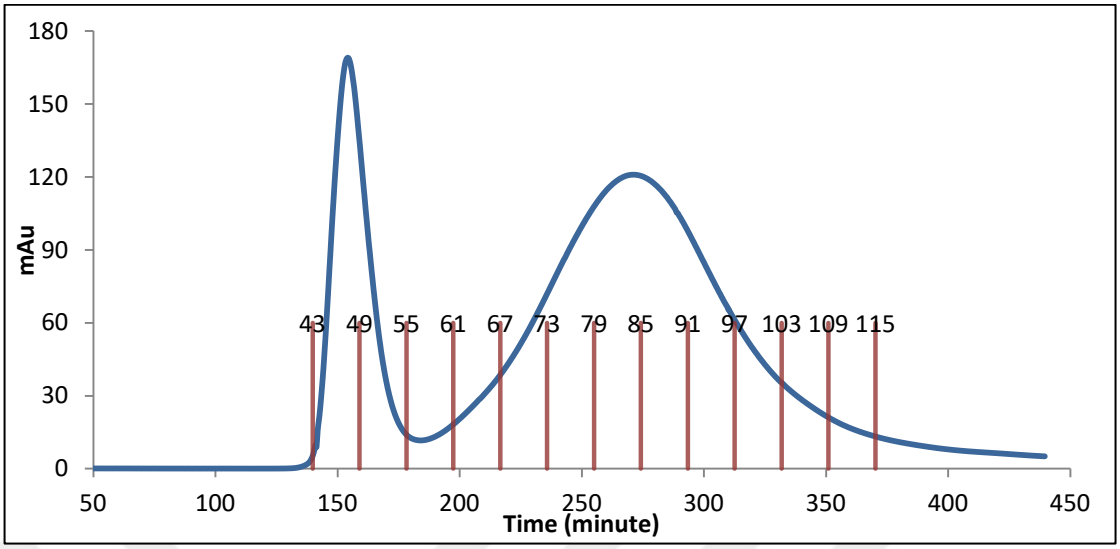

Figure 4.28. Polishing of affinity purified AtXTH3 protein using Superdex 75 16/100 column.

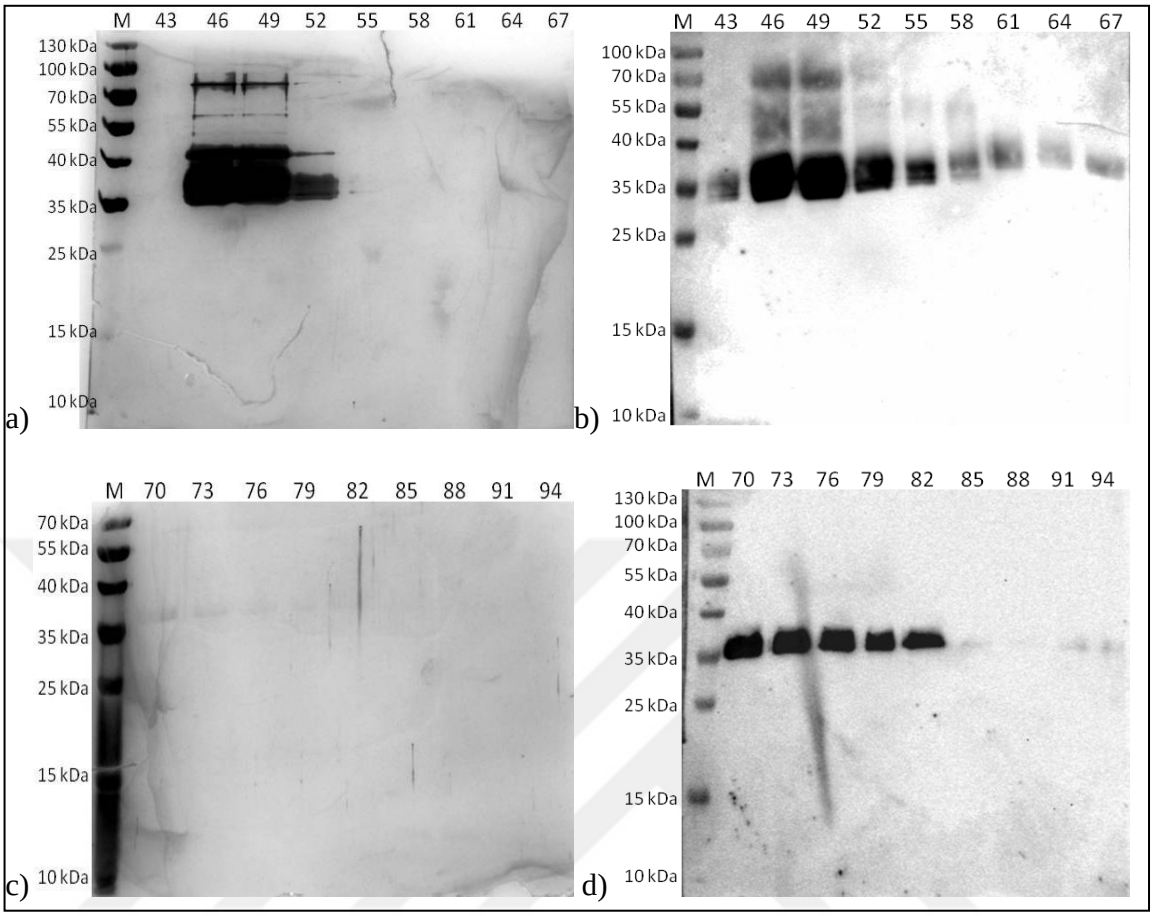

Figure 4.29. SDS-PAGE and Western blotting analysis result of AtXTH3 SEC fractions. a)Silver staining image of fractions 43-67, b)Western blotting image of fractions 43-67 using Anti6X-His antibody, c) Silver staining image of fractions 70-94, d) Western blotting image of fractions 70-94 using Anti6X-His antibody. Fraction numbers and protein size marker band sizes are indicated in the figure.

Fractions between 43-114 were tested for XET activity using TXG-XGO donor-acceptor couples. Hybrid products produced during activity test were quantified by HPLC analysis (Figure 4.30).

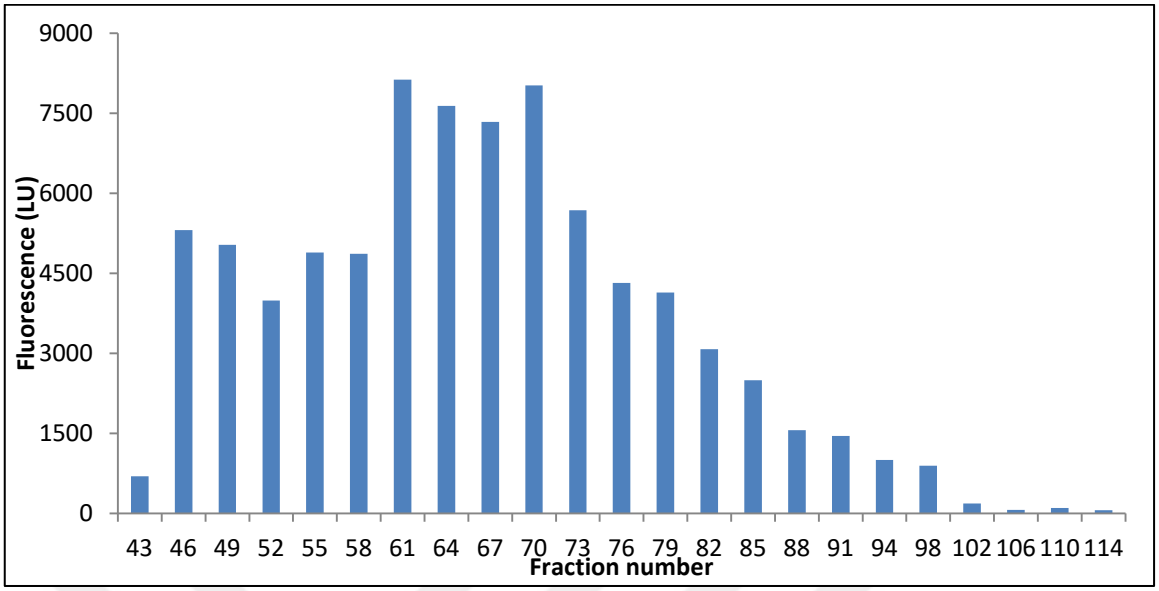

Figure 4.30. Florescence amounts of hybrid TXG-XGO products generated by AtXTH polishing fractions.

Results of AtXTH3 polishing step were evaluated together. During polishing step, protein sample was separated into 2 peaks, one sharper and other one wider. First peak, consisting of fractions 43-56, had some high molecular weight smear that can be result of protein aggregates. Fractions coming after fraction 58 are purer and additionally, some have higher XET activity compared to fractions prior to 58. Thus, all these fractions were separated into 2 pools regarding their purity; Pool 1 consisting of fractions 43-56 and Pool 2 consisting of fractions 57-115. Pools were concentrated and their protein concentrations were studied by BCA assay. Also their specific XET activity were calculated after TXG-XGO enzyme activity test (Table 4.8). With a lower protein concentration, Pool 2 have a higher XET activity, meaning that this pool is purer.

Table 4.8. Protein concentrations and specific XET activities of AtXTH3 polishing pools Pool 1 and Pool 2.

Sample name	**Protein concentration (mg/ml)**	**Specific XET activity (picokatal/mg enzyme)**
AtXTH3 Pool1	6.11	0.186
AtXTH3 Pool2	5.30	0.7952

SDS-PAGE analysis was done for AtXTH3 concentrated pools in order to visualize their protein content (Figure 4.31). Gels were stained by silver nitrate staining. As expected, Pool 1 have high molecular weight smear and bands whereas Pool 2 shows a pure profile. Thus, Pool 2 was used in substrate specificity and enzyme kinetic studies.

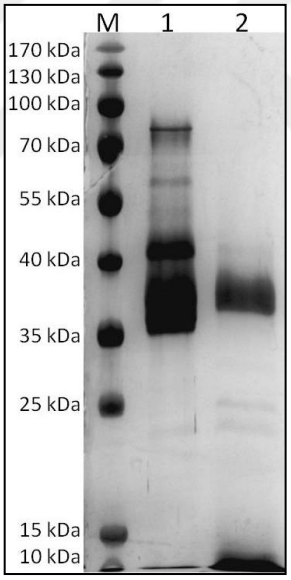

Figure 4.31. Protein compositions of AtXTH3 Pool 1 and Pool 2 analysed by SDS-PAGE silver nitrate staining. M; protein size marker. Pool numbers are indicated on figure.

4.6.2. AtXTH4

As an initial AtXTH4 synthesis trial, 100 mL BMMY culture of *P. pastoris AtXTH4-7* transformant was induced for 5 days. After induction period was over, cells were separated by centrifugation and supernatant was filtered through 0.45 RC syringe filter. Prior to affinity chromatography, 50 mL of the sample was loaded on HiPrep DeSalting 26/10 column and proteins were eluted in Binding buffer that was used as mobile phase. Protein bearing fractions were loaded onto HisTrap FF column for affinity purification of heterologously synthesized AtXTH4 and eluted by elution buffer. Fractions showing protein presence were pooled down together and loaded onto HiPrep DeSalting 26/10 column for buffer exchange into 0.1 M ammonium acetate pH 6.0 buffer. Proteins eluted from the column were collected as fractions and they were concentrated with Millipore Amicon Ultra 15 mL centrifugal filters. Purified AtXTH4 protein synthesized by AtXTH4-7 colony was analysed by loading 1.3 µg on polyacrylamide gel and performing SDS-PAGE. Gel was stained with coomassie blue stain however no bands were visible (Figure 4.32). Also, no XET activity was observed on TXG-XGO donor-acceptor couple.

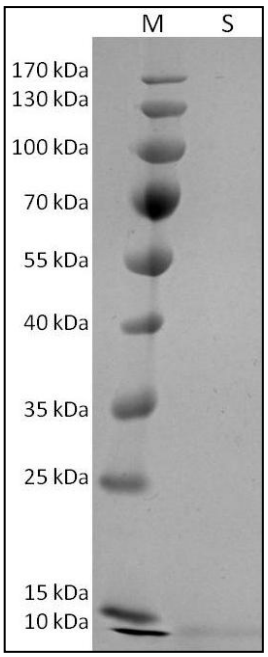

Figure 4.32. SDS-PAGE analysis of purified AtXTH4-7 sample. M; protein molecular size marker.

A new *AtXTH4* transformant colony was chosen for induction and purification studies. Colony AtXTH4-6 was induced in 100 mL BMMY for 5 days. Cells were separated by centrifugation and supernatant was analysed for XET activity prior to purification using TXG-XGO acceptor-donor couple. Activity results were positive however SDS-PAGE analysis and Western blotting results were negative.

AtXTH4-9 colony was induced in 1 L BMMY media for 5 days by 1 per cent v/v methanol addition every 24 hour. At the end of incubation period cells were separated by centrifugation. Supernatant was passed through 0.22 μm RC syringe filter in order to eliminate any cells and proteins were precipitated by ammonium sulphate precipitation method. After dialysis of sample to remove ammonium sulphate, 6X-His tagged AtXTH4 protein was separated by loading sample onto HisTrapFF affinity purification column. 6X-His tagged AtXTH4 was recovered from column in elution buffer and buffer was changed into 0.1 M ammonium acetate pH 6.0 by using HiPrep 26/10 DeSalting column. AtXTH4 protein sample was concentrated and used in specific activity studies. Protein concentration was measured by Bradford assay, and calculated as 1.4 mg/ml protein.

Large scale AtXTH4 protein production was also carried using AtXTH4-18 colony. Transformant yeast cells were grown in 2 L BMMY media for 5 days, with 1 per cent v/v methanol addition every 24 hour. Cells were separated by centrifugation and proteins in growth media were precipitated using ammonium sulphate precipitation with 85 per cent ammonium sulphate saturation. Sample was dialysed into 20 mM sodium phosphate pH 7.4 buffer and polyhistidine tagged AtXTH4 enzymes were purified by HisTrap FF column. Sample was desalted into 0.1 M ammonium acetate pH 6.0 buffer and concentrated. Enzyme concentration was measured by Bradford assay and calculated as 0.65 mg/ml. This enzyme was used in initial substrate screening and pH optimization trials.

For specificity tests, AtXTH4 enzyme was reproduced using AtXTH4-18 colony and inducing cells in 2.5 L BMMY media for 5 days with 1 per cent v/v methanol addition every 24 hour. At the end of induction period cells were centrifuged and proteins in supernatant were precipitated using ammonium sulphate precipitation method. Polyhistidine tagged AtXTH4 was affinity purified using HisTrap FF column and polished using HiPrep 26/60 Sephacryl S-200 HR column (Figure 4.33). While polishing, column outcomes were collected as fractions of 1.5 mL. Fractions were further combined and concentrated for protein content analysis via SDS-PAGE silver nitrate staining (Figure

4.34) and XET enzyme activity analysis by TXG-XGO substrate couple. Enzyme activity reactions were blotted on Whatman paper and visualized (Figure 4.35).

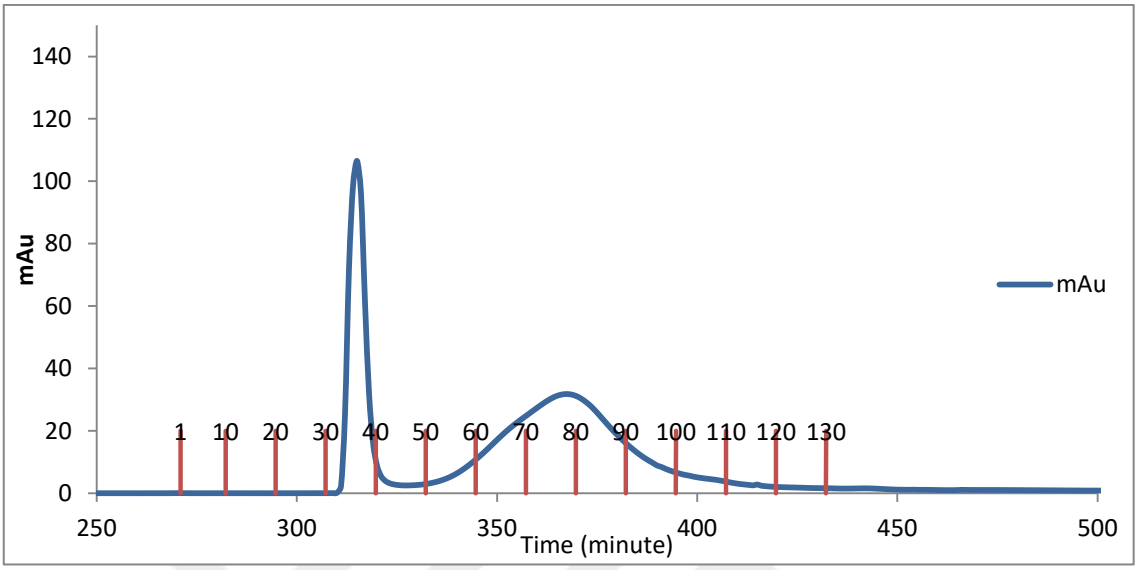

Figure 4.33. HiPrep 26/60 polishing chromatography of affinity purified 6X His tagged AtXTH4. Fraction numbers are shown on graph.

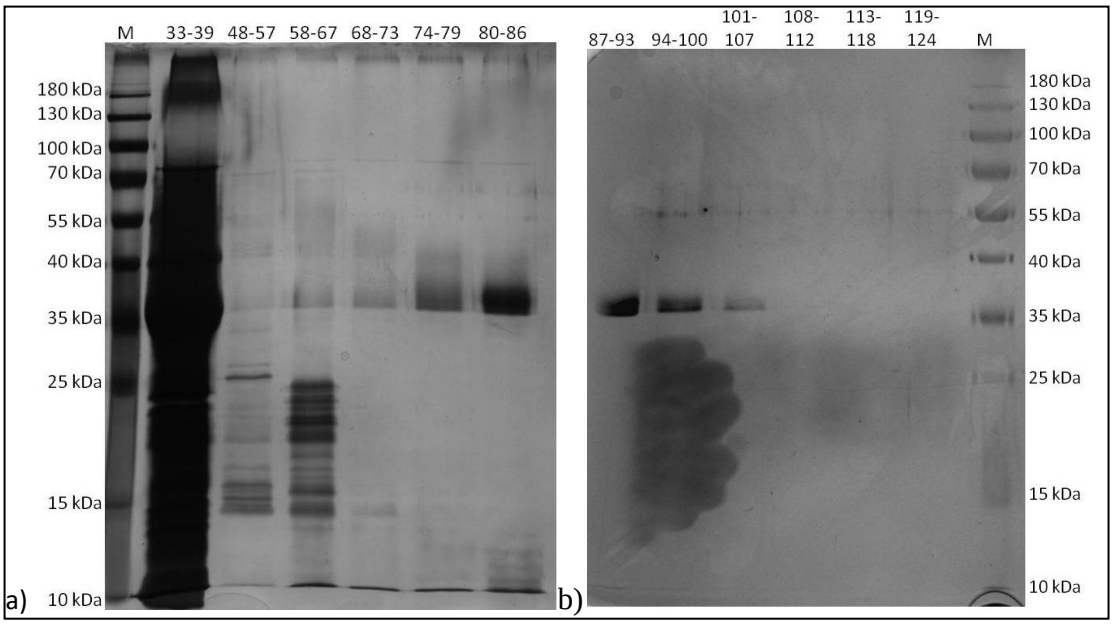

Figure 4.34. SDS-PAGE silver nitrate staining of 6X-His tagged AtXTH4 HiPrep 26/60 polishing column fractions. Fraction numbers and protein size marker bands are shown in image. M; protein size marker.

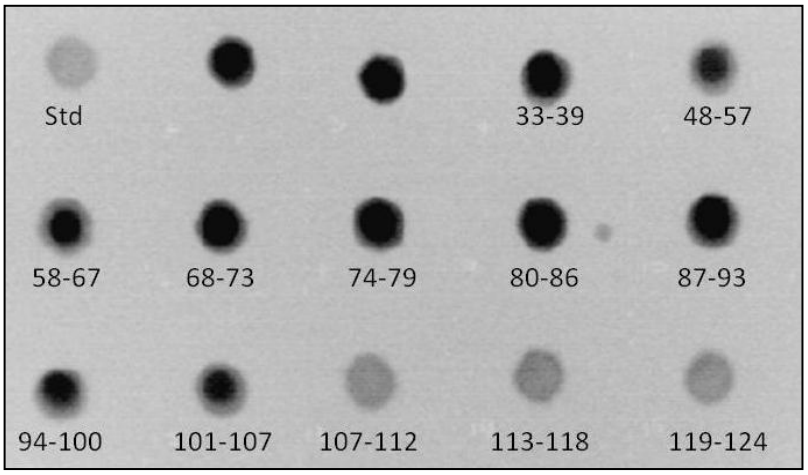

Figure 4.35. 6X-His tagged AtXTH4 HiPrep 26/60 polishing column fractions TXG-XGO enzyme reactions dot blot results. Fraction numbers are shown in figure.

In Figure 4.34, it is clearly seen fractions 33-67 doesn't contain pure protein but rather looks like protein bulk passing through the void volume of column without interacting with column. Fractions 74-107 are showing XET activity and representing a pure profile on SDS-PAGE analysis. Thus, fractions 74-107 were pooled together and fraction 33-39 were reloaded on HiPrep 26/60 column for a second polishing trial. Fractions were collected and analysed by SDS-PAGE silver nitrate staining and TXG-XGO activity analysis (Figure 4.36, Figure 4.37).

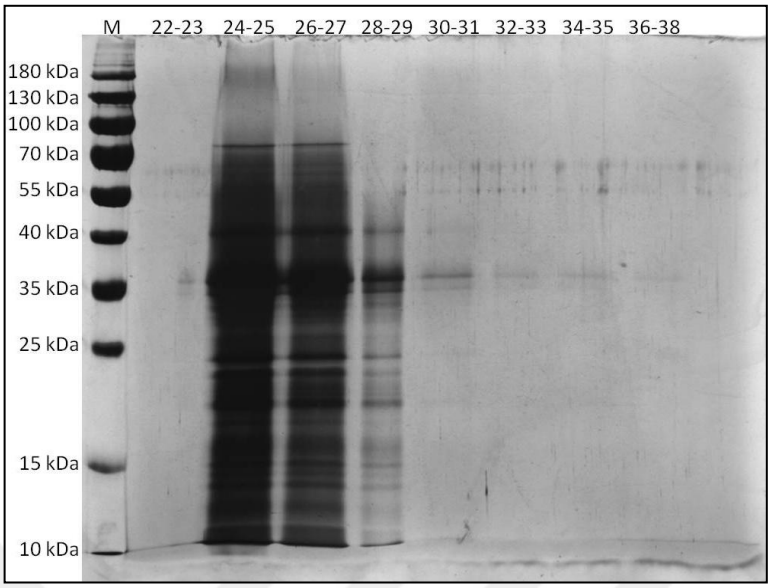

Figure 4.36. SDS-PAGE analysis of AtXTH4 HiPrep 26/60 re-polishing fractions, proteins visualized by silver nitrate staining. M; protein size marker. Fraction numbers are indicated on figure.

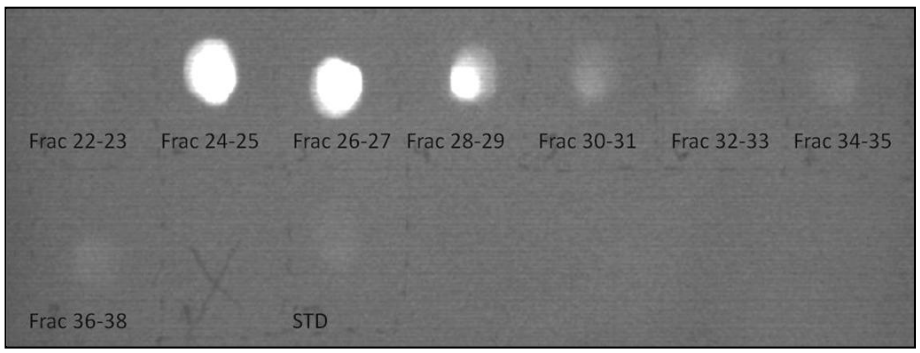

Figure 4.37. Dot-blot analysis of enzyme activity reactions done for repolishing fractions of AtXTH4 using TXG-XGO substrate couples. Fraction numbers are indicated on figure.

Second polishing results were evaluated and fractions 30-38 are the fractions with pure protein. They were pooled together and combined with fractions 74-107 from first polishing run. Protein concentration of 2nd product and polished AtXTH4was measured by Bradford assay and calculated as 0.2593 mg/ml. Enzyme was used in substrate specificity

trials using TXG, HEC, BBG, WA donors and various acceptors, however after two repeats enzyme was all used up. Thus, AtXTH4 was heterologously produced for a 3rd time.

AtXTH4 enzyme was produced for a 3rd time by inducing 2.5 L BMMY for 5 days by addition of 1 per cent v/v methanol every 24 hours. Cells were separated from growth media by centrifugation at the end of induction period and growth media was processed in order to purify produced 6X-His tagged AtXTH4. Proteins were precipitated by saturating supernatant to 90 per cent ammonium sulphate saturation. Pelleted proteins were dialysed and loaded onto HisTrapFF column and eluted by elution buffer. Flow-through during protein loading was collected and repurified on HisTrap FF column for maximum recovery of 6X his tagged proteins. Buffer exchange into 0.1 M ammonium acetate pH 6.0 was performed and then polishing was carried using HiPrep 26/60 Sephacryl S-200 HR column. Protein sample was separated into 1.5 mL fractions. Collected fractions were pooled and concentrated and analysed by SDS-PAGE silver nitrate staining and TXG-XGO activity dot-blot analysis (Figure 4.38).

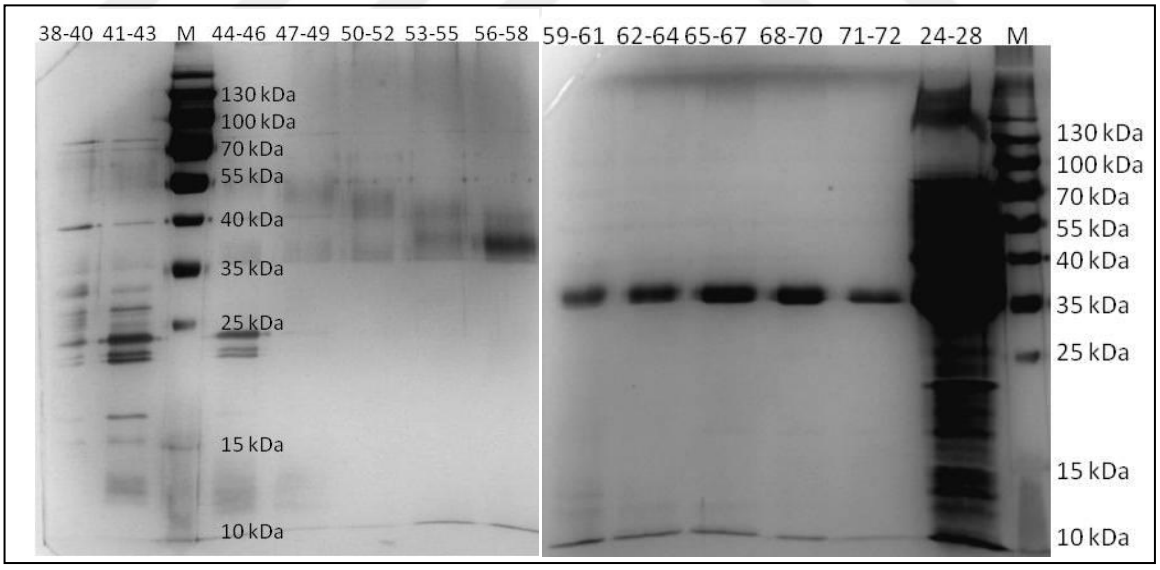

Figure 4.38. SDS-PAGE analysis of AtXTH4 (3rd batch trial) HiPrep 26/60 polishing fractions, proteins visualized by silver nitrate staining. M; protein size marker. Fraction numbers are indicated on figure.

SDS-PAGE results of 3rd time AtXTH4 polishing were evaluated. Fractions 24-28 represent proteins that pass through the column without being separated. Contaminant proteins were visual between fraction 38-55 and purest AtXTH4 was seen between fraction 56-72. Thus these pure fractions were combined and concentrated via Amicon centrifugal filter units. Protein concentration was measured by Bradford assay and found out to be 0.2731 mg/ml. Enzyme was used in specific activity trials however no correlation was observed between the repeats thus AtXTH4 was produced for one more time.

As a fourth AtXTH4 enzyme production, AtXTH4-18 colony was induced by 1 per cent v/v methanol addition every 24 hours in 3.6 L BMMY medium for 5 days. Cells were separated by centrifugation and supernatant was processed for protein purification. Firstly proteins were precipitated by ammonium sulphate precipitation, using 90 per cent saturation point. Pellets were dissolved in 20 mM sodium phosphate buffer pH 7.4 and filtered through 0.22 μm RC syringe filter. Sample was dialysed in order to remove ammonium sulphate salt and then loaded onto HisTrap FF column for affinity purification of 6X His tagged AtXTH4. Affinity purification was carried out in 3 batches, dividing dialysed sample into 3 and loading them separately in order to increase binding change and efficiency of the sample. Flow-through during sample loading was collected and repurified for maximum protein recovery from affinity purification step. Elution buffer was replaced with 0.1 M ammonium acetate pH 6.0 buffer by performing chromatography with HiPrep DeSalting 26/10 column. Then, affinity purified AtXTH4 was further polished by loading on HiPrep 26/60 Sephacryl S-200 HR column in three batches. Fractions were collected during polishing and they were concentrated for analysis via SDS-PAGE silver nitrate staining and Western blotting (Figure 4.39, Figure 4.40). Also, XET enzyme activity was tested by activity test using TXG-XGO donor-acceptor couple and performing dot-blot in order to visualize results (Figure 4.41).

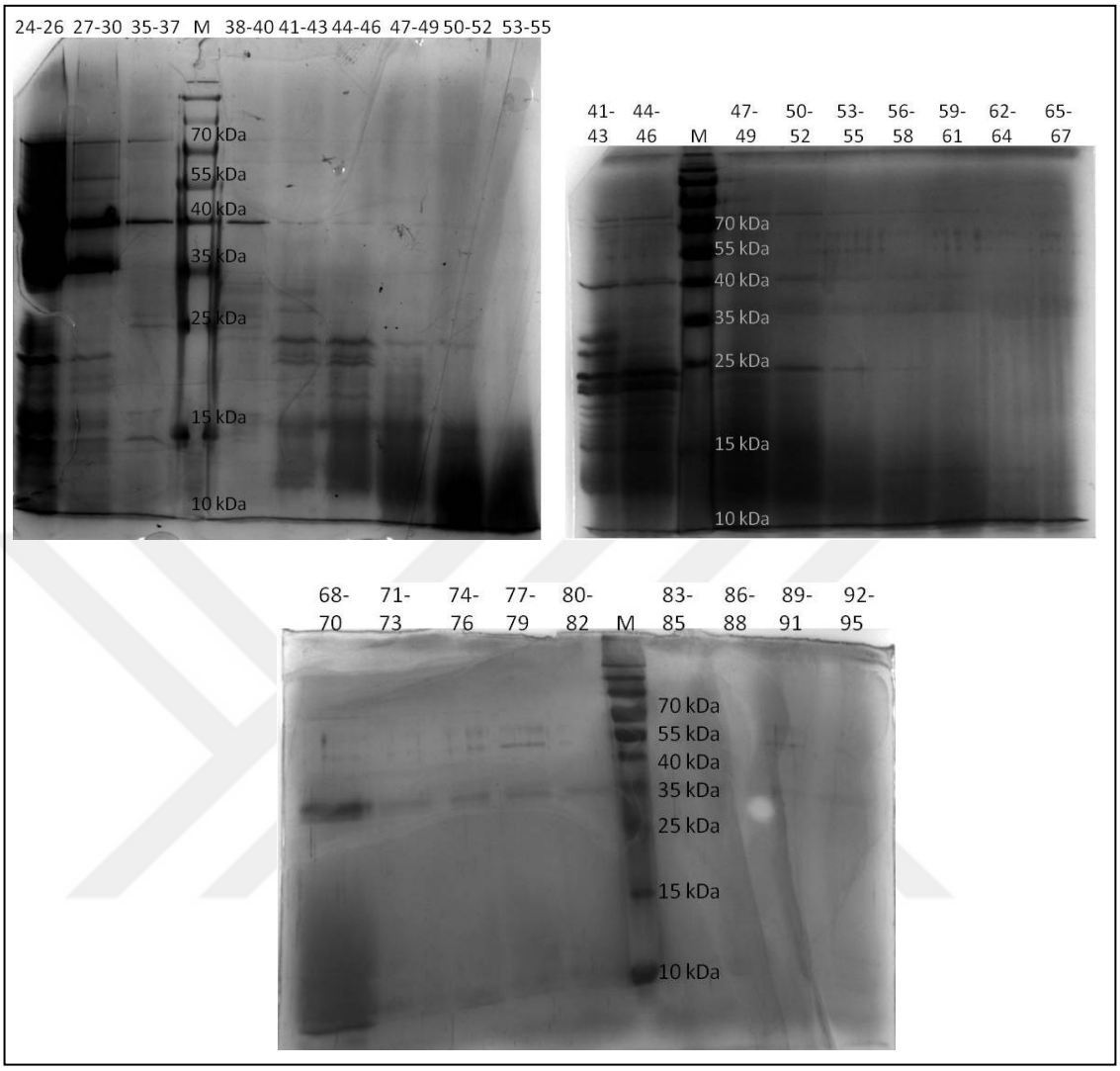

Figure 4.39. AtXTH4 4th product polishing fractions SDS-PAGE silver nitrate staining. Fraction numbers and protein size marker bands are given in figure.

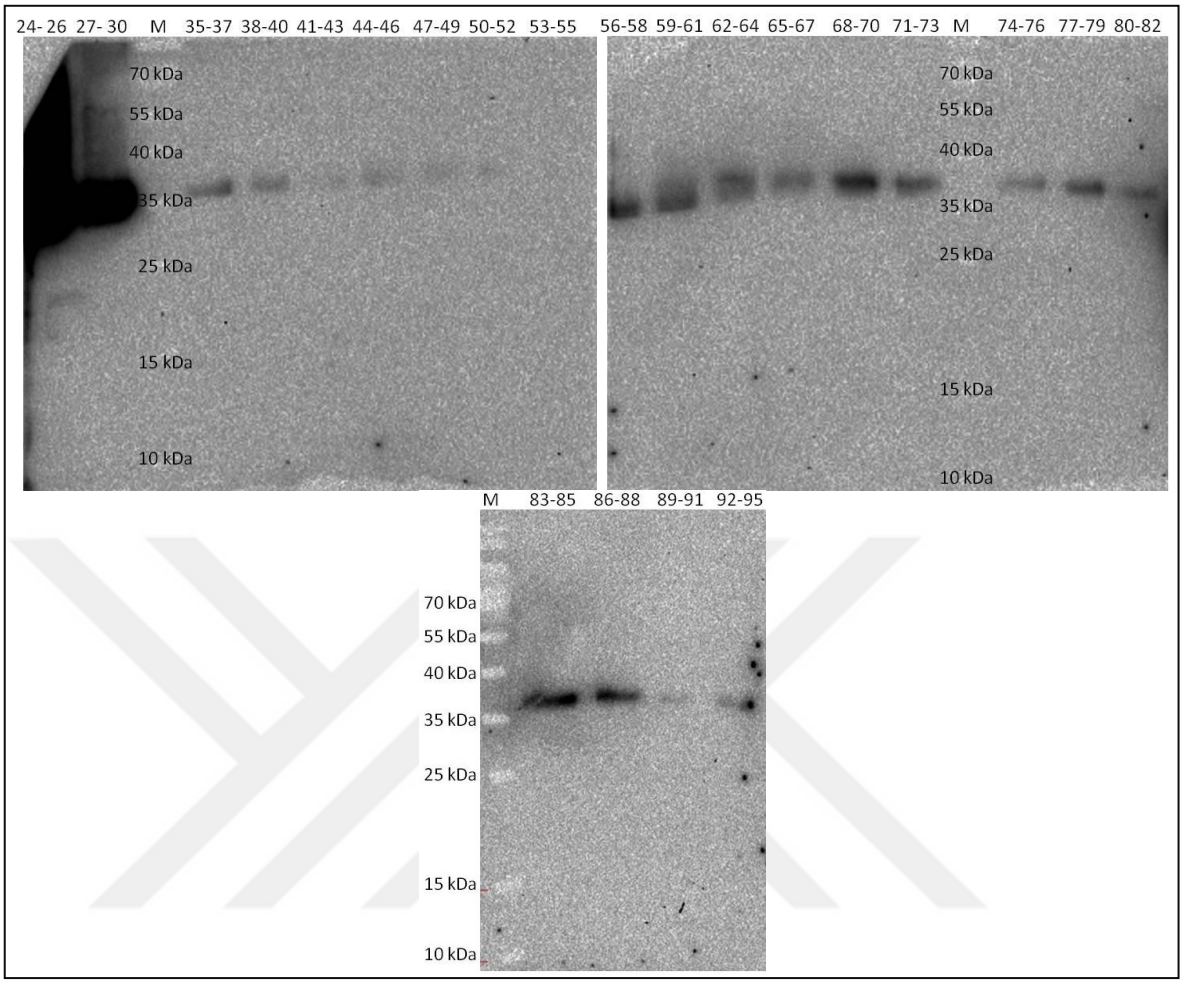

Figure 4.40. AtXTH4 4th product polishing fractions SDS-PAGE Western blotting. Fraction numbers and protein size marker bands are given in figure.

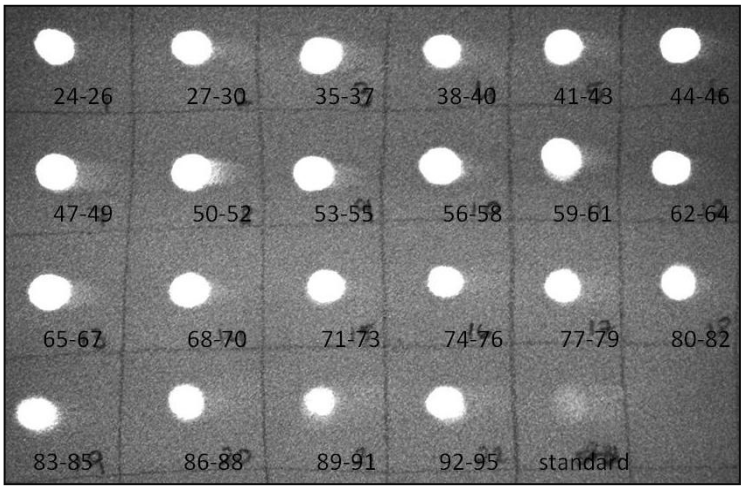

Figure 4.41. 6X-His tagged AtXTH4 4th product HiPrep 26/60 polishing column fractions TXG-XGO enzyme reactions dot blot results. Fraction numbers are shown in figure.

AtTH4 protein polishing results suggest that, by gel filtration chromatography step, contaminating proteins were removed and pure protein was seen between fraction 56-95. These fractions also gave one pure band in Western blotting and they all showed XET activity in dot-blot analysis. Thus, fractions 56-95 were pooled together and further concentrated to be used in enzymatic analysis. Protein concentration of pure AtXTH4 enzyme was measured by Bradford assay and calculated as 0.151 mg/ml.

4.6.3. BdXTH2

Large scale production with BdXTH2-14 colony was carried as 2 batches in total of 3L. For both of the batches, BMMY cultures were induced for 3 days, with 1 per cent v/v methanol addition every 24 hours. Cells were separated by centrifugation and proteins in supernatant were precipitated with ammonium sulphate protein precipitation method, applying ammonium sulphate salt to 90 per cent saturation. After dialysis, protein sample was loaded onto HisTrap FF column and 6X-His tagged BdXTH2 protein was purified. Flow-through collected during affinity chromatography was also loaded onto HisTrap FF column for maximum protein recovery. Buffer exchange of protein samples was performed using HiPrep DeSalting 26/10 column into 0.1 M ammonium acetate pH 6.0 buffer. Affinity purified BdXTH2 sample was loaded on Superdex 75 XK 16/100 column for

polishing. During size exclusion of BdXTH2, sample was separated into 2 mL fractions (Figure 4.42).

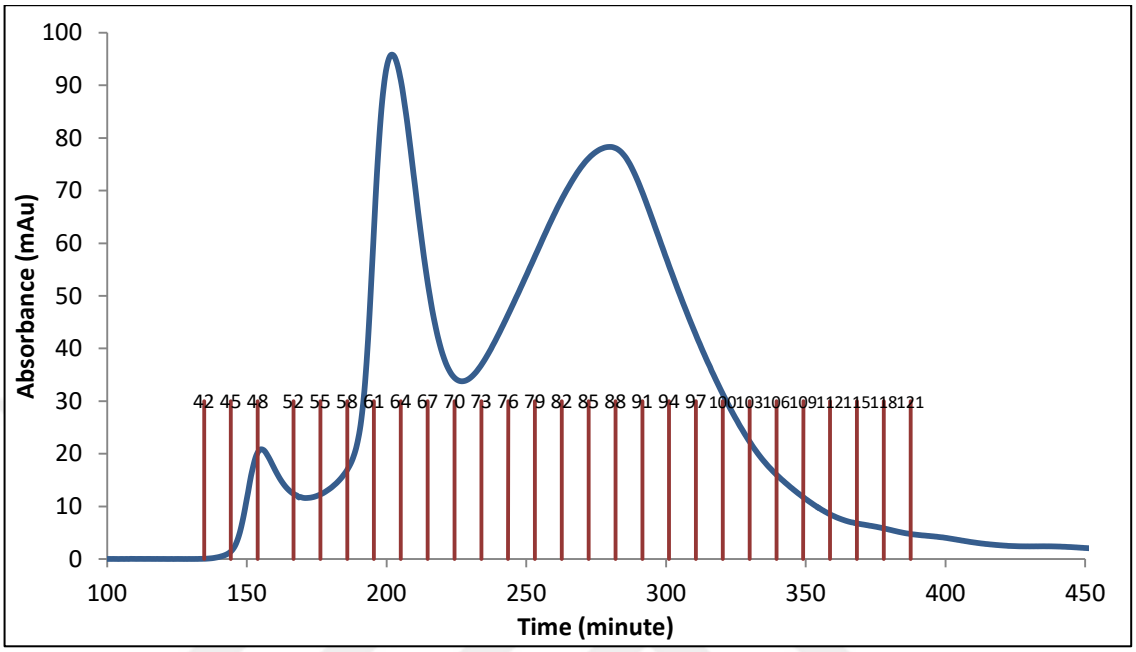

Figure 4.42. Superdex 75 XK 16/100 column polishing of affinity purified BdXTH2.

Fractions with proteins (fractions 42-121) were collected and 1 in every 3 fractions were concentrated prior to analysis. TXG-XGO activity analysis was performed using concentrated fractions. Amounts of hybrid products were analysed by HPLC analysis (Figure 4.43). Also, protein profiles of fractions were visualised by SDS-PAGE and silver nitrate staining (Figure 4.44). 6X-His tagged BdXTH2 in fractions was detected by SDS-PAGE Western blotting (Figure 4.44).

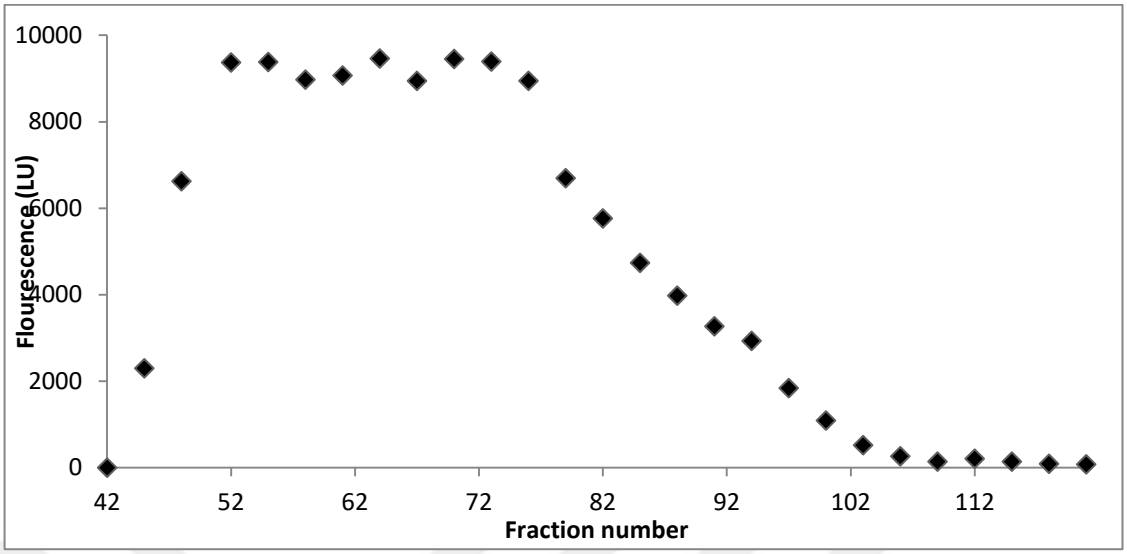

Figure 4.43. HPLC analysis of hybrid TXG-XGO products produced by BdXTH2 polishing fractions.

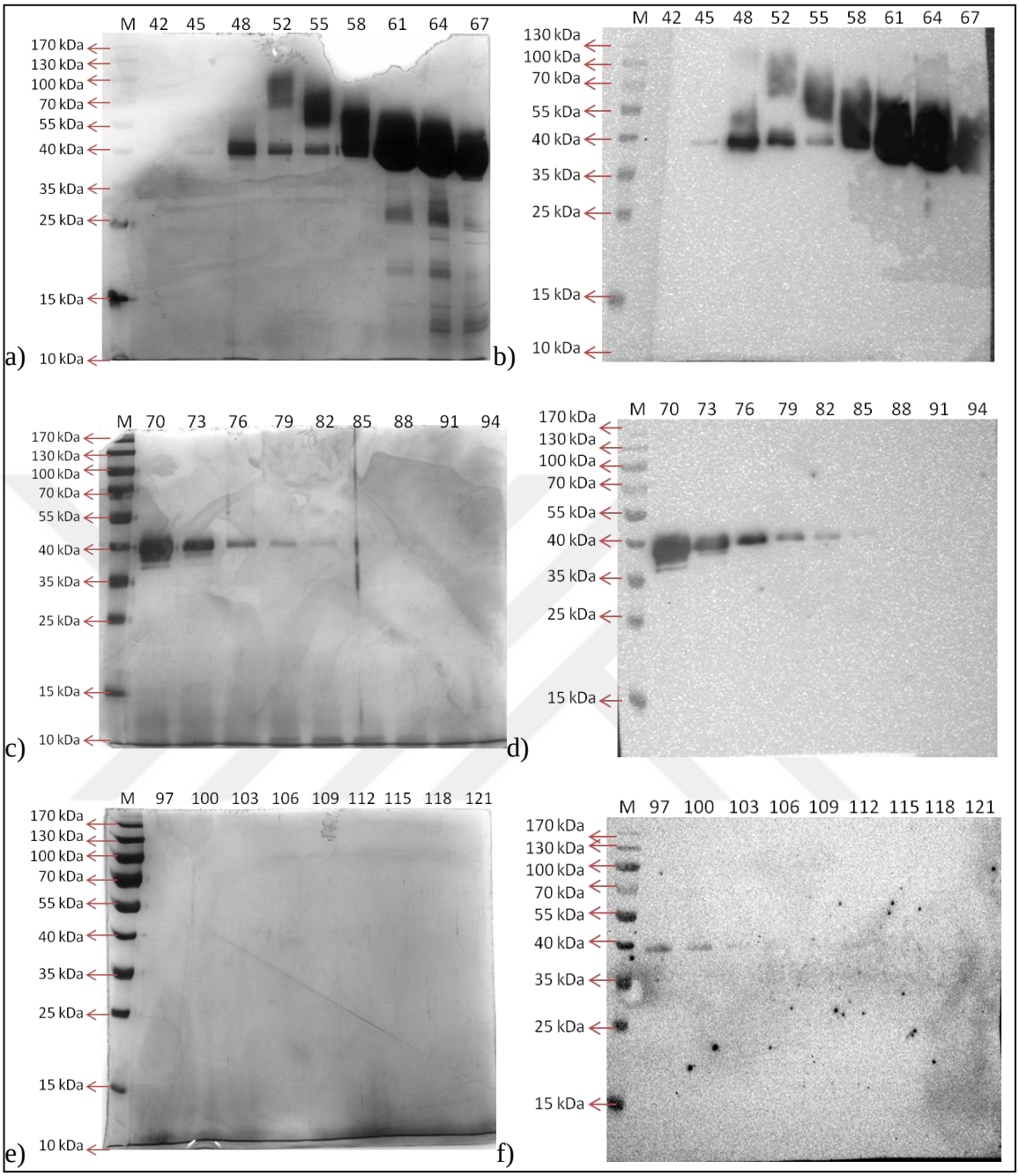

Figure 4.44. SDS-PAGE silver nitrate staining and Western blotting analysis of affinity purified BdXTH2 polishing fractions. a) SDS-PAGE silver nitrate staining of fractions 42-67, b)Western blotting of fractions 42-67, c) SDS-PAGE silver nitrate staining of fractions 70-94, d)Western blotting of fractions 70-94, e) SDS-PAGE silver nitrate staining of fractions 97-121, f)Western blotting of fractions 97-121. M; protein size marker. Fraction numbers are indicated on figure.

Results regarding BdXTH2 polishing fractions were analysed together and they were grouped into 3 groups depending on their purities. Fractions 45-58 are fractions with high molecular weight protein contamination, thus they were pooled down together to give BdXTH2_Pool 1. Fractions 59-69 are fractions with some low molecular weight contamination and high XET activity, thus they are pooled down together to give BdXTH2_Pool 2. Finally, fractions 70-90 are fractions with highest purity regarding silver nitrate staining, so they were pooled together to give BdXTH2_Pool 3. Fractions after fraction 90 showed XET activity at activity test (Figure 4.43), however they do not present presence of protein on silver stained gels, thus they were kept separately. All of the pools were concentrated down to ~ 1 mL and analysed for protein purity via SDS-PAGE silver nitrate staining (Figure 4.45). Like expected, Pool 2 and Pool 3 showed a pure profile whereas Pool 1 showed a profile with smear.

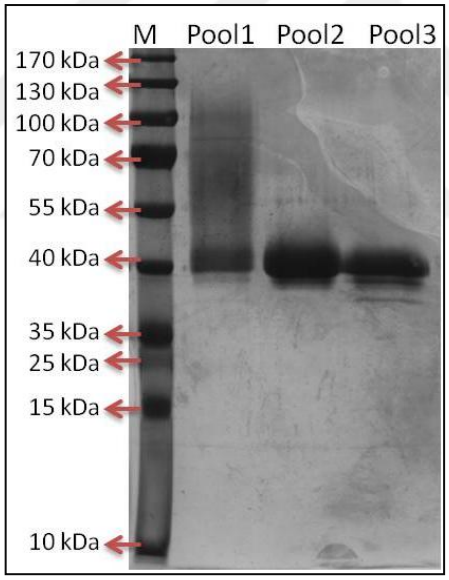

Figure 4.45. SDS-PAGE silver nitrate staining analysis of BdXTH2 polishing pools. M; protein size marker. Pool numbers are indicated in figure.

Specific activities and protein concentrations of BdXTH2 pools were also studied by Bradford assay and TXG-XGO enzyme activity assay respectively (Table 4.9). Pool 3 is the pool with lowest protein concentration but highest specific activity, meaning it is the purest pool. Thus it is planned to be used for enzyme kinetic studies. Whereas pool with lowest specific activity, Pool 1, was meant to be used in pH optimization and pool 2 used

during enzyme substrate specificity characterization. All BdXTH2 enzymatic analysis using the purified and polished pools were carried by another member of Plant Biotechnology lab as her MSc thesis.

Table 4.9. Protein concentrations and TXG-XGO specific XET activities of BdXTH2 polishing pools.

Sample Name	Protein concentration (mg/ml)	Specific activity pkatal / mg enzyme
Pool 1	1.356	14.523
Pool 2	10.868	33.445
Pool 3	0.421	47.844

4.6.4. GhXTH2

A pilot large scale production of *P. pastoris GhXTH2* transformant colony 10 was performed. Transformant was grown and induced in 100 mL BMMY media for 5 days, with 1 per cent v/v methanol addition every 24 hours. Synthesized and secreted GhXTH2 protein was separated from supernatant. Supernatant was filtered through 0.45µm RC syringe filter and proteins were precipitated by ammonium sulphate precipitation with 90 per cent saturation. Protein sample was desalted from ammonium sulphate by loading sample on HiPrep DeSalting 26/10 column with Binding Buffer mobile phase. His-tagged GhXTH2 proteins were purified by loading sample on HisTrap FF column. Eluted GhXTH2 proteins were desalted into 0.1 M ammonium acetate pH 6.0 by HiPrep DeSalting 26/10 column. GhXTH2 protein sample volume was reduced using Amicon Ultra-15 centrifugal filter units. Protein amount measurement was done by Bradford assay and calculated as 0.328 mg/ml protein. This sample was used to investigate substrate specificity of GhXTH2 enzyme, however more enzyme production was necessary in order to perform characterization studies.

GhXTH2 enzyme was heterologously produced twice in 1 L BMMY media, by inducing transformant cells for 5 days via addition of 1 per cent v/v methanol every 24 hours. After the induction period, cells were separated by centrifugation and proteins in supernatant

were precipitated by 90 per cent ammonium sulphate precipitation. Buffer exchange of samples prior to affinity chromatography, into Binding buffer, was carried using HiPrep DeSalting 26/10 column. Protein purification was carried by loading samples on HisTrap FF affinity column. His-tagged GhXTH2 proteins were recovered from column by eluting using Elution Buffer. As a last chromatographic step, buffer exchange of purified GhXTH2 was done into 0.1 M ammonium acetate pH 6.0 buffer using HiPrep DeSalting 26/10 column. Sample volumes were reduced with Amicon Ultra-15 centrifugal filter units. Obtained pure GhXTH2 samples were used in pH optimization and in initial characterization trials. However, after pH optimisation and carrying first time interval studies, a contamination problem occurred in the pure enzyme, thus GhXTH2 was reproduced by inducing 2.6 L BMMY media for 5 days by 1 per cent v/v methanol addition every 24 hours.

P. pastoris GhXTH2 transformant colony 10 was induced in 2.6 L BMMY media for 5 days and after induction period, cells were separated by centrifugation. Supernatant was filtered through 0.22 μm RC syringe filter and proteins were precipitated by 90 per cent ammonium sulphate precipitation. Protein sample was dialysed against 20 mM sodium phosphate buffer pH 7.4 to get rid of ammonium sulphate salt. Then, sample buffer composition was made up to Binding buffer and loaded onto HisTrap FF column for affinity purification of his-tagged GhXTH2. Flow-through during sample loading was also collected and repurified on the column for maximum recovery. Proteins were then polished on HiPrep 26/60 Sephacryl S-200 HR column and fractionated. Fractions with proteins were collected and concentrated for analysis. Protein content of polishing fractions were analysed by SDS-PAGE silver nitrate staining (Figure 4.46) and XET activity of fractions were analysed by activity test with TXG-XGO and dot-blot (Figure 4.47).

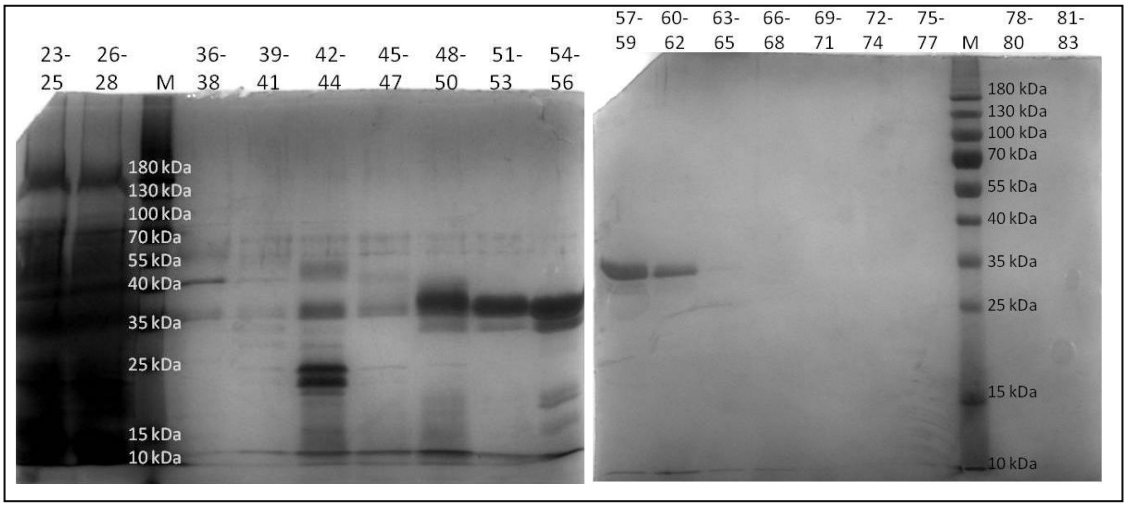

Figure 4.46. SDS-PAGE silver nitrate staining analysis of GhXTH2 polishing fractions. M; protein size marker. Fraction numbers are indicated in figure.

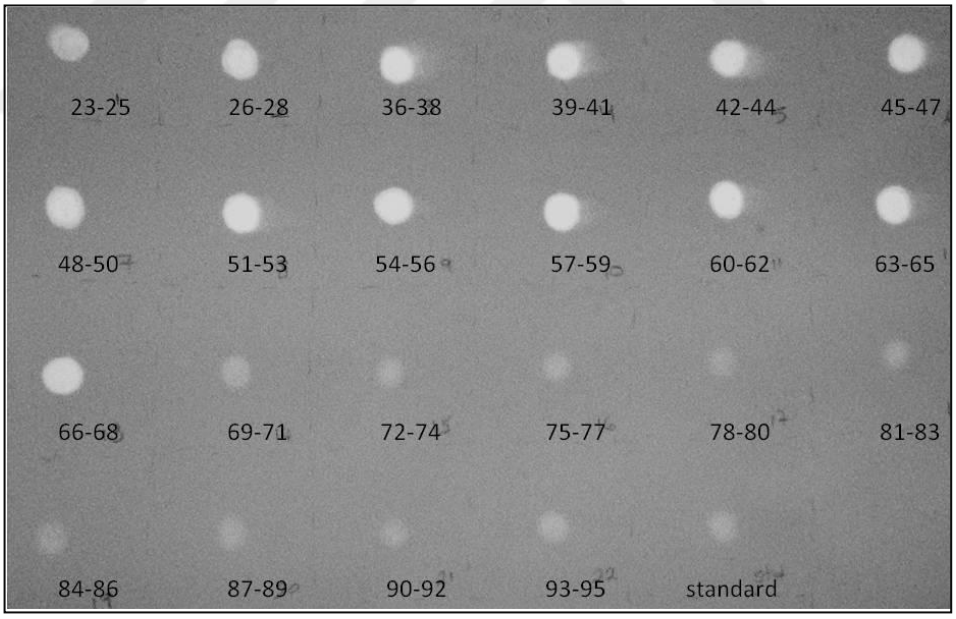

Figure 4.47. Dot-blot analysis of TXG-XGO enzyme activity reactions of GhXTH2 polishing fractions.

Dot-blot activity analysis revealed that fractions 23-68 are showing XET activity however, depending on SDS-PAGE silver nitrate analysis, only fractions 51-65 have pure protein. Thus fractions 51-65 were pooled down concentrated to be used in characterization studies.

4.6.5. PtXTH3

Large scale production of PtXTH3 enzyme was carried out by inducing the cells in 2.4 L BMMY media for 5 days with 1 per cent v/v methanol addition every 24 hours. When induction was over, cells were separated from supernatant by centrifugation and supernatant was filtered through 0.2 µm RC syringe filter. Proteins in induction media were separated and concentrated by ammonium sulphate precipitation method using 90 per cent ammonium sulphate saturation point. Prior to affinity purification, ammonium sulphate salt was removed from protein solution via dialysis and sample buffer was replaced by elution buffer.

Protein sample was loaded onto HisTrap FF column for affinity purification of 6X-His tagged PtXTH3. Flow-through during sample column loading was collected and purified on affinity column for maximum PtXTH3 recovery. In each run, protein sample was eluted from column via elution buffer (Figure 4.48) and divided into fractions. Fractions with protein were collected and pooled down for second liquid chromatography step.

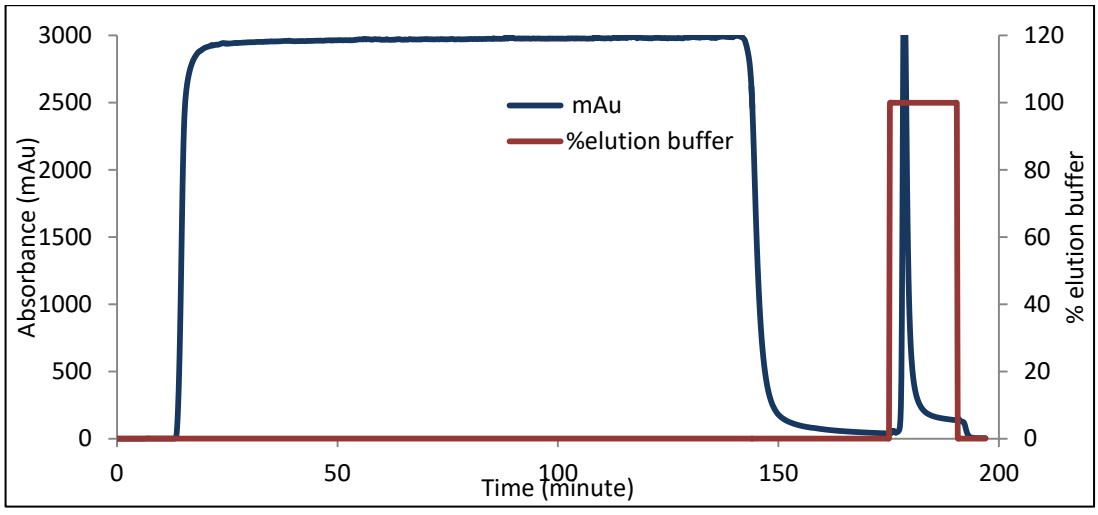

Figure 4.48. Affinity chromatography of heterologously produced 6X-His tagged PtXTH3 with HisTrap FF column.

Buffer of affinity purified PtXTH3 was changed from elution buffer to 0.1 M ammonium acetate pH 6.0 by performing size exclusion chromatography using HiPrep DeSalting 26/10 column. Then, protein was polished by size exclusion chromatography on Superdex 75 16/100 column (Figure 4.49). Sample was divided into three distinct peaks. During polishing step, all of the column outcome was divided into different fraction. Fractions with proteins were detected by increase in absorbance and these fractions were collected for further analysis.

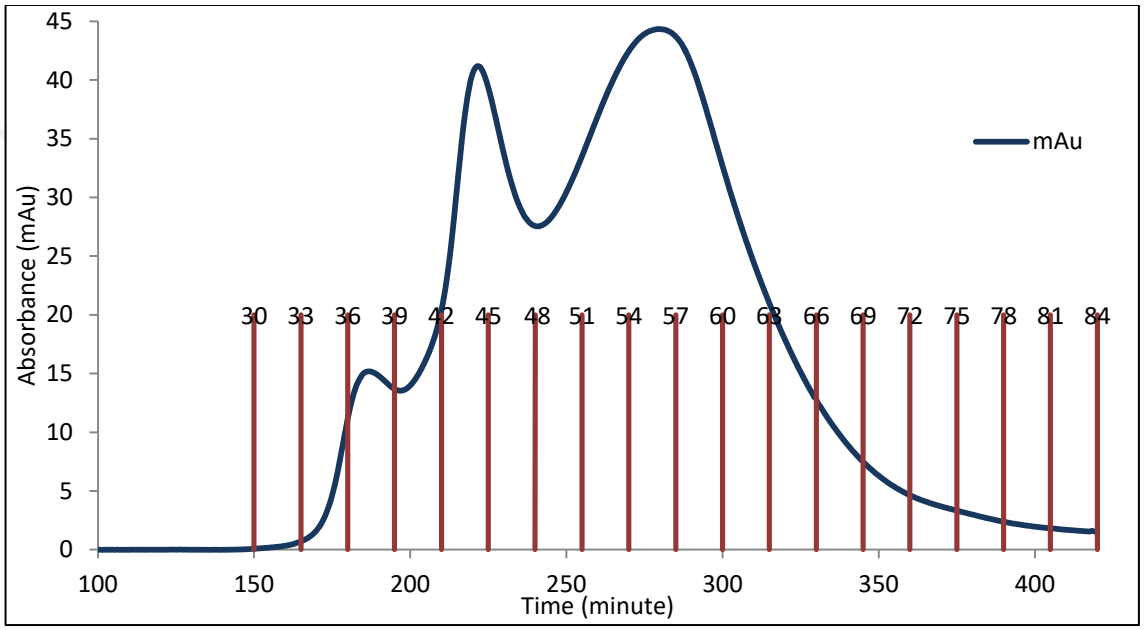

Figure 4.49. Size exclusion chromatography polishing of affinity purified PtXTH3 protein.

Polishing step fractions were investigated for their protein profiles and XET activities. One in every 3 fractions between 31 to 82 were concentrated by Amicon ultra centrifugal filter units, denatured and separated by SDS-PAGE. Gels were both stained by silver nitrate to visualize all proteins in the fractions and blotted onto nitrocellulose membrane in order to detect 6X-His tagged PtXTH3 (Figure 4.50). Silver nitrate stained gels suggest fractions 37-46 have an additional protein band between 55-70 kDa along target PtXTH3 band which is between 35-40 kDa. Western blotting results indicate another 6X-His tagged protein between 25-15 kDa, which can be incomplete protein product or degraded PtXTH3. Fractions 49-58 are purer fractions with high protein content, regarding thickness and brightness of bands on both stained gel and western membrane. Lastly, fractions 59-82

are not showing any contamination on gel and membrane, thus they are pure and less concentrated.

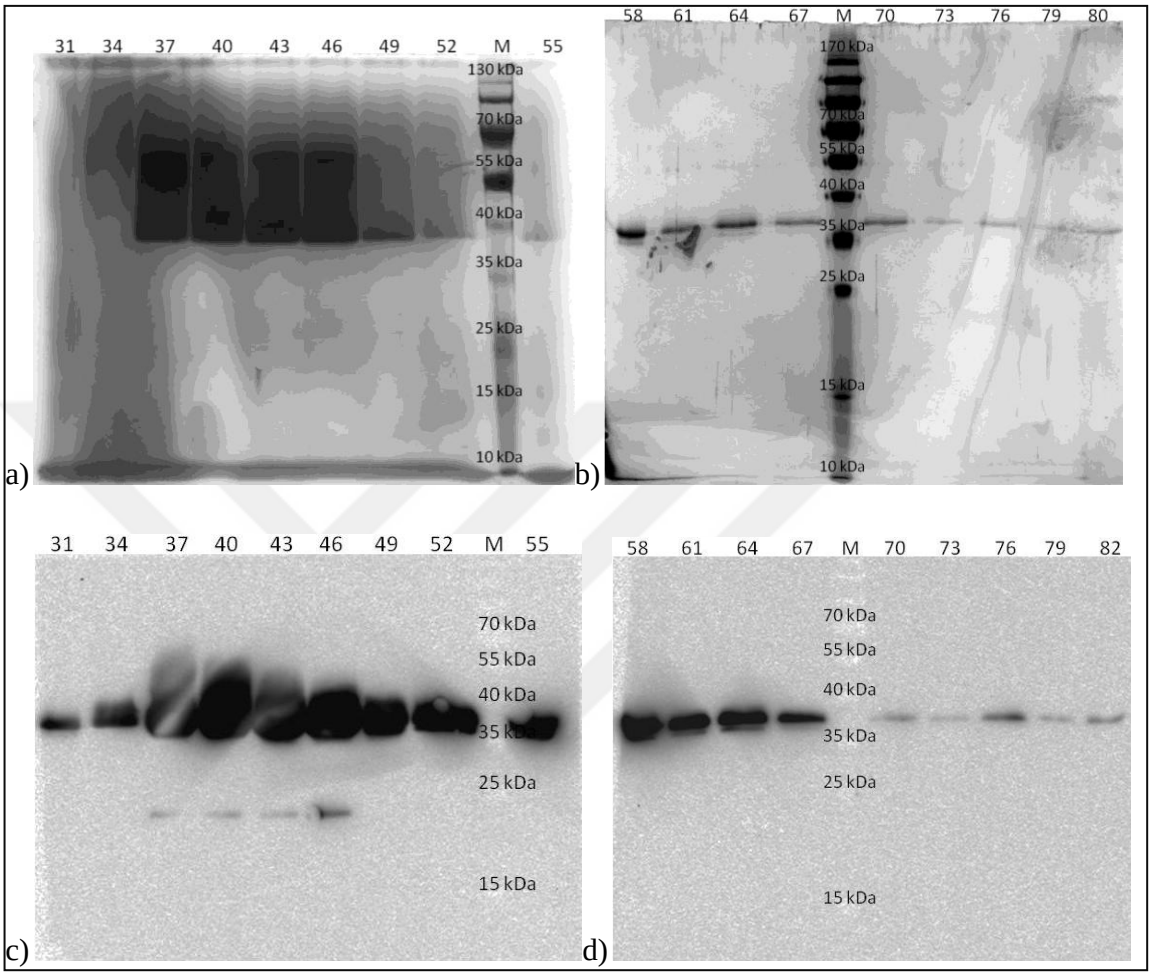

Figure 4.50. SDS-PAGE Western blotting analysis of polishing fractions of PtXTH3 protein sample. a) SDS-PAGE silver staining of PtXTH3 polishing fractions 31-55, b) SDS-PAGE silver staining of PtXTH3 polishing fractions 58-80, c) SDS-PAGE Western blotting of PtXTH3 polishing fractions 31-55, d) SDS-PAGE Western blottingof PtXTH3 polishing fractions 58-80. M; protein size marker. Fraction numbers are indicated on figures.

XET activities of fractions were studied by setting enzyme activity reactions with TXG-XGO donor-acceptor couples and quantifying amount of hybrid product by HPLC system (Figure 4.51). All of the fractions were showing XET activity, decreasing as fraction number increase beyond fraction 61.

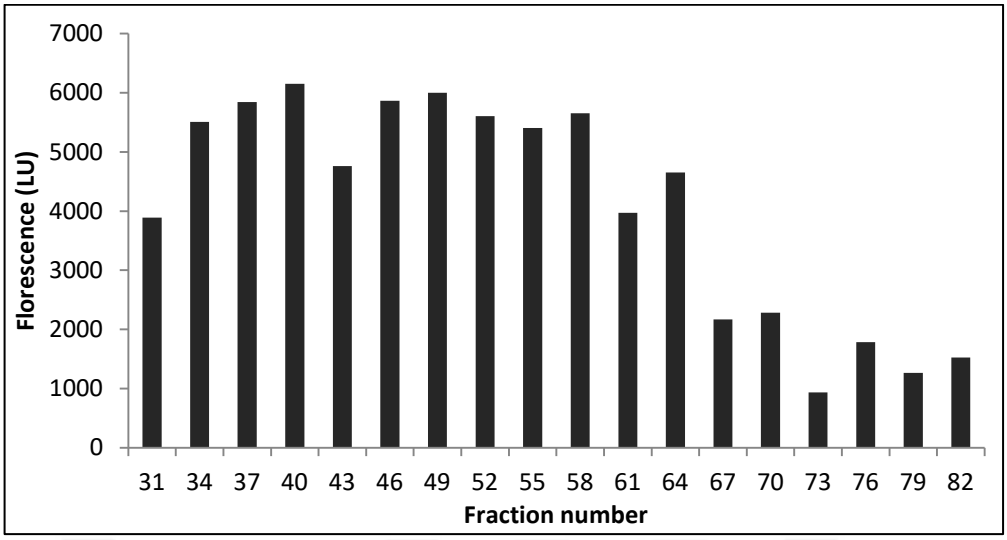

Figure 4.51. Florescence amounts of TXG-XGO enzyme activity reaction result hybrid products generated via PtXTH3 polishing reactions.

Polishing fractions SDS-PAGE, Western blotting and XET activity test results were evaluated together and fractions were divided into 3 pools; Pool 1 consisting of 37-48, Pool 2 consisting of 49-58 and Pool 3 consisting of 59-82. These pools were concentrated using Amicon ultra centrifugal filter units. Protein concentrations of pools were determined by Bradford assay (Table 4.10). Also samples from each pool were analysed by SDS-PAGE silver nitrate staining to see protein profiles (Figure 4.52).

Table 4.10. Protein concentrations and specific TXG-XGO activities of PtXTH3 polishing pools.

Sample name	**Protein concentration (mg/ml)**	**Specific TXG-XGO activity (pkatal/mg protein)**
Pool 1	1.56	402.12
Pool 2	0.20	462.51
Pool 3	0.08	208.20

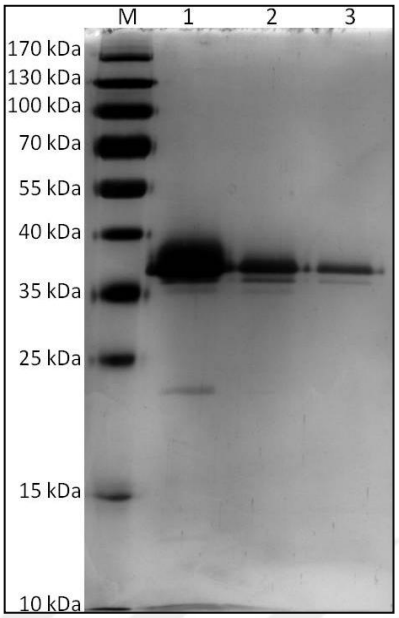

Figure 4.52. SDS-PAGE silver nitrate staining gel image of PtXTH3 polishing pools. M; protein size marker. Pool numbers are given in figure.

It was concluded that Pool 1 can be used for substrate specificity analysis, since it doesn't has any contaminant regarding Figure 4.52. Pool2, being purer and having more specific activity, will be used for enzyme kinetic studies.

4.6.6. TaXTH5

Transformant *TaXTH5 P.pastoris* colonies were obtained as a result of performed transformations. Firstly, a pilot scale induction trial was done using colony 13 in 100 mL BMMY media. Induction was carried for 5 days, by addition of 1 per cent v/v methanol every 24 hours. Cells were centrifuged and separated and supernatant was passed through a 0.45 μm syringe filter. Enzyme activity assay using TXG-XGO was carried using filtered supernatant in order to visualize XET activity, however no positive results were obtained.

Large scale production trial was carried using colony 46 in 1 L BMMY. Cells were induced in BMMY media for 5 days, with 1 per cent v/v methanol addition every 24 hours. When induction period was over, cells were separated by centrifugation and proteins in growth media were precipitated using ammonium sulphate precipitation 90 per cent

saturation point. After dialysis of protein sample, 6X-His tagged TaXTH5 protein was purified by affinity chromatography. Sample was loaded on HisTrap FF column and eluted by high imidazole concentration. Purified TaXTH5 was desalted into 0.1 M ammonium acetate buffer using HiPrep DeSalting 26/10 column. Protein concentration was studied via Bradford assay and found as 0.707 mg/ml. Enzyme was used in pH optimization study.

After pH optimization of TaXTH5 enzyme, heterologously produced first batch of enzyme was lost due to protein degradation. Thus, a second large scale production was carried by inducing colony 46 in 1 L BMMY media for 5 days, with 1 per cent v/v methanol addition every 24 hours. At the end of induction period, cells were centrifuged and supernatant was processed for protein purification. Ammonium sulphate precipitated protein sample was dialysed and loaded onto HisTrap FF column for affinity purification of 6X-His tagged TaXTH5 protein. Affinity purified TaXTH5 was buffer exchanged into 0.1 M ammonium acetate prior to being used. By Bradford assay, concentration was measured as 0.812 mg/ml. Substrate specificity trials were carried using this purified TaXTH5 enzyme. Different substrate couples were screened via purified TaXTH5 however, a new production was carried in order to obtained purified and polished TaXTH5 for complete characterization and kinetic studies.

As a new production, 3.3 L *P. pastoris TaXTH5* transformant colony number 46 in BMMY was induced by 1 per cent v/v methanol addition every 24 hours for 5 days. During induction period, cell growth continued with a decreasing rate over the whole process (Figure 4.53).

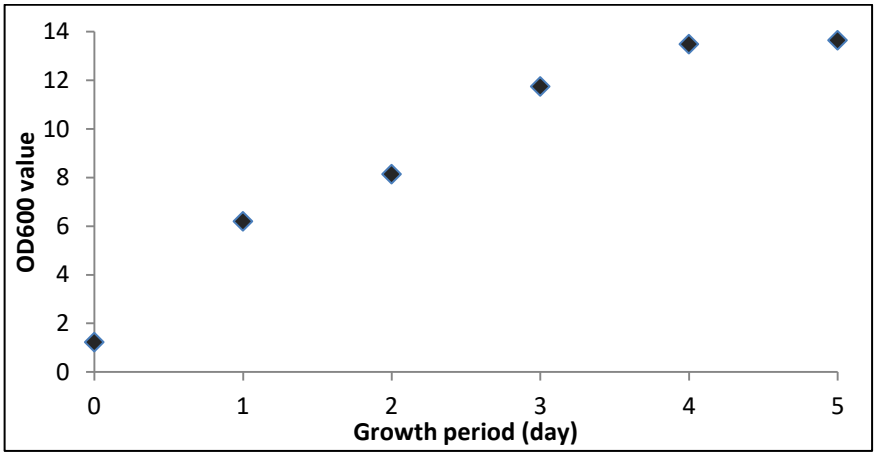

Figure 4.53. OD600 absorbance values of *P. pastoris TaXTH5* transformant culture during large scale gene expression induction period.

Cells were separated from growth media by centrifugation. Prior to protein precipitation by ammonium sulphate precipitation, supernatant was filtered through 0.22 µm RC syringe filter in order to remove any remaining yeast cell in the supernatant. Proteins were precipitated using 90 per cent ammonium sulphate saturation. After resuspending with 20 mM sodium phosphate pH 7.4 buffer, protein sample was dialysed against 20 mM sodium phosphate pH 7.4 for removal of excess salts. Then, 6X-His tagged TaXTH5 proteins were affinity purified by loading on HisTrap FF column. Non-bound proteins were collected as flow-through during affinity purification and they were also loaded on HisTrap FF column for a second round of purification and maximum recovery.

Affinity purified 6X-His tagged TaXTH5 was further purified by polishing on HiPrep 26/60 Sephacryl S-200 HR size exclusion column. Protein sample components were separated into fractions of relying on their molecular sizes (Figure 4.54). Fractions with protein were collected and concentrated using Amicon centrifugal filter units prior to analysis. Protein content and purity of TaXTH5 polishing fractions were examined by SDS-PAGE silver nitrate staining and Western blotting (Figure 4.55). 6X-His tagged TaXTH5 enzyme was detected using anti 6X-His tag antibody. Also, XET capacity of concentrated fractions were tested by enzyme activity using TXG-XGO donor-acceptor couple.

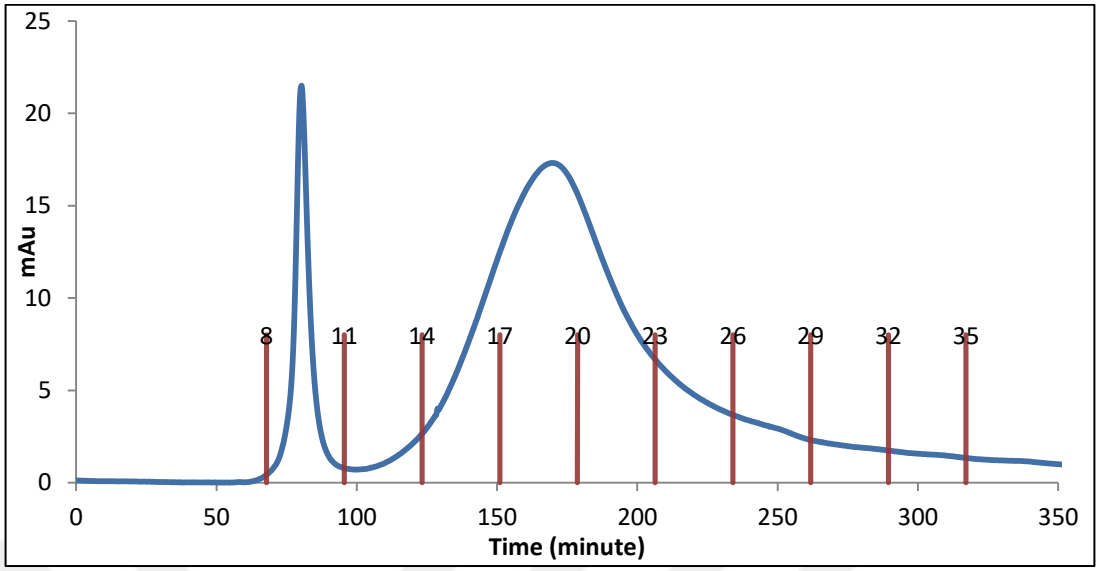

Figure 4.54. HiPrep 26/60 Sephacryl S-200 HR polishing pf affinity purified TaXTH5. Fraction numbers are indicated as red bars on x-axis.

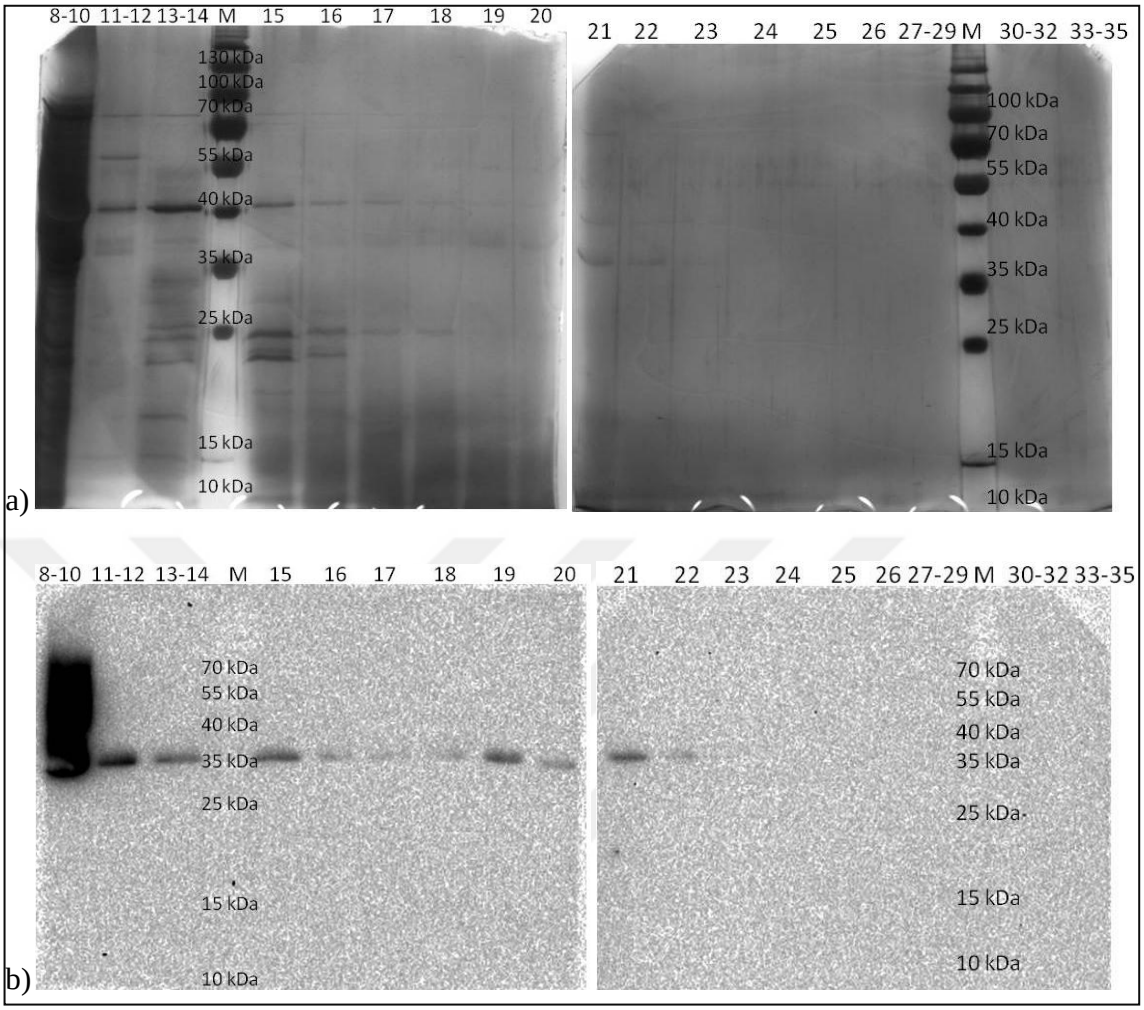

Figure 4.55. SDS-PAGE Western blotting analysis of polishing fractions of TaXTH5 protein sample. a) SDS-PAGE silver staining of PtXTH3 polishing fractions 8-20, b) SDS-PAGE silver staining of PtXTH3 polishing fractions 21-35, c) SDS-PAGE Western blotting of PtXTH3 polishing fractions 8-20, d) SDS-PAGE Western blottingof PtXTH3 polishing fractions 21-35. M; protein size marker. Fraction numbers are indicated on figures.

SDS-PAGE results were evaluated and it was observed that fractions after 15 are purer compared to previous fractions. Fractions 11-12 have high molecular weight contamination whereas fractions 13-14 have lower molecular weight contaminations. Thus, it was concluded to combine fractions into 3 pools as Pool 1 consisting of fractions 11 and 12; Pool 2 consisting of fractions 13-22. Pool 2 of TaXTH5 enzyme was used in substrate

specificity tests and kinetic trials. For activity analysis, a proportion of TaXTH5 Pool 2 sample was further concentrated using Amicon centrifugal filter and both non-concentrated and concentrated sample's protein concentrations were measured and calculated using Bradford assay. Concentration of non-concentrated sample was calculated as 0.136 mg/ml and concentration of concentrated sample was calculated as 0.337 mg/ml.

4.7. ENZYME CHARACTERIZATION, ACTIVITY ANALYSIS AND KINETIC STUDIES

4.7.1. pH optimization

4.7.1.1. AtXTH4

pH optimization of AtXTH4 was carried using AtXTH4-18 enzyme, diluted 1/10 times. A pH range from pH 4.0 to pH 8.0 was tested by preparing donor TXG with McIlvaine buffer at different pH values. Enzyme incubation was carried for an hour and produced hybrid TXG-XGO products were analysed by HPLC system (Figure 4.56). Highest amount of hybrid product was obtained using donor with pH 6.1.

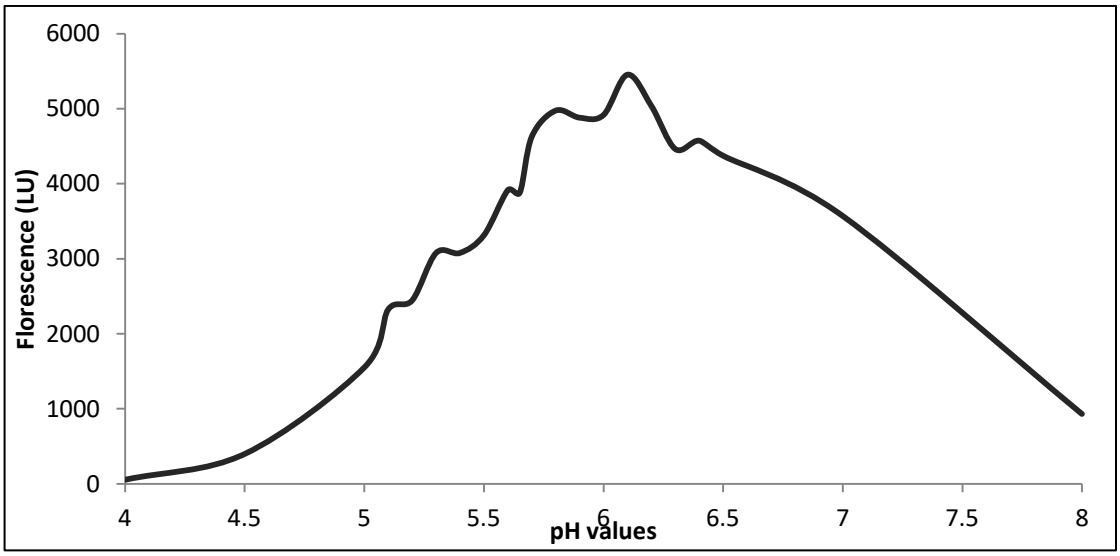

Figure 4.56. pH optimization study of AtXTH4 enzyme between pH 4.0 to pH 8.0 using McIlvaine buffer.

It is known that buffering range of McIlvaine buffer and ammonium acetate buffer are different from each other. Enzymes are in ammonium acetate buffer and reaction environment is ammonium acetate buffer. Thus, a second pH optimisation was carried using ammonium acetate buffer between pH 4.5 to pH 7.0. AtXTH4-18 enzyme was diluted 1/10 and TXG donors were diluted to 0.4 per cent w/v working concentration with ammonium acetate buffers at different pHs. After 1 hour incubation, hybrid TXG-XGO product amounts were analysed by HPLC system (Figure 4.57). pH optima was pH 6.5 when ammonium acetate buffer was used.

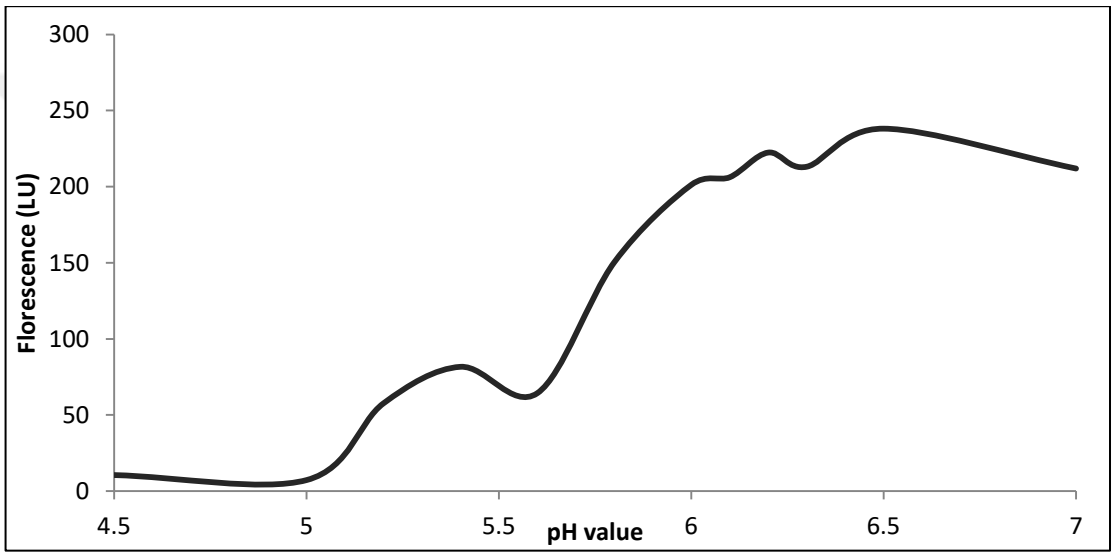

Figure 4.57. pH optimization study of AtXTH4 enzyme between pH 4.5 to pH 7.0 using ammonium acetate buffer.

4.7.1.2. GhXTH2

McIlvaine buffer system was used to create different pH values between pH 4.0 to pH 8.0. TXG donors were prepared using McIlvaine buffers, resulting in donors with different pH values. Using these donors and XGO acceptor, reactions were prepared and hybrid product amounts at the end of incubation period were measured by HPLC system. When plotted on a graph, it was observed that most product was produced in pH 5.2 tube (Figure 4.58).

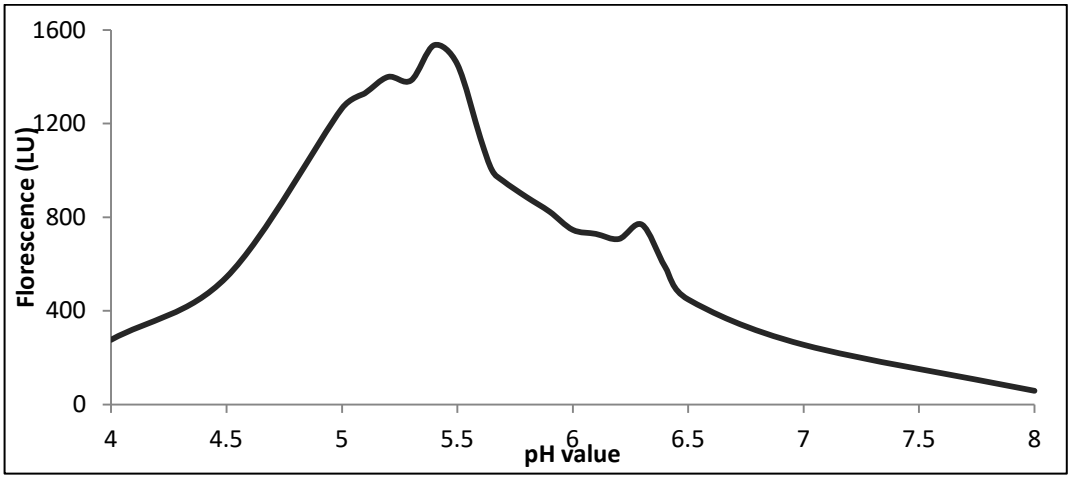

Figure 4.58. pH optimization of GhXTH2 enzyme between pH 4.0 to pH 8.0 using McIlvaine buffer.

It is known that different buffer systems have a variable pH buffering capacities at different pH values. pH optimization with McIlvaine buffers give a correct idea about pH optima of enzymes however reactions all characterization reactions are carried using ammonium acetate buffer and ammonium acetate solutions have a different pH buffering capacity. Thus, in order to carry reactions in an optimum pH, an additional optimisation was done using ammonium acetate buffer between pH 5.0 and pH 6.5. Trial with ammonium acetate buffer revealed enzyme was showing the highest XET activity at pH 6.0, thus characterization studies were carried at pH 6.0 (Figure 4.59).

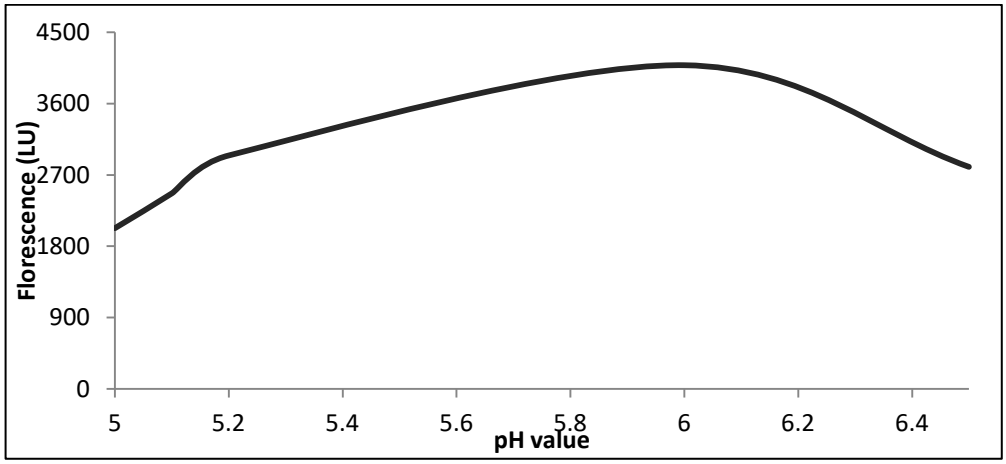

Figure 4.59. pH optimization of GhXTH2 enzyme between pH 5.0 to pH 6.5 using ammonium acetate buffer.

4.7.1.3. PtXTH3

As an initial step of characterization, pH optima were studied for PtXTH3 enzyme between pH 4.0 to 7.0 using McIlvaine buffer. For each pH values, pH of TXG donors was arranged using matching McIlvaine buffers and these TXG donors were used in enzyme activity analysis with XGO acceptors. Amount of hybrid product amount was measured by HPLC system and plotted on a graph (Figure 4.60). The highest amount of TXG-XGO hybrid product was produced using TXG pH 4.5, thus making pH 4.5 as optimum pH with McIlvaine buffer. However, ammonium acetate is used as the buffer in enzyme reaction environment and ammonium acetate buffer and McIlvaine buffer have different buffering capacities. Thus pH optimization studies were repeated with a narrower range of pH values using ammonium acetate buffer.

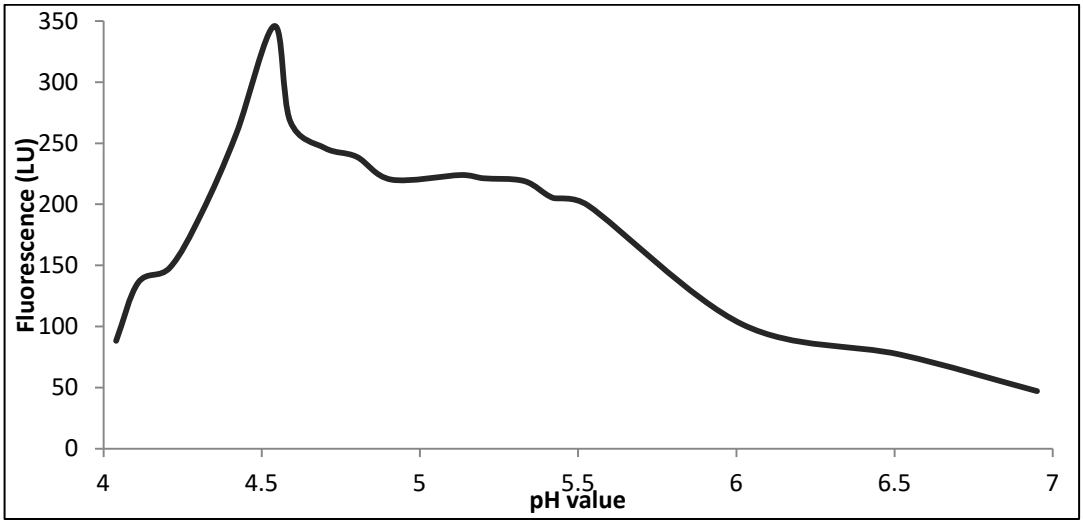

Figure 4.60. pH optimization of PtXTH3 enzyme between pH 4.0 to pH 7.0 using McIlvaine buffer.

pH optimization with ammonium acetate buffer was performed between pH 4.0 to 5.5. TXG donors were prepared with ammonium acetate buffers at different pH values and they were used as donors in enzyme activity reaction. Amount of hybrid products were analysed and highest amount of hybrid TXG-XGO was observed at pH 5.0 (Figure 4.61). Thus, pH optima of PtXTH3 was concluded as pH 5.0. All of the characterization studies were carried at pH 5.0.

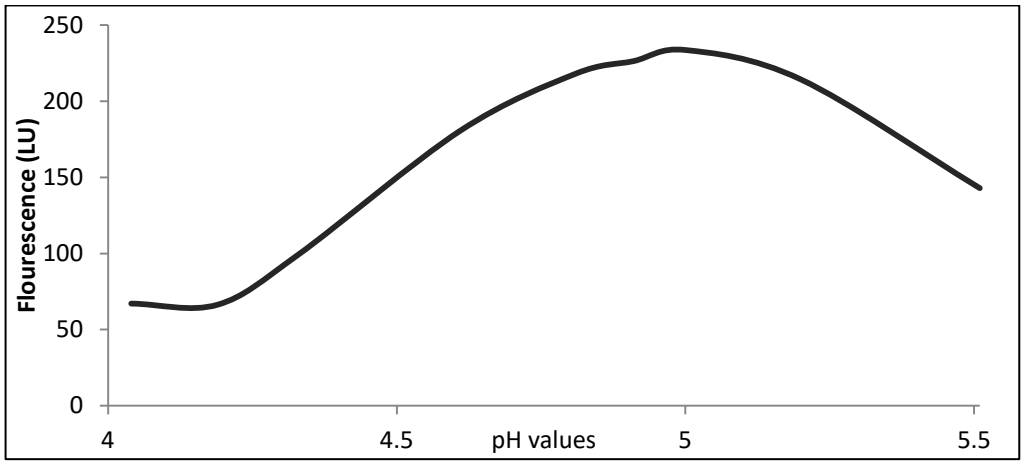

Figure 4.61. pH optimization of PtXTH3 enzyme between pH 4.0 to pH 5.5 using ammonium acetate buffer.

4.7.1.4. TaXTH5

TaXTH5 pH optimization study was carried using McIlvaine buffer between pH 4.0 to pH 8.0. TXG donors possessing different pH values were used in enzyme reaction tests and amounts of hybrid products produced by each TXG donor were measured by HPLC system. These hybrid product values were used to generate a pH optima plot (Figure 4.62). The highest amount of hybrid product was obtained with pH 6.4.

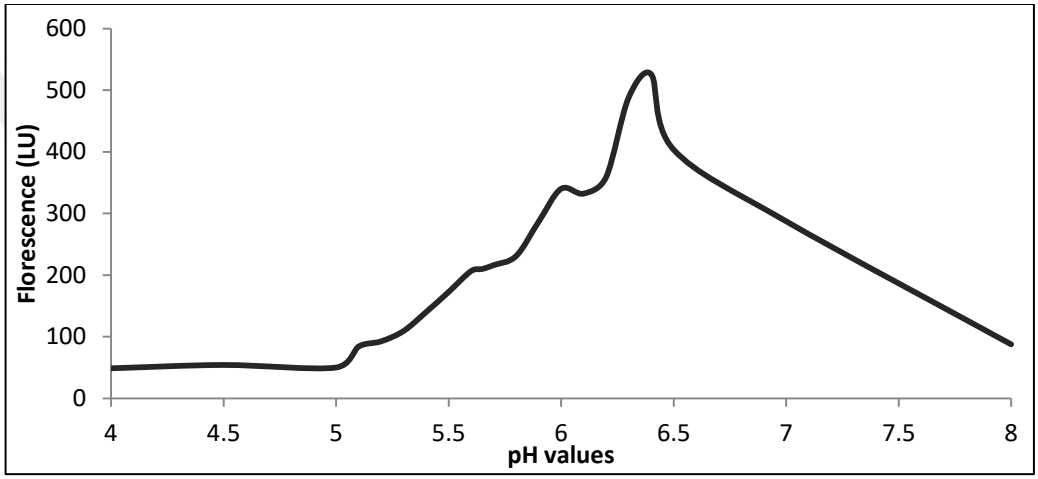

Figure 4.62. pH optimization of TaXTH5 enzyme between pH 4.0 to pH 8.0 using McIlvaine buffer.

4.7.2. Acceptor-Donor specificity

4.7.2.1. AtXTH3

Heterologously produced and purified AtXTH3 enzyme's substrate specificity characterization was carried at pH5.5 since this pH value is pH optima for AtXTH3. Different donor-acceptor couples were screened as possible substrates for AtXET3's XET activity and it was observed that AtXET3 can catalyse endotransglycosylation between many different donors and acceptors (Table 4.11). Donor-acceptor couples indicated as positive target for AtXTH3's XET activity were used in time interval studies.

Table 4.11. Donor-acceptor couples that AtXTH3 can use as substrate in endotransglycosylation. Acceptor names are given in the first raw and donor names are given in the first column. (+) sign indicate AtXTH3 is active on that specific substrate couple whereas (-) indicated AtXTH3 is not active on that specific substrate couple. Empty cells indicate that those couples haven't been checked.

	BA	**BB**	**BC**	**CT**	**LT**	**XT**	**X7**	**XGO**
TXG	+	+	+	+	+	+	+	+
BBG	+	+	+	+	+	+	+	+
HEC	+	+	+	+	+	+	+	+
WA								-
KM								+
MC							+	+
CMC							+	+

4.7.2.2. AtXTH4

AtXTH4-9 enzyme was used in AtXTH4 acceptor-donor specificity studies. 8 different donors (BBG, WA, LG, CM, GM, KM, TXG, HEC) and 11 different acceptors (BA, BB, BC, GM, CT, DGM, MT, LT, X7, XT, XGO), giving 88 substrate couple, were used. The enyzme showed XET activity with the acceptor-donor couples given in table 4.12.

Table 4.12. Acceptor-donor couples AXTH4 is showing XET activity with.

TXG-BA	TXG-BB	TXG-BC	TXG-CT	TXG-GM	TXG-DGM	TXG-MT	TXG-LT	TXG-X7	TXG-XT	TXG-XGO
HEC-BA	HEC-BB	HEC-BC	HEC-CT	HEC-GM	HEC-DGM	HEC-MT	HEC-LT	HEC-X7	HEC-XT	HEC-XGO

Second time produced and polished AtXTH4-18 was also used in substrate specificity trials and results revealed a different matrix (Table 4.13). The difference between first enzyme's ad second enzyme's substrate specificity can be due to difference in enzyme purity and concentration.

Table 4.13. Acceptor-donor couples AXTH4 (2nd product) is showing XET activity with.

TXG-BA	TXG-BB	TXG-BC	TXG-CT	TXG-GM	TXG-LT	TXG-X7	TXG-XT	TXG-XGO
HEC-BA	HEC-BB	HEC-BC	HEC-CT	HEC-GM	HEC-LT	HEC-X7	HEC-XT	HEC-XGO
BBG-CT	BBG-XT	BBG-XGO	BBG-X7	BBG-BA	BBG-BB	WA-CT	WA-X7	

Third time produced AtXTH4-18 enzyme was investigated for substrate specificity prior to enzymatic analyses and resulted in showing activity on TXG-X7, TXG-XGO, TXG-BA, TXG-BB, TXG-BC, TXG-CT, HEC-X7, HEC-XGO, HEC-CT acceptor-donor couples. Enzyme didn't show any activity with BBG, WA, GM, KM or LT donors. Thus, enzyme characterization studies were carried using these donor-acceptor couples.

4.7.2.3. GhXTH2

GhXTH2 enzyme was tested using 8 different donors and 11 different acceptors to reveal substrate specificity of the enzyme. Activity tests result in a wide range of substrate usage comprising TXG, HEC and BBG donors (Table 4.14).

Table 4.14. Donor-acceptor couples GhXTH2 enzyme is showing activity with.

TXG-BA	TXG-BB	TXG-BC	TXG-CT	TXG-GM	TXG-XT
TXG-X7	TXG-XGO	HEC-BB	HEC-BC	HEC-CT	HEC-XT
HEC-X7	HEC-XGO	BBG-BB	BBG-X7	BBG-XGO	

Specific enzyme activity trials were carried using donor-acceptor couples mentioned in Table X for GhXTH2 characterization.

4.7.2.4. PtXTH3

Heterologously synthesized and purified PtXTH3 enzyme Pool 1 was used activity tests with different donor-acceptor combinations in order to reveal substrate couples enzyme shows activity with. Activity test results were analysed by HPLC and donor-acceptor couples' enzyme can catalyse endotransglcyosylation between are given in Table 4.15. These donor-acceptor couples were further used in time interval studies for enzyme specific activity calculations.

Table 4.15. Matrix of donors and acceptors used in enzyme activity test with PtXTH3. Substrate couples PtXTH3 enzyme is showing activity with are indicated with '+' sign.

	BA	**BB**	**BC**	**CT**	**LT**	**GM**	**DGM**	**MT**	**XT**	**X7**	**XGO**
TXG	+	+	+	+	+	+	-	-	+	+	+
BBG	+	+	+	+	+	+	-	-	+	+	+
HEC	+	+	+	+	+	+	-	-	+	+	+
WA											-
KM											+

4.7.2.5. TaXTH5

Heterologous expression trials for TaXTH5 were carried for a couple of times. Enzyme produced and purified at second batch was used to investigate substrate preference of TaXTH5 enzyme. TXG, BBG, HEC and WA donors were coupled with BA, BB, BC, CT, XT, GM, DGM, MT, XT ,X7 and XGO acceptors and KM, CM, GM and LG donors were coupled only with XGO acceptor during enzyme activity analysis and used as substrate couples. Produced hybrid products were analysed via HPLC system. Enzyme catalysed endotransglycosylation reactions between TXG donor and BB, CT , X7 and XGO acceptors and HEC donor and BB, X7 and XGO acceptors. However, TaXTH5 didn't catalysed endotransglycosylation between HEC,BBG, WA, KM, CM, GM, LG donors and any acceptors tested. Thus, characterization was carried with TXG and HEC donors and BB, CT, X7 and XGO acceptors.

4.7.3. Substrate specificity analysis

Substrate specificity calculations per each substrate couple were carried by analysing amount of product produced by the enzyme within a given time. At least 4 time points, one of them being 0 time point, were used for all enzyme and substrate couples in order to achieve a linear increase in hybrid product amount through screened time intervals for a reliable reaction rate and reaction specific activity calculation.

4.7.3.1. AtXTH3

AtXTH3 enzyme has a wide substrate specificity through many couples. 28 different donor-acceptor couples were used with at least 4 different time intervals and as at least 3 repeats. Amount of hybrid products produced during enzyme activity tests were quantified by HPLC system and plotted in graph to visualize linear increase in product amount throughout the analysis period (Figure 4.63). Amount of hybrid product generated for one time point for each acceptor-donor couple was chosen and converted into pkatal / mg protein specific activity (Table 4.16).

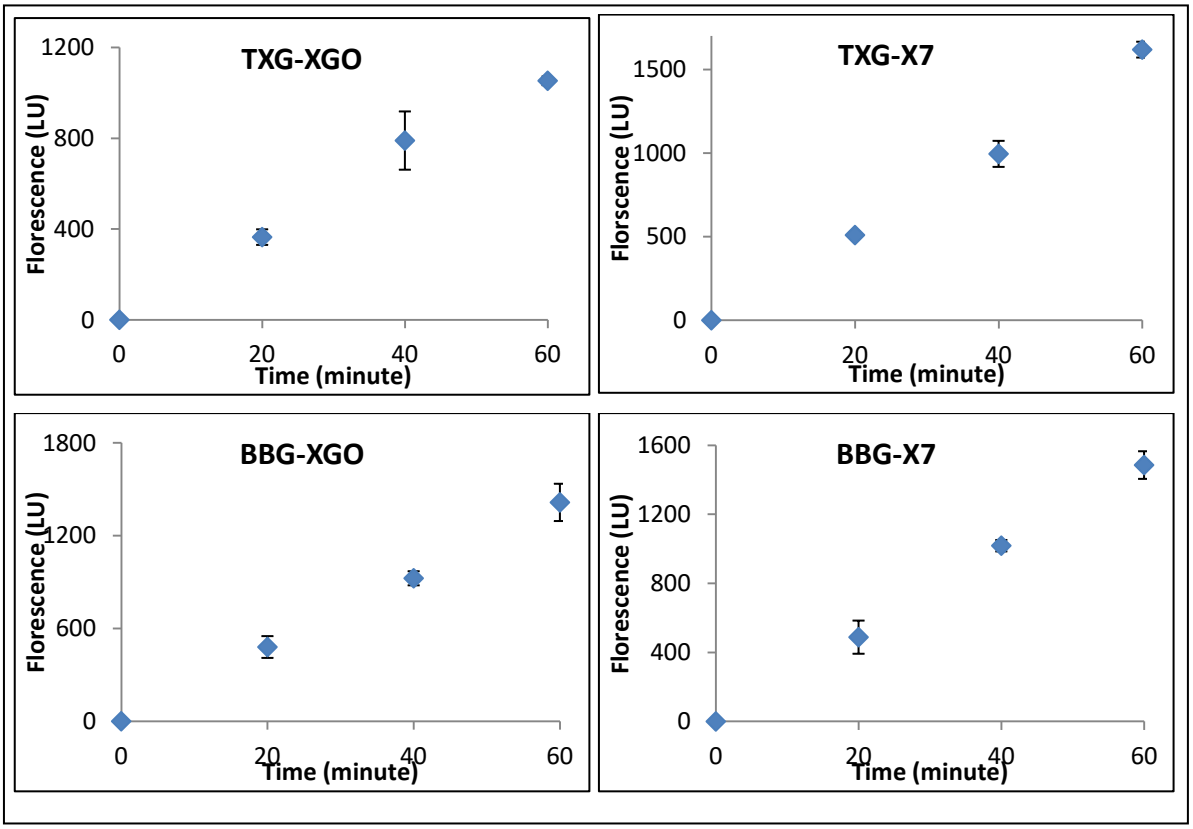

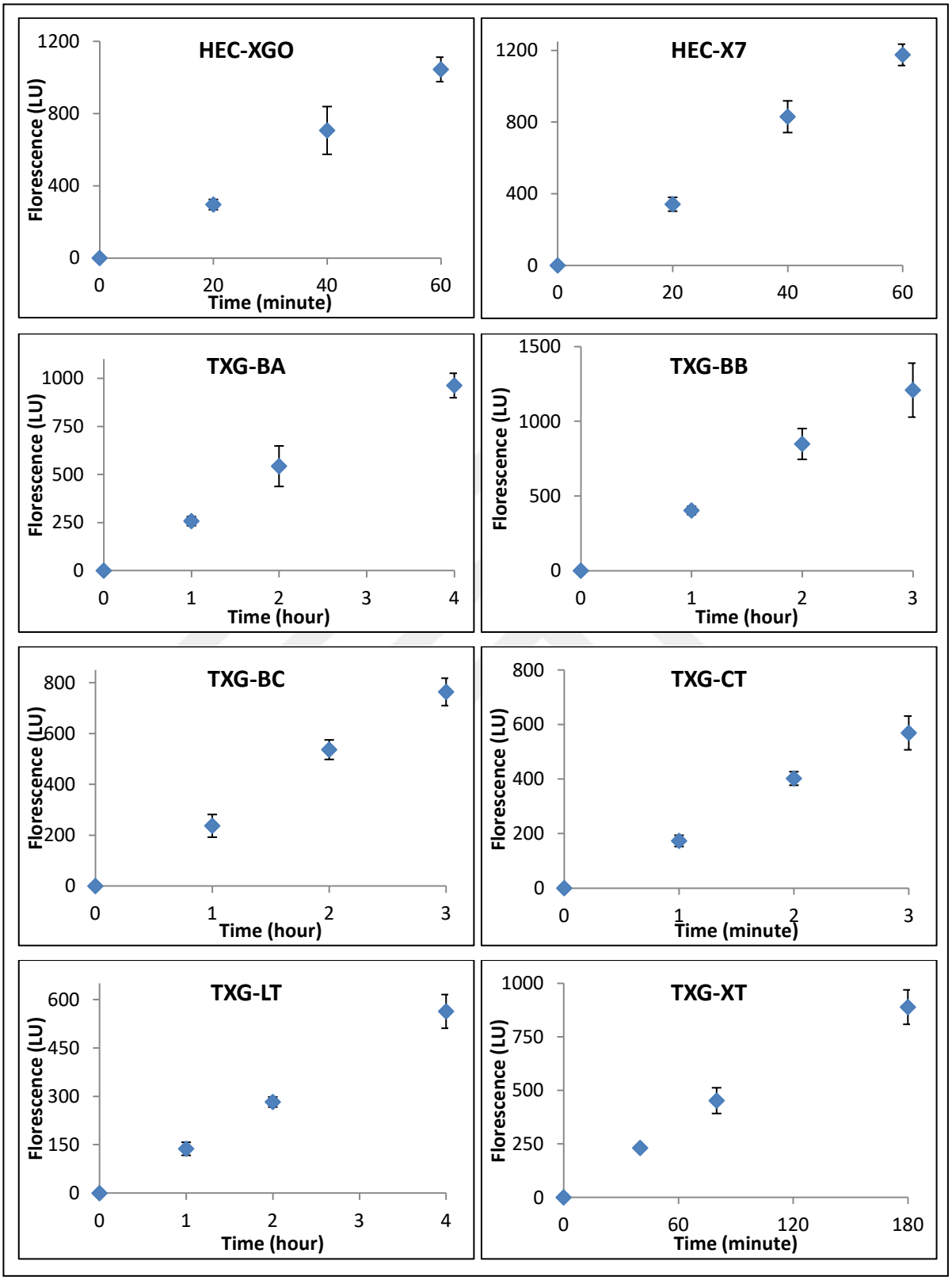
HEC-XGO
Florescence (LU)
1200
800
400
0
0
20
40
60
Time (minute)
HEC-X7
1200
800
400
0
0
20
40
60
TXG-BA
Florescence (LU)
1000
750
500
250
0
0
1
2
3
4
Time (hour)
TXG-BB
Florescence (LU)
1500
1000
500
0
0
1
2
3
Time (hour)
TXG-BC
Florescence (LU)
800
600
400
200
0
0
1
2
3
Time (hour)
TXG-CT
Florescence (LU)
800
600
400
200
0
0
1
2
3
Time (minute)
TXG-LT
Florescence (LU)
600
450
300
150
0
0
1
2
3
4
Time (hour)
TXG-XT
Florescence (LU)
1000
750
500
250
0
0
60
120
180
Time (minute)

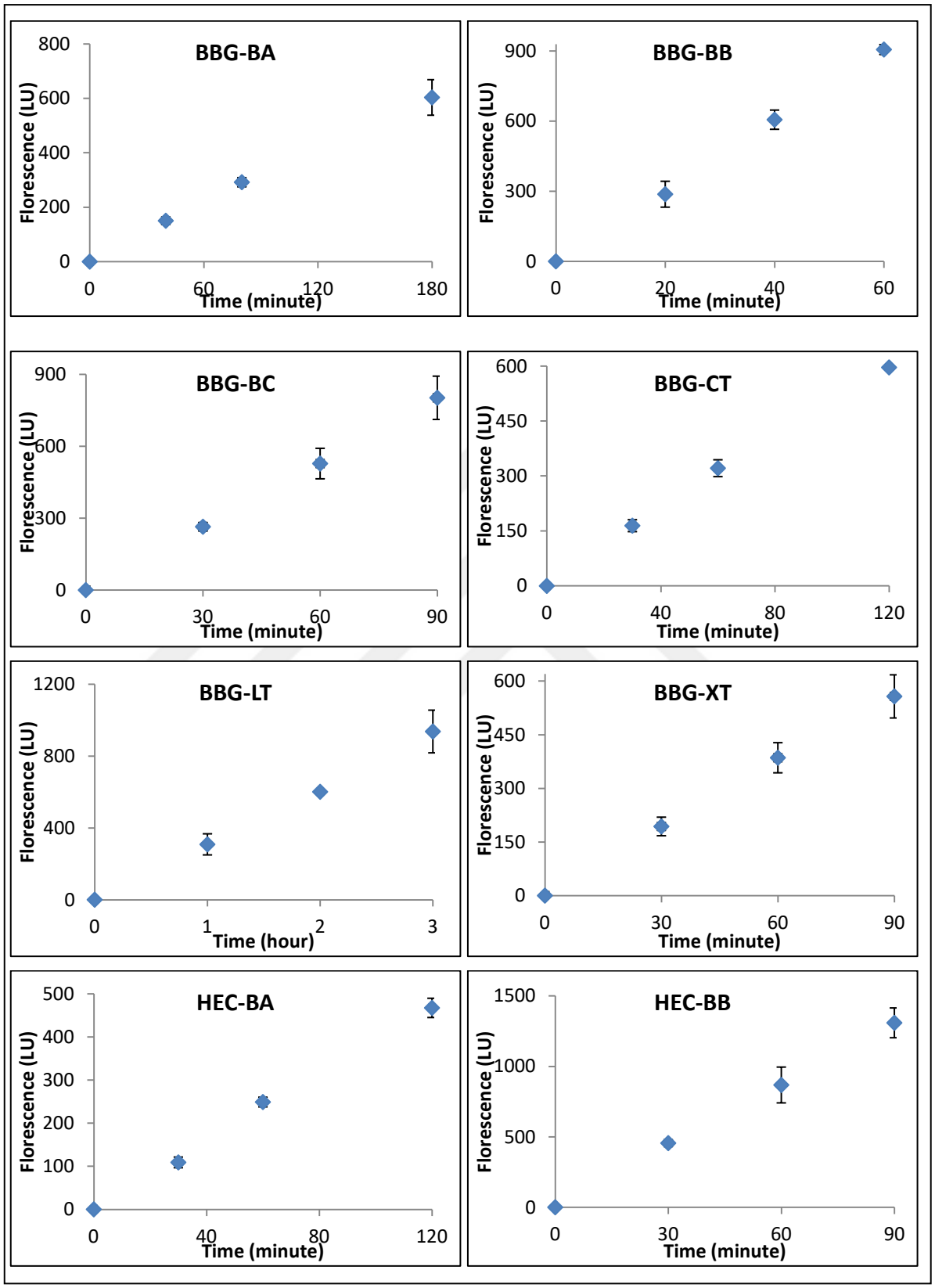
BBG-BA
Florescence (LU)
800
600
400
200
0
0
60
120
180
Time (minute)
BBG-BB
Florescence (LU)
900
600
300
0
0
20
40
60
Time (minute)
BBG-BC
Florescence (LU)
900
600
300
0
0
30
60
90
Time (minute)
BBG-CT
Florescence (LU)
600
450
300
150
0
0
40
80
120
Time (minute)
BBG-LT
Florescence (LU)
1200
800
400
0
0
1
2
3
Time (hour)
BBG-XT
Florescence (LU)
600
450
300
150
0
0
30
60
90
Time (minute)
HEC-BA
Florescence (LU)
500
400
300
200
100
0
0
40
80
120
Time (minute)
HEC-BB
Florescence (LU)
1500
1000
500
0
0
30
60
90
Time (minute)

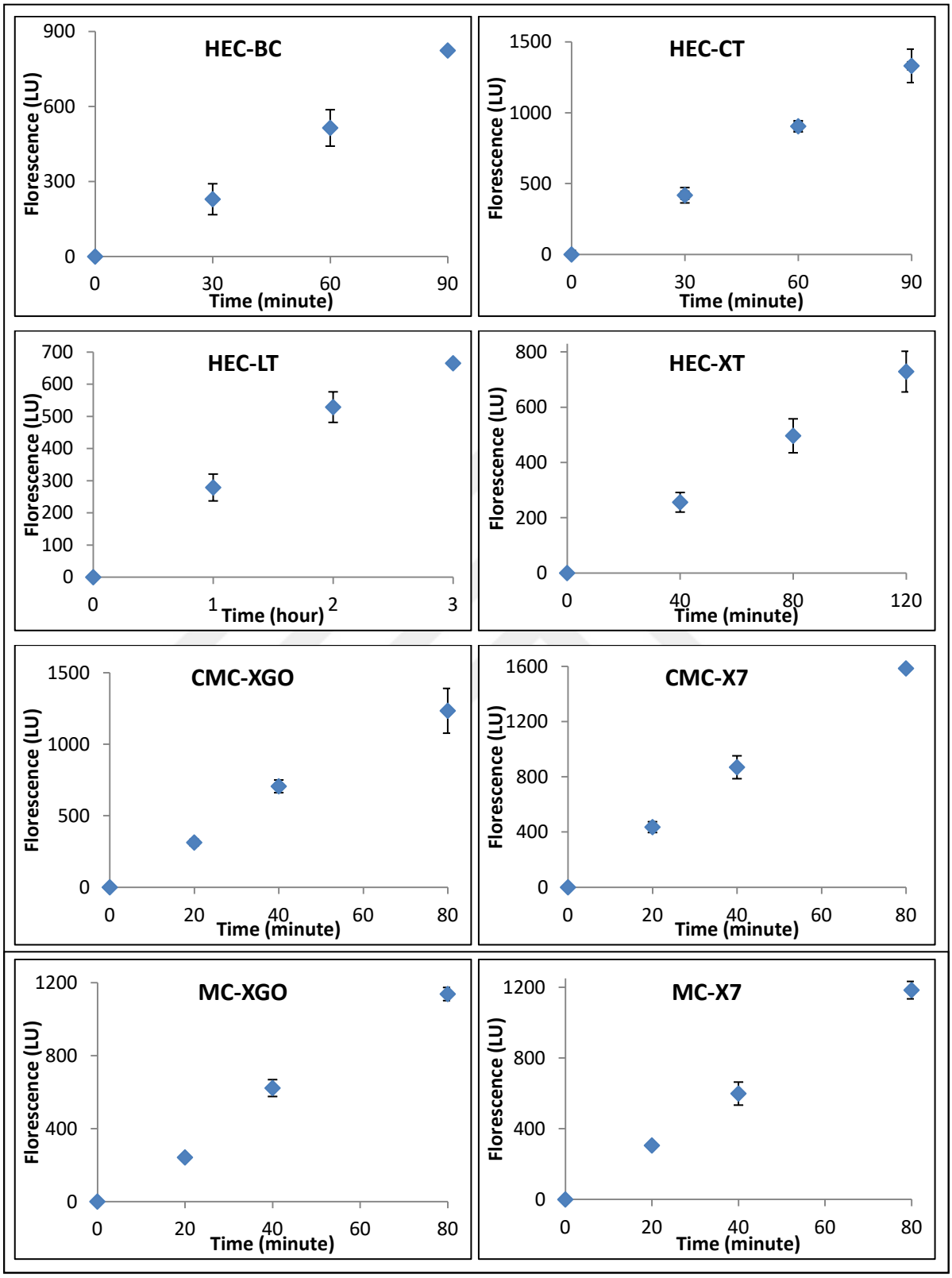

Figure 4.63. Time interval enzyme activity studies of AtXTH3 with different donor-acceptor couples. Florescence amounts of generated hybrid products were studied by HPLC. Donor-acceptor couples and error bars are indicated on graphs.

Table 4.16. Specific enzyme activity of AtXTH3 on various donor-acceptor couples and ratios of specific activities to TXG-XGO, BBG-XGO and HEC-XGO couples' activities.

	Pkatal/mg protein	**per centTXG-XGO**	**per centBBG-XGO**	**per centHEC-XGO**
TXG-XGO	0.842	100.00		
TXG-X7	0.998	118.52		
TXG-BA	0.063	7.47		
TXG-BB	0.396	47.02		
TXG-BC	0.193	22.97		
TXG-CT	0.188	22.28		
TXG-LT	0.028	3.33		
TXG-XT	0.072	8.56		
BBG-XGO	2.773	329.12	100.02	
BBG-X7	2.392	284.00	86.31	
BBG-BA	0.101	12.05	3.66	
BBG-BB	0.849	100.83	30.64	
BBG-BC	0.381	45.22	13.74	
BBG-CT	0.300	35.61	10.82	
BBG-LT	0.060	7.08	2.15	
BBG-XT	0.082	9.73	2.96	
HEC-XGO	2.043	242.46		100.02
HEC-X7	2.033	241.38		99.58
HEC-BA	0.115	13.69		5.65
HEC-BB	0.810	96.16		39.67
HEC-BC	0.353	41.90		17.29
HEC-CT	0.338	40.10		16.54
HEC-LT	0.105	12.47		5.15
HEC-XT	0.079	9.40		3.88
CMC-XGO	2.055	244.01		
CMC-X7	2.897	343.89		
MC-XGO	1.996	236.89		
MC-X7	2.031	241.09		

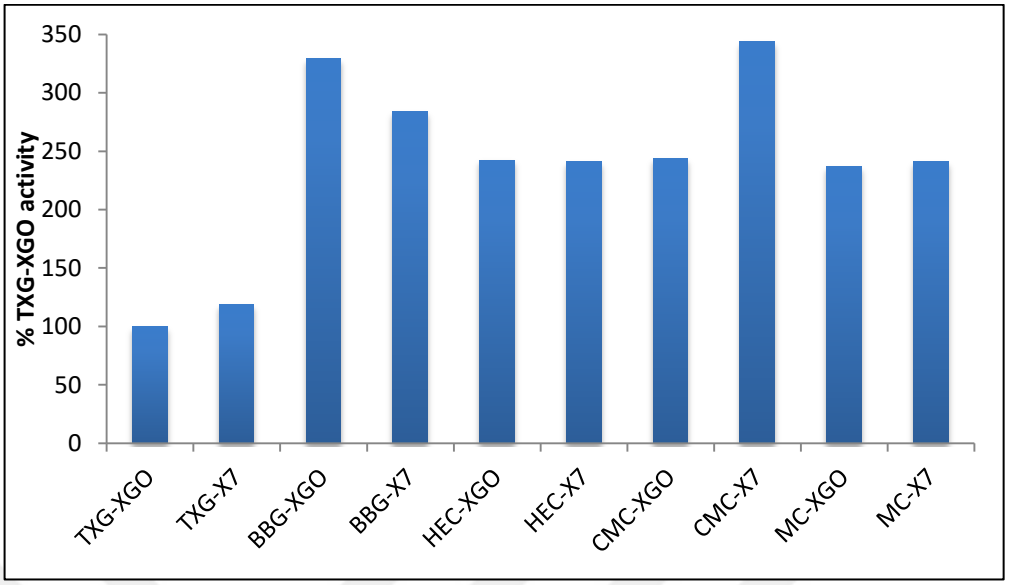

Figure 4.64. Activity ratio pf AtXTH3 on various donors and X7 and XGO acceptors compared to TXG-XGO specific activity value.

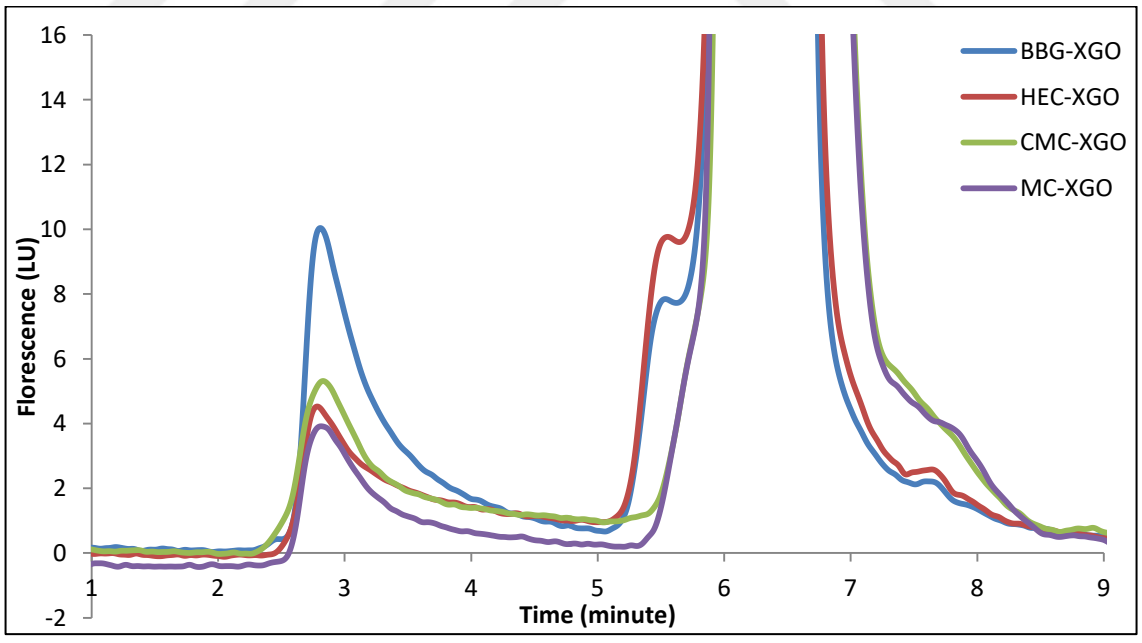

Figure 4.65. HPLC chromatograms of AtXTH3 enzyme activity reactions with BBG-XGO, HEC-XGO, CMC-XGO and MC-XGO substrate couples for 20 minutes of incubation.

AtXTH3 enzyme is a member of ancestral clade in XTH phylogenetic tree. It is known that Group I and Group II members are true and dominant XET enzymes, capable of showing relatively low activity on other donor-acceptor couples. Surprisingly, being an ancestral clade member, AtXTH3 enzyme shows higher specific activity with mixed-linked glucan (BBG) and cellulose analogues (HEC, CMC, MC) donors (Figure 4.64, Figure 4.65). Enzyme's activity on TXG-XGO and BBG-BB, HEC-BB couples are almost equal. These data suggest, AtXTH3 enzyme has a very unique activity pattern as a XET enzyme. AtXTH3 catalyse endotransglycosylation reaction between BBG donor and xyloglucan acceptor ~ 3 times faster than endotransglycosylation between xyloglucan donor and acceptors. Also, enzyme catalyses endotransglycosylation between cellulose analogue donor and xyloglucan acceptor ~2.4 times faster than endotransglycosylation between xyloglucan donor and acceptor.

During activity tests, three different cellulose analogues were used in order to analyse whether structural change in cellulose effect enzyme activity or not. Except, CMC-X7 couple, all cellulose analogues (HEC, CMC, MC) are showing same amount of activity with XGO acceptor.

Another interesting and curious point is, independent of donor used, AtXTH3 enzyme showed higher activity rate with BB acceptor when BA, BB and BC acceptors are compared using same donor. Enzyme prefer BA the least from these 3 acceptor. Difference between them is the 1,3-β-glycosidic bond position; in BA, it is at the 1^{st} position, in BB it is at the 3^{rd} position and in BC it is at the 2^{nd} position. Difference of 1,3-β-glycosidic bond effects glucotetraose chain structure by changing the 'kink' in the chain, thus it effects substrate binding to active site of AtXTH3. Since substrate binding and stability during substrate binding is effected, this process totally effects enzyme activity rate.

Alongside those interesting points about AtXTH3 enzyme, another curious result is endotransglycosylation reaction rate using HEC-CT substrate couple. Both HEC and CT are representing cellulose donor and acceptor within our studies and AtXTH3 is capable of using this donor-acceptor couple with a 40 per cent rate compared to TXG-XGO. This finding adds another question mark as to how this enzyme evolved and in which tissues, *AtXTH3* expression is seen in actual Arabidopsis plants.

Substrate specificity calculations revealed many interesting points about AtXTH3 enzyme. To be able to make more precise and real comparison between AtXTH3 and other enzymes and between different donors, kinetic values need to be calculated. Enzyme kinetics were further studied with TXG, BBG and HEC donors in order to make comparisons and enlighten catalytic capacity of AtXTH3 with different donors.

Firstly, optimum working concentrations of donor substrates were investigated by testing donor concentrations between 0.8 per cent w/v to 0.05 per cent w/v in activity tests with X7 acceptor. The donor concentration at which enzyme is producing the most hybrid molecule is optimum donor concentration for particular donor. Thus, hybrid TXG-X7, BBG-X7 and HEC-X7 product amounts were analysed by HPLC system and plotted on graphs (Figure 4.66). Enzyme activity showed a similar layout for all substrate couples tested. Amount of hybrid product amount increased exponentially for all three donors and reached maximum product amount with 0.6 per cent w/v donor. When donor concentration was further increase to 0.8 per cent w/v, this change didn't have a positive effect on reaction rate, on the contrary it caused a decrease in produced hybrid product amount for donors tested. This decrease in product amount compared to 0.6 per cent w/v donor can be a result of adverse effect caused by decrease in viscosity with increasing donor polysaccharide concentration. Thus, for proper kinetic studies, 0.6 per cent w/v TXG, BBG and HEC donors were used.

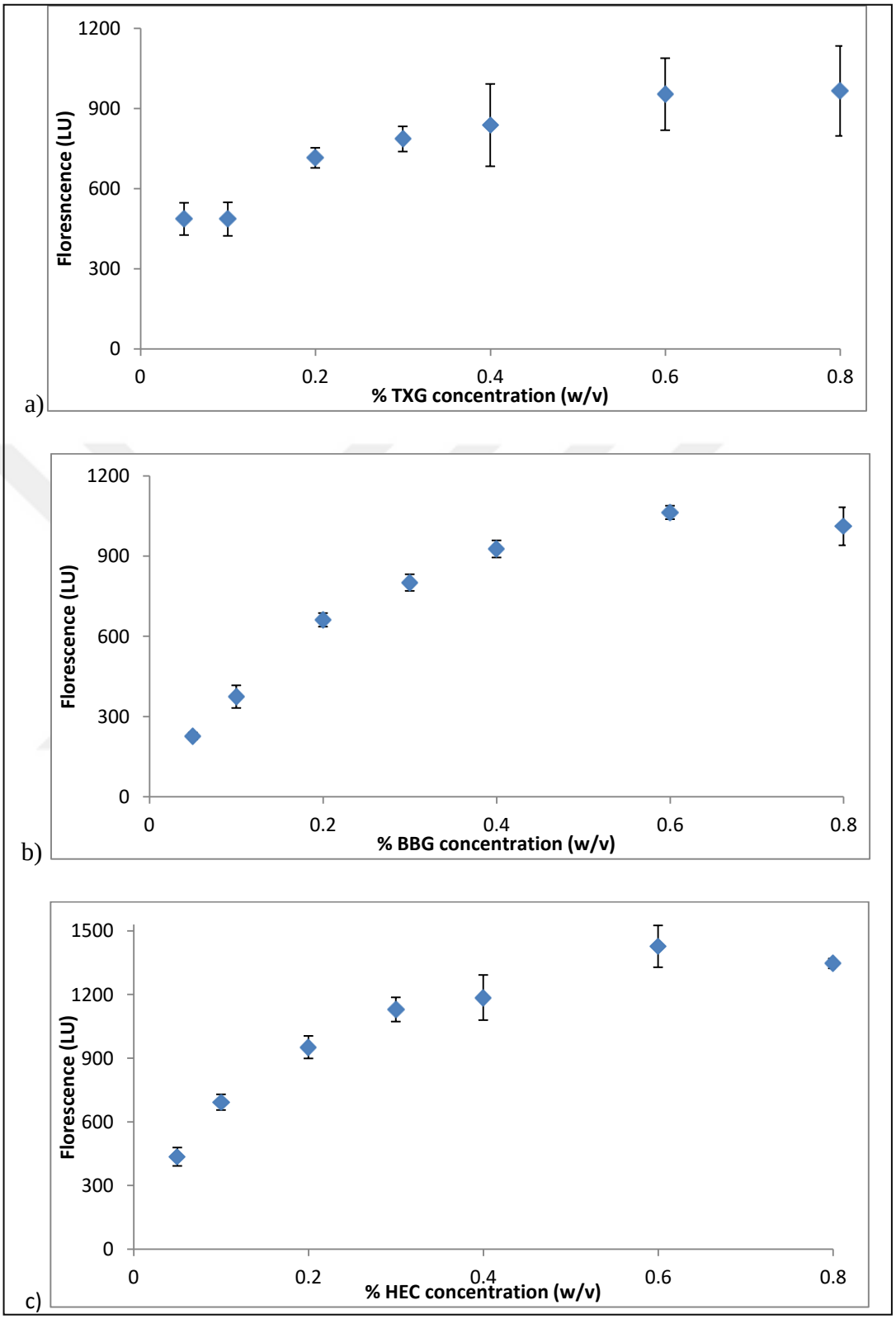

Figure 4.66. Effect of TXG, BBG and HEC donor concentrations on AtXTH3 enzyme activity amount via measurement of hybrid products generated.. a) Effect of TXG donor, b) Effect of BBG donor, c) Effect of HEC donor.

TXG-X7 kinetics were studied with 0.6 per cent w/v TXG concentration and various X7 concentrations ranging from 1 μM to 400 μM. Hybrid product amounts were measured by HPLC system and converted to reaction rate for each donor-acceptor couple (Table 4.17). Reaction rates versus X7 concentrations were plotted on a graph to give Michaelis-Menten graph of TXG-X7 substrate couple. With increasing X7 concentration, reaction rate started to increase until 80 μM X7 acceptor. Then, linearity started to bend and reaction rate reached a plateau phase after 250 μM X7 concentration (Figure 4.67). Michaelis-Menten plot was turned into Lineweaver-Burke graph for calculation of kinetic values (Figure 4.68). Using Lineweaver Burke graph and slope equation V_{max} was calculated as 0.036 μM/minute, K_m was calculated as 8.772 μM and K_{cat} as 0.014 min^{-1}.

Table 4.17. Enzyme activity rates of AtXTH3 with 0.6 per cent w/v TXG and various acceptor concentrations.

Final X7 concentration (μM)	**Stock X7 concentration (μM)**	**μM product / minute**
0.033	1	0.0004
0.133	4	0.0006
0.267	8	0.0014
0.533	16	0.0021
1.000	30	0.0035
1.333	40	0.0050
1.667	50	0.0065
2.333	70	0.0074
2.667	80	0.0086
3.333	100	0.0103
4.000	120	0.0120
5.000	150	0.0136
6.667	200	0.0159
8.333	250	0.0179
10.000	300	0.0186
11.667	350	0.0190
13.333	400	0.0194

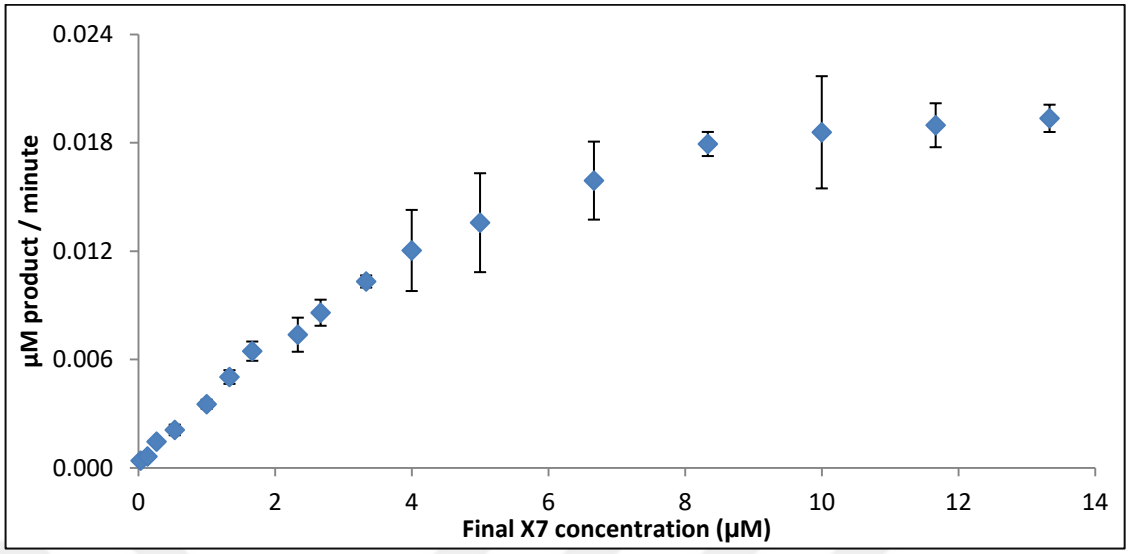

Figure 4.67. AtXTH3 enzyme 0.6 per cent w/v TXG and various X7 concentrations reaction rate Michaelis-Menten plot.

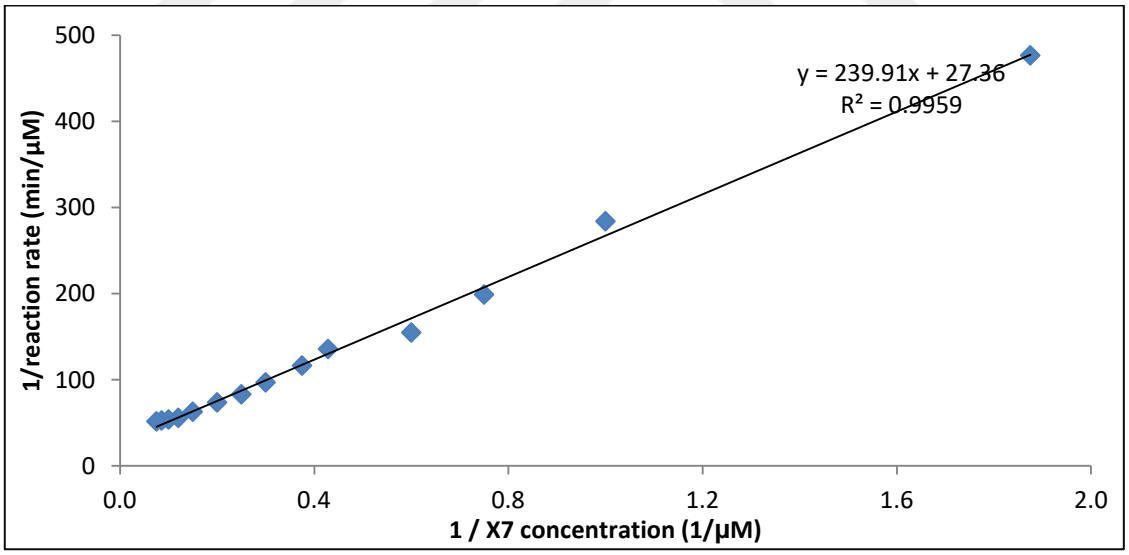

Figure 4.68. AtXTH3 enzyme 0.6 per cent w/v TXG and various X7 concentrations reaction rate Lineweaver-Burke plot.

Another set of enzyme kinetic measurements and calculations were done in order to find out preference of AtXTH3 for BBG-X7 substrate couple. As a donor, 0.6 per cent w/v BBG was used and 15 different X7 concentration were used between 1 µM X7 to 300 µM

X7. Amount of hybrid product produced within a certain time period was measured for each donor-acceptor couple and these values were converted to reaction rate for each X7 concentration (Table 4.18). By plotting these values on a graph, Michaelis-Menten plot was obtained (Figure 4.69). AtXTH3 reaction rate with BBG-X7 substrate couple reaches a plateau phase after 150 μM X7 concentration. Reaction rate values were used to prepare a Lineweaver-Burke plot (Figure 4.70) and by using Lineweaver-Burke plot, kinetic values were calculated. AtXTH3 enzyme's V_{max} for BBG-X7 donor acceptor couple is 0.036 μM/minute, K_m is 8.391 μM and K_{cat} is 0.258 min^{-1}.

Table 4.18. Enzyme activity rates of AtXTH3 with 0.6 per cent w/v BBG and various acceptor concentrations.

Final X7 concentration (μM)	**Stock X7 concentration (μM)**	**μM product / minute**
0.033	1	0.0003
0.067	2	0.0003
0.167	5	0.0011
0.267	8	0.0013
0.400	12	0.0014
0.533	16	0.0019
0.667	20	0.0031
1.000	30	0.0051
1.333	40	0.0056
1.667	50	0.0077
2.667	80	0.0085
3.333	100	0.0100
5.000	150	0.0111
6.667	200	0.0118
8.333	250	0.0113

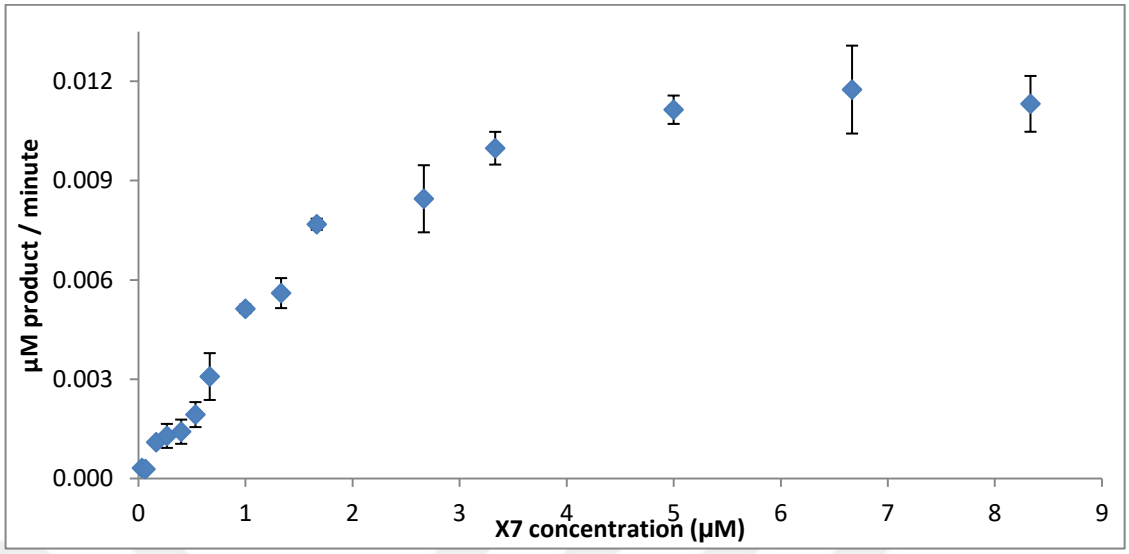

Figure 4.69. AtXTH3 enzyme 0.6 per cent w/v BBG and various X7 concentrations reaction rate Michaelis-Menten plot.

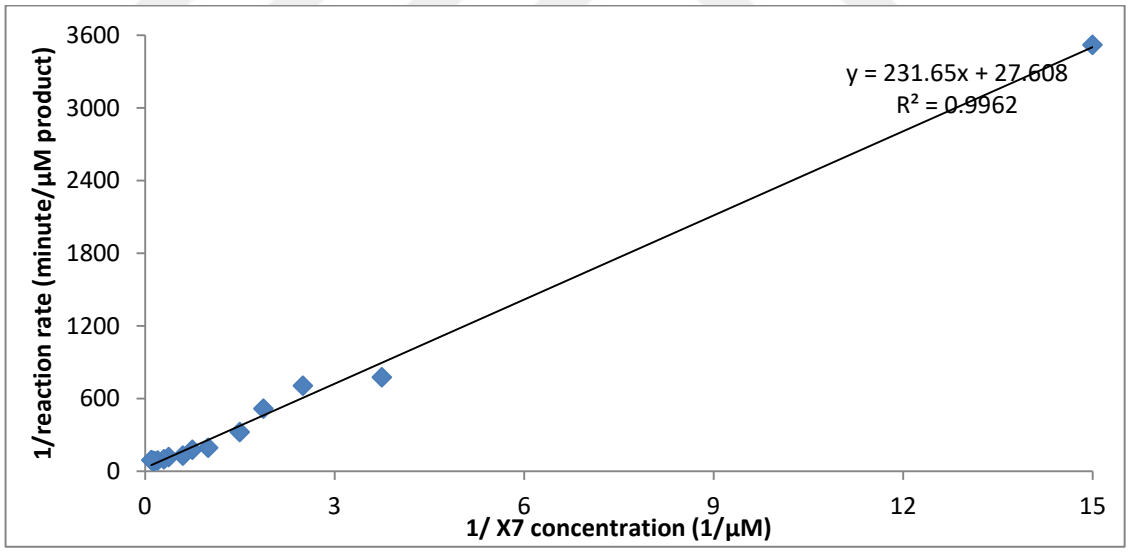

Figure 4.70. AtXTH3 enzyme 0.6 per cent w/v BBG and various X7 concentrations reaction rate Lineweaver-Burke plot.

HEC-X7 kinetics were studied with 17 different X7 concentrations ranging from 1 µM to 250 µM. Reaction rates for each X7 concentration were calculated (Table 4.19) and used to plot a Michaelis-Menten graph. Reaction rate of AtXTH3 reaches a plateau phase after 120

μM X7 concentration (Figure 4.71). Reaction rates and X7 concentrations were used to draw Lineweaver-Burke plot and slope equation of Lineweaver-Burke plot was used to do calculations of kinetic values (Figure 4.72). AtXTH3 enzyme's HEC-X7 donor-acceptor couple V_{max} value is 0.015 μM/minute, K_m value is 4.579 μM and K_{cat} value is 0.109 min^{-1} (Table 4.20).

Table 4.19. Enzyme activity rates of AtXTH3 with 0.6 per cent w/v HEC and various acceptor concentrations.

Final X7 concentration (μM)	**Stock X7 concentration (μM)**	**μM product / minute**
0.033	1	0.0001
0.067	2	0.0002
0.133	4	0.0004
0.267	8	0.0010
0.400	12	0.0012
0.533	16	0.0016
0.667	20	0.0025
1.000	30	0.0028
1.333	40	0.0036
1.667	50	0.0043
2.333	70	0.0048
2.667	80	0.0052
3.333	100	0.0055
4.000	120	0.0062
5.000	150	0.0064
6.667	200	0.0064
8.333	250	0.0063

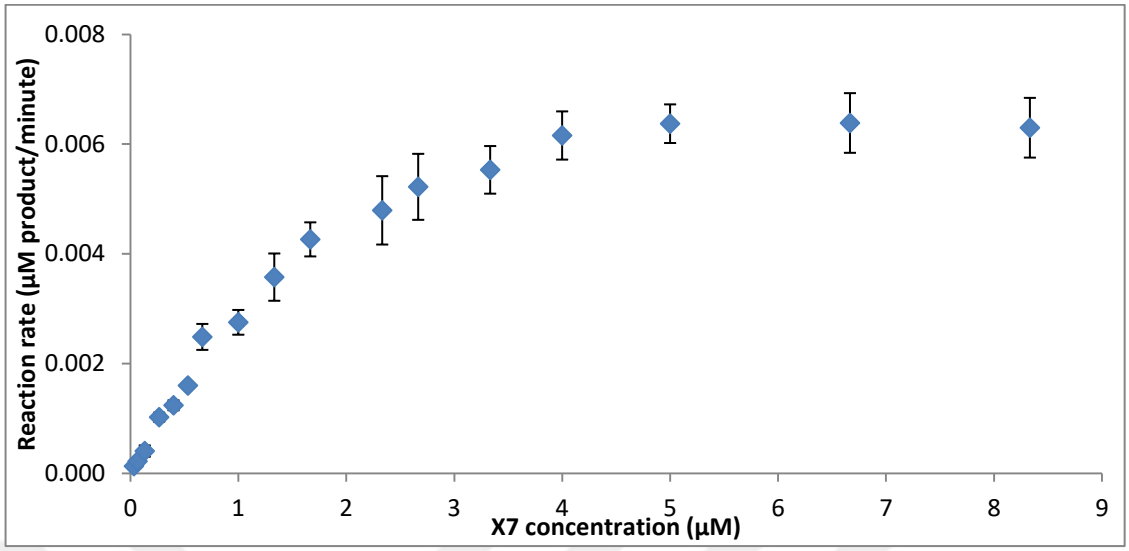

Figure 4.71. AtXTH3 enzyme 0.6 per cent w/v HEC and various X7 concentrations reaction rate Michaelis-Menten plot.

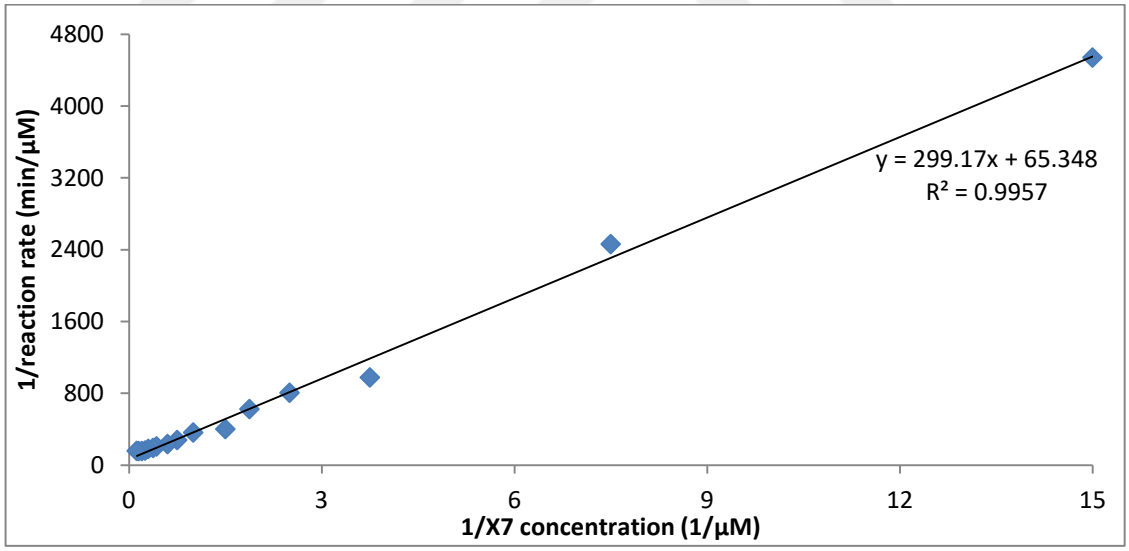

Figure 4.72. AtXTH3 enzyme 0.6 per cent w/v HEC and various X7 concentrations reaction rate Lineweaver-Burke plot.

Table 4.20. V_{max}, K_m and K_{cat} values of AtXTH3 reactions with TXG-X7, BBG-X7 and HEC-X7 donor-acceptor couples.

	V_{max} (µM/min)	**K_m (µM)**	**K_{cat} (min^{-1})**
TXG-X7	0.036	8.772	0.014
BBG-X7	0.036	8.391	0.258
HEC-X7	0.015	4.578	0.109

4.7.3.2. AtXTH4

AtXTH4-9 was used in substrate specificity studies in order to calculate AtXTH4 specific activity on different acceptor-donor couples. Time interval studies on donor-acceptor couples with 4 different time points were used. However, it was observed that enzyme lost activity in between trials.

AtXTH4-18 first production was used in time interval studies. It was observed that enzyme was showing low activity with TXG-CT, TXG-XT, HEC-BA, HEC-BB, HEC-BC, HEC-CT substrate couples to the contrary of seeing a wider range of substrate specificity with AtXTH4-9 enzyme. Thus, a new enzyme production was carried.

Second time produce AtXTH4-18 enzyme (June July 2014) was used in specific enzyme activity studies with various donor-acceptor couples. Trials were carried as 2 repeats and at least 4 different time points per each donor-acceptor couple and hybrid products produced by AtXTH4 XET activity were analysed using HPLC system florescence detector (Figure 4.73). Obtained data was converted to pkatals/mg enzyme specific enzyme activity (Table 4.21).

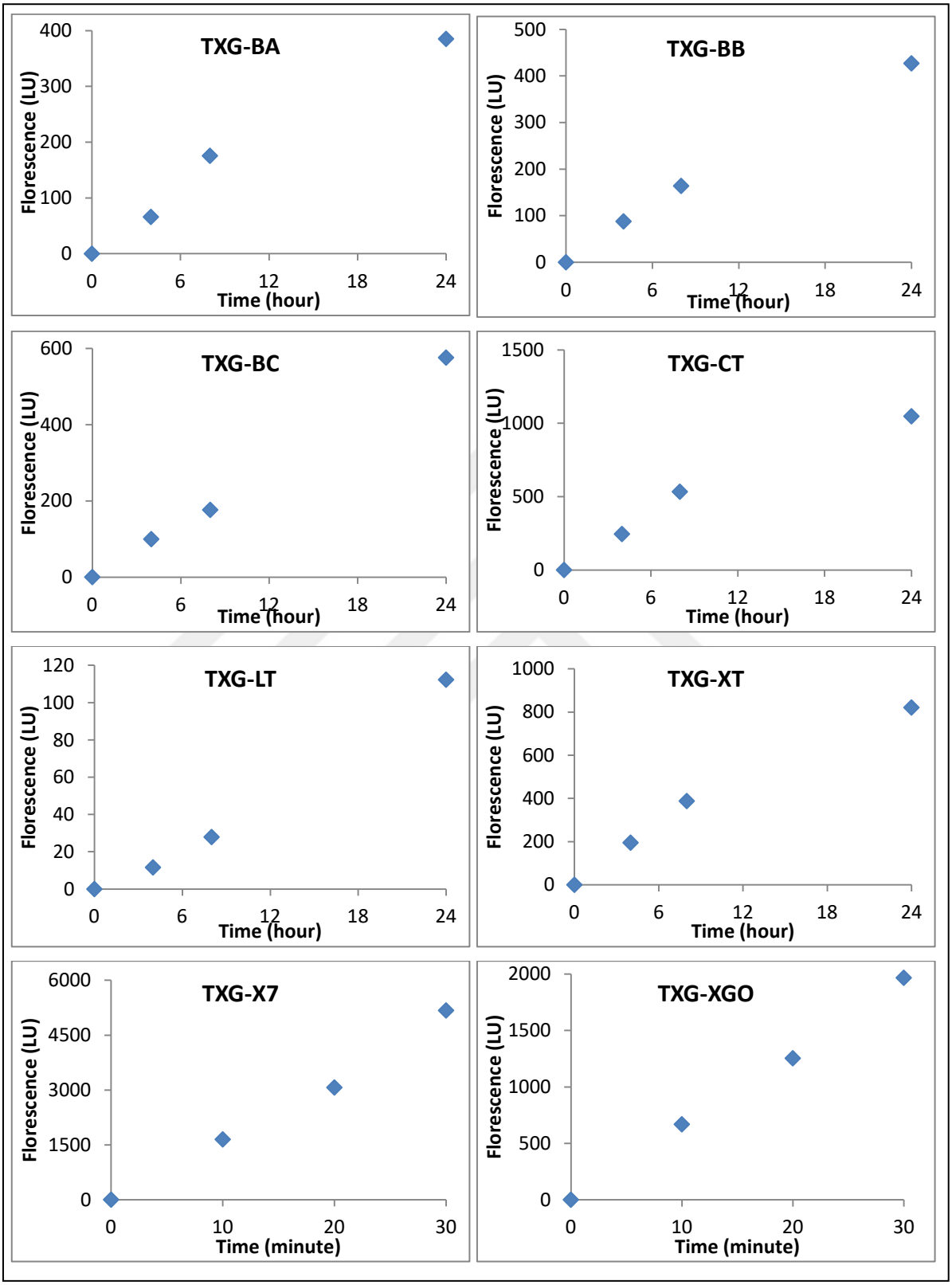
TXG-BA
Florescence (LU)
Time (hour)
TXG-BB
Florescence (LU)
Time (hour)
TXG-BC
Florescence (LU)
Time (hour)
TXG-CT
Florescence (LU)
Time (hour)
TXG-LT
Florescence (LU)
Time (hour)
TXG-XT
Florescence (LU)
Time (hour)
TXG-X7
Florescence (LU)
Time (minute)
TXG-XGO
Florescence (LU)
Time (minute)

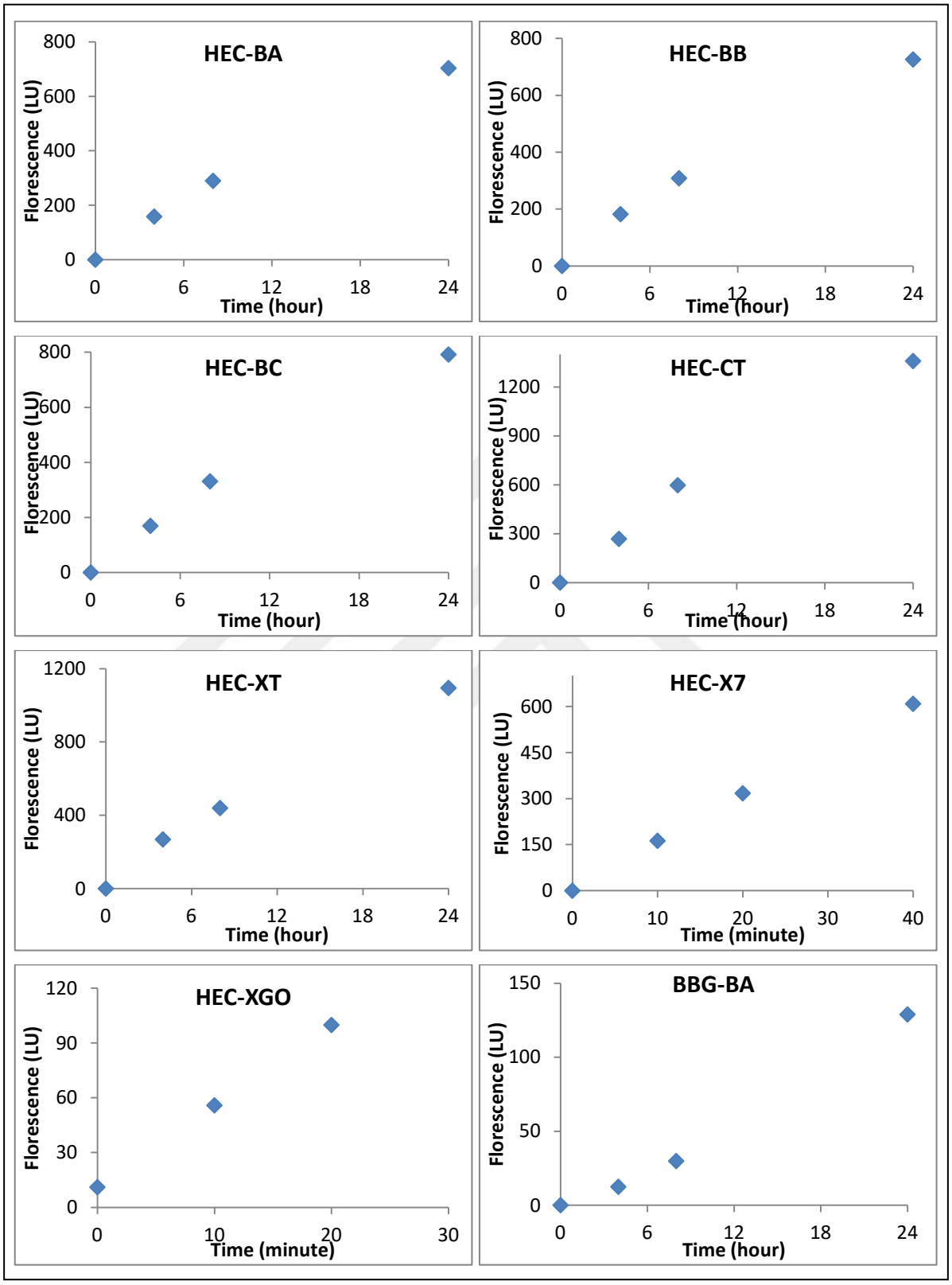
HEC-BA
Florescence (LU)
800
600
400
200
0
0
6
12
18
24
Time (hour)
HEC-BB
Florescence (LU)
800
600
400
200
0
0
6
12
18
24
Time (hour)
HEC-BC
Florescence (LU)
800
600
400
200
0
0
6
12
18
24
Time (hour)
HEC-CT
Florescence (LU)
1200
900
600
300
0
0
6
12
18
24
Time (hour)
HEC-XT
Florescence (LU)
1200
800
400
0
0
6
12
18
24
Time (hour)
HEC-X7
Florescence (LU)
600
450
300
150
0
0
10
20
30
40
Time (minute)
HEC-XGO
Florescence (LU)
120
90
60
30
0
0
10
20
30
Time (minute)
BBG-BA
Florescence (LU)
150
100
50
0
0
6
12
18
24
Time (hour)

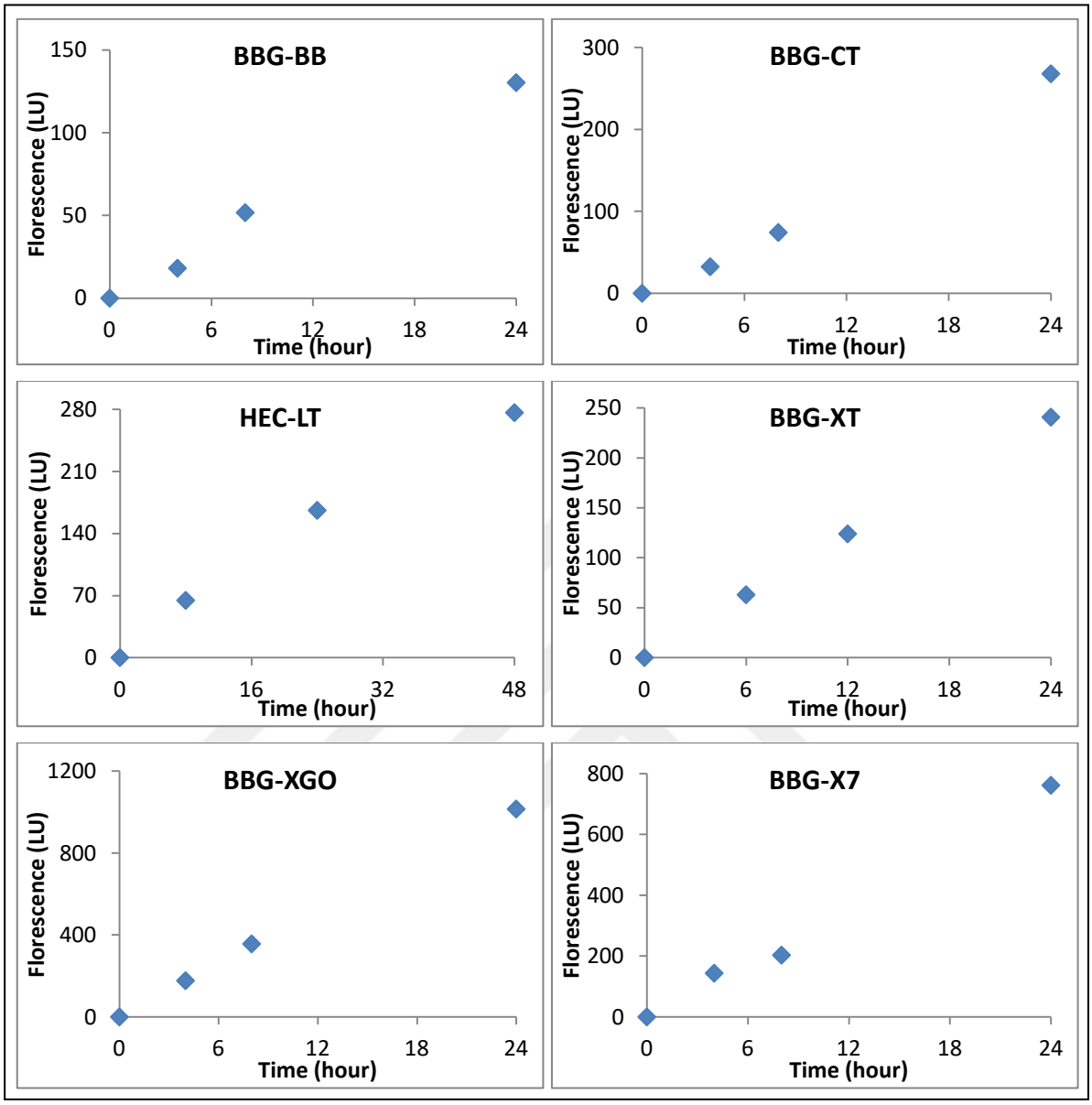

Figure 4.73. HPLC analysis of time interval AtXTH4 (second product) activity on different donor-acceptor couples. Florescence amounts of generated hybrid products were studied by HPLC. Donor-acceptor couples are indicated as graph titles.

Table 4.21. Specific activities as pkatals/mg enzyme of AtXTH4 (second product) on various donor-acceptor couples.

Donor-acceptor couple	pkatal/mg enzyme	per cent TXG-XGO activity
TXG-BA	0.136	0.044
TXG-BB	0.190	0.061
TXG-BC	0.123	0.040
TXG-CT	0.606	0.196
TXG-LT	trace	trace
TXG-XT	0.293	0.095
TXG-X7	304.041	98.157
TXG-XGO	309.750	100.000
HEC-BA	0.235	0.076
HEC-BB	0.390	0.126
HEC-BC	0.229	0.074
HEC-CT	0.856	0.276
HEC-LT	0.050	0.016
HEC-XT	0.405	0.131
HEC-X7	7.578	2.447
HEC-XGO	23.093	7.455
HEC-LT	0.060	0.019
BBG-BA	0.021	0.007
BBG-BB	0.048	0.016
BBG-CT	0.077	0.025
BBG-XT	0.007	0.002
BBG-XGO	0.337	0.109
BBG-X7	0.131	0.042

Specific enzyme activity data obtained from second product AtXTH4 enzyme is not enough for the studies because only 2 repeats were able to be performed and no further studies considering enzyme kinetics were done. Thus, another production of AtXTH4 was carried using AtXTH4-18 colony.

AtXTH4 specific enzyme activity studies were re-done using AtXTH4 produced for the third time. Experiments were carried out as 3 repeats and calculations were done for each repeat separately (Table 4.22). When these 3 repeats were compared with each other, it

was seen that there is a significant difference between them. Thus, it was concluded that these results were not reliable to be used.

Table 4.22. Specific activities as pkatals/mg enzyme of AtXTH4 (third product) on various donor-acceptor couples.

Donor-acceptor couple	**1st repeat**	**2nd repeat**	**3rd repeat**
TXG-BA	0.217	0.227	0.385
TXG-BB	0.508	0.342	0.618
TXG-BC	0.392	0.142	0.182
TXG-CT	0.486	0.713	0.870
TXG-LT	0.063	0.045	0.056
TXG-XT	0.291	0.456	0.903
TXG-X7	594.591	539.784	1219.570
TXG-XGO	618.855	740.339	939.837
HEC-BA	0.425	0.383	0.568
HEC-BB	0.875	0.522	1.231
HEC-BC	0.898	0.436	0.593
HEC-CT	1.011	1.909	1.042
HEC-XT	1.156	0.816	1.364
HEC-X7	42.143		19.275
HEC-XGO	28.125		18.087
HEC-LT	0.123	0.094	0.151
WA-XGO	0.047	0.186	0.208
WA-CT	0.043		
WA-X7		0.172	0.236
BBG-BA	0.090	0.092	0.106
BBG-BB	0.190	0.102	0.228
BBG-CT	0.291	0.506	0.334
BBG-XT	0.149	0.154	0.171
BBG-XGO	1.094	0.481	0.562
BBG-X7	0.728	0.556	0.846

AtXTH4 enzyme was synthesized by transformant *P. pastoris* cells for a 4th time and purified enzyme was used for characterization and kinetic studies. Enzyme activity assays were performed with TXG-X7, TXG-XGO, TXG-BA, TXG-BB, TXG-BC, TXG-CT, HEC-X7, HEC-XGO, HEC-CT donor-acceptor couples, using at least 3 different time points as at least 3 repeats (Figure 4.74). Hybrid product florescence amount was measured via HPLC system (Figure 4.75). Hybrid product amounts were used for pkatal/mg enzyme calculations (Table 4.23).

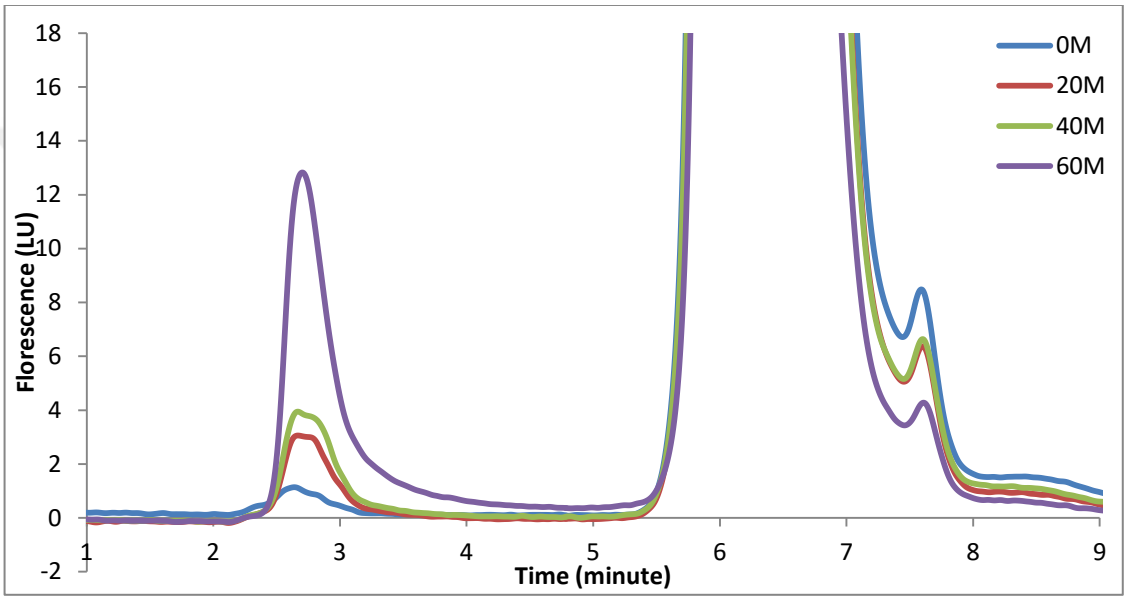

Figure 4.74. HPLC chromatogram of AtXTH4 time interval enzyme activity reaction using TXG-XGO substrate couple. Incubation times of each line is indicated on graph.

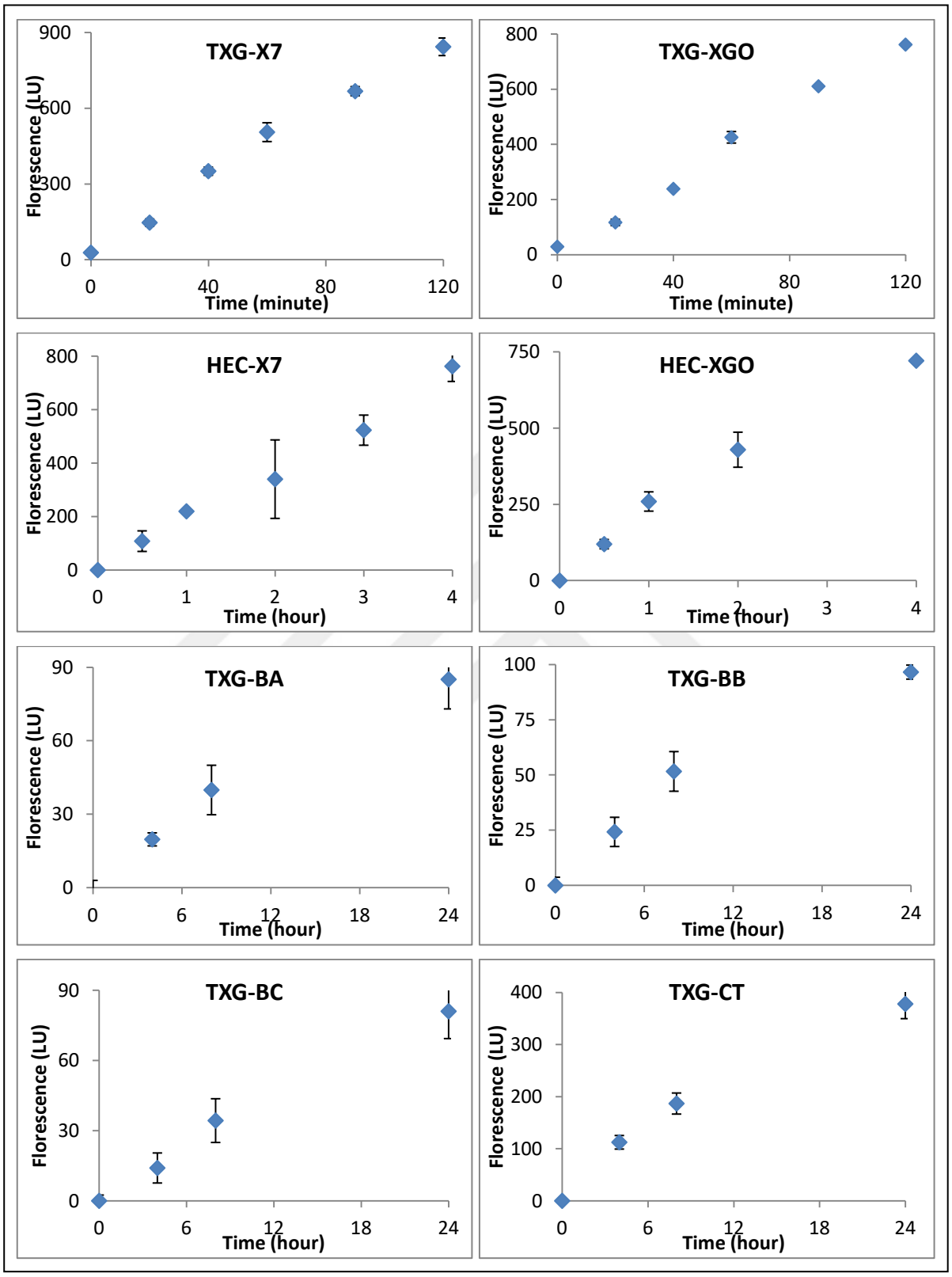
TXG-X7
Florescence (LU)
Time (minute)
TXG-XGO
Florescence (LU)
Time (minute)
HEC-X7
Florescence (LU)
Time (hour)
HEC-XGO
Florescence (LU)
Time (hour)
TXG-BA
Florescence (LU)
Time (hour)
TXG-BB
Florescence (LU)
Time (hour)
TXG-BC
Florescence (LU)
Time (hour)
TXG-CT
Florescence (LU)
Time (hour)

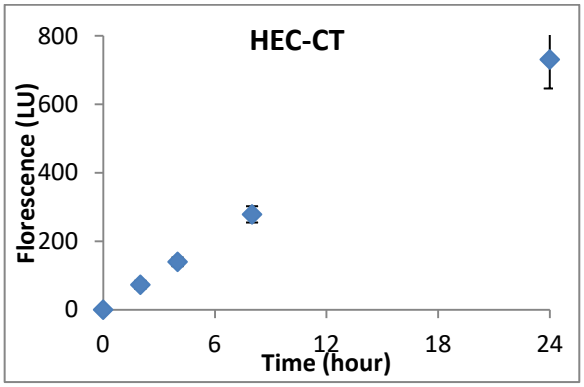

Figure 4.75. HPLC analysis of time interval AtXTH4 (fourth product) activity on different donor-acceptor couples. Florescence amounts of generated hybrid products were studied by HPLC. Donor-acceptor couples are indicated as graph titles.

Table 4.23. Specific activities as pkatals/mg enzyme of AtXTH4 (fourth product) on various donor-acceptor couples.

	pkatals/mg enzyme	**per centTXG-XGO**	**per centHEC-XGO**
TXG-X7	18.953	109.561	
TXG-XGO	17.299	100.000	
TXG-BA	0.020	0.117	
TXG-BB	0.027	0.157	
TXG-BC	0.015	0.085	
TXG-CT	0.093	0.536	
HEC-X7	1.168	6.752	88.795
HEC-XGO	1.315	7.604	100.000
HEC-CT	0.145	0.837	11.010

As a result of substrate specificity calculations, it was seen that AtXTH4 enzyme prefers xyloglucan as both acceptor and donor over other polysaccharides that are represented in the cell wall. On the other hand, AtXTH4 enzyme can bind and use HEC as donor too. AtXTH4 enzyme's specific activity on TXG-XGO couple is 17.29 pkatal/mg whereas its specific activity on HEC-XGO is 1.315 pkatak/mg. When these two values are compared, enzyme's HEC donor preference is 7.6 per cent enzyme's TXG donor preference. In

addition to using a cellulose analogue as a donor, AtXTH4 enzyme is capable of catalysing detectable amount of endotransglycosylation reaction between HEC cellulose analogue and CT acceptor, suggesting AtXTH4 enzyme can be able to modify cellulose backbone or it can have a role in coating and/or connecting cellulose microfibrils with xyloglucan chains. This opinion can be supported by enzyme's really low activity on TXG-CT couple compared to HEC-XGO couple. AtXTH4 enzyme also showed small amount of activity with BA, BB, BC acceptors. Enzyme can also connect xyloglucan chains to glucan chains with 1,3-β-glycosidic bond *in muro.*

Enzyme kinetics of AtXTH4 were studied using TXG and HEC as donors. Optimum donor concentrations of both TXG and HEC were studied because donor viscosity can have an indirect effect on enzyme kinetics due to their effect on reaction environment viscosity. Enzyme kinetics were studied with xyloglucan acceptor after donor concentrations were optimized to give the highest activity.

TXG concentrations between 0.4 per cent w/v to 0.05 per cent w/v and HEC concentrations between 0.4 per cent w/v to 0.05 per cent w/v were used in donor concentration optimization. AtXTH4 enzyme reaction with TXG-XGO donor-acceptor couple reach a plateau phase between 0.2 per cent and 0.4 per cent w/v donor concentration (Figure 4.76). Increasing donor concentration higher that 0.2 per cent w/v doesn't have significant increase in specific enzyme activity, thus 0.2 per cent w/v TXG was used in further kinetic studies (Table 4.24).

Table 4.24. AtXTH4 reaction rates on various TXG concentrations and 50 μM XGO.

Donor stock concentration (per cent w/v)	**Donor final concentration (per cent w/v)**	**Fluorescence of TXG-XGO hybrid molecule**	**uM product formed/min**
0.4	0.308	1531.8	0.025
0.2	0.154	1418	0.023
0.1	0.077	1090.9	0.018
0.05	0.038	841.7	0.014

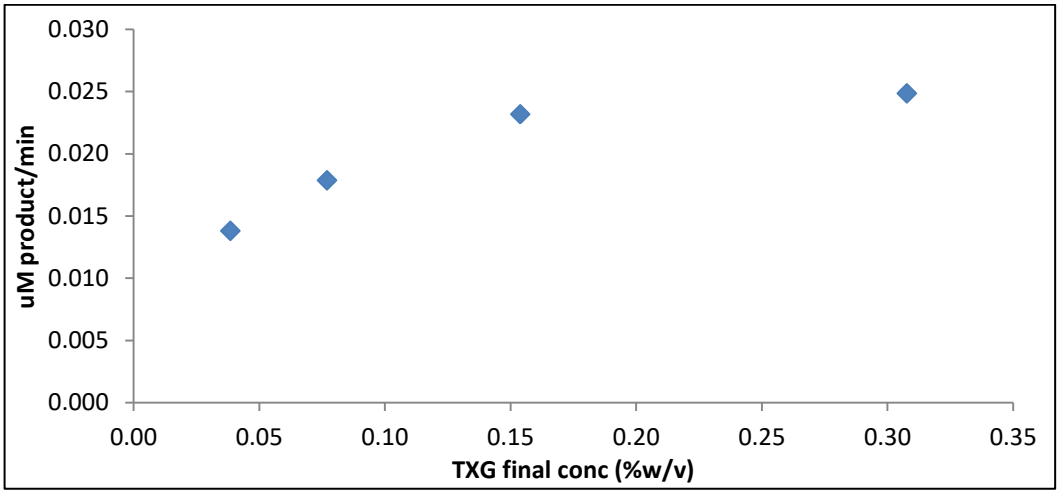

Figure 4.76. AtXTH4 reaction rates graph on various TXG concentrations and 50 µM XGO. Error bars are given on graph.

HEC donor concentration optimization was carried by testing concentrations between 0.4 per cent w/v to 0.05 per cent w/v (Figure 4.77, Table 4.25). AtXTH4 reaction rate continue to increase linearly through 0.05-0.4 per cent w/v donor range however more concentrated donors weren't tested because viscosity of reaction environment would decrease when more concentrated HEC donor was used. Decrease in reaction environment viscosity can affect reaction rate by causing molecules to interact slower. Also, viscous sample can clog HPLC system and HPLC column. Highest reaction rate was achieved with 0.4 per cent w/v HEC, thus donor was used at this concentration during kinetic studies.

Table 4.25. AtXTH4 reaction rates on various HEC concentrations and 50 µM XGO.

Donor stock concentration (per cent w/v)	**Donor final concentration (per cent w/v)**	**Fluorescence of HEC-XGO hybrid molecule**	**pM product formed/min**
0.4	0.308	444.07	14.920
0.3	0.231	310.80	10.435
0.2	0.154	211.17	7.120
0.1	0.077	120.03	4.048
0.05	0.038	54.50	1.868

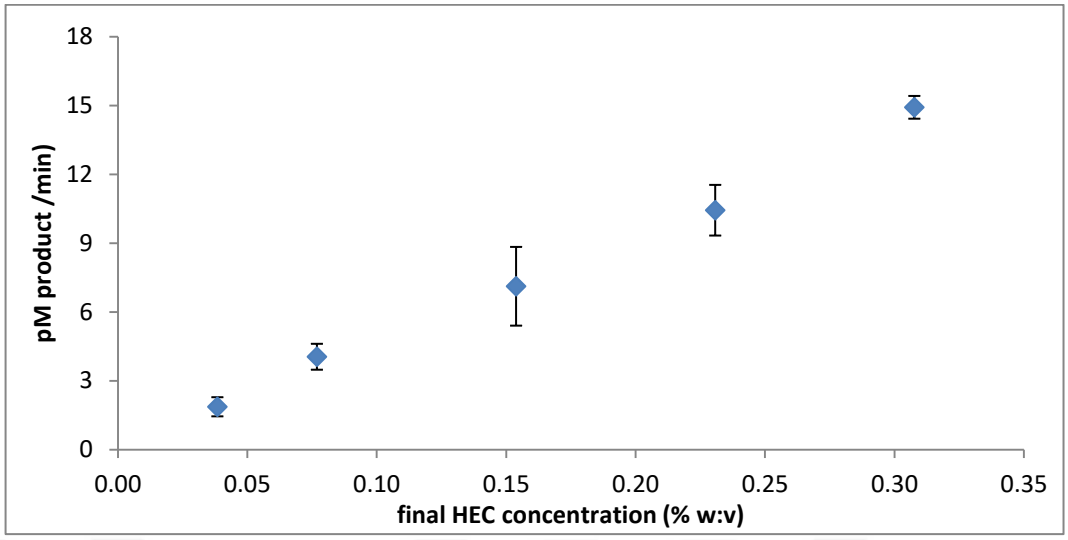

Figure 4.77. AtXTH4 reaction rates graph on various HEC concentrations and 50 µM XGO. Error bars are given on graph.

In order to do kinetic value calculations, AtXTH4 reaction rate was calculated through a wide range of acceptor concentrations. By using different acceptor concentrations, enzyme reactions were prepared for TXG-XGO substrate couple. Amount of formed hybrid product was measured by HPLC system and converted to µM product formed in a minute (Table 4.26). Obtained values were plotted on a graph to give Michaelis-Menten curve of AtXTH4 enzyme with TXG-XGO donor-acceptor couple (Figure 4.78). The curve reaches plateau phase when 250 µM XGO was used as acceptor and plateau phase continues even though more concentrated acceptors were used.

Table 4.26. Enzyme reaction rates of AtXTH4 with 0.2 per cent w/v TXG and various acceptor concentrations.

Stock XGO concentration (uM)	Final XGO concentration (uM)	uM product/min
400	13.333	0.02977
350	11.667	0.02806
300	10.000	0.03036
250	8.333	0.02833
200	6.667	0.02523
150	5.000	0.02184
100	3.333	0.01751
70	2.333	0.01298
50	1.667	0.01052
30	1.000	0.00623
10	0.333	0.00238
1	0.033	0.00009

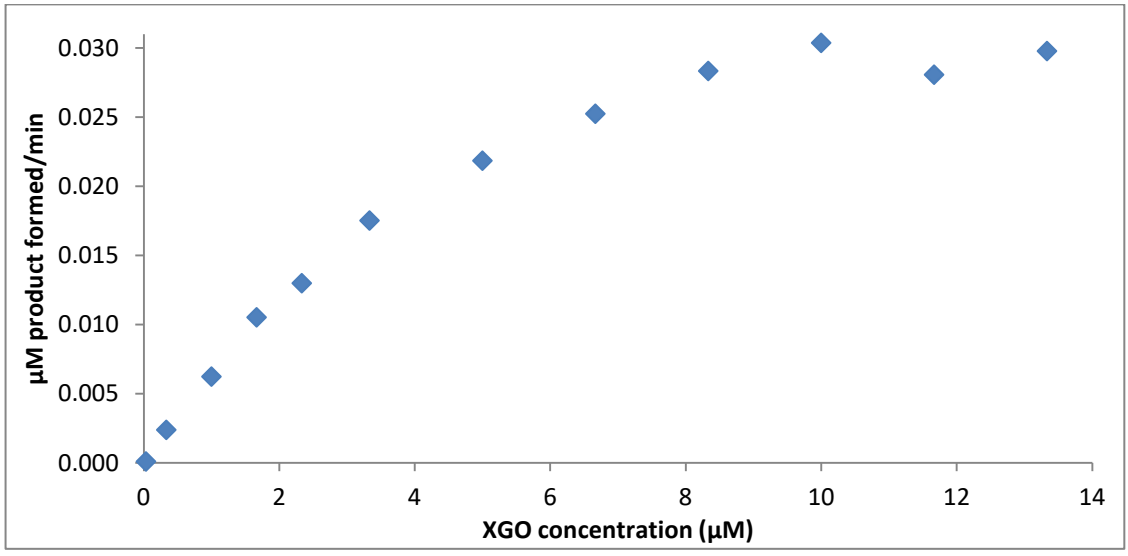

Figure 4.78. Michaelis-Menten plot of AtXTH4 enzyme with 0.2 per cent w/v TXG and various XGO concentrations.

Michaelis-Menten plot was converted to Lineweaver Burke plot and kinetic values K_m, K_{cat} and V_{max} were calculated using Lineweaver Burke plot (Figure 4.79). From the plot, V_{max} was found as 0.0492 µM/min, K_m was calculated as 6.5763 µM and K_{cat} as 0.0742 min^{-1}.

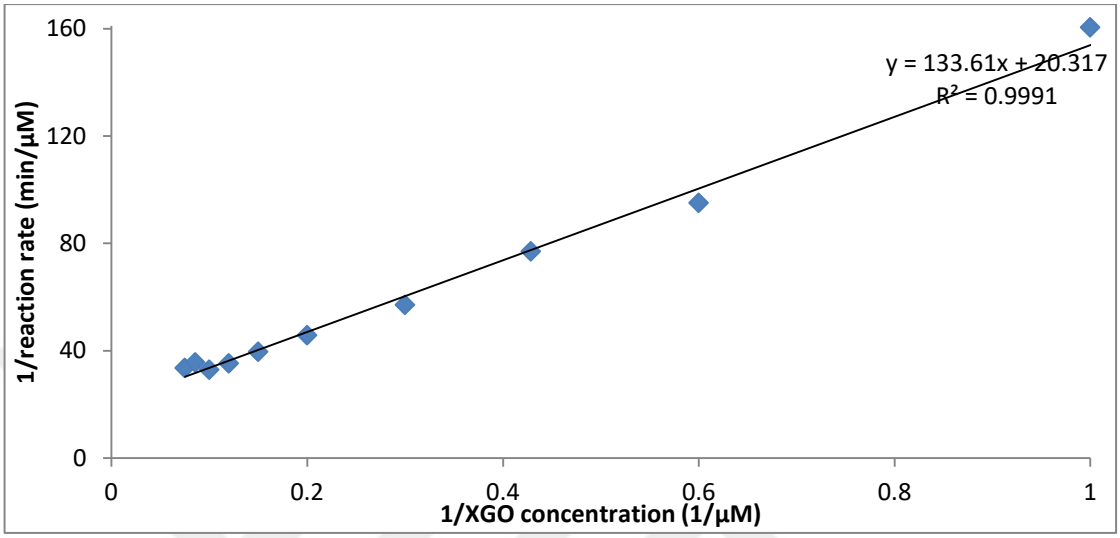

Figure 4.79. Lineweaver-Burke plot of AtXTH4 enzyme with 0.2 per cent w/v TXG and various XGO concentrations.

Reaction rate calculations were also performed for HEC-XGO donor-acceptor couple. Enzyme reactions were set with 0.4 per cent w/v HEC donor and various XGO with concentrations ranging from 1µM to 30 µM. Amount of hybrid product produced during incubation period was measured by HPLC system and reaction rates were calculated as nM product produced per minute (Table 4.27). Values were plotted and a Michaelis-Menten plot was generated (Figure 4.80). It was observed that reaction rate of AtXTH4 reached a plateau even though acceptor concentration increased more than 10 µM.

Table 4.27. Enzyme reaction rates of AtXTH4 with 0.4 per cent w/v HEC and various acceptor concentrations.

Stock XGO concentration (uM)	Final XGO concentration (uM)	nM product/min
30	1.000	0.701
20	0.667	0.700
10	0.333	0.613
8	0.267	0.492
6	0.200	0.413
5	0.167	0.349
4	0.133	0.249
2	0.067	0.126
1	0.033	0.062

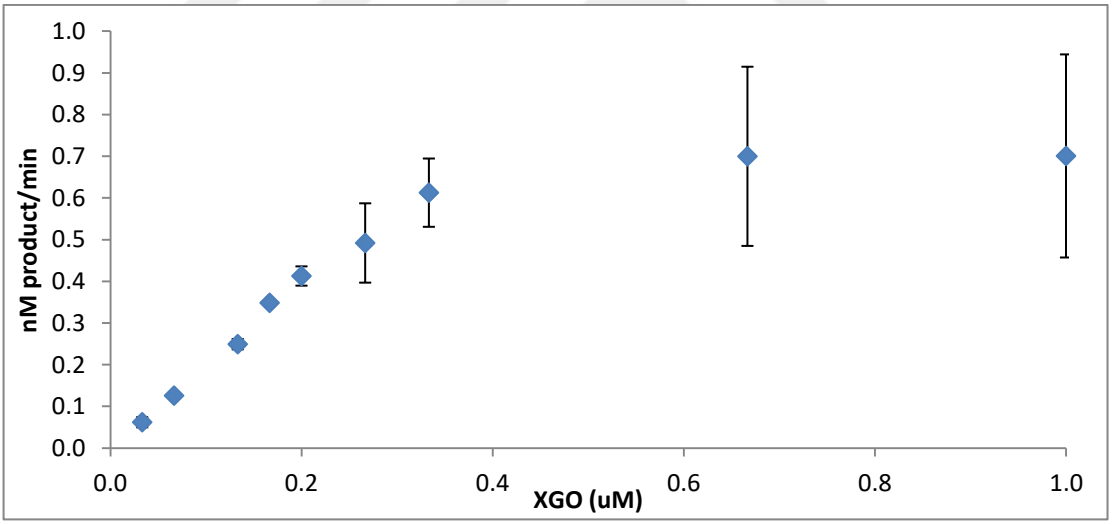

Figure 4.80. Michaelis-Menten plot of AtXTH4 enzyme with 0.4 per cent w/v HEC and various XGO concentrations.

Lineweaver-Burke plot was generated for AtXTH4 enzyme and HEC-XGO donor-acceptor couple using Michaelis-Menten plot (Figure 4.81). Using Lineweaver-Burke plot, V_{max} was found as 0.021 µM/min, K_m was calculated as 11.076 µM and K_{cat} as 0.032 min^{-1}.

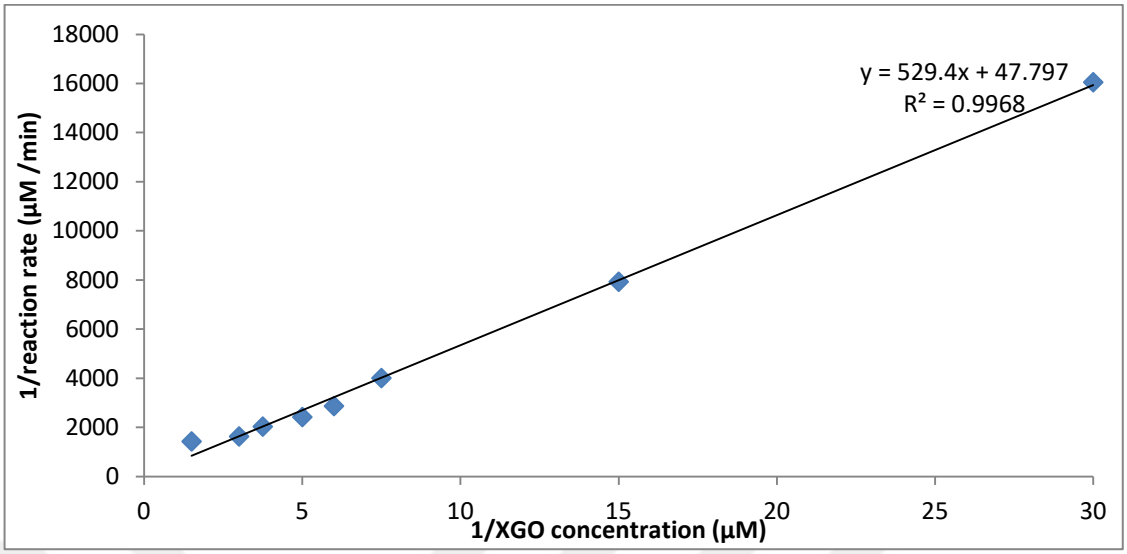

Figure 4.81. Lineweaver-Burke plot of AtXTH4 enzyme with 0.4 per cent w/v HEC and various XGO concentrations.

4.7.3.3. GhXTH2

GhXTH2 enzyme is another member of Group I XTH enzymes. Heterologously produced non-polished GhXTH2 enzyme was used in initial substrate characterization studies. Enzyme showed detectable activity on TXG-BA, TXG-BB, TXG-BC, TXG-CT, TXG-XT, TXG-X7, TXG-XGO, HEC-X7 and HEC-XGO donor acceptor couples. At least 4 different time points were used as incubation periods for each substrate couple in 3 repeats and obtained hybrid products were analysed by HPLC system (Figure 4.82). Hybrid product amounts were used to generate specific activity picokatal / mg enzyme values (Table 4.28).

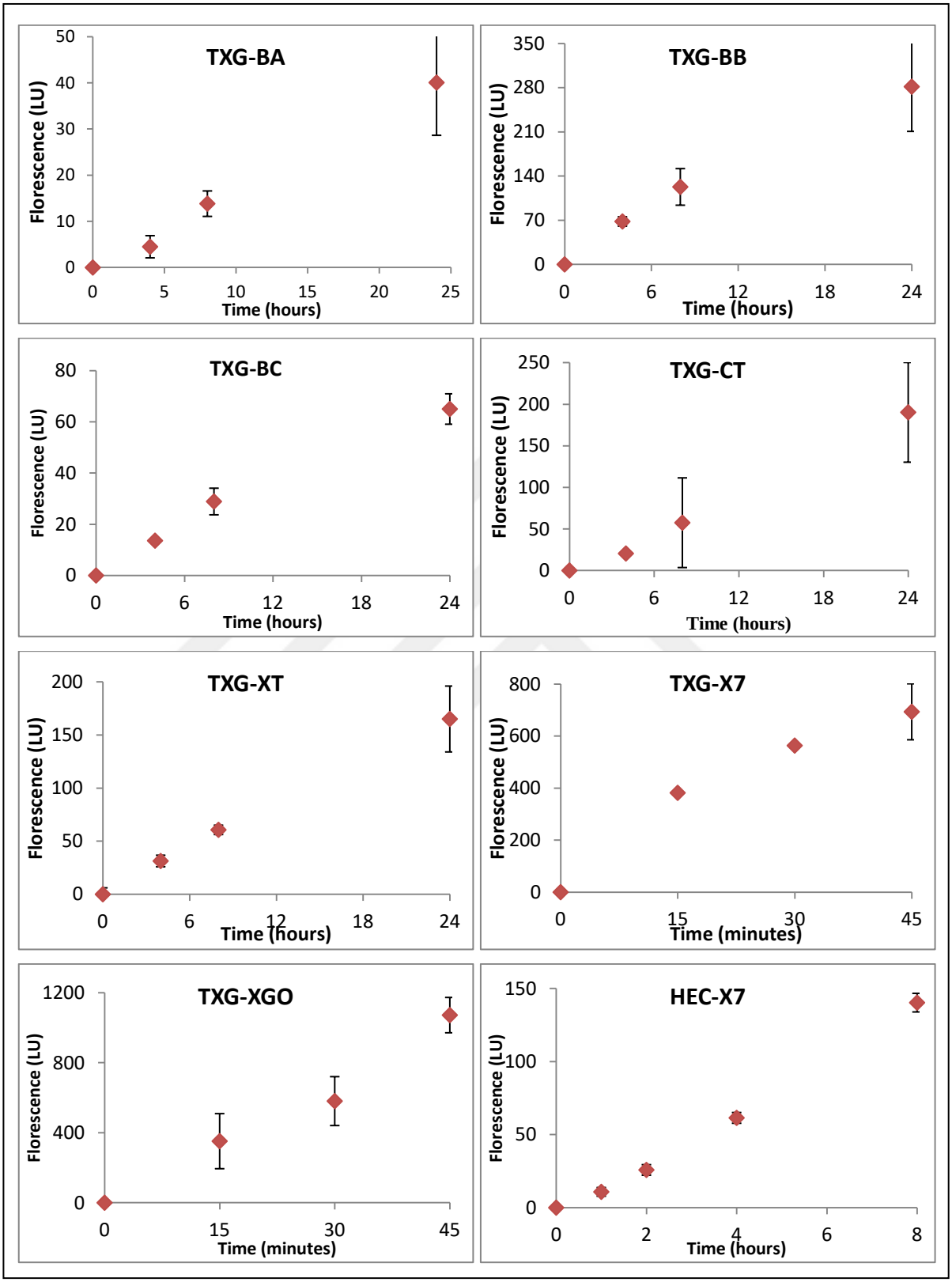
TXG-BA
Florescence (LU)
Time (hours)
TXG-BB
Florescence (LU)
Time (hours)
TXG-BC
Florescence (LU)
Time (hours)
TXG-CT
Florescence (LU)
Time (hours)
TXG-XT
Florescence (LU)
Time (hours)
TXG-X7
Florescence (LU)
Time (minutes)
TXG-XGO
Florescence (LU)
Time (minutes)
HEC-X7
Florescence (LU)
Time (hours)

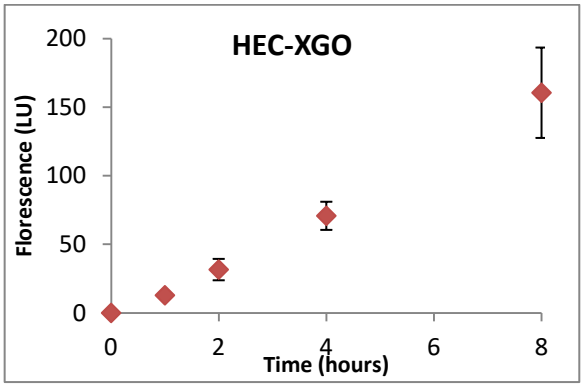

Figure 4.82. Time interval enzyme activity studies of unpolished GhXTH2 with different donor-acceptor couples. Florescence amounts of generated hybrid products were studied by HPLC. Donor-acceptor couples and error bars are indicated on graphs.

Table 4.28. GhXTH2 specific activity on various donor-acceptor couples with unpolished affinity purified GhXTH2 and ratios of different specific activities compared to TXG-XGO specific activity.

	Pkatals/mg enzyme	**per centTXG-XGO**
TXG-BA	0.0033	0.0123
TXG-BB	0.0364	0.1348
TXG-BC	0.0072	0.0265
TXG-CT	0.0266	0.0985
TXG-XT	0.0237	0.0877
TXG-X7	36.3145	134.5983
TXG-XGO	26.9799	100.0000
HEC-X7	0.0410	0.1517
HEC-XGO	0.0388	0.1438

After contamination of non-polished GhXTH2, new GhXTH2 enzyme was produced heterologously and polished. This new and purer enzyme was used in main characterization studies. Polished GhXTH2 enzyme shows activity on more diverse donor-acceptor couples. Time interval studies on each substrate couple was done as at least 3

repeats and 3 time points. Hybrid product amounts were measured by HPLC system and converted to specific activity values (Figure 4.83, Figure 4. 84, Table 4.29).

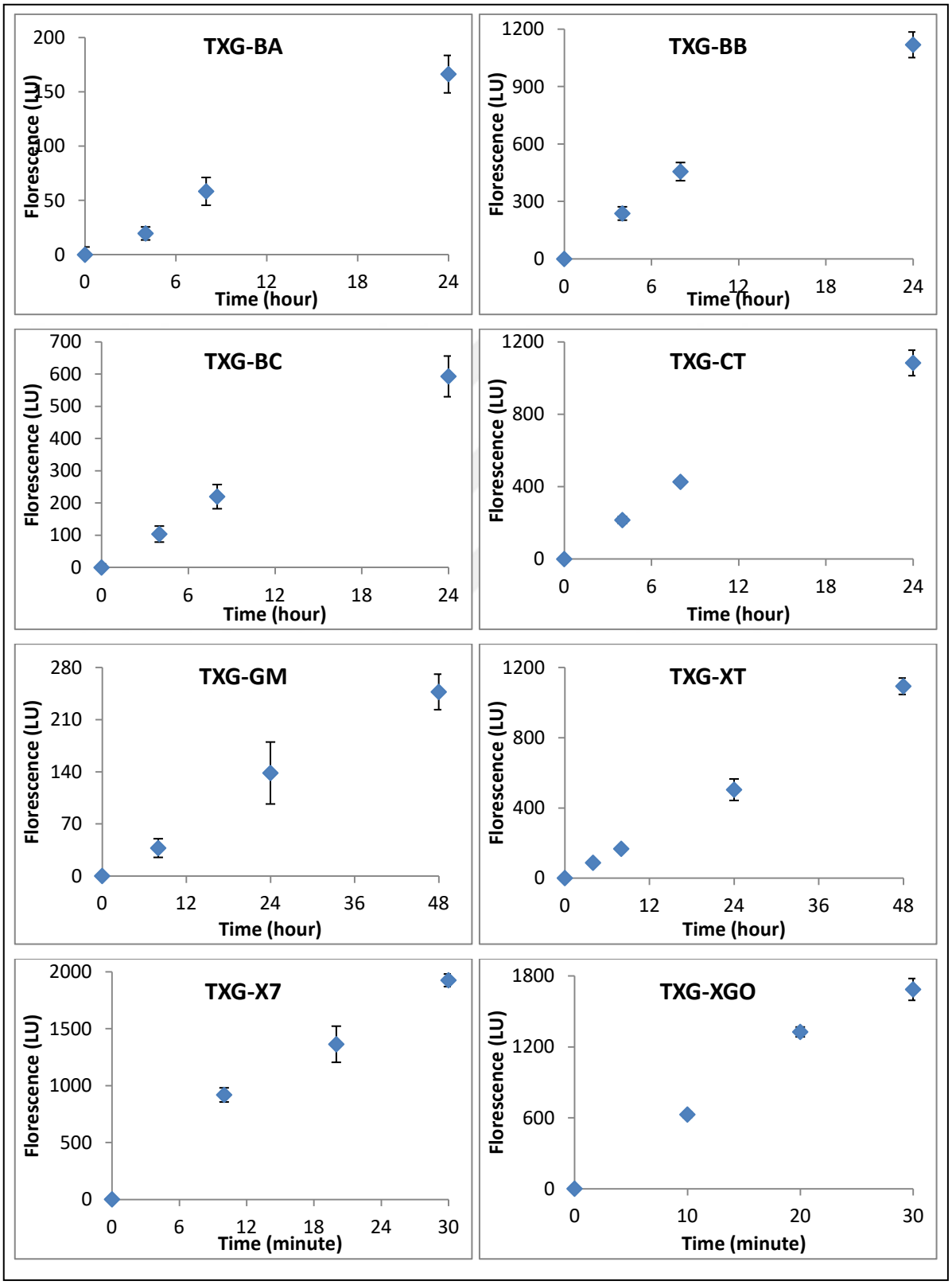

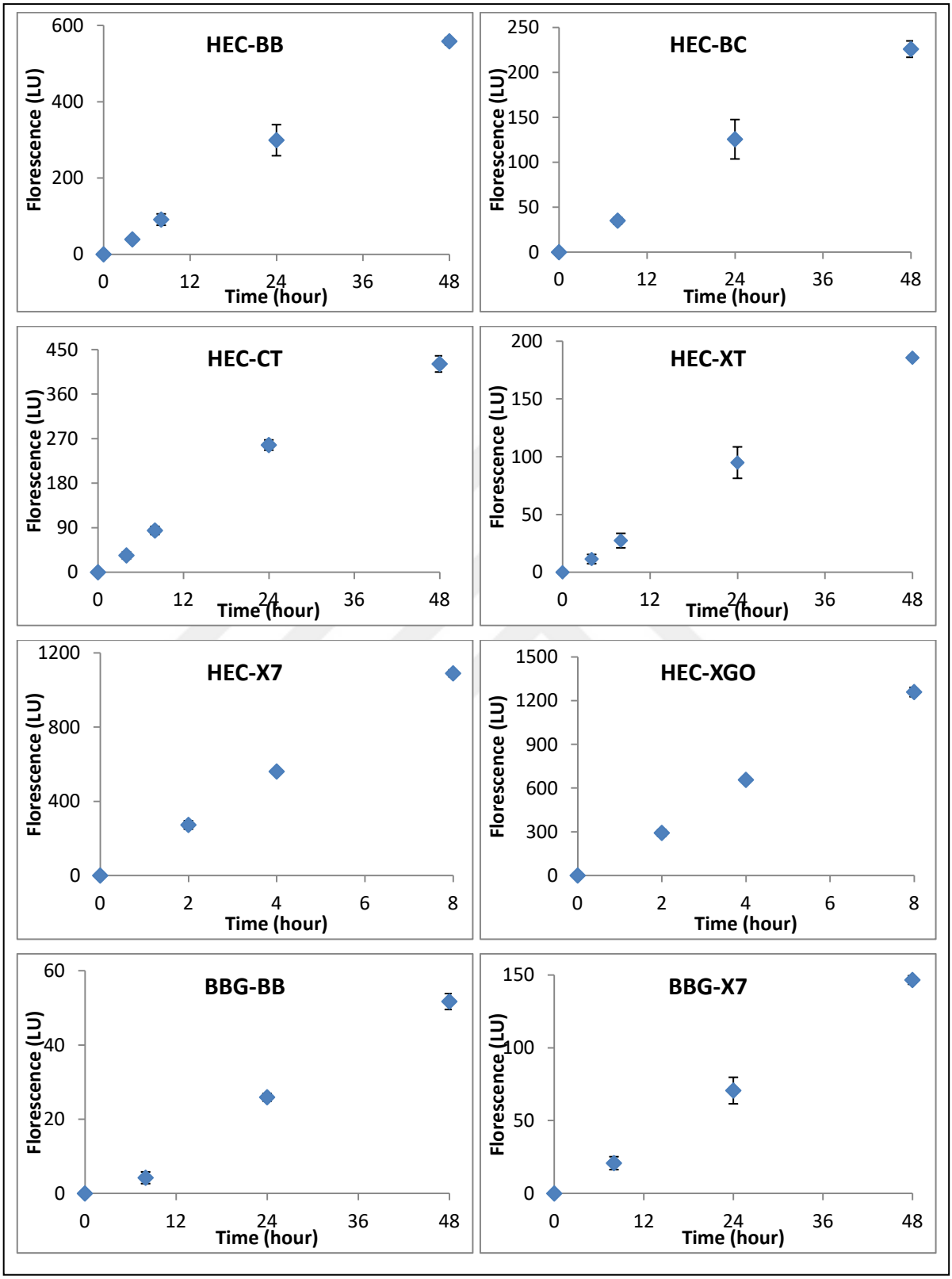
HEC-BB
Florescence (LU)
Time (hour)
HEC-BC
Florescence (LU)
Time (hour)
HEC-CT
Florescence (LU)
Time (hour)
HEC-XT
Florescence (LU)
Time (hour)
HEC-X7
Florescence (LU)
Time (hour)
HEC-XGO
Florescence (LU)
Time (hour)
BBG-BB
Florescence (LU)
Time (hour)
BBG-X7
Florescence (LU)
Time (hour)

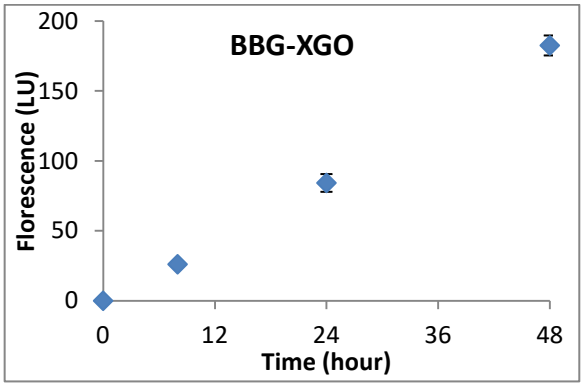

Figure 4.83. Time interval enzyme activity studies of polished GhXTH2 with different donor-acceptor couples. Florescence amounts of generated hybrid products were studied by HPLC. Donor-acceptor couples and error bars are indicated on graphs.

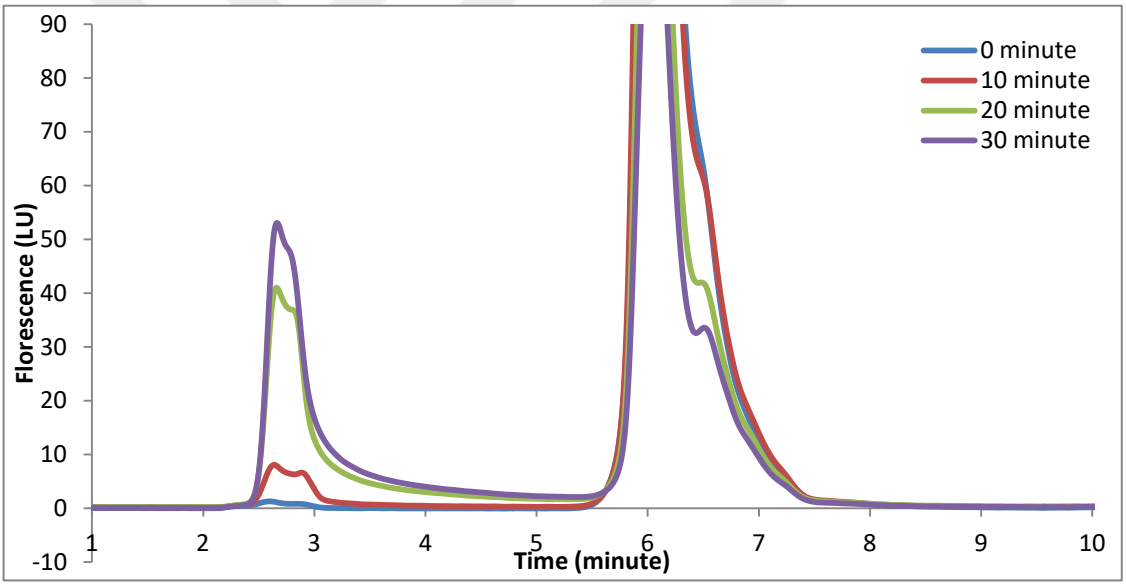

Figure 4.84. HPLC chromatogram of GhXTH2 time interval enzyme activity reaction using TXG-XGO substrate couple. Incubation times of each line is indicated on graph.

Table 4.29. Specific enzyme activity of GhXTH2 on various donor-acceptor couples and ratios of specific activities to TXG-XGO, BBG-XGO and HEC-XGO couples' activities.

	Pkatals / mg enyzme	**per cent TXG-XGO**	**per cent HEC-XGO**	**per cent BBG-XGO**
TXG-BA	0.0155	0.0071		
TXG-BB	0.1799	0.0828		
TXG-BC	0.0593	0.0273		
TXG-CT	0.1206	0.0555		
TXG-GM	0.0108	0.0050		
TXG-XT	0.0620	0.0285		
TXG-X7	219.8488	101.1413		
TXG-XGO	217.3681	100.0000		
HEC-BB	0.0345	0.0159	7.696	
HEC-BC	0.0120	0.0055	2.664	
HEC-CT	0.0236	0.0109	5.263	
HEC-XT	0.0113	0.0052	2.509	
HEC-X7	0.3670	0.1688	81.800	
HEC-XGO	0.4486	0.2064	100.000	
BBG-BB	0.0033	0.0015		34.117
BBG-X7	0.0079	0.0036		82.560
BBG-XGO	0.0096	0.0044		99.997

Specific activity calculations of GhXTH2 revealed that enzyme is showing highest endotransglycosylase activity on xyloglucan donor and acceptor. Since GhXTH2 is a Group I member, this is an expected result. However, activity on other substrate couples is surprising. GhXTH2 enzyme's specific activity on TXG-X7 couple is 219.85 and 0.367 on HEC-X7, meaning enzyme is per cent0.168 active on HEC-X7 compared to TXG-X7. This ratio can seem low, yet it can still be remarkably important when cotton plant and plant product cotton ball's cellulose amount is taken in account. Another interesting point is enzyme activities on TXG-BB and BBG-X7 substrate couples. When xyloglucan is used as donor and mixed-linked glucan subunit as acceptor, enzyme's specific activity is 0.179. However, when the case is opposite, mixed-linked glucan is used as donor and xyloglucan

subunit as acceptor, enzyme's specific activity is 0.0079. There is a 22.66 times different between TXG-BB and BBG-X7, meaning enzyme's catalytic site is highly specific for donors and acceptors.

GhXTH2 enzyme kinetics were studied using polished GhXTH2 with TXG-XGO and HEC-XGO donor -acceptor couples. Firstly, donor concentrations at which enzyme is showing highest activity were determined. TXG concentrations between 0.4 per cent w/v to 0.05 per cent w/v were screened. Produced hybrid product amounts and reaction rates were calculated for each TXG concentration (Table 4.30, Figure 4.85). When these values are plotted, it is observed that reaction rate reaches a plateau at 0.2 per cent w/v TXG concentration. Increasing TXG concentration beyond this point doesn't have any positive effect on enzyme reaction rate, thus 0.2 per cent w/v TXG is used for kinetic studies.

Table 4.30. GhXTH2 reaction rates on various TXG concentrations and 50 μM XGO.

Donor stock concentration (per cent w/v)	**Donor final concentration (per cent w/v)**	**Fluorescence of TXG-XGO hybrid molecule**	**nM product formed/min**
0.4	0.308	439.30	5.112
0.3	0.231	432.75	5.035
0.2	0.154	400.67	4.662
0.1	0.077	298.77	3.476
0.05	0.038	182.80	2.127

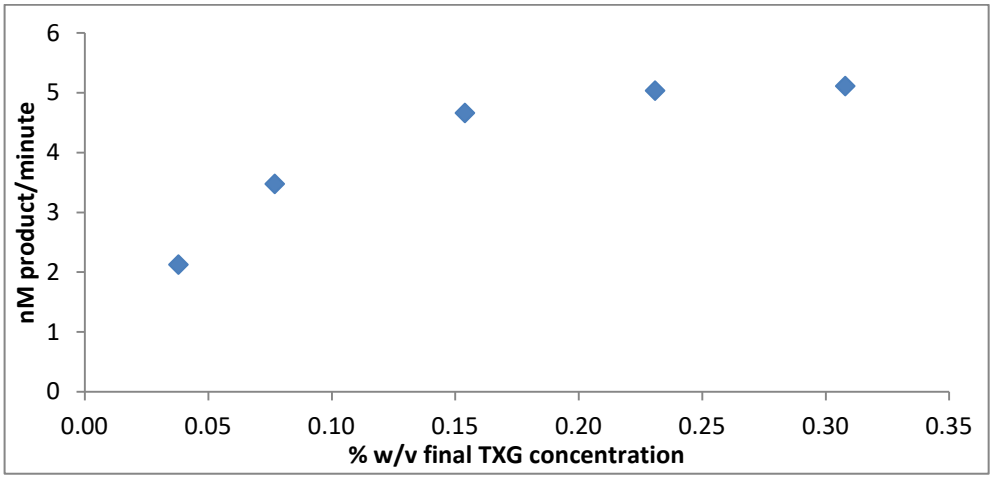

Figure 4.85. GhXTH2 reaction rates graph on various TXG concentrations and 50 µM XGO. Error bars are given on graph.

In case of HEC concentration optimization, 0.4 per cent w/v to 0.05 per cent w/v HEC concentrations were studied. GhXTH2 reaction rate continued to increase by increasing HEC w/v concentration (Table 4.31). Among concentrations tested, reaction rate plot didn't reach a plateau phase (Figure 4.86). This means enzyme reaction rate is expected to increase with increasing HEC concentration, however it is not possible to increase donor concentration beyond a point due to clogging problem of HPCL system. In kinetic studies, 0.2 per cent w/v HEC donor was used.

Table 4.31. GhXTH2 reaction rates on various HEC concentrations and 50 µM XGO.

Donor stock concentration (per cent w/v)	**Donor final concentration (per cent w/v)**	**Fluorescence of HEC-XGO hybrid molecule**	**nM product formed/min**
0.4	0.308	617.53	1.136
0.3	0.231	452.13	0.832
0.2	0.154	272.35	0.501
0.1	0.077	148.53	0.273
0.05	0.038	76.23	0.140

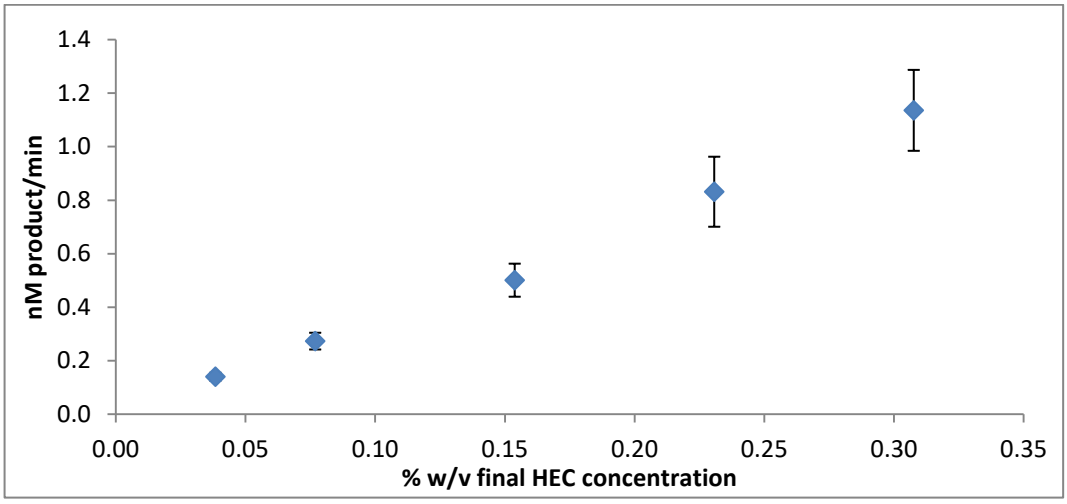

Figure 4.86. GhXTH2 reaction rates graph on various HEC concentrations and 50 µM XGO. Error bars are given on graph.

GhXTH2 kinetic studies were carried depending on acceptor concentration and reaction rate. 10 different XGO concentration ranging between 1 µM to 200 µM were used with 0.2 per cent w/v TXG donor and hybrid product amounts were analysed. Hybrid product amounts were converted to reaction rate and plotted on a graph to give Michaelis-Menten plot (Figure 4.87). From this plot, Lineweaver-Burke graph was generated and used for kinetic value calculations (Figure 4.88, Table 4.32).

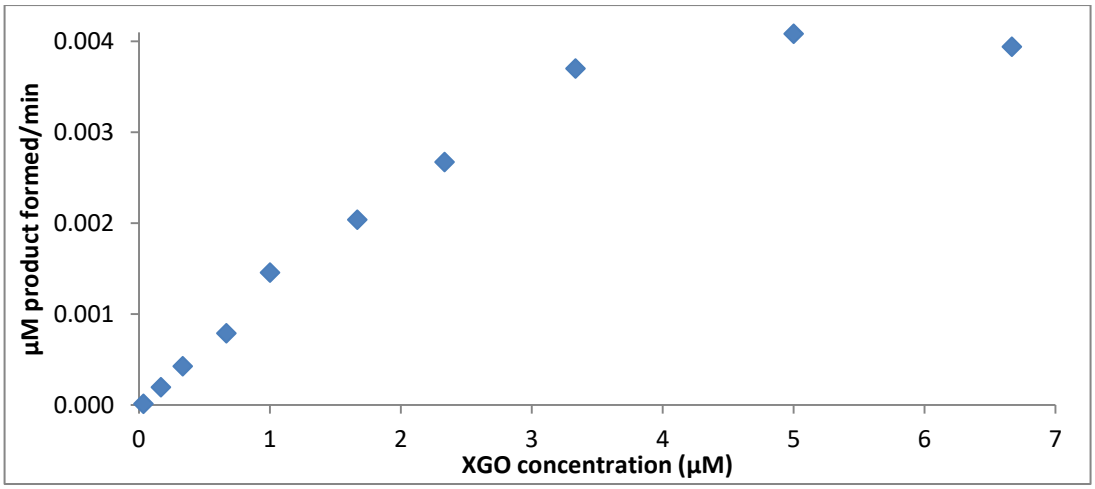

Figure 4.87. Michaelis-Menten plot of GhXTH2 enzyme with 0.2 per cent w/v TXG and various XGO concentrations.

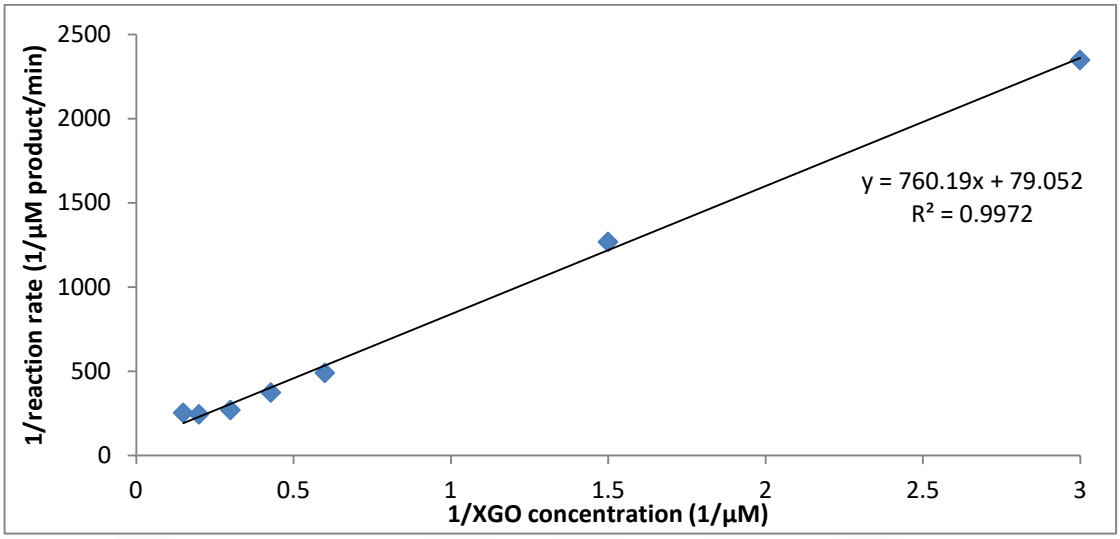

Figure 4.88. Lineweaver-Burke plot of GhXTH2 enzyme with 0.2 per cent w/v TXG and various XGO concentrations.

Enzyme kinetics of GhXTH2 enzyme was also studied with 0.2 per cent w/v HEC donor concentration and 1-10 µM XGO acceptor solutions. Different reactions were set and hybrid product amounts were measured via HPLC. Those values were used to calculate reaction rates and Michaelis-Menten plot was generated for GhXTH2 enzyme on HEC-XGO (Figure 4.89). From this plot, Lineweaver-Burke graph was generated and used for kinetic value calculations (Figure 4.90, Table 4.32).

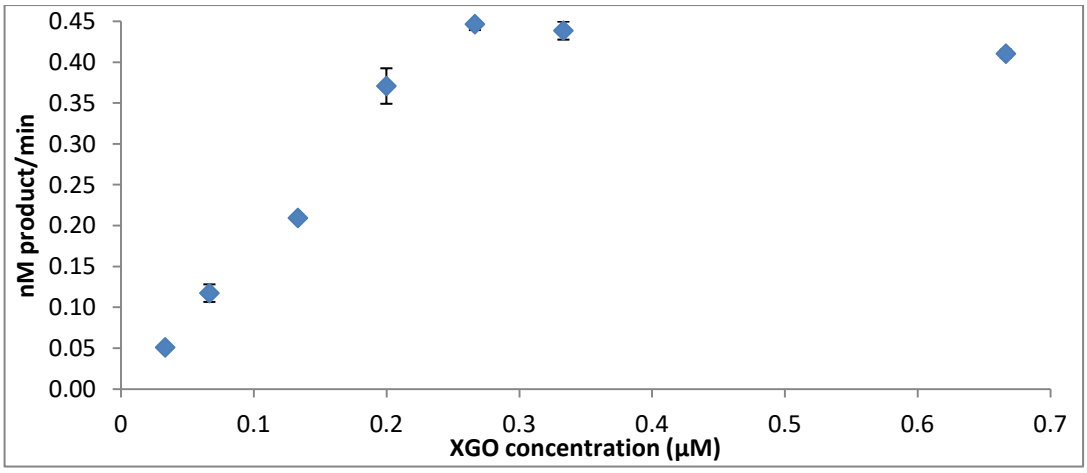

Figure 4.89. Michaelis-Menten plot of GhXTH2 enzyme with 0.2 per cent w/v HEC and various XGO concentrations.

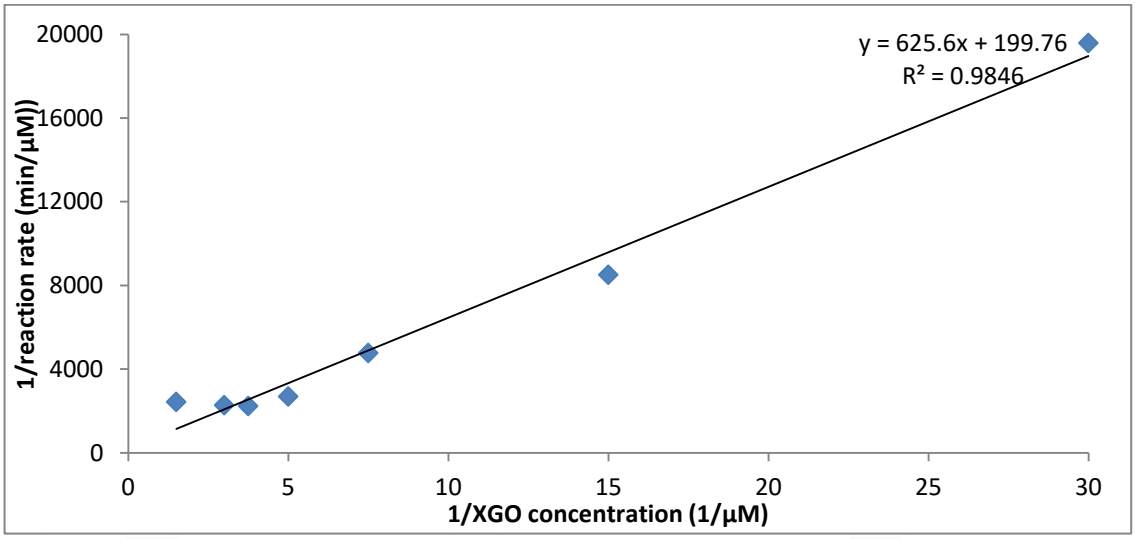

Figure 4.90. Lineweaver-Burke plot of GhXTH2 enzyme with 0.2 per cent w/v HEC and various XGO concentrations.

Table 4.32. V_{max}, K_m and K_{cat} values of GhXTH2 reactions with TXG-XGO and HEC-XGO donor-acceptor couples.

	TXG-XGO	**HEC-XGO**
V_{max}	0.013 µm/min	0.005 µM/min.
K_m	9.616 µM	3.132 µM
K_{cat}	0.068 min^{-1}	0.005 min^{-1}

4.7.3.4. PtXTH3

PtXTH3 is one of the enzymes analysed within the concept of this thesis that shows a wide substrate specificity over broad spectrum of donor-acceptors. TXG, BBG, HEC and KM donors were used with different acceptors. Enzyme reactions were carried with at least three time points and as at least three repeats for each donor-acceptor couple. Amount of hybrid products were measured for each trial by HPLC florescence detector (Figure 4.91). Average florescence values were plotted on florescence- incubation time graphs (Figure

4.92). These values were used to calculate specific enzyme activity as picokatal / mg enzyme (Table 4.33).

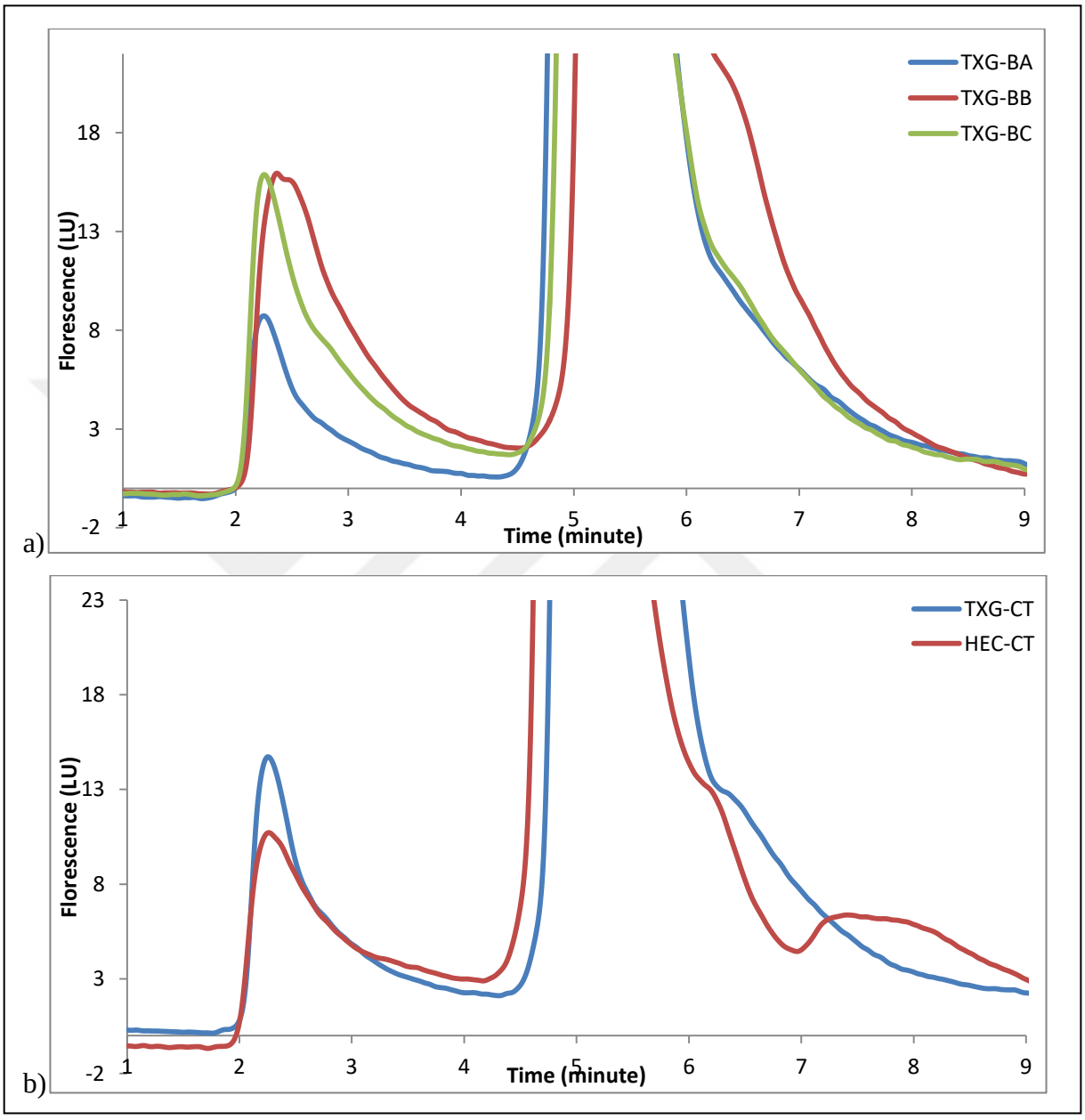

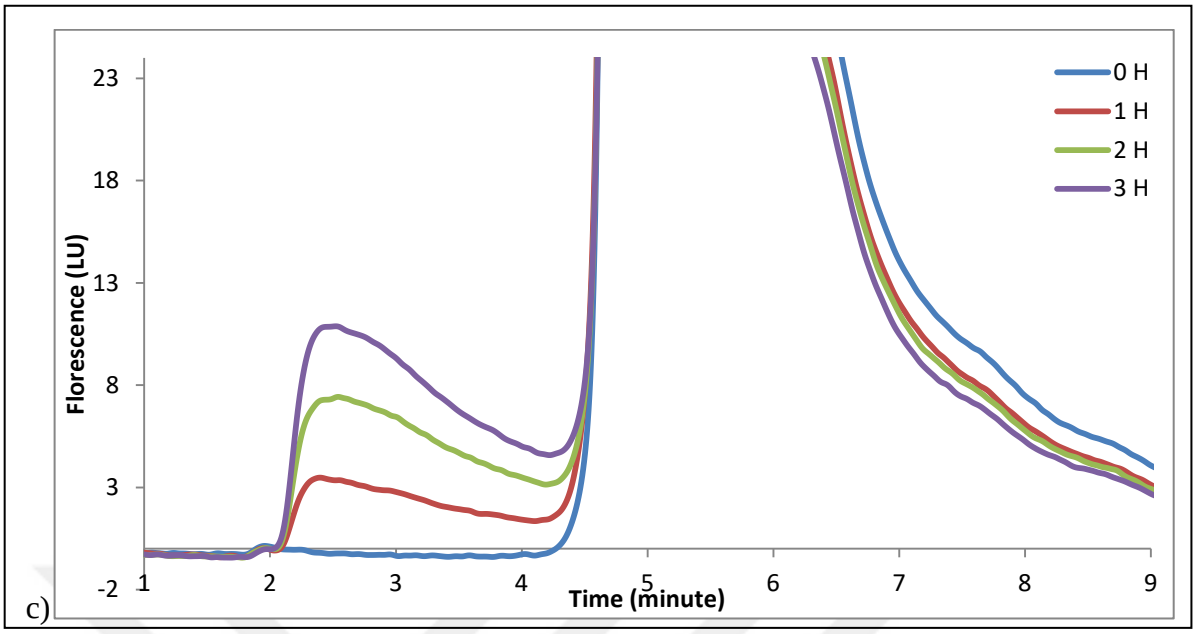

Figure 4.91. HPLC chromatogram of PtXTH3 time interval enzyme activity reaction using various substrate couple. a) Comparison of chromatograms of 1H enzyme reactions with TXG-BA, TXG-BB and TXG-BC donor-acceptor couples, b) Comparison of chromatograms of 1H enzyme reactions with TXG-CT and HEC-CT donor-acceptor couples, c) Time interval chromatograms with KM-XGO substrate couple.

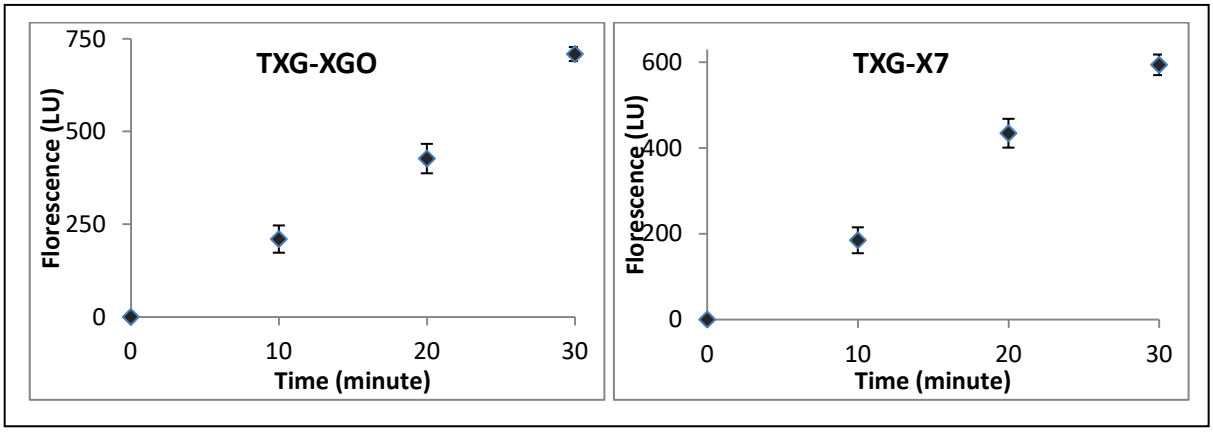

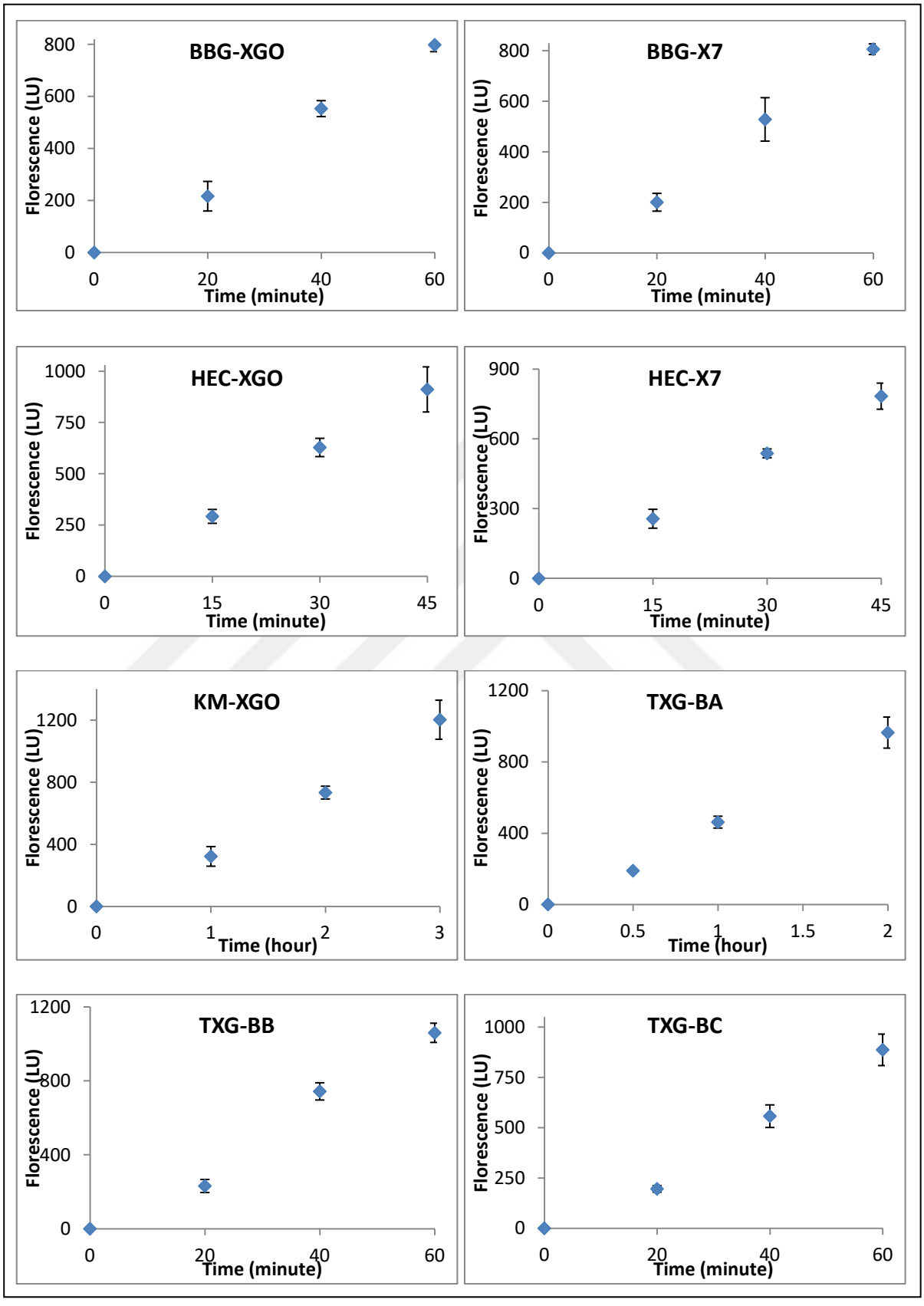
BBG-XGO
Florescence (LU)
800
600
400
200
0
0
20
40
60
Time (minute)
BBG-X7
Florescence (LU)
800
600
400
200
0
0
20
40
60
Time (minute)
HEC-XGO
Florescence (LU)
1000
750
500
250
0
0
15
30
45
Time (minute)
HEC-X7
Florescence (LU)
900
600
300
0
0
15
30
45
Time (minute)
KM-XGO
Florescence (LU)
1200
800
400
0
0
1
2
3
Time (hour)
TXG-BA
Florescence (LU)
1200
800
400
0
0
0.5
1
1.5
2
Time (hour)
TXG-BB
Florescence (LU)
1200
800
400
0
0
20
40
60
Time (minute)
TXG-BC
Florescence (LU)
1000
750
500
250
0
0
20
40
60
Time (minute)

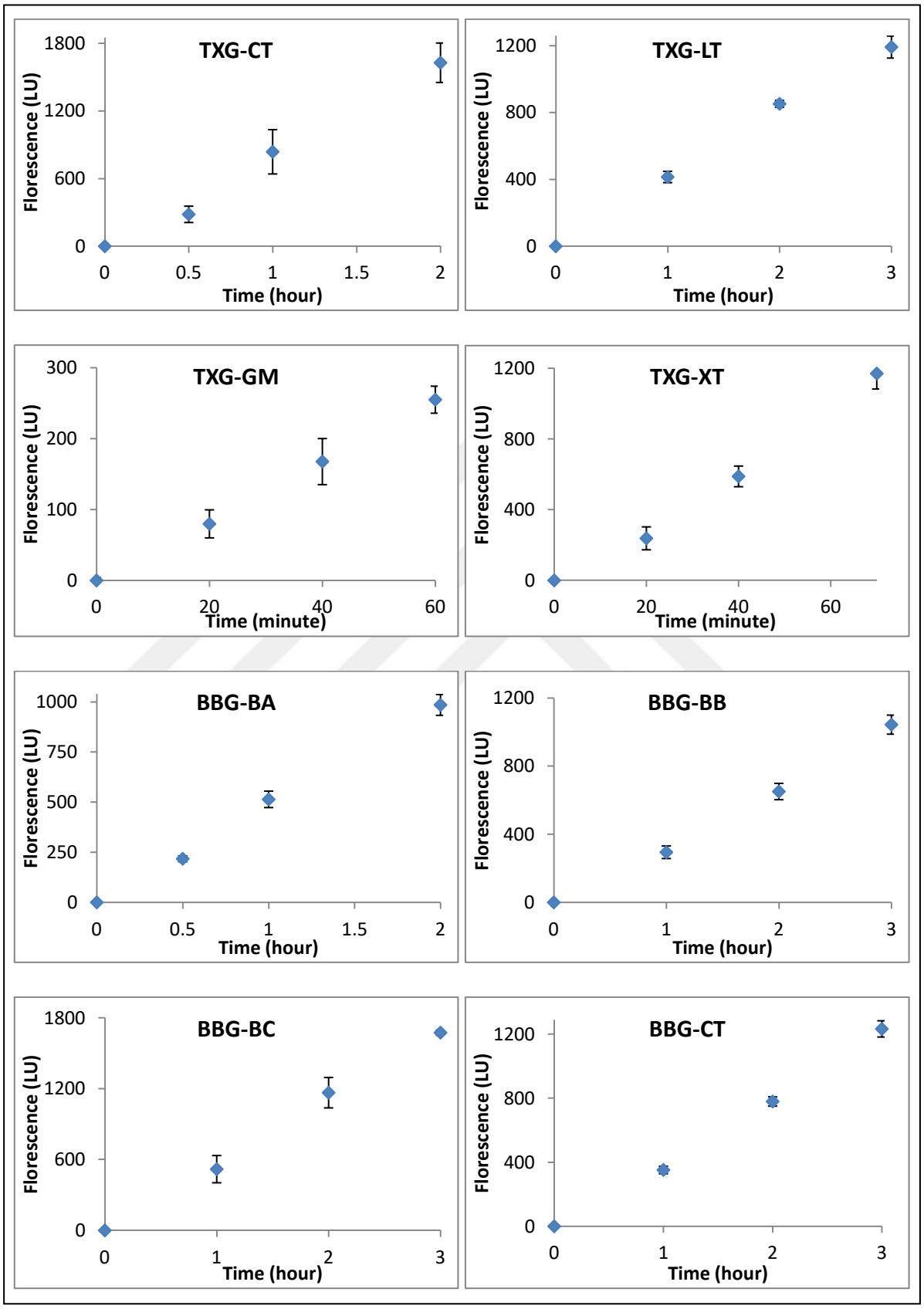
TXG-CT
Florescence (LU)
1800
1200
600
0
0
0.5
1
1.5
2
Time (hour)
TXG-LT
Florescence (LU)
1200
800
400
0
0
1
2
3
Time (hour)
TXG-GM
Florescence (LU)
300
200
100
0
0
20
40
60
Time (minute)
TXG-XT
Florescence (LU)
1200
800
400
0
0
20
40
60
Time (minute)
BBG-BA
Florescence (LU)
1000
750
500
250
0
0
0.5
1
1.5
2
Time (hour)
BBG-BB
Florescence (LU)
1200
800
400
0
0
1
2
3
Time (hour)
BBG-BC
Florescence (LU)
1800
1200
600
0
0
1
2
3
Time (hour)
BBG-CT
Florescence (LU)
1200
800
400
0
0
1
2
3
Time (hour)

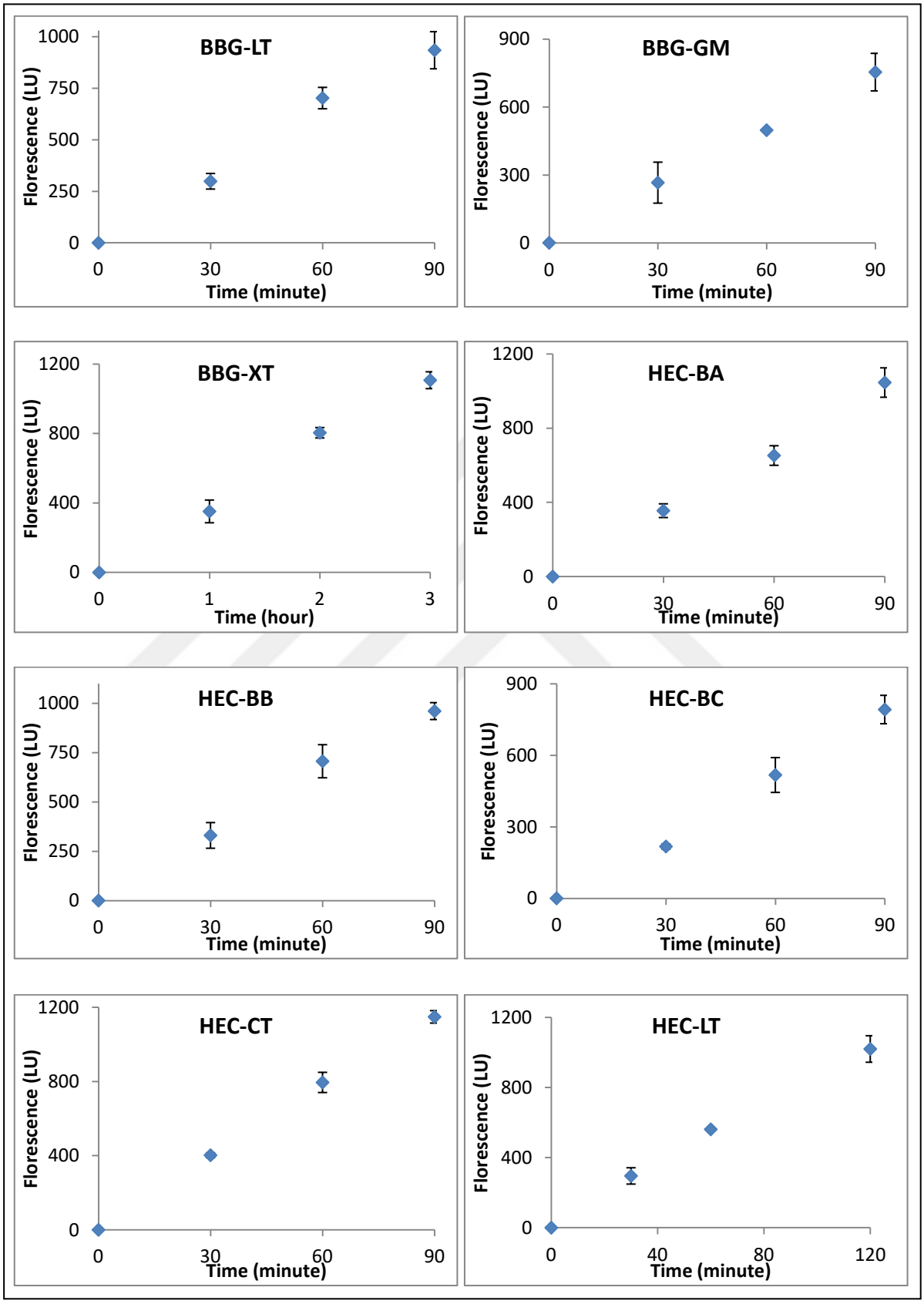
BBG-LT
Florescence (LU)
1000
750
500
250
0
0
30
60
90
Time (minute)
BBG-GM
Florescence (LU)
900
600
300
0
0
30
60
90
Time (minute)
BBG-XT
Florescence (LU)
1200
800
400
0
0
1
2
3
Time (hour)
HEC-BA
Florescence (LU)
1200
800
400
0
0
30
60
90
Time (minute)
HEC-BB
Florescence (LU)
1000
750
500
250
0
0
30
60
90
Time (minute)
HEC-BC
Florescence (LU)
900
600
300
0
0
30
60
90
Time (minute)
HEC-CT
Florescence (LU)
1200
800
400
0
0
30
60
90
Time (minute)
HEC-LT
Florescence (LU)
1200
800
400
0
0
40
80
120
Time (minute)

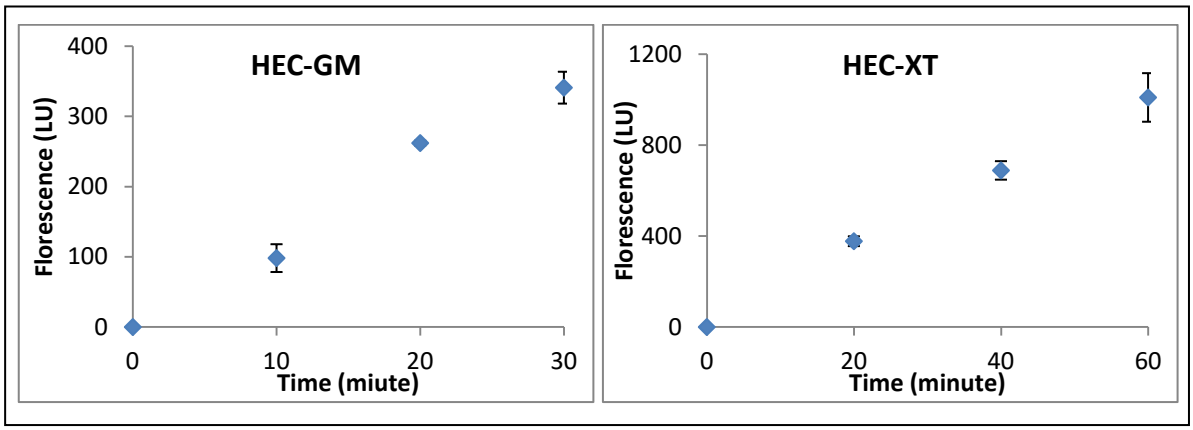

Figure 4.92. Time interval enzyme activity studies of PtXTH3 with different donor-acceptor couples. Florescence amounts of generated hybrid products were studied by HPLC. Donor-acceptor couples and error bars are indicated on graphs.

Table 4.33. Specific enzyme activity of PtXTH3 on various donor-acceptor couples and ratios of specific activities to TXG-XGO, BBG-XGO and HEC-XGO couples' activities.

Donor-acceptor couple	**Pkatal / mg enzyme**	**per cent TXG-XGO**	**per cent HEC-XGO**	**per cent BBG-XGO**
TXG-BA	14.18	1.76		
TXG-BB	35.35	4.40		
TXG-BC	21.78	2.71		
TXG-CT	46.23	5.75		
TXG-GM	6.97	0.87		
TXG-LT	5.31	0.66		
TXG-XT	61.51	7.65		
TXG-X7	876.14	108.94		
TXG-XGO	804.24	100.00		
HEC-BA	21.82	2.71	6.83	
HEC-BB	41.92	5.21	13.13	
HEC-BC	26.95	3.35	8.44	
HEC-CT	44.36	5.52	13.89	
HEC-GM	6.54	0.81	2.05	
HEC-LT	9.46	1.18	2.96	
HEC-XT	78.88	9.81	24.70	
HEC-X7	327.34	40.70	102.51	
HEC-XGO	319.31	39.70	100.00	
BBG-BA	7.88	0.98		37.41
BBG-BB	10.32	1.28		48.96
BBG-BC	6.07	0.76		28.83
BBG-CT	10.75	1.34		51.03
BBG-GM	2.76	0.34		13.10
BBG-LT	3.82	0.48		18.14
BBG-XT	12.25	1.52		58.13
BBG-X7	24.11	3.00		114.40
BBG-XGO	21.07	2.62		100.00
KM-XGO	0.93	0.12		

PtXTH3 enzyme XET activity on TXG-XGO and TXG-X7 donor-acceptor couples are above 400 pkatals / mg enzyme. In addition to this, enzyme's specific activity with HEC-XGO and HEC-X7 donor-acceptor couples are 159.66 and 163.67 respectively. These values are ~ 40 per cent compared to TXG-XGO and the highest specific activity observed (Figure 4.93). Enzyme's activity amounts on TXG-CT and HEC-CT donor acceptor couples are almost the same and this outcome suggests as a member of XTH enzyme family PtXTH3 enzyme has a specific substrate preference. When activity values with TXG and HEC were compared, except XGO and X7 acceptors, enzyme catalyse reactions between HEC and tested acceptors almost at the same speed or faster than TXG and tested acceptors. Specific activity values between BBG and acceptors are lower compared to TXG and HEC, yet pkatal / mg enzyme values are still high when evaluated with other enzymes.

BA, BB and BC are three representatives of mixed-linked glucan structural glucotetraose subunits. Regardless of donor, PtXTH3 enzyme showed higher activity with BB acceptor compared to BA and BC. This suggests BB acceptor has the best conformation for active cleft of the enzyme.

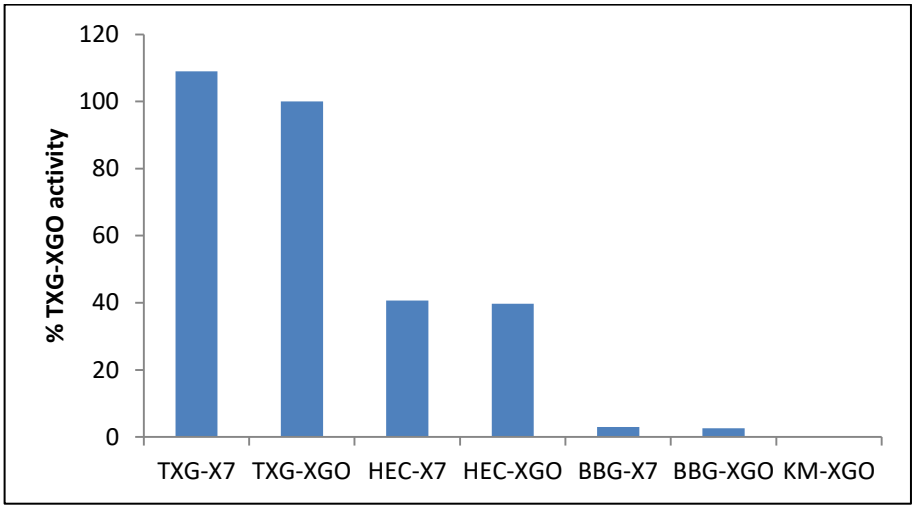

Figure 4.93. Ratios of specific activities of PtXTH3 on TXG-X7, HEC-X7, HEC-XGO, BBG-X7, BBG-XGO and KM-XGO to specific activity on TXG-XGO.

PtXTH3 enzyme kinetics were studied separately for TXG, BBG and HEC donors and X7 acceptor. Donor concentration optimization was performed for each donor. For TXG

optimization, 14 different TXG concentrations between 0.8 per cent w/v to 0.005 per cent w/v were used and amounts of TXG-XGO hybrid products produced with each substrate couple were measured by HPLC system (Table 4.34). Then, these product values were used to calculate reaction rate and plotted on a graph (Figure 4.94). PtXTH3 reaction rates with TXG donors showed a profile with two peak points at 0.08 per cent w/v and 0.2 per cent w/v TXG concentration, 0.2 per cent w/v TXG concentration being the highest. Thus, kinetic calculations will be carried using 0.2 per cent w/v TXG as donor in order to eliminate any concentration based limiting effect of donor substrate.

Table 4.34. PtXTH3 reaction rates on various TXG concentrations and 50 µM XGO.

TXG Donor stock concentration (w/v per cent)	**Donor final concentration (per cent w/v)**	**Fluorescence of TXG-XGO hybrid molecule**	**µM product formed/min**
0.8	0.347	314.1	0.0032
0.6	0.260	316.3	0.0033
0.4	0.173	441.0	0.0046
0.3	0.130	499.2	0.0052
0.2	0.087	714.8	0.0074
0.18	0.078	686.2	0.0071
0.16	0.069	673.0	0.0070
0.14	0.061	618.2	0.0064
0.12	0.052	562.1	0.0058
0.1	0.043	514.3	0.0053
0.08	0.035	636.9	0.0066
0.06	0.026	683.7	0.0071
0.04	0.017	608.6	0.0063
0.02	0.009	333.8	0.0035
0.01	0.004	193.8	0.0020
0.005	0.002	89.7	0.0009

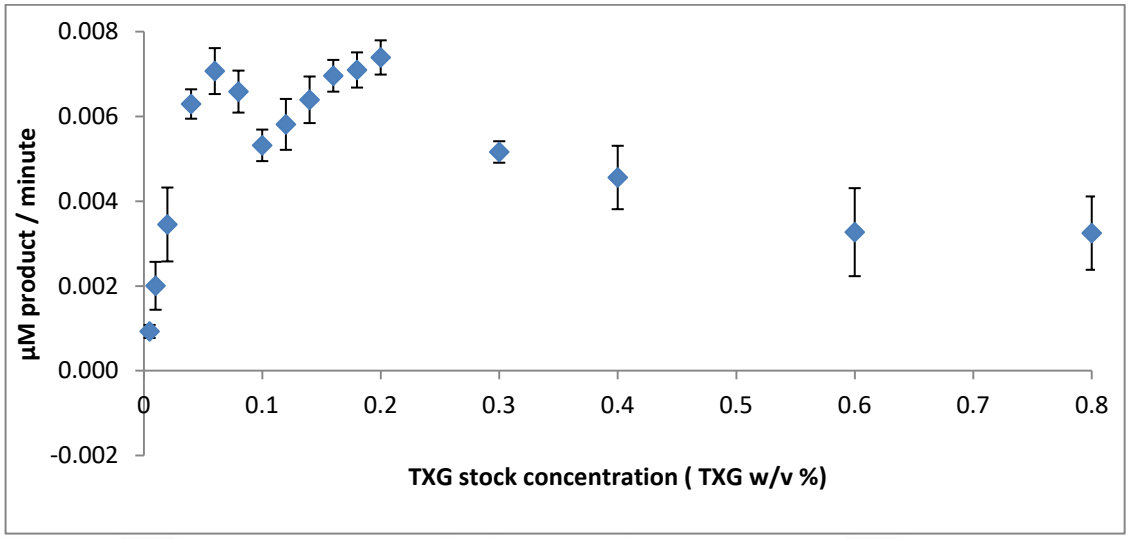

Figure 4.94. PtXTH3 reaction rates graph with various TXG concentrations and 50 µM XGO. Error bars are given on graph.

HEC donor concentration optimization for kinetic studies was carried using 7 different concentrations (w/v) between 0.8 to 0.05. Hybrid product amounts were measured by HPLC and converted into µM product formed/min reaction rate for each donor concentration (Table 4.35). When these values were plotted, a bell shape graph of reaction rate vs. HEC donor concentration was achieved, with a peak point at 0.4 per cent w/v HEC (Figure 4.95). Thus, 0.4 per cent w/v HEC was used for kinetic calculations.

Table 4.35. PtXTH3 reaction rates on various HEC concentrations and 50 µM XGO.

Donor stock concentration (w/v per cent)	**Donor final concentration (per cent w/v)**	**Fluorescence of HEC-XGO hybrid molecule**	**µM product formed/min**
0.8	0.35	324.0	0.0034
0.6	0.26	415.9	0.0043
0.4	0.17	458.8	0.0047
0.3	0.13	302.4	0.0031
0.2	0.09	224.0	0.0023
0.1	0.04	132.2	0.0014
0.05	0.02	113.0	0.0012

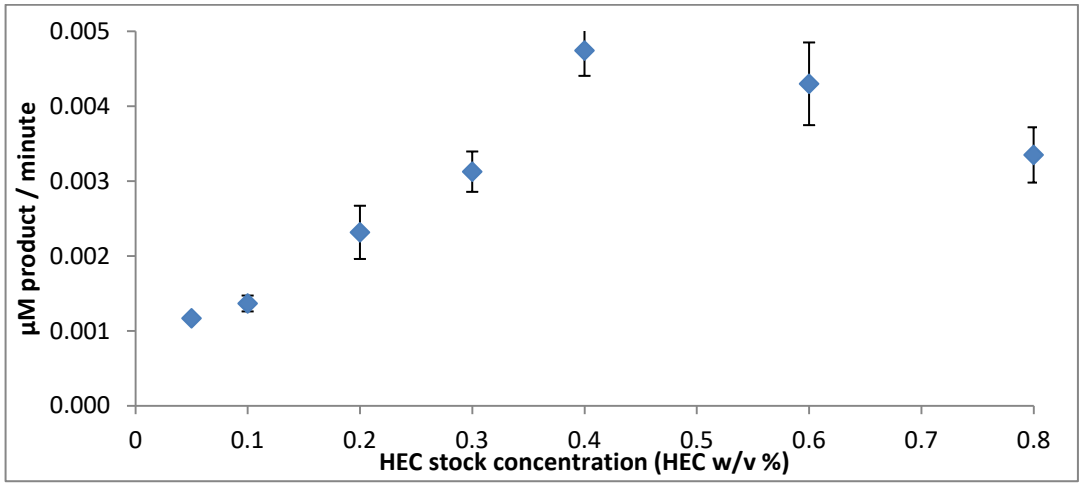

Figure 4.95. PtXTH3 reaction rates graph with various HEC concentrations and 50 µM XGO. Error bars are given on graph.

BBG donor concentration optimization was carried using 7 different BBG concentrations between 0.8 per cent w/v to 0.05 per cent w/v in enzyme activity reactions. Amounts of hybrid products generated by PtXTH3 within a particular incubation period were quantified by HPLC system and converted into µM product formed/min reaction rate for each donor concentration (Table 4.36). Then, these values were plotted on a graph, giving a peak point of reaction rate at concentration 0.3 per cent w/v (Figure 4.96). Thus, 0.3 per cent w/v BBG concentration was used for kinetic studies in order to eliminate any concentration based limiting effect of donor substrate.

Table 4.36. PtXTH3 reaction rates on various BBG concentrations and 50 µM XGO.

BBG donor stock concentration (w/v per cent)	**Donor final concentration (per cent w/v)**	**Fluorescence of BBG-XGO hybrid molecule**	**µM product formed/min**
0.8	0.35	238.95	0.0025
0.6	0.26	326	0.0034
0.4	0.17	420.8	0.0044
0.3	0.13	444.4	0.0046
0.2	0.09	239.5	0.0025
0.1	0.04	109.3	0.0011
0.05	0.02	45.3	0.0005

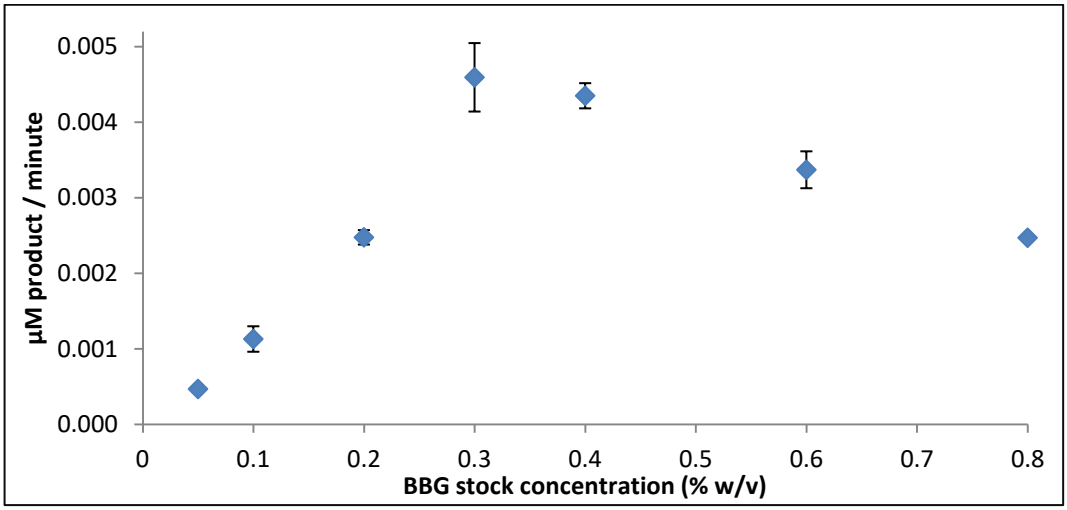

Figure 4.96. PtXTH3 reaction rates graph with various BBG concentrations and 50 µM XGO. Error bars are given on graph.

PtXTH3 kinetic calculations were carried for three different donors; TXG, HEC and BBG through reactions with X7 acceptor. Effect of X7 concentration on enzyme reaction rates using all three donors were studied. With TXG, X7 concentrations ranging between 1-1000 µM were used and reaction rates were plotted onto a graph to give Michaelis Menten plot (Figure 4.97). Using this plot, Lineweaver-Burke plot of PtXTH3 on TXG was generated and kinetic value calculations were done accordingly (Figure 4.98, Table 4.37).

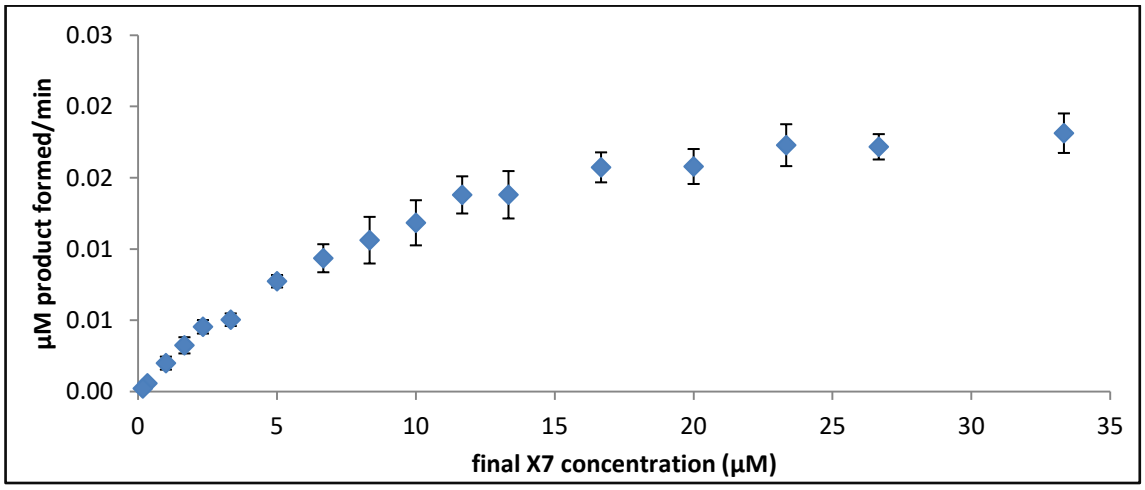

Figure 4.97. Michaelis-Menten plot of PtXTH3 enzyme with 0.2 per cent w/v TXG and various X7 concentrations.

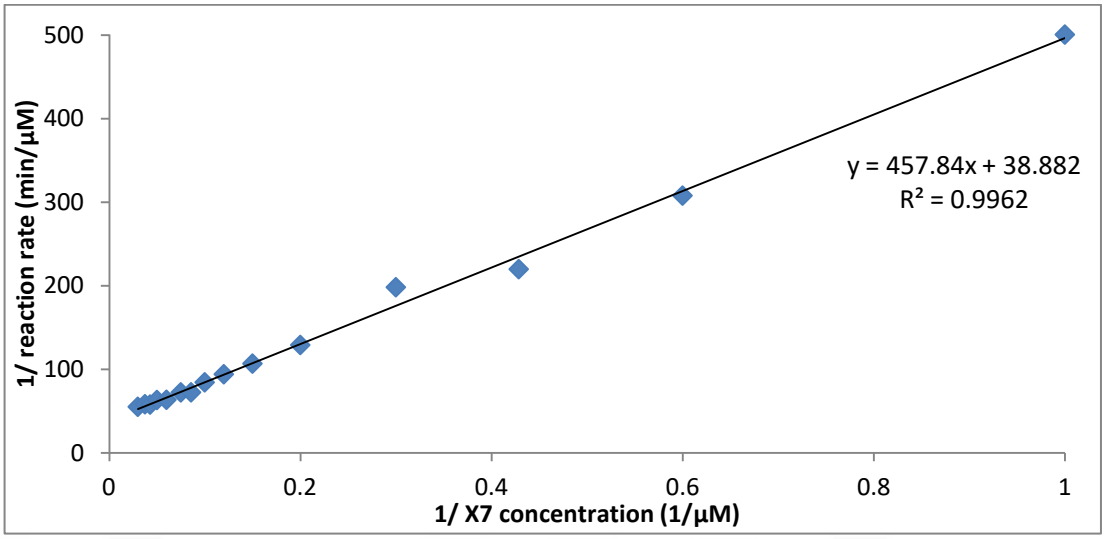

Figure 4.98. Lineweaver-Burke plot of PtXTH3 enzyme with 0.2 per cent w/v TXG and various X7 concentrations.

With HEC donor, X7 concentrations ranging between 1-150 µM were used and reaction rates were plotted onto a graph to give Michaelis Menten plot (Figure 4.99). Using this plot, Lineweaver-Burke plot of PtXTH3 on TXG was generated and kinetic value calculations were done accordingly (Figure 4.100, Table 4.37).

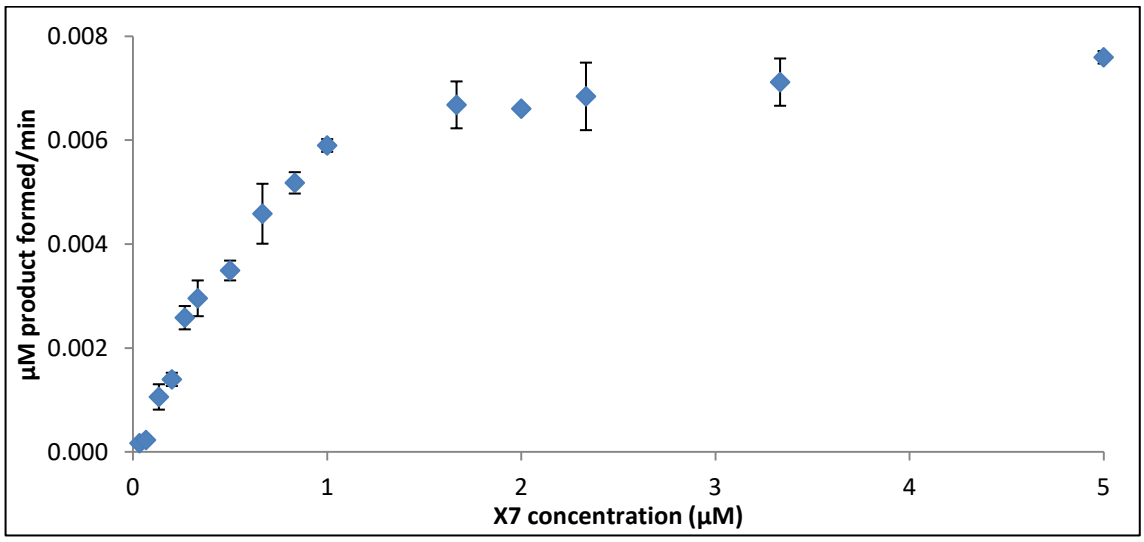

Figure 4.99. Michaelis-Menten plot of PtXTH3 enzyme with 0.4 per cent w/v HEC and various X7 concentrations.

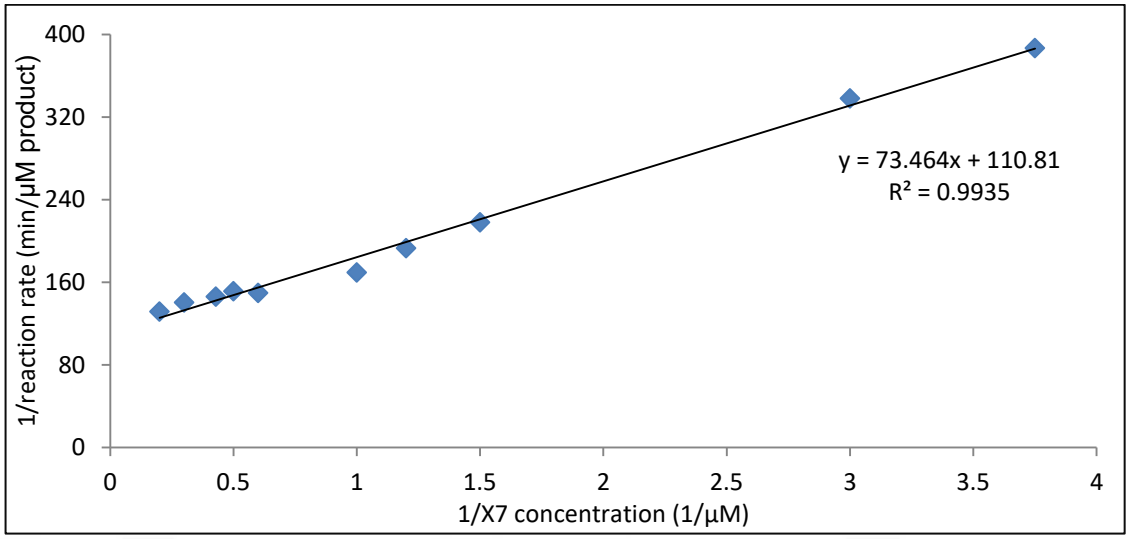

Figure 4.100. Lineweaver-Burke plot of PtXTH3 enzyme with 0.4 per cent w/v HEC and various X7 concentrations.

With BBG donor, X7 concentrations ranging between 1-80 µM were used and reaction rates were plotted onto a graph to give Michaelis Menten plot (Figure 4.101). Using this plot, Lineweaver-Burke plot of PtXTH3 on TXG was generated and kinetic value calculations were done accordingly (Figure 4.102, Table 4.37).

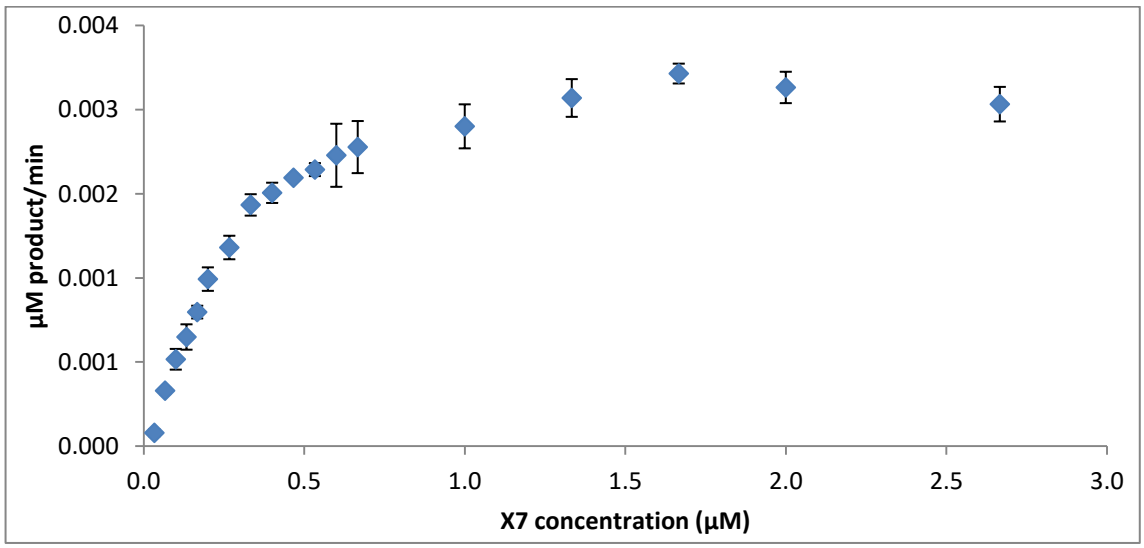

Figure 4.101. Michaelis-Menten plot of PtXTH3 enzyme with 0.3 per cent w/v BBG and various X7 concentrations.

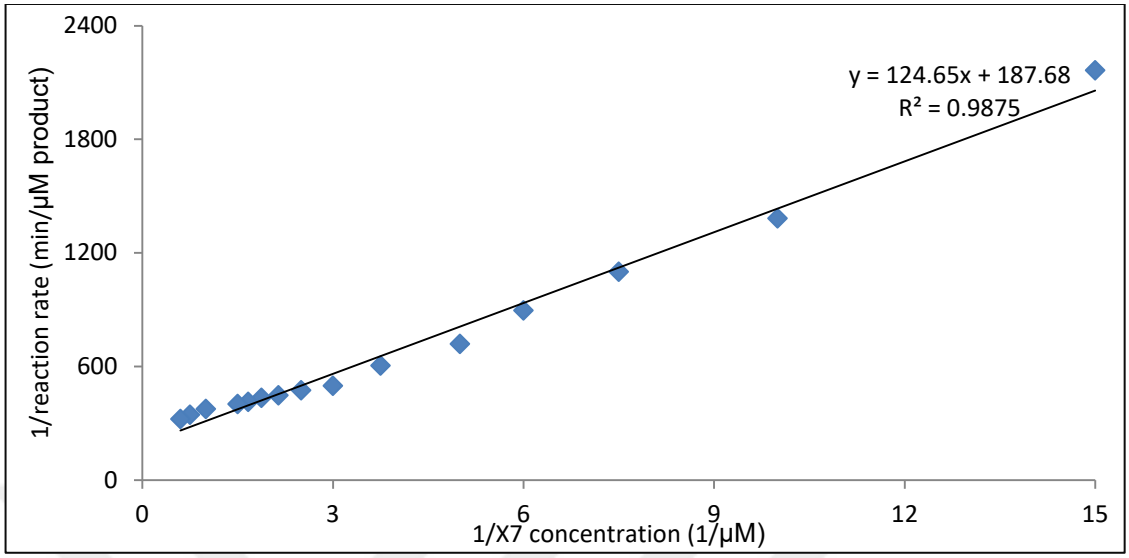

Figure 4.102. Lineweaver-Burke plot of PtXTH3 enzyme with 0.3 per cent w/v BBG and various X7 concentrations.

Table 4.37. V_{max}, K_m and K_{cat} values of PtXTH3 reactions with TXG-X7, BBG-X7 and HEC-X7 donor-acceptor couples.

	TXG-X7	**HEC-X7**	**BBG-X7**
V_{max}	0.026 µm/min	0.009 µM/min.	0.005 µM/min.
K_m	11.776 µM	0.663 µM	0.664 µM
K_{cat}	2.903 min^{-1}	0.407 min^{-1}	0.060 min^{-1}

4.7.3.5. TaXTH5

TaXTH5 enzyme is another Group I member, showing XET activity. As a monocot representative of Group I XTH enzymes, enzymic analyses were carried out using a third batch of purified and polished TaXTH5 enzyme. Enzyme was showing endotransglycosylation activity between TXG-XGO, TXG-X7, TXG-BB, TXG-CT, HEC-XGO, HEC-X7, HEC-BB donor-acceptor couples. At least 3 different time points were

used during activity tests with 3 repeats. Endotransglycosylation activity of TaXTH5 enzyme on TXG-BB, TXG-CT and HEC-BB couples were very low and specific activity calculations were not carried with these couples due to low amounts of activity. On the other hand, activity calculations were finalized for other substrate couples under inspection (Figure 4.103, Figure 4.104). Hybrid product amounts of TaXTH5 XET activity with different substrate couples during different incubation periods were measured by HPLC system and converted into pkatal / mg enzyme activity (Table 4.38).

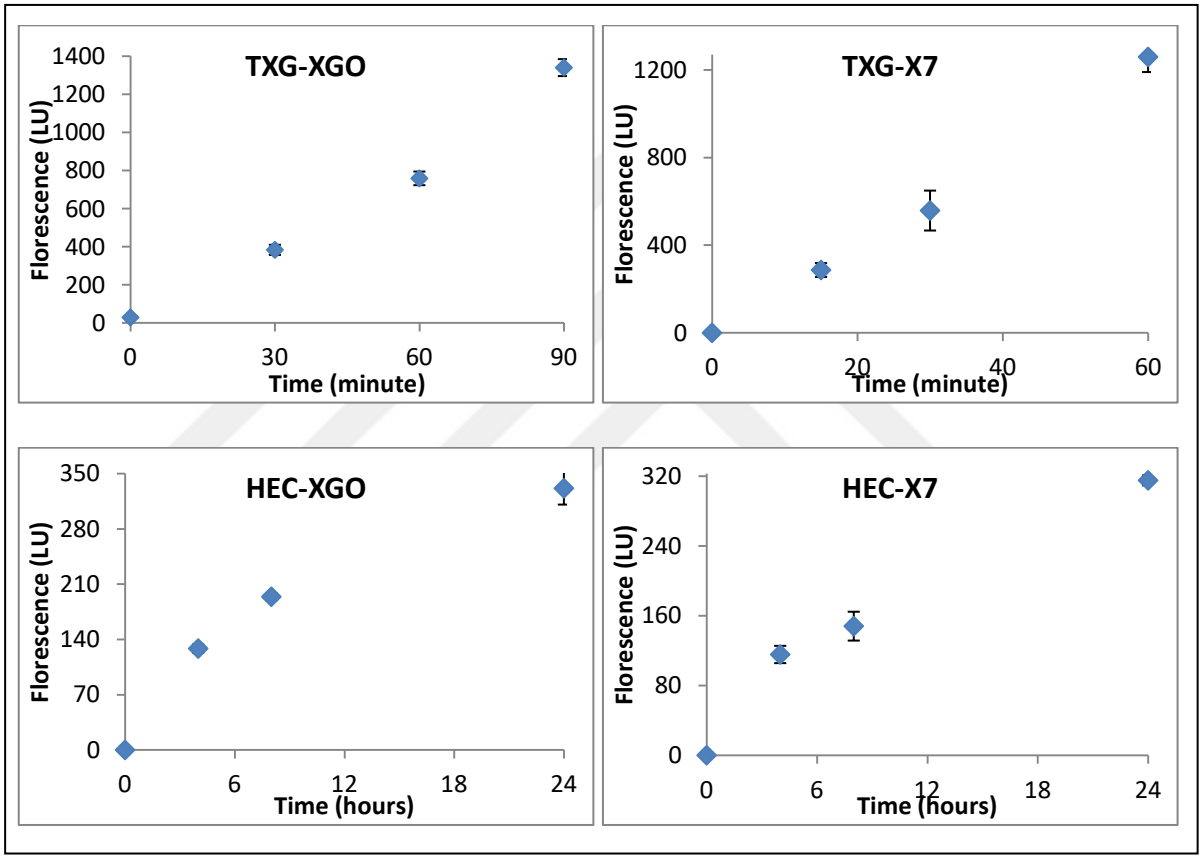

Figure 4.103. Time interval enzyme activity studies of TaXTH5 with different donor-acceptor couples. Florescence amounts of generated hybrid products were studied by HPLC. Donor-acceptor couples and error bars are indicated on graphs.

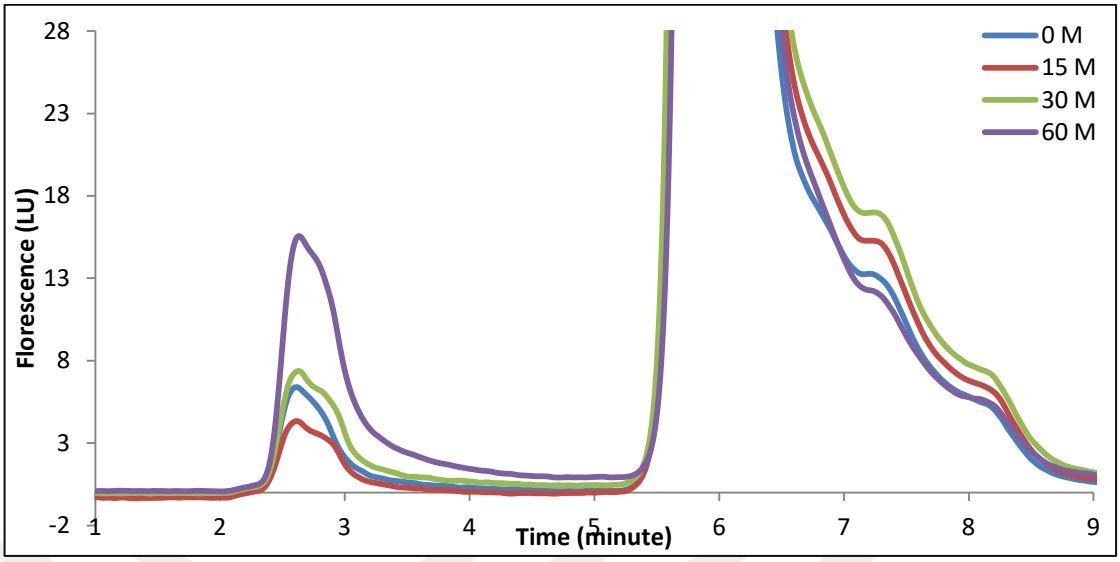

Figure 4.104. HPLC chromatogram of GhXTH2 time interval enzyme activity reaction using TXG-XGO substrate couple. Incubation times of each line is indicated on graph.

Table 4.38. Specific enzyme activity of PtXTH3 on various donor-acceptor couples and ratios of specific activities to TXG-XGO and HEC-XGO couples' activities.

	Pkatals / mg enzyme	**per cent TXG-XGO**	**per cent HEC-XGO**
TXG-XGO	5.698	100	
TXG-X7	7.435	130.475	
TXG-BB	trace		
TXG-CT	trace		
HEC-XGO	0.104	1.828	100
HEC-X7	0.035	0.620	33.913
HEC-BB	trace		

TaXTH5 enzyme was observed to be a loyal XET enzyme, showing only 1.8 per cent activity with HEC donor compared to TXG donor. These findings suggest TaXTH5 enzyme is metabolically more active in xyloglucan remodelling *in muro* compared to remodelling of other plant cell wall components.

Analysis of substrate specificity revealed donors and acceptors TaXTH5 is showing activity with. However, in order to compare activity with other known XTH enzymes, kinetic values needed to be studied. Thus, TaXTH5 enzyme kinetics were examined using TXG donor and XGO acceptor. Firstly, TXG donor concentration was optimized in order to facilitate the fastest XET activity of enzyme on TXG-XGO donor-acceptor couple, without effects of donor viscosity on enzyme reaction. TXG concentrations between 0.4 per cent w/v to 0.05 per cent w/v were used as donors and hybrid TXG-XGO amount were measured (Table 4.39). Amount of hybrid product continue to increase with increasing donor concentration (Figure 4.105). However, this increase wasn't directly proportional to increase in reaction rate. Also, increasing donor concentration can have negative effects on HPLC system. Taking all of these considerations into account, 0.1 per cent w/v TXG donor was used during kinetic experiments.

Table 4.39. TaXTH5 reaction rates on various TXG concentrations and 50 µM XGO.

TXG Donor stock concentration (w/v per cent)	**Donor final concentration (per cent w/v)**	**Fluorescence of TXG-XGO hybrid molecule**	**µM product formed/min**
0.4	0.308	724.9	0.0073
0.3	0.231	623.6	0.0062
0.2	0.154	520.6	0.0051
0.1	0.077	436.8	0.0043
0.05	0.038	301.9	0.0029

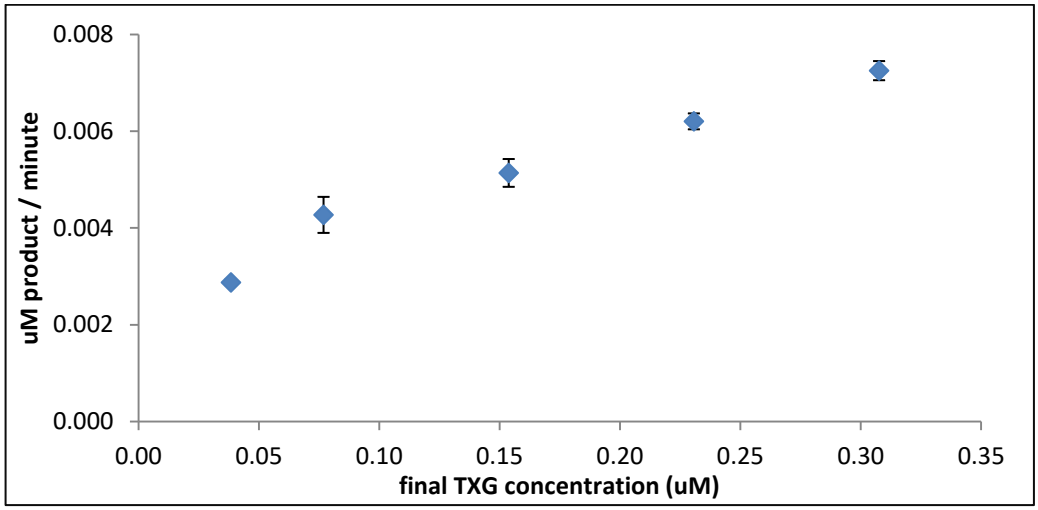

Figure 4.105. TaXTH5 reaction rates graph with various BBG concentrations and 50 µM XGO. Error bars are given on graph.

TaXTH5 enzyme activity rate was tested with 14 different XGO concentrations ranging from 1 µM to 400 µM XGO. Reaction rate of TaXTH5 with each acceptor concentration was studied by measuring hybrid product amount by HPLC and converting that amount into reaction rate. When these reaction rate values are plotted on a graph versus XGO concentration, it was observed that TaXTH5 reaction rate reaches a plateau phase at 300 µM XGO concentration (Figure 4.106), giving Michaelis-Menten graph. Using values on Michaelis-Menten graph, Lineweaver-Burke plot was generated for TaXTH5 enzyme and kinetic calculations were carried (Figure 4.107). V_{max} was calculated as 0.0211 µM / min, K_m was calculated as 4.9628 µM and K_{cat} was calculated as 0.0525 min^{-1}.

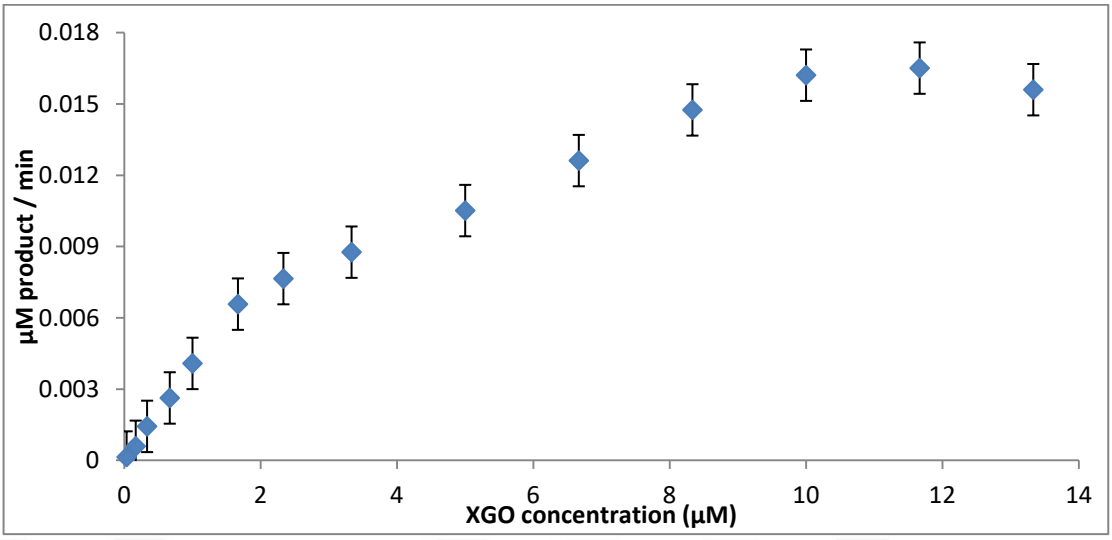

Figure 4.106. Michaelis-Menten plot of TaXTH5 enzyme with 0.3 per cent w/v BBG and various X7 concentrations.

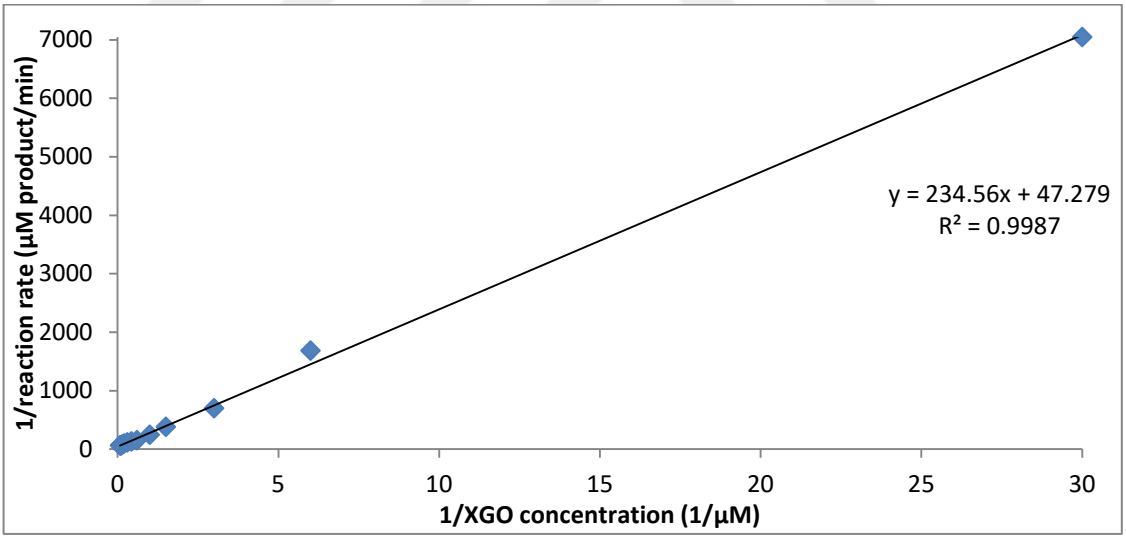

Figure 4.107. Lineweaver-Burke plot of TaXTH5 enzyme with 0.3 per cent w/v BBG and various X7 concentrations.

4.8. EQUISETUM SAMPLE COLLECTION AND SPECIES IDENTIFICATION

Equisetum species distribution through Turkey was investigated. Only 9 *Equisetum* species were reported to exist in Turkey; *Equisetum hyemale, Equisetum ramosissimum, Equisetum variegatum, Equisetum fluviatile, Equisetum palustre, Equisetum sylvaticum, Equisetum arvense, Equisetum telmateia* and *Equisetum x litorale* (www.tubives.com, Turkish Plant Data Service version 2.0 Beta). These species show a variable distribution between different geographical regions within Turkey.

Equisetum samples were found and collected from 2 different areas; Balıkesir and Istanbul_Belgrad Forest Neşet Suyu Parkuru. In both regions, plant samples were naturally growing in forest, next to many different native plant species, in shadowy areas and moist lands that are close to creeks. Out of 9 *Equisetum* species reported in Turkey, only 6 are found in Istanbul and these are *E. hyemale, E. ramosissimum, E. palustre, E. sylvaticum, E. arvense, E. telmateia* (Figure 4.108).

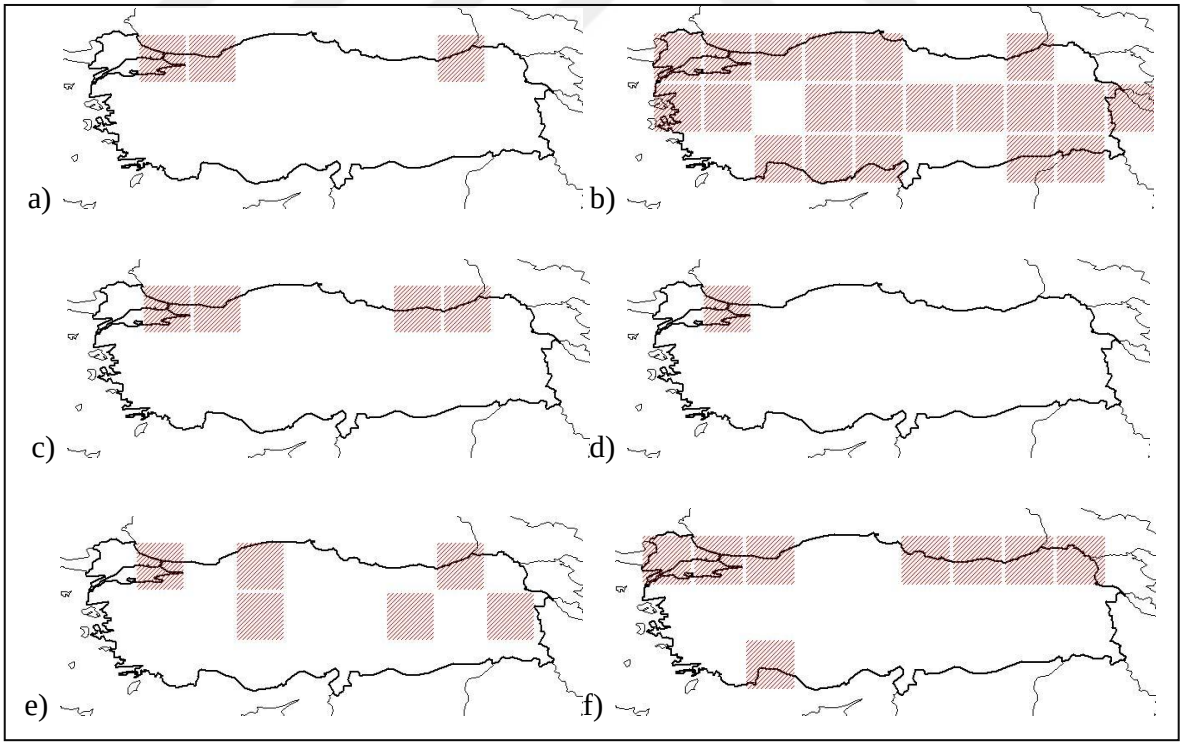

Figure 4.108. Geographical distribution of several *Equisetum* species in Turkey. a) *E. hyemale*, b) *E. ramosissimum*, c) *E. palustre*, d) *E. sylvaticum*, e) *E. arvense*, f) *E. telmateia*.

Plant samples were collected during different time periods in order to visualize growth pattern on *Equisetum* sample. During every sample collection, plants were pulled out of soil without harming or breaking stem of individual samples in order to inhibit any change in cell wall metabolism. *Equisetum* species don't have true root systems however they have under soil stems with rhizomes. Plants were pulled from the soil with their underground stems, so that they won't dry before extraction. Sampling was done twice from Balıkesir region, once in spring and once during autumn. Sampling from Istanbul was done more frequently, due to access ease of the area from Yeditepe University (Table 4.40). Another reason for preference of Istanbul for sampling is short time requirement for transportation of samples to the Plant Biotechnology laboratory for processing.

Table 4.40. List of *Equisetum* sampling dates and places.

Sampling Date (month, year)	**Sampling Region**
May, 2014	Balıkesir
September, 2014	Belgrad Forest Bahçeköy situs, Neşetsuyu track
October, 2014	Balıkesir
June, 2015	Belgrad Forest Bahçeköy situs, Neşetsuyu track
November, 2015	Belgrad Forest Bahçeköy situs, Neşetsuyu track
April, 2016	Belgrad Forest Bahçeköy situs, Neşetsuyu track
June, 2016	Belgrad Forest Bahçeköy situs, Neşetsuyu track
July, 2016	Belgrad Forest Bahçeköy situs, Neşetsuyu track
September, 2016	Belgrad Forest Bahçeköy situs, Neşetsuyu track

Belgrad Forest Neşetsuyu track region was investigated during different visits for plant collection throughout the year. It was observed that *Equisetum* plants starts growing early April and they are observed as 40-80 cm during April-May months. Towards the end of May and during June, July and August plants reaching up to 1.5-2 m in height were observed as close populations. As the end of August and beginning of September, other species in forest ground start to over populate *Equisetum* plants, thus *Equisetum*s start dying because of nutrient depletion caused by other plant growths. It is possible to find newly sprouting relatively short plants (20-60 cm) between April-September months,

regardless of the season. As fall season takes over the summer and as weather starts getting colder, *Equisetum* population dies, until sprouting again in early spring.

Samples collected from Istanbul Belgrad Forest Neşetsuyu Parkuru examined phenotypically for species determination. Examinations were carried both by bare eyes and under stereomicroscope (Figure 4.109). The species we were working with was identified as *Equisetum telmateia* using data from the TUBIVES database and with kind help of Prof. Dr. Tamer Ozcan (Istanbul University Department of Biology Botany).

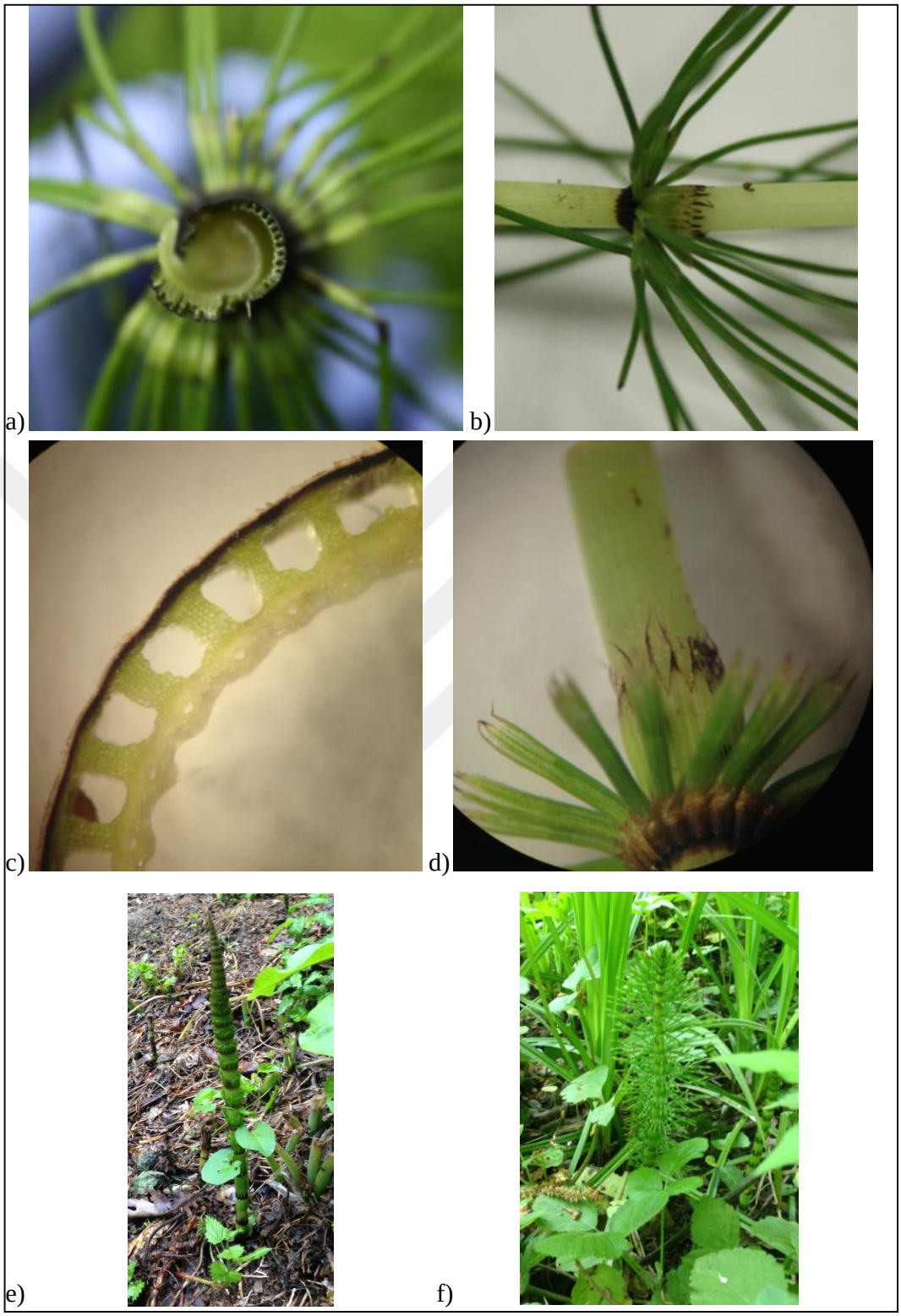

Figure 4.109. Images of *Equisetum* collected from Istanbul Belgrad Forest. a) Transversal section of internode, b) internode and leaf section, c) Transversal section of internode under stereomicroscope, 32X magnification, d) internode and leaf section internode and leaf section, e) on site imaging of newly sprouting plant, f) on site image of young plant.

4.9. EQUISETUM EXTRACT PREPARATION AND PROTEIN PURIFICATION

Equisetum extract preparations were carried using fresh samples. For extraction method optimization, two methods, Fry method and Fincher method, were compared. Extracts obtained were used in TXG-XG0 and BBG-XGO enzyme reactions and formed hybrid TXG-XGO and BBG-XGO product amounts were measured by HPLC and compared in order to interpret efficiency and usefulness of both methods (data not shown). Amount of hybrid TXG-XGO product will reflect XET activity whereas amount of hybrid BBG-XGO will reflect MXE activity. Obtaining higher amounts of hybrid BBG-XGO compared to TXG-XGO will result in higher amount of target MXE enzyme compared to other endotransglycosylases.

Extract prepared according to Fry method resulted in higher amounts of hybrid products. Also, extraction buffer used in Fry method was less toxic and safer to use. Thus, all of the following protein extractions were carried according to Fry method.

Other concerns about protein purification from *Equisetum* are to find the plant section with the highest target enzyme activity in the right growth stage and the best chromatographic approach to fully purify target *Equisetum* enzyme from any contaminant proteins. Thus, as a first step in optimizing purification process, young stem part and rhizomes of May 2014 plants were separated and extracts of these samples were prepared separately. Extracts were tested using TXG-XGO and BBG-XGO donor-acceptor couples for presence of MXE enzyme activity. Hybrid product amounts were measured by HPLC system (Table 4.41) and ratios of BBG-XGO hybrid product florescence over TXG-XGO hybrid product florescence of both plant sections were evaluated. None of the samples showed higher ratio of MXE compared to XET. This highly likely to be the consequence of gradual protein degradation during sample transportation from Balıkesir and sample storage during protein extraction method optimization.

Table 4.41. Florescence amounts of TXG-XGO and BBG-XGO hybrid products generated by May 2014 Balıkesir *Equisetum* extracts.

Sample name	**TXG-XGO hybrid product florescence**	**BBG-XGO hybrid product florescence**	**BBG-XGO/ TXG-XGO**
May 2014 Balıkesir young stem	357.6	319.2	0.893
May 2014 Balıkesir rhizome	200.9	240.8	1.198

September 2014 and October 2014 *Equisetum* samples were freshly used after sample collection. Young stem, mature stem and leaf tissues of September 2014 sample were used for protein extraction whereas stem and leaf parts of October 2014 were used for the same purpose. Tissue extracts were prepared according to Fry method, using 62 gr September 2014 young stem, 200 gr September 2014 mature stem, 100 gr September 2014 leaves, 200 gr October 2014 stem and 200 gr October 2014 leaves. Extracts were analysed for the presence of target MXE enzyme by performing enzyme activity test using TXG-XGO and BBG-XGO donor-acceptor couples. Hybrid product amounts were measured by HPLC and BBG-XGO florescence values were proportioned over TXG-XGO florescence values in order to interpret MXE activity in the specific plant parts (Table 4.42). It was observed that September young stem and leaf parts are promising as MXE sources whereas October samples showed low XET and MXE activity. September 2014 mature stem sample showed more XET activity compared to MXE activity however this sample was chosen for initial MXE purification trial. There are couple of reasons for such a sample selection. Firstly, protein amount of September 2014 mature stem sample was higher compared to other September 2014 extract samples (Table 4.43). Protein concentration was studied by Bradford assay. Also, since we don't have any insights about chemical structure of target MXE enzyme, it would take some trials before optimizing chromatographic purification steps. Thus, in order to eliminate risk of losing a valuable sample during optimization steps, a less significant sample was chosen for purification steps optimization.

Table 4.42. Florescence amounts of TXG-XGO and BBG-XGO hybrid products generated by September and October 2014 Balıkesir *Equisetum* extracts.

Name of the sample	**TXG-XGO hybrid product florescence**	**BBG-XGO hybrid product florescence**	**BBG-XGO/ TXG-XGO**
September, 2014-young stem	159.27	202.57	1.27
September,2014-mature stem	346.87	220.27	0.64
September, 2014-leaf	117.57	161.27	1.37
October, 2014-stem	132.05	106.75	0.81
October, 2014-leaf	38.55	46.35	1.20

Table 4.43. Protein amounts of September 2014 *Equisetum* extracts.

Sample name	**Protein amount (mg)**
September 2014 mature stem	102
September 2014 young stem	48.2
September 2014 leaves	17.6

Firstly, ammonium sulphate precipitation using 90 per cent ammonium sulphate saturation was performed with September 2014 mature stem extract. Protein pellet was dissolved in 20 mM Tris-HCl pH 8.0 buffer and dialysed against 20 mM Tris-HCl pH 8.0 buffer in order to remove excessive salts. Then, protein sample was loaded onto HiScreen Capto Q column for an initial anion exchange step. Proteins were eluted from column depending on their total surface charges using linear salt gradient (20 mM Tris HCl, 1 M NaCl, pH 8.0) from no NaCl to 1 M NaCl (Figure 4.110). Outcomes of column were divided into fractions of 2 mL. Flow-through during sample loading onto column and fractions were tested for XET and MXE activity using TXG-XGO and BBG-XGO donor-acceptor couples. Enzyme activity reactions products were analysed by HPLC system (Figure 4.111).

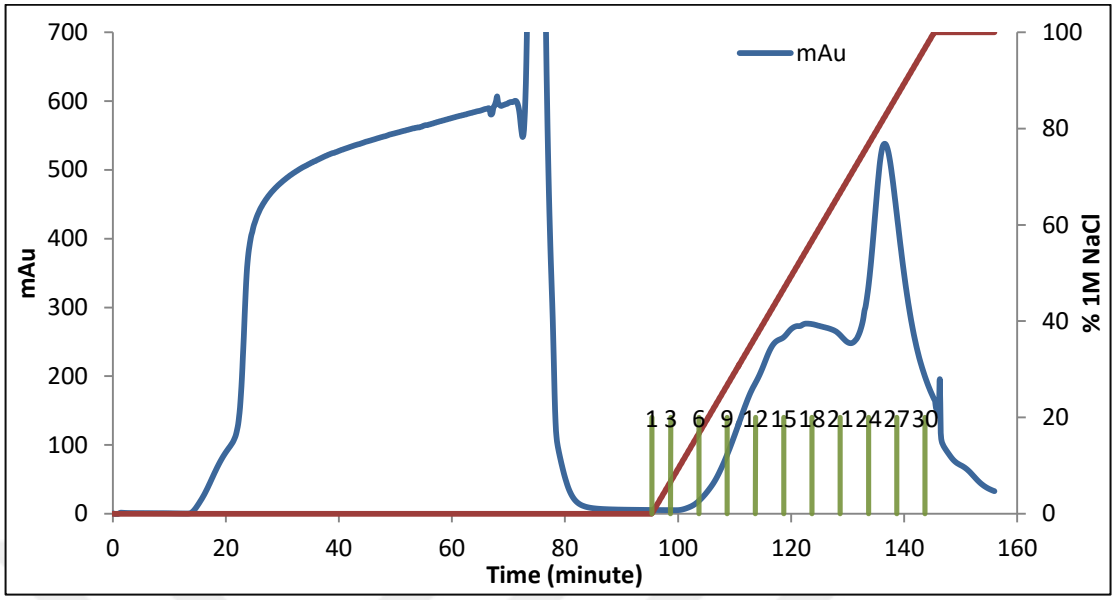

Figure 4.110. September 2014 *Equisetum* mature stem HiScreen Capto Q anion exchange column chromatogram.

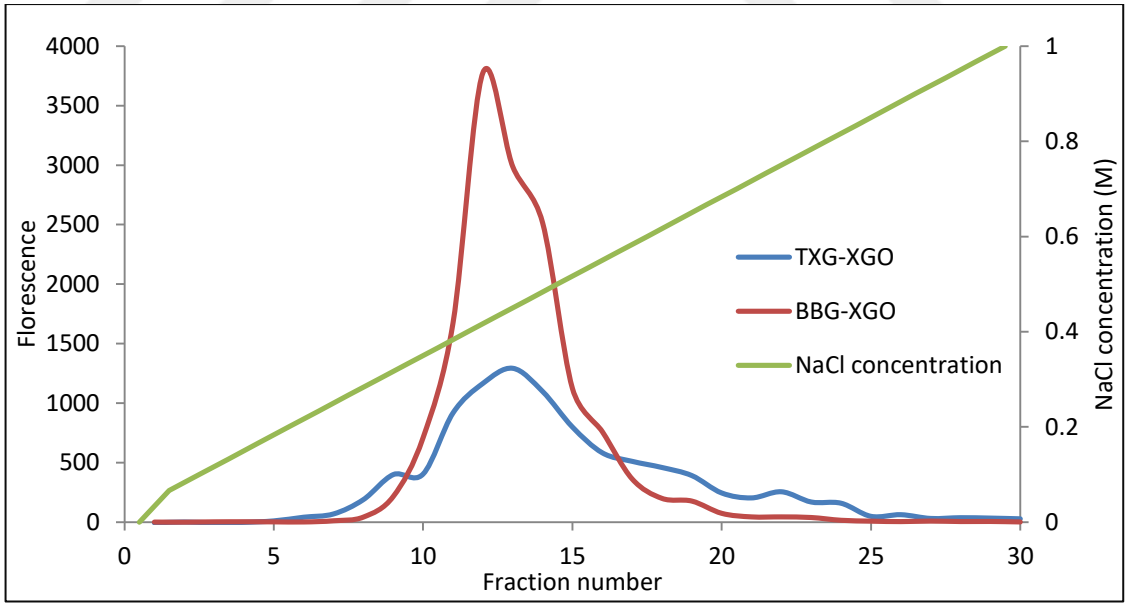

Figure 4.111. Florescence amounts of TXG-XGO and BBG-XGO hybrid products generated during enzyme activity reactions with September 2014 *Equisetum* Capto Q elution fractions.

When XET and MXE activities of fractions were compared, fractions 10-16 showed higher amounts of hybrid BBG-XGO product compared to hybrid TXG-XGO product, meaning target MXE enzyme was eluted in fractions 10-16. Thus, these fractions were pooled together and buffer exchanged into 50 mM sodium phosphate 1.7 M ammonium sulphate pH 7.0 buffer using HiPrep DeSalting 26/10 column for the second chromatographic separation step. As second chromatography step, hydrophobic interaction chromatography was carried by HiScreen Capto Butyl column. Loaded sample was eluted by 20 mM sodium phosphate pH 7.0 buffer into 2 mL fractions. These fractions were tested by enzyme activity test using both TXG-XGO and BBG-XGO donor-acceptor couples, yet no positive results were obtained for neither any fraction nor flow-through during column loading. This situation might be due to loss of enzyme activity/stability during hydrophobic interaction chromatography, high amounts of ammonium sulphate in starting buffer of this chromatographic step might have been detrimental for protein since it was purer than total extract while loading to HIC column.

Equisetum September 2014 young stem extract was used as a second sample for purification optimization study. Proteins within the extract were precipitated by 90 per cent ammonium sulphate saturation and dissolved in 20 mM Tris-HCl pH 8.0 buffer. Excessive ammonium sulphate salt was removed by dialysing against 20 mM Tris-HCl pH 8.0 buffer. Prepared protein sample was firstly loaded onto HiScreen Capto DEAE column for a weak anion exchange separation. Elution was carried using linear salt gradient by 20 mM Tris-HCl 1M NaCl pH 8.0 buffer from no NaCl to 1M NaCl and column outcomes during elution were collected as 3 mL fractions (Figure 4.112). Both the fractions and flow-through during sample loading was used in an enzyme activity test with TXG-XGO and BBG-XGO donor-acceptor couples. However, no activity with neither of the substrate couples was observed. It was concluded that amount of protein was diluted during chromatographic separation and fraction concentration wasn't enough for activity analysis. Thus sample was way too diluted and was lost during separation.

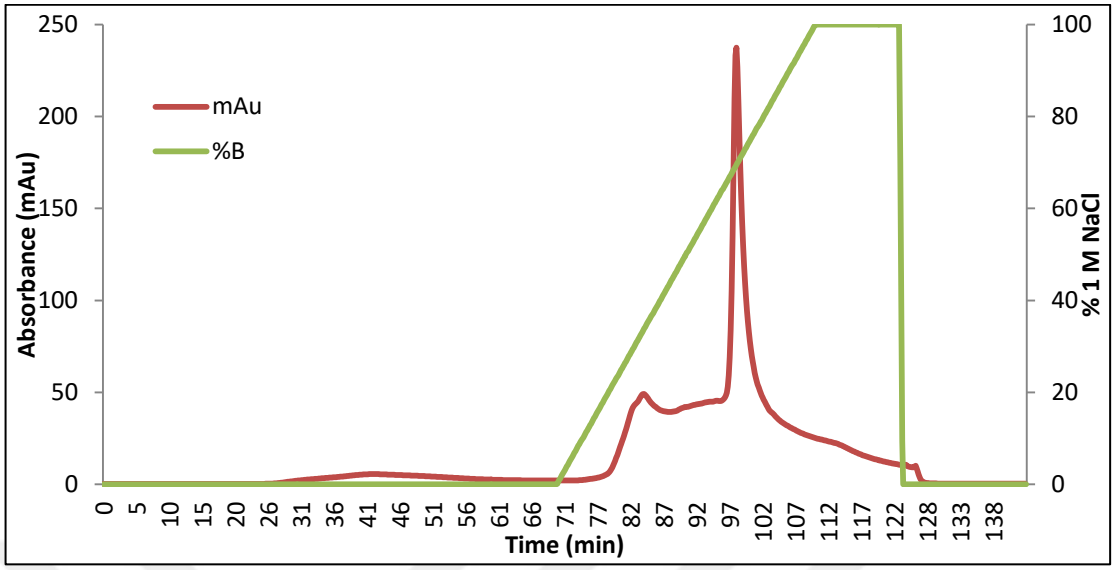

Figure 4.112. September 2014 young stem *Equisetum* protein sample HiScreen Capto DEAE weak anion exchange chromatography chromatogram.

Next trial for developing a protein purification strategy was carried by freshly collected *Equisetum* sample on June, 2015 from Belgrad forest, Istanbul. Extracts of both leaf and whole stem tissue were prepared according to Fry method using 200 gr of each tissues. Total plant extracts were screened for MXE activity by setting up enzyme activity reactions with TXG-XGO and BBG-XGO substrate couples in order to select target tissue for protein purification (Table 4.44). BBG-XGO/TXG-XGO ratio suggested that leaf sample is more likely to have higher amounts of MXE compared to XET, thus this sample was chosen for protein purification trials.

Table 4.44. TXG-XGO and BBG-XGO hybrid molecule fluorescence amounts of enzyme reaction carried with June 2015 Belgrad *Equisetum* extracts.

Tissue name	**TXG-XGO hybrid molecule fluorescence**	**BBG-XGO hybrid molecule fluorescence**	**BBG-XGO fluorescence /TXG- XGO fluorescence**
leaf	124.6	284.6	2.28
Whole stem	1330.,5	329.5	0.25

Proteins in June 2015 Belgrad *Equisetum* extract were precipitated using 90 per cent ammonium sulphate saturation. Pelleted proteins were resuspended in 50 mM sodium acetate pH 5.0 and excessive amount of ammonium sulphate salt in protein solution was removed carrying size exclusion chromatography using HiPrep 26/10 DeSalting column. Afterwards, sample was loaded on HiScreen Capto S column for cation exchange chromatography. Flow-through during sample loading was collected and positively charged proteins that are sticking onto column were eluted using 50 mM sodium acetate 1 M NaCl pH 5.0 buffer by a linear salt gradient from no NaCl to 1 M NaCl (Figure 4.113).

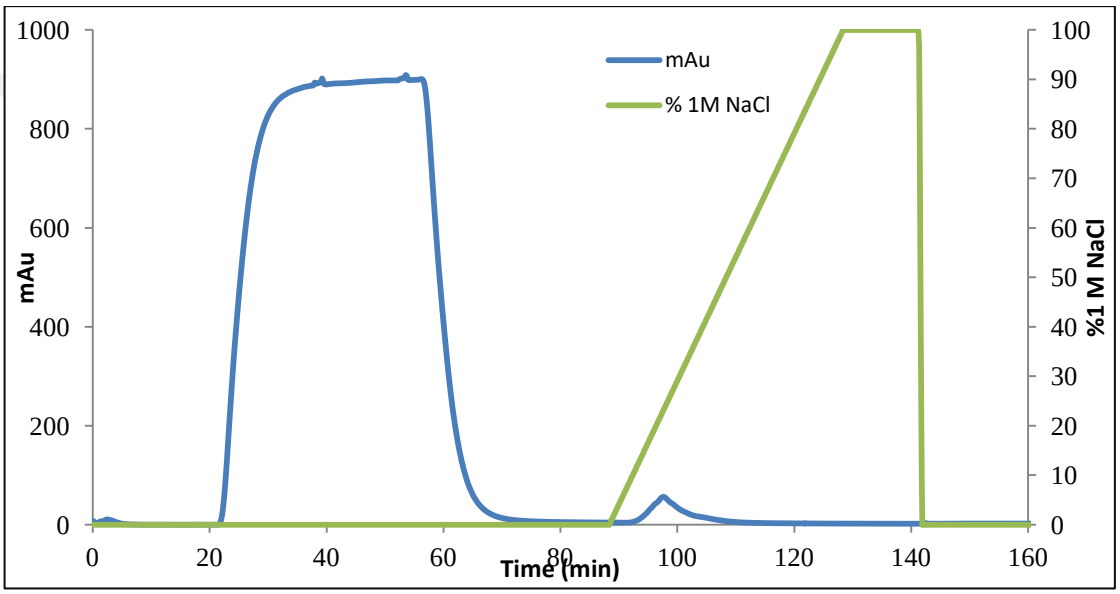

Figure 4.113. Capto S cation exchange chromatography of June 2015 Belgrad leaf *Equisetum* sample.

Since MXE and XET enzymes have a slightly acidic pI, they are expected to run through a cation exchange column at an acidic pH value without binding to the column. In order to test this phenomenon, enzyme activity test with BBG-XGO and TXG-XGO donor-acceptor couples were carried using Capto S column fractions and flow-through. Reactions were analysed with HPLC system (Figure 4.114). As expected, both MXE and XET activities were observed in flow-through but not in any fractions, MXE activity being more than XET activity.

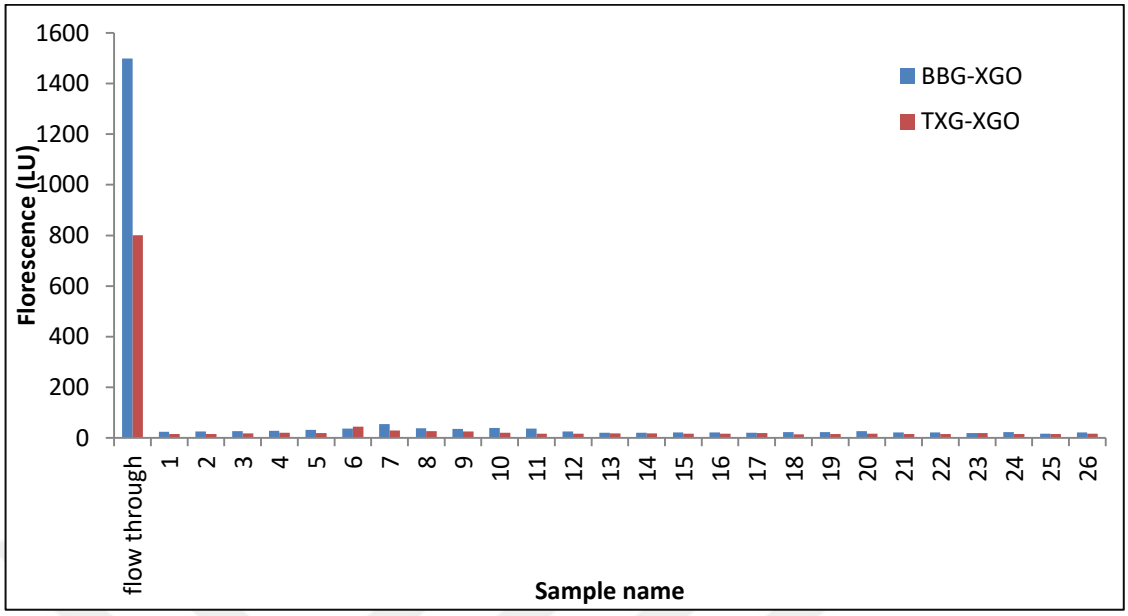

Figure 4.114. HPLC detection of enzyme activity test of June 2015 Belgrad *Equisetum* sample Capto S cation exchange column fractions and flow-through. TXG-XGO and BBG-XGO donor-acceptor couples were used in tests.

June 2015 Belgrad *Equisetum* leaf sample Capto S cation exchange column flow-through sample was buffer exchanged into 20 mM Tris-HCl pH 8.0 buffer using HiPrep 26/10 DeSalting column and carrying size exclusion chromatography. Then, sample was applied onto HiScreen Capto Q column for anion exchange chromatography and proteins bound to column were eluted depending on their charge via NaCl gradient as 1.5 mL fractions (Figure 4.115). Elution buffer, 20 mM Tris-HCl, 1M NaCl pH 8.0 was used to create linear salt gradient from no NaCl to 1M NaCl. Salt gradient result in protein separation, seen as multiple peaks on chromatogram (Figure 4.115). All fragments and flow-through during sample loading were analysed by enzyme activity test using TXG-XGO and BBG-XGO donor-acceptor couples in order to enlighten presence of MXE enzyme within the fragments. Reaction results were run on HPLC system. Flow-through showed no activity on any of the substrate couples (data not shown). Fractions 20-29 showed presence of MXE enzyme, by resulting in more BBG-XGO hybrid product compared to TXG-XGO hybrid product. When these fractions' activity traces are investigated closely, it is observed that two peaks, one big and one small, that are intertwined into each other. Fractions 24-29 seem to result in a shoulder near fractions 20-23. Also, fractions 20-23 and fractions 24-29

results in two different peaks as seen in Capto Q column chromatogram (Figure 4.116). Thus, fractions 20-23 and fractions 24-29 were pooled separately and handled as two different samples.

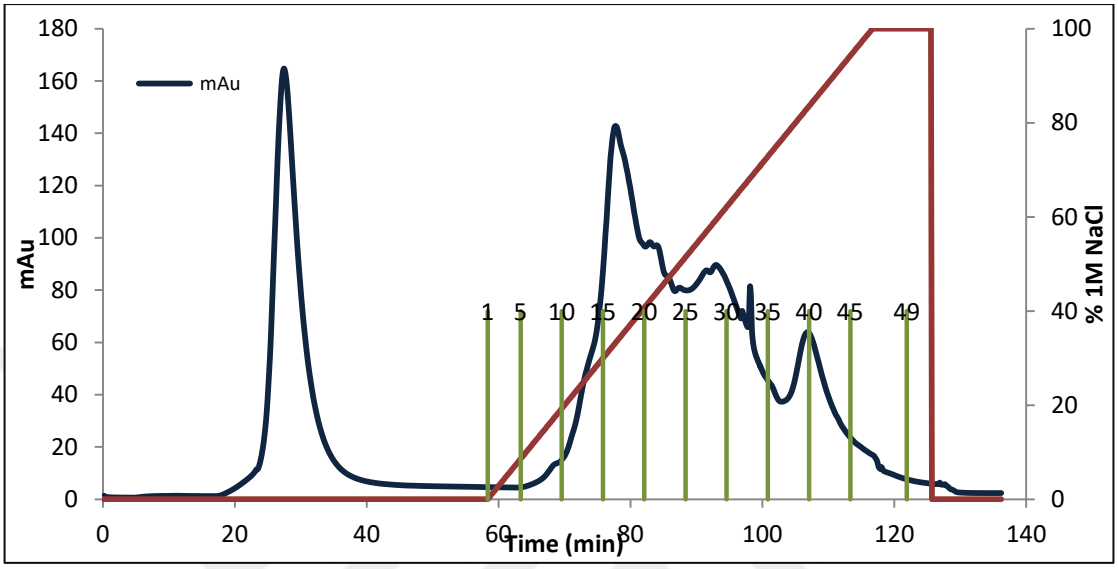

Figure 4.115. Capto Q anion exchange chromatography of June 2015 Belgrad leaf *Equisetum* sample.

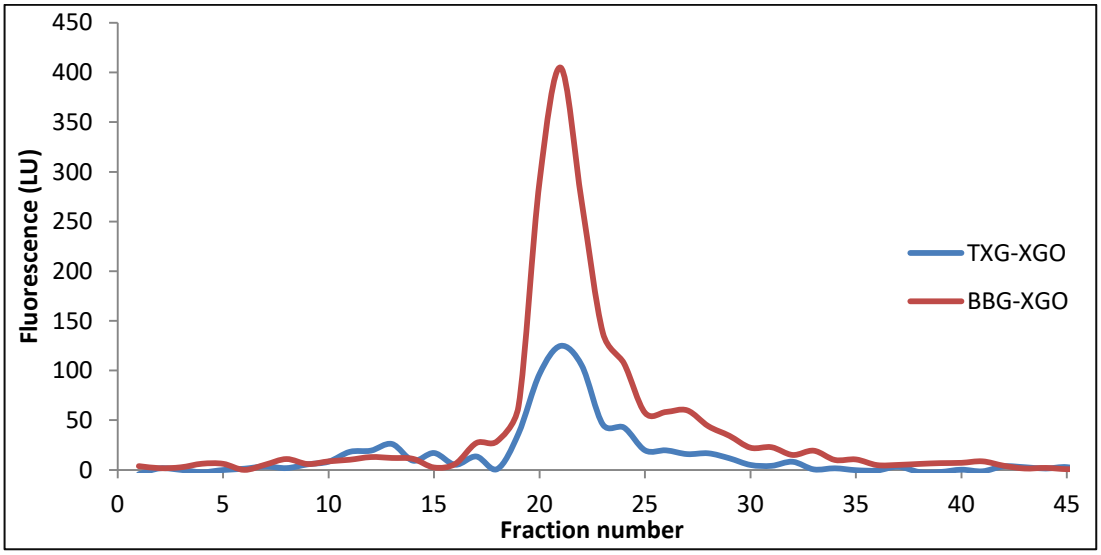

Figure 4.116. Florescence of TXG-XGO and BBG-XGO hybrid molecules generated during enzyme activity test of June 2015 Belgrad *Equisetum* leaf sample Capto Q anion exchange chromatography fractions.

Two fraction pools coming from Capto Q column anion exchange chromatography were separately loaded onto GE Superdex 75 16/100 column and polished. During runs of both pools, proteins were separated into different peaks depending on their 3D molecule sizes (Figure 4.117). Samples were fractionated during chromatography runs as 1.6 mL fractions.

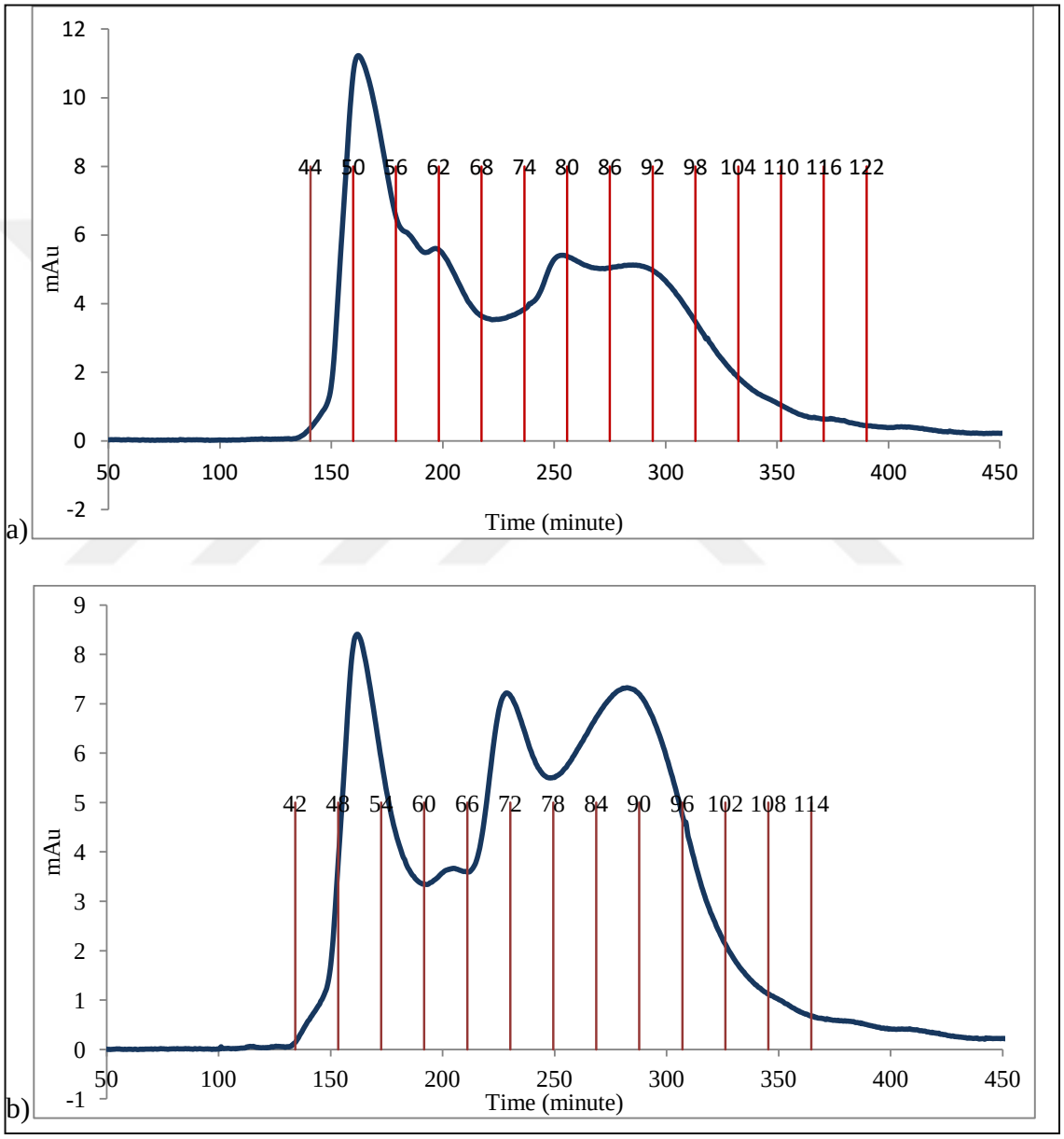

Figure 4.117. Superdex 75 16/100 column polishing of June 2015 Belgrad *Equisetum* leaf sample. a) June 2015 Belgrad *Equisetum* leaf sample Capto Q fraction 20-23, b) June 2015 Belgrad *Equisetum* leaf sample Capto Q fraction 24-29.

Fractions showing protein presence (increase in UV absorbance) were collected during polishing runs of Capto Q pools. Every one in three fraction were tested for MXE and XET enzyme activity by enzyme activity test using both BBG-XGO and TXG-XGO donor-acceptor couples. Activity test results were analysed by HPLC run in order to see amounts of BBG-XGO and TXG-XGO hybrid molecule amounts generated during enzyme activity test. On the other hand, protein concentrations of fractions were measured spectrophotometrically at 280 nm using nanodrop. HPLC data and protein concentration results were plotted together on graphs and polishing fractions showing MXE activity were interpreted through these graphs (Figure 4.118).

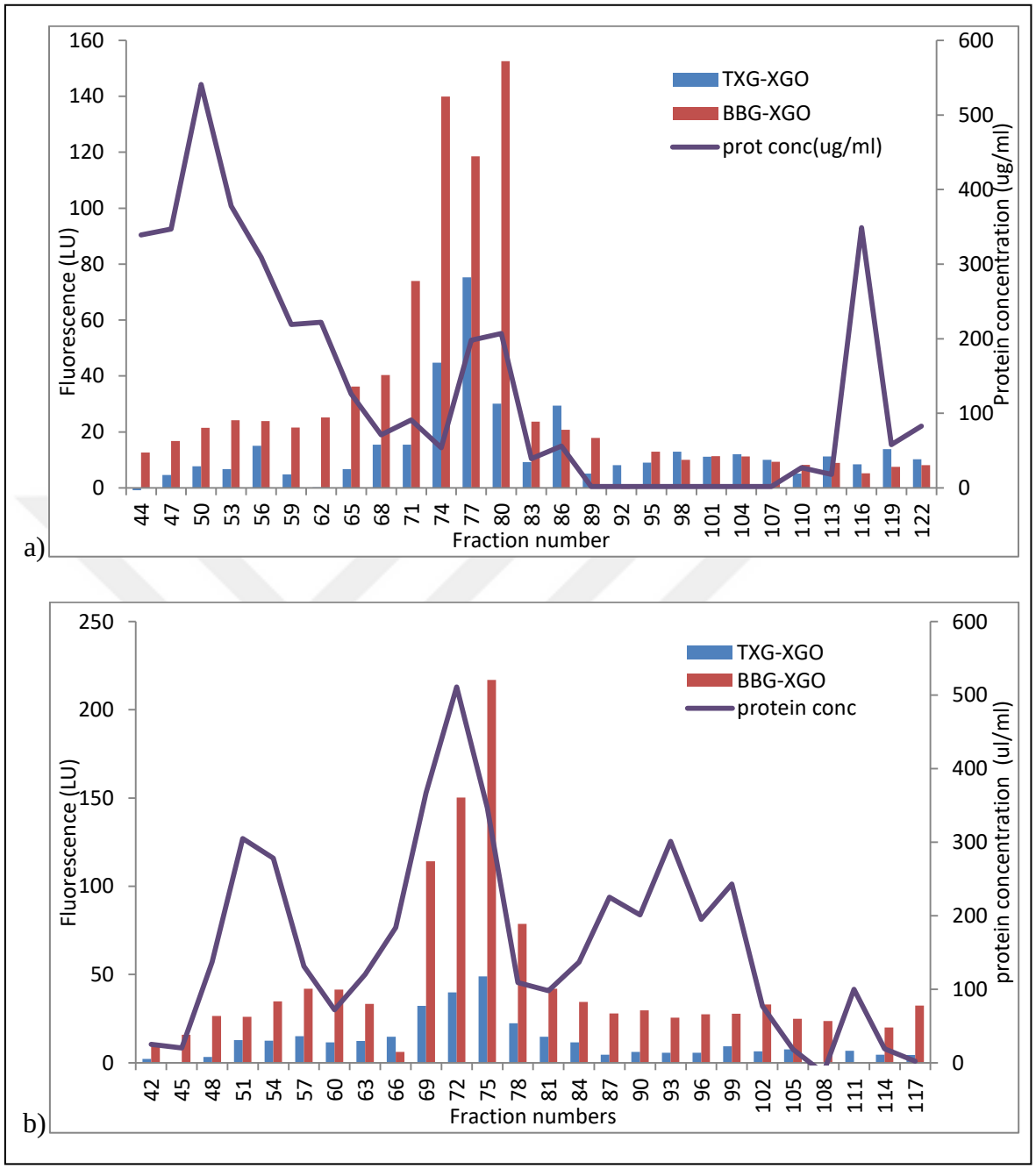

Figure 4.118. June 2015 *Equisetum* leaf protein sample Capto Q fractions 20-23 and 24-29 polishing results activity tests using TXG-XGO and BBG-XGO donor-acceptor couples and protein concentrations, a) Capto Q fractions 20-23, b) Capto Q fractions 24-29.

Fractions 74-80 from Capto Q fractions 20-23 and fractions 68-78 from Capto Q fractions 24-29 resulted in more BBG-XGO hybrid product compared to TXG-XGO hybrid product as seen in Figure 4.118. MXE activity was also observed with Capto Q 20-23 fractions 44-71 yet their amounts were too low to be considered as target activity. Also Capto Q

fractions 42-63 and 81-108 showed more MXE activity compared to XET activity, yet activity amounts were too low and protein chromatogram on Figure 4.117 and concentration measurements on Figure 4.118 were showing different peaks. Protein data was interpreted as, although MXE activity was more than XET activity, what is causing those activities were different proteins, thus pooling fractions which are resulting in low activity and different peaks would have caused protein contamination in the sample.

Fractions 74-80 from polishing of Capto Q fractions 20-23 were renamed as Pool X and fractions 68-78 from polishing of Capto Q fractions 24-29 were renamed as Pool Y. Both these pools were further investigated by SDS-PAGE and silver nitrate staining in order to see protein profiles (Figure 4.119) and by enzyme activity analysis using both TXG-XGO and BBG-XGO donor-acceptor couples (Table 4.45).

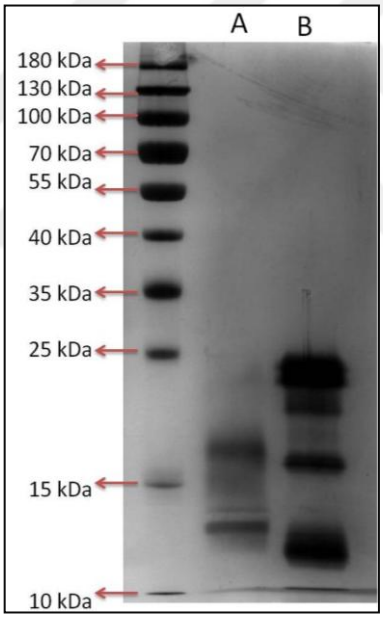

Figure 4.119. SDS-PAGE silver nitrate staining of June 2015 Belgrad *Equisetum* leaf sample polishing pools Pool X and Pool Y.

Table 4.45. TXG-XGO and BBG-XGO hybrid molecule fluorescence amounts of enzyme reaction carried with June 2015 Belgrad *Equisetum* leaf polishing pools X and Y.

Sample Name	**BBG-XGO hybrid molecule fluorescence**	**TXG-XGO hybrid molecule fluorescence**	**BBG-XGO/ TXG-XGO**
Pool X	739.4	149.6	4.94
Pool Y	416.2	153.1	2.72

Expected molecular weight of a putative *Equisetum* MXE is ~30 kDa, yet SDS-PAGE analysis of purified and polished sample showed no bands around 30 kDa, and showed multiple bands sizes ranging between 25 kDa-10 kDa. Even if activity results suggest a strong possibility of MXE enzyme in both Pool A and Pool B samples, more purification studies were carried for purer enzyme.

An additional step was added to protein purification flow from *Equisetum* after a new report was published by Simmons et al., 2015. Preliminary studies regarding the article were carried by formed member of Plant Biotechnology lab, Beyza Mat, and it was concluded to use a stepwise ammonium sulphate precipitation during protein precipitation in order to eliminate some of the unwanted proteins. Different ammonium sulphate saturations ranging from 10 per cent to 90 per cent were tested on June 2015 *Equisetum* Belgrad whole stem sample, since it was the fresh sample in hand during experimenting despite low BBG-XGO / TXG-XGO florescence value (Table 4.44). As proposed by Simmons et al., 2015 and as visualized by Beyza Mat (data not shown), 20 per cent ammonium sulphate saturation was applied during protein precipitation of June 2015 *Equisetum* Belgrad whole stem sample because of being a better saturation value compared 90 per cent as being used in previous trials.

Equisetum protein sample precipitated by 20 per cent ammonium sulphate saturation was used in further protein purification studies. Firstly, excessive amounts of ammonium sulphate salts were removed and sample buffer was changed to 50 mM sodium acetate buffer pH 5.0 using HiPrep DeSalting 26/10 column. Then, sample was loaded onto HiScreen Capto S cation exchange column and flow through during sample application to the column was collected. Interacting proteins were eluted from the column with a linear

NaCl gradient from no NaCl to 1M NaCl applied by 50 mM sodium acetate 1 M NaCl pH 5.0 elution buffer (Figure 4.120). As seen previously, MXE enzyme is expected to be in flow-through of Capto S column because of having a relatively positive charge at pH 5.0, a pH value lower than its possible theoretical pI.

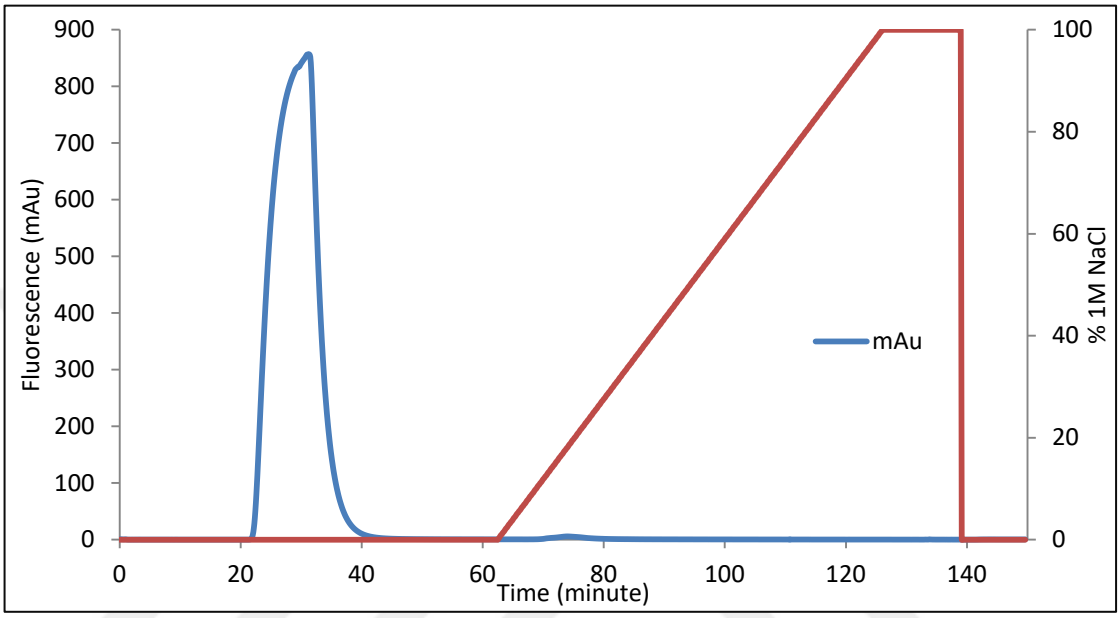

Figure 4.120. June 2015 *Equisetum* whole stem sample 20 per cent $(NH_4)_2SO_4$ saturation protein precipitation HiScreen Capto S cation exchange chromatography.

Flow-through coming from cation exchange chromatography was buffer exchanged into 20 mM Tris-HCl pH 8.0 buffer by a buffer exchange step using Amicon centrifugal filter units. Then sample was loaded onto Capto Q column for anion exchange step and proteins bound to column were separated and eluted by a linear NaCl gradient (Figure 4.121). Proteins were separated as 1.5 mL fractions based on their net charge by applying salt gradient from no NaCl to 1 M NaCl with 20 mM Tris-HCl 1 M NaCl pH 8.0 elution buffer. All fractions were tested for presence of MXE and XET enzymes by enzyme activity test using both TXG-XGO and BBG-XGO donor-acceptor couples. Results were evaluated by HPLC run and florescence amounts of hybrid products generated by fractions were enlightened (Figure 4.122).

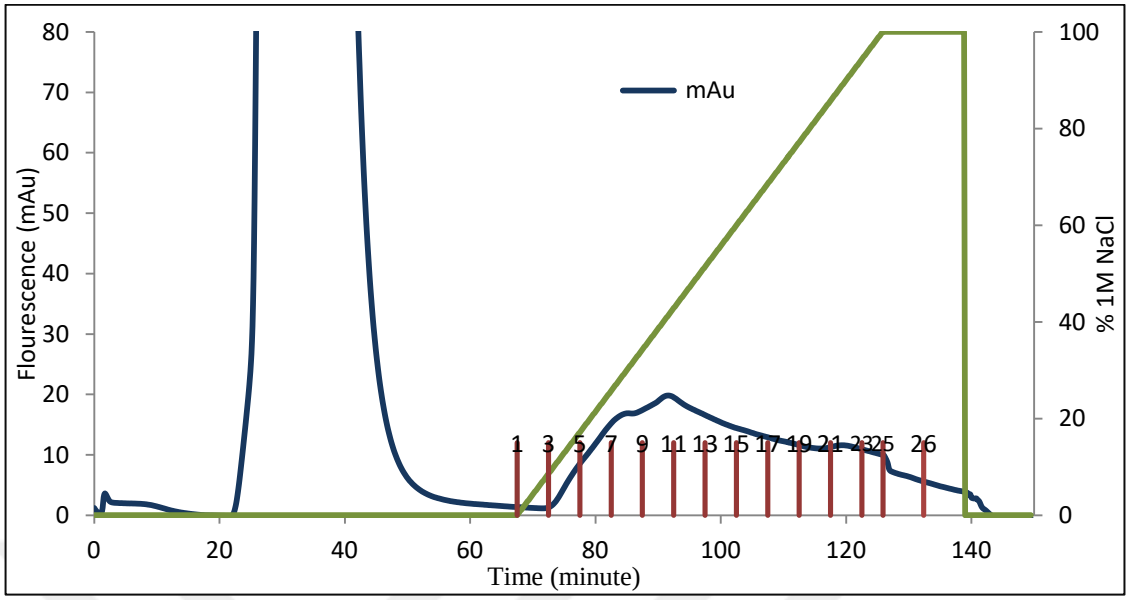

Figure 4.121. June 2015 *Equisetum* whole stem sample Capto S column flow-through HiScreen Capto Q anion exchange chromatography. Fractions are indicated on graph with red rods.

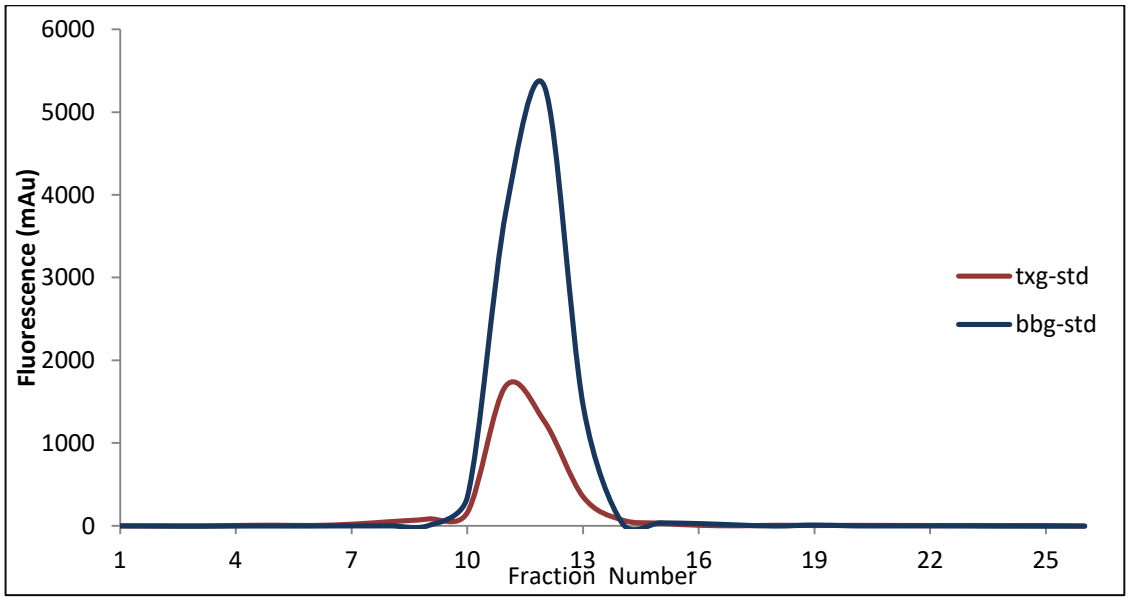

Figure 4.122. Florescence of TXG-XGO and BBG-XGO hybrid molecules generated during enzyme activity test of June 2015 Belgrad *Equisetum* whole stem sample Capto Q anion exchange chromatography fractions.

As seen in Figure 4.122, both TXG-XGO and BBG-XGO hybrid product amounts showed a similar trend in means of increasing and decreasing at same fraction samples. This means Capto Q anion exchange step showed no XET-MXE separation yet it still helped with separation of other proteins seen as peaks in Figure 4.121 that showed neither XET nor MXE activity. As a third chromatography step, fractions 10-14 showing higher MXE activity compared to XET activity, coming from Capto Q column anion exchange chromatography, were pooled and loaded onto Superdex 75 16/100 column for polishing step. During size exclusion separation of sample, column outcomes were divided into fractions of 1.5 mL (Figure 4.123).

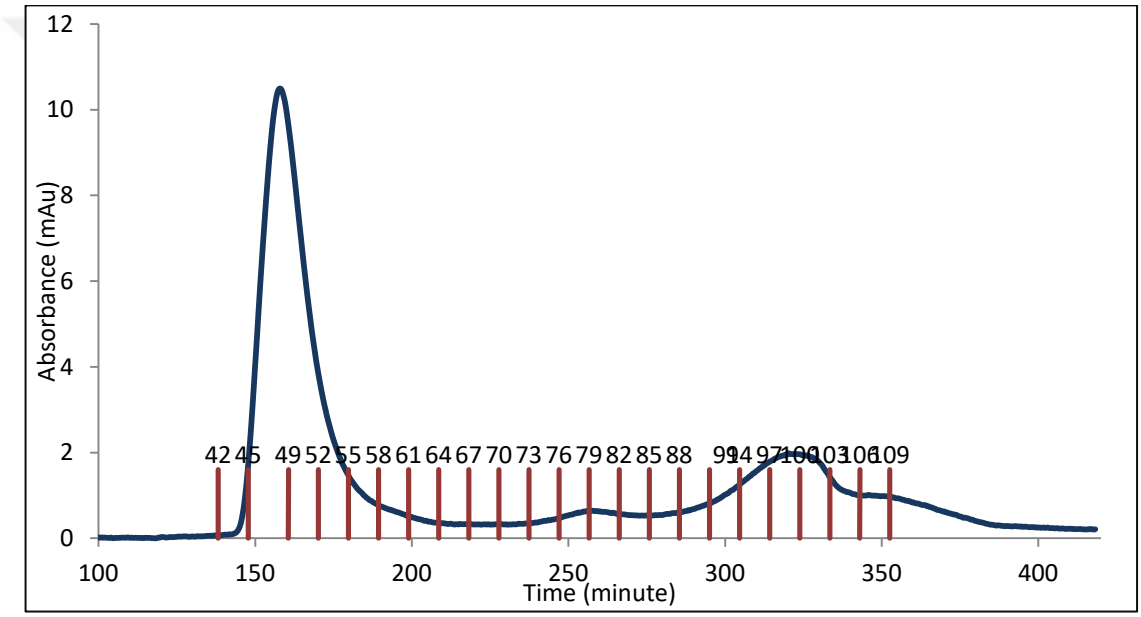

Figure 4.123. June 2015 *Equisetum* whole stem sample polishing with Superdex 75 16/100 column. Fractions are indicated on graph with red rods.

Polishing step resulted in three distinct protein peaks represented as fractions 44-56, fractions 57-63 and fractions 76-82. Due to scantiness of protein amounts in fractions, enzyme activity assay wasn't carried with fractions because it would have been hard to visualize enzyme activity with such diluted protein fractions. Instead, fractions were pooled regarding protein chromatogram of polishing step, resulting in three pools as Pool 1 (fractions 44-56), Pool 2 (fractions 57-63) and Pool 3 (fractions 76-82). These generated pools were tested for presence of MXE enzyme by enzyme activity using TXG-XGO and

BBG-XGO donor-acceptor couples (Table 4.46). Also, protein purity profiles of pools were investigated by SDS-PAGE and silver nitrate staining (Figure 4.124).

Table 4.46. TXG-XGO and BBG-XGO hybrid molecule fluorescence amounts of enzyme reaction carried with June 2015 Belgrad *Equisetum* whole stem polishing pools 1, 2 and 3.

Sample name	**BBG-XGO hybrid molecule fluorescence**	**TXG-XGO hybrid molecule fluorescence**	**BBG-XGO /TXG-XGO**
Pool 1	102.8	41.2	2.49
Pool 2	56.7	56.5	1.00
Pool 3	2123.6	5515.8	0.38

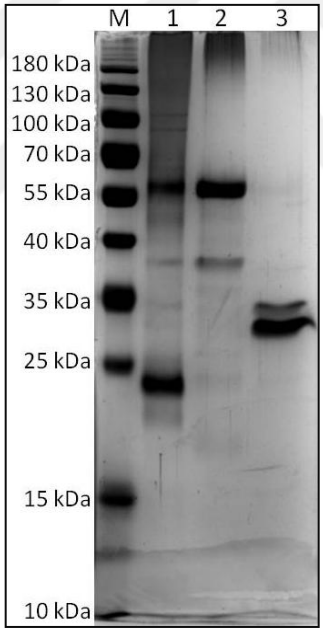

Figure 4.124. SDS-PAGE silver nitrate staining of June 2015 Belgrad *Equisetum* whole stem sample polishing pools Pool 1, 2 and Pool 3.

When equal volumes of samples were used, Pool 1 gave the most promising results in means of enzyme activity. Pool 1 resulted in more BBG-XGO hybrid product than TXG-XGO compared to other two pools, yet amounts of hybrid products Pool 1 gave are low. This means MXE is present in Pool 1 more than XET enzyme however overall amounts of

the enzymes are low. Additionally, Pool 1 showed many contaminant proteins in SDS-PAGE analysis. Pool 3 gave the purest protein profile when SDS-PAGE image was analysed yet this pool showed more than 2 times more XET activity compared to XET activity. These results suggest that *Equisetum* sample collected in September has many contaminating enzymes which are hard to be separated from target MXE, due to similarities in chemical features.

Another visit was paid to Belgrad forest during the end of November 2015 in order to investigate physiological stages of *Equisetum* plants and to collect some more sample for extraction. Plants were almost covered with other common forest wild plants such as ivies, brier roses. Also, most of the plants were fading away, meaning as weather is becoming cooler, *Equisetum* plants are dying. Alive and healthy looking plants were gathered and extract preparation was carried. 400 gr of stem and 100 gr of leaf was used for extraction. Extracts of these two samples were used in enzyme activity assays with both TXG-XGO and BBG-XGO donor acceptor couples in order to see MXE and XET activity potential of the tissues. Assay results were analysed by HPLC and neither XET nor MXE activity was detected in any of the extracts (data not shown). This trial resulted that late season plants are not suitable samples for MXE enzyme purification and MXE enzyme don't have a role in late season plants.

New *Equisetum* plant material was collected in April, 2016 from Belgrad forest region during early development of plants. Collected plants were young ones, which are between 30-60 cm in height. Underground stem parts were cut and leaves were cleared before processing of samples. 400gr whole young stem was used for extract preparation according to Fry method. Extract was tested for the presence of MXE enzyme by enzyme activity test using TXG-XGO and BBG-XGO donor-acceptor couples. Incubation time was 24 hours and results were analysed by HPLC system (Table 4.47). April 2016 *Equisetum* extract resulted in more BBG-XGO hybrid product compared to TXG-XGO hybrid product. This result indicates that there is a huge chance of MXE being present in high quantities in April 2016 extract. Thus, protein purification was carried.

Table 4.47. Fluorescence of hybrid TXG-XGO and BBG-XGO products obtained by enzyme activity assay using April 2016 Belgrad *Equisetum* sample.

TXG-XGO	**BBG-XGO**	**BBG-XGO/TXG-XGO**
200.2	354.7	1.77

Ammonium sulphate protein precipitation was carried in stepwise fashion. Firstly 20 per cent ammonium sulphate saturation was applied to the sample and proteins were precipitated. Then, ammonium sulphate saturation was increased to 80 per cent and more proteins were precipitated at this saturation value. Protein content obtained at both saturation values were tested by enzyme activity test for presence of XET and MXE activity using TXG-XGO and BBG-XGO donor-acceptor couples. Activity test results were analysed by HPLC system and the amout of hybrid products were reflected as florscence amounts (Table 4.48). Protein pool obtained with 20 per cent$(NH_4)_2SO_4$ saturation protein precipitation didn't show any XET or MXE activity. On the other hand, protein pool obtained with 80 per cent $(NH_4)_2SO_4$ saturation showed ~2 times higher MXE activity compared to XET activity, thus 80 per cent $(NH_4)_2SO_4$ saturation sample was used in further protein purification studies. Step-wise protein precipitation helped with eliminating some of the contaminating proteins.

Table 4.48. Florescence amounts of hybrid TXG-XGO and BBG-XGO products generated by 20 per cent $(NH_4)_2SO_4$ saturated and 80 per cent $(NH_4)_2SO_4$ saturated protein pools of April 2016 Belgrad *Equisetum* sample.

20 per cent $(NH_4)_2SO_4$ saturation		**80 per cent $(NH_4)_2SO_4$ saturation**	
TXG-XGO	BBG-XGO	TXG-XGO	BBG-XGO
4.35	8.35	574.2	1092.1

Prior to proceeding with purification steps, 80 per cent $(NH_4)_2SO_4$ saturated sample was fiktered through 0.22 μM RC syringe filter and buffer exchanged into 50 mM sodium acetate pH 5.0 buffer using Amicon Centrifugal Filter Units. Protein sample was loaded onto HiScreen Capto S cation exchange column in order to exclude proteins with

positively charge at pH 5.0 value. Bounds proteins were eluted from the column into 4 mL fractions with a linear NaCl gradient from no NaCl to 1 M NaCl that is created using 50 mM sodium acetate 1M NaCl pH 5.0 elution buffer (Figure 4.125). Both elution fractions and flow-through composed of non-bound proteins during sample loading were analysed for the presence of MXE enzyme by enzyme activity test using TXG-XGO and BBG-XGO donor-acceptor couples. Results were analysed by HPLC system and as expected, no XET or MXE activity was visible with elution fractions. Both MXE and XET activities were expected to be seen in flow-through of Capto S column and as expected, flow-through resulted in more than 3 times more BBG-XGO hybrid product compared to TXG-XGO hybrid product amount (Figure 4.126).

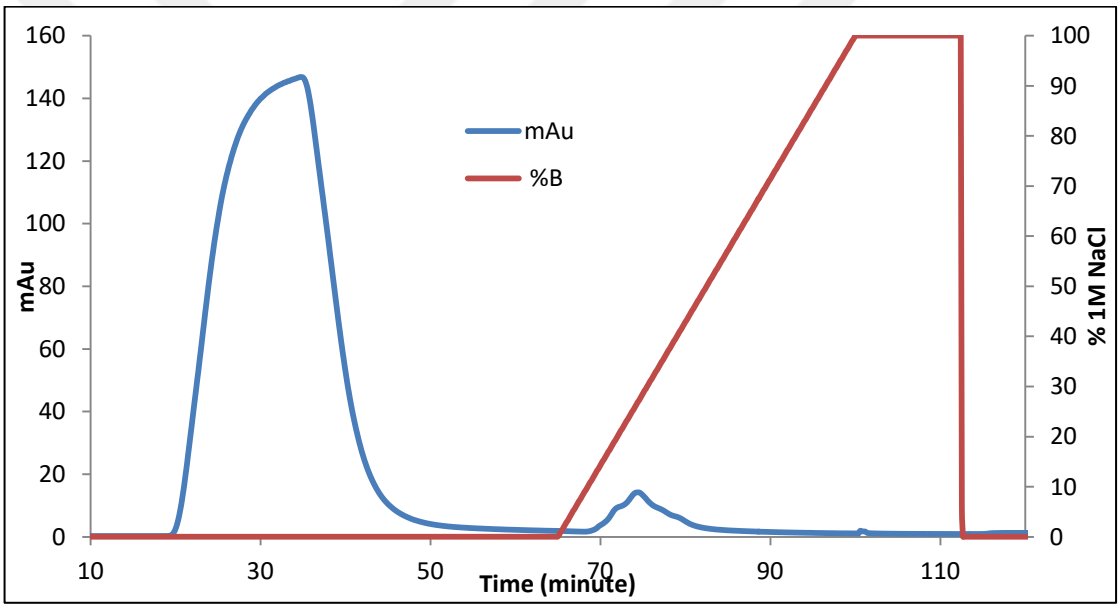

Figure 4.125. April 2016 *Equisetum* sample 80 per cent $(NH_4)_2SO_4$ saturated protein pool HiScreen Capto S cation exchange chromatography.

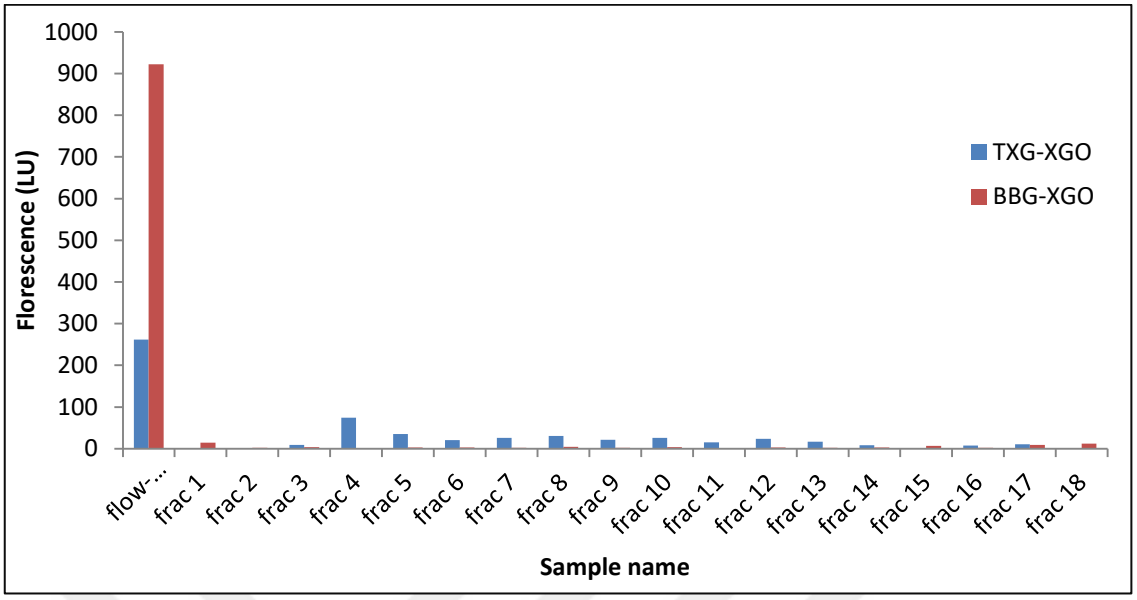

Figure 4.126. Florescence of TXG-XGO and BBG-XGO hybrid molecules generated during enzyme activity test of April 2016 Belgrad *Equisetum* sample Capto S cation exchange chromatography fractions.

Flow-through from Capto S cation exchange column was used in the second chromatographic purification step, anion exchange chromatography. Prior to that, buffer of the sample was changed to 20 mM Tris-HCl pH8.0 using Amicon Ultra centrifugal filters. Protein sample was loaded onto HiScreen Capto Q anion exchange column. Bound proteins were eluted from column and divided into fractions of 1.4 mL based on their net surface charge amount. Elution was carried by a linear NaCl gradient from no NaCl to 1M NaCl applied by 20 mM Tris-HCl 1M NaCl pH 8.0 elution buffer (Figure 4.127).

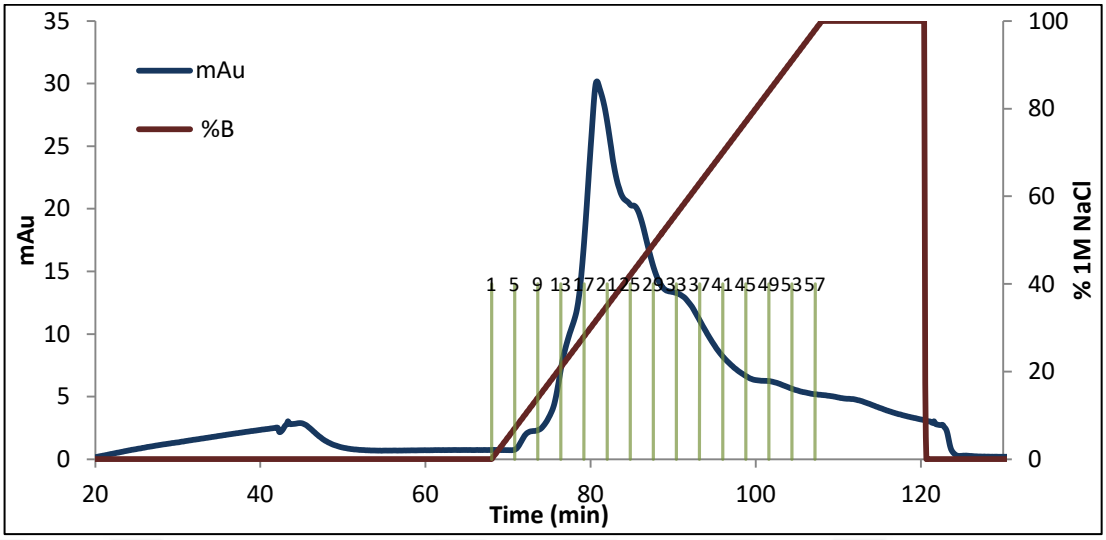

Figure 4.127. April 2016 *Equisetum* sample Capto S column flow-through HiScreen Capto Q anion exchange chromatography. Fractions are indicated on graph with green rods.

Flow-through and elution fractions of Capto Q column was subjected to enzyme activity test to see any present MXE and XET activity using BBG-XGO and TXG-XGO donor-acceptor couples. Activity reactions were analysed using HPLC system after 24 hour incubation time and florescence amounts of hybrid products were measured (Figure 4.128).

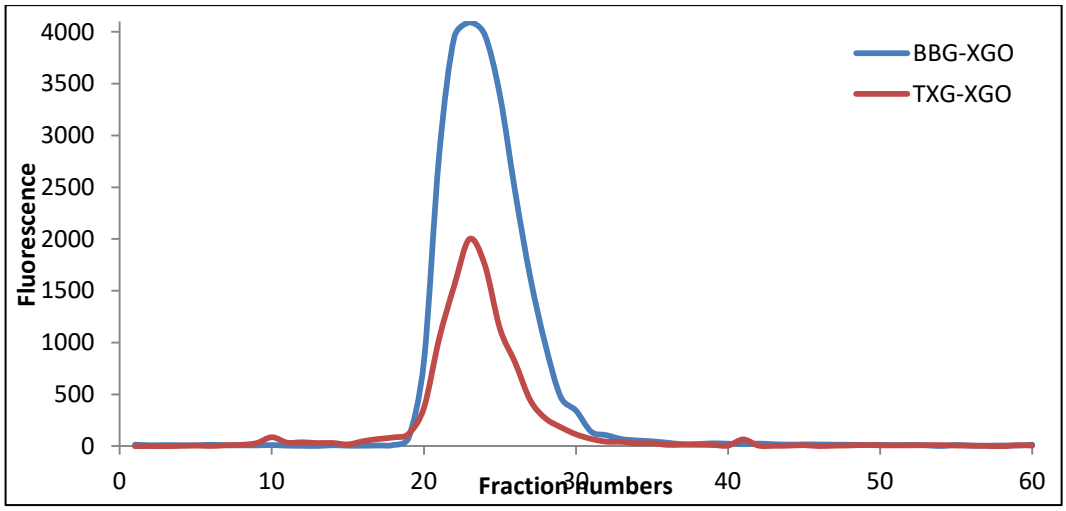

Figure 4.128. Florescence of TXG-XGO and BBG-XGO hybrid molecules generated during enzyme activity test of April 2016 Belgrad *Equisetum* sample Capto Q anion exchange chromatography fractions.

Amounts of hybrid products generated by the Capto Q fractions gave us a hit that fractions 16-19 have XET activity but no MXE activity whereas fractions 20-33 are showing a strong MXE activity over XET activity. Fractions 20-33 were represented by a separate peak in Capto Q anion exchange chromatogram. Also fractions 29-31 are giving a shoulder profile in means of BBG-XGO hybrid product amounts which is reflecting separation of MXE from XET. To summarize, Capto Q anion exchange step result in further separation of MXE enzyme. Fractions 20-33 were pooled down and concentrated and buffer exchanged into 20 mM sodium citrate 100 mM NaCl pH 5.5 buffer using Amicon Ultra centrifugal filters. As the third chromatographic separation step, sample was loaded onto Superdex 75 16/100 column for size-exclusion chromatography and separated into 1.5 mL fractions depending on molecule size of proteins (Figure 4.129).

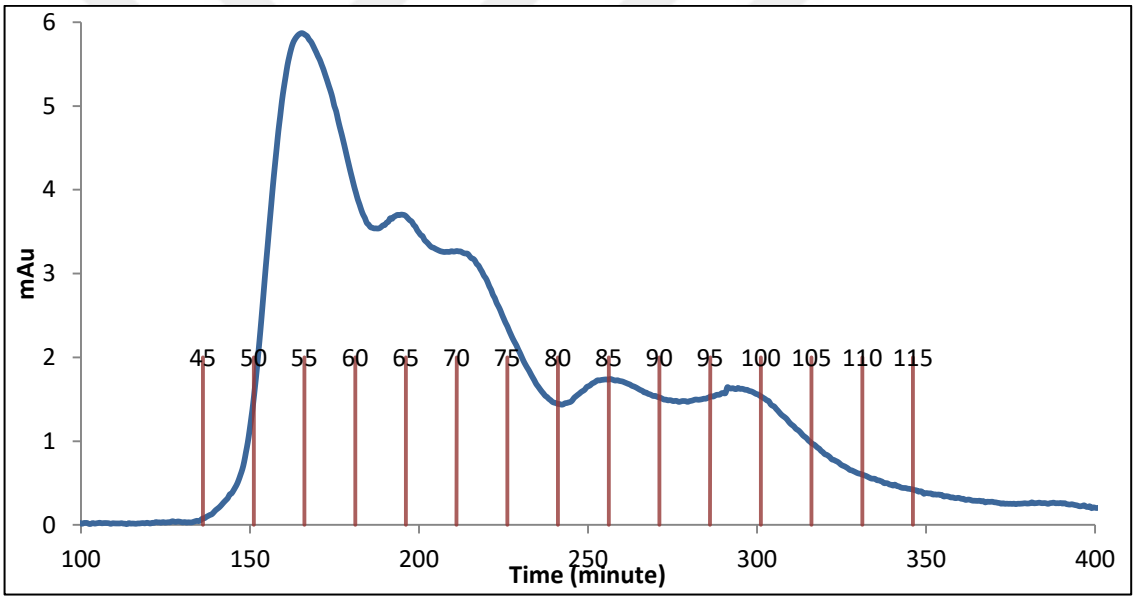

Figure 4.129. April 2016 *Equisetum* sample polishing with Superdex 75 16/100 column. Fractions are indicated on graph with red rods.

Fractions 45-112 which are showing protein content were collected and tested for the presence of MXE enzyme by enzyme activity test using BBG-XGO and TXG- XGO substrate couples. Reaction results were analysed using HPLC system and hybrid product amounts were plotted on a graph merged with protein absorbance recorded during size exclusion step (Figure 4.130a).

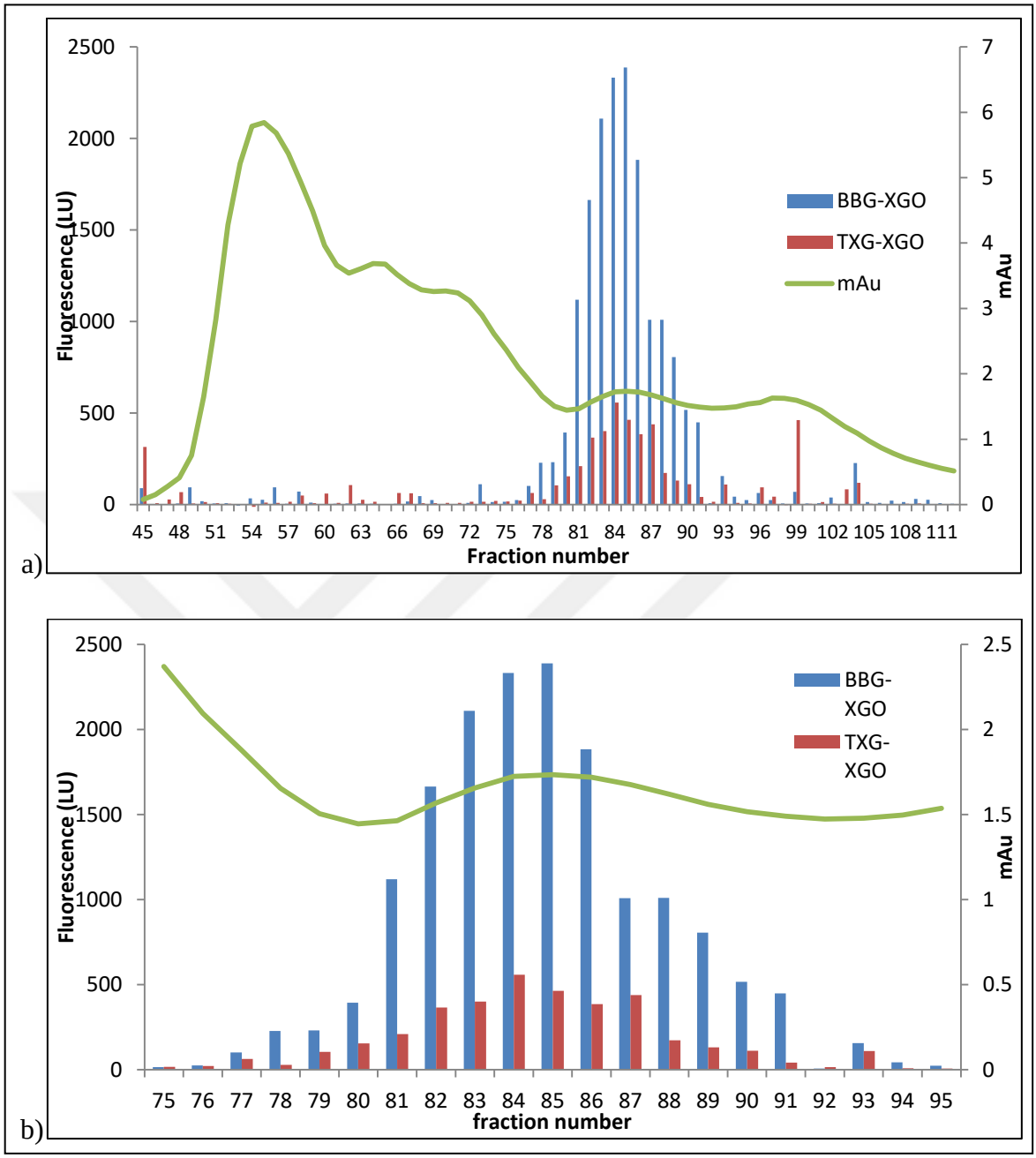

Figure 4.130. Florescence of TXG-XGO and BBG-XGO hybrid molecules generated during enzyme activity test of April 2016 Belgrad *Equisetum* sample polishing fractions. a) Fractions 45-111, b) fractions 75-95.

Size exclusion chromatography fractions 78-91 showed presence of MXE activity. When data belonging to these fractions were investigated closely (Figure 4.130b), these fractions can be divided into 4 different pools regarding the ratio between BBG-XGO and TXG-

XGO hybrid product amounts and protein peak curl. These pools are Pool 1 composing of fractions 78-80, Pool 2 composed of fractions 81-83, Pool 3 composed of fractions 84-86 and Pool 4 composed of fractions 87-91. These fractions were brought together and concentrated using Amicon Ultra centrifugal filters. Newly formed pools were subjected to BCA assay in order to find protein concentrations. Enzyme activity test using BBG-XGO and TXG-XGO donor-acceptor couples were carried with April 2016 Belgrad *Equisetum* pools and hybrid product amounts were measured by HPLC analysis. Then, specific activities of these pools were calculated on both BBG-XGO and TXG-XGO donor-acceptor couples (Table 4.49). Also, protein profiles were investigated by SDS-PAGE and silver nitrate analysis (Figure 4.131).

Table 4.49. Protein concentrations and specific XET and MXE activities of April 2016 *Equisetum* sample polishing pools Pool 1, 2, 3 and 4.

Sample name	**Protein concentration (mg protein/ml)**	**Specific XET activity (pkatal/ mg enzyme)**	**Specific MXE activity (pkatal/ mg enzyme)**	**MXE activity / XET activity**
Equisetum Pool 1	0.043	0.088	0.570	6.48
Equisetum Pool 2	0.058	0.434	2.340	5.39
Equisetum Pool 3	0.040	0.780	2.920	3.74
Equisetum Pool 4	0.052	0.355	1.956	5.51

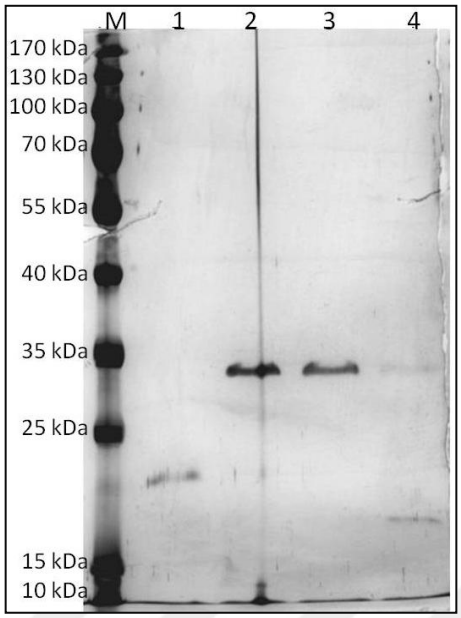

Figure 4.131. SDS-PAGE silver nitrate analysis of April 2016 *Equisetum* sample polishing pools Pool 1, 2, 3 and 4. M; protein size marker, pool numbers are indicated on figure.

All generated *Equisetum* April 2016 pools have characteristics of MXE enzyme, showing higher MXE specific activity compared to XET specific activity. Though their protein concentrations were low, activities were easily monitored. On the other hand, low concentrations mean low protein amount and this situation makes samples very precious. When these precious samples were analysed by SDS-PAGE, it was observed that Pool 2 and Pool 3 show single strong band at possible theoretical molecular size which is similar to identified XETs within phylogenetic tree. Pool 4 also shows this band between 25 kDa to 35 kDa, yet it also shows presence of a low molecular non-specific band. Pool 1, contrarily, only showed a low protein molecular weight band between 15 kDa to 25 kDa. More, Pool 1showed low MXE activity compared to other pools. This situation coincides with not seeing the band seen in Pool 2 & 3 in Pool 1 sample; low MXE protein ratio in Pool 1 protein mix results in low MXE enzyme activity.

New plant sample was collected form Belgrad forest region at the first half of June 2016 and extracts were prepared separately from 300 gr leaf and 300 gr stem tissue. Extracts of different tissues were used in enzyme activity test to visualize any present MXE and XET activity. Produced hybrid products were analysed by HPLC system (Table 4.50). Leaf

sample showed no XET or MXE activity. Stem sample showed domineering XET activity, thus this sample was set aside since XET activity product was higher than MXE activity product.

Table 4.50. Florescence amounts of TXG-XGO and BBG-XGO hybrid product amounts generated during enzyme activity test with June 2016 *Equisetum* extracts.

	TXG-XGO hybrid product florescence amount	**BBG-XGO hybrid product florescence amount**
Leaf	1.55	1.6
Stem	359.35	240.1

Equisetum sample was collected during the end of July 2016 from Belgrad region in order to monitor presence of MXE through lifespan of the plants. 200 gr of leaf and 400 gr of leaf-free stems were used in extraction. Prepared extracts were used in enzyme activity tests with TXG-XGO and BBG-XGO donor-acceptor couples to monitor the sample with more MXE activity compared to XET activity. Hybrid polysaccharides produced during activity assays were analysed using HPLC system (Table 4.51). Leaf extract showed trace XET and MXE activity, thus this extract was not used in further purification studies. Stem extract showed both XET and MXE activity, MXE being more than XET. Thus, stem sample is a good donor for MXE purification.

Table 4.51. Florescence amounts of TXG-XGO and BBG-XGO hybrid product amounts generated during enzyme activity test with July 2016 *Equisetum* extracts.

	TXG-XGO hybrid product fluorescence	**BBG- XGO hybrid product fluorescence**	**BBG-XGO/ TXG-XGO**
Stem extract	119.6	178.45	1.49
Leaf extract	9.45	3.45	no activity

Starting the process of protein purification, firstly sequential ammonium sulphate precipitation was carried; solution was saturated to 20 per cent ammonium sulphate firstly,

proteins were pelleted and then remaining proteins in the supernatant were saturated to 85 per cent and precipitated. Both 20 per cent and 85 per cent $(NH_4)_2SO_4$ saturation pools were used in enzyme activity test using TXG-XGO and BBG-XGO donor-acceptor couples. Enzyme reactions were analysed by HPLC system (Table 4.52). 20 per cent $(NH_4)_2SO_4$ saturated pool doesn't include any XET or MXE activity whereas 85 per cent $(NH_4)_2SO_4$ saturated pool showed both XET and MXE activity, MXE being higher than XET. Therefore 85 per cent $(NH_4)_2SO_4$ saturated protein pool was desalted into 50 mM sodium acetate pH 5.0 buffer prior to cation exchange chromatography.

Table 4.52. Fluorescence amounts of hybrid products produced by ammonium sulphate precipitated Equisetum July'16 stem extracts. Sequential ammonium sulphate precipitation as 20 per cent and 85 per cent was done with the sample.

	TXG-XGO hybrid product fluorescence	**BBG- XGO hybrid product fluorescence**	**BBG-XGO/ TXG-XGO**
20 per cent $(NH_4)_2SO_4$	40.25	12.2	0.30
85 per cent $(NH_4)_2SO_4$	709.65	949.65	1.34

July 2016 *Equisetum* protein sample was loaded onto HiScreen Capto S column, flow-through during sample loading was collected and bound proteins were eluted by linear NaCl gradient from no NaCl up to 1 M NaCl into fractions of 2.5 mL (Figure 4.132). Elution fractions and flow-through were tested for the presence of XET and MXE enzymes by enzyme activity test using both TXG-XGO and BBG-XGO donor-acceptor couples. These reactions were analysed by HPLC system. None of the fractions showed any activity where as both XET and MXE activities were monitored in Capto S column flow-through, MXE activity being 2.72 times more than XET activity (data not shown).

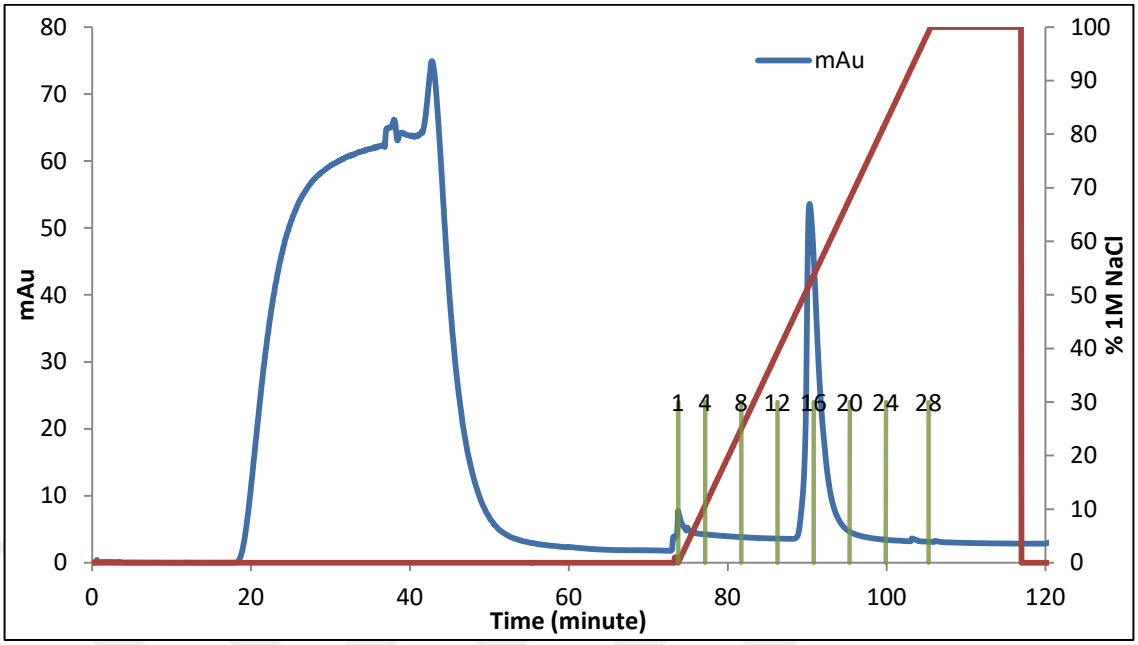

Figure 4.132. July 2016 *Equisetum* sample 85 per cent $(NH_4)_2SO_4$ saturated protein pool HiScreen Capto S cation exchange chromatography.

Capto S column flow-through was buffer exchanged into 20 mM Tris-HCl pH 8.0 and then loaded onto Capto Q column for anion exchange chromatograph. Protein sample of June 2016 *Equisetum* were separated based on their total charge using a linear salt gradient elution from no NaCl to 1 M NaCl (Figure 4.133). Elution step resulted in separation of protein, by resulting in different protein peaks seen in Figure 4.133. During elution, sample was separated into 1.5 mL fractions depending on their net surface charge. All the fractions and flow-through during sample loading were subjected to enzyme activity test with TXG-XGO and BBG-XGO donor-acceptor couples. Activity test reactions were analysed by HPLC system and florescence amounts of hybrid products generated by fractions were merged with UV chromatogram from Capto Q anion exc hange step (Figure 4.134). Flow-through of CaptoQ anion exchange step didn't generate any hybrid products as expected.

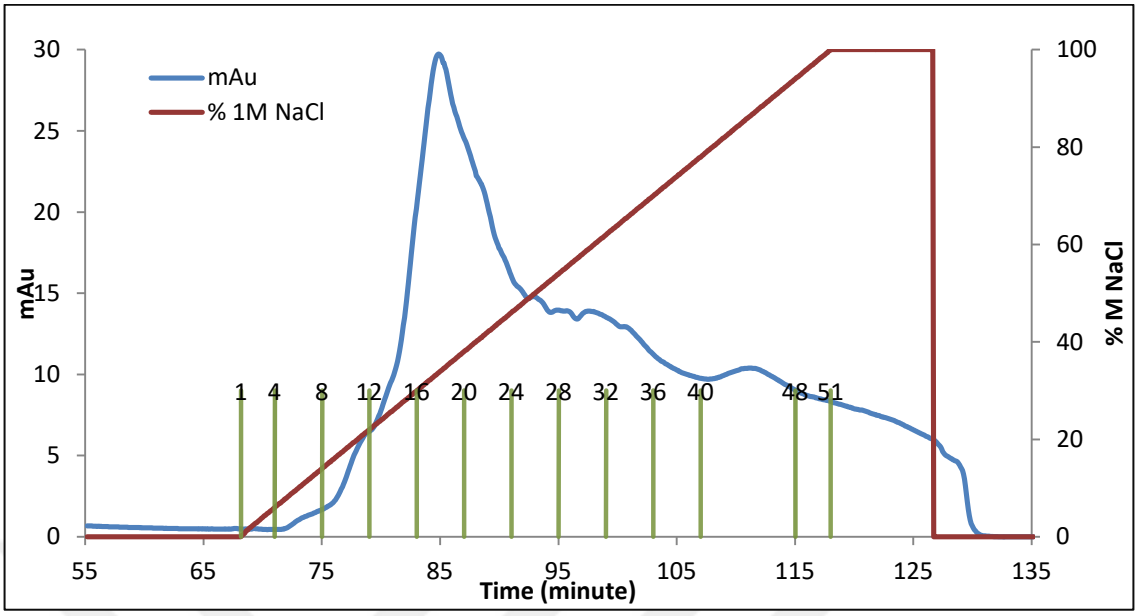

Figure 4.133. July 2016 *Equisetum* sample Capto S column flow-through HiScreen Capto Q anion exchange chromatography. Fractions are indicated on graph with green rods.

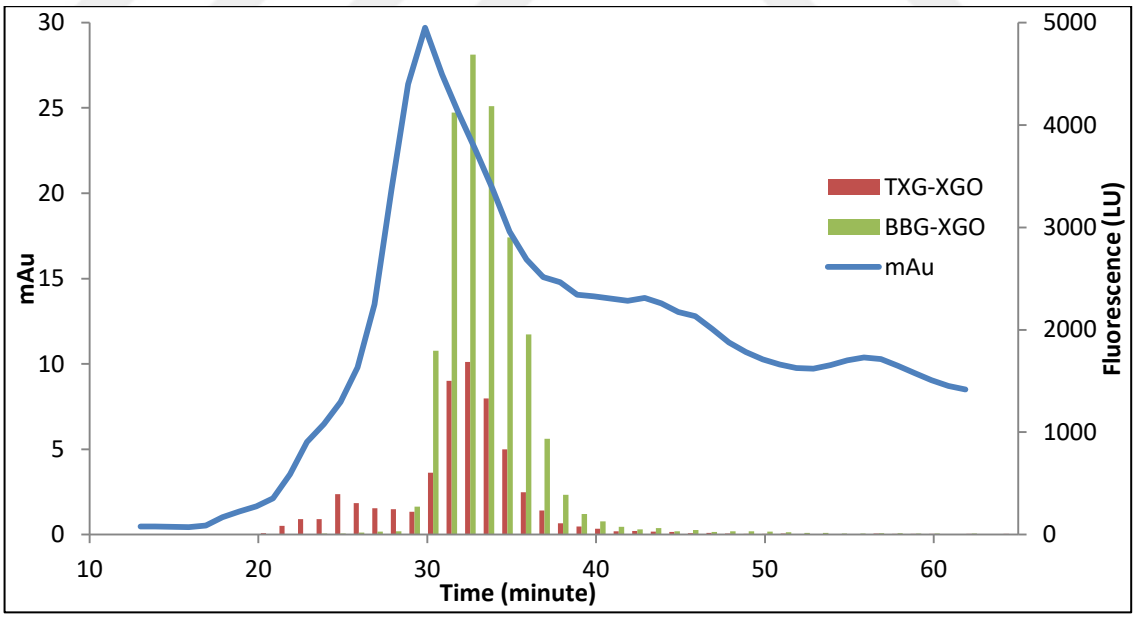

Figure 4.134. Florescence of TXG-XGO and BBG-XGO hybrid molecules generated during enzyme activity test of July 2016 Belgrad *Equisetum* sample Capto Q anion exchange chromatography fractions.

Activity assay revealed that Capto Q column fractions 19-26 have > 2.5 times activity on BBG-XGO compared to TXG-XGO substrate couple. Thus, fractions 19-26 were pooled down and concentrated using Amicon Centrifugal filters as preparation for size exclusion chromatography step. On the other hand, both Capto S flow-through sample and Capto Q fractions 19-26 pool were subjected to SDS-PAGE and silver nitrate gel staining in order to visualize use of Capto Q anion exchange step in protein separation and purification (Figure 4.135). Capto Q purified fractions 19-26 pools shows a purer profile compared to Capto S flow-through, it is seen that Capto Q protein sample doesn't harbour many proteins bands yet still it shows more than one band profile. Thus, polishing step with size exclusion chromatography step was carried to further purify target protein.

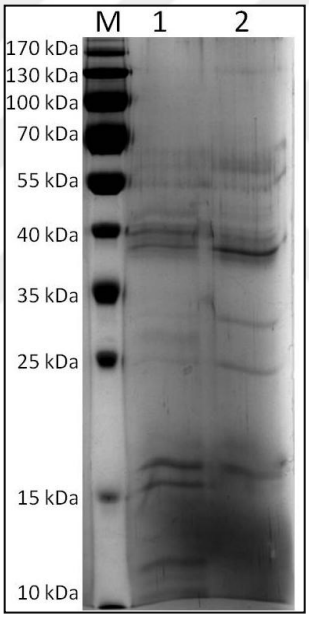

Figure 4.135. Silver nitrate staining of *Equisetum* July' 16 protein purification step samples. Sample 1 is flow-through of Capto S cation exchange column, Sample 2 is Capto Q anion exchange column fractions 19-26 pooled down.

Capto Q fraction pool was loaded onto Superdex 75 16/100 size exclusion column and separated hinge upon molecules 3D sizes. Sample was divided into 1.5 mL fractions (Figure 4.136a) and fractions with protein content (fractions 30-108) were analysed by enzyme activity test using BBG-XGO and TXG-XGO donor-acceptor couples. Hybrid product amounts generated during activity test were quantified by HPLC system (Figure

4.136b). Fractions between 71-87 showed valued activity by resulting in more BBG-XGO hybrid product compared to TXG-XGO hybrid product.

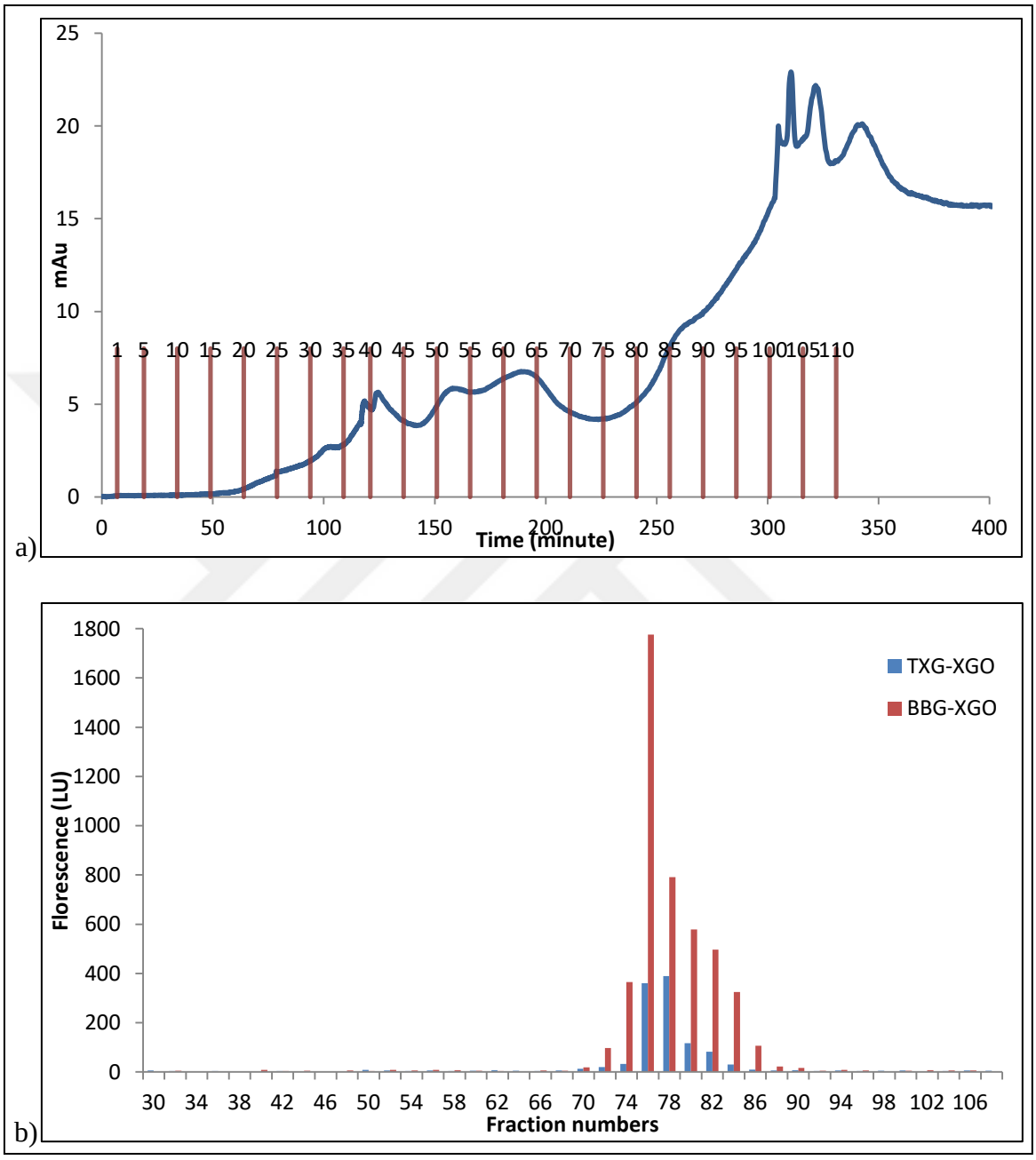

Figure 4.136. *Equisetum* July'16 sample Superdex 75 16/100 polishing separation. a) *Equisetum* July'16 protein sample size exclusion separation on Superdex 75 16/100 column. Fraction numbers are shown as red bars on x-axis, b) Fluorescence amounts of TXG-XGO and BBG-XGO hybrid products generated by size-exclusion chromatography fractions of *Equisetum* July'16 protein sample.

Polishing step chromatogram and enzyme activity results were evaluated together. Fractions showing dominant MXE activity are represented as end of a protein peak, start of a protein peak and a nested peak. This peak separation is also reflected in BBG-XGO / TXG-XGO hybrid products ratio. Regarding these observations, polishing step fractions were merged into 3 pools. These pools are Pool A fractions 71-76, Pool B fractions 77-80 and Pool C fractions 81-87. Protein concentrations of Pool A, Pool B and Pool C were studied by BCA assay. Also, their MXE/XET activity ratios were studied by carrying enzyme activity reactions using TXG-XGO and BBG-XGO donor acceptor couples and measuring florescence generated by hybrid products (Table 4.53). Also, purity of the pools were control by SDS-PAGE silver nitrate staining (Figure 4.137). Pool B is the pool with highest activity amount whereas Pool C harbours more of MXE activity compared to XET activity. Unfortunately, all the pools have distinct 2 contamination bans; the size of one of the contaminating band is ~25 kDa and the size of the other contaminating band is between 15-25 kDa. Target MXE enzyme is expected to be around 35 kDa and all pools harbour a band around 35 kDa which is indicated with a red star on the image. Pool B is the July 2016 *Equisetum* protein sample with the highest amount of target MXE when protein band intensities and thicknesses are compared on silver stained gel image.

Table 4.53. Protein concentrations and specific XET and MXE activities of July 2016 *Equisetum* sample polishing pools Pool A, B and C.

	TXG-XGO hybrid fluorescence	**BBG-XGO hybrid fluorescence**	**BBG-XGO/ TXG-XGO**	**Protein concentration (mg/ml)**
Pool A	81.65	346.75	4.25	0.110
Pool B	93.3	429.15	4.60	0.065
Pool C	42.1	234.5	5.57	0.134

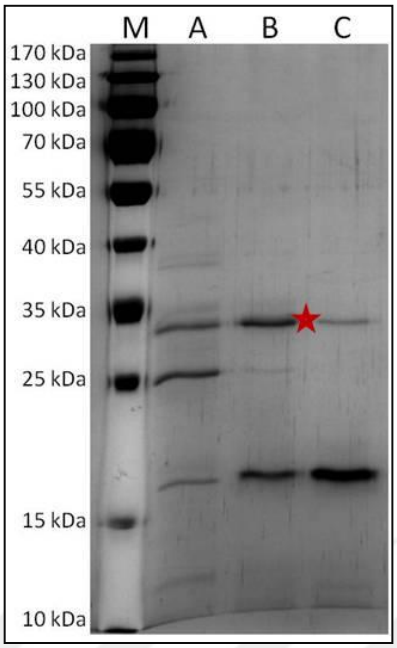

Figure 4.137. SDS-PAGE silver nitrate staining analysis of *Equisetum* July'16 SEC protein pools. M;protein size marker. Pool names are indicated on figure. Red star stands for the probable putative MXE enzyme.

One of the aims during protein purification from *Equisetum* samples is to monitor amount and activity of target MXE during an annual lifespan of *Equisetum* plants. Thus, a sample representing late stage was collected on September 2016 from Belgrad region. Extract preparation from this sample was carried in 2 separate batches; 240 gr mature plants as mature tissue extract and 720 gr of younger and smaller plants as young tissue. Prepared plant extracts were tested for presence of MXE enzyme via enzyme activity test using TXG-XGO and BBG-XGO substrate couples. Reactions were analysed by HPLC system and composed hybrid BBG-XGO products were compared to hybrid TXG-XGO products (Table 4.54). Young plant extract was the one with higher MXE activity compared to XET activity since it is the one with >1 BBG-XGO/TXG-XGO ratio. Thus, young plant extract was used in protein purification studies.

Table 4.54. Florescence amounts of TXG-XGO and BBG-XGO hybrid product amounts generated during enzyme activity test with September 2016 *Equisetum* extracts, old plants and young plants extracts.

	TXG-XGO hybrid product fluorescence	**BBG-XGO hybrid product fluorescence**	**BBG-XGO/ TXG-XGO**
Old plants	157.5	158.05	1.00
Young plants	75.15	357.65	4.76

Ammonium sulphate protein precipitation was carried as first step of MXE purification. Protein precipitation was carried in a stepwise manner; solution was first of all saturated to 20 per cent $(NH_4)_2SO_4$ concentrations and proteins were precipitated at this ratio. Then solution was further saturated to 85 per cent $(NH_4)_2SO_4$ point and proteins were again precipitated. Both 20 per cent and 85 per cent $(NH_4)_2SO_4$ pools were tested for presence of MXE and XET activities by enzyme activity test using BBG-XGO and TXG-XGO substrate couples. 20 per cent $(NH_4)_2SO_4$ pool showed equal amounts of XET and MXE activity whereas 85 per cent $(NH_4)_2SO_4$ pool showed more XET activity compared to MXE activity (data not shown). This situation can be explained by growth-related role of MXE enzyme. *Equisetum* plants have an annual germination cycle; they sprout in early spring, continue growing through summer and start dying as weather becomes colder in fall. September corresponds to a later stage in their annual cycle and depending on our activity data from different extracts, it can be interpreted that MXE enzyme has a more active role during stem elongation.

Even though MXE activity was not the dominant XET activity in 85 per cent $(NH_4)_2SO_4$ protein pool, it was processed for protein purification. 85 per cent $(NH_4)_2SO_4$ protein pool was buffer exchanged into 50 mM sodium acetate pH 5.0 buffer using Amicon centrifugal filters and then loaded onto HiScreen Capto S column for cation exchange chromatography. Flow-through during sample loading onto column was collected and bound proteins were eluted by linear NaCl gradient from no NaCl to 1M NaCl (Figure 4.138). Elution was separated into 2.5 mL fractions and all these fractions plus flow-through were used in enzyme activity test using TXG-XGO and BBG-XGO donor-acceptor couples in order to visualise MXE enzyme's movement during cation exchange

chromatography step. Reactions were analysed by HPLC system (Figure 4.138). The major XET and MXE activities were visualised in flow-through of Capto S column, XET activity being ~ 2 times more than MXE activity.

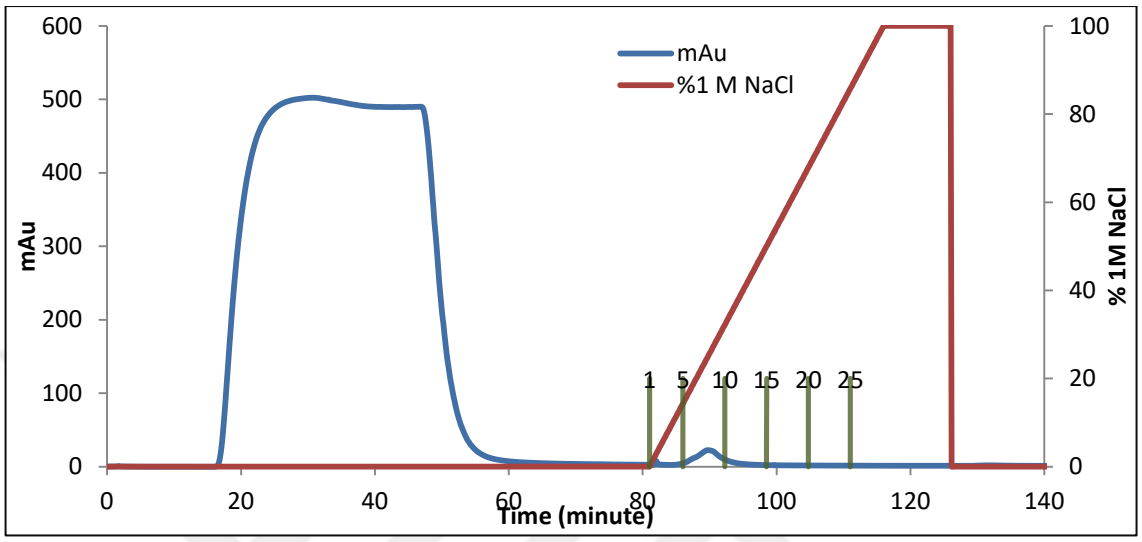

Figure 4.138. September 2016 *Equisetum* young plants sample 85 per cent $(NH_4)_2SO_4$ saturated protein pool HiScreen Capto S cation exchange chromatography.

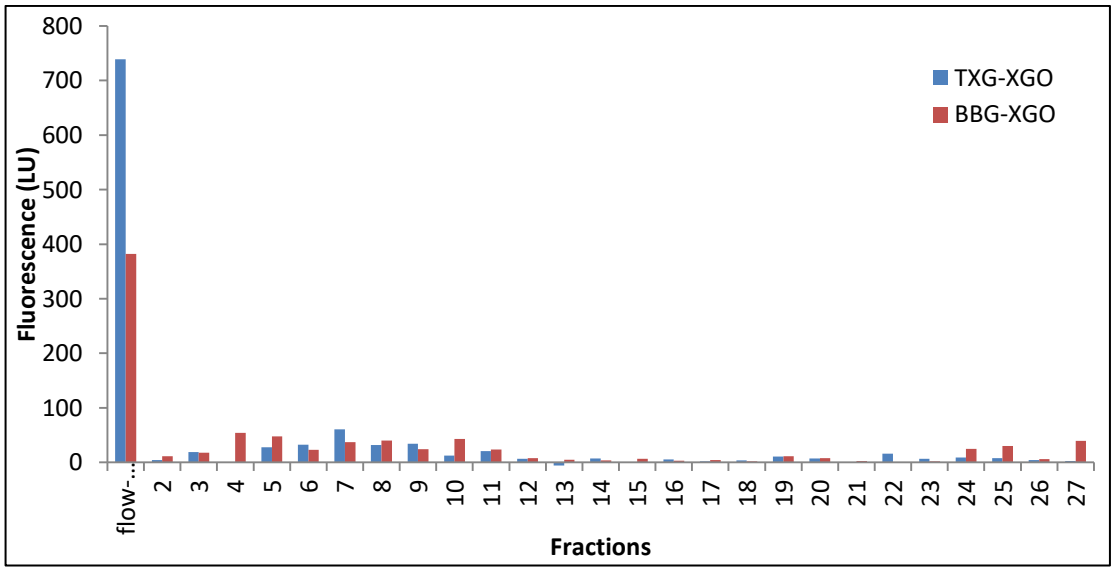

Figure 4.139. Florescence of TXG-XGO and BBG-XGO hybrid molecules generated during enzyme activity test of September 2016 Belgrad *Equisetum* young plants sample Capto S cation exchange chromatography fractions and column flow-through.

During the first 2 steps of optimized protein purification procedure, MXE activity amount was observed to be less than XET activity amount. Despite these outcomes, it was decided to continue on with purification because optimized purification procedure was used successfully before in separating MXE from XET. As the next step, Capto S flow-through was buffer exchanged into 20 mM Tris-HCl pH 8.0 buffer using Amicon Centrifugal filters and then loaded onto HiScreen Capto Q column for anion exchange chromatography step. Flow-through was collected during sample loading. Bound proteins were eluted from column based on their charges by a linear salt gradient from no NaCl to 1 M NaCl and separated into 1.5 mL fractions (Figure 4.140). Flow-through and elution fractions were tested for MXE and XET activity by enzyme activity test using BBG-XGO and TXG-XGO donor acceptor couples. Reactions were analysed by HPLC system and plotted on a graph (Figure 4.141). Hybrid product amounts showed two peak profile; fractions 16-21 showed lower BBG-XGO/TXG-XGO ratio whereas fractions 22-30 showed higher BBG-XGO/TXG-XGO ratio. Thus Capto Q fractions were combined into 2 pools; Sample 1 (S1) composed of fractions 16-21 and Sample 2 (S2) composed of fractions 22-30. In order to visualise protein composition differences, SDS-PAGE and silver nitrate staining was performed using S1 and S2 (Figure 4.142).

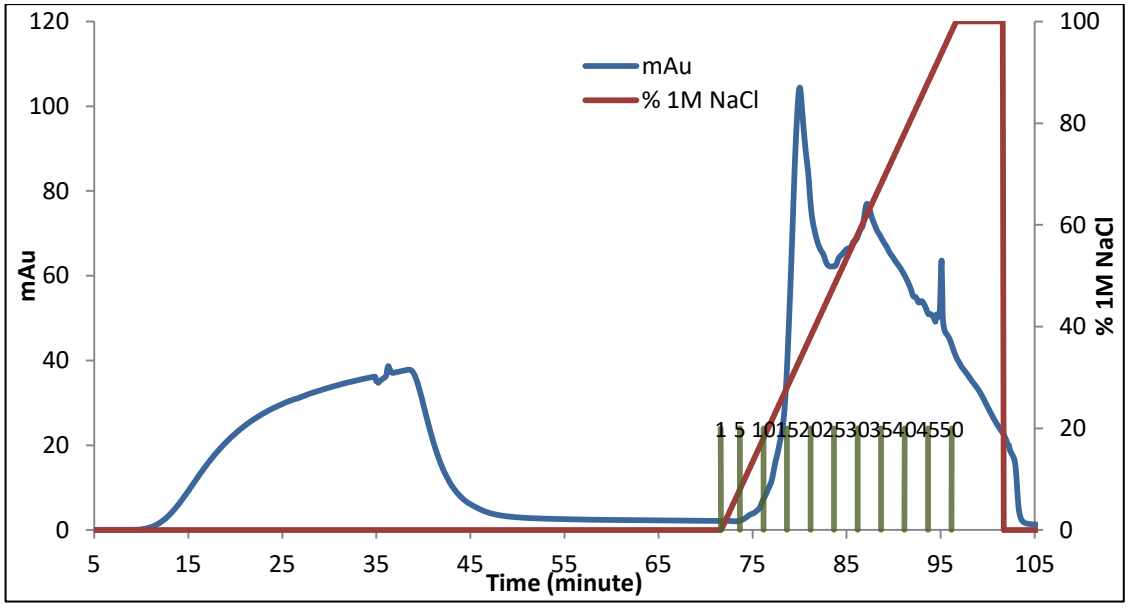

Figure 4.140. September 2016 *Equisetum* sample Capto S column flow-through HiScreen Capto Q anion exchange chromatography. Fractions are indicated on graph with green bars on x-axis.

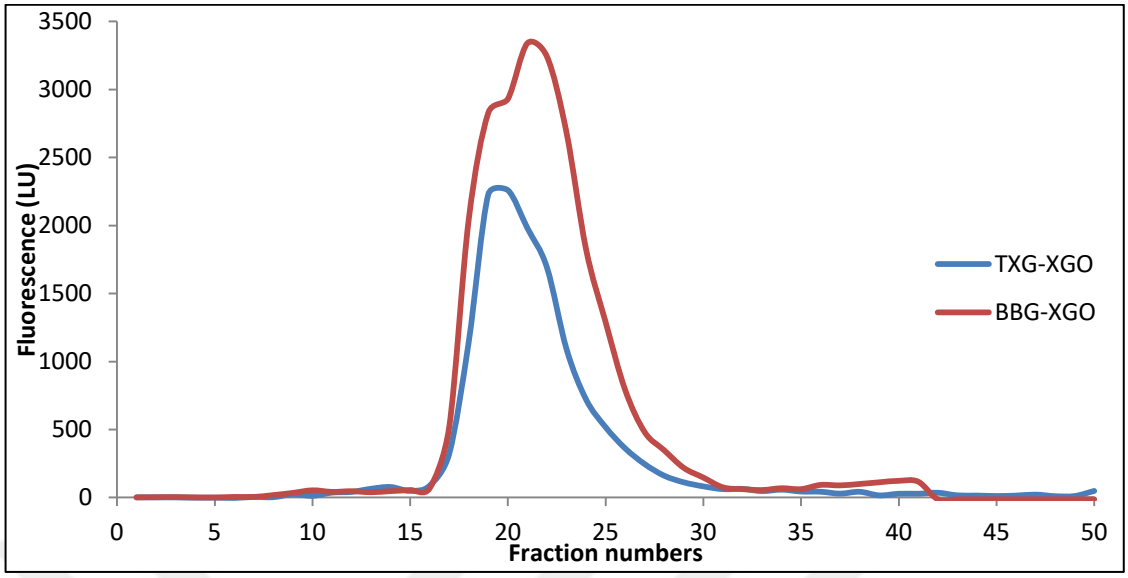

Figure 4.141. Florescence of TXG-XGO and BBG-XGO hybrid molecules generated during enzyme activity test of September 2016 Belgrad *Equisetum* sample Capto Q anion exchange chromatography fractions.

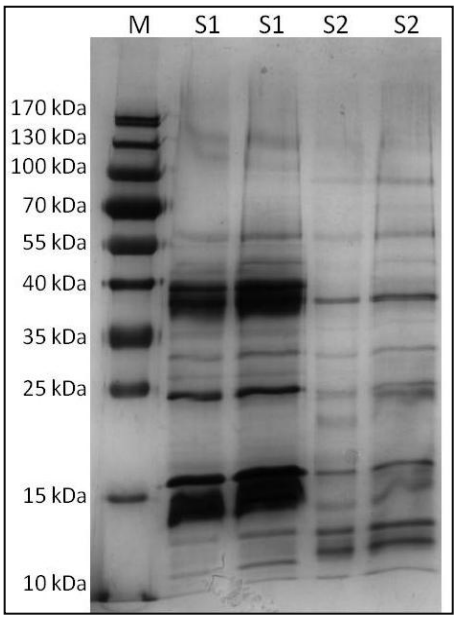

Figure 4.142. *Equisetum* September'16 Capto Q anion exchange chromatography Sample 1 (S1) and Sample 2 (S2) SDS-PAGE silver nitrate analysis. M; protein size marker. Sample names are indicated on figure.

S1 and S2 samples showed differences in their protein compositions. S1 has some bands that S2 is missing and S2 has some extra bands compared to S1. An important difference is S1has 2 major bands between 35-40 kDa whereas S2 only has one of those bands. Also, S2 has less protein bands between 25-35 kDa. Since expected MXE size is between 25-35 kDa, sample with less protein bands at 25-35 kDa range is purer sample. Their activities on different donor-acceptor couples were tested by enzyme activity test using TXG-XGO, BBG-XGO and HE-XGO donor-acceptor couples. Reaction results were analysed by HPLC system (Table 4.55). Both S1 and S2 samples showed activity on all tested substrate couples and S1 shows 2 time more activity compared to S2. This divergence can be due to protein concentration differences. Since S2 showed purer protein profile on SDS-PAGE analysis, it was chosen as working sample.

Table 4.55. Florescence of TXG-XGO, BBG-XGO and HEC-XGO hybrid molecules generated during enzyme activity test of September 2016 Belgrad *Equisetum* sample Capto Q anion exchange chromatography sample 1 and 2. Incubation duration 1 H.

	TXG-XGO	**BBG-XGO**	**HEC-XGO**	**BBG-XGO/ TXG-XGO**
Sept'16 Capto Q *Equisetum* sample 1	216.6	944.9	45.3	4.36
Sept'16 Capto Q *Equisetum* sample 2	106.4	448.4	21.4	4.21

September 2016 *Equisetum* Capto Q S2 sample was loaded onto Superdex 75 16/100 size exclusion chromatography for polishing step. Protein sample was divided into 1.5 mL fractions based on their molecule sizes (Figure 4.143). Fractions 48-107 that are showing protein existence were collected for further analysis. Enzyme activity test using TXG-XGO and BBG-XGO substrate couples were done with SEC fractions. Reactions were analysed by HPLC (Figure 4.144).

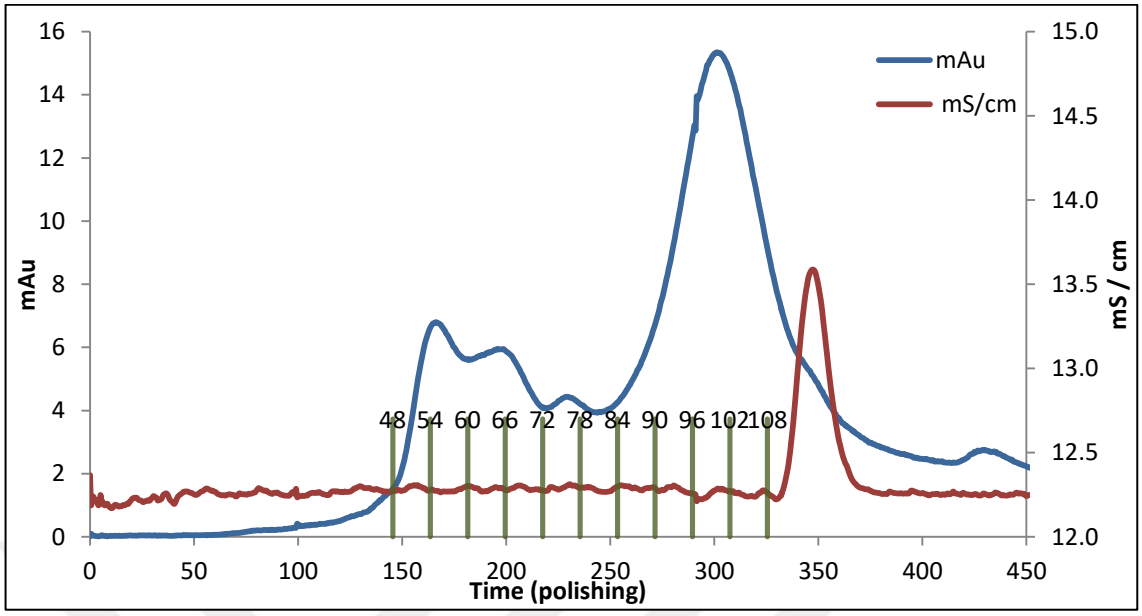

Figure 4.143. September 2016 *Equisetum* sample Capto Q S2 polishing using Superdex 75 16/100 column. Fractions are indicated on graph with green bars on x-axis.

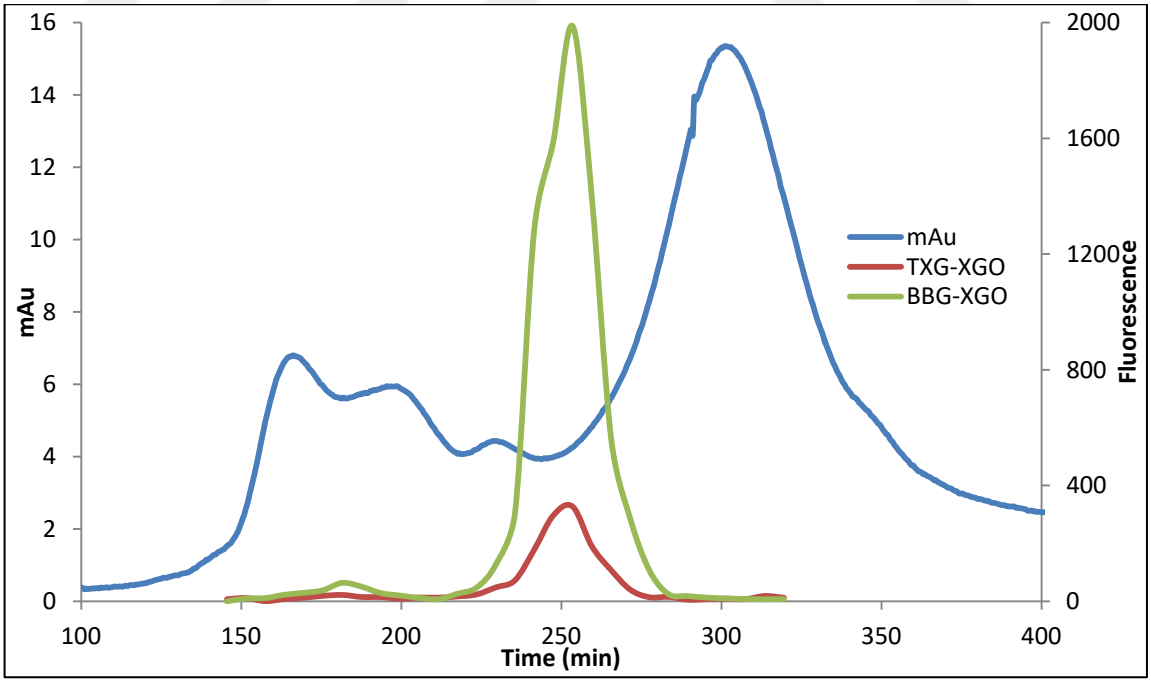

Figure 4.144. Fluorescence amounts of TXG-XGO and BBG-XGO hybrid products generated by polishing step fractions of *Equisetum* September 2016 protein sample.

Based on generated hybrid product amounts and SEC chromatogram, fractions were combined into 3 pools; Pool α composed of fractions 76-81, Pool β composed of fractions 82-87 Pool γ composed of fractions 88-92. Samples taken during protein purification procedure and SEC pool of September 2016 *Equisetum* young plant extract were analysed by SDS-PAGE silver nitrate staining for protein purity (Figure 4.145). A big difference, in means of protein band profile, was seen between Capto Q S2 and SEC pools. Superdex 75 16/100 provided useful separation of sample. Polishing step pools were quantified in means of protein concentration via BCA assay. They were also used in enzyme activity tests with TXG-XGO and BBG-XGO donor-acceptor couples in order to see MXE and XET activity ratios of Pools α, β and γ (Table 4.56).

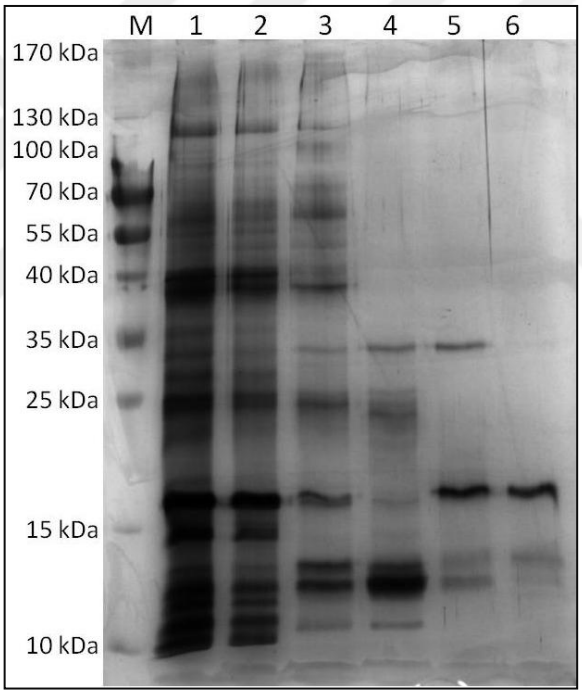

Figure 4.145. SDS-PAGE silver staining of *Equisetum* September'16 samples. 1; Sample before Capto S chromatography, 2; Capto S column flow-through, 3; Capto Q column sample 2, 4; SEC sample α, 5; SEC sample β, 6; SEC sample γ.

Table 4.56. Protein concentrations and florescence amounts of TXG-XGO and BBG-XGO hybrid products generated by enzyme activity test using September 2016 *Equisetum* polishing samples α, β, γ.

Sample name	Protein concentration (mg/ml)
Equis Sept'16 Sample α	0.044
Equis Sept'16 Sample β	0.029
Equis Sept'16 Sample γ	0.021

4.10. SPECIFIC ENZYME ACTIVITIES AND ENZYME KINETICS OF PURIFIED EQUISETUM MXES

As the first step in activity tests, pH optimization of *Equisetum* MXE was performed in order to find the pH value at which enzyme is showing the maximum activity so that a more accurate specific activity calculation can be performed. pH optimization of MXE was carried between pH values 4.0 and 6.4 with BBG-XGO donor-acceptor couples. pH of donor substrate was adjusted using ammonium acetate buffer with specific pH values between 4.0 and 6.8. Hybrid products amounts generated by MXE enzyme using donors with different pH values were analysed by HPLC system and it was concluded that enzyme is producing highest amount of product at pH 5.4, thus pH optima of the enzyme is pH 5.4 (Figure 4.146).

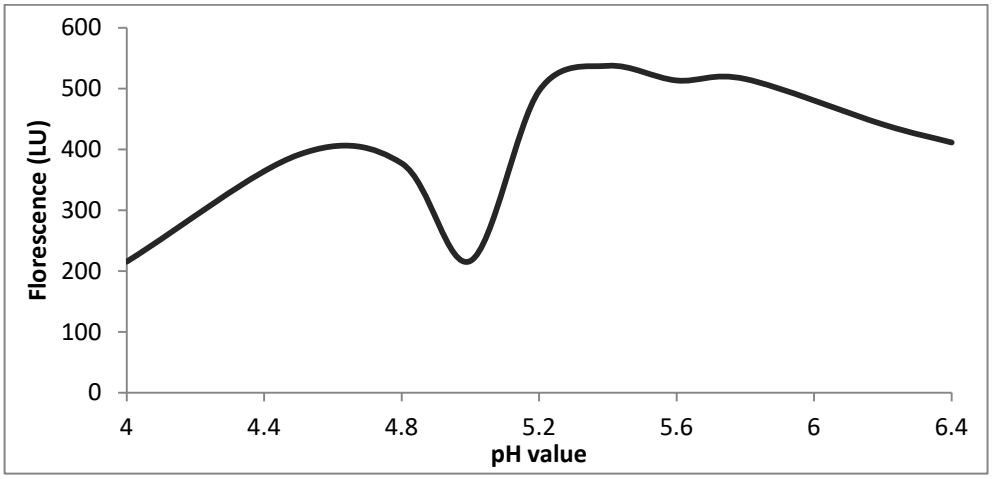

Figure 4.146. pH optimization study of *Equisetum* MXE enzyme between pH 4.0 to pH 6.4 using ammonium acetate buffer.

Purified *Equisetum* MXE enzymes from plants collected on different months were subjected to various analysis in order to identify the protein and some of the sample pools were all used up during mentioned identification tests, before enzyme activity tests were done. On the other hand, it is necessary to carry specific activity calculations of enzyme samples too. Thus, one remaining pool with visible MXE band around 30-35 kDa was chosen for activity tests. Pool 3 of April 2016 sample, Pool B of July 2016 sample and Pool β of September 2016 sample was used for specific activity calculations. Using these enzyme pools, time interval studies were carried with TXG-X7, TXG-XGO, BBG-X7, BBG-XGO, HEC-X7 and HEC-XGO as at least 3 repeats. Hybrid products generated during enzyme activity tests were analysed by HPLC system and data were used to calculate picokatals / mg enzyme specific activities (Table 4.57). All tested enzyme samples are showing preferentially more activity endotransglycosylation activity with BBG donor compared to TXG or HEC donor. This situation confirms MXE activity. Enzymes are showing activity on HEC donor too, yet this activity is less than both BBG and TXG.

Table 4.57. Specific enzyme activities of pure September 2016, July 2016 and September 2016 *Equisetum* MXE samples. Given values are pkatals / mg enzyme.

	April 2016 Pool3	**July 2016 Pool B**	**September 2016 Pool β**
TXG-X7	1.397	20.876	9.020
TXG-XGO	1.003	21.269	8.106
HEC-X7	0.436	4.797	2.412
HEC-XGO	0.430	4.729	5.682
BBG-X7	3.486	98.404	30.279
BBG-XGO	5.264	75.108	29.784

Specific enzyme activity studies revealed that protein sample purified from July 2016 *Equisetum* explants shows highest specific activity per mg protein with tested substrate couples TXG-X7, TXG-XGO, HEC-X7, HEC-XGO, BBG-X7 and BBG-XGO. Although samples from all different explants showed expected MXE band at the same size, activity amounts showed significant difference. This difference can be caused by positive or negative effect of other proteins in the surrounding environment on stability and reaction catalysing ability of *Equisetum* MXE. Due to protein-protein or protein-peptide interactions, MXE from a particular explant might be more active than others, considering residual contaminant protein bands after all chromatographic separation steps.

Enzyme sample with the highest activity, July 2016, was chosen for enzyme kinetics studies. These calculations were carried with BBG-X7 and TXG-X7 substrate couples because the enzyme activity in scope of this work is MXE activity. Firstly, donor concentrations ranging between 0.05 per cent w/v to 0.6 per cent w/v were tested with enzyme activity test and results were analysed by HPLC system (Figure 4.147). When change in enzyme reaction rates (μM product/minute) values were evaluated for each donor, it was seen that reaction rate increases with increasing donor concentration, yet these increases tail off as donor concentration is reaching the highest tested value 0.6 per cent w/v. Thus, for kinetic value calculations, 0.6 per cent w/v donors were used.

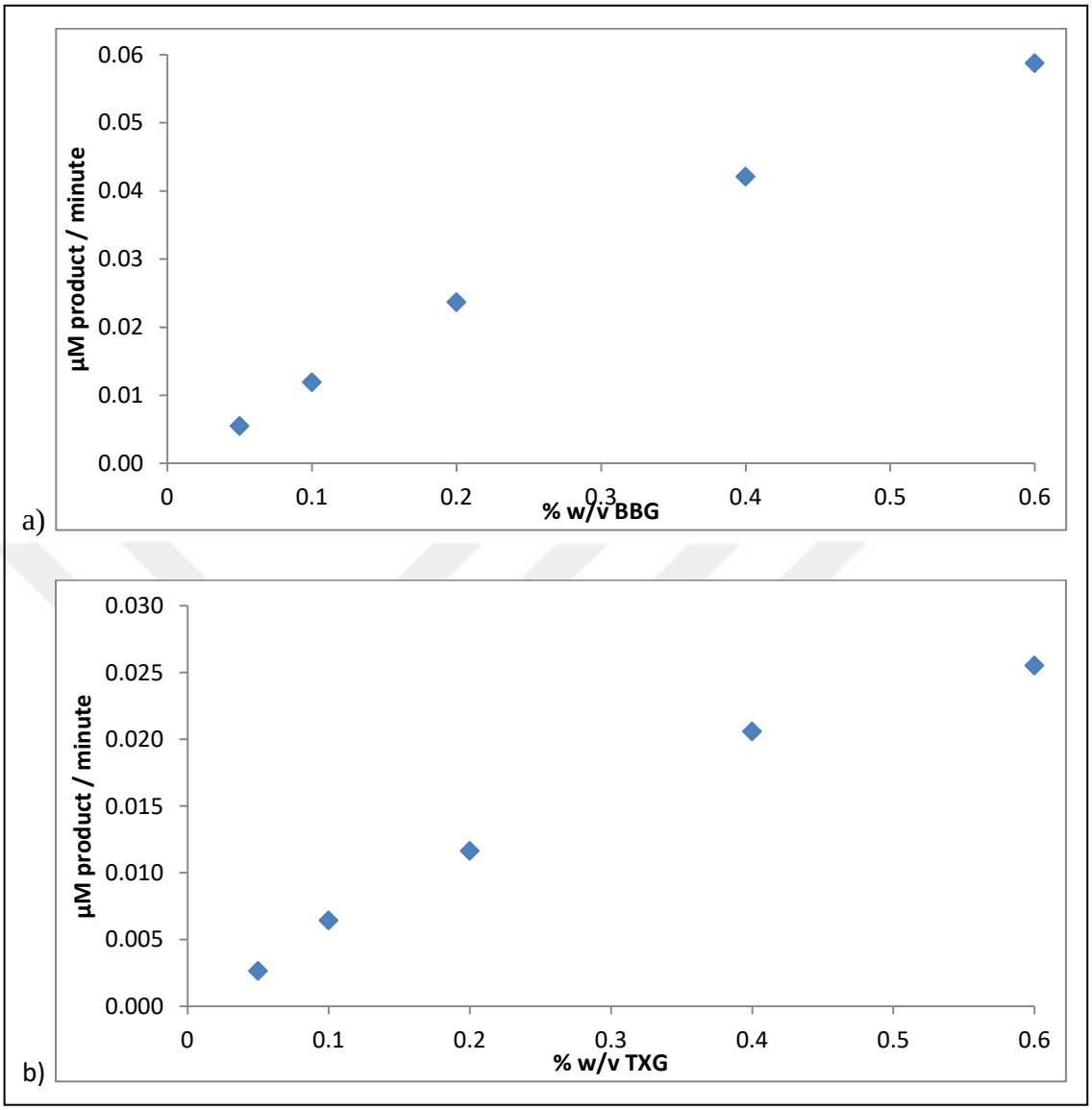

Figure 4.147. *Equisetum* MXE reaction rates graph with various donor concentrations and 50 µM XGO. a) Various BBG concentrations, b) Various TXG concentrations.

Enzyme kinetic calculations were done by generating Michaelis-Menten plots for TXG-X7 and BBG-X7 substrate couples separately. For TXG-X7 couple, acceptor concentrations between 1-200 µM were tested and amount of hybrid product generated by each acceptor concentration was quantified via HPLC analysis (Figure 4.148a). Using Michaelis-Menten plot, Lineweaver-Burke plot was generated for TXG-X7 substrate couple (Figure 4.148b). Same studies were also carried using BBG donor and varying X7 concentration between 150 µM. Michaelis-Menten (Figure 4.149a) and Lineweaver-Burke (Figure 4.149b) plots

were generated. Using slope equations of Lineweaver-Burke plots for each donor, kinetic value calculations were done (Table X).

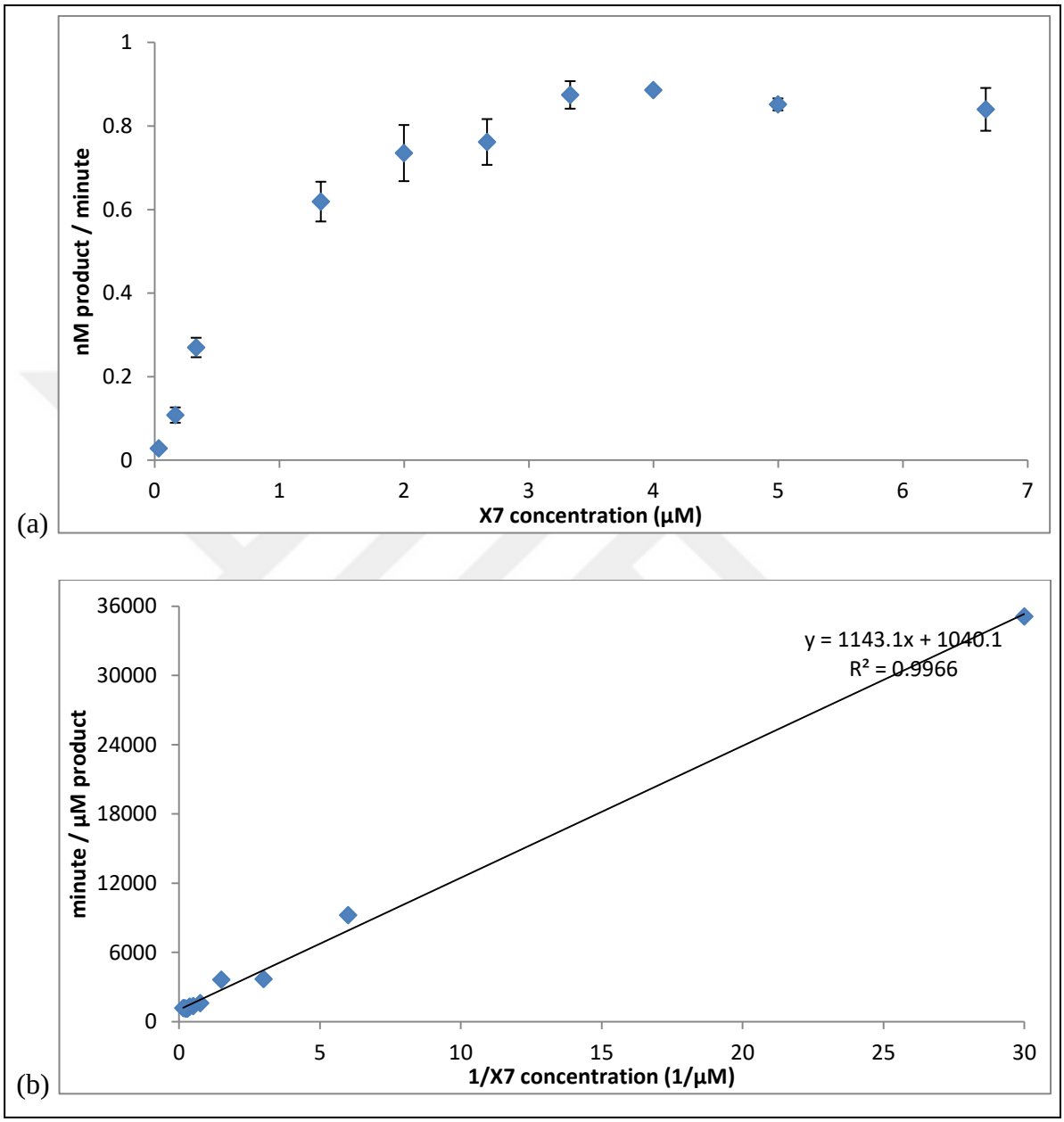

Figure 4.148. *Equisetum* MXE enzyme rate with 0.6 per cent w/v TXG and various X7. a) Michaelis-Menten plot, b) Lineweaver-Burke plot

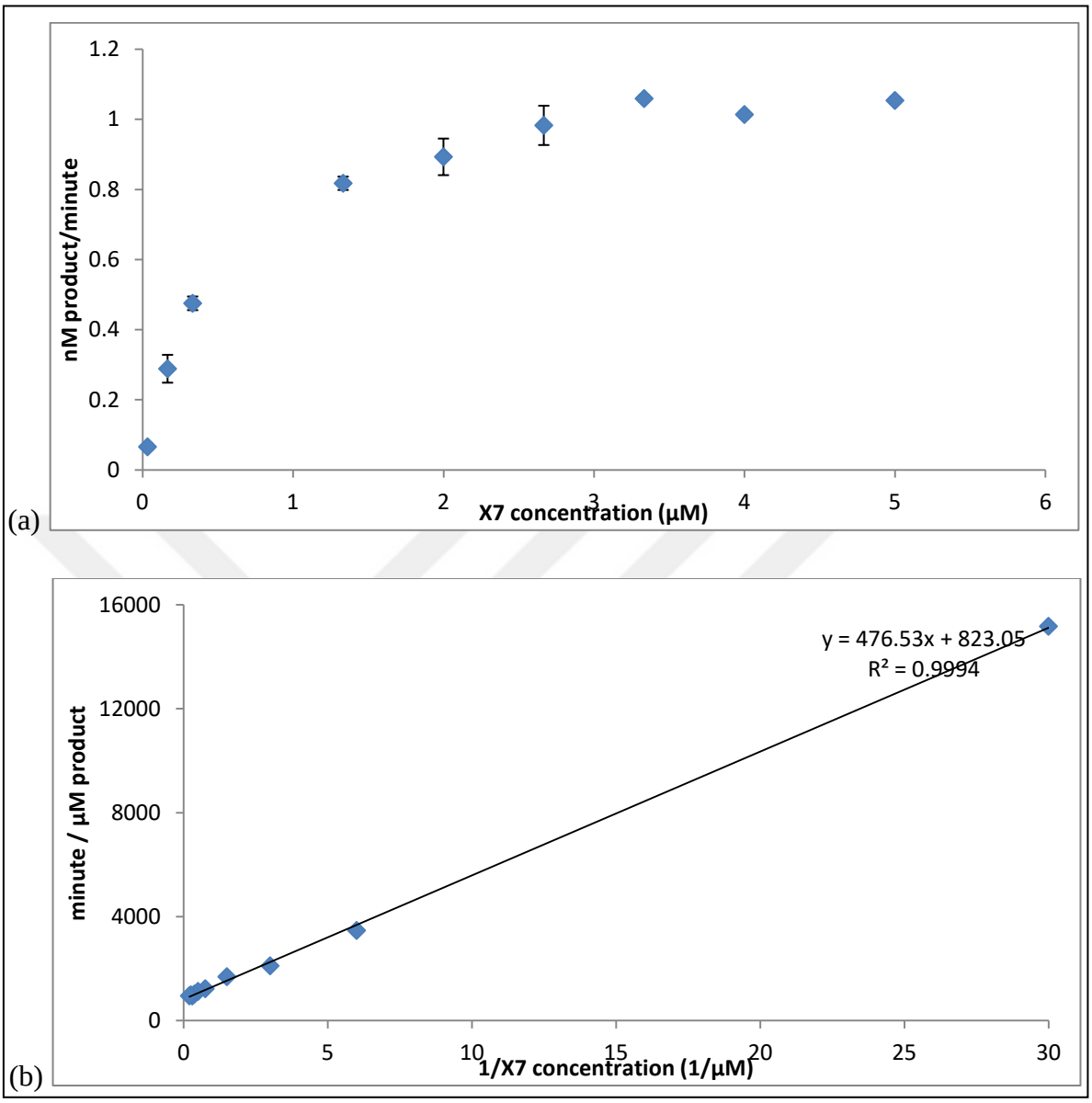

Figure 4.149. *Equisetum* MXE enzyme rate with 0.6 per cent w/v BBG and various X7. a) Michaelis-Menten plot, b) Lineweaver-Burke plot

Table 4.58. V_{max}, K_m values of *Equisetum* MXE enzyme on TXG-X7 and BBG-X7 donor-acceptor couples.

	TXG-X7	**BBG-X7**
V_{max}	$9.61 * 10^{-4}$ µM/min	$1.22 * 10^{-3}$ µM/min
K_m	1.09 µM	0.58 µM

4.11. 2D-PAGE TRIAL WITH PURIFIED EQUISETUM MXE ENZYME

Further proteomic analysis was carried in order to identify potential target MXE protein band observed in Pool 2&3 samples. Firstly, 2D-PAGE trials were carried to investigate any non-specific protein band that is impossible to visualize in 1D SDS-PAGE such as an unrelated protein with same molecular weight but different pI value. 2D-PAGE trials were started with using 800 ng April 2016 Belgrad *Equisetum* Pool 3 sample. Protein sample was used in rehydration mixture and 17 cm pH 4-7 IPG strip was rehydrated for 16 hours at room temperature. Isoelectric focusing of proteins on strip was carried using Bio-rad Protean IEF system with 0 → 10 000 volt rapid ramping and 40 000 VH total. Then, focused strip was equilibrated and second dimension run was done. Gel was stained with coomassie blue staining solution and destained with ultrapure water until background is cleared. Gel was visualized and examines (Figure 4.150). No protein dots were visible on first 2D-PAGE trial gel. Method optimization is one of the difficulty of 2D-PAGE along with sample handling yet additionally, protein amount was low and this can be one of the main reasons of not achieving a successful result in the first 2D-PAGE trial.

Figure 4.150. First 2D-PAGE analysis of April 2016 Belgrad *Equisetum* Pool 3 sample, coomassie brilliant blue stained. M; protein size marker.

Second 2D-PAGE trial was carried with 8µg *Equisetum* April 2016 Pool 3 which is 10 times more than the one used in first trial. Also, 5 µg BSA was added in order to visualize success of the separation. Target *Equisetum* protein and BSA mix was used with rehydration buffer to rehydrate 17 cm pH 4-7 IPG strip. The strip was focused at room temperature in Bio-rad Protean IEF system with 0 → 10 000 volt rapid ramping and 40 000 VH total. Second dimension separation was carried after equilibration of the strip. Proteins on the isoelectric focusing strip were separated based on their molecular weight in vertical system and gel was stained with coomassie blue dye for 3 hours. Unbound dye molecules were removed by destaining solution and gel was visualised (Figure 4.151). Result of second 2D-PAGE was fruitless too like the first trial. Neither the BSA nor target protein spots were visible even though sample amounts and staining period was more than previous trial. This outcome makes us conclude that 2D-PAGE analysis is indeed a tough method to apply and needs detailed optimization. Due to fewness of precious *Equisetum* purified protein sample, 2D-PAGE trials were set aside and alternative methods were applied to identify protein band(s).

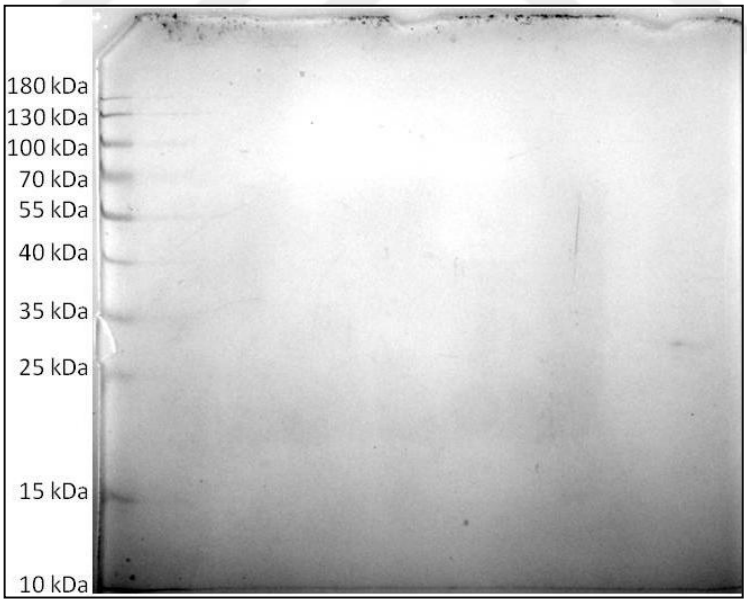

Figure 4.151. Second 2D-PAGE analysis of April 2016 Belgrad *Equisetum* Pool 3 sample, coomassie brilliant blue stained. M; protein size marker.

4.12. IN-GEL TRYPTIC DIGESTION AND MALDI-TOF ANALYSIS OF PURIFIED EQUISETUM PROTEIN

2D-PAGE trials failed, yet previous 1D SDS-PAGE trial (Figure 4.131) indicate that Pool 2 and Pool 3 of April 2016 *Equisetum* sample are pure since they are showing one band profile with silver nitrate staining method which is a very sensitive staining method. Thus, April 2016 *Equisetum* sample Pool 2 was decided to be used in In-Gel digestion and MS analysis approach. By such a proteomic analysis, we aimed to achieve insights about amino acid sequence of target MXE enzyme in *Equisetum telmateia*. 17µL of April 2016 *Equisetum* Pool 2 sample was concentrated using Amicon Centrifugal Filters and vacuum concentrator. After denaturation, protein sample was run in polyacrylamide gel. Gel was stained with coomassie brilliant blue dye and destained to visualize protein bands (Figure 4.152). Two bands were visualized by staining and destainig of the gel; band 1 is larger in size and excess in quantity compared to band 2. Both of the bands were cut out of the gel and processed with in-gel tryptic digestion protocol in order to prepare tryptic fragments for MS analysis. Prepared fragments were analysed by TOF/TOF 5800 system (ABSciex) and peptide fragments' masses were discovered. Data acquired from instrument was analysed using Mascot software. Peptide fragment were compared against prepared database (Appendix A). The best match was with AtXTH22 (protein ID NP_200564.1; CDS accession number NM_125137.4) which is a Group II XTH enzyme from *Arabidopsis thaliana*. Only total of 6 tryptic fragments of April 2016 *Equisetum* sample band 1 showed match with four different Equisetum proteins within the database. These outcomes are not sufficient for identification of protein sample band 1. Thus, a different approach was chosen for identification.

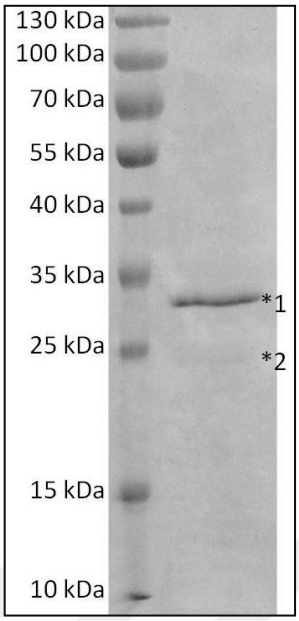

Figure 4.152. April 2016 *Equisetum* Pool 2 sample SDS-PAGE gel stained with coomassie brilliant blue for mass spectrometry analysis. Proteins size marker bands and sample band are indicated on the figure.

4.13. N-TERMINAL EDMAN DEGRADATION OF PURIFIED EQUISETUM MXE PROTEIN

Another approach performed to identify target protein is N-terminal Edman degradation assay. April 2016 *Equisetum* sample Pool 3 was prepared for this assay. 12 µg protein sample was desalted into 5 mM sodium citrate 10 mM NaCl pH 5.5 buffer and denatured by mixing with laemmli buffer. Then it was run on polyacrylamide gel. Gel was blotted onto PVDF membrane in the presence of 50 mM sodium borate pH 9.0 buffer. Membrane was visualized with coomassie brilliant blue staining and destained. Protein band on the membrane was faint (Figure 4.153). This can be due to short staining period of the membrane, yet protein band indicated with a rectangle in Figure 4.153 was cut and sent to Proteome Factory AG Belin Germany for N-terminal Edman sequencing. Reply from the company was negative, they stated that they couldn't detect any valid sequence in the first 6 amino acid and this can be due to N-terminal blockage of the sample (Appendix B).

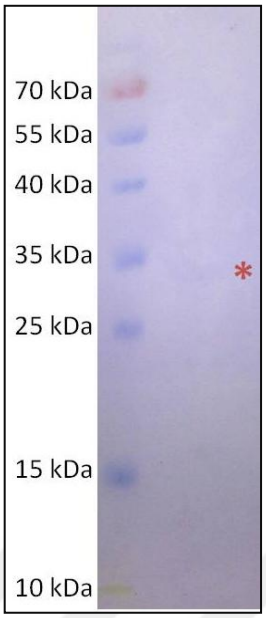

Figure 4.153. April 2016 Belgrad *Equisetum* Pool 3 sample SDS-PAGE gel blotted on PVDF membrane and stained with coomassie brilliant blue for N-Terminal Edman degradation sequencing.

4.14. NATIVE-PAGE AND IN GEL ACTIVITY ASSAY OF PURIFIED EQUISETUM MXE

Purified *Equisetum* protein samples (July 2016 and September 2016 Belgrad samples) are showing multiple band profiles in silver nitrate stained SDS-PAGE gels. Putative MXE enzyme is thought to be ~35 kDa, and it is highly likely to be causing both XET and MXE activity. Native-PAGE & in-gel activity assay protocols were developed and optimized in order to prove both XET and MXE activities belong to same enzyme.

When a protein sample is separated on a native polyacrylamide gel, fragments will mostly preserve their native conformational state. *Equisetum* September'16 sample shows a profile consisting of multiple bands on SDS-PAGE analysis. When this protein sample is separated by Native-PAGE technique, fragments will most probably separate, even if this separation is not based only on molecular sizes. All the proteins making up Equisetum september'16 sample will be in their native state, meaning it will be possible to detect activity they are showing. Thus, if the native-PAGE gel is prepared including MXE donor

BBG, putative Equisetum MXE enzyme will show activity when there are excessive amounts of acceptor in reach of the enzyme, integrating X7 acceptor in the environment onto BBG chains, resulting in binding of X7 acceptors onto BBGs within gel matrix and causing fluorescence bands on the gel.

September 2016 *Equisetum* samples Pools α and β were used in Native-PAGE and in-gel activity assay trials. 400 ng of each protein sample was mixed with Native-PAGE sample loading buffer and they were loaded into both native gel w/ BBG donor and native gel w/o BBG donor. After running the gels, both gels were visualised by silver nitrate staining and It was observed that *Equisetum* protein samples run into gel and showed separation into different bands (Figure 4.154).

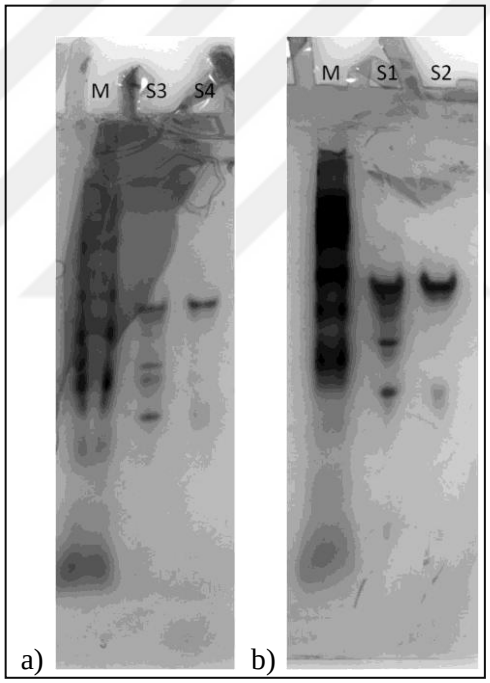

Figure 4.154. Native-PAGE separation of *Equisetum* September'16 protein samples, a) Samples loaded on w/ BBG gel, b) samples loaded on w/o BBG gel. Gels were visualized by silver-nitrate staining.

After observing separation of *Equisetum* protein sample with Native-PAGE technique, in gel activity assay was performed. Both September 2016 *Equisetum* Pool α and β samples were separated in w/ BBG donor polyacrylamide native gel and then gel was incubated

with X7 acceptor. Next, gel was washed and visualised using ChemiDoc instrument different methods since a specific wavelength arrangement setting is not available in ChemiDoc (Figure 4.155). A clear sharp band is visible in each image gathered using different filters. When silver nitrate stained gel image and in-gel activity assay image of Pools α and β were compared (Figure 4.155e), it can be clearly seen that protein band on top in both samples is the source of MXE activity.

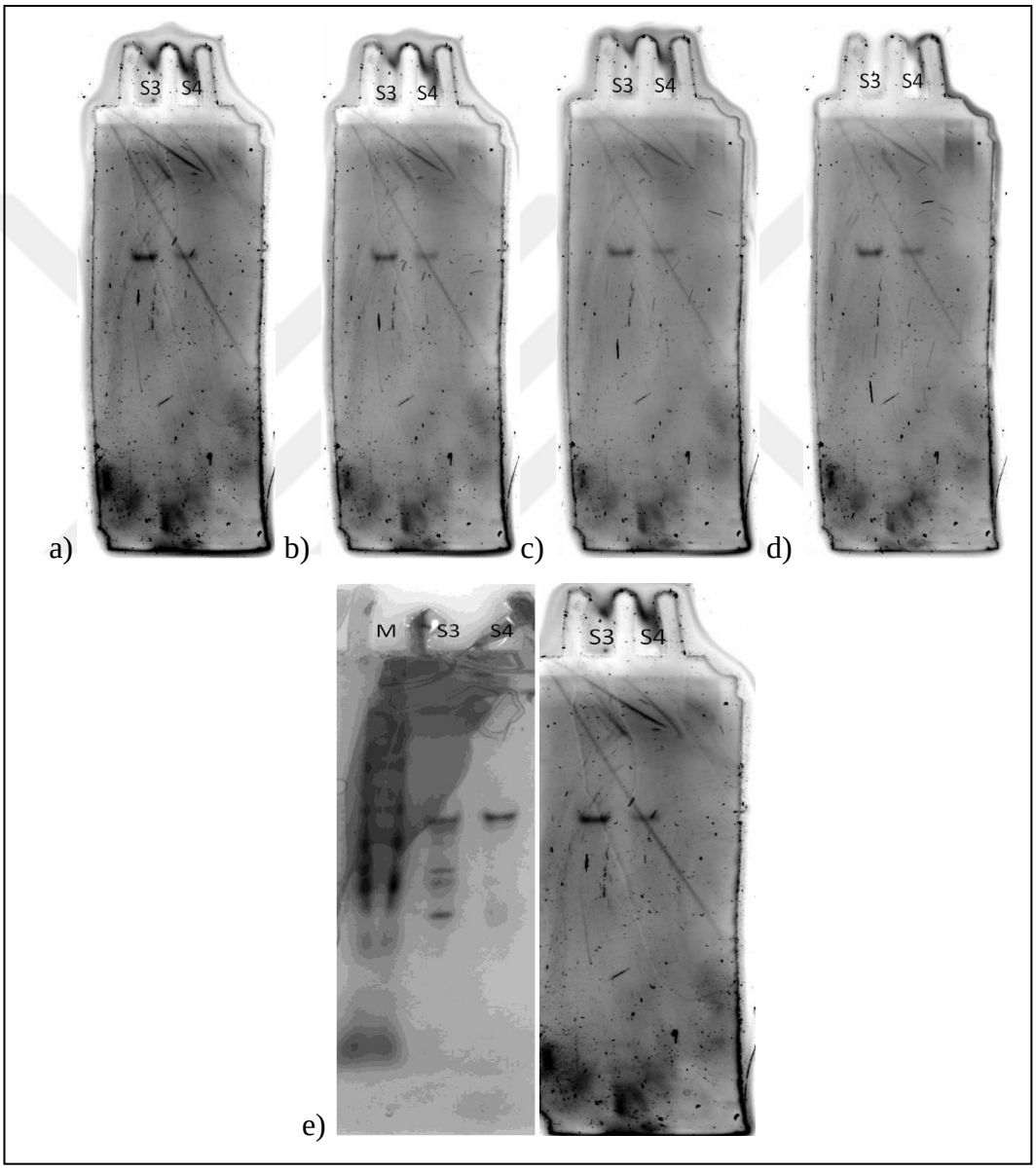

Figure 4.155. Equisetum September'16 protein sample Native-PAGE in-gel activity results visualization by various ChemiDoc filters, a)Sypro Ruby filter, b) Coomassie fluor orange filter, c) fluorescein filter, d) Qdot 565 nm filter. e) Alignment of silver stained samples and in-gel activity result of same samples.

4.15. RANDOM AMPLIFIED CDNA ENDS (RACE)

Equisetum telmateia, unlike *Equisetum diffusum, Equisetum hyemale, Equisetum arvense* and *Equisetum fluviatile*, doesn't have any genomic/proteomic information in publicly available databases. Thus, in order to have more information, we aimed to combine both proteomic and genomic approaches to enlighten MXE enzyme from *E. telmateia*. Analysis of tryptic fragments gives some information about possible sequence of protein, yet available protein sequences in databases are sequences of other *Equisetum* species (such as *E. diffusum, E. hyemale*), thus a mass spectrometry approach for tryptic fragments will not be enough. To overcome this drawback, RACE strategy was employed.

4.15.1. 3'-RACE

The idea of 3'-RACE is fishing out unknown 3' end of a sequence by using a primer couple composed of a primer for 5' region of the sequence and an adaptor primer for 3' end of the unknown sequence (3'-RACE system for rapid amplification of cDNA ends, Invitrogen Life Technologies). Adaptor region at 3' end is added next to polyA tail region during cDNA synthesis via using oligo-d-(T) primer with the adaptor region. As 5' PCR primers, degenerate primers were designed using coding region sequences of publicly available *Equisetum* MXE/XET sequences. 2 sets of degenerate primers were designed (a 5' PCR primer and a nested primer) for 3 different Equisetum groups, Equisetum Group, Group I and GroupIIIB.

As the first step of 3'-RACE system, RNA extraction from 3 different tissue samples were done. IntronBio easyspin II RNA extraction kit was used, however due to the high silica and polysaccharide content of Equisetum plants, RNA extraction didn't result in high efficiency (Table 4.59). Despite low concentrations and 260/280 and 260/230 absorbance ratios, extracted RNAs were used in cDNA synthesis by oligodT adapter primer.

Table 4.59. Concentration and purity of extracted RNAs from different frozen *Equisetum* tissue samples.

Sample abbreviation	Sample name	RNA concentration (ng/µl)	A260/ A280	A260/ A230
1 / cDNA_1	Equisetum Apr'16 whole young plant 1	43.6	1.45	0.59
2 / cDNA_2	Equisetum Apr'16 whole young plant 2	26.0	1.39	0.54
3 / cDNA_3	Equisetum Sept'16 whole young plant	7.9	1.44	0.58
4 / cDNA_4	Equisetum June'16 young stem	11.9	1.35	0.61

Synthesized cDNAs were used as templates in first PCR. AUAP-3'-RACE primer was used as reverse primer and 3 different degenerate primers were used as forward primers separately (Table 4.60). For each primer couple, 3 annealing temperatures were tested and all of these primer couple-annealing temperature combinations were utilized separately for 4 different cDNAs. Generated PCR products were loaded on agarose gel and analysed (Figure 4.156).

Table 4.60. Abbreviations of primer couples used for first PCR amplification in 3'-RACE.

Primer couple abbreviation	5' primer	3' primer
A	EqOnlyDegI	AUAPIIIRACE
B	GrpIOnlydegI	AUAPIIIRACE
C	GrpIIIBOnlydegI	AUAPIIIRACE

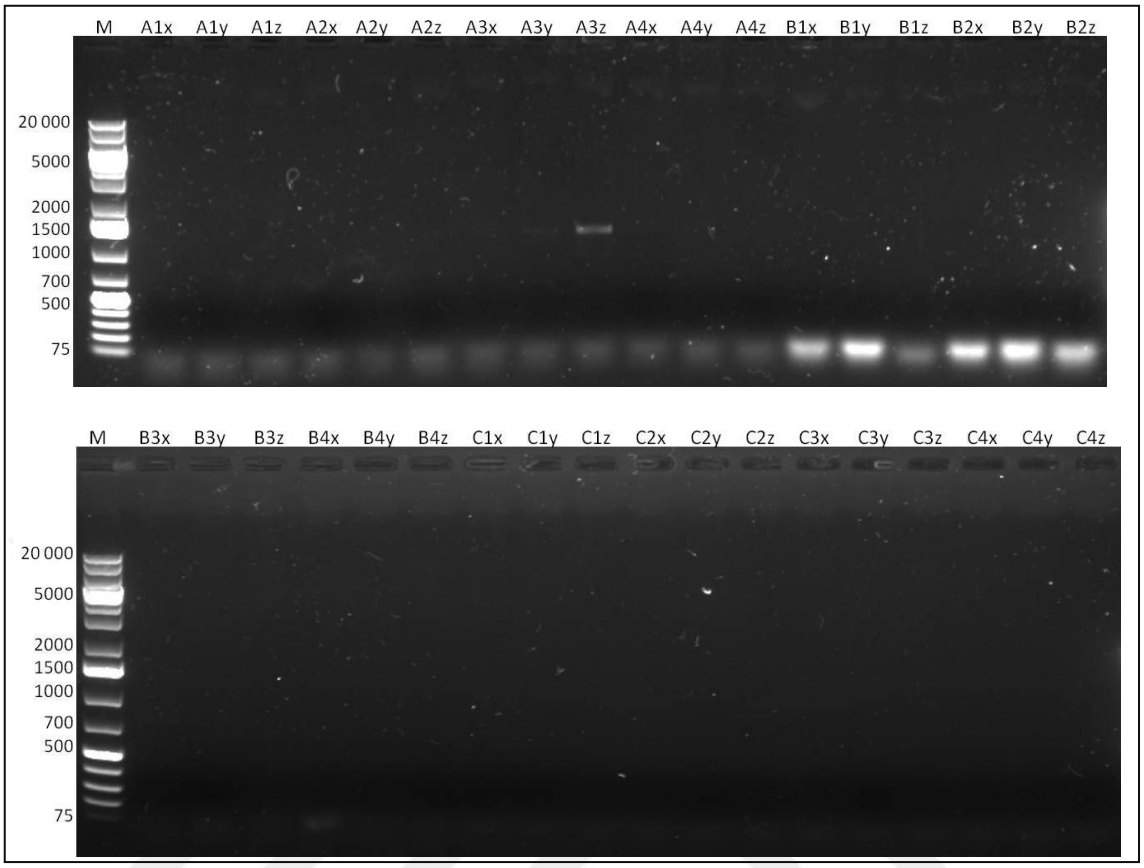

Figure 4.156. First 3'-RACE PCR results using primer couples stated in Table 4.60. Sample names and molecular size marker is given in the figure. Sample names are coded as first letter for primer couple, second number for cDNA template and last letter for annealing temperature.

Only EqusetumOnlyDegenerateI primer gave a band when used with September'16whole young plant cDNA. Thus, another gradient PCR was done with same cDNA samples and primer couples, which is named as second PCR. More PCR products were obtained when annealing temperatures were lowered (Figure 4.157). DNA fragments were generated using EquisetumOnlyDegenerateI primer and GroupIOnlyDegenerateI primer with cDNA_3 and cDNA_4 at lower annealing temperatures.

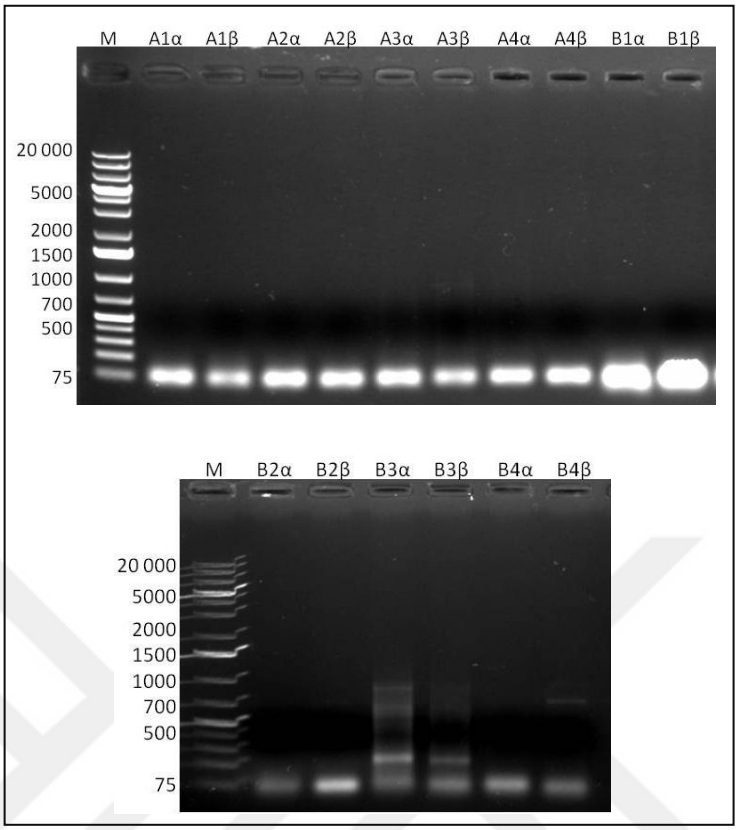

Figure 4.157. Second 3'-RACE PCR results using primer couples stated in Table 4.60. Sample names and molecular size marker is given in the figure. Sample names are coded as first letter for primer couple, second number for cDNA template and last letter for annealing temperature.

PCR products A3z, A3β, B3α and B4β were used as templates and a nested PCR with EquisetumOnlyDegenerateII and GroupIOnlyDegenerateII primers were carried out. EquisOnlyDegII primer was used with A3z PCR product and GrpIOnlyDegII primer was used with A3β, B3α and B4β PCR products. Gradient PCR was done and PCR products were loaded on agarose gel for analyses (Figure 4.158).

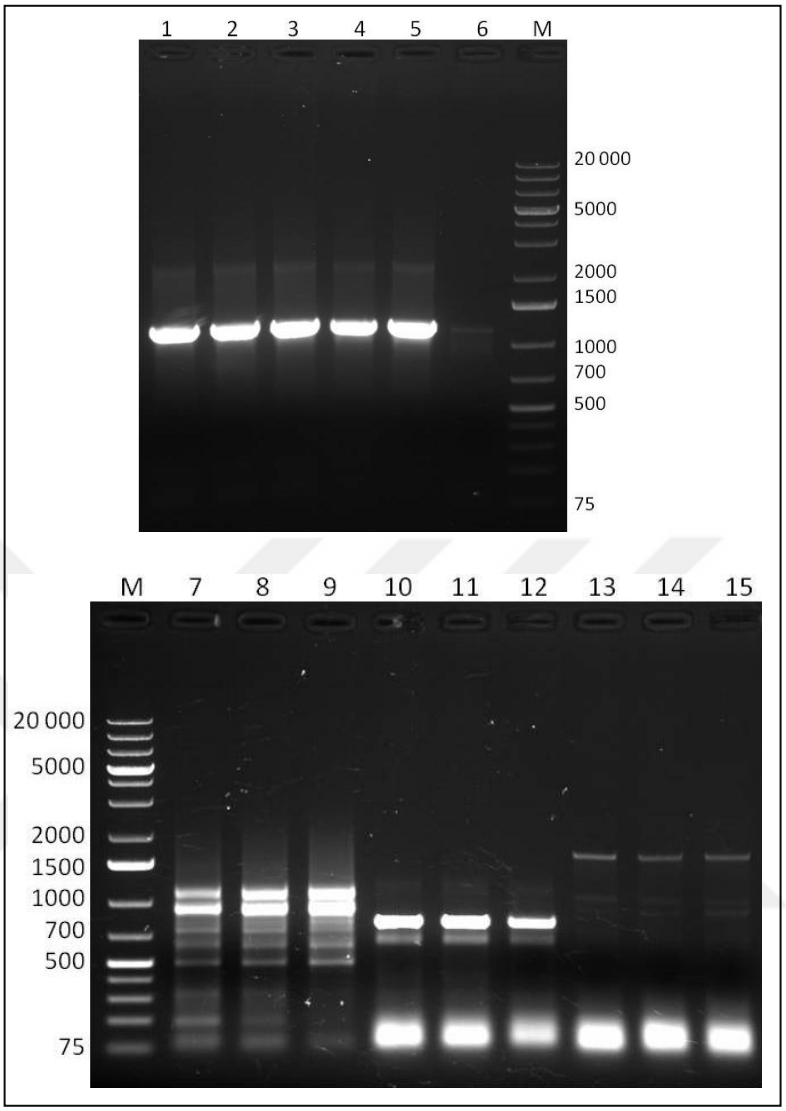

Figure 4.158. Nested PCR results. Samples 1-5; template is A3z PCR products, primers are EquisOnlyDegII-AUAP, Samples 7-9; template is A3β, primers are EquisOnlyDegII-AUAP, Samples 10-12; template B3α, primers are GroupIOnlyDegII-AUAP, Samples 13-15; template is B4β, primers are GroupIOnlyDegII-AUAP. Molecular size marker bands are given in the figure.

Nested PCR trial resulted in many PCR products. All of those products were planned to cloned separately into pCR8 vector for sequencing. Both first round PCR products and nested PCR products were re-produced for cloning. They were loaded onto agarose gels and labelled, then labelled bands were sliced out of agarose gel (Figure 4.159) and gel

purified using Macherey-Nagel gel purification kit. Recovered DNA amounts and purities were quantified by Nanodrop analysis.

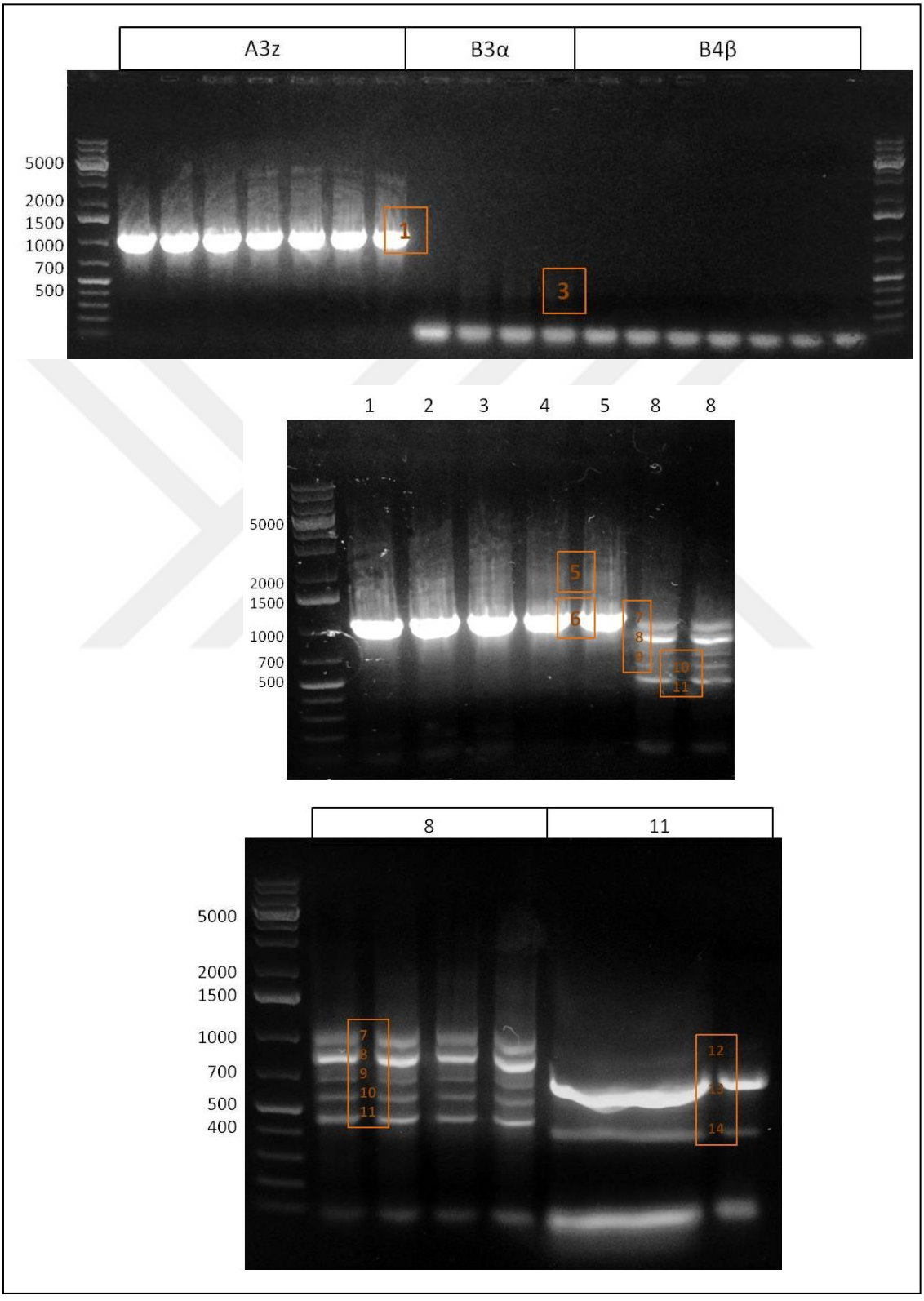

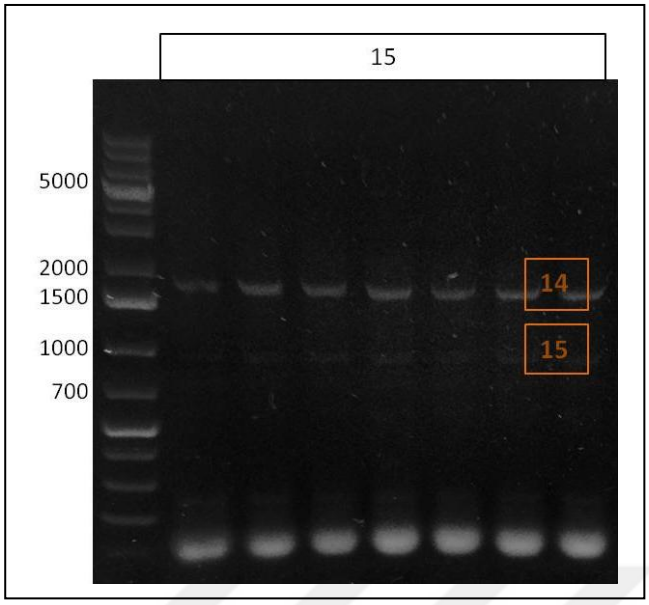

Figure 4.159. Agarose gel loading of nested PCR products regenerated for cloning. Sample names are given above images. Cut and gel purified bands are indicated and labelled on figures. Molecular marker band sizes are indicated on figures.

Gel purified fragments were cloned into pCR8 TOPO cloning vector and chemically competent *DH5α E. coli* cells were transformed by ligation products. However, no colonies were seen as a result of this transformation event. Thus, purified fragments were further concentrated by sodium acetate & ethanol precipitation method. Then, they were cloned into pCR8 TOPO cloning vector one more time and then transformed into competent *DH5α E. coli* cells. However, no positive results were obtained in the second trial. Hence, concentrated PCR fragments were cloned into pGEM-T easy cloning vector as a new approach and then these ligation products were transformed into freshly prepared competent cells. Transformant colonies were selected on LBA+amp+X-gal+IPTG plates and more than 5 positive transformant colonies were obtained per fragment. Three positive white colonies were chosen per fragment and inoculated in LB+amp broth for plasmid isolation. Isolated plasmids were digested with NotI restriction endonuclease enzyme for verification of insert and visualisation of insert length. Digestion results were loaded on agarose gel and analysed (Figure 4.160).

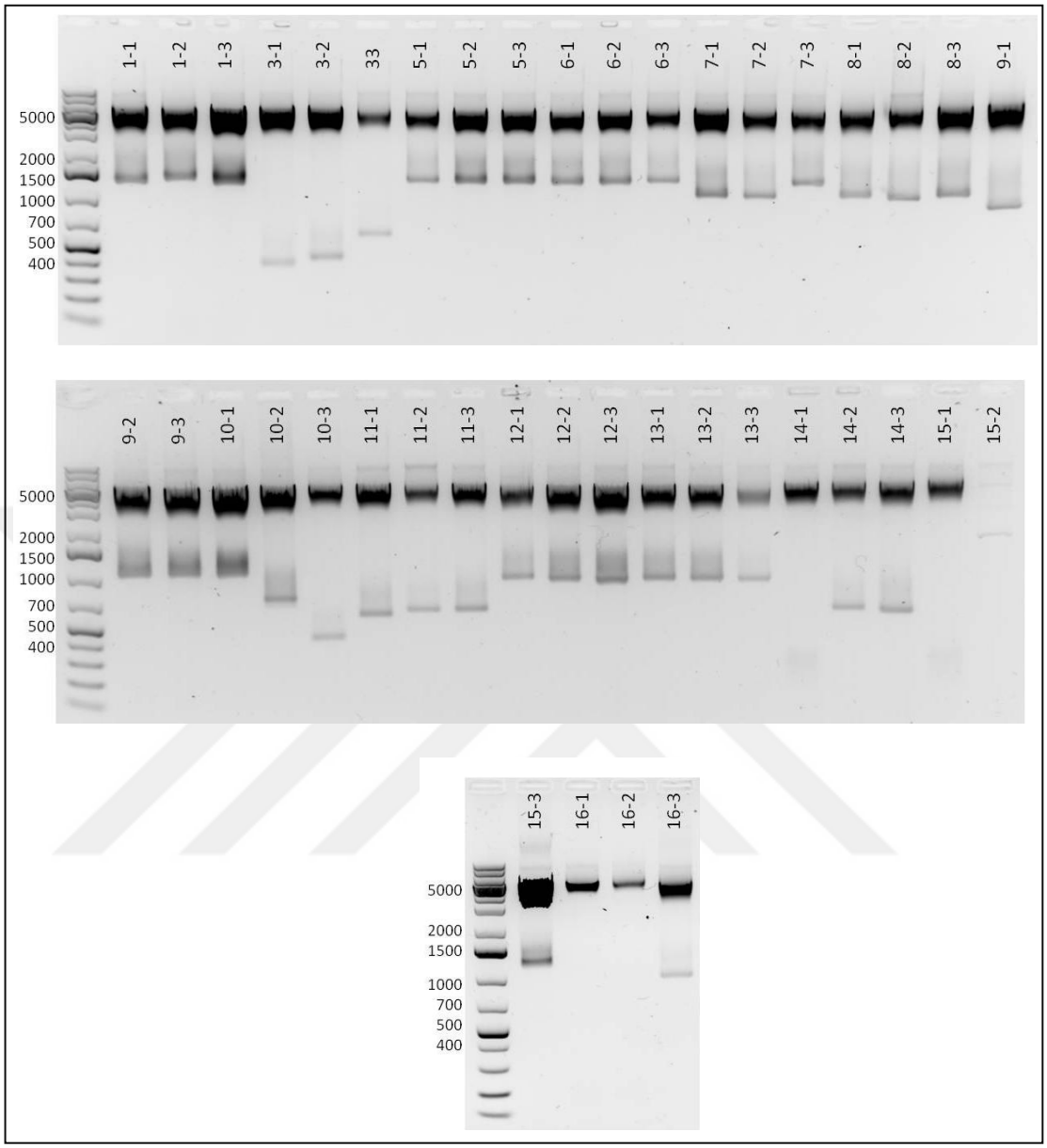

Figure 4.160. NotI digestion of pGEM-t easy with different DNA fragment inserts. Sample names and molecular size marker bands are indicated on figure.

As seen in Figure 4.160, some inserts result in various sizes of restriction fragment. Thus, plasmids 1-1, 1-3, 3-1, 3-2, 3-3, 5-3, 6-1, 7-1, 7-3, 8-1, 8-3, 9-1, 9-2, 10-1, 10-2, 10-3, 11-1, 11-2, 12-1, 12-2, 13-1, 13-2, 14-2, 14-3, 15-3, 16-3 were sent for sequencing.

Insert sequences were insulated from plasmid sequencing results and all were translated into amino acid sequences in different ORFs using Swiss Institute of Bioinformatics, Bioinformatics Resource Portal Translate Tool. Conserved active site sequence of XTHs,

DEIDFEFLG, was searched within translated sequences. Three inserts, fragment 9, fragment 10-3 and fragments 12/13/16-3 (all gave the same sequence) had the conserved domain (Table 4.61).

Table 4.61. Translations of DNA fragments that are giving conserved coding region that is common amongst XTH enzymes. Translations are in reading frames that are giving the meaningful results.

Fragment name	**Amino Acid Sequence**
Fragment 9	DELDFEFLGNYSGDPYLLHTNIFASGVGNREQQFFLWFDPTADFHD YTIIWNPQQILFLVDGRAVRSFPNNEAIGVPYLKSQWMNVHASLW NGETWATLGGLRRIDWNSAPFVASYSEFVGDSCFDSADSPCMASK WWNQPAYQFLSTNDASSIQWVRANYLKYDYCYDTKLYPNGFPAE CSNRGF
Fragment 10-3	DELDFEFLGNVSGQPYIVQTNVYASGVGGREQRIYLWFDPTADFHT YSLSWNKDHIIFLIDGTPIRVYANNENMGVPNPNNQPMQIFSSLWK SSWCPCTSRRVA
Fragment 12	ELDFEFLGNRSGQPYVVQTNMFVNGVGEREQRIYLWFDPTAEFHT YSILWNTHQTVFYVDRVPIRVHVNTPETRNAFPWQPMYVFSSIWN GDQWATRGGLEKINWLSAPFVSSYEKFHADACGGGFCVPSSTTPW WDQPSAWSLSPQEKQKYAWVKSKLTVYDYCTDKARYPSLPADC MVHI

All positive results were from September'16 *Equisetum* cDNA, thus this sample was used in 5'-RACE trials. Using sequencing results and other available *Equisetum hyemale* and *Equisetum diffusum* XET sequences, new 5'-RACE primers that are only specific to fragment-9, 10-3 and 12 were designed. These primers are specific to only the stated fragments, but did align to other Equisetum species available transcripts.

4.15.2. 5'-RACE

Positive results obtained during 3'-RACE trials were all acquired from September 2016 *Equisetum* cDNA. This indicated that September 2016 *Equisetum* cDNA should be used to discover 5' end of putative MXE DNA sequences.

As the first step of 5'-RACE, cDNA synthesis was done using gene specific primers. New RNA extraction was carried from frozen September 2016 *Equisetum* tissue samples using Norgen plant/fungi RNA extraction kit. RNAs were quantified by Nanodrop measurements (Table 4.62).

Table 4.62. *Equisetum* September 2016 RNAs concentrations and purities.

	RNA concentration (ng/µl)	**A2600/A280**	**A260/A230**
September 2016 *Equisetum*_1	107.7	2.04	1.96
September 2016 *Equisetum*_2	76.8	1.99	1.73
September 2016 *Equisetum*_3	81.3	2.00	1.80

Gene specific primers for Fragment 9, Fragment 10-3 and Fragment 12 were designed for using during cDNA synthesis. Also, nested PCR primers specific to each fragment were designed too. Using September 2016 *Equisetum*_1 RNA and GSP1 for fragments 9, 10-3 and 12, 5' cDNAs of fragments 9, 10-3 and 12 (3'-RACE results) were synthesized individually. They were purified by S.N.A.P. column purification protocol. Purified cDNAs were dCTP tailed by TdT tailing step. Then, they were used in PCR with GSP2 for fragments 9, 10-3 and 12. For each template and primer couple, two annealing temperatures were tested and results were analysed after agarose gel electrophoresis of PCR products (Figure 4.161). This first PCR trial resulted in many non-specific bands with some grade of smear image. Exact size of expected band is unknown, yet it can be said that there are many non-specific PCR products in Figure 4.161.

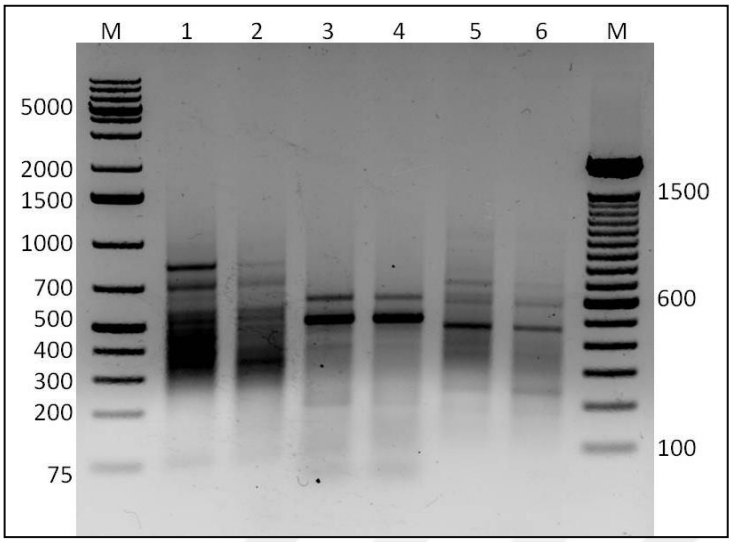

Figure 4.161. Agarose gel electrophoresis results of dCTP tailed cDNAs and GSPs of fragments 9, 10-3, 12. M; marker, 1; Fragment 9 at 58°C, 2; Fragment 9 at 60.5°C, 3; Fragment 10-3 at 60.5°C, 4; Fragment 10-3 at 64.5°C, 5; Fragment 12 at 58°C, 6; Fragment 12 at 60.5°C. DNA size marker band is indicated on figure.

Another gradient PCR was carried by increasing annealing temperatures of primers in order to reduce amount of non-specific PCR bands. Also, in this second trial $MgCl_2$ amount, primer amounts and template cDNA amounts were reduced too. Results were visualised by agarose gel electrophoresis (Figure 4.162). Non-specific PCR products were less visible, though for fragments 9 and 12, dominant PCR product bands were also weak. Thus, a third PCR trial was carried.

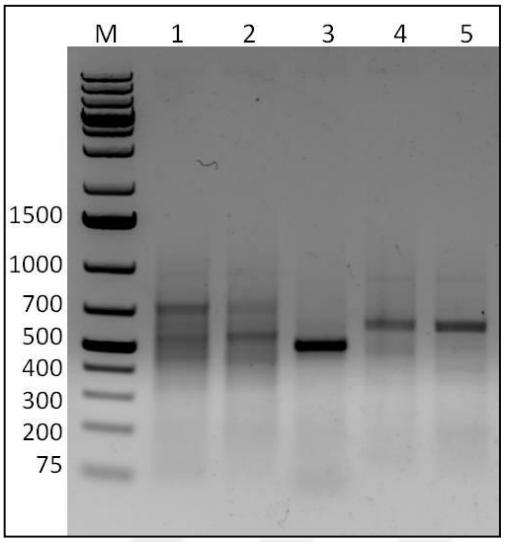

Figure 4.162. Agarose gel electrophoresis results of dCTP tailed cDNAs and GSPs of fragments 9, 10-3, 12. M; marker, 1; Fragment 9 at 58.8°C, 2; Fragment 9 at 61.2°C, 3; Fragment 10-3 at 62°C, 4; Fragment 12 at 58.8°C, 5; Fragment 12 at 61.2°C. DNA size marker band is indicated on figure.

For the third PCR trial, annealing temperatures were varied and PCR products of previous PCR runs were used as templates (Table 4.63). PCR results were run in agarose gel and analysed (Figure 4.163). Changed conditions and compositions didn't make much difference in means of achieving single PCR products. All three PCR trials were evaluated and 5 different combinations were concluded to be used for PCR band production.

Table 4.63. Details of third PCR trial for 5'-RACE. Sample names, primers names, templates and annealing temperatures are given.

	Primer	**Template**	**Annealing temperature**
1	Frg9 GSP2	PCR1st_tube1	61.6°C
2	Frg9 GSP2	PCR1st_tube1	64.9°C
3	Frg10-3 GSP2	PCR1st_tube3	66.4°C
4	Frg10-3 GSP2	PCR2nd_tube3	68°C
5	Frg10-3 GSP2	PCR2nd_tube3	64.9°C
6	Frg12 GSP2	PCR1st_tube5	60°C
7	Frg12 GSP2	PCR1st_tube5	61.6°C
8	Frg12 GSP2	PCR1st_tube5	64.9°C
9	Frg12 GSP2	PCR2nd_tube5	61.6°C
10	Frg12 GSP2	PCR2nd_tube5	64.9°C

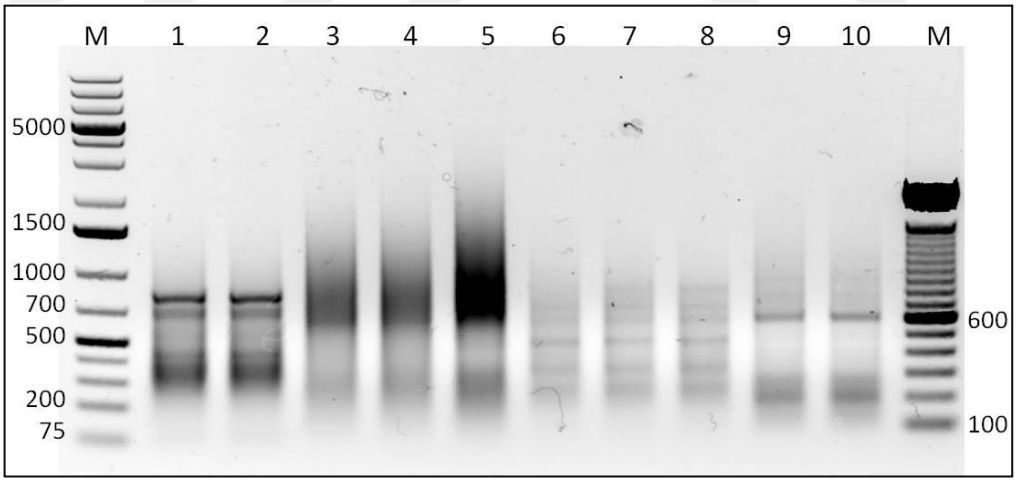

Figure 4.163. Agarose gel electrophoresis result of third PCR trial. Sample names are indicated on figure. Details about sample abbreviations are given in table X. M; DNA size marker.

Different PCR products of Fragments 9, 10-3 and 12 were produced to be sequenced. Production of these bands were done according to combinations given in Table 4.64. PCR

products were run on agarose gel, separated depending on their lengths (Figure 4.164). Bright bands indicated on Figure 4.164 were cut out by a scalpel blade and PCR fragments were recovered using Macherey-Nagel Nucleospin Gel and PCR Clean-up kit.

Table 4.64. PCR combinations for sequencing sample preparation. Abbreviation of PCR sample and their primers, template DNAs and annealing temperatures are given.

Abbreviation	5' primer name	Template DNA	Annealing temperature (°C)
S1	Fragment 10-3 GSP2	dc-tailed cDNA	62
S2	Fragment 9 GSP2	dc-tailed cDNA	58
S3	Fragment 9 GSP2	dc-tailed cDNA	58.8
S4	Fragment 12 GSP2	dc-tailed cDNA	58
S5	Fragment 12 GSP2	dc-tailed cDNA	61.2

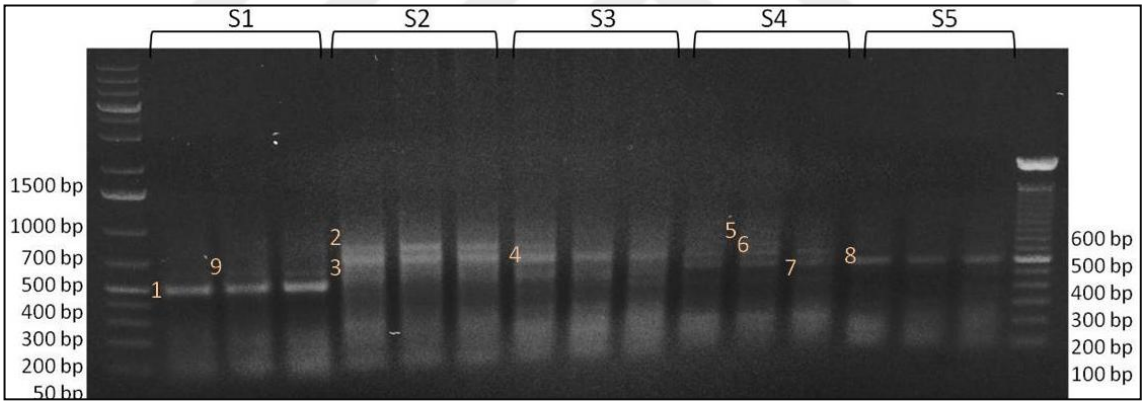

Figure 4.164. Agarose gel electrophoresis of PCR trial done for generating sequencing samples. Sample names are given above images. Cut and gel purified bands are indicated and labelled on figures. Molecular marker band sizes are indicated on figures.

Gel purified PCR bands were concentrated by sodium acetate & ethanol precipitation. Then, they were ligated into pGEM-T easy cloning vector and transformed into *E. coli* DH5α cells. More than 5 white transformant colonies were obtained for each fragment except fragment 5 and fragment 6; only 2 transformant colonies were obtained for fragment 5 and fragment 6. For fragments other than fragment 5 and 6, 4 different

transformants were inoculated and plasmid isolation was performed using Invitrogen Purelink Quick Plasmid Miniprep Kit. Plasmids were quantified by nanodrop instrument and insert presences and sizes were control by NotI digestion. Restriction digestion products were visualised by agarose gel analysis (Figure 4.165).

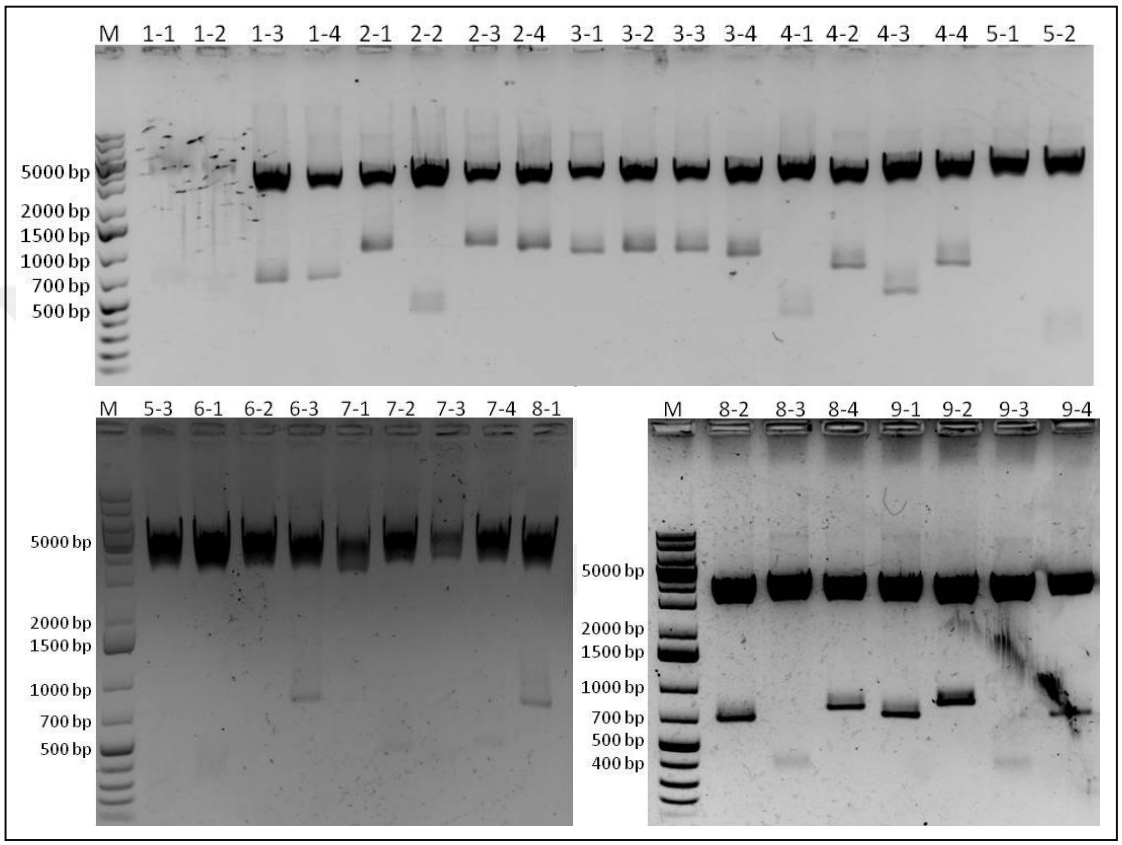

Figure 4.165. NotI digestion of pGEM-t easy with different DNA fragment inserts as result of 5'-RACE trials. Sample names and molecular size marker bands are indicated on figure.

Different colonies of the same fragment resulted in various insert sizes and some restriction digestion didn't show any insert bands. Thus, samples showing various insert sizes, 1-1, 1-3, 2-1, 2-2, 2-4, 3-1, 3-4, 4-1, 4-2, 4-3, 5-2, 6-3, 7-2, 7-4, 8-1, 8-2, 8-3, 8-4, 9-1, 9-2, 9-3, were sent for sequencing. Sequencing results were evaluated by translating DNA sequences into amino acid sequences and searching for the conserved region. Samples with positive results were aligned with 3'-RACE results and full sequences of fragments 10-3 and fragments 12 were constructed (Table 4.65). However, no full-length result was obtained for fragment 9 in the first sequencing run. 5'-RACE trial for Fragment

9 doesn't resulted in a translation with conserved region. Thus, more transformant colonies were chosen and new sequencing reactions were performed to enlighten 5' end of fragment 9.

Table 4.65. Translations of DNA fragments that have conserved coding region which is common amongst XTH enzymes. Translations are in reading frames that are giving the meaningful results. Underlined sequence is conserved region. Yellow highlighted amino acids are the differences between 3' and 5' results.

	Fragment 10-3	**Fragment 12**
3'-RACE result	DELDFEFLGNVSGQPYIVQTNV YASGVGGREQRIYLWFDPTADF HTYSLSWNKDHIIFLIDGTPIRVY ANNENMGVPNPNNQPMQIFSSL WKSSWCPCTSRRVA	ELDFEFLGNRSGQPYVVQTNMF VNGVGEREQRIYLWFDPTAEFH TYSILWNTHQTVFYVDRVPIRV HVNTPETRNAFPWQPMYVFSSI WNGDQWATRGGLEKINWLSAP FVSSYEKFHADACGGGFCVPSS TTPWWDQPSAWSLSPQEKQKY AWVKSKLTVYDYCTDKARYPS LPADCMVHI
5'-RACE result	MASLAASPCLSLVIGLGMVLVA CSSAKVSPVATSSFYTDFDVTW SPSKVQILNGGQELHLTLDSSSG SGFVSKKSYLHGNIDMQIKLVP GNSAGTATAYYLSSTGANHDEL DFEFLGNVSGQPYIVQTNV	MWADDHVQTSQDGTTWHLVL DQSSGSGFQSKNSYLHGWFSMK LKLVPGDSAGVVTAYYMSSNN EKHDELDFEFLGNRSGQPYVVQ TNMFVNGVGEREQRIYLWFDPT AEFHTYSILRNTHQTVFYVDRVP
Complete amino acid sequence	MASLAASPCLSLVIGLGMVLVA CSSAKVSPVATSSFYTDFDVTW SPSKVQILNGGQELHLTLDSSSG SGFVSKKSYLHGNIDMQIKLVP GNSAGTATAYYLSSTGANHDEL DFEFLGNVSGQPYIVQTNVYAS GVGGREQRIYLWFDPTADFHTY SLSWNKDHIIFLIDGTPIRVYAN NENMGVPNPNNQPMQIFSSLWK SSWCPCTSRRVA	MWADDHVQTSQDGTTWHLVL DQSSGSGFQSKNSYLHGWFSMK LKLVPGDSAGVVTAYYMSSNN EKHDELDFEFLGNRSGQPYVVQ TNMFVNGVGEREQRIYLWFDPT AEFHTYSILWNTHQTVFYVDRV PIRVHVNTPETRNAFPWQPMYV FSSIWNGDQWATRGGLEKINWL SAPFVSSYEKFHADACGGGFCV PSSTTPWWDQPSAWSLSPQEKQ KYAWVKSKLTVYDYCTDKARY PSLPADCMVHI

In total, 22 more colonies were chosen for Fragment 9 and plasmid isolation was carried using Invitrogen Purelink Quick Plasmid Miniprep Kit. Isolated plasmids were digested by

NotI restriction enzymes and digestion results were visualized by agarose gel electrophoresis (Figure 4.166). When these results were investigated, samples 2-1, 2-5, 2-6, 2-7, 3-1, 3-2, 3-3, 3-4, 3-5, 3-6, 4-1, 4-4, 4-5, 4-6, 4-7 and 4-8 were sequenced since they were showing different product sizes. None of the sequencing result turn out to be a positive one.

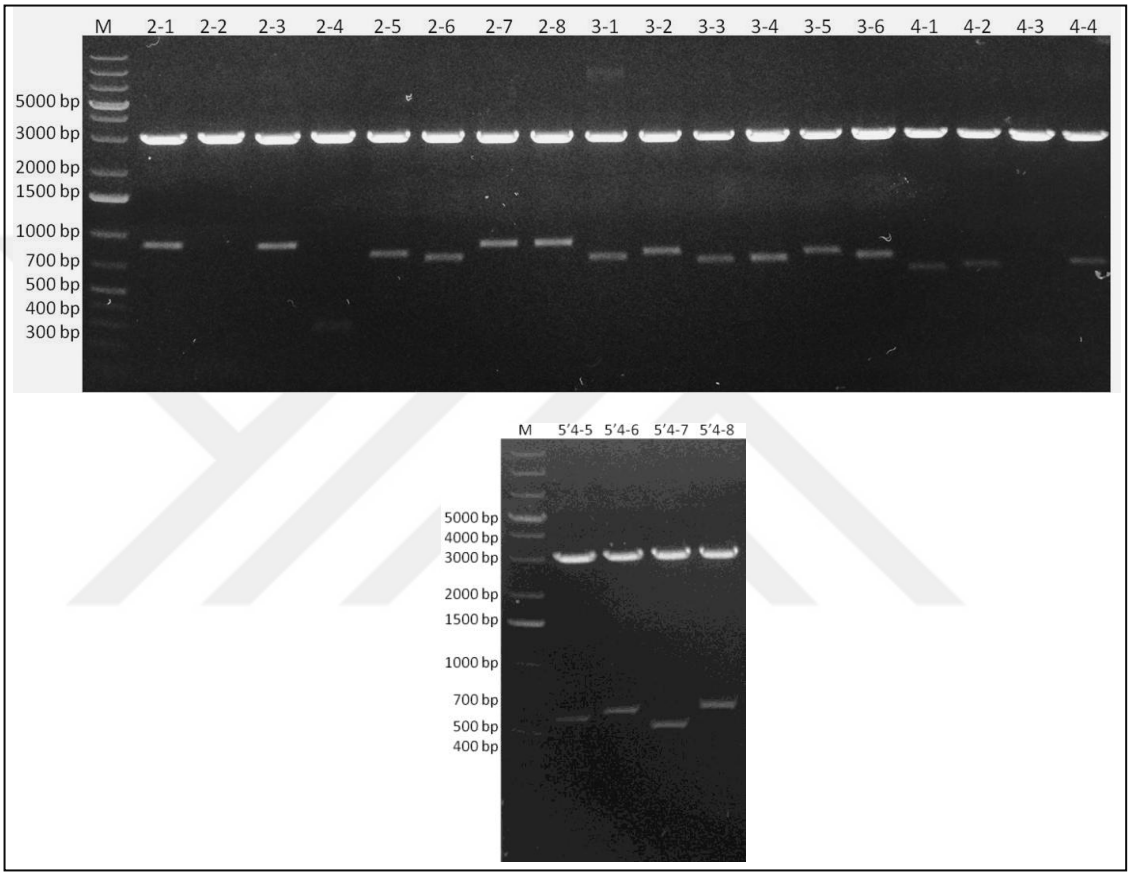

Figure 4.166. NotI digestion of second lot of pGEM-t easy with different DNA fragment inserts as result of 5'-RACE trials. Sample names and molecular size marker bands are indicated on figure.

5. DISCUSSION

Life is a mysterious and mesmerizing *omni* of chemical reactions. The concept humankind named as energy is so beautifully arranged that even though everything can collapse at any given moment, life continue to flow with harmony. An important feature contributing to harmony in our crowded universe is 'margins'. In plant kingdom, these margins are seen in two scales. In major scale, bark forms border of an independent multicellular organism whereas in minor scale, plant cell walls surround cells individually, creating a separate environment for biochemical reactions of a cell.

Plant cell wall, the structural component keeping plant cells intact, is a very important distinctive feature for plant cells. Throughout plant kingdom, cell wall structure, composition and arrangement differs between different families, species and cell types, yet a central point is they are constructed of cellulose microfibrils embedded in a gel like matrix accompanied with structural and/or functional proteins [130]. In most of agriculturally important plants, cellulose microfibrils are cross-linked by non-cellulosic β-linked polysaccharides and embedded in a matrix of pectins.

Cell walls can be grouped as primary cell walls and secondary cell walls; primary cell walls can further be divided into two groups as Type I cell walls (seen in dicot plants) and Type II cell walls (seen in monocots). Despite having an important role as creating margins of individual plant cells, cell walls must be flexible, adaptive and changeable in order to compensate to the changing environment. Modifications in cell walls are actualised by cell wall modifying enzymes. Expansins, hydrolases and transglycosylases can be listed as examples of important cell wall modifying enzymes.

Xyloglucan endotransglycosylases/hydrolases (XTHs) are a group of glycoside hydrolases and they are the scope of this work. XTH enzymes are member of GH16 (glycoside hydrolase 16) family that have action as xyloglucan modifiers. Xyloglucan is one of the non-cellulosic β-linked polysaccharides found in cell walls of plants. They are found in primary cell walls of dicots with a higher ratio and of monocots with a lower ratio. Also, their presence was visualised in secondary cell walls of gymnosperms and angiosperms. Also, members of Polypodiopsida contain structural xyloglucan chains in their cell walls.

Being an important structural component of plant cell walls have driven a lot of attention to xyloglucan and its metabolism in the last two decades. Another interesting and intriguing point is both monocots and dicots that are studied so far possess multi member *XTH* gene families. This situation is especially important in case of grasses (such as rice, wheat and barley) because xyloglucan is commonly < 10% of total polysaccharide weight yet they house > 30 member *XTH* multigene families [131]. Expression profile analysis and immunohistological studies provide information about different *XTH* genes and gene products. It was observed that members of *XTH* families show variable expression profiles in different tissues, during different development stages and under various environmental conditions. For example, when expression levels of *GhXTH1, GhXTH2* and *GhXTH3* were compared within various cotton tissues, *GhXTH2*and *GhXTH3*expression levels were higher in petal tissue whereas *GhXTH1* was showing the highest expression level in 15 day post-anthesis fibre tissue. These findings propose an important role for GhXTH1 enzyme in fibre elongation and development and developmental role of GhXTH2 and GhXTH3 in petal tissues [91]. Another study with *Populus XTH* genes revealed that these genes show variable expression in different tissues with most of the investigated members showing highest relative expression in vascular tissues [132]. Different plant hormones can change expression levels of *XTH* genes. They can have an upregulation or down regulation effect on expression profiles. For example IAA upregulated *VaXTH1* and *VaXTH2* gene expressions whereas abscisic acid downregulated expression of both genes significantly in azuki bean [133]. Drought and heat stresses cause a change in *XTH* expression too. In a study with *T. durum* cultivars that are sensitive and tolerant to heat stress, total *XTH* expression was observed as decreasing in root apical region as a result of heat treatment. On the other hand, especially in heat tolerant cultivar, extractable XET activity increased during heat application, indicating a heat response role of XTHs in *T. durum* [134]. A member of 25 (all showing tissue and developmental stage specific expression) identified tomato *XTH*s, *SlXTH5*, was found to be expressed in ripening fruit and the expression was observed to be increasing during development of fruit [106].

When members of *XTH* multigene families' products were compared and aligned based on their amino acid similarities, XTH proteins grouped into 6 groups; Group I, Group II, Group IIIA, Group IIIB, EG16, Ancestral Group. Functional features of each group were proposed to be different between different groups; Group I and Group II have domineering

XET activity whereas Group IIIA members show XEH activity. EG16 members are introduced with endoglucanase activity. All these grouping create an question mark about ancestral clade members; why do they form a separate group?

Xyloglucan structure and function in plant cell wall and role and characteristics of XTH enzymes are still riveting areas of research with a lot of new information waiting to be revealed. The fact that *XTH* genes appear as multigene families is intriguing, especially in grasses with low xyloglucan levels in their cell walls.

During course of this work, a report about xyloglucan presence in *Equisetum* plants and a new enzyme named as MXE in *Equisetum* plants were reported. Thus, in order to systematically answer questions of;

- What is characteristics of Ancestral Clade XTH enzymes?
- How do XTHs evolve and differentiated into different phylogenetic groups?
- Can *Equisetum* be a step in XTH evolution from bacterial licheninases?

We aimed to unravel enzymatic properties of representatives of true XETs (from Group I) and Ancestral Clade members. At the same time, we investigated *Equisetum* MXE from genomic, proteomic and enzymatic points of view.

Group I members AtXTH4, GhXTH2 and TaXTH5 were chosen to represent XET catalytic activity whereas Ancestral Clade members AtXTH3, AtXTH11, BdXTH2 and PtXTH3 were chosen to enlighten role of ancestral clade in XTH evolution. Stable transgenic *P. pastoris* lines with each gene were created and using those lines in heterologous expression studies, pure gene products were obtained. Except AtXTH11 and BdXTH2 (which was used by another member of Plant Biotechnology Group as master thesis project), *in vitro* substrate specificity characterization and enzyme kinetic measurements were done with AtXTH3, AtXTH4, GhXTH2, PtXTH3 and TaXTH5. Donor polysaccharides and sulforhodamine-labelled acceptor oligosaccharides were used to represent cell wall polysaccharide composition. Specific enzyme activities on different donor-acceptor couples were given as picokatals/mg enzyme (Table 5.1). Enzyme kinetic measurements and calculations were carried for each enzyme with different donors and X7 acceptor (Table 5.2).

Firstly, all screened heterologously expressed enzymes possess XET activity by catalysing endotransglycosylation between TXG-XGO substrates. Group I representatives TaXTH5 also has a low activity on HEC donor and XGO acceptor. In case of position switch, TaXTH5 enzyme shows traceable activity around detection level, suggesting TaXTH5 enzyme might have a physiological role of attaching xyloglucan chains on cellulose microfibrils. Another monocot enzyme, HvXET5, was reported to have 3.63 picokatals/mg enzyme activity on TXG-XGO, similar to activity observed with TaXTH5 on TXG-XGO. HvXET5 enzyme was reported as showing 44.2 per cent relative TXG-XGO activity on HEC-XGO, which is more than what's observed with TaXTH5, most likely due to differences in physiological roles of two enzymes [128].

As another member of Group I, AtXH4 enzyme shows faster XET activity compared to TaXTH5 (17.299 and 5.698 picokatals/mg enzyme specific activities respectively). Substrate specificity of AtXTH4 is also wider compared to TaXTH5; enzyme can catalyse endotransglycosylation using both TXG and HEC donors, with a preference to TXG. Other *A. thaliana* XET enzymes, AtXTH12, AtXTH13, AtXTH14 AtXTH17, AtXTH18, AtXTH19 and AtXTH26 were also reported to be using different cellulose analogues as donors, with a very low ratio compared to TXG donor [99, 135]. Surprisingly, endotransglycosylation was also observed between HEC donor and CT acceptor, pointing to a possible role of AtXTH4 in crosslinking of cellulose fibrils. Also, ability of AtXTH4 to catalyse reaction with TXG donor and BA, BB, BC acceptors in a very low level is surprising because to our knowledge, as a dicotyledonous plant, *A. thaliana* doesn't have any MLG in its cell wall. Thus, this newly discovered activity can be an evolutionary residue from proposed licheninase ancestors.

AtXTH4 expression was observed highest at shoot apical meristem, cotyledon and leaf pavement cells and lowest at endosperm and upregulated during germination (Genevestigator AT_AFFY_ATH1-0, [136]). Upregulation during germination proposes *AtXTH4* is likely to have an important role during cell wall maturation and this can correspond to the faster enzyme activity observed. Catalytic activity on HEC-XGO and HEC-X7 of AtXTH4 was proven *in vitro* and observed activity strengthens the idea of AtXTH4 having a role in fast growing tissues as cell wall modifier and crosslinking cellulose microfibrils to xyloglucan chains in order to create invulnerable structure.

Cotton GhXTH2 enzyme is also a member of Group I XTHs. A different activity motif is observed with GhXTH2 enzyme. Firstly, when compared with other analysed enzymes in this study, it is highly active on TXG-XGO substrate couple. Compared to activity on TXG-XGO, other activities are ≤ 0.21 per cent of TXG-XGO activity, indicating a strong preference to TXG-XGO because reaction rate is higher on TXG-XGO. Enzyme shows endotransglycosylation activity on TXG-BA, TXG-BB and TXG-BC, with a preference as BB > BC > BA, like other enzymes tested in this study. Activities on TXG-CT, HEC-XGO and HEC-CT are important in case of cotton because cotton fibers are high in cellulose content, which is also used as raw material for many industrial applications. Compared to TXG-XGO activity, they are low however important point is TXG-CT and HEC-XGO comparison. Interestingly GhXTH2 enzyme's reaction rate with HEC-XGO is 3.7 times more than TXG-CT. This indicates that in case of cross-linking cellulose microfibrils and xyloglucan polysaccharide within the cell wall, GhXTH2 enzyme would prefer cellulose microfibrils as donors and xyloglucan chains as acceptors, graphing xyloglucans on cellulose microfibrils. Even if such a physiological event is happening, it is happening with a slow rate because *GhXTH2* have highest expression in petal of cotton flower and expression of it decreases after anthesis event [91].

In focus group of the study, there are three Ancestral Clade members which are AtXTH3, AtXTH11 and PtXTH3. When these members are aligned together with several other XTH group members (Figure 4.11), AtXTH11 display an interesting profile. Unlike other XTHs that have conserved 'DE-I/V-DFEFLG' domain, AtXTH11 has 'DELCFQILG' amino acid sequence in active site. Also, AtXTH11 lacks another motif that is observed in other XTHs but not EG16 member, towards C-terminal that is usually represented with 'D/A/S-WAT-R/A/D-GGL-E/I/T' amino acids. These two differences in amino acid sequences are reflected in protein model. A model of AtXTH11 was generated by SWISS-MODEL online tool using 1un1.2 as template (Figure 5.1). Template 1un1.2 was created by crystallographic studies on PttXET16A with proven XET activity (GenBank accession number AF515607) [137]. When models of these two enzymes are compared from same angle (as seen in Figure 5.1 a and Figure 5.1 c), it is possible to observe that active cleft of template 1un1.2 s wider compared to modelled AtXTH11. Also, α-helix structure is different between two models and this can also contribute to helping the substrate interact with the enzyme. Pit seen in Figure 5.1 d where trisaccharide ligand is bond is not

observed as hallow in Figure 5.1 b as in Figure 5.1 d and this structural difference can also contribute to lack of XET activity seen with AtXTH11 enzyme. In order to understand this phenomenon better, docking studies needs to be done. Prior to any docking studies, heterologous expression of *AtXTH11* in *P. pastoris* host was done and colonies were screened for XET activity using TXG-XGO substrate couple. None of the colonies showed any XET activity. Difference in active site effected enzyme activity in a negative way and these findings prove function and importance of conserved active site.

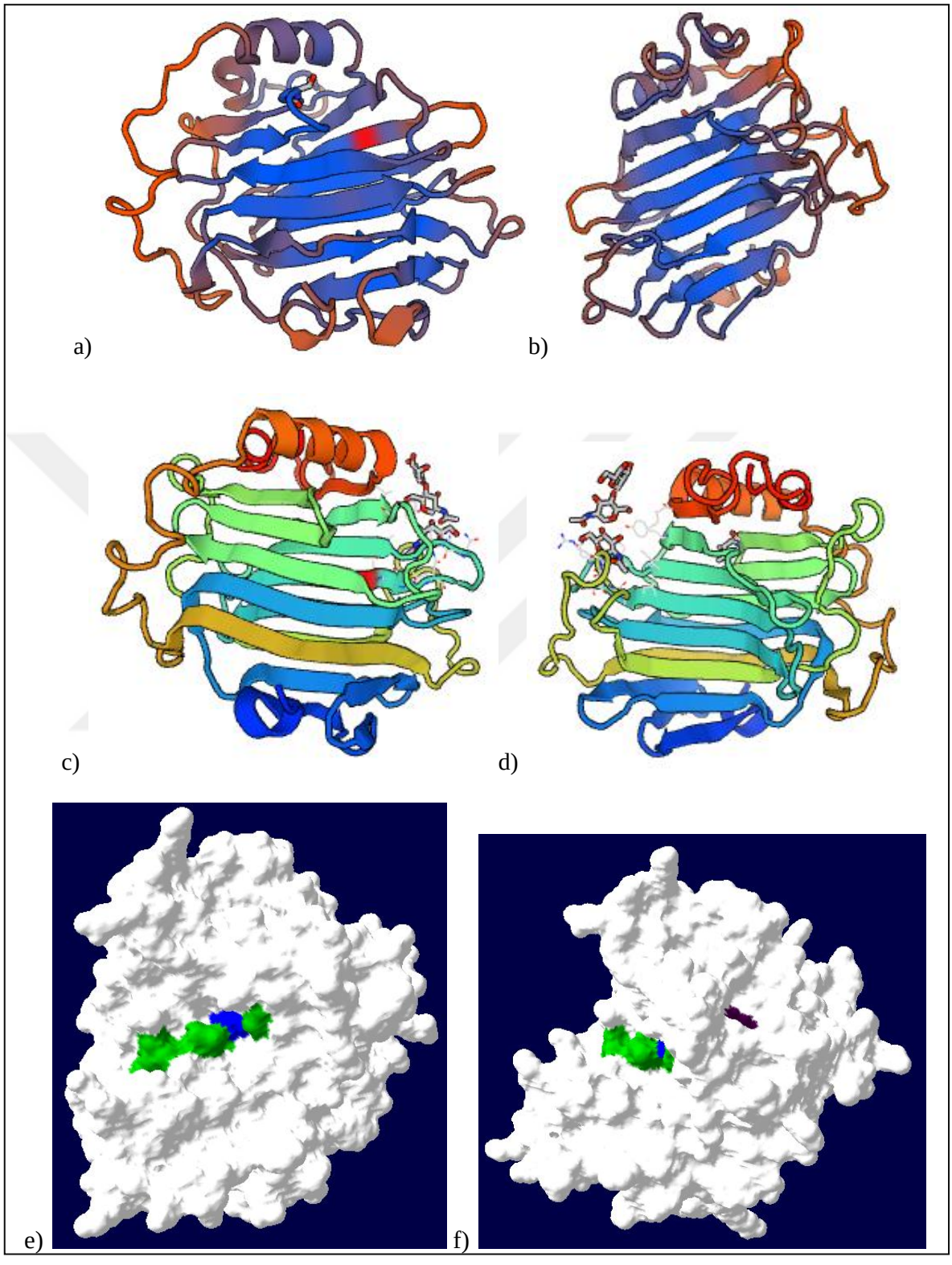

Figure 5.1. Surface models of AtXTH11 and 1un1.2 (PDB no). a) Model of AtXTH11 created using 1un1.2 as template, b) Model of AtXTH11 created using 1un1.2 as template , c) Model created for template 1un1.2 by crystal structure studies, d) Model created for template 1un1.2 by crystal structure studies with a trisaccharide ligand. Amino acids

indicated in red are the last leucines in the active site of the proteins, e) Surface model generated based on 1un1 PDB template, green amino acids indicating active site and blue amino acid indicating Cys residue, f) Surface model generated based on 1un1 PDB template, purple amino acid indicating second Asp in active site.

Other two ancestral group members, AtXTH3 and PtXTH3, showed a wider activity profile compared to analysed Group I members. Out of tested donors, AtXTH3 enzyme was able to use TXG, BBG, HEC, CMC and MC as donor substrate and unlike other analysed XET enzymes, AtXTH3 has more preference to BBG, HEC, CMC and MC as donor compared to TXG. This is the first report about such a donor preference of a XET enzyme. AtXTH3 enzyme has the best activity on CMC-X7 substrate couple and BBG-XGO comes at the second place. Enzyme's reaction rate with BBG and CMC are more than three times faster compared TXG donor. Even more, reaction rate between BBG-BB is more than reaction rate between TXG-XGO. When models of a XET (PttXET16A, 1umz.1) and AtXTH3 are compared, substrate binding site of AtXTH3 is monitored wider compared to 1umz.1 template (Figure 5.2). This difference can contribute to binding of a donor with kinks in its structure such as BBG. Analogy between enzyme's activity with BBG and cellulose analogues tested points to hypothesis that enzyme can bind a donor without substitutions as in TXG. This hypothesis can be strengthened by visualisation of active site from another angle (Figure 5.2 b and Figure 5.2 d); in 1umz.1 the active site looks hollower whereas in AtXTH3 model, active site is tightened by a β-sheet.

Additionally, with BA, BC, CT, LT, XT acceptors, enzyme prefers HEC and BBG donors. Another interesting point is comparison between BA, BB and BC acceptors. Irrelevant of donor, enzyme always shows better activity with BB, then BC and least activity with BA acceptors. Active site structure permits binding of glucotetraose molecule with G4G4G3G structure more than G4G3G4G and least with G3G4G4G. Position of β-1,3-glycosidic bond effects linearity of glucotetraose acceptor, thus chance of acceptor landing in active site while enzyme is attached to donor will be affected. This is why enzyme can act better when kink in the chain is in the last position of acceptor.

Differences between reaction rates of AtXTH3 enzyme with same donor and XGO or X7 acceptor was observed. Reaction rates with XGO and X7 don't follow a pattern, with TXG,

CMC and MC donors, X7 reaction rate is higher whereas with HEC and BBG donors, XGO reaction rate is higher. In case of TXG, HEC and MC these differences can be assumed as experimental variation, yet with BBG and CMC reaction rate difference is a little higher. Still, since over all reaction rates are slow, these differences can be omitted and we can conclude enzyme acts more or less the same on X7, X8 and X9 acceptors.

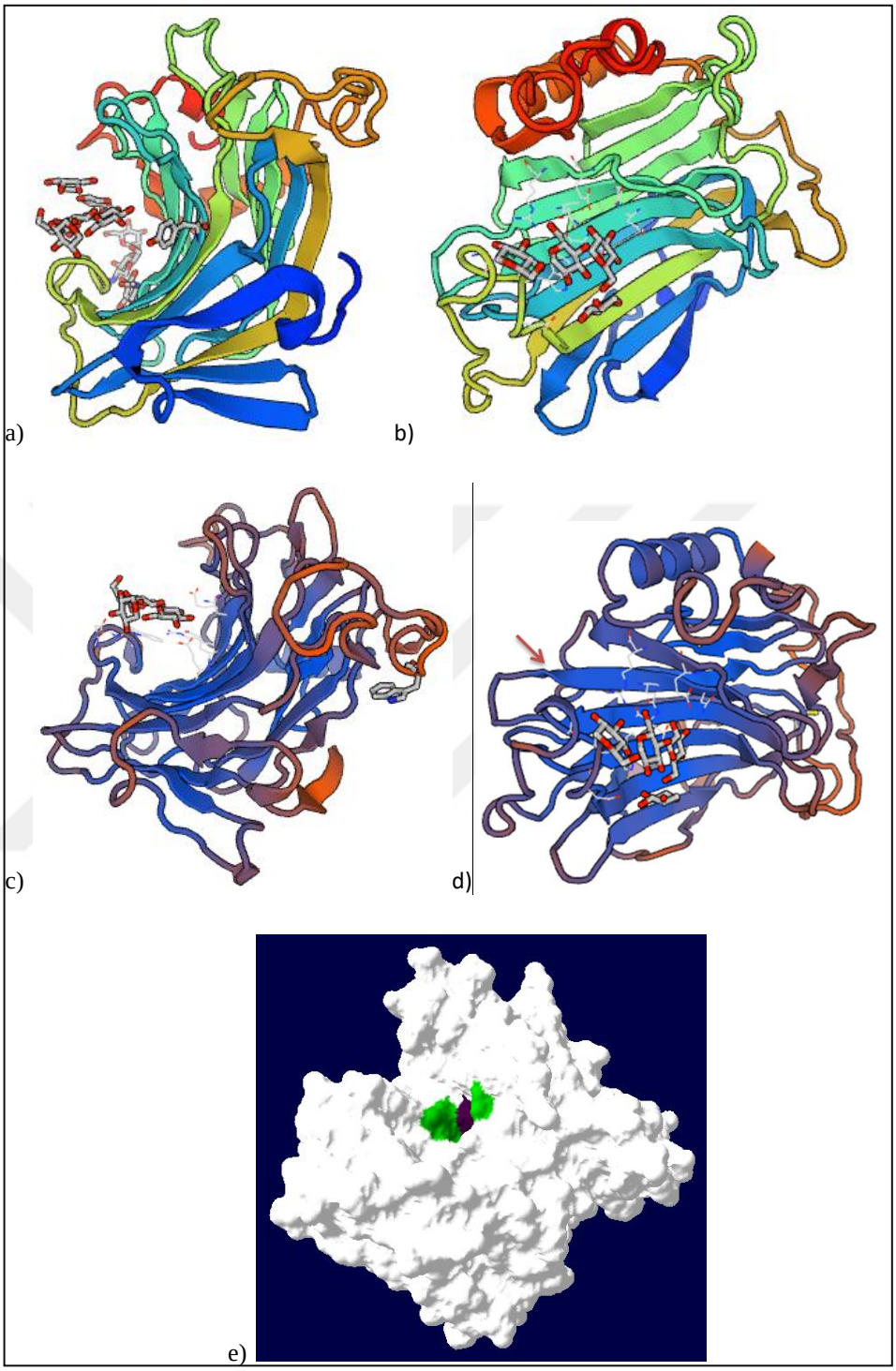

Figure 5.2. Surface models of AtXTH3 and 1umz.2 (PDB no). a and b) Model created for template 1umz.1 by crystal structure studies with a tetrasaccharide ligand, c) Model of AtXTH11 created using 1umz.1 as template with a tetrasaccharide ligand, d) Model of AtXTH11 created using 1umz.1 as template with a tetrasaccharide ligand, β-sheet narrowing the active site is indicated with a red arrow, e) Surface model made on 1umz1 PDB template, green atoms indicating active site, purple is second Asp in active site.

Genevestigator data mining revealed that *AtXTH3* expression is usually low throughout life span of an *A. thaliana* plant in different tissues except flower tissue and flower development stage. This expression profile makes *AtXTH3* a unique gene, having a very specific expression. Since floral tissue hosts reproductive organs of a flower, their structure and orientation to the environment is highly important. If a change of mutation happening in floral tissues don't correspond to fitness of reproduction of the plant, that change won't become a new trait. Thus, evaluating AtXTH3 substrate specificity from its 'duty station', we can comment that AtXTH3 enzyme can still carry mark of its ancestors in its catalytic fashion. Having role in cell walls of a reproductive tissue makes AtXTH3more unsuitable to changes during evolution of *A. thaliana* plant. Also, reproductive system cells like pollens have a different structural polysaccharide in their cell walls; callose [138, 139]. AtXTH3 enzyme can have a big impact in functionalizing and remodelling callose in the cell wall. Even though *A. thaliana* don't have MLG in its cell walls, ability of AtXTH3 acting on BBG-XGO, BBG-BB, HEC-XGO and HEC-BB can have impact on functionalizing plant raw material from grass species for industrial applications.

PtXTH3 is the only XET enzyme from a tree species that is investigated within this study and it is the enzyme with fastest specific activity investigated in the study. As a member of Ancestral clade, PtXTH3 shows the widest substrate specificity in the research. This enzyme is capable of catalysing endotransglycosylation between TXG, HEC and BBG donors and XGO, X7, BA, BB, BC, CT, GM, LT and XT acceptors and between KM-XGO substrate couple.

PtXTH3 enzyme's activity on TXG-XGO is ~2.5 times more than its activity on HEC-XGO and ~38 times more than its activity on BBG-XGO. Regarding these findings, PtXTH3 is an enzyme with dominant XET activity, yet on the other hand, when activities were compared horizontally in-between enzymes, we observe that activity of PtXTH3 on BBG-XGO is ~25 times more than activity of AtXTH3 on TXG-XGO. This makes PtXTH3 a more functional enzyme in plant cell wall material modification for industrial applications.

Specific enzyme activity of PtXTH3 TXG and HEC as donor and BA, BB, BC as acceptor follows a pattern BB>BC>BA like AtXTH3 activity. Comparing three different glucotetraose structures and position of β-1,3 link, G4G4G3G structure is more favourable for PtXTH3 activity compared to G4G3G4G and G3G4G4G structures when used with

TXG or HEC donor. But when it comes to donor with its own of β-1,3 links, BBG, enzyme preferences are BB>BA>BC. This phenomenon can be explained by positions of β-1,3 links in a three-dimensional space and docking studies would favour this.

Enzyme's specific activity on both TXG-XT and HEC-XT are higher than BBG-XGO. Ability to use XT as acceptor gives us clues about enzyme's role in cell wall remodelling. PtXTH3 might be forming bridges between xyloglucan and xylans and cellulose fibrils and xylans, contributing to strength of the cell wall. Enzyme is also able to catalyse endotransglycosylation between TXG-GM, HEC-GM, BBG-GM and KM-XGO, meaning it can use galactosyl mannotriose as acceptor and bind a galactomannan found in the cell wall with either other non cellulosic β-linked polysaccharides or crosslink it with cellulose fibrils. Also, glucomannan can bind to enzyme as donor and it can crosslink this glucomannan to xyloglucan network.

Observing highest activity of *PtXTH3* gene with probe set PtpAffx.202676.1.S1 in midday samples of female and male catkin points to cell wall modifying role of PtXTH3 in reproductive tissues of poplar tree [140]. Other focus of the research from Ancestral clade, *AtXTH3*, had higher expression in floral tissues too. This points to ancestral clade members having role in floral tissues and cells with different cell wall composition. Also, having ability to catalyse endotransglycosylation reaction between different donors and acceptors other than TXG-XGO points to place of ancestral clade members as evolutionary steps from β-1,3-glucanases to XETs.

Table 5.1. Specific activities of enzymes AtXTH3, AtXTH4, GhXTH2, PtXTH3 and TaXTH5 on different donor-acceptor couples tested. Values are given as pkatals/mg enzyme. Grey boxes indicate that enzyme did not showed any detectable activity on donor-acceptor couple.

	AtXTH3	**AtXTH4**	**GhXTH2**	**PtXTH3**	**TaXTH5**
TXG-XGO	0.842	17.299	217.368	804.241	5.698
TXG-X7	0.998	18.953	219.849	876.136	7.435
TXG-BA	0.063	0.020	0.015	14.182	
TXG-BB	0.396	0.027	0.180	35.351	trace
TXG-BC	0.193	0.015	0.059	21.778	
TXG-CT	0.188	0.093	0.121	46.233	trace
TXG-GM			0.011	6.972	
TXG-LT	0.028			5.308	
TXG-XT	0.072		0.062	61.507	
HEC-XGO	2.773	1.315	0.449	319.312	0.104
HEC-X7	2.392	1.168	0.367	327.339	0.035
HEC-BA	0.115			21.820	
HEC-BB	0.810		0.034	41.922	trace
HEC-BC	0.353		0.012	26.950	
HEC-CT	0.338	0.145	0.024	44.361	
HEC-GM				6.536	
HEC-LT	0.105			9.464	
HEC-XT	0.079		0.011	78.880	
BBG-XGO	2.773		0.009	21.073	
BBG-X7	2.392		0.008	24.109	
BBG-BA	0.101			7.884	
BBG-BB	0.849		0.003	10.318	
BBG-BC	0.381			6.075	
BBG-CT	0.300			10.753	
BBG-GM				2.760	
BBG-LT	0.060			3.823	
BBG-XT	0.082			12.251	
CMC-XGO	2.055				
CMC-X7	2.897				
MC-XGO	1.996				
MC-X7	2.031				
KM-XGO				0.93100	

Table 5.2. Kinetic values of enzyme reactions catalysed by AtXTH3, AtXTH4, GhXTH2, PtXTH3 and TaXTH5 enzymes. Donor-acceptor couples of reactions are given in the second column of the table.

		V_{max} (µM/minute)	**K_m (µM)**	**K_{cat} (min^{-1})**	**K_{cat}/ K_m**
AtXTH3	TXG-X7	0.0366	8.7719	0.0139	0.00158
	BBG-X7	0.0362	8.3907	0.2583	0.03078
	HEC-X7	0.0153	4.5780	0.1090	0.02381
AtXTH4	TXG-XGO	0.0492	6.5763	0.0742	0.01128
	HEC-XGO	0.0209	11.0760	0.0315	0.00285
GhXTH2	TXG-XGO	0.0126	9.6163	0.0683	0.00710
	HEC-XGO	0.0050	3.1318	0.0047	0.00150
PtXTH3	TXG-X7	0.0257	11.7758	2.9028	0.24651
	HEC-X7	0.0090	0.6630	0.4074	0.61455
	BBG-X7	0.0053	0.6642	0.0601	0.09055
TaXTH5	TXG-XGO	0.0212	4.9612	0.0525	0.01058

Specific enzyme activity provides valuable information about substrate preference of an enzyme and reaction rates of an enzyme on different donor-acceptor couples. However, comparison through kinetic values are more reliable, in case of differences in molecular weights of compared enzymes. Even though most of XTHs studied have similar molecular weights, it is better to do comparison through kinetic values to minimize any error caused by molecular weight, thus mole number differences. When each enzyme's k_m values are evaluated together, it is possible to see that k_m value is higher for substrate couple that enzyme is showing higher activity with. For example, with GhXTH2, enzyme specific activity is higher with TXG-XGO yet k_m value is higher for this substrate couple, which can indicate that if an enzyme is acting fast on a substrate couple it would have a weaker binding affinity for that couple. The important value for evaluating enzyme's catalytic efficiency is k_{cat} / k_m. When characterized enzymes are compared to each other, PtXTH3 is showing the highest ratio with HEC-XGO substrate couple, indicating PtXTH3 is the most efficient and fastest enzyme with HEC-XGO within analysed combinations. Importance of this data is due to importance of poplar trees in forestry area, with discovery of a fast and

efficient cell wall modifying enzyme, lignocellulosic material can become easier to process.

k_{cat} / k_m ratios of AtXTH3 activity on different substrate couples mimic specific activity rate, highest with BBG-XGO and lowest with TXG-XGO, proving that AtXTH3 enzyme is acting more efficiently with the BBG donor. This also proves ancestral role of AtXTH3 enzyme in evolution of XET catalytic activity. AtXTH4 and GhXTH2 enzymes ratios are low and their specific enzyme activity values were also low, meaning those two enzymes are not fast enzymes. In a previous study with AtXTH3 enzyme, its k_{cat} / k_m ratio was calculated as 0.079 on TXG-XGO which is similar to AtXTH4 [99]. Even though being an immature thought, we might be able to say *Arabidopsis* XTH enzymes might be acting slow and less efficiently compared to other XTHs analysed.

During evolution of *XTH* multigene families, members end up with a degree of diversification in their amino acid sequences and these changes were reported to cause two distinct types of enzymatic activities; endotransglycosylase and hydrolase activity [82], yet considering substrate specificity analysis and catalytic activity calculations done with representatives of XTH phylogenetic groups, we can conclude that specific amino acid alterations change catalytic function of the mentioned enzymes.

Another focus point of the project was fishing, purifying, identifying and characterization of *Equisetum* MXE from native host. As described in previously published reports, newly discovered *Equisetum* enzyme shows MLG: xyloglucan endotransglycosylase (MXE) activity [119]. We propose *Equisetum* MXE can fill in the gap between bacterial licheninases and plant XTHs in evolutionary order. Being an evolutionary distant species to domineering land plants makes *Equisetum* more likely to harbour an ancestral enzyme which is an intermediate form between bacterial licheninases and XTHs. Also, observed activity of catalysing reaction better between MLG and XGO compared to TXG and XGO intensify this hypothesis [119, 120] because bacterial licheninases have β-1,3-glucanase activity. As being a bridge between these two groups of enzymes, *Equisetum* MXE has domineering MXE activity and less XET activity. Thus, we aim to provide more information and prove this linkage.

Different *Equisetum* species are widely distributed around Turkey geography (www.tubives.com, Turkish Plant Data Service version 2.0 Beta). Plant samples for protein

purification can be picked up from native sources or can be grown in trial greenhouse in order to always have plant material in hand. Istanbul Bahçeköy Belgrad Forest Neşetsuyu Region was reported as having a native *Equisetum* population, thus this location was defined as plant material sampling point due to its closeness to our research facility. During multiple plant sampling visits, young plants were collected with their underground shoots and soil covering them in order to grow them in our greenhouse however, trials were unsuccessful even if plants were frequently watered and planted with their own soil. Thus, cultivating trials were set aside and plant sampling was carried every time protein purification was planned to be done.

Equisetum sampled from Belgrad Forest were identified as *Equisetum telmateia* and there are no reports nor sequence information about or related to this species in publicly available databases.

In previous reports, *Equisetum* MXE was observed and purified from mature, late season *E. fluviatile* and *E. arvense* plants [120, 121]. Thus, MXE potential of *E. telmateia* was screened during growth season of the plant. In order to do so, plant samples were collected in different months, ranging from April to November. While screening for best growth stage of plants for MXE purification, purification strategy optimization was carried with the samples. Serial application of HiScreen Capto S cation exchange chromatography, HiScreen Capto Q anion exchange chromatography, Superdex 75 16/100 size exclusion chromatography was found to be the best strategy for purification of MXE protein. On the other hand, unlike previously reported [120, 121], early season, young and small plants resulted in a higher MXE: XET enzymatic ratio, meaning collected young *E. telmateia* harbour more MXE compared to mature older *E. telmateia* plant or MXE enzyme is no longer produced by mature *E. telmateia* plants. During course of this work, *E. fluviatile* MXE was purified, sequenced and characterized from late season plants by The Edinburgh Cell Wall Group and during characterization, name of enzyme was changed to hetero-trans-β-glucanase (HTG) due to enzyme's additional activity of catalysing endotransglycosylation between cellulose and xyloglucan, an activity named as cellulose: xyloglucan endotransglycosylase (CXE), alongside MXE and XET activities [121]. Also, HTG purification from plant crude extract was done by applying 20% ammonium sulphate precipitation meaning target HTG in late season *E. fluviatile* is slightly hydrophobic [121].

When overall procedure of HTG host, purification and catalytic activity is evaluated, we can confidently conclude that target MXE is totally different compared to HTG.

First of all, plant species and their growth stage is different in both cases; HTG is from late season *E. fluviatile* whereas MXE is from early season *E. telmateia.* Secondly, no MXE activity was observed from 20% saturated ammonium sulphate precipitated fraction of *E. telmateia* crude extract whereas, HTG from *E. fluviatile* was detected in 20% saturated ammonium sulphate precipitated fraction, indicating MXE is more hydrophilic compared to HTG. As the last important difference, HTG from *E. fluviatile* showed CXE activity exceeding XET and MXE activity [121] whereas MXE from *E. telmateia* activities align as MXE>XET>CXE. All these differences points identified and characterized HTG is totally different than our target, MXE.

E. telmateia plants were screened during their growth season starting from April and continuing until November for MXE activity. Samples collected during October and November don't possess distinguishable XET or MXE activity and on the contrary, samples collected between April to September resulted in target MXE activity. These findings indicate that MXE activity is abundantly found in early season plants or younger plants in middle-season. Thus, after purification work-flow optimization, three main samples were gathered and processed; April 2016, July 2016 and September 2016. The last step of chromatographic separation is size exclusion polishing step and for each sample, pure protein samples were aimed. Purest protein sample was obtained from *Equisetum* September'16 pool 2 and 3, a single band between 25kDa and 35 kDa molecular marker bands. Seeing a single protein band on silver nitrate stained SDS-PAGE gel strongly indicates presence of pure protein, although there is a change and risk of contaminant protein that is similar in size but different in pI point. Ion exchange chromatography steps decrease the risk of a different pI contaminant, yet in order to be confident, 2D-PAGE trials were carried. If there is a contaminant, 2D-PAGE will have a higher resolution rate and will visualize the contaminant. Different trials with variable protein amounts were carried, however none of them resulted in any protein profiles. Since *Equisetum* MXE protein sample is low in amount and growth related, it is very valuable for the research. It would require lot of protein sample for optimizing isoelectric focusing optimization, which is hard to acquire from plants. Regarding technical difficulties, 2D-PAGE trials were paused till unidentified time point in future.

As detailed identification methods, N-terminal Edman Degradation and in-gel tryptic digestion and MALDI-TOF MS analysis strategies were 'tracked'. *Equisetum* September 2016 sample analysed for *de novo* protein amino acid sequencing by Proteome Factory, Inc. company. As company reported, the sequencing was unsuccessful due to N-terminal blockage of protein. Thus, as an alternative, protein sample was analysed by in-gel tryptic digestion accompanied with MALDI-TOF MS. Analysed peptide fragments were searched against a database composed of Ancestral clade XTHs, *H. vulgare, O. sativa* and *A. thaliana* XTHs, putative *E. telmateia* MXEs and XETs mined from RNA sequencing data using MASCOT software. The best hit, yet not enough to identify target protein with certainty, was AtXTH22 protein which is a Group II member. Regarding substrate preference of *Equisetum* MXE, it is unexpected to observe such a match. When putative *E. telmateia* MXEs and XETs mined from RNA sequencing data were aligned with XTHs from other plants (*H. vulgare, O. sativa* and *A. thaliana, G. hirsutum, B. distachyon*), they grouped with Group I and Group II enzymes, meaning *Equisetum* MXEs have high amino acid similarities to XTHs with dominant xyloglucan preference (Data not shown). This phenomenon can be explained in several ways. Evolution of traits is a complex mechanism. With today's fund of knowledge, it can be suggested that during separate co-evolution of *Equisetum* MXEs and flowering plant XTHs, *Equisetum* MXEs have conserved MXE function due to the presence of both XyG and MLG in their cell walls whereas dicot plants don't contain MLG in their cell wall. From another point of view, it can be thought that due to ancient conservatism of *Equisetum* species [141-143], MXE could have evolved separately from XET back in history whereas in cotyledonous plants, change and evolution is still ongoing. Also, crowded genuses with many members adds to evolution rate of dicotyledonous species, resulting in isoenzymes to co-exist.

MALDI-TOF MS analysis results were not enough to identify protein or unravel probable peptide sequences and reasons for such problematic analysis can be due to incomplete tryptic digestion or fewness of sample loaded for analysis. Thus, this analysis is aimed to be repeated with freshly isolated and purified protein sample. Problems encountered during MS analyses can be overcome by several different approaches. Firstly, the protein starting material amount can be changed in order to facilitate a more efficient enzymatic digestion. More, common protease enzymes other than trypsin can be used for protein digestion, thus identification of peptide fragments could be carried more effectively. Tryptic digestion and

analysis of other contaminating protein bands seen in samples can also be studied since they can be degradation products of target MXE. Another drawback that can be faced during MS analysis can be caused by post-translational modifications. Most of the XTH enzymes possess an N-terminal glycosylation site. Presence of glycan motif(s) on protein structure can negatively affect enzymatic digestion of proteins and/or glycopeptides exhibit poor ionization efficiency [144]. Removal of glycan residues from peptide chains can be an alternative approach and Peptide-*N*-Glycosidase F (PNGase F) enzyme can be used for such an approach. This enzyme is an amidase, capable of catalysing a cleavage between the innermost GlcNAc and asparagine residues [145]. Thus, it can be used to fully remove glycan residues and prepare proteins for enzymatic digestion. Another post-translational modification mentioned to be seen in XTH family enzymes, especially EfHTG (UniProt KB A0A0K2WA62_EQUFL), is intrachain disulfide bond(s). These disulfide bonds are necessary for folding and enzymatic activity of proteins. Yet, presence of these bonds can be an obstacle during both enzymatic protein digestion and sample analysis in MS. Partial reduction of disulfide bonds during sample preparation or over alkylation can hinder analyses. Presence of one disulfide bond in the structure causes 2-Da reduction of molecular weight and this would affect result interpretation of tryptic fragments. Thus, optimization of reduction-alkylation procedure prior to enzymatic digestion can be a strategy as well as investigating usage of other reduction agents like guanidine hydrochloride or desalting after SDS treatment and alkylation agents like *N*-ethylmaleimide [146]. Other post translational modifications that are frequently observed in plants such as phosphorylation, deamidation, ubiquination and methylation were not reported for XTHs and remains to be discovered [147].

Different from April 2016 samples, *Equisetum* July 2016 samples possess low molecular weight contaminants after polishing step of purification. Same low molecular weighted protein band was also visible in September 2016 samples, indicating that after early season, an additional protein can be chaperoning MXE, that is impossible to separate under native and mild chromatographic conditions applied within this study. In case of denaturing conditions of SDS-PAGE, it is possible to visualize low molecular weight band.

A novel approach employed during this work to verify only one protein band is responsible for MXE activity was native-PAGE and in-gel activity assay. When September 2016 protein sample was separated by native-PAGE, it formed a multiband profile although

protein samples are not separated based on their molecular weights in native-PAGE. Native-PAGE experiment was repeated using a gel casted with BBG donor and as a result of acceptor incubation, hybrid BBG-X7 product band was visualized on gel, indicating only one of the bands seen in SDS-PAGE gel (the top band in native-PAGE) is responsible for MXE activity (Figure 4.155). This finding proves that, even if protein sample is not pure, activity is caused only by one of the proteins find in polished sample.

The purest protein sample, April 2016 was mostly employed for proteomic work, thus most of the characterization studies were carried using July 2016 *Equisetum* sample. Specific activities of all three pure samples were calculated for TXG-X7, TXG-XGO, BBG-X7, BBG-XGO, HEC-X7 and HEC-XGO. Highest activities were observed with July 2016 Pool B sample (Table 4.57), 28 times of April 2016 Pool 3 activity and 3.25 times of September 2016 Pool β activity on BBG-X7 substrate couple. All the enzyme samples are showing a dominant preference for BBG donor, although acceptor preferences differ between X7 or XGO. Enzymes show least preference for HEC donor. Ratios of preferences are between 31.23-22.97 per cent TXG-X7 for HEC-X7. Variability in activity ratios are more in case of activity with BBG. With April 2016 sample, BBG-X7 activity is 2.49 times more of TXG-X7 activity whereas it is 4.71 times more with July 2016 sample and 3.35 times more with September 2016 sample. The purest sample was obtained from April 2016 sample yet specific activities and TXG-X7/ BBG-X7 ratio are the least with this sample. Both specific activities and TXG-X7/ BBG-X7 ratio are the highest with July 2016, indicating impurities seen in SDS-PAGE can actually contribute to enzyme activity.

HTG enzyme from *E. fluviatile* was characterized for kinetics using heterologously expressed enzyme. With TXG-X7 substrate couple, k_m was measured as 3.9 μM and with BBG-X7 is was measured as 1.4 μM [121] whereas k_m values for *E. telmateia* are 1.09 μM and 0.58 μM respectively for TXG-X7 and BBG-X7 substrate couples. Regarding these values, we can conclude *E. telmateia* MXE is binding to stronger to substrates compared to *E. fluviatile* HTG. This difference also indicates these enzymes are different from each other. However, it was not possible to do any k_{cat} calculations with *E. telmateia* MXE due to lack of sequence data and uncertainty of molecular weight. AtXTH3 k_m values can be compared to MXE since a similar activity pattern was observed with AtXTH3 enzyme. AtXTH3 enzyme k_m value with TXG-X7 substrate couple is 5.20 and it is 8.40 with BBG-X7, implying a weaker bound between AtXTH3 and its substrate compared to MXE. This

phenomenon can be due to place of action of enzymes. On the other hand, differences in k_m values of BBG-X7 substrate couple can be due to loss-of-function of mixed-linked glucan: xyloglucan endotransglycosylase in a dicot model, *Arabidopsis*, caused by absence of MLG in its cell walls.

After proteomic approaches were not successful to identify sequence of *Equisetum* MXE protein, RACE trials from 3' and 5' ends were carried explore coding sequence for *MXE*. Firstly 3'-RACE was done and then, using that sequence information, 5'-RACE was carried. Full length mRNA sequences and amino acid sequences for two different enzymes were obtained, named Fragment 10-3 and Fragment 12. Both these fragments were also used to analyse and interpret MALDI-TOF MS data, yet tryptic fragments don't match with neither Fragment 10-3 nor Fragment 12.

When pieced together, two sequences unravelled with RACE studies and MALDI-TOF data point that more work needs to be done for identification of novel *E. telmateia* MXE protein as soon as possible. After acquiring amino acid sequence, it would be very exciting to compare both amino acid sequences and 3D models of AtXTH3 and *E. telmateia* MXE against true XET enzymes studied in this thesis, AtXTH4, GhXTH2 and TaXTH5.

6. CONCLUSION

Plant cell wall are very unique micro environments when evaluated on their own because they are the first layer where a plant cell's interaction with changing environment happens. In order to protect the cell and adapt to changing environment, it should be robust and changeable. Controlled loosening and strengthening of the cell wall is provided by cell wall modifying enzyme, which XTHs are a type of.

Within the content of this thesis, six different XTHs from various plants were heterologously produced and characterized. AtXTH4, GhXTH2 and TaXTH5 ar Group I XTH enzymes whereas AtXTH3, AtXTH11 and PtXTH3 are Ancestral XTH enzymes. Phylogenetic grouping of these enzymes is based on their amino acid sequences, but the groupings are also reflected in their substrate specificities, as shown in this work. Group I members have dominant preferences for xyloglucan donor and acceptors, yet they can use some other polysaccharides with very low ratios compared to xyloglucan. Interestingly, dominant donor preferences were variable within the ancestral group members and they also have a wider substrate specificity. AtXTH3 enzyme was able to use BBG-XGO substrate couple more efficient compared to TXG-XGO substrate couple whereas TXG-XGO couple was dominant preference of PtXTH3 yet this enzyme was catalysing reactions faster than AtXTH3. Thus, in general, the Ancestral group genes can be seen as having broad substrate specificities.

Amino acid differences in the active site of ancestral clade member AtXTH11 resulted in total loss of XET activity. The change of an aspartic acid to cysteine residue and a glutamic acid to glutamine is highly likely to be responsible of such an outcome.

Ancestral clade members, with their amino acid differences and substrate specificities, fills in the gap between bacterial licheninases (hydrolases) and plant XTHs in the evolution of genes and traits.

While working on XTH enzymes, discovery of firstly MLG, then MXE/HTG in *E. fluviatile* plants were thrilling because *Equisetum* is an evolutionary distant family of ferns and they possess a cell wall component that is similar to that seen in graminaceous species like wheat and barley. Thus, we hypothesize that *Equisetum* MXE can also be a step in

evolution of XTHs. For this purpose, *E. telmateia* was used as an explant and MXE purification and identification work was carried out. Purified MXE protein showed a dominant donor preference for MLG, yet grouped with Group I/II XTHs. Initial sample purified from *E. telmateia* were not sufficient for protein identification by Edman sequencing or MALDI-TOF MS analysis. Protein sequence analysis would be repeated to enlighten all of the sequence information since similarities and differences in amino acid sequences of different enzymes should be compared for correct identification and for XTH evolution. Addition or deletion of a region in protein structure might be causing a significant difference in substrate specificity and more detailed interpretations can only be made after full recovery of MXE sequence. Enlightening the protein structure of these fascinating enzymes will help us understand the role and function of MXE in evolution and plant physiology. Also, further modelling and docking studies will support building an argument about the role of amino acids and change of amino acids through evolution to share in substrate preferences.

Revealing substrate specificities of XTHs can lead to a new era where these enzymes can be used in industrial application. Without any harsh chemical conditions, especially ancestral clade members, are capable of crosslinking different polysaccharides to each other. This feature can also be used in crosslinking different substrates (dye molecules, active pharmaceutical molecules, special tags) onto plant based materials such as paper, and textiles. They can alo have important application in processing plant raw material for the biofuel industry.

REFERENCES

1. M. Pauly, S. Gille, L. Liu, N. Mansoori, A. de Souza, A. Schultink and G. Xiong. Hemicellulose Biosynthesis. *Planta*, 238, 4:627-642, 2013.

2. P. R. Moghaddam and D. Wilman. Cell Wall Thickness and Cell Dimensions in Plant Parts of Eight Forage Species. *Journal of Agricultural Science*, 131:59-67, 1998.

3. C. Somerville, S. Bauer, G. Brininstool, M. Facette, T. Hamann, J. Milne, E. Osborne, A. Paredez and S. Perssonand. Toward a Systems Approach to Understanding Plant Cell Walls. *Science*, 306, 5705:2206-2211, 2004.

4. A. Bacic, P. J. Harris and B. A. Stone. Structure and Function of Plant Cell Walls a Comprehensice Treatise. In: J. Preiss, editor, *The Biochemistry of Plants*, pages 297-358. San Diego California: Academic Press; 1988.

5. D. J. Cosgrove. Catalysts of Plant Cell Wall Loosening. *F1000Res*, 5, 2016.

6. R. J. Dyson, L. R. Band, O. E. Jensen. A Model of Crosslink Kinetics in the Expanding Plant Cell Wall: Yield Stress and Enzyme Action. *J Theor Biol*, 307:125-136, 2012.

7. K. Keegstra. Plant Cell Walls. *Plant Physiology*, 154, 2:483-486, 2010.

8. P. B. White, T. Wang, Y. B. Park, D. J. Cosgrove and M. Hong. Water-Polysaccharide Interactions in the Primary Cell Wall of Arabidopsis Thaliana from Polarization Transfer Solid-State Nmr. *Journal of American Chemical Society*, 136, 29:10399-10409, 2014.

9. A. H. Liepman, R. Wightman, N. Geshi, S. R. Turner and H. V. Scheller. Arabidopsis - a Powerful Model System for Plant Cell Wall Research. *Plant Journal*, 61, 6:1107-1121, 2010.

10. E. Miedes, I. Zarra, T. Hoson, K. Herbers, U. Sonnewald and E. P. Lorences. Xyloglucan Endotransglucosylase and Cell Wall Extensibility. *Journal Plant Physiology*, 168, 3:196-203, 2011.

11. K. J. Lee, S. E. Marcus and J. P. Knox. Cell Wall Biology: Perspectives from Cell Wall Imaging. *Molecular Plant*, 4, 2:212-219, 2011.

12. D. Bellincampi, F. Cervone and V. Lionetti. Plant Cell Wall Dynamics and Wall-Related Susceptibility in Plant-Pathogen Interactions. *Frontiers Plant Science*, 5:228, 2014.

13. J. C. Mollet, S. Y. Park, E. A. Nothnagel and E. M. Lord. A Lily Stylar Pectin Is Necessary for Pollen Tube Adhesion to an in Vitro Stylar Matrix. *Plant Cell*, 12, 9:1737-1750, 2000.

14. M. S. Doblin, F. Pettolino and A. Bacic. Plant Cell Walls: The Skeleton of the Plant World. *Functional Plant Biology*, 37, 5:357-381, 2010.

15. I. M. Saxena and R. M. Brown, Jr. Cellulose Biosynthesis: Current Views and Evolving Concepts. *Annals of Botany*, 96, 1:9-21, 2005.

16. L. Saulnier, F. Guillon and A. L. Chateigner-Boutin. Cell Wall Deposition and Metabolism in Wheat Grain. *Journal of Cereal Science*, 56, 1:91-108, 2012.

17. D. J. Cosgrove. Growth of the Plant Cell Wall. *Nature Review Molecular Cell Biology*, 6, 11:850-861, 2005.

18. D. J. Cosgrove and M. C. Jarvis. Comparative Structure and Biomechanics of Plant Primary and Secondary Cell Walls. *Frontiers in Plant Sciences*, 3:204, 2012.

19. S. C. Fry. Primary Cell Wall Metabolism: Tracking the Careers of Wall Polymers in Living Plant Cells. *New Phytologist*, 161, 3:641-675, 2004.

20. G. Müse, T. Schindler, R. Bergfeld, K. Ruel, G. Jacquet, C. Lapierre, V. Speth and P. Schopfer. Structure and Distribution of Lignin in Primary and Secondary Cell Walls of Maize Coleoptiles Analyzed by Chemical and Immunological Probes. *Planta*, 201, 2:146-159, 1997.

21. W. D. Reiter. Biosynthesis and Properties of the Plant Cell Wall. *Current Opinion in Plant Biology*, 5, 6:536-542, 2002.

22. L. E. Del Bem and M. G. Vincentz. Evolution of Xyloglucan-Related Genes in Green Plants. *BMC Evolutionary Biology*, 10:341, 2010.

23. M. Albert, M. Werner, P. Proksch, S. C. Fry and R. Kaldenhoff. The Cell Wall-Modifying Xyloglucan Endotransglycosylase/Hydrolase Lexth1 Is Expressed During the Defence Reaction of Tomato against the Plant Parasite Cuscuta Reflexa. *Plant Biology (Stuttgart)*, 6, 4:402-407, 2004.

24. G. Bethke, R. E. Grundman, S. Sreekanta, W. Truman, F. Katagiri and J. Glazebrook. Arabidopsis Pectin Methylesterases Contribute to Immunity against Pseudomonas Syringae. *Plant Physiology*, 164, 2:1093-1107, 2014.

25. Y. B. Liu, S. M. Lu, J. F. Zhang, S. Liu and Y. T. Lu. A Xyloglucan Endotransglucosylase/Hydrolase Involves in Growth of Primary Root and Alters the Deposition of Cellulose in Arabidopsis. *Planta*, 226, 6:1547-1560, 2007.

26. A. M. D. Mbeguie, O. Hubert, F. C. Baurens, T. Matsumoto, M. Chillet, B. Fils-Lycaon and S. Sidibe-Bocs. Expression Patterns of Cell Wall-Modifying Genes from Banana During Fruit Ripening and in Relationship with Finger Drop. *Journal of Experimenal Botany*, 60, 7:2021-2034, 2009.

27. M. A. O'Neill, D. Warrenfeltz, K. Kates, P. Pellerin, T. Doco, A. G. Darvill and P. Albersheim. Rhamnogalacturonan-Ii, a Pectic Polysaccharide in the Walls of Growing Plant Cell, Forms a Dimer That Is Covalently Cross-Linked by a Borate Ester. In Vitro Conditions for the Formation and Hydrolysis of the Dimer. *Journal of Biological Chemistry*, 271, 37:22923-22930, 1996.

28. J. E. Thompson and S. C. Fry. Evidence for Covalent Linkage between Xyloglucan and Acidic Pectins in Suspension-Cultured Rose Cells. *Planta*, 211, 2:275-286, 2000.

29. J. Vogel. Unique Aspects of the Grass Cell Wall. *Current Opinions in Plant Biology*, 11, 3:301-307, 2008.

30. L. Lei, S. Li and Y. Gu. Cellulose Synthase Complexes: Composition and Regulation. *Frontiers in Plant Science*, 3:75, 2012.

31. E. J. Mellerowicz and B. Sundberg. Wood Cell Walls: Biosynthesis, Developmental Dynamics and Their Implications for Wood Properties. *Current Opinions in Plant Biology*, 11, 3:293-300, 2008.

32. J. F. Vincent. From Cellulose to Cell. *Journal of Experimental Biology*, 202, 23:3263-3268, 1999.

33. T. Doco, P. Williams, M. Pauly, M. A. O'Neill and P. Pellerin. Polysaccharides from Grape Berry Cell Walls. Part Ii. Structural Characterization of the Xyloglucan Polysaccharides. *Carbohydrate Polymers*, 53, 3:253-261, 2003.

34. G. B. Fincher. Revolutionary Times in Our Understanding of Cell Wall Biosynthesis and Remodeling in the Grasses. *Plant Physiology*, 149, 1:27-37, 2009.

35. S. Y. Yong and R. Wickneswari. Molecular Characterization of a Cellulose Synthase Gene (Aaxmcesa1) Isolated from an Acacia Auriculiformis X Acacia Mangium Hybrid. *Plant Molecular Biology Report*, 31:303-313, 2013.

36. D. P. Delmer. Cellulose Biosynthesis: Exciting Times for a Difficult Field of Study. *Annual Reviews in Plant Physiology Plant Molecular Biology*, 50:245-276, 1999.

37. M. S. Doblin, I. Kurek, D. Jacob-Wilk and D. P. Delmer. Cellulose Biosynthesis in Plants: From Genes to Rosettes. *Plant Cell Physiology*, 43, 12:1407-1420, 2002.

38. A. H. Liepman, C. J. Nairn, W. G. Willats, I. Sorensen, A. W. Roberts and K. Keegstra. Functional Genomic Analysis Supports Conservation of Function among Cellulose Synthase-Like a Gene Family Members and Suggests Diverse Roles of Mannans in Plants. *Plant Physiology*, 143, 4:1881-1893, 2007.

39. T. A. Richmond and C. R. Somerville. The Cellulose Synthase Superfamily. *Plant Physiology*, 124, 2:495-498, 2000.

40. R. A. Burton, S. M. Wilson, M. Hrmova, A. J. Harvey, N. J. Shirley, A. Medhurst, B. A. Stone, E. J. Newbigin and A. Bacicand. Cellulose Synthase-Like Cslf Genes Mediate the Synthesis of Cell Wall (1,3;1,4)-Beta-D-Glucans. *Science*, 311, 5769:1940-1942, 2006.

41. K. S. Dhugga, R. Barreiro, B. Whitten, K. Stecca, J. Hazebroek, G. S. Randhawa, M. Dolan, A. J. Kinney and D. Tomesand. Guar Seed Beta-Mannan Synthase Is a Member of the Cellulose Synthase Super Gene Family. *Science*, 303, 5656:363-366, 2004.

42. A. H. Liepman, C. G. Wilkerson and K. Keegstra. Expression of Cellulose Synthase-Like (Csl) Genes in Insect Cells Reveals That Csla Family Members Encode Mannan Synthases. *Proceedings of the National Academy of Sciences of the Unites States of America*, 102, 6:2221-2226, 2005.

43. J. R. Pear, Y. Kawagoe, W. E. Schreckengost, D. P. Delmer and D. M. Stalker. Higher Plants Contain Homologs of the Bacterial Cela Genes Encoding the Catalytic Subunit of Cellulose Synthase. *Proceedings of the National Academy of Sciences of the Unites States of America*, 93, 22:12637-12642, 1996.

44. E. F. Crowell, M. Gonneau, Y. D. Stierhof, H. Hofte and S. Vernhettes. Regulated Trafficking of Cellulose Synthases. *Current Opinions in Plant Biology*, 13, 6:700-705, 2010.

45. E. Chanliaud, J. De Silva, B. Strongitharm, G. Jeronimidis and M. J. Gidley. Mechanical Effects of Plant Cell Wall Enzymes on Cellulose/Xyloglucan Composites. *Plant Journal*, 38, 1:27-37, 2004.

46. C. Xiao, T. Zhang, Y. Zheng, D. J. Cosgrove and C. T. Anderson. Xyloglucan Deficiency Disrupts Microtubule Stability and Cellulose Biosynthesis in Arabidopsis, Altering Cell Growth and Morphogenesis. *Plant Physiology*, 170, 1:234-249, 2016.

47. D. U. Lima, W. Loh and M. S. Buckeridge. Xyloglucan-Cellulose Interaction Depends on the Sidechains and Molecular Weight of Xyloglucan. *Plant Physiology and Biochemistry*, 42, 5:389-394, 2004.

48. H. Hilz, L. E. de Jong, M. A. Kabel, R. Verhoef, H. A. Schols and A. G. Voragen. Bilberry Xyloglucan--Novel Building Blocks Containing Beta-Xylose within a Complex Structure. *Carbohydrate Research*, 342, 2:170-181, 2007.

49. J. K. Rose, J. Braam, S. C. Fry and K. Nishitani. The Xth Family of Enzymes Involved in Xyloglucan Endotransglucosylation and Endohydrolysis: Current Perspectives and a New Unifying Nomenclature. *Plant Cell Physiology*, 43, 12:1421-1435, 2002.

50. N. C. Carpita and D. M. Gibeaut. Structural Models of Primary Cell Walls in Flowering Plants: Consistency of Molecular Structure with the Physical Properties of the Walls During Growth. *Plant Journal*, 3, 1:1-30, 1993.

51. A. Zykwinska, J.-F. Thibault and M.-C. Ralet. Competitive Binding of Pectin and Xyloglucan with Primary Cell Wall Cellulose. *Carbohydrate Polymers*, 74, 4:957-961, 2008.

52. T. Takeda, Y. Furuta, T. Awano, K. Mizuno, Y. Mitsuishi and T. Hayashi. Suppression and Acceleration of Cell Elongation by Integration of Xyloglucans in Pea Stem Segments. *Proceedings of the National Academy of Sciences of the Unites States of America*, 99, 13:9055-9060, 2002.

53. M. Hoffman, Z. Jia, M. J. Pena, M. Cash, A. Harper, A. R. Blackburn, 2nd, A. Darvill and W. S. York. Structural Analysis of Xyloglucans in the Primary Cell Walls of Plants in the Subclass Asteridae. *Carbohydrate Research*, 340, 11:1826-1840, 2005.

54. J. C. Cocuron, O. Lerouxel, G. Drakakaki, A. P. Alonso, A. H. Liepman, K. Keegstra, N. Raikhel and C. G. Wilkerson. A Gene from the Cellulose Synthase-Like C Family Encodes a Beta-1,4 Glucan Synthase. *Proceedings of the National Academy of Sciences of the Unites States of America*, 104, 20:8550-8555, 2007.

55. I. M. Sims, S. L. Munro, G. Currie, D. Craik and A. Bacic. Structural Characterisation of Xyloglucan Secreted by Suspension-Cultured Cells of Nicotiana Plumbaginifolia. *Carbohydrate Research*, 293, 2:147-172, 1996.

56. J. Davis, F. Brandizzi, A. H. Liepman and K. Keegstra. Arabidopsis Mannan Synthase Csla9 and Glucan Synthase Cslc4 Have Opposite Orientations in the Golgi Membrane. *Plant Journal*, 64, 6:1028-1037, 2010.

57. D. M. Cavalier, O. Lerouxel, L. Neumetzler, K. Yamauchi, A. Reinecke, G. Freshour, O. A. Zabotina, M. G. Hahn and I. Burgertand. Disrupting Two Arabidopsis Thaliana Xylosyltransferase Genes Results in Plants Deficient in Xyloglucan, a Major Primary Cell Wall Component. *Plant Cell*, 20, 6:1519-1537, 2008.

58. O. A. Zabotina, W. T. van de Ven, G. Freshour, G. Drakakaki, D. Cavalier, G. Mouille, M. G. Hahn, K. Keegstra and N. V. Raikhel. Arabidopsis Xxt5 Gene Encodes a Putative Alpha-1,6-Xylosyltransferase That Is Involved in Xyloglucan Biosynthesis. *Plant Journal*, 56, 1:101-115, 2008.

59. R. M. Perrin, A. E. DeRocher, M. Bar-Peled, W. Zeng, L. Norambuena, A. Orellana, N. V. Raikhel and K. Keegstra. Xyloglucan Fucosyltransferase, an Enzyme Involved in Plant Cell Wall Biosynthesis. *Science*, 284, 5422:1976-1979, 1999.

60. M. Madson, C. Dunand, X. Li, R. Verma, G. F. Vanzin, J. Caplan, D. A. Shoue, N. C. Carpita and W. D. Reiter. The Mur3 Gene of Arabidopsis Encodes a Xyloglucan Galactosyltransferase That Is Evolutionarily Related to Animal Exostosins. *Plant Cell*, 15, 7:1662-1670, 2003.

61. L. Frankova and S. C. Fry. Trans-Alpha-Xylosidase, a Widespread Enzyme Activity in Plants, Introduces (1-->4)-Alpha-D-Xylobiose Side-Chains into Xyloglucan Structures. *Phytochemistry*, 78:29-43, 2012.

62. Y. S. Hsieh and P. J. Harris. Xyloglucans of Monocotyledons Have Diverse Structures. *Molecular Plant*, 2, 5:943-965, 2009.

63. S. Romo, T. Jimenez, E. Labrador and B. Dopico. The Gene for a Xyloglucan Endotransglucosylase/Hydrolase from Cicer Arietinum Is Strongly Expressed in Elongating Tissues. *Plant Physiology and Biochemistry*, 43, 2:169-176, 2005.

64. A. Ebringerova and T. Heinze. Xylan and Xylan Derivatives - Biopolymers with Valuable Properties, 1 - Naturally Occurring Xylans Structures, Procedures and Properties. *Macromolecular Rapid Communications*, 21, 9:542-556, 2000.

65. A. Rakha, L. Saulnier, P. Aman and R. Andersson. Enzymatic Fingerprinting of Arabinoxylan and Beta-Glucan in Triticale, Barley and Tritordeum Grains. *Carbohydrate Polymers*, 90, 3:1226-1234, 2012.

66. C. Rodriguez-Gacio Mdel, R. Iglesias-Fernandez, P. Carbonero and A. J. Matilla. Softening-up Mannan-Rich Cell Walls. *Journal of Experimental Botany*, 63, 11:3976-3988, 2012.

67. F. Goubet, C. J. Barton, J. C. Mortimer, X. Yu, Z. Zhang, G. P. Miles, J. Richens, A. H. Liepman and K. Seffenand. Cell Wall Glucomannan in Arabidopsis Is Synthesised by Csla Glycosyltransferases, and Influences the Progression of Embryogenesis. *Plant Journal*, 60, 3:527-538, 2009.

68. R. A. Burton and G. B. Fincher. (1,3;1,4)-Beta-D-Glucans in Cell Walls of the Poaceae, Lower Plants, and Fungi: A Tale of Two Linkages. *Molecular Plant*, 2, 5:873-882, 2009.

69. G. B. Fincher. Exploring the Evolution of (1,3;1,4)-Beta-D-Glucans in Plant Cell Walls: Comparative Genomics Can Help! *Current Opinions in Plant Biology*, 12, 2:140-147, 2009.

70. S. C. Fry, B. H. Nesselrode, J. G. Miller and B. R. Mewburn. Mixed-Linkage (1-->3,1-->4)-Beta-D-Glucan Is a Major Hemicellulose of Equisetum (Horsetail) Cell Walls. *New Phytologist*, 179, 1:104-115, 2008.

71. J. A. Trethewey, L. M. Campbell and P. J. Harris. (1->3),(1->4)-{Beta}-D-Glucans in the Cell Walls of the Poales (Sensu Lato): An Immunogold Labeling Study Using a Monoclonal Antibody. *American Journal of Botany*, 92, 10:1660-1674, 2005.

72. H. Henriksson, S. E. Denman, I. D. Campuzano, P. Ademark, E. R. Master, T. T. Teeri and H. Brumer, 3rd. N-Linked Glycosylation of Native and Recombinant Cauliflower Xyloglucan Endotransglycosylase 16a. *Biochemical Journal*, 375, 1:61-73, 2003.

73. G. J. Davies, T. M. Gloster and B. Henrissat. Recent Structural Insights into the Expanding World of Carbohydrate-Active Enzymes. *Current Opinion in Structural Biology*, 15, 6:637-645, 2005.

74. J. M. Eklof and H. Brumer. The Xth Gene Family: An Update on Enzyme Structure, Function, and Phylogeny in Xyloglucan Remodeling. *Plant Physiology*, 153, 2:456-466, 2010.

75. J. M. Eklof, S. Shojania, M. Okon, L. P. McIntosh and H. Brumer. Structure-Function Analysis of a Broad Specificity Populus Trichocarpa Endo-Beta-Glucanase Reveals an Evolutionary Link between Bacterial Licheninases and Plant Xth Gene Products. *Journal of Biological Chemistry*, 288, 22:15786-15799, 2013.

76. B. L. Cantarel, P. M. Coutinho, C. Rancurel, T. Bernard, V. Lombard and B. Henrissat. The Carbohydrate-Active Enzymes Database (Cazy): An Expert Resource for Glycogenomics. *Nucleic Acids Research*, 37: 233-238, 2009.

77. V. Lombard, H. Golaconda Ramulu, E. Drula, P. M. Coutinho and B. Henrissat. The Carbohydrate-Active Enzymes Database (Cazy) in 2013. *Nucleic Acids Research*, 42: 490-495, 2014.

78. J. L. Yang, X. F. Zhu, Y. X. Peng, C. Zheng, G. X. Li, Y. Liu, Y. Z. Shi and S. J. Zheng. Cell Wall Hemicellulose Contributes Significantly to Aluminum Adsorption and Root Growth in Arabidopsis. *Plant Physiology*, 155, 4:1885-1892, 2011.

79. A. Tabuchi, H. Mori, S. Kamisaka and T. Hoson. A New Type of Endo-Xyloglucan Transferase Devoted to Xyloglucan Hydrolysis in the Cell Wall of Azuki Bean Epicotyls. *Plant Cell Physiology*, 42, 2:154-161, 2001.

80. K. Nishitani and R. Tominaga. Endo-Xyloglucan Transferase, a Novel Class of Glycosyltransferase That Catalyzes Transfer of a Segment of Xyloglucan Molecule to Another Xyloglucan Molecule. *Journal of Biological Chemistry*, 267, 29:21058-21064, 1992.

81. R. Schroder, R. G. Atkinson, G. Langenkamper and R. J. Redgwell. Biochemical and Molecular Characterisation of Xyloglucan Endotransglycosylase from Ripe Kiwifruit. *Planta*, 204, 2:242-251, 1998.

82. R. Yokoyama and K. Nishitani. A Comprehensive Expression Analysis of All Members of a Gene Family Encoding Cell-Wall Enzymes Allowed Us to Predict Cis-Regulatory Regions Involved in Cell-Wall Construction in Specific Organs of Arabidopsis. *Plant Cell Physiology*, 42, 10:1025-1033, 2001.

83. T. Harada, Y. Torii, S. Morita, R. Onodera, Y. Hara, R. Yokoyama, K. Nishitani and S. Satoh. Cloning, Characterization, and Expression of Xyloglucan Endotransglucosylase/Hydrolase and Expansin Genes Associated with Petal Growth and Development During Carnation Flower Opening. *Journal of Experimental Botany*, 62, 2:815-823, 2011.

84. K. Vissenberg, I. M. Martinez-Vilchez, J. P. Verbelen, J. G. Miller and S. C. Fry. In Vivo Colocalization of Xyloglucan Endotransglycosylase Activity and Its Donor Substrate in the Elongation Zone of Arabidopsis Roots. *Plant Cell*, 12, 7:1229-1237, 2000.

85. I. N. Saab and M. M. Sachs. A Flooding-Induced Xyloglucan Endo-Transglycosylase Homolog in Maize Is Responsive to Ethylene and Associated with Aerenchyma. *Plant Physiology*, 112, 1:385-391, 1996.

86. W. Xu, M. M. Purugganan, D. H. Polisensky, D. M. Antosiewicz, S. C. Fry and J. Braam. Arabidopsis Tch4, Regulated by Hormones and the Environment, Encodes a Xyloglucan Endotransglycosylase. *Plant Cell*, 7, 10:1555-1567, 1995.

87. C. Catala, J. K. Rose, W. S. York, P. Albersheim, A. G. Darvill and A. B. Bennett. Characterization of a Tomato Xyloglucan Endotransglycosylase Gene That Is Down-Regulated by Auxin in Etiolated Hypocotyls. *Plant Physiology*, 127, 3:1180-1192, 2001.

88. S. J. Ji, Y. C. Lu, J. X. Feng, G. Wei, J. Li, Y. H. Shi, Q. Fu, D. Liu and J. C. Luoand. Isolation and Analyses of Genes Preferentially Expressed During Early Cotton Fiber Development by Subtractive Pcr and Cdna Array. *Nucleic Acids Research*, 31, 10:2534-2543, 2003.

89. K. Vissenberg, V. Van Sandt, S. C. Fry and J. P. Verbelen. Xyloglucan Endotransglucosylase Action Is High in the Root Elongation Zone and in the Trichoblasts of All Vascular Plants from Selaginella to Zea Mays. *Journal of Experimental Botany*, 54, 381:335-344, 2003.

90. G. Michailidis, A. Argiriou, N. Darzentas and A. Tsaftaris. Analysis of Xyloglucan Endotransglycosylase/Hydrolase (Xth) Genes from Allotetraploid (Gossypium Hirsutum) Cotton and Its Diploid Progenitors Expressed During Fiber Elongation. *Journal of Plant Physiology*, 166, 4:403-416, 2009.

91. J. Lee, T. H. Burns, G. Light, Y. Sun, M. Fokar, Y. Kasukabe, K. Fujisawa, Y. Maekawa and R. D. Allen. Xyloglucan Endotransglycosylase/Hydrolase Genes in Cotton and Their Role in Fiber Elongation. *Planta*, 232, 5:1191-1205, 2010.

92. V. Bourquin, N. Nishikubo, H. Abe, H. Brumer, S. Denman, M. Eklund, M. Christiernin, T. T. Teeri and B. Sundbergand. Xyloglucan Endotransglycosylases Have a Function During the Formation of Secondary Cell Walls of Vascular Tissues. *Plant Cell*, 14, 12:3073-3088, 2002.

93. N. Nishikubo, T. Awano, A. Banasiak, V. Bourquin, F. Ibatullin, R. Funada, H. Brumer, T. T. Teeri and T. Hayashiand. Xyloglucan Endo-Transglycosylase (Xet) Functions in Gelatinous Layers of Tension Wood Fibers in Poplar--a Glimpse into the Mechanism of the Balancing Act of Trees. *Plant Cell Physiology*, 48, 6:843-855, 2007.

94. J. Munoz-Bertomeu, E. Miedes and E. P. Lorences. Expression of Xyloglucan Endotransglucosylase/Hydrolase (Xth) Genes and Xet Activity in Ethylene Treated Apple and Tomato Fruits. *Journal of Plant Physiology*, 170, 13:1194-1201, 2013.

95. S. K. Cho, J. E. Kim, J. A. Park, T. J. Eom and W. T. Kim. Constitutive Expression of Abiotic Stress-Inducible Hot Pepper Caxth3, Which Encodes a Xyloglucan Endotransglucosylase/Hydrolase Homolog, Improves Drought and Salt Tolerance in Transgenic Arabidopsis Plants. *FEBS Letters*, 580, 13:3136-3144, 2006.

96. J. Y. Choi, Y. S. Seo, S. J. Kim, W. T. Kim and J. S. Shin. Constitutive Expression of Caxth3, a Hot Pepper Xyloglucan Endotransglucosylase/Hydrolase, Enhanced Tolerance to Salt and Drought Stresses without Phenotypic Defects in Tomato Plants (Solanum Lycopersicum Cv. Dotaerang). *Plant Cell Reports*, 30, 5:867-877, 2011.

97. Y. Han, W. Wang, J. Sun, M. Ding, R. Zhao, S. Deng, F. Wang, Y. Hu and Y. Wangand. Populus Euphratica Xth Overexpression Enhances Salinity Tolerance by the Development of Leaf Succulence in Transgenic Tobacco Plants. *Journal of Experimental Botany*, 64, 14:4225-4238, 2013.

98. C. Wagstaff, G. J. Clarkson, F. Zhang, S. D. Rothwell, S. C. Fry, G. Taylor and M. S. Dixon. Modification of Cell Wall Properties in Lettuce Improves Shelf Life. *Journal of Experimental Botany*, 61, 4:1239-1248, 2010.

99. A. Maris, N. Kaewthai, J. M. Eklof, J. G. Miller, H. Brumer, S. C. Fry, J. P. Verbelen and K. Vissenberg. Differences in Enzymic Properties of Five Recombinant Xyloglucan Endotransglucosylase/Hydrolase (Xth) Proteins of Arabidopsis Thaliana. *Journal of Experimental Botany*, 62, 1:261-271, 2011.

100. Z. Sulova and V. Farkas. Kinetic Evidence of the Existence of a Stable Enzyme-Glycosyl Intermediary Complex in the Reaction Catalyzed by Endotransglycosylase. *General Physiology and Biophysics*, 17, 2:133-142, 1998.

101. A. Yan and W. J. Lennarz. Unraveling the Mechanism of Protein N-Glycosylation. *Journal of Biological Chemistry*, 280, 5:3121-3124, 2005.

102. G. Vaaje-Kolstad, V. Farkas, M. Hrmova and G. B. Fincher. Xyloglucan Xyloglucosyl Transferases from Barley (Hordeum Vulgare L.) Bind Oligomeric and Polymeric Xyloglucan Molecules in Their Acceptor Binding Sites. *Biochimica et Biophysica Acta*, 1800, 7:674-684, 2010.

103. M. Strohmeier, M. Hrmova, M. Fischer, A. J. Harvey, G. B. Fincher and J. Pleiss. Molecular Modeling of Family Gh16 Glycoside Hydrolases: Potential Roles for Xyloglucan Transglucosylases/Hydrolases in Cell Wall Modification in the Poaceae. *Protein Science*, 13, 12:3200-3213, 2004.

104. D. W. Meinke, J. M. Cherry, C. Dean, S. D. Rounsley and M. Koornneef. Arabidopsis Thaliana: A Model Plant for Genome Analysis. *Science*, 282, 5389:662, 679-682, 1998.

105. L. H. Hartwell. *Genetics : From Genes to Genomes*. McGraw-Hill Higher Education Boston, MA, 2008.

106. M. Saladie, J. K. Rose, D. J. Cosgrove and C. Catala. Characterization of a New Xyloglucan Endotransglucosylase/Hydrolase (Xth) from Ripening Tomato Fruit and Implications for the Diverse Modes of Enzymic Action. *Plant Journal*, 47, 2:282-295, 2006.

107. R. Yokoyama, J. K. Rose and K. Nishitani. A Surprising Diversity and Abundance of Xyloglucan Endotransglucosylase/Hydrolases in Rice. Classification and Expression Analysis. *Plant Physiology*, 134, 3:1088-1099, 2004.

108. J. Geisler-Lee, M. Geisler, P. M. Coutinho, B. Segerman, N. Nishikubo, J. Takahashi, H. Aspeborg, S. Djerbi and E. Masterand. Poplar Carbohydrate-Active Enzymes. Gene Identification and Expression Analyses. *Plant Physiology*, 140, 3:946-962, 2006.

109. A. Matsui, R. Yokoyama, M. Seki, T. Ito, K. Shinozaki, T. Takahashi, Y. Komeda and K. Nishitani. Atxth27 Plays an Essential Role in Cell Wall Modification During the Development of Tracheary Elements. *Plant Journal*, 42, 4:525-534, 2005.

110. M. J. Baumann, J. M. Eklof, G. Michel, A. M. Kallas, T. T. Teeri, M. Czjzek and H. Brumer, 3rd. Structural Evidence for the Evolution of Xyloglucanase Activity from Xyloglucan Endo-Transglycosylases: Biological Implications for Cell Wall Metabolism. *Plant Cell*, 19, 6:1947-1963, 2007.

111. G. Michel, L. Chantalat, E. Duee, T. Barbeyron, B. Henrissat, B. Kloareg and O. Dideberg. The Kappa-Carrageenase of P. Carrageenovora Features a Tunnel-Shaped Active Site: A Novel Insight in the Evolution of Clan-B Glycoside Hydrolases. *Structure*, 9, 6:513-525, 2001.

112. K. M. Pryer, H. Schneider, A. R. Smith, R. Cranfill, P. G. Wolf, J. S. Hunt and S. D. Sipes. Horsetails and Ferns Are a Monophyletic Group and the Closest Living Relatives to Seed Plants. *Nature*, 409, 6820:618-622, 2001.

113. A. L. Nothnagel and E. A. Nothnagel. Primary Cell Wall Structure in the Evolution of Land Plants. *Journal of Integrative Plant Biology*, 49, 8:1271-1278, 2007.

114. I. Sorensen, F. A. Pettolino, S. M. Wilson, M. S. Doblin, B. Johansen, A. Bacic and W. G. Willats. Mixed-Linkage (1-->3),(1-->4)-Beta-D-Glucan Is Not Unique to the Poales and Is an Abundant Component of Equisetum Arvense Cell Walls. *Plant Journal*, 54, 3:510-521, 2008.

115. X. Xue and S. C. Fry. Evolution of Mixed-Linkage (1 -> 3, 1 -> 4)-Beta-D-Glucan (Mlg) and Xyloglucan in Equisetum (Horsetails) and Other Monilophytes. *Annals of Botany*, 109, 5:873-886, 2012.

116. M. J. Hodson, P. J. White, A. Mead and M. R. Broadley. Phylogenetic Variation in the Silicon Composition of Plants. *Annals of Botany*, 96, 6:1027-1046, 2005.

117. L. Sapei, N. Gierlinger, J. Hartmann, R. Noske, P. Strauch and O. Paris. Structural and Analytical Studies of Silica Accumulations in Equisetum Hyemale. *Analytical and Bioanalytical Chemistry*, 389, 4:1249-1257, 2007.

118. M. J. Pena, A. G. Darvill, S. Eberhard, W. S. York and M. A. O'Neill. Moss and Liverwort Xyloglucans Contain Galacturonic Acid and Are Structurally Distinct from the Xyloglucans Synthesized by Hornworts and Vascular Plants. *Glycobiology*, 18, 11:891-904, 2008.

119. S. C. Fry, K. E. Mohler, B. H. Nesselrode and L. Frankova. Mixed-Linkage Beta-Glucan : Xyloglucan Endotransglucosylase, a Novel Wall-Remodelling Enzyme from Equisetum (Horsetails) and Charophytic Algae. *Plant Journal*, 55, 2:240-252, 2008.

120. K. E. Mohler, T. J. Simmons and S. C. Fry. Mixed-Linkage Glucan:Xyloglucan Endotransglucosylase (Mxe) Re-Models Hemicelluloses in Equisetum Shoots but Not in Barley Shoots or Equisetum Callus. *New Phytologist*, 197, 1:111-122, 2013.

121. T. J. Simmons, K. E. Mohler, C. Holland, F. Goubet, L. Frankova, D. R. Houston, A. D. Hudson, F. Meulewaeter and S. C. Fry. Hetero-Trans-Beta-Glucanase, an Enzyme Unique to Equisetum Plants, Functionalizes Cellulose. *Plant Journal*, 83, 5:753-769, 2015.

122. R. Daly and M. T. Hearn. Expression of Heterologous Proteins in Pichia Pastoris: A Useful Experimental Tool in Protein Engineering and Production. *Journal of Molecular Recognition*, 18, 2:119-138, 2005.

123. T. Ito, S. Fujimura, M. Uchino, N. Tanaka, Y. Matsufuji, T. Miyaji, K. Takano, T. Nakagawa and N. Tomizuka. Distribution, Diversity and Regulation of Alcohol Oxidase Isozymes, and Phylogenetic Relationships of Methylotrophic Yeasts. *Yeast*, 24, 6:523-532, 2007.

124. S. Macauley-Patrick, M. L. Fazenda, B. McNeil and L. M. Harvey. Heterologous Protein Production Using the Pichia Pastoris Expression System. *Yeast*, 22, 4:249-270, 2005.

125. M. A. Larkin, G. Blackshields, N. P. Brown, R. Chenna, P. A. McGettigan, H. McWilliam, F. Valentin, I. M. Wallace and A. Wilmand. Clustal W and Clustal X Version 2.0. *Bioinformatics*, 23, 21:2947-2948, 2007.

126. T. N. Petersen, S. Brunak, G. von Heijne and H. Nielsen. Signalp 4.0: Discriminating Signal Peptides from Transmembrane Regions. *Nature Methods*, 8, 10:785-786, 2011.

127. O. Kosik and V. Farkas. One-Pot Fluorescent Labeling of Xyloglucan Oligosaccharides with Sulforhodamine. *Analytical Biochemistry*, 375, 2:232-236, 2008.

128. M. Hrmova, V. Farkas, J. Lahnstein and G. B. Fincher. A Barley Xyloglucan Xyloglucosyl Transferase Covalently Links Xyloglucan, Cellulosic Substrates, and (1,3;1,4)-Beta-D-Glucans. *Journal of Biological Chemistry*, 282, 17:12951-12962, 2007.

129. N. Kaewthai, A. J. Harvey, M. Hrmova, H. Brumer, I. Ezcurra, T. T. Teeri and G. B. Fincher. Heterologous Expression of Diverse Barley Xth Genes in the Yeast Pichia Pastoris. *Plant Biotechnology*, 27, 3:251-258, 2010.

130. P. J. Harris and B. A. Stone. Chemistry and Molecular Organization of Plant Cell Walls. In: M. E. Himmel, editor, *Biomass Recalcitrance*, pages 61-93, Blackwell Publishing Ltd., London, 2009.

131. D. M. Gibeaut, M. Pauly, A. Bacic and G. B. Fincher. Changes in Cell Wall Polysaccharides in Developing Barley (Hordeum Vulgare) Coleoptiles. *Planta*, 221, 5:729-738, 2005.

132. N. Nishikubo, J. Takahashi, A. A. Roos, M. Derba-Maceluch, K. Piens, H. Brumer, T. T. Teeri, H. Stalbrand and E. J. Mellerowicz. Xyloglucan Endo-Transglycosylase-Mediated Xyloglucan Rearrangements in Developing Wood of Hybrid Aspen. *Plant Physiology*, 155, 1:399-413, 2011.

133. T. Nakamura, R. Yokoyama, E. Tomita and K. Nishitani. Two Azuki Bean Xth Genes, Vaxth1 and Vaxth2, with Similar Tissue-Specific Expression Profiles, Are Differently Regulated by Auxin. *Plant Cell Physiology*, 44, 1:16-24, 2003.

134. A. Iurlaro, M. De Caroli, E. Sabella, M. De Pascali, P. Rampino, L. De Bellis, C. Perrotta, G. Dalessandro and G. Piroand. Drought and Heat Differentially Affect Xth Expression and Xet Activity and Action in 3-Day-Old Seedlings of Durum Wheat Cultivars with Different Stress Susceptibility. *Frontiers in Plant Science*, 7:1686, 2016.

135. A. Maris, D. Suslov, S. C. Fry, J. P. Verbelen and K. Vissenberg. Enzymic Characterization of Two Recombinant Xyloglucan Endotransglucosylase/Hydrolase (Xth) Proteins of Arabidopsis and Their Effect on Root Growth and Cell Wall Extension. *Journal of Experimental Botany*, 60, 13:3959-3972, 2009.

136. T. Hruz, O. Laule, G. Szabo, F. Wessendorp, S. Bleuler, L. Oertle, P. Widmayer, W. Gruissem and P. Zimmermann. Genevestigator V3: A Reference Expression Database for the Meta-Analysis of Transcriptomes. *Advances in Bioinformatics*, 2008:420747, 2008.

137. P. Johansson, H. Brumer, 3rd, M. J. Baumann, A. M. Kallas, H. Henriksson, S. E. Denman, T. T. Teeri and T. A. Jones. Crystal Structures of a Poplar Xyloglucan Endotransglycosylase Reveal Details of Transglycosylation Acceptor Binding. *Plant Cell*, 16, 4:874-886, 2004.

138. Y. Chebli, M. Kaneda, R. Zerzour and A. Geitmann. The Cell Wall of the Arabidopsis Pollen Tube--Spatial Distribution, Recycling, and Network Formation of Polysaccharides. *Plant Physiology*, 160, 4:1940-1955, 2012.

139. J. C. Mollet, C. Leroux, F. Dardelle and A. Lehner. Cell Wall Composition, Biosynthesis and Remodeling During Pollen Tube Growth. *Plants (Basel)*, 2, 1:107-147, 2013.

140. O. Wilkins, H. Nahal, J. Foong, N. J. Provart and M. M. Campbell. Expansion and Diversification of the Populus R2r3-Myb Family of Transcription Factors. *Plant Physiology*, 149, 2:981-993, 2009.

141. K. Vanneste, L. Sterck, A. A. Myburg, Y. Van de Peer and E. Mizrachi. Horsetails Are Ancient Polyploids: Evidence from Equisetum Giganteum. *Plant Cell*, 27, 6:1567-1578, 2015.

142. A. Channing, A. Zamuner, D. Edwards and D. Guido. Equisetum Thermale Sp. Nov. (Equisetales) from the Jurassic San Agustin Hot Spring Deposit, Patagonia: Anatomy, Paleoecology, and Inferred Paleoecophysiology. *American Journal of Botany*, 98, 4:680-697, 2011.

143. C. Husby. Biology and Functional Ecology of Equisetum with Emphasis on the Giant Horsetails. *Botanical Review*, 79, 2:147-177, 2013.

144. J. Irungu, E. P. Go, Y. Zhang, D. S. Dalpathado, H.-X. Liao, B. F. Haynes and H. Desaire. Comparison of Hplc/Esi-Fticr Ms Versus Maldi-Tof/Tof Ms for Glycopeptide Analysis of a Highly Glycosylated Hiv Envelope Glycoprotein. *Journal of the American Society for Mass Spectrometry*, 19, 8:1209-1220, 2008.

145. W. Morelle and J.-C. Michalski. Analysis of Protein Glycosylation by Mass Spectrometry. *Nature Protocols*, 2, 7:1585-1602, 2007.

146. L. Tsai Pei, S.-F. Chen and Y. Huang Sheng. Mass Spectrometry-Based Strategies for Protein Disulfide Bond Identification. *Reviews in Analytical Chemistry*, 4, 32:257, 2013.

147. G. Friso and K. J. van Wijk. Posttranslational Protein Modifications in Plant Metabolism. *Plant Physiology*, 169, 3:1469, 2015.

APPENDIX A: MALDI-TOF MS Result

Table A.1. MALDI-TOF MS reads MASCOT search of trytic fragments of *Equisetum* April 2016 Pool 2 sample.

	Accession	Mass	Score	Description
1	gnl|unk|AtXTH22	32073	10	AT5G57560 xyloglucan:xyloglucosyl transferase / xyloglucan endotransglycosylase / endo-xyloglucan transferase (TCH4)
2	gnl|unk|OsXTH7	32167	9	OS04G51510 OSINDICA_04G43260 9632.m04978 predicted protein
3	gnl|unk|AtXTH33	34622	8	AT1G10550 xyloglucan:xyloglucosyl transferase, putative / xyloglucan endotransglycosylase, putative / endo-xyloglucan transferase, putative
4	gnl|unk|EgXTH_3697	25635	8	Transcript_1_1_m.8190
5	gnl|unk|HvXET37	22159	8	FGENESH:[mRNA] 1 3 exon (s) 852 - 1606 591 bp, chain +
6	gnl|unk|EgXTH_15921	37107	8	Transcript_1_1_m.29972
7	gnl|unk|HvXET39	31612	7	FGENESH:[mRNA] 1 3 exon (s) 865 - 1925 864 bp, chain +
8	gnl|unk|OsXTH5	33381	6	OS08G14210 OSINDICA_08G12980 9636.m01414 predicted protein
9	gnl|unk|AtXTH25	32552	6	AT5G57550 xyloglucan:xyloglucosyl transferase / xyloglucan endotransglycosylase / endo-xyloglucan transferase (XTR3)
10	gnl|unk|TmQ41614	33950	6	Xyloglucan endotransglycosylase. nasturtium

Table A.2. Details of best hit; gnl|unk|AtXTH22 Mass: 32073 Score: 10 Expect: 17 Matches: 4

Observed	Mr(expt)	Mr(calc)	Miss	Ions	Peptide
723.3705	722.3632	722.3455	0	---	K.VSMQMK.L
755.342	754.3347	754.3353	0	---	K.VSMQMK.L + 2 Oxidation (M)
1453.7072	1452.6999	1452.6456	0	---	R.GFQQEACVWSNGK.S
3591.6018	3590.5945	3590.6744	2	---	K.NMESLGTLFPKNKPMRMY SSLWNADDWATR.G + 2 Oxidation (M)

APPENDIX B: EDMAN DEGRADATION SEQUENCING REPORT

Figure B.1. N-terminal Edman Sequencing result report from Proteome Factory Company.

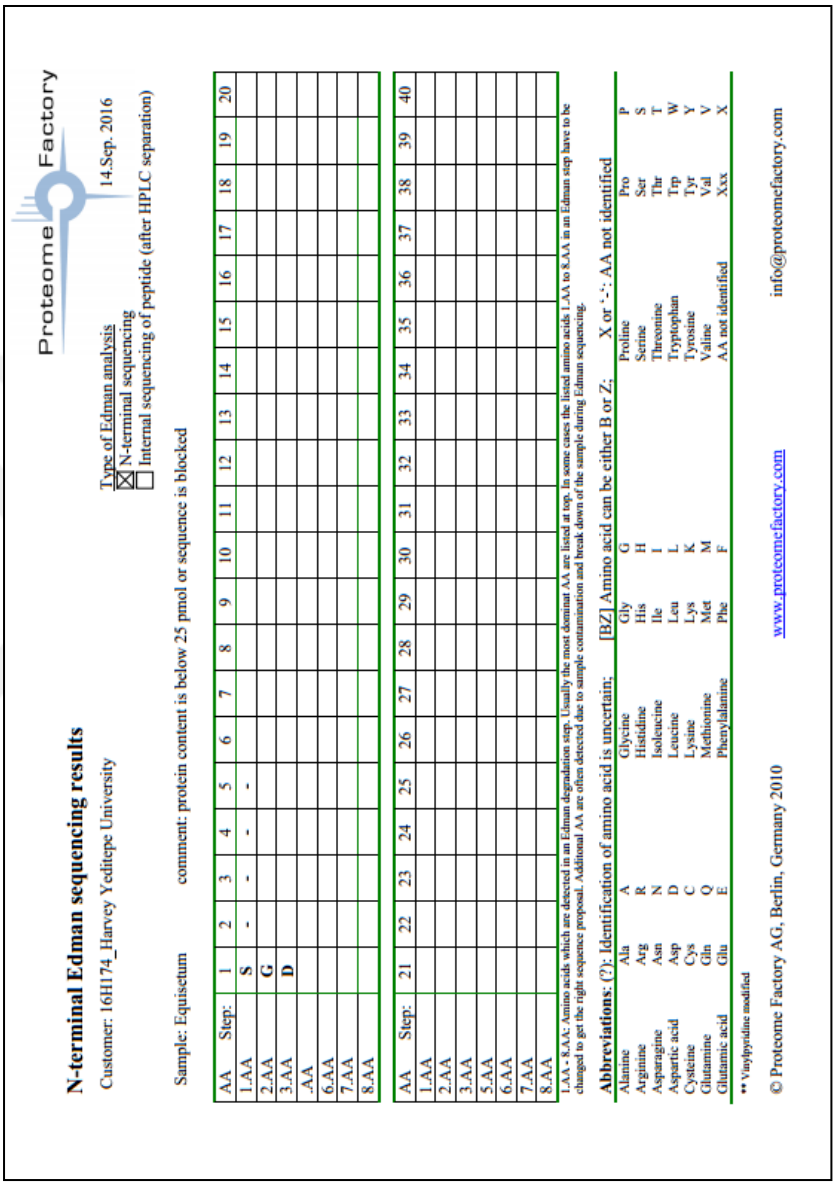

Proteome Factory

N-terminal Edman sequencing results

Customer: 16H174_Harvey Yeditepe University

Type of Edman analysis
☒ N-terminal sequencing
☐ Internal sequencing of peptide (after HPLC separation)

14.Sep. 2016

Sample: Equisetum comment: protein content is below 25 pmol or sequence is blocked

AA	Step:	1	2	3	4	5	6	7	8	9	10	11	12	13	14	15	16	17	18	19	20
1.AA		S	-	-	-	-															
2.AA		G																			
3.AA		D																			
.AA																					
6.AA																					
7.AA																					
8.AA																					

AA	Step:	21	22	23	24	25	26	27	28	29	30	31	32	33	34	35	36	37	38	39	40
1.AA																					
2.AA																					
3.AA																					
5.AA																					
6.AA																					
7.AA																					
8.AA																					

1.AA - 8.AA: Amino acids which are detected in an Edman degradation step. Usually the most dominat AA are listed at top. In some cases the listed amino acids 1.AA to 8.AA in an Edman step have to be changed to get the right sequence proposal. Additional AA are often detected due to sample contamination and break down of the sample during Edman sequencing.

Abbreviations: (?): Identification of amino acid is uncertain; [BZ] Amino acid can be either B or Z; X or '-': AA not identified

Alanine	Ala	A	Glycine	Gly	G	Proline	Pro	P
Arginine	Arg	R	Histidine	His	H	Serine	Ser	S
Asparagine	Asn	N	Isoleucine	Ile	I	Threonine	Thr	T
Aspartic acid	Asp	D	Leucine	Leu	L	Tryptophan	Trp	W
Cysteine	Cys	C	Lysine	Lys	K	Tyrosine	Tyr	Y
Glutamine	Gln	Q	Methionine	Met	M	Valine	Val	V
Glutamic acid	Glu	E	Phenylalanine	Phe	F	AA not identified	Xxx	X

** Vinylpyridine modified

www.proteomefactory.com info@proteomefactory.com